



UNIVERSITAT
POLITÈCNICA
DE VALÈNCIA

Departamento de Ingeniería Textil y Papelera (DITEXPA)

PhD in Textile Engineering

**Assessment of novel Advanced Oxidation
Processes for the simultaneous disinfection
and decontamination of water**

Memory presented for the title of Doctor:

Ilaria Berruti

Almería, March 2022

THESIS SUPERVISORS:

Dr. María Inmaculada Polo López

Research Fellow OPI

CIEMAT-Plataforma Solar de Almería,

Almería, Spain

Dr. Marcello Manfredi

Researcher

University of Piemonte Orientale,

Novara, Italy



*"Success is not final; failure is not fatal:
it is the courage to continue that counts."*

Winston Churchill

ACKNOWLEDGMENT

Throughout the PhD, I have received a great deal of support and assistance. Doing a PhD abroad is a challenge, leading sometimes to have mixed feeling provoked by separation from family, cultural differences and language barriers, that have to be overcome. At this point, I can say, without any doubt, that it was the best decision of my life. I will be always grateful to each person that I had the opportunity and the luck to meet in these years, which make me feel like at home. I am happy to have another big family and Almería will always be in my heart.

I would like first to thank my supervisor, Dr. M. Inmaculada Polo López; gracias Inma, por tus aportaciones y participación en el desarrollo de esta tesis. Estaré siempre agradecida por todo lo que me has enseñado, por la paciencia, por el cariño, por tu apoyo, por tu disponibilidad, por la pasión que pones en tu trabajo y por ser tan buena personal y profesionalmente. Gracias por escucharme, por preocuparte por mí, y por estar siempre presente. Espero que estés satisfecha del trabajo final que hemos conseguido; el desarrollo de esta tesis no hubiera sido posible sin ti y estoy muy contenta de nuestro trabajo en equipo. I would also like to thank Dr. Isabel Oller; Isa, gracias por la disponibilidad, el apoyo, el cariño y por aceptarme en el grupo desde el principio, sin que me sintiera en ningún momento fuera de lugar.

A special thank to Prof. Paola Calza; grazie per le opportunità che mi hai dato e per credere in me, molto di piú di quanto abbia mai fatto io stessa.

I would like to acknowledge also Prof. Sixto Malato for sharing his knowledge and experience. Thank to Prof. Ana Agüera for the collaboration, availability and help and to my tutor at UPV Prof. Antonio Arques.

I would also like to thank my tutors for their valuable guidance and support during the several secondment, Prof. Elisa Robotti and Prof. Fabio Gosetti in UPO/ISALIT, Prof. M. Luisa Marín, Prof. Francisco Boscá, Prof. María Ángeles Castillo, Prof. Consuelo Sabater in UPV, Dr. Ulrich Pretsch, Dr. Peter Bondgaard Mortensen, Dr. Pia Bøgelund in Eurofins and Prof. Marco Minella in UNITO.

It has been a pleasure to be involved in the doctoral programme Marie-Skłodowska-Curie Actions' (MSCA) Innovative Training Network (ITN), funded by the European Union (EU). I had the opportunity to conduct research in an international, challenging and stimulating environment, collaborating and interacting with various experts in water field, performing several secondments and training and attending project meeting and conferences.

Thank you to all the AQUALity project members, a special thanks to the fifteen Early-Stage Researchers and in particular to Nuno, Masho (for the help and for all the moments; the secondment in Denmark would have not been the same without you), Iván (por todos los momentos compartido juntos, por todos los viajes en España y por los meses de tu estancia en Almería), Dimitra and to my colleague at PSA Dennis (for the support and help). It was a pleasure to know each of you and to share nice moments all around Europe.

It is essential to acknowledge each one of the PSA colleagues, for the constant support and for sharing work, pleasure, and tired times.

Tengo sólo palabras de agradecimiento para cada uno de vosotros.

A Samira, mi apoyo desde el primer minuto y una amiga con la cual puedo contar. Gracias, mi Sami, por creer en mí, por enseñarme los primeros pasos en ese camino, por ayudarme y por el cariño.

A mi mami española, gracias Isa por la ayuda cuando mi cabezonería creía poder con todo. Gracias por plantarte allí de todas formas y hacerme la vida más fácil. Gracias por entenderme en el silencio, sabiendo que algo no iba bien con tan solo mirarme a los ojos y por estar presente por lo que me hacía falta.

Gracias Azahara, por estar siempre disponible, gracias por los consejos, por las ayudas en las cosas burocráticas y por todo lo que me has enseñado. Ha sido importante para mi encontrar la manera de entendernos, para trabajar bien juntas, ayudándonos mutuamente.

Gracias Meli, por todos los buenos momentos, por tener siempre una sonrisa, una buena actitud y por tu maravillosa voz que nos ha alegrado los días (aunque mis oídos no estén totalmente de acuerdo jajaja).

Gracias Chus, por cada momento pasado juntas y por el apoyo mutuo, he agradecido mucho tu llegada en la recta final de mi doctorado.

Gracias Alba R., por tu amabilidad, por tu buen ser y por los momentos compartidos. Gracias Eli, por ayudarme siempre con una sonrisa (y gracias por todos los eppendorfs que has rellenado con PBS jejeje) y Panchy por estar siempre disponible a echarme una mano y por todos los momentos dentro y fuera del laboratorio.

Gracias a Irene, Ana, Gracia, Joyce y a los compañeros de otras unidades Aurelio, Sergio e Isa Requena.

Gracias a Anita por la paciencia, la disponibilidad y el apoyo.

Un agradecimiento especial a mi compañera de despacho preferida. Alba, en poco tiempo te has convertido en alguien muy importante en mi vida y has sido fundamental en esta

última etapa, que no hubiese sido igual sin ti. Gracias por animarme, por apoyarme, por hacerme desconectar, por entenderme sin que haga falta hablar y por estar siempre presente. PSA provides an international and stimulating environment and I had the opportunity to meet several people from different places in the world with different cultures, way of thinking, backgrounds and languages, sharing with each of them nice and unforgettable moments.

I will always be grateful to Giusy, Cristina, Lis, Gema, Belén, Leonor, Yeney, Antonino, Massimo and Burcu.

A special thank to Elizangela and Isaac. Gracias por todos los momentos compartidos, por los cafés, las charlas y por los viajes. Os echo muchos de menos.

Grazie alla mia piccolina Gulnara. Grazie per essere sempre stata presente, per le nostre passeggiate, per gli aperitivi nella spiaggia e per tutti i pranzi della domenica che abbiamo preparato insieme. Sapevo che la vita ad Almería non sarebbe stata più la stessa, non avendoti più a 5 minuti da casa mia, ma ricorderò sempre con tanto affetto tutti i momenti che abbiamo vissuto insieme.

A cada uno de vosotros tengo también que daros las gracias por compartir buenos momentos fuera del trabajo, por las tapas y los vinos en buena compañía, y sobre todo por hacer que no me sintiera sola en ningún momento.

An acknowledgment to all the people that I met during the several secondments. Thank you to Mattia, Maria, Damiano, Ximo, Jenny, Mauricio, Oscar, Cristina, Paloma, Pia, Johannes, and Luca.

Grazie ad Alessandro per essere sempre presente, nonostante la distanza.

Grazie alla mia famiglia per l'amore, il costante sostegno, per non avermi mai fatto sentire sola e per credere in me. Grazie a mia mamma e a mio papà per tutti i sacrifici fatti per permettermi di arrivare a questo punto e soprattutto per aver appoggiato incondizionatamente qualsiasi mia scelta. Grazie a mia sorella e a mio fratello, su cui si può sempre contare. Grazie ai miei zii e a mia cugina e un grazie speciale a mia nonna che ha sempre aspettato con ansia il mio ritorno, contando i mesi, i giorni e i minuti.

Last, but not least, I would like to thank to myself for considering the possibility to get out for the comfort zone, challenging myself and completely changing my life.

I lived an unforgettable experience that has allowed me to improve my skills and knowledge and to expand my horizons, enhancing myself from both personal and professional point of view.

Thesis framework and scientific production

The research presented in this thesis has been developed in the framework of the European Union's Horizon 2020 research and innovation programme under the Marie Skłodowska-Curie Grant Agreement No 765860 (AQUALity) and it was carried out at CIEMAT-Plataforma Solar de Almeria facilities (Almeria, Spain).

Moreover, several secondments were conducted in partner's laboratories within AQUALity consortium (academic and non-academic) for a total duration of 10 months:

- Isalit S.r.l./Università of Piemonte Orientale (UPO) (Italy): for 2 months under the supervision of Prof. Elisa Robotti.
- Universitat Politècnica de València (UPV) at Instituto de Tecnología Química (ITQ) and at Dpto Biotecnología (Spain): for 3 months under the supervision of Prof. M. Luisa Marin.
- Eurofins (Denmark): for 2 months under the supervision of Dr. Ulrich Precht.
- Università di Torino (UNITO) (Italy): for 3 months under the supervision of Prof. Marco Minella.

In addition, another collaboration involves the research group FQM374 "Análisis ambiental y tratamiento de aguas", belonging to the research centre CIESOL (joint research centre formed by University of Almería (UAL) and CIEMAT).

The results shown in this memory have been published or are in process of being published in international journals with high scientific impact factor:

1. Berruti, I., Oller, I., Polo-López, M.I., 2021. **Direct oxidation of peroxymonosulfate under natural solar radiation: Accelerating the simultaneous removal of organic contaminants and pathogens from water.** Chemosphere 279. <https://doi.org/10.1016/j.chemosphere.2021.130555>
2. Berruti, I., Nahim-Granados, S., Abeledo-Lameiro, M.J., Oller, I., Polo-López, M.I., 2021. **UV-C peroxymonosulfate activation for wastewater regeneration: Simultaneous inactivation of pathogens and degradation of contaminants of emerging concern.** Molecules 26. <https://doi.org/10.3390/molecules26164890>
3. Berruti, I., Nahim-Granados, S., Abeledo-Lameiro, M.J., Oller, I., Polo-López, M.I., 2022. **Recent advances in solar photochemical processes for water and wastewater disinfection.** Chemical Engineering Journal Advances. 100248.
4. Berruti, I., Gonçalves, N., Calza, P., Paganini, M.C., Oller, I., Polo-López, M.I. **Natural solar activation of modified zinc oxides with rare earth elements (Ce, Yb and Fe) for the simultaneous disinfection and decontamination of urban wastewater.** Submitted in Chemosphere

5. Berruti, I., Polo-López, M.I.; Oller I., Laurenti, E., Calza, P., Minella, M. **New insights into the mechanism of peroxymonosulfate activity for the removal of aqueous pollutants.** To be submitted in Catalysis Today.
6. Berruti I., Polo-López, M.I.; Oller I., Flores, J., Marin, M.L., Bosca, F. **Sulfate radical anion: Laser flash photolysis study and application in water disinfection and decontamination.** Submitted in Applied Catalysis B: Environmental.
7. Berruti, I., Nahim-Granados, S., Abeledo-Lameiro, M.J., Oller, I., Polo-López, M.I. **Combination between natural solar radiation and peroxymonosulfate for urban wastewater regeneration.** To be submitted in Science of Total Environment.
8. Berruti I., Polo-López, M.I.; Oller I., Martínez-Piernas, A. B. Agüera, A. **Identification and occurrence of diclofenac, sulfamethoxazole and trimethoprim transformation products by solar and UV-C peroxymonosulfate systems in urban wastewater.** In preparation.

Additional activities of dissemination have been carried out by the PhD candidate, including scientific contributions in conferences, seminars, workshop, among others (see Curriculum Vitae).

INDEX OF CONTENTS

SUMMARY	3
1. INTRODUCTION.....	21
1.1. The water availability: towards a circular economy.....	21
1.2. The European water framework	25
1.2.1. Drinking water legislation	27
1.2.2. Reclamation of urban wastewater legislation	29
1.3. Water pollutants of emerging concern	30
1.3.1. Microbial targets.....	30
1.3.2. Contaminants of Emerging Concern	33
1.3.3. Disinfection by Products formation.....	36
1.4. Water treatment plants.....	38
1.4.1. Drinking water treatment plants	39
1.4.2. Urban wastewater treatment plants.....	40
1.5 Water purification treatments	42
1.5.1. Chlorination.....	43
1.5.2. Ozonation	43
1.5.3. UV-C radiation	45
1.5.4. Solar water disinfection.....	46
1.6 Advances Oxidation Processes.....	48
1.6.1. Solar heterogeneous photocatalysis.....	54
1.7 Sulfate radical Advanced Oxidation Processes	59
1.8. Photo-reactors employed for water processes	63
1.8.1. Compound Parabolic Collector	63
1.8.2. UV-C plant	64
1.9. Transformation products and toxicity	65
2. OBJECTIVES AND EXPERIMENTAL PLAN.....	71
2.1 Objectives.....	71
2.2 Experimental plan	72
3. MATERIALS AND METHODS	79
3.1. Chemicals.....	79
3.2. Microbial targets	81
3.2.1 Description of bacterial strains investigated.....	81
3.2.2. Bacterial enumeration and quantification procedure.....	82
3.2.3. Antibiotic resistant genes detection procedure	87
3.3 Organic chemical targets	91
3.3.1 Contaminants of Emerging Concern description.....	91
3.3.2. CECs preparation and quantification.....	92
3.4. Water matrices.....	95

Index of contents

3.4.1 Isotonic water	95
3.4.2 Well water	96
3.4.3 Simulated Urban Wastewater	96
3.4.4 Urban Wastewater	97
3.5 Water characterization.....	97
3.5.1. Conductivity, pH, and turbidity	98
3.5.2 Dissolved organic carbon	98
3.5.3. Ion chromatography.....	100
3.6. Reactors for water purification.....	101
3.6.1. 200-mL solar vessel reactor.....	101
3.6.2. 10-L Compound Parabolic Collector reactor.....	102
3.6.3. 80-L UV-C pilot plant	103
3.7. Water disinfection and decontamination tests	105
3.7.1. Experimental procedure.....	105
3.7.2. Solar radiation analysis.....	106
3.7.3. Analytical determination of PMS in water	106
3.7.4. Photocatalysts	107
3.8. Kinetics analysis models	108
3.9. Transformation Products analysis and quantification	109
3.10. Toxicity tests	113
3.10.1. <i>Aliivibrio fischeri</i>	113
3.10.2. Phytotoxicity.....	114
3.11. Laser Flash Photolysis technique	115
3.12. Radical's generation analysis	117
3.12.1. Radical scavenger's tests	117
3.12.2. Electron paramagnetic resonance	118
4. ASSESSMENT OF SIMULTANEOUS DISINFECTION AND DECONTAMINATION OF WATER BY SOLAR HETEROGENEOUS PHOTOCATALYSIS	123
4.1. Proof-of-principle studies in isotonic water	124
4.1.1. Dark assessment of ZnO materials.	124
4.1.2. Photocatalytic activity in isotonic water.....	125
4.1.3. Interpretation of modified ZnO photocatalytic activity.....	130
4.2. Proof-of principle in simulated urban wastewater.....	132
4.3. Disinfection and decontamination of urban wastewater	137
4.4. Concluding remarks	142
5. ASSESSMENT OF PEROXYMONOSULFATE AND SULFATE RADICAL REACTIVITY	147
5.1 Peroxymonosulfate reactivity.....	148
5.1.1 Parameters affecting PMS reactivity under dark conditions	148
5.1.2. Reactive Oxygen Species determination by scavenger experiments.....	154

5.1.2.1	Reactive species under dark condition.....	155
5.1.2.2	Reactive species under simulated solar radiation	156
5.1.2.3	Reactive species under UV-C radiation.....	157
5.1.3.	Electron paramagnetic resonance detection	158
5.2	Radical sulfate reactivity	162
5.2.1	Radical sulfate $\text{SO}_4^{\cdot-}$ generation	162
5.2.2	Elucidation of the $\text{SO}_4^{\cdot-}$ mechanism of reaction	163
5.2.2.1	H-abstraction reaction.....	164
5.2.2.2	Electron transfer reaction.....	165
5.2.3.	Determination of the bimolecular rate constants ($k_{\text{SO}_4^{\cdot-}}$) between cell wall constituents and $\text{SO}_4^{\cdot-}$	166
5.2.4.	Determination of the bimolecular rate constants between $\text{SO}_4^{\cdot-}$ and CECs.....	173
5.3	Concluding remarks	175
6.	ASSESSMENT OF PEROXYMONOSULFATE FOR WATER PURIFICATION UNDER NATURAL SOLAR RADIATION	179
6.1	PMS/Dark system.....	179
6.2	PMS/Solar system	184
6.3	Interpretation of abatement mechanisms by PMS/Solar radiation	187
6.4	Disinfection and decontamination performances in natural well water	190
6.5.	Effect of inorganic species on PMS/Solar system performance.....	192
6.6	Concluding remarks	193
7.	ACTUAL WASTEWATER PURIFICATION BY PEROXYMONOSULFATE AND SOLAR RADIATION AT PILOT PLANT SCALE	197
7.1	PMS/Solar process performance in simulated urban wastewater.....	198
7.1.1	Assessment of microbial and CECs abatement	198
7.1.2	Assessment of organic matter influence	201
7.2	PMS/Solar process performance in actual urban wastewater.....	203
7.2.1	Bacterial inactivation kinetics	204
7.2.2	CECs degradation kinetics	206
7.2.3	Antibiotic Resistant Bacteria and Genes removal	208
7.3	Photocatalytic performance of ZnO-Ce with peroxymonosulfate in UWW	210
7.4	Conclusions	213
8.	WATER AND WASTEWATER PURIFICATION BY PEROXYMONOSULFATE AND UV-C RADIATION	217
8.1	Disinfection and decontamination performances in isotonic water.....	218
8.2	Disinfection and decontamination performances in simulated urban wastewater.....	222
8.3	Disinfection and decontamination performances in urban wastewater	224
8.4	Comparison of process performance: analysing the effect of natural organic matter and inorganic species	228
8.5	Antibiotic Resistant Bacteria and Genes removal	230
8.6	Concluding remarks	232

Index of contents

9. COMPARATIVE EVALUATION OF PHOTO-CHEMICAL PROCESSES	237
9.1 Transformation Products assessment	238
9.1.1 Identification of TPs and degradation routes	238
9.1.2 TPs detection during PMS/Solar <i>versus</i> PMS/UV-C process	244
9.2 Eco-toxicological assessment of treated UWW	247
9.3 Annual Treatment Cost	250
9.3.1 PMS/Solar	250
9.3.2 PMS/UV-C	252
9.4 Comparative evaluation and concluding remarks	253
10. CONCLUSIONS	259
11. REFERENCES.....	265
12. ANNEXES	291
ANNEX A. Modified ZnO photocatalyst characterization	291
ANNEX B. Kinetic constants evaluation	294
ANNEX C. TPs identification.....	303

INDEX OF FIGURES

Figure 1.1 World map of water stress condition in 2040, according to a World Resource Institute (Luo, 2015).

Figure 1.2. Linear *versus* circular vision of the urban water cycle.

Figure 1.3. Framework of European water legislation.

Figure 1.4. CECs classification, sources and accumulation in soil, water and air, impacting on animals, plants and humans.

Figure 1.5. Occurrence of DBPs.

Figure 1.6. Treatment processes train of (a) surface water and (b) groundwater to obtain drinking water.

Figure 1.7. Treatment processes train in UWWTPs and influent and effluent main chemical and microbiological parameters of concern (Data according to Wang, 2020).

Figure 1.8. Water treatment processes.

Figure 1.9. Spectrum of solar radiation at the top of Earth and at sea level.

Figure 1.10. Sunlight mediated inactivation mechanism involving photoinactivation of endogenous cell constituents' chromophore (a) direct effects, (b) indirect effects and (c) indirect photoinactivation of exogenous chromophore. Adapted from (Nelson, 2018).

Figure 1.11. Mechanism of photocatalysis.

Figure 1.12. Mechanism of photocatalysis in the presence of PMS.

Figure 1.13. Frequency of reports by year (2000 - 2021), dealing with SR-AOPs for water treatment. The search was based on Scopus database using as keywords 'advanced oxidation processes; sulfate radicals; water including articles, reviews, books, and book chapters.

Figure 1.14. Dissociation equilibrium for peroxymonosulfate and corresponding pKa.

Figure 1.15. Schematic drawing of a CPC. Adapted from (Malato, 2002).

Figure 1.16. Water treatment by UV-C radiation.

Figure 3.1. (a) Laminar flow cabinet and (b) autoclave used in this work and available at the laboratory of Solar Treatment of Water (CIEMAT-PSA).

Figure 3.2. Rotary shaking incubator used for growing of bacteria in liquid culture media.

Figure 3.3. Example of a stock plate containing *E. coli* colonies.

Figure 3.4. Microfil®filtration system.

Figure 3.5. (a) *E. coli* O157:H7 cultivated in Chromocult agar, (b) *E. faecalis* in SB agar and (c) *P. aeruginosa* in Pseudomonas chromogenic agar.

Figure 3.6. DNA extraction of water samples for PCR analysis, according to the commercial DNeasy® PowerWater® Kit.

Figure 3.7. Amplification plot obtained over the duration of a real-time PCR experiment. ΔR_n : baseline-corrected normalized reporter.

Figure 3.8. UPLC-UV-DAD used for CECs quantification.

Figure 3.9. Calibration lines of DCF, SMX and TMP (0-120 $\mu\text{g/L}$).

Figure 3.10. (a) Conductometer, (b) pH meter and (c) turbidimeter.

Figure 3.11. Shimadzu Total Organic Carbon analyzer TOC-L with an autosampler ASI-L.

Figure 3.12. TC, IC and DOC measurements.

Figure 3.13. 850 Professional IC.

Figure 3.14. (a) 200-mL vessel reactor used in a photocatalytic test under natural sunlight. (b) Outside and inside natural solar irradiance profile, measured through the solar-glass vessel reactor used in this study. Measurements obtained with a spectrometer (AvaSpec-ULS2048 AVANTES) at 10:50 am local time in a sunny day at CIEMAT-PSA location (South East of Spain).

Index of contents

Figure 3.15. (a) 10-L CPC installed at PSA-CIEMAT facilities and used in this work and (b) reactor flow diagram.

Figure 3.16. (a) Schematic configuration of the reactor containing the UV-C lamp and (b) UV-C pilot plant installed at PSA-CIEMAT facilities.

Figure 3.17. Irradiance profiles of UV-C lamp in different water matrices (DW, SUWW, UWW).

Figure 3.18. (a) UV-A pyranometer located at PSA facilities and (b) typical solar irradiance profile at the PSA location.

Figure 3.19. (a) Oxidation of DPD by PMS and (b) spectrophotometer Evolution 220.

Figure 3.20. UV-visible absorbance profiles of the different photocatalysts at 100 mg/L and solar emission spectrum at ground level (measured at CIEMAT-PSA facilities).

Figure 3.21. SPE procedure: (a) sample filtration, (b) cartridge conditioning, equilibration, loading and elution, (c) cartridge drying under N₂ and (d) sample evaporation.

Figure 3.22. (a) HPLC 1260 Infinity- QTOF mass analyzer Triple TOF 5600+ and (b) scheme of a QTOF instrument.

Figure 3.23. Suspect screening workflow.

Figure 3.24: Germination of *Lepidium sativum* (a), *Sinapis alba* (b) and *Sorghum saccharatum* (c).

Figure 3.25: (a) LFP diagram and (b) ND:YAG SL404G-10 Spectron Laser System.

Figure 3.26. (a) X-band Bruker EMX spectrometer and (b) the SpinFit window.

Figure 4.1: (a) Viability of sum of bacteria and (b) adsorption of total CECs in IW in the presence of modified ZnO with Ce, Fe and Yb at 500 mg/L. Tests performed in the dark, at room temperature and under constant agitation (350 rpm).

Figure 4.2. T, pH and UV-A irradiance profiles during solar experiments.

Figure 4.3. Inactivation profiles of *E. coli*, *E. faecalis* and *P. aeruginosa* (left) and sum of bacteria with solar inactivation (for comparison purposes) (right) by modified ZnO with Ce (a), Yb (b), and Fe (c) at 100, 200 and 500 mg/L under natural solar radiation in IW.

Figure 4.4. Degradation profiles of DCF, SMX and TMP (left) and total CECs with solar photolysis (for comparison purpose) (right) by modified ZnO with Ce (a), Yb (b) and Fe (c) at 100, 200 and 500 mg/L in IW under natural solar radiation.

Figure 4.5. (a) Inactivation kinetic constants of *E. coli*, *P. aeruginosa* and *E. faecalis* and (b) CECs degradation kinetic constants in the presence of modified ZnO modified with Ce, Yb and Fe at concentration of 100, 200 and 500 mg/L in IW under natural solar radiation.

Figure 4.6. Schematic representation of ROS generation by the modified ZnO catalysts with Ce, Yb and Fe in water and irradiated by natural solar radiation.

Figure 4.7. SMX degradation curves (C₀=25 mg/L) under simulated sunlight (photolysis), in the presence of ZnO-Ce at 50 mg/L, with or without MeOH and TBA at 0.1 M.

Figure 4.8. Inactivation profiles of *E. coli* (a), *P. aeruginosa* (b) and *E. faecalis* (c) in SUWW in the presence of ZnO modified with Ce, Fe and Yb and TiO₂-P25 at 100 (left) and 500 mg/L (right).

Figure 4.9. Degradation profiles of DCF (a), SMX (b) and TMP (c) in the presence of ZnO modified with Ce, Yb and Fe and TiO₂-P25 at concentration of 100 (left) and 500 mg/L (right) in SUWW under natural solar radiation.

Figure 4.10. (a) Pseudo first-order inactivation kinetic constants of *E. coli*, *P. aeruginosa* and *E. faecalis* and (b) degradation constants of DCF, SMX and TMP in the presence of ZnO modified with Ce, Yb and Fe and TiO₂-P25 at concentration of 100 and 500 mg/L in SUWW under natural solar radiation.

Figure 4.11. Inactivation profiles of *E. coli* (a), Total coliforms (b), *Pseudomonas* spp. (c) and *Enterococcus* spp. (d) in UWW in the presence of TiO₂-P25 and modified ZnO-Ce at 100 and 500 mg/L.

Figure 4.12. Degradation profiles of DCF (a), SMX (b) and TMP (c) in the presence of modified ZnO-Ce and TiO₂-P25 at concentration of 100 and 500 mg/L in UWW under natural solar radiation.

Figure 4.13. (a) Inactivation kinetic constants of natural occurring in UWW *E. coli*, Total coliforms, *Enterococcus* spp., and *Pseudomonas* spp., (b) inactivation bacteria summation profiles, (c) degradation kinetic constants of DCF, SMX and TMP and (d) total CECs degradation curves in the presence of ZnO-Ce and TiO₂-P25 at concentration of 100 and 500 mg/L under natural solar radiation.

Figure 4.14. Ratio between kinetic constants in UWW and SUWW of DCF, SMX and TMP in the presence of ZnO-Ce and TiO₂-P25 at concentration of 100 and 500 mg/L.

Figure 5.1: SMX ($C_0 = 1 \cdot 10^{-5}$ M) degradation profiles under dark conditions in the presence of different (a) concentration of PMS, (b) T and (c) pH.

Figure 5.2: Acid-base speciation for SMX (a) and for PMS (b).

Figure 5.3: SMX ($C_0 = 1 \cdot 10^{-5}$ M) degradation profiles under dark conditions in the presence of different concentration of (a) Cl⁻ and Cl⁻ in the presence of phenol ($1 \cdot 10^{-3}$ M) and (b) HCO₃⁻ $4 \cdot 10^{-3}$ M, adding different concentrations of 3-Chloroaniline ($2 \cdot 10^{-5}$, $4 \cdot 10^{-5}$ and $1 \cdot 10^{-3}$ M), and in the presence of PMS alone $1 \cdot 10^{-3}$ M (in milliQ water at pH 3) and at pH 7 for phosphate buffer.

Figure 5.4. SMX degradation profiles in the presence of PMS $1 \cdot 10^{-3}$ M (a) under dark condition and (i) without scavengers, (ii) with MeOH 1 M, (iii) with TBA 1 M, (iv) NaN₃ $1.5 \cdot 10^{-2}$ M and (v) FFA $1 \cdot 10^{-5}$ M; (b) under simulated solar radiation (280 nm filter) and (i) without scavengers, (ii) with MeOH 0.5 M, (iii) with TBA 0.5 M and at 50°C under dark conditions and SMX (c) and TMP (d) degradation profiles under UV-C light in the presence PMS $3 \cdot 10^{-3}$ M and MeOH 0.1 M or TBA 0.1 M.

Figure 5.5. (a) Absorption spectra of SMX $1 \cdot 10^{-5}$ M and PMS $1 \cdot 10^{-3}$ M on an optical length ($b=1$ cm) and solar emission spectrum at ground level (measured at CIEMAT-PSA facilities) and (b) SMX degradation profiles in the presence of PMS $1 \cdot 10^{-3}$ M in dark at 60 °C and with and without MeOH and TBA 0.5 M as radical's scavengers.

Figure 5.6. Reactions between the spin trap (a) DMPO and HO[•], SO₄^{•-} and HClO and (b) TEMP and ¹O₂.

Figure 5.7. EPR spectra of DMPO adducts formed by PMS in the dark (a) at pH 3; (b) pH 11; (c) in the presence of NaN₃ ($1.5 \cdot 10^{-2}$ M) at different times, (d) simulation by Spinfit software and (e) EPR spectra of DMPOX formed by PMS in the dark and in the presence of chloride ions $1.5 \cdot 10^{-1}$ M at different times.

Figure 5.8. (a) EPR spectra of DMPO adducts formed by PMS under UV-C radiation at different times; (b) its simulation by Spinfit software as sum of two species: DMPO-OH[•] and DMPO-SO₄^{•-} adducts. Simulated spectra of the two species are also shown separately in the lower part of the figure.

Figure 5.9. EPR spectra of DMPOX formed by PMS under simulated sunlight at different times.

Figure 5.10. EPR spectra of TEMP adducts formed by PMS at different times in the dark (a) at pH=3 and (b) at pH = 11.

Figure 5.11. (a) Transient absorption spectra of SO₄^{•-}, generated upon LFP irradiation ($\lambda_{exc} = 266$ nm) of aqueous solutions of PS (0.1 M) and (b) decay of SO₄^{•-} monitored at 450 nm in the absence or presence of air.

Figure 5.12. Left: Decay of SO₄^{•-}, monitored at 450 nm, obtained from laser flash excitation ($\lambda_{exc} = 266$ nm) of aerated solutions of PS (0.1 M), in the presence of increasing concentrations of isopropanol (a) or methanol (b). Right: Corresponding Stern-Volmer plots.

Figure 5.13. (a) Decay of SO₄^{•-}, monitored at 450 nm, obtained from laser flash excitation ($\lambda_{exc} = 266$ nm) of deaerated solutions of PS (0.1 M), in the presence of increasing concentrations of NaN₃. (b) Corresponding Stern-Volmer plot.

Figure 5.14. Structure of the muramic acid subunit in the peptidoglycan of *E. coli*.

Figure 5.15. Left: Decay of SO₄^{•-}, monitored at 450 nm, obtained from laser flash excitation ($\lambda_{exc} = 266$ nm) of deaerated solutions of PS (0.1 M), in the presence of increasing concentrations of cell wall constituents: *N*-acetylmuramic acid (a); *N*-acetyl-*L*-alanine (b); 2,6-Diaminopimelic acid

Index of contents

(c); *N*-acetyl-*D*-glucosamine (d); *N*-acetyl-*L*-lysine (e); *N*-acetyl-*D,L*-glutamic acid (f). Right: corresponding Stern-Volmer plots.

Figure 5.16: (a) Transient absorption spectra obtained from a solution of PS (0.1 M) in the presence of Trp ($2 \cdot 10^{-4}$ M), recorded at different times after the laser pulse ($\lambda_{\text{exc}} = 266$ nm). (b) Oxidation of *L*-tryptophan methyl ester by e^- transfer followed by proton transfer (PCET mechanism). (c) Left: Transient absorption traces monitored at 550 nm, obtained upon laser pulse ($\lambda_{\text{exc}} = 266$ nm) from a solution of PS (0.1 M) with different concentrations of Trp. Right: Corresponding Stern-Volmer plot.

Figure 5.17: Left: Decay of $\text{SO}_4^{\cdot-}$, monitored at 450 nm, obtained from laser flash excitation ($\lambda_{\text{exc}} = 266$ nm) of aerated solutions of PS (0.1 M), in the presence of increasing concentrations of tyrosine (a) and phenylalanine (b). Right: Corresponding Stern-Volmer plot.

Figure 5.18: Schematic drawing of gram-negative and gram-positive bacteria cell wall and $\text{SO}_4^{\cdot-}$ main attack sites.

Figure 5.19: Left: Decay of $\text{SO}_4^{\cdot-}$, obtained from laser flash excitation ($\lambda_{\text{exc}} = 266$ nm) of a solution of PS (0.1 M), in the presence of different concentrations of DCF (a), SMX (b) and TMP (c), monitored at 450 nm. Right: corresponding Stern-Volmer plot.

Figure 6.1. Inactivation profiles of (a) *E. coli*, (b) *P. aeruginosa*, (c) *E. faecalis* and (d) the sum of bacteria in the presence of different concentrations of PMS (0-0.01 mM) at 25 °C in IW and in the dark.

Figure 6.2. Degradation profiles of (a) DCF, (b) SMX, (c) TMP and (d) total CECs in the presence of different concentrations of PMS (0-0.01 mM) at 25 °C in IW and in the dark

Figure 6.3: Kinetic constant values (min^{-1}) of (a) bacterial inactivation and (b) CEC degradation by PMS/Dark in IW.

Figure 6.4: Temperature, pH and UV-A irradiance profiles during solar experiments.

Figure 6.5. Inactivation profiles of (a) *E. coli*, (b) *E. faecalis*, (c) *P. aeruginosa* and (d) sum of bacteria by PMS/Solar system at different PMS concentrations (0-0.01 mM) in IW and under natural sunlight.

Figure 6.6. Degradation profiles of (a) DCF, (b) SMX, (c) TMP and (d) total CECs by PMS/Solar system at different PMS concentrations in IW and under natural solar radiation.

Figure 6.7. Kinetic constant values of bacterial inactivation at 0.005 mM of PMS and CECs degradation at 0.01 mM of PMS, in the dark and under natural solar radiation in IW.

Figure 6.8. Proposed inactivation mechanism of bacteria by PMS/Solar treatment.

Figure 6.9: Inactivation profiles of *E. coli* (a), *P. aeruginosa* (b), *E. faecalis* (c) and degradation profiles of DCF (d), SMX (e), TMP (f) in diluted well water (d-WeW) and well water (WeW) by PMS/Solar at 0.01 mM of oxidant.

Figure 6.10. (a) Inactivation profiles of the sum of all bacteria and (b) degradation profiles of total CECs in in DW, IW, d-WeW and WeW by solar only radiation and PMS/Solar at 0.01 mM under natural solar radiation.

Figure 7.1: Inactivation profiles of *E. coli* (a), *P. aeruginosa* (b), *E. faecalis* (c) and sum of bacteria (d) in SUWW by PMS/Solar (0-0.5 mM).

Figure 7.2: Degradation profiles of DCF (a), SMX (b), TMP (c) and total CECs (d) in SUWW by PMS/Solar (0-0.5 mM).

Figure 7.3. (a) Inactivation profiles of the total concentration of bacteria, (b) total CECs degradation and inactivation (c) and degradation (d) kinetic constant values in SUWW by PMS at 0.5 mM under darkness and under natural solar radiation.

Figure 7.4. PMS concentration profiles along: (a) all solar treatments in SUWW (0.01-0.5 mM); (b) at 0.05 mM in the dark and with different water matrixes (DW, SUWW and UWW); (c) at 0.05 mM with different organic matter components (concentration according to SUWW recipe).

Figure 7.5: PMS concentration profiles measured along PMS/Solar treatments in UWW (0.1- 1 mM).

Figure 7.6: Inactivation profiles of *E. coli* (a), Total coliforms (b), *Pseudomonas* spp. (c), *Enterococcus* spp. (d) and sum of bacteria (e) in UWW by PMS/Solar (0-1 mM).

Figure 7.7: Degradation profiles of DCF (a), SMX (b), TMP (c) and total CECs (d) in UWW by PMS/Solar (0-1 mM).

Figure 7.8. (a) Inactivation profiles of *E. coli*, *Enterococcus* spp. and *Pseudomonas* spp. and their resistant TMP, AMP and CPX counterparts and (b) ARGs removal in the presence of 1 mM of PMS under natural solar radiation in UWW.

Figure 7.9: Comparison of the inactivation constants for *E. coli* (a), *Pseudomonas* spp. (b), *Enterococcus* spp. (c), DCF (d), SMX (e) and TMP (f) by ZnO-Ce (100 mg/L), PMS/Solar (0.2, 0.3 and 0.4 mM) and their combination PMS/ZnO-Ce (0.2, 0.3, 0.4 mM with 100 mg/L) under natural solar radiation.

Figure 8.1. Linear fitting of the inactivation profiles of (a) *E. coli*, (b) *P. aeruginosa*, (c) *E. faecalis* and (d) sum of bacteria by PMS/UV-C system at different PMS concentrations (0-0.005 mM) in IW under UV-C radiation.

Figure 8.2. Degradation profiles of (a) DCF, (b) SMX, (c) TMP and (d) total CECs by PMS/UV-C system at different PMS concentrations (0-0.01 mM) in IW and under UV-C radiation.

Figure 8.3. Inactivation profiles of (a) *E. coli*, (b) *P. aeruginosa*, (c) *E. faecalis* and (d) sum of bacteria by PMS/UV-C system at different PMS concentrations (0-0.5 mM) in SUWW and under UV-C radiation.

Figure 8.4. PMS concentration decrease in function of time (minutes) and accumulative UV energy Q_{UV} (kJ/L) under UV-C treatment at different PMS concentrations in SUWW (0.01-0.5 mM).

Figure 8.5. Degradation profiles of (a) DCF, (b) SMX, (c) TMP and (d) total CECs by PMS/UV-C system at different PMS concentrations (0-0.5 mM) in SUWW under UV-C radiation.

Figure 8.6. Inactivation profiles of (a) *E. coli*, (b) *Pseudomonas* spp., (c) *Enterococcus* spp., (d) Total coliforms and (e) sum of bacteria by PMS/UV-C system at different PMS concentrations (0-1 mM) in UWW under UV-C radiation.

Figure 8.7. PMS concentration decrease in function of time (minutes) and accumulative UV energy Q_{UV} (kJ/L) under UV-C treatment at different PMS concentrations in UWW (0.1-1 mM).

Figure 8.8. Degradation profiles of (a) DCF, (b) SMX, (c) TMP and (d) total CECs by PMS/UV-C system at different PMS concentrations (0-1 mM) in UWW under UV-C radiation.

Figure 8.9. Bacteria inactivation (a) and CECs degradation (b) profiles by PMS/UV-C in IW, SUWW and UWW in the presence of PMS concentration necessary to achieve > 5 LRV in 20 minutes and 80 % of CECs removal in 10 minutes.

Figure 8.10. Inactivation of *E. coli*, *Enterococcus* spp., and *Pseudomonas* spp. and their AMP, CPX and TMP-AR counterpart by PMS/UV-C with 1 mM in UWW.

Figure 8.11. Relative abundance of ARGs detected by PMS/UV-C (1 mM) and UV-C alone.

Figure 9.1: Degradation pathway of DCF.

Figure 9.2: Degradation pathway of SMX.

Figure 9.3: Degradation pathway of TMP.

Figure 9.4: Degradation of DCF, SMX and TMP (a) and evolution of their major photolytic TPs (b, c and d) in UWW with 1 mM of PMS under natural solar radiation (left) and UV-C radiation (right) in SPE-enriched sample.

Figure 9.5. BI results towards *A. fischeri* in untreated and treated UWW by PMS/Solar and PMS/UV-C (1 mM).

Figure 9.6: Phytotoxicity results for *S. saccharatum*, *S. alba* and *L. sativum* in the positive (+) control (Zn²⁺ solution at 100 mg/L), negative (-) control (untreated UWW), and treated UWW by PMS/Solar and PMS/UV-C (1 mM).

Figure A.1. XRD patterns of several rare earth ions modified ZnO and among them (a) ZnO-Ce (trace c) and ZnO-Yb (trace f). Inset: enlargement of the ZnO-Ce pattern and of (b) ZnO-Fe with different iron contents; ZnO-Fe (0.5 %) (trace b). Adapted from (Cerrato, 2018; Paganini, 2019).

Index of contents

Figure A.2. (a) SEM micrographs, (b) TEM images of ZnO-Ce. Adapted from (Cerrato, 2018; Cerrato, 2020).

Figure A.3. (a) SEM micrographs, (b) TEM images and (c) High Resolution TEM (HR-TEM) image of ZnO-Yb. Adapted from (Cerrato, 2018; Cerrato, 2020).

Figure A.4. EPR spectra recorded at 77 K of activated samples before (Panel A) and during (Panel B) UV irradiation of several rare earth ions modified ZnO and among of them: c) ZnO-Ce and ZnO-Yb. Adapted from (Cerrato, 2018).

INDEX OF TABLES

Table 1.1. Benefits and drawbacks of the systems based on the principles of linear and circular economy.

Table 1.2. Watch lists of substances for Union-wide monitoring.

Table 1.3. Drinking water minimum requirements as established by the Directive (EU) 2020/2184.

Table 1.4. Reclaimed water quality for agricultural irrigation established by the Regulation (EU) 2020/741.

Table 1.5. Relevant pathogens typically detected in aqueous ecosystems (WHO, 2021; WHO, 2006).

Table 1.6.: Average concentrations of different pharmaceuticals measured in different water matrices in several countries. Adapted from (Montes-Grajales, 2017; Pereira, 2020).

Table 1.7. List of 12 CECs indicators, class and abatement during ozonation or PAC treatment, according to the New Swiss Water Protection Act.

Table 1.8. Maximum Contaminant Level (MCL) ($\mu\text{g/L}$) of regulated DBPs, according to USEPA, WHO and European guidelines in drinking water.

Table 1.9. Properties of peroxymonosulfate, persulfate, hydrogen peroxide and free chlorine. References: (Kiejza, 2021; Lee, 2020; Yang, 2019; Wang, 2018; Waclawek, 2017; Guan, 2011; Herrmann, 2007).

Table 1.10. Summary of conventional (ozonation, chlorination and UV-C) and advanced water treatment technologies (heterogeneous photocatalysis with $\text{TiO}_2\text{-P25}$, $\text{H}_2\text{O}_2/\text{UV-C}$ and $\text{H}_2\text{O}_2/\text{Solar}$) performances, with main advantages, drawbacks and possible solutions.

Table 1.11. PMS/UV-C literature studies for removal of chemical and microbial targets.

Table 1.12. Classification of the main toxicity bioassays.

Table 3.1. Chemical used in the experimental work.

Table 3.2. CECT number, culture medium, growth temperature and incubation time for each culture-type bacterium.

Table 3.3. Conditions used in qPCR Real-Time assays.

Table 3.4. Physicochemical properties and detection parameters of DCF, SMX and TMP.

Table 3.5. Physicochemical characteristics of the water matrices used in this work.

Table 3.6. Technical characteristics and specification of solar water reactors used in this experimental work.

Table 3.7. 80-L UV-C pilot plant main technical specifications.

Table 3.8. Working conditions used for TPs analysis in HPLC.

Table 3.9. ESI source parameters.

Table 5.1. Second order kinetic constants for the reaction with OH^\bullet and $^1\text{O}_2$ with the different SMX species at different pH (Ge, 2019).

Table 5.2. Radicals, quenching agent and corresponding $k_{\text{ROS}, \text{Q}}$ ($\text{M}^{-1} \text{s}^{-1}$) (Acero, 2005; Neta, 1988; Appiani, 2017).

Table 5.3. Experimentally measured first order kinetic constants.

Table 5.4. Second order rate constants $k_{\text{SO}_4^{\bullet-}, \text{Q}}$ ($\text{M}^{-1} \text{s}^{-1}$) between $\text{SO}_4^{\bullet-}$ and cell wall constituents investigated.

Table 7.1. ARGs mean and standard deviation of the ratio detected in this study.

Table 7.2: Synergistic factor calculated for microbial and chemical targets in the presence of the different concentrations of PMS.

Table 8.1. Main parameters related to optical absorption characteristics of DCF, SMX, TMP (at 1 mg/L) and PMS (at 1 mM) of concentration.

Table 8.2. ARGs mean and standard deviation of the ratio detected in this study.

Table 9.1. List of TPs tentatively identified in samples for DCF, SMX and TMP.

Index of contents

Table 9.2. Annual treatment costs to disinfect and remove CECs from UWW by the PMS/Solar process at 0.5, 0.75 and 1 mM.

Table 9.3. Estimated ATC for UWW treatment by UV-C and PMS/UV-C in a continuous flow reactor.

Table 9.4. Summary of the comparative evaluation of PMS/Solar and PMS/UV-C processes in the actual UWW from El Bobar (Almería).

Table A.1. Crystallite's size, and calculated energy gap for ZnO and modified samples (Cerrato, 2018b; 2020b; Paganini, 2019).

Table B.1. Bacteria inactivation kinetic constants in IW, SUWW and UWW at different concentrations of modified ZnO catalysts under natural sunlight (Data belong to Chapter 4).

Table B.2. CECs degradation constants in IW, SUWW and UWW at different concentrations of modified ZnO catalysts under natural sunlight (Data belong to Chapter 4).

Table B.3. Bacteria inactivation and CECs degradation pseudo-first order kinetic constants (k , min^{-1}) by PMS/Dark in the presence of several oxidant concentrations in IW and SUWW (Data belong to Chapter 6 and 7).

Table B.4. Bacteria inactivation pseudo-first order kinetic constants (k , min^{-1}) by PMS/Solar in the presence of several oxidant concentrations in IW, SUWW and UWW (Data belong to Chapter 6 and 7).

Table B.5. CECs degradation pseudo-first order kinetic constants (k , min^{-1}) by PMS/Solar in the presence of several oxidant concentrations in IW, SUWW and UWW (Data belong to Chapter 6 and 7).

Table B.6. Kinetics data of bacteria and CECs obtained in isotonic water (IW), diluted well water (d-WeW) and well water (WeW) under natural sunlight with and without 0.01 mM of PMS (Data belong to Chapter 6).

Table B.7. Bacteria and CECs kinetic constants in UWW at different concentrations of PMS (0, 0.2, 0.3 and 0.4 mM) in the absence and in the presence of ZnO-Ce in UWW under natural sunlight (Data belong to Chapter 7).

Table B.8. Bacteria inactivation kinetic constants (k , min^{-1}) by PMS/UV-C in the presence of several oxidant concentrations in IW, SUWW and UWW (Data belong to Chapter 8).

Table B.9. CECs degradation pseudo-first order kinetic constants (k , min^{-1}) by PMS/UV-C in the presence of several oxidant concentrations in IW, SUWW and UWW (Data belong to Chapter 8).

Table C.1. List of TPs tentatively identified in samples. Chromatographic and spectral information.

ABBREVIATIONS

ACN	Acetonitrile
AMP	Ampicillin
AOPs	Advanced Oxidation Processes
APCI	Atmospheric Pressure Chemical Ionization
AR	Antibiotic Resistance
ARB	Antibiotic Resistant Bacteria
ARGs	Antibiotic Resistant Genes
ATC	Annual Treatment Cost
BI	Bioluminescence Inhibition
BET	Brunauer–Emmett–Teller
BOD	Biological Oxygen Demand
CAS	Conventional Activated Sludge
CB	Conduction Band
CECs	Contaminants of Emerging Concern
CEPT	Colección Española de Cultivos Tipo
CFU	Colony Forming Unit
CPC	Compound Parabolic Collector
CPDs	Cyclobutane Pyrimidine Dimers
CPS	Count Per Second
CPX	Ciprofloxacin
CRF	Capital Recovery Factor
Ct	Cycle Threshold
DBE	Double Bond Equivalents
DBPs	Disinfection by Products
DCF	Diclofenac
DFT	Density Functional Theory
DL	Detection limit
DNA	DeoxyriboNucleic Acid
DOC	Dissolved Organic Carbon
DPD	N,N'-diethyl-p-phenylenediamine
DR	Diffuse Reflectance
DW	Demineralized Water
d-WeW	Diluted Well Water
DWTPs	Drinking Water Treatment Plants
EC	Equipment cost
ECHA	European Chemicals Agency
EDCs	Endocrine Disrupting Compounds
EEC	European Economic Community
EPR	Electron Paramagnetic Resonance
EPS	Extracellular Polymeric Substances
ESI	Electrospray Ionization
EQS	Environmental Quality Standard
EUCAST	European Committee on Antimicrobial Susceptibility Testing
FAO	Food and Agriculture Organization
FFA	Furfuryl Alcohol
FBR	Fixed Bed Bioreactors
HAAs	Haloacetic Acids
HETP	Height Equivalent to the Theoretical Plate
HFS	Hyper Fine Splittings
HPLC	High-Performance Liquid Chromatography
ISO	International Organization for Standardization
IC	Inorganic Carbon
InC	Investment Cost

Index of contents

IW	Isotonic Water
IDA	Information Dependent Acquisition
K _{ow}	Octanol-Water Partition Constant
LB	Luria-Bertani
LC-QTOF-MS	Liquid Chromatography-Quadrupole Time of Flight-Mass Spectrometry
LED	Light-Emitting Diode
LFP	Laser Flash Photolysis
LOQ	Limit of Quantification
LP	Low-pressure mercury-vapour lamps
LRV	Logarithm Reduction Values
MeOH	Methanol
MBBR	Moving Bed Biofilm Reactor
MBR	Membrane Bioreactors
MC	Maintenance Cost
MCL	Maximum Contaminant Level
MGD	Million Gallons per Day
MIC	Minimum Inhibitory Concentration
MP	Medium-pressure mercury-vapor lamps
NDIR	Non-Dispersive Infrared
NHE	Normal Hydrogen Electrode
NOM	Natural Organic Matter
NORMAN	Network of reference laboratories, research centres and related organizations for monitoring of emerging environmental substances
NSAID	Non-Steroidal Anti-Inflammatory Drugs
NTU	Nephelometric Turbidity Units
OC	Operation Cost
OECD	Organisation for Economic Co-operation and Development
PABA	Para-aminobenzoic acid
PBS	Phosphate-Buffered Saline
PC	Poly-Carbonate
PCET	Proton Coupled Electron Transfer
PCPs	Personal Care Products
PCR	Polymerase Chain Reaction
PFAS	Perfluoroalkyl and Polyfluoroalkyl Substances
PE	Population Equivalent
PET	PolyEthylene Terephthalate
Phe	Phenylalanine
PMS	Peroxymonosulfate
PS	Persulfate
PTFE	Polytetrafluoroethylene
PZC	Point of Zero Charge
RBMP	River Basin Management Plan
RGI	Relative Growth Index
ROS	Reactive Oxygen Species
RP-LC	Reversed-Phase Liquid Chromatography
RPM	Revolutions Per Minute
QL	Quantification Limit
QTOF	Quadrupole time-of-flight
SB	Slanetz and Bartley
SDG	Sustainable Development Goal
SEM	Scanning Electron Microscopy
SI	Synergy Index
SMX	Sulfamethoxazole
SODIS	Solar Water Disinfection

SPCM	Standard Plate Counting Method
SPE	Solid Phase Extraction
SR-AOPs	Sulfate radical-based Advanced Oxidation Processes
SSB	Single Strand Breaks
SSRIs	Selective Serotonin Reuptake Inhibitors
STEC	Shiga Toxin-producing <i>E. coli</i>
SUWW	Simulated Urban Wastewater
TBA	Tert Butanol
TC	Total Carbon
TEM	Transmission Electron Microscopy
THM	Trihalomethanes
Tyr	Tyrosine
TMP	Trimethoprim
TPs	Transformation products
Trp	Tryptophan
TSS	Total Suspended Solids
TTC	Triphenyl Tetrazolium Chloride
UN	United Nations
UPLC-UV-DAD	Ultra-Performance Liquid Chromatography with Ultraviolet-Diode Array Detection
USEPA	U.S. Environmental Protection Agency
UWW	Urban Waste Water
UWWTPs	Urban Waste Water Treatment Plants
VB	Valence Band
WeW	Well Water
WHO	World Health Organization
WL	Watch List
WFD	Water Framework Directive
XRD	X-rays powder diffraction

SUMMARY/RESUMEN/RESUM

SUMMARY

Currently, it is well recognized that the world is facing a water crisis, caused by population growth, economic development, climate change and water contamination. The reuse of urban wastewater (UWW) in different activities, especially in agriculture, has been gaining attention as a reliable solution to address this problem, enhancing water balance, limiting water withdrawal from natural bodies (surface water and groundwater), promoting water savings according to the principle of circular economy, but also ensuring environmental and human health protection. In fact, it is mandatory to promote the safe water reuse and minimum water quality limits could be achieved by upgrading the Urban Wastewater Treatment Plants (UWWTPs), through the addition of an efficient tertiary treatment. Currently, the microbiological safety of treated UWW must be assured by using *E. coli* as the main indicator, but additional requirements, not included in the (EU) 2020/741 regulation, could be of concern for human health and for the environment: (i) Contaminants of Emerging Concern (CECs) and their Transformation Products (TPs), (ii) Disinfection by-Products (DBPs) and (iii) anti-microbial resistance (Antibiotic Resistant Bacteria (ARB) and Antibiotic Resistant Genes (ARGs)), whose removal is not achieved in a conventional UWWTP.

Conventional tertiary treatments include ozonation, chlorination and UV-C radiation, but important drawbacks still need to be faced, mainly associated to high cost (for ozonation), the DBPs formation (for ozonation and chlorination), the limited CECs removal efficiency (for chlorination and UV-C) and bacterial post-treatment reactivation (for ozonation and UV-C radiation).

In the last decades, Advanced Oxidation Processes (AOPs) have been raised as alternative to conventional treatments for both water disinfection and decontamination. These processes rely on the potential generation of highly oxidant, reactive and non-selective Reactive Oxygen Species (ROS), such as hydroxyl radical HO^\bullet , sulfate radical $\text{SO}_4^{\bullet-}$, superoxide radical $\text{O}_2^{\bullet-}$ and singlet oxygen $^1\text{O}_2$, that can attack organic compounds in water with diffusion-limited kinetics (10^9 - $10^{10} \text{ M}^{-1}\text{s}^{-1}$).

The general aim of this study is the assessment of novel AOPs for the simultaneous disinfection and decontamination of water and of secondary effluents from UWWTPs. The following AOPs were investigated: (i) solar heterogeneous photocatalysis, involving modified ZnO with Ce, Yb and Fe and the benchmark TiO_2 -P25, (ii) peroxymonosulfate

(PMS) under natural solar radiation (PMS/Solar), (iii) Sulfate radical-based AOPs (SR-AOPs) involving PMS and UV-C radiation (PMS/UV-C) and (iv) combination of the best-performing photocatalytic material with PMS (PMS/modified ZnO).

The parameters analyzed and selected in this study for further establishing the UWW tertiary water treatments investigated as promising and suitable were the following: (i) capability to perform simultaneous disinfection and chemical decontamination, (ii) absence of bacteria regrowth, guaranteeing water safety during post-treatment storage, (iii) effectiveness to control antibiotic resistant phenomenon by reducing ARB and ARGs, (iv) TPs generation and process capability to attain their efficient degradation, (v) eco-toxicity of treated UWW effluent and (vi) the techno-economic evaluation for process implementation.

The involved biological and chemical targets in this study were selected due to their frequent detection in natural freshwater and wastewater resources: three human health impact pathogens (two gram-negative bacteria *Escherichia coli*, *Pseudomonas* spp. and the gram-positive *Enterococcus* spp.) and three CECs (Diclofenac-DCF, Sulfamethoxazole-SMX and Trimethoprim-TMP).

The proof-of-principle was performed for all processes in simple matrix (isotonic water (IW)), the potential effect of organic and inorganic chemical compounds on treatment performances was evaluated in simulated urban wastewater (SUWW) and well water (WeW) and finally the process capability was assessed in an actual secondary effluent (UWW) from the UWWTP of El Bobar, Almeria, Spain.

Firstly, photoactivity of modified ZnO with Ce, Yb or Fe was assessed in 200-mL vessel reactors, in suspension mode and under natural sunlight in IW with a wide range of concentrations (0-500 mg/L). The simultaneous analysis of biological and chemical contaminants highlights an enhancement in all target removal, compared to only solar radiation, being 100 mg/L the best load for the bacteria inactivation and 500 mg/L for CECs removal in IW.

The bacteria inactivation and CECs degradation mechanism was postulated based on the HO[•] generation, confirmed by electron paramagnetic resonance (EPR) and scavengers' experiments. In fact, upon photo-excitation, ROS (mainly HO[•]) were generated at the semiconductor particle-solution interface, and they further reacted with organic compounds and components of microorganisms in water, favouring their abatement.

Subsequently, the potential effect of organic and inorganic chemical compounds on photocatalytic performances was performed in SUWW, finding that the presence of natural organic matter (NOM) and inorganic ions negatively affected photocatalytic performances, obtaining lower kinetic rates compared to IW. ZnO-Fe and Zn-Yb showed lower removal rates in comparison with the benchmark TiO₂-P25 and the best performing material was ZnO-Ce, which was selected for a further investigation in actual UWW. Best results were obtained in the presence of ZnO-Ce at 500 mg/L, at which 80 % of the mixture of CECs was removed after 45 minutes (4.4 kJ/L of accumulated UV energy (Q_{UV})), while inactivation of wild bacteria present in UWW was achieved after 120 min (14 kJ/L of Q_{UV}), obtaining similar results with TiO₂-P25. Nevertheless, treatment effectiveness did not outperform TiO₂-P25, nor other conventional treatments, therefore, considering the high treatment cost (correlated to photocatalyst' production), its feasibility for a further up-scaling was discarded.

Moreover, the strategy of ZnO-Ce photocatalyst activity enhancement *via* the combination with PMS under natural sunlight was assessed and, despite it showed a good preliminary treatment performance, it was also considered not suitable, due to an important post contamination related with an up to 20 mg/L release of Zn²⁺.

Subsequently, PMS alone was chosen as oxidant agent for water purification and a deep study of its reactivity was conducted using SMX as model substrate, evaluating the effect of increased oxidant concentration, T, pH and common water ions (Cl⁻ and HCO₃⁻). Target removal was enhanced in all operational conditions tested. Furthermore, proper reactive species scavengers, together with the recorded EPR spectra, allowed to give an insight into the radical species involved in SMX degradation under dark, simulated solar light and UV-C radiation. For solar light, a non-radical pathway, involving direct electron transfer as responsible for targets removal, without the generation of SO₄^{-•} and HO[•], was elucidated, not discarding the increment of the water T as a parameter for enhancing the oxidation capability of PMS. On the other hand, UV-C wavelengths are able to break O-O bond with the formation of the strong SO₄^{-•} and HO[•], generated with a ratio 1.2:1, experimentally evaluated comparing the EPR DMPO-SO₄^{-•}/DMPO-HO[•] signals, and being therefore this radical pathway the main responsible for target degradation.

Moreover, a mechanistic understanding on water disinfection and decontamination by SR-AOPs has been provided by Laser Flash Photolysis (LFP), a valuable time-resolved technique to determine reaction rate constants and to investigate the operating mechanism.

Therefore, $\text{SO}_4^{\bullet-}$ has been assessed on the base of the detection and kinetic analysis of short-lived excited states and intermediates, usually in the microsecond time-scale. $\text{SO}_4^{\bullet-}$ was generated by laser irradiation of persulfate (PS) with UV-C wavelengths and its reactivity was determined with specific cell-wall model compounds of gram-positive (such as *E. faecalis*) and gram-negative (such as *E. coli*) bacteria cell walls and with the three CECs (DCF, SMX and TMP) under investigation.

LFP results revealed that $\text{SO}_4^{\bullet-}$ reacts with typical constituents of bacteria cell wall via H-abstraction mechanism (10^6 - $10^7 \text{ M}^{-1}\text{s}^{-1}$). Meanwhile, an additional electron transfer at higher rate ($10^9 \text{ M}^{-1}\text{s}^{-1}$) could occur with the aromatic amino acid (Tryptophan (Trp), Tyrosine (Tyr) and Phenylalanine (Phe)) contained in the skeleton of porins (proteins of outer membrane of gram-negative bacteria), suggesting a higher susceptibility of these types of bacteria to $\text{SO}_4^{\bullet-}$ treatments. On the other hand, CECs also quickly react with $\text{SO}_4^{\bullet-}$ by the electron transfer mechanism ($k_{\text{SO}_4^{\bullet-}, \text{CECs}}, 10^9 \text{ M}^{-1}\text{s}^{-1}$).

On the basis of PMS reactivity, its effectiveness without any type of external activation was assessed for water purification in the absence and in the presence of natural solar radiation for the simultaneous inactivation of three pathogens (*E. coli*, *E. faecalis* and *P. aeruginosa*) and for the degradation of three CECs (DCF, SMX and TMP) at laboratory scale in several water matrices.

It has been demonstrated that PMS/Solar process efficiency: (i) increased in the presence of high content of chloride ions (IW – due to HClO formation), (ii) decreased in the presence of a complex inorganic chemical water composition (WeW), not being influenced by the concentration of HCO_3^- (WeW vs diluted-WeW) and (iii) decreased in the presence of organic matter content (SUWW - due to oxidant consumption).

Then, the capability of the process was evaluated in actual UWW at pilot plant scale in 10-L Compound Parabolic Collector (CPC), by inactivating several natural occurring bacteria (*E. coli*, Total coliforms, *Enterococcus* spp. and *Pseudomonas* spp.), and degrading the three CECs (DCF, SMX and TMP) in the presence of different PMS concentrations (0-1 mM) under natural solar radiation. Optimal load of PMS was found to be 1 mM, at which an 80 % of total CECs removal was reached after 27 minutes (2.0 kJ/L of Q_{UV}) and the detection limit (2 CFU/mL) for all microbial targets (including the antibiotic resistant counterpart) was attained after 30 minutes (2.6 kJ/L of Q_{UV}) treatment time. No bacterial regrowth after 48h was detected, but low removal of ARGs (16S rRNA, *intI1* and selected

ARGs commonly found in UWW (*sul1*, *qnrS*, *blaTEM*, *blaCTX-M32*, *tetM*) and TPs was obtained.

The effectiveness of SR-AOPs was evaluated for water and UWW wastewater purification, generating $\text{SO}_4^{\cdot-}$ and HO^{\cdot} in solution through the activation of PMS by UV-C irradiation at pilot plant scale (80 L). Its effectiveness was tested with the already mentioned water matrices, highlighting the same fundamental treatment performance trend than the observed in PMS/Solar, but in all cases exhibiting higher pollutant kinetics, attributed to the baseline effect of UV-C wavelengths over the biological and chemical tested targets abatement.

Results in UWW showed that the best PMS concentration was also found to be 1 mM, at which all bacteria (including ARB) reached a concentration < 10 CFU/100 mL after 6 minutes of treatment (0.01 kJ/L of Q_{UV}), without observing regrowth after 48h. Regarding organic chemical pollutants, CECs were degraded after 12 minutes (0.13 kJ/L of Q_{UV}), while their TPs were removed within 90 minutes of treatment, except for the refractory SMX-TP 283. The quantification limit of all ARGs was reached within 60 minutes (1.4kJ/L of Q_{UV}), except for 16S rRNA and *intI1*, with only 50 % of removal.

Reclaimed UWW obtained by both PMS/Solar and PMS/UV-C process showed no toxicity towards *Aliivibrio fischeri*, excluding a harmful effect towards the receiving aquatic environment after effluent discharge, and a very slightly phytotoxic effect for growth of two out of the three tested seeds (*L. sativum* and *S. alba*), indicating the suitability of this water for its subsequent reuse for agriculture.

Finally, the techno-economic evaluation of both processes, supported the feasibility of PMS/Solar process as an attractive, suitable and sustainable option to be applied for the treatment of small water volumes in decentralized systems in low-income countries with a high solar radiation incidence, saving energy costs by using natural solar radiation. PMS/UV-C process could be a suitable option to be implemented in an already working UWWTPs, provided with UV-C treatment, allowing to obtain a high-quality of water.

RESUMEN

Actualmente el planeta se enfrenta a una crisis global del agua provocada por el crecimiento demográfico, el desarrollo económico, el cambio climático y la contaminación de los recursos hídricos. La reutilización de aguas residuales urbanas en diferentes actividades, especialmente en agricultura, ha surgido como una solución real para enfrentar este problema, mejorando el equilibrio hídrico, reduciendo la extracción de agua dulce de aguas superficiales y subterráneas, promoviendo el ahorro de agua de acuerdo con el principio de economía circular, y al mismo tiempo garantizando la protección del medio ambiente y la salud humana. De hecho, promover la reutilización segura del agua se impone como obligatoriedad a través de la implantación de tratamientos terciarios eficientes en las Estaciones Depuradoras Aguas Residuales Urbanas (EDAR) para alcanzar los límites mínimos de calidad requeridos. De acuerdo a la nueva normativa europea (reglamento (UE) 2020/741), la seguridad microbiológica se debe garantizar mediante el seguimiento fundamentalmente de *Escherichia coli* como indicador bacteriano. No obstante, existen otra serie de requisitos no incluidos en este reglamento, pero que se consideran, por la comunidad científica, como factores de preocupación para la salud humana y el medio ambiente, tales como: (i) Contaminantes de preocupación emergente (CE) y sus productos de transformación, (ii) subproductos de desinfección y (iii) resistencia antimicrobiana (bacterias y genes resistentes a antibióticos, ARB y ARGs, por sus siglas en inglés, respectivamente), y cuya eliminación no se logra en una EDAR convencional.

Los tratamientos terciarios convencionales incluyen ozonización, cloración y radiación UV-C, pero éstos aún presentan importantes inconvenientes o limitaciones principalmente asociadas al alto costo (ozonización), formación de subproductos de desinfección (en ozonización y cloración), limitada eficiencia de eliminación de CE (en cloración y UV-C) y reactivación bacteriana post-tratamiento (en ozonización y UV-C). En las últimas décadas, los Procesos de Oxidación Avanzada (POA) se han planteado como alternativa a los tratamientos convencionales tanto para la desinfección como para la descontaminación de aguas. Estos procesos se basan en la generación de especies reactivas de oxígeno altamente oxidantes y no selectivas, como el radical hidroxilo HO[•], el radical sulfato SO₄^{•-}, el radical superóxido O₂^{•-} y el oxígeno singlete ¹O₂, que pueden atacar compuestos en agua con cinéticas de difusión limitada (10⁹-10¹⁰ M⁻¹s⁻¹).

El objetivo general de este estudio es la evaluación de nuevos POA para la desinfección y descontaminación simultánea de agua y efluentes secundarios de EDAR. Para ello se investigaron los siguientes procesos: (i) fotocátalisis solar con ZnO modificado con Ce, Yb o Fe en comparación con TiO₂-P25 como referencia, (ii) peroxymonosulfato (PMS) bajo radiación solar natural (PMS/Solar), (iii) POA basados en generación de radical sulfato (RS-POA) utilizando PMS y radiación UV-C (PMS/UV-C) y (iv) combinación del mejor material fotocatalítico con PMS (PMS/ZnO modificado).

Los parámetros analizados y seleccionados en este estudio para el posterior establecimiento de los tratamientos terciarios en EDAR investigados como prometedores y adecuados fueron los siguientes: (i) capacidad para realizar simultáneamente desinfección y descontaminación química del agua, (ii) ausencia de recrecimiento de bacterias, garantizando la seguridad del agua durante el post-tratamiento, (iii) eficacia para controlar el fenómeno de resistencia a los antibióticos mediante la reducción de ARB y ARGs, (iv) generación de productos de transformación y capacidad de proceso para lograr su degradación eficiente, (v) eco-toxicidad del efluente de EDAR tratado y (vi) la evaluación económica de los procesos para su implementación.

Los objetivos biológicos y químicos analizados fueron seleccionados en base a la frecuente detección en fuentes naturales de agua dulce y aguas residuales, estos son: tres patógenos con impacto en la salud humana (dos bacterias gram-negativas *E. coli*, *Pseudomonas* spp. y una bacteria gram-positiva *Enterococcus* spp.) y tres CE (Diclofenaco-DCF, Sulfametoxazol-SMX y Trimetoprim-TMP).

El análisis de la eficiencia de los procesos seleccionados se realizó en diferentes matrices, partiendo de una matriz simple (agua isotónica), continuando con la evaluación en presencia de materia orgánica y compuestos inorgánicos utilizando agua residual simulada (S-EDAR) y agua de pozo y finalmente investigando su capacidad directamente en el efluente secundario real de la EDAR El Bobar (Almería, España).

Respecto a los tratamientos, en primer lugar, se investigó la fotoactividad de un amplio rango de concentraciones (0-500 mg/L) de ZnO modificado con Ce, Yb o Fe en suspensión, a escala de laboratorio (200 mL) y bajo luz solar natural. Los resultados en agua isotónica demostraron una clara mejora en la eliminación de los microorganismos y CE en comparación con el mero efecto de la radiación solar, siendo 100 y 500 mg/L la

concentración de catalizador que alcanzó el mejor resultado para la eliminación de los objetivos biológicos y químicos, respectivamente.

El mecanismo de inactivación bacteriana y degradación de CE mediante estos fotocatalizadores se estableció en base a la generación de HO[•] en la interfase del semiconductor-solución tras la foto-excitación del mismo, confirmado por resonancia paramagnética electrónica (espectros RPE) y ensayos de secuestro de radicales.

Posteriormente, la eficiencia de los fotocatalizadores se analizó en presencia de materia orgánica y elementos inorgánicos en S-EDAR, encontrando un efecto negativo en términos de cinéticas de degradación más bajas en comparación con agua isotónica, aunque no totalmente limitante. Las tasas de degradación más bajas se obtuvieron con los fotocatalizadores ZnO-Fe y Zn-Yb en comparación con TiO₂-P25, mientras que ZnO-Ce se seleccionó por su mejor rendimiento de tratamiento para su posterior análisis en efluente de EDAR. En esta matriz compleja y real de agua, el mejor resultado de tratamiento se obtuvo en presencia de 500 mg/L de ZnO-Ce, donde el 80 % del total de CE se eliminó tras 45 minutos de tratamiento (4,4 kJ/L de energía UV acumulada (Q_{UV})), y la completa inactivación bacteria (límite detección) en 120 minutos (14 kJ/L de Q_{UV}), siendo estos resultados similares a los obtenidos con TiO₂-P25. Sin embargo, y dado que la eficiencia no superó al fotocatalizador de referencia TiO₂-P25, ni tampoco los resultados obtenidos son competitivos frente a los típicos tratamientos convencionales y considerando el coste (producción del fotocatalizador), esta tecnología se descartó como potencialmente interesante para trasladarla a una mayor escala de tratamiento.

Además, se evaluó la estrategia de mejora de la actividad del fotocatalizador ZnO-Ce mediante la combinación con PMS bajo luz solar natural y, a pesar del buen rendimiento que se observó inicialmente, también se consideró como no adecuado debido a un importante efecto de post-contaminación relacionado con la liberación de Zn²⁺ (hasta 20 mg/L) durante el tratamiento.

En cuanto al uso de PMS como agente oxidante para la purificación de agua, en primer lugar, se realizó un detallado estudio de su reactividad usando SMX como sustrato modelo, evaluando el efecto del aumento de la concentración de oxidante, temperatura, pH e iones comunes del agua (Cl⁻ y HCO₃⁻), y obteniendo mejoras en la cinética de degradación de SMX. Además, se llevaron a cabo ensayos de secuestro de radicales junto con el análisis de espectros RPE, permitiendo determinar las especies radicales involucradas en la

degradación de SMX bajo luz solar simulada, radiación UV-C y en oscuridad. En presencia de luz solar, se pudo establecer la degradación mediante una vía no radical (sin generación de $\text{SO}_4^{\bullet-}$ y HO^{\bullet}) atribuida principalmente a la transferencia directa de electrones, no descartándose el incremento de la temperatura del agua como parámetro para mejorar la capacidad de oxidación de PMS. Por otro lado, las longitudes de onda de la radiación UV-C son capaces de romper el enlace O-O del oxidante con la consecuente formación de los $\text{SO}_4^{\bullet-}$ y HO^{\bullet} , generados con una proporción de 1.2:1, confirmado experimentalmente mediante espectros RPE DMPO- $\text{SO}_4^{\bullet-}$ /DMPO- HO^{\bullet} , y siendo, por tanto, la vía radical la principal responsable de la degradación del contaminante modelo.

La herramienta '*Laser Flash Photolysis*' (LFP) es una técnica de resolución que permite determinar constantes de velocidad e investigar mecanismos de reacción, y en este estudio, su uso ha proporcionado una mejor comprensión del mecanismo de desinfección y descontaminación de agua mediante RS-POA. Para ello, se ha evaluado la formación de $\text{SO}_4^{\bullet-}$ mediante LFP en base de su detección y análisis cinético de estados excitados e intermedios de corta duración (escala de microsegundos). El $\text{SO}_4^{\bullet-}$ se generó por radiación láser (longitudes de onda UV-C) partiendo de persulfato (PS) como sustrato y determinándose su reactividad con compuestos modelo de la pared celular de bacterias gram-positivas (*E. faecalis*) y gram-negativas (*E. coli*) y con los tres CE (DCF, SMX y TMP) investigados.

Los resultados de LFP revelaron que el radical $\text{SO}_4^{\bullet-}$ reacciona con los constituyentes de la pared celular bacteriana a través de un mecanismo de abstracción de H (10^6 - $10^7 \text{ M}^{-1}\text{s}^{-1}$), mientras que velocidades más alta ($10^9 \text{ M}^{-1}\text{s}^{-1}$, atribuidas a mecanismos de transferencia de electrones) se detectaron con el análisis de aminoácidos aromáticos (triptófano (Trp), tirosina (Tyr) y fenilalanina (Phe)) presentes en el esqueleto de porinas, proteínas de la membrana externa de bacterias gram-negativas, sugiriendo una mayor susceptibilidad de este tipo de bacterias en comparación con las gram-positivas al radical $\text{SO}_4^{\bullet-}$. Los CE también reaccionaron con velocidades altas asociadas al mecanismo de transferencia de electrones ($k_{\text{SO}_4^{\bullet-}, \text{CECs}}, 10^9 \text{ M}^{-1}\text{s}^{-1}$).

En base a la reactividad del PMS, a continuación, se llevó a cabo el análisis de su eficacia para la depuración de aguas en ausencia y en presencia de radiación solar natural, evaluando la inactivación simultánea de los tres patógenos microbianos (*E. coli*, *E. faecalis* y *P. aeruginosa*) y la degradación de los tres CE (DCF, SMX y TMP) de este estudio a escala de laboratorio y en varias matrices de agua.

En general, la eficiencia del proceso PMS/Solar: (i) aumentó en presencia de un alto contenido de iones cloruro (agua isotónica, debido a la formación de HClO), (ii) disminuyó en presencia de una composición química inorgánica compleja (agua de pozo), no siendo influenciada por la concentración de HCO_3^- (agua de pozo *versus* agua de pozo diluida) y (iii) disminuyó en presencia de materia orgánica (S-EDAR, debido al consumo de oxidante).

Tras ello, la capacidad del proceso se evaluó en efluente de EDAR real a escala de planta piloto en un colector parabólico compuesto (CPC) de 10L, siguiendo la inactivación de bacterias presentes de manera natural en este efluente (*E. coli*, coliformes totales, *Enterococcus* spp. y *Pseudomonas* spp.), y la degradación de los tres CE (adicionados) en presencia de diferentes concentraciones de PMS (0-1 mM) bajo radiación solar natural. Se encontró que la concentración óptima de PMS fue de 1 mM, alcanzándose el 80 % de la eliminación total de CE en 27 minutos (2,0 kJ/L de Q_{UV}) y el límite de detección (2UFC/mL) para todos los objetivos microbianos (incluidas ARB) en 30 minutos (2,6 kJ/L de Q_{UV}) de tratamiento. No se detectó recrecimiento bacteriano tras 48 h, pero tanto el análisis genético (16S rRNA, *intI1* y ARGs comúnmente presentes en efluente de EDAR *sull1*, *qnrS*, *blaTEM*, *blaCTX-M32*, *tetM*) como la degradación de los productos de transformación formados no se eliminaron de manera significativa.

Por otro lado, la eficiencia del proceso RS-POA para la depuración de agua y aguas residuales, generando $\text{SO}_4^{\cdot-}$ y HO^{\cdot} en solución, se investigó mediante la activación de PMS por irradiación UV-C a escala de planta piloto (80 L). La influencia del tipo de matriz de agua sobre la eficiencia del proceso también se investigó en este caso, destacando la misma tendencia fundamental de rendimiento del tratamiento que la observada en PMS/Solar, pero en todos los casos exhibiendo cinéticas de degradación más altas, atribuido al efecto de base de la radiación UV-C sobre los objetivos biológicos y químicos investigados.

Los resultados en efluente de EDAR mostraron que la mejor concentración de PMS también fue 1 mM, a la cual todas las bacterias (incluidas ARB) alcanzaron una concentración < 10 UFC/100 mL en 6 minutos de tratamiento (0,01 kJ/L de Q_{UV}), sin observar recrecimiento tras 48 h. En cuanto a los CE, éstos se degradaron en 12 minutos (0,13 kJ/L de Q_{UV}), mientras que sus productos de transformación se eliminaron a los 90 minutos de tratamiento, excepto el refractario SMX-TP 283. El límite de cuantificación de todos los ARGs se alcanzó en 60 minutos (1,4 kJ/L de Q_{UV}), excepto en el caso de 16S rRNA e *intI1*, con solo un 50 % de eliminación.

El análisis de eco-toxicidad del efluente de EDAR tratado con los procesos PMS/Solar y PMS/UV-C no mostró toxicidad para *Aliivibrio fischeri*, excluyendo un efecto nocivo para el medio ambiente acuático receptor, y un muy leve efecto fitotóxico para el crecimiento de dos de las tres semillas ensayadas (*L. sativum* y *S. alba*), indicando la idoneidad de este efluente tratado para su posterior reutilización en agricultura.

Finalmente, la evaluación técnico-económica realizada para ambos procesos demuestra que el proceso PMS/Solar es una opción atractiva, adecuada y sostenible para ser aplicada en sistemas descentralizados (pequeños volúmenes de agua) en áreas con alta incidencia de radiación solar, dado el consecuente ahorro de costes energéticos por el uso de radiación solar natural. Mientras que el proceso PMS/UV-C podría ser una opción adecuada para implementarse en EDAR, ya provistas con sistemas de tratamiento basado en UV-C, dado la alta calidad química y microbiológica del efluente obtenido.

RESUM

Actualment el planeta s'enfronta a una crisi global de l'aigua provocada pel creixement demogràfic, el desenvolupament econòmic, el canvi climàtic i la contaminació dels recursos hídrics. La reutilització d'aigües residuals urbanes en diferents activitats, especialment en agricultura, ha sorgit com una solució real per a enfrontar aquest problema, millorant l'equilibri hídric, reduint l'extracció d'aigua dolça d'aigües superficials i subterrànies, promovent l'estalvi d'aigua d'acord amb al principi d'economia circular, i al mateix temps garantint la protecció del medi ambient i la salut humana. De fet, promoure la reutilització segura de l'aigua s'imposa com a obligatorietat a través de la implantació de tractaments terciaris eficients en les Estacions Depuradores Aigües Residuals Urbanes (EDAR) per a aconseguir els límits mínims de qualitat requerits. D'acord amb la nova normativa europea (reglament (UE) 2020/741), la seguretat microbiològica s'ha de garantir mitjançant el seguiment fonamentalment d'*Escherichia coli* com a indicador bacterià. No obstant això, existeixen una altra sèrie de requisits no inclosos en aquest reglament, però que es consideren, per la comunitat científica, com a factors de preocupació per a la salut humana i el medi ambient, com ara: (i) Contaminants de preocupació emergent (CE) i els seus productes de transformació, (ii) subproductes de desinfecció i (iii) resistència antimicrobiana (bacteris i gens resistents a antibiòtics, ARB i ARGs, per les seues sigles en anglés, respectivament), l'eliminació dels quals no s'aconsegueix en una EDAR convencional.

Els tractaments terciaris convencionals inclouen l'ozonització, la cloració i la radiació UV-C, però aquests encara presenten importants inconvenients o limitacions principalment associats a l'alt cost (ozonització), formació de subproductes de desinfecció (en ozonització i cloració), limitada eficiència d'eliminació de CE (en cloració i UV-C) i reactivació bacteriana post-tractament (en ozonització i UV-C). En les últimes dècades, els Processos d'Oxidació Avançada (POA) s'han plantejat com a alternativa als tractaments convencionals tant per a la desinfecció com per a la descontaminació d'aigües. Aquests processos es basen en la generació d'espècies reactives d'oxigen altament oxidants i no selectives, com el radical hidroxil $\cdot\text{HO}$, el radical sulfat $\text{SO}_4^{\cdot-}$, el radical superòxid $\text{O}_2^{\cdot-}$ i l'oxigen singlet $^1\text{O}_2$, que poden atacar compostos en aigua amb cinètiques limitades per la difusió (10^9 - $10^{10} \text{ M}^{-1}\text{s}^{-1}$). L'objectiu general d'aquest estudi és l'avaluació de nous POA per a la desinfecció i descontaminació simultània d'aigua i efluent secundaris d'EDAR. Per a això es van investigar els següents processos: (i) fotocatalisi solar amb ZnO modificat amb Ce, Yb o Fe

en comparació amb TiO₂-P25 com a referència, (ii) peroximonosulfat (PMS) baix radiació solar natural (PMS/Solar), (iii) POA basats en la generació de radical sulfat (RS-POA) utilitzant PMS i radiació UV-C (PMS/UV-C) i (iv) combinació del millor material fotocatalític amb PMS (PMS/ZnO modificat).

Els paràmetres analitzats i seleccionats en aquest estudi per a la posterior selecció dels tractaments terciaris d'EDAR investigats com a prometedors i adequats van ser els següents: (i) capacitat per a realitzar simultàniament desinfecció i descontaminació química de l'aigua, (ii) absència de recreixement de bacteris, garantint la seguretat de l'aigua durant el post-tractament, (iii) eficàcia per a controlar el fenomen de resistència als antibiòtics mitjançant la reducció d'ARB i ARGs, (iv) generació de productes de transformació i capacitat del procés per a aconseguir la seua degradació eficient, (v) eco-toxicitat de l'efluent d'EDAR tractat i (vi) l'avaluació econòmica dels processos per a la seua implementació.

Els objectius biològics i químics analitzats van ser seleccionats sobre la base de la freqüent detecció en recursos naturals d'aigua dolça i aigües residuals. Aquests són: tres patògens amb impacte en la salut humana (dos bacteris gram-negatius *E. coli*, *Pseudomonas* spp. i un gram-positiu *Enterococcus* spp.) i tres CE (Diclofenac-DCF, Sulfametoxazol-SMX i Trimetoprim-TMP). L'anàlisi de l'eficiència dels processos seleccionats es va realitzar en diferents matrius, partint d'una matriu simple (aigua isotònica), continuant amb l'avaluació en presència de matèria orgànica i compostos inorgànics utilitzant aigua residual simulada (S-EDAR) i aigua de pou i finalment investigant la seua capacitat directament sobre l'efluent secundari real de l'EDAR El Bobar (Almeria, Espanya).

Respecte als tractaments, en primer lloc, es va investigar la fotoactivitat d'un ampli rang de concentracions (0-500 mg/L) de ZnO modificat amb Ce, Yb o Fe en suspensió, a escala de laboratori (200 ml) i baix llum solar natural. Els resultats en aigua isotònica van demostrar una clara millora en l'eliminació dels microorganismes i CE en comparació amb el mer efecte de la radiació solar, sent 100 i 500 mg/L la concentració de catalitzador que va aconseguir el millor resultat per a l'eliminació dels objectius biològics i químics, respectivament.

El mecanisme d'inactivació bacteriana i degradació de CE mitjançant aquests fotocatalitzadors es va establir sobre la base de la generació de HO[•] en la inter-fase del semiconductor-solució després de la foto-excitació d'aquest, confirmat per ressonància paramagnètica electrònica (espectres RPE) i assajos de segrest de radicals.

Posteriorment, l'eficiència dels fotocatalitzadors es va analitzar en presència de matèria orgànica i elements inorgànics en S-EDAR, trobant un efecte negatiu en termes de

cinètiques de degradació més baixes en comparació amb aigua isotònica, encara que no totalment limitant. Les taxes de degradació més baixes es van obtenir amb els fotocatalitzadors ZnO-Fe i Zn-Yb en comparació amb TiO₂-P25, mentre que ZnO-Ce es va seleccionar pel seu millor rendiment de tractament per a la seua posterior anàlisi en efluent d'EDAR. En aquesta matriu complexa i real d'aigua, el millor resultat de tractament es va obtenir en presència de 500 mg/L de ZnO-Ce, on el 80 % del total de CE es va eliminar després de 45 minuts de tractament (4,4 kJ/L d'energia UV acumulada (Q_{UV})), i la completa inactivació de bacteris (al límit detecció) en 120 minuts (14 kJ/L de Q_{UV}), sent aquests resultats similars als obtinguts amb TiO₂-P25. No obstant això, i atés que l'eficiència no va superar al fotocatalitzador de referència TiO₂-P25, ni tampoc els resultats obtinguts són competitiu enfront de típics tractaments convencionals i considerant el cost (producció del fotocatalitzador), aquesta tecnologia es va descartar com potencialment interessant per a traslladar-la a una major escala de tractament.

A més, es va avaluar l'estratègia de millora de l'activitat del fotocatalitzador ZnO-Ce mitjançant la combinació amb PMS baix llum solar natural i, malgrat el bon rendiment que es va observar inicialment, també es va considerar com no adequat a causa d'un important efecte de post-contaminació relacionat amb l'alliberament de Zn²⁺ (fins a 20 mg/L) durant el tractament.

Quant a l'ús de PMS com a agent oxidant per a la purificació d'aigua, en primer lloc, es va realitzar un detallat estudi de la seua reactivitat utilitzant SMX com a substrat model, avaluant l'efecte de l'augment de la concentració d'oxidant, temperatura, pH i ions comuns en l'aigua (Cl⁻ i HCO³⁻), i obtenint en general millores en la cinètica de degradació de SMX. A més, es van dur a terme assajos de segrest de radicals juntament amb l'anàlisi d'espectres RPE, permetent determinar les espècies radicals involucrades en la degradació de SMX baix llum solar simulada, radiació UV-C i en foscor. En presència de llum solar, es va poder establir la degradació mitjançant una via no radicalària (sense generació de SO₄^{•-} i HO•) atribuïda principalment a la transferència directa d'electrons, no descartant-se l'increment de l' temperatura de l'aigua com a paràmetre per a millorar la capacitat d'oxidació de PMS. D'altra banda, les longituds d'ona de la radiació UV-C són capaces de trencar l'enllaç O-O de l'oxidant amb la conseqüent formació dels SO₄^{•-} i HO•, generats amb una proporció d'1.2:1, confirmat experimentalment mitjançant espectres RPE DMPO-SO₄^{•-}/DMPO-HO•, i sent, per tant, la via radical la principal responsable de la degradació del contaminant model.

L'eina 'Laser Flash Photolysis' (LFP) és una tècnica de resolució que permet determinar constants de velocitat i investigar mecanismes de reacció, i en aquest estudi, el seu ús ha proporcionat una millor comprensió del mecanisme de desinfecció i descontaminació d'aigua mitjançant RS-POA. Per a això, s'ha avaluat la formació de $\text{SO}_4^{\bullet-}$ mitjançant LFP en base de la seua detecció i anàlisi cinètica d'estats excitats i intermedis de curta duració (escala de microsegons). El $\text{SO}_4^{\bullet-}$ es va generar per radiació làser (longituds d'ona UV-C) partint de persulfat (PS) com a substrat i determinant-se la seua reactivitat amb compostos model de la paret cel·lular de bacteris gram-positius (*E. faecalis*) i gram-negatius (*E. coli*) i amb els tres CE (DCF, SMX i TMP) investigats.

Els resultats de LFP van revelar que el radical $\text{SO}_4^{\bullet-}$ reacciona amb els constituents de la paret cel·lular bacteriana a través d'un mecanisme d'abstracció d'H (10^6 - $10^7 \text{ M}^{-1}\text{s}^{-1}$), mentre que velocitats més altes ($10^9 \text{ M}^{-1}\text{s}^{-1}$, atribuïdes a mecanismes de transferència d'electrons) es van detectar amb l'anàlisi d'aminoàcids aromàtics (triptòfan (Trp), tirosina (Tyr) i fenilalanina (Phe)) presents en l'esquelet de porines, proteïnes de la membrana externa de bacteris gram-negatius, suggerint una major susceptibilitat d'aquesta mena de bacteris en comparació amb als gram-positius al radical $\text{SO}_4^{\bullet-}$. Els CE també van reaccionar amb velocitats altes associades al mecanisme de transferència d'electrons ($k_{\text{SO}_4^{\bullet-}, \text{CECs}}, 10^9 \text{ M}^{-1}\text{s}^{-1}$). Sobre la base de la reactivitat del PMS, a continuació, es va dur a terme l'anàlisi de la seua eficàcia per a la depuració d'aigües en absència i en presència de radiació solar natural, avaluant la inactivació simultània dels tres patògens microbians (*E. coli*, *E. faecalis* i *P. aeruginosa*) i la degradació dels tres CE (DCF, SMX i TMP) a escala de laboratori i en diverses matrius d'aigua.

En general, l'eficiència del procés PMS/Solar: (i) va augmentar en presència d'un alt contingut d'ions clorur (aigua isotònica, a causa de la formació de HClO), (ii) va disminuir en presència d'una composició química inorgànica complexa (aigua de pou), no sent influenciada per la concentració de HCO_3^- (aigua de pou *versus* aigua de pou diluïda) i (iii) va disminuir en presència de matèria orgànica (S-EDAR - a causa del consum d'oxidant).

Després d'això, la capacitat del procés es va avaluar en efluent d'EDAR real a escala de planta pilot en un col·lector parabòlic compost (CPC) de 10 L, seguint la inactivació de diversos bacteris naturalment presents en UWW (*E. coli*, coliformes totals, *Enterococcus* spp. i *Pseudomonas* spp.), i la degradació dels tres CE (addicionats) en presència de diferents concentracions de PMS (0-1 mM) baix radiació solar natural. Es va trobar que la concentració òptima de PMS va ser d'1 mM, aconseguint-se el 80 % de

l'eliminació total de CE en 27 minuts (2,0 kJ/L de Q_{UV}) i el límit de detecció (2 UFC/ml) per a tots els objectius microbians (inclosos ARB) en 30 minuts (2,6 kJ/L de Q_{UV}) de tractament. No es va detectar recreixement bacterià després de 48 h, però tant l'anàlisi genètica (16S rRNA, *intI1* i ARGs comunament presents en UWW *sul1*, *qnrS*, *blaTEM*, *blaCTX-M32*, *tetM*) com la degradació dels productes de transformació formats indiquen que no es van eliminar de manera significativa.

D'altra banda, l'eficiència del procés RS-POA per a la depuració d'aigua i aigües residuals, generant $SO_4^{\cdot-}$ i HO^{\cdot} en solució, es va investigar mitjançant l'activació de PMS per irradiació UV-C a escala de planta pilot (80 L). La influència sobre la eficiència del procés de les matrius d'aigua ja esmentades també es va investigar en aquest cas, destacant la mateixa tendència fonamental de rendiment del tractament que l'observada en PMS/solar, però en tots els casos exhibint cinètiques de degradació més altes, atribuït a l'efecte de base de la radiació UV-C sobre els objectius biològics i químics investigats.

Els resultats en efluent d'EDAR van mostrar que la millor concentració de PMS també va ser 1 mM, a la qual tots els bacteris (inclosos ARB) van aconseguir una concentració < 10UFC/100 mL en 6 minuts de tractament (0,01 kJ/L de Q_{UV}), sense observar recreixement després de 48 h. Quant als CE, aquests es van degradar en 12 minuts (0,13 kJ/L de Q_{UV}), mentre que els seus TP es van eliminar als 90 minuts de tractament, excepte el refractari SMX-TP 283. El límit de quantificació de tots els ARGs es va aconseguir en 60 minuts (1,4 kJ/L de Q_{UV}), excepte en el cas de 16S rRNA i *intI1*, amb només un 50 % d'eliminació.

L'anàlisi d'eco-toxicitat del efluent d'EDAR tractada amb els processos PMS/Solar i PMS/UV-C no van mostrar toxicitat per a *Aliivibrio fischeri*, exclouent un efecte nociu per al medi ambient aquàtic receptor, i un efecte molt lleument tòxic per al creixement de dos de les tres llavors assajades (*L. sativum* i *S. alba*), indicant la idoneïtat d'aquest efluent tractat per a la seua posterior reutilització en agricultura.

Finalment, l'avaluació tecnicoeconòmica realitzada per a tots dos processos demostra que el procés PMS/Solar és una opció atractiva, adequada i sostenible per a ser aplicada en sistemes descentralitzats (xicotets volums d'aigua) en àrees amb alta incidència de radiació solar, donat el conseqüent estalvi de costos energètics per l'ús de radiació solar natural. Mentre que el procés PMS/UV-C podria ser una opció adequada per a implementar-se en EDAR, proveïdes amb sistemes de tractament basat en UV-C, donat l'alta qualitat química i microbiològica de l'efluent obtingut.

CHAPTER 1
INTRODUCTION

1. INTRODUCTION

1.1. The water availability: towards a circular economy

Freshwater is defined as a natural, renewable but finite resource, exploitable and available for beneficial uses, such as agriculture (70 % of total amount), industry (20 %) and domestic applications (10 %) (Boretti, 2019). 70 % of Earth' surface is covered by water, from which 97.5 % is salt water and only 3 % is freshwater, being 2.5 % trapped in glaciers, atmosphere and soil. Therefore, only 0.5 % is exploitable and accessible to human uses.

Freshwater availability affects directly human well-being, ecosystems and sustainable development, being therefore its protection a worldwide goal. Nevertheless, currently it is well recognized that the world is facing a water crisis, that it could get even worse in the future (Figure 1.1), because of population growth, economic development, climate change and water contamination.

All these components are inter-linked and a synergistic effect exacerbates the water stress conditions and the water imbalance, with water demand exceeds water resource exploitability under sustainable conditions.

1. Introduction

- Economic development implies population growth, industrial and agricultural activities expansion, provoking both an increase in global water demand and an increase in pollutant load.
- Global climate induces an alteration to the hydrological cycle, provoking higher variability in precipitation and increasing frequency and intensity of extreme events, such as storms, floods and droughts. Moreover, an increased risk of water pollution could be due to a reduced dilution of discharge effluent pollutant load, caused by lower water levels in rivers, lakes and streams.
- Water pollution typically refers to microbial pathogens, chemicals or other substances present in the environment in concentrations higher than the one under natural conditions.

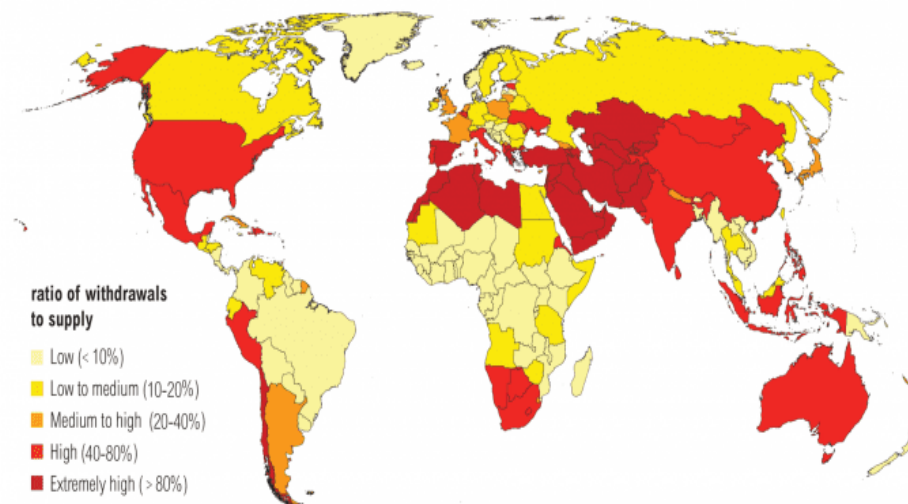


Figure 1.1. World map of water stress condition in 2040, according to the World Resource Institute (Luo, 2015).

From the different uses of fresh-water, two elemental needs could be highlighted as vital for humans: drinking and food production, involving domestic and irrigation water, respectively. Today, it is well recognized that both needs are far from to be properly covered, due to a clear and promulgated lack of access and rights of every human in the world to safe drinking water and food. United Nations (UN) five-year sustainable freshwater strategy (2017 to 2021) aimed to preserve the world's freshwater and the human health (UNEP, 2017). In line, the Sustainable Development Goal (SDG) number 6 (United Nations, 2018), which is part of the 2030 Agenda for Sustainable Development, claims that access to safe drinking water and sanitation must be guaranteed for all within ten years. This will be a considerable challenge because currently 2.2 billion people lack

access to safe drinking water, 4.2 billion have little or no sanitation, millions of people die annually, with more than 297 000 children under five who die annually for diseases transmitted through unsafe water or human excreta (United Nations, 2019). Regarding the human nutrition, UN estimated that 2.37 billion people are without access to food or unable to eat a healthy balanced diet. Regarding this topic, the SDG number 2 seeks sustainable solutions to end hunger, achieve food security, improve nutrition, through the promotion of sustainable and resilient agricultural practices, that increase productivity and production, where water plays also a mayor role. According to the Food and Agriculture Organization (FAO), 2 litres of water are often sufficient for daily drinking water requirements, but 3000-L are necessary to produce the daily food needs of a person (FAO, 2011), being, therefore, agriculture the largest user of water globally. Moreover, population growth implies also a growing food demand, and it is estimated that agricultural production will need to be expanded by approximately 70 % by 2050, increasing even more water consumption in agriculture.

To respond to the increasing pressures on hydric resources, the principle of circular economy could be applied to water, dissolved and sludge nutrients and energy (Guerra-Rodríguez, 2020). Up to now, the water uses system is mostly based on the principles of linear economy, characterized by take-make-use-dispose (Giakoumis, 2020). As it can be observed in Figure 1.2, water is taken from the natural environment and it is treated in Drinking Water Treatment Plants (DWTPs), by a 4 steps processes, including coagulation, sedimentation, filtration and disinfection. Then, drinking water is distributed and consumed in houses, workplaces, industries and in some sectors of the agrofood industry. After its use, it is collected through the sewer system and conducted to an Urban Wastewater Treatment Plant (UWWTPs), where it is treated in different steps (namely, primary and secondary treatment) and finally it is discharged back in the environment. However, currently, the water circular economy promotes the solution to reduce the demand for potable water based on considering Urban Wastewater (UWW) as a resource, that can be recycled and reused in different activities, involving irrigation, industry and recreational activities. In this sense, after the primary use of the freshwater and the treatment in UWWTPs, an additional tertiary treatment could be applied to allow its reuse for different application, especially for agriculture (75-80 % of water resource is used for crops irrigation), as it can be observed in Figure 1.2. A wide reuse of treated wastewater allows to limit the water withdrawal from natural bodies (surface water and groundwater), reducing

1. Introduction

environmental impact, promoting water savings and ensuring environmental and human health protection.

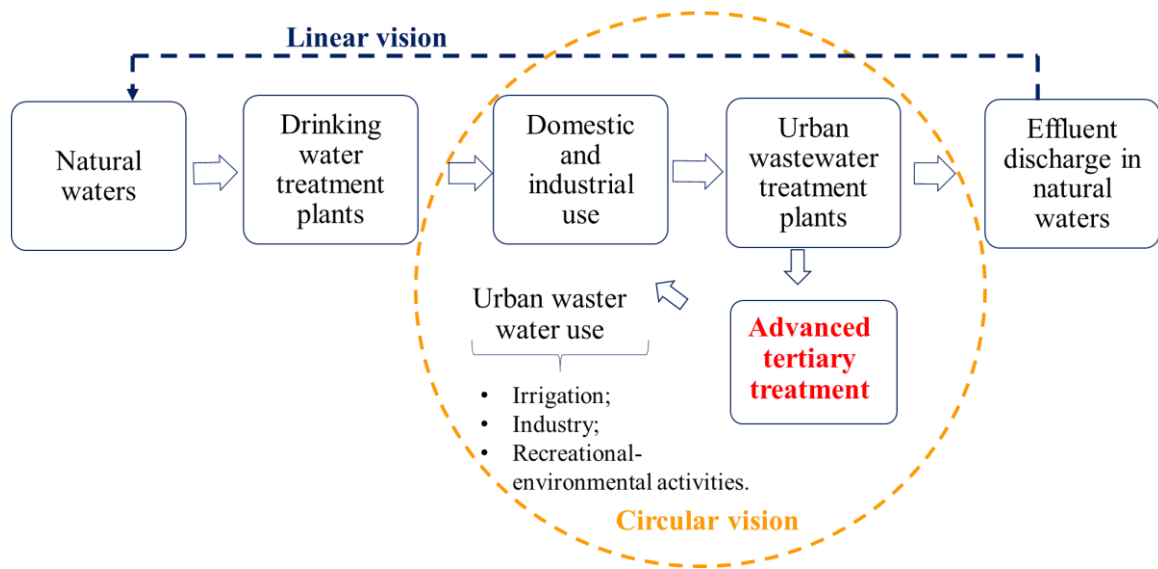


Figure 1.2. Linear *versus* circular vision of the urban water cycle.

Benefits and drawbacks of the two systems are listed in Table 1.1 (Guerra-Rodríguez, 2020; Giakoumis, 2020).

Table 1.1. Benefits and drawbacks of the water use systems based on the principles of linear and circular economy.

	Principles of Linear Economy	Principles of Circular Economy
<i>Benefits</i>	<ul style="list-style-type: none"> • Use of higher quality water in agriculture, industry and recreational activities. 	<ul style="list-style-type: none"> • Water resource savings, reduction of hydric stress and of waste. • Increase of water resource availability by reducing withdrawal. • Sustainable management of resources by increasing water use efficiency. • Potable water demand reduction. • Nutrient's recovery and reduction of the demand of mineral fertilizers. • Possible valorisation of sewage sludge and recovery of energy. • Contribution to achieve UN SDG12 on sustainable consumption and production.
<i>Drawbacks</i>	<ul style="list-style-type: none"> • Continuous extraction of finite water resources. • Contamination of natural water, due to the discharge of inappropriately treated or untreated UWW. 	<ul style="list-style-type: none"> • Risks to human health associated to an inappropriately treated UWW. • Lack of social acceptance and public confidence in wastewater reuse. • High investment cost of UWW reuse systems.

Currently, UWW reuse practice is still carried out to a limited extent in the European Union, because opposite to the large numbers of European water legislations implemented during

last decades (described in next section), a harmonization of requirements has been just come into force with the regulation (EU) 2020/741, by setting minimum requirements for water reuse. Minimum health standard for agriculture products, irrigated with reclaimed UWW, could allow their free movement in all member state. Moreover, the lack of social acceptance could be overcome by providing clear, update and comprehensive information to the public about water safeness for human health and environment. Financial incentives to upgrade UWWTPs could help to cover high investment needed to implement efficient and sustainable tertiary treatments. Therefore, the water treatment appears in the scheme as one of the most important key factors on the water circular economy to encourage the water reuse as real practice (Figure 1.2), *via* the removal of all types of chemical and biological pollution from the contaminated water.

1.2. The European water framework

At European level, over the years, different legislations that aim to protect and manage the community hydric resources have been implemented, as it is shown in Figure 1.3.

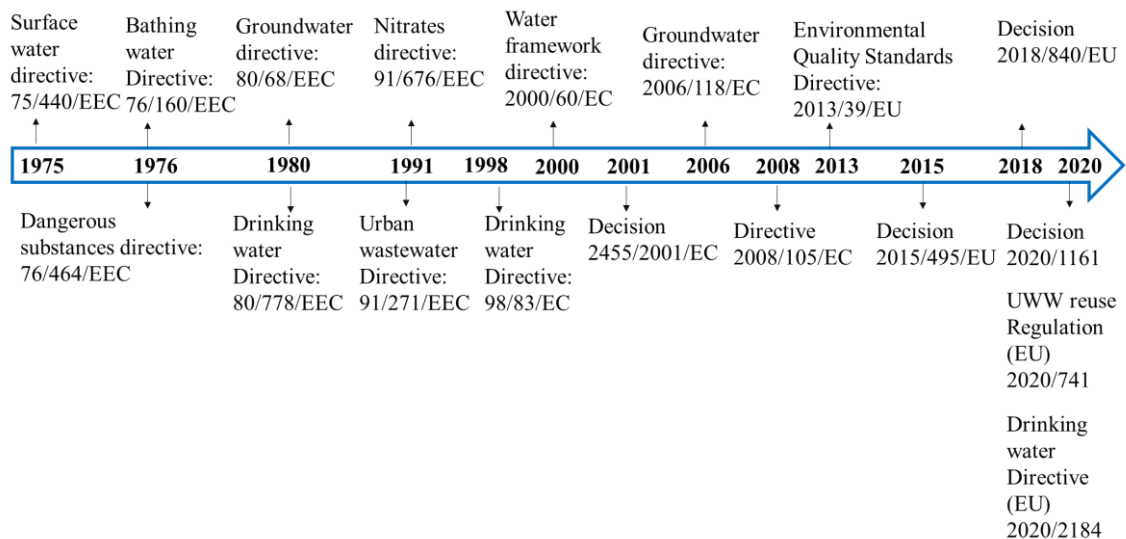


Figure 1.3. Framework of European water legislation.

The first directive concerning the quality required of surface water intended for the abstraction of drinking water was established in 1975, followed by others on bathing water, discharges of hazardous substances, groundwater, drinking water and urban wastewater (and their revisions). In 2000, the Water Framework Directive (WFD 2000/60/EC) was introduced with the implementation of an integrative River Basin Management Plan (RBMP), aiming at achieving good quality for all water bodies. A list of 33 priority substances was established on the base of a risk-based assessment procedure. 11 out of 33

1. Introduction

were considered priority hazardous substances and subjected to cessation or to reduce emissions and losses, within an appropriate timetable not exceeding 20 years. Monitoring of priority substances, whose concentration must be in compliance with the established Environmental Quality Standard (EQS) limits, could assure a good chemical status. Different amendments were followed, revising the priority substances list and the EQS limits. Moreover, substances that may pose a significant risk, but for which monitoring data are not sufficient, were included in the Watch List (WL), gathering data for future prioritization process. Table 1.2 shows the different substances included in the WLs, established in the decisions.

Table 1.2. Watch lists of substances for Union-wide monitoring.

Class	Substance		
	<i>DECISION (EU) 2015/495</i>	<i>DECISION (EU) 2018/840</i>	<i>DECISION (EU) 2020/1161</i>
<i>Hormone</i>	17- α -ethinylestradiol (EE2) 17- β -estradiol (E2) Estrone (E1)	17- α -ethinylestradiol (EE2) 17- β -estradiol (E2) Estrone (E1)	
<i>Antibiotic</i>	Macrolide antibiotics	Macrolide antibiotics Amoxicillin Ciprofloxacin	Amoxicillin Clotrimazole Ciprofloxacin Fluconazole Miconazole Sulfamethoxazole Trimethoprim
<i>Pesticide</i>	Methiocarb	Methiocarb	Imazalil Ipconazole Metconazole Penconazole Prochloraz Tebuconazole Tetraconazole
<i>Herbicide</i>	Oxadiazon Tri-allate	-	-
<i>Insecticide</i>	-	Metaflumizole	Metaflumizone
<i>Fungicide</i>	-	-	Dimoxystrobin Famoxadone
<i>Personal care products</i>	2-Ethylhexyl-4-methoxycinnamate	-	-
<i>Nonsteroidal anti-inflammatory drug</i>	Diclofenac	-	-
<i>Endocrine disruptor</i>	2,6-Di-tert-butyl-4-methylphenol	-	-
<i>Anti-depressant</i>	-	-	Venlafaxine O-desmethylvenlafaxine

The first WL was established in the Decision 2015/495 and it contained 10 substances, an indication of the monitoring matrix, possible analytical methods (not entailing excessive costs) and maximum acceptable method detection limits. This list must be updated every two years, by removing the substances for which a risk-based assessment can be concluded (monitoring obligation shall not exceed 4 years) or including the hazardous ones to the priority substances list.

1.2.1. Drinking water legislation

The first drinking water directive (80/778/EEC) entered into force in 1980, and mandatory requirements for about 60 microbiological, organoleptic and physical-chemical parameters for all Member States of the European Economic Community (EEC) were established, without taking into account requirements for materials and substances used in the distribution of drinking water. In 1998 the EU adopted the Second Drinking Water Directive (98/83/EC), covering also those substances and materials. Recently, legislation on drinking water has been revised and the Directive (EU) 2020/2184 of the European Parliament and of the Council of 16 December 2020 on the quality of water intended for human consumption has entered into force on the past 12/01/2021.

The main objective is to protect human health from adverse effects of any contamination of water intended for human consumption, by ensuring that it is wholesome and clean, preventing chemical and microbiological risk, and to improve access to safe water. Besides, water must be palatable, clear, colorless, odorless and it must contain certain amounts of natural minerals and essential elements.

Minimum biological (part A), chemical parameters (part B) and ones relevant for domestic distribution systems (part D) are established and the maximum allowable concentrations for each parameter are shown in Table 1.3 (according to precautionary principles).

Regarding the Contaminants of Emerging Concern (CECs, for the definition see below the Section 1.3.2), only pesticide, bisphenol A and Perfluoroalkyl and Polyfluoroalkyl Substances (PFAS) are included in the legislation. However, in order to address growing public concern about the effects of these emerging compounds, such as endocrine-disrupting compounds, pharmaceuticals and microplastics, on human health, a WL mechanism was introduced, including the monitoring of water pollutants, that could pose a potential risk to human health. β -estradiol and nonylphenol are potential candidates to be included in the

1. Introduction

first WL in view of their endocrine-disrupting properties and the risk they pose to human health (the first WL shall be established by 12 January 2022, including guidance values and analytical methods). Moreover, regular monitoring of the quality of water intended for human consumption involves also the evaluation of parameters reported in Part A, B, C (indicator parameters) and D (Annex 1 of the Directive), with a minimum frequency of sampling and analysis set out (depending also on volume of water distributed or produced each day within a supply zone), performing also operational monitoring to provide a rapid insight of water quality (including turbidity and somatic coliphages analysis).

Table 1.3. Drinking water minimum requirements established by the Directive (EU) 2020/2184.

Minimum requirements for water intended for human consumption			
Microbiological parameter (Part A) (number/100 mL) (number/250 mL for water put into bottles or containers)			
	<i>E. coli</i>		0
	Intestinal enterococci		0
Chemical parameters (Part B) (µg/L)			
Acrylamide	0.10	Haloacetic acids	60
Antimony	10	Lead	5
Arsenic	10	Mercury	1
Benzene	1	Microcystin_LR	1
Benzo(a)pyrene	0.01	Nickel	20
Bisphenol A	2.5	Nitrate	50000
Boron	1500	Nitrite	500
Bromate	10	Pesticides	0.1
Cadmium	5	Pesticides Total	0.5
Chlorate	250	PFAS Total	0.5
Chlorite	250	Sum of PFAS	0.1
Chromium	25	Polycyclic Aromatic Hydrocarbons	0.1
Copper	2000	Selenium	20
Cyanide	50	Tetrachloroethene and Trichloroethene	10
1,2 dichloroethane	3	Trihalomethanes Total	100
Epichlorohydrin	0.1	Uranium	30
Fluoride	1500	Vinyl chloride	0.5
Parameters relevant for the risk assessment of domestic distribution systems (Part D)			
	<i>Legionella</i> (CFU/L)		< 1000
	Lead (µg/L)		10

Furthermore, a risk-based approach, that covers the whole supply chain from the catchment area, abstraction, treatment, storage and distribution of water, is introduced, identifying and preventing hazards and hazardous events by defining and implementing control measures for the prevention and mitigation of the risks.

1.2.2. Reclamation of urban wastewater legislation

At European level, Regulation (EU) 2020/741 establishes the minimum requirements for the safe use of reclaimed water for agricultural irrigation, with the aim of guaranteeing environmental and human health protection and addressing water scarcity. Reclaimed water is defined as UWW, that has been collected in a collecting system, treated in UWWTPs (in accordance with the Directive 91/271/EEC) and that undergoes additional treatment, in order to fit the quality parameters, set out in this regulation. The type of treatment and the quality requirements depend on the final reuse application. Different uses were defined, involving mainly agricultural irrigation of raw, processed and non-food crops, but also other possible uses are not discarded, such as industrial applications and urban and environmental purposes. Different biological (*E. coli* and in specific cases *Legionella* spp. and intestinal nematodes) and physicochemical parameters (Biological Oxygen Demand-BOD₅, Total Suspended Solid-TSS and turbidity) were considered to set out the minimum quality requirements (Table 1.4). On the bases of the values of these parameters 4 minimum reclaimed water quality class (A, B, C or D) were established, used to irrigate certain crops categories with a specific irrigation method.

Table 1.4. Reclaimed water quality for agricultural irrigation established by the Regulation (EU) 2020/741.

Reclaimed water quality class	Quality requirements				
	<i>E. coli</i> (CFU/mL)	BOD ₅ (mg/L)	TSS (mg/L)	Turbidity (NTU)	Other
A	≤ 10	≤ 10	≤ 10	≤ 5	In the case of risk of aerosolization <i>Legionella</i> spp.: < 1000 CFU/L
B	≤ 100	25*	35*	-	
C	≤ 1000	25*	35*	-	In the case of irrigation of pastures or forage: Intestinal nematodes ≤ 1 egg/L
D	≤ 10000	25*	35*	-	

* In accordance with Directive 91/271/EEC

Moreover, minimum routine monitoring with a minimum frequency was set out, to verify that the reclaimed water is in compliance with the minimum water quality requirements set out. As novelty in the new EU regulation, treatment performances should be validated by assessing the Logarithm Reduction Values (LRV) of different indicator microorganisms associated with each group of pathogens: bacteria (*E. coli* ≥ 5-LRV), viruses (Total coliphages/F-specific coliphages/somatic coliphages/coliphages ≥ 6-LRV) and protozoa (*Clostridium perfringens* spores ≥ 4 LRV or spore-forming sulfate-reducing bacteria ≥

1. Introduction

5 LRV). Finally, a water reuse risk management plan is established, identifying hazards, risks and appropriate preventive and/or possible corrective measures.

Nevertheless, CECs, Antibiotic Resistant Bacteria and Genes (ARB and ARGs) have not been yet included. However, they are considered as additional requirements of particular concern, as it is defined in the regulation (EU) 2020/741 text body as follows: “...when necessary to ensure adequate protection of the environment and of human and animal health, in particular when there is clear scientific evidence that the risk originates from reclaimed water and not from other sources.”

1.3. Water pollutants of emerging concern

1.3.1. Microbial targets

Waterborne pathogen can be defined as an agent that causes disease transmitted, through water, to a host. The most common and relevant waterborne pathogens, the concentrations typically detected in different aquatic ecosystems and the main diseases generated in humans are shown in Table 1.5.

Nevertheless, the determination of microbiological safety of water is based on the use of indicator organisms, being impossible all pathogens detection as routine monitoring. They are defined as microorganisms whose detection in water indicates probable presence of pathogens (disease-causing organisms). Ideally, such microorganisms should (i) be nonpathogenic, (ii) occur in high concentration in pathogen-contaminated water, (iii) not multiply in waters, (iv) be reliably and easily detectable and (v) have similar survival times than pathogens. This approach generally involves the monitoring of enteric bacterial coliforms, belonging to the family of Enterobacteriaceae. *E. coli* is the first organism of choice in legislation and in water quality monitoring programs, whose presence provides evidence of recent faecal contamination, while intestinal enterococci group could also be used as an indicator of faecal pollution. However, for the more infective viruses and protozoa, this approach is insufficient, and the related bacterial indicators are not suitable for water quality assessment. Bacteriophages (phages), viruses that use only bacteria as hosts for replication are divided into (i) somatic coliphages and (ii) F-RNA coliphages. Somatic coliphages are not suitable for verification and surveillance monitoring, because there is no direct correlation between coliphages and enteric virus's occurrence (enteric

viruses contaminated water could not contain coliphages) and they are mostly used in validation testing.

Table 1.5. Relevant pathogens typically detected in aqueous ecosystems (WHO, 2021; WHO, 2006).

Pathogens	Disease	Numbers per 100 mL			
		Lakes	Rivers	Groundwater	Raw sewage
Bacteria					
<i>Campylobacter</i> spp.	Gastroenteritis	2-50	9-250	0-1	10 ⁴ -10 ⁵
<i>C. perfringens</i> spores	Diarrhea	-	-	-	6·10 ⁴ - 8·10 ⁴
<i>E. coli</i>	Gastrointestinal illness	10 ³ -10 ⁵	3·10 ³ -10 ⁵	0-10	10 ⁶ -10 ⁷
<i>Faecal streptococci/</i> <i>Intestinal streptococci</i>	Pneumonia/Ear infection/Meningitis	-	-	-	4.7·10 ³ - 4·10 ⁵
<i>Salmonella</i> spp.	Gastroenteritis	-	0.3-5800	-	0.2-8·10 ³
<i>Shigella</i> spp.	Bacillary dysentery	-	-	-	0.1-·10 ³
<i>Leptospira</i> spp.	Leptospirosis	-	-	-	-
<i>Vibrio cholera</i>	Diarrhea	-	-	-	-
<i>Yersinia enterocolitica</i>	Yersiniosis	-	3-6	0-0.2	0.1- 10 ⁴
Viruses					
Polioviruses	Poliomyelitis	-	-	-	1.8·10 ² -5·10 ⁵
Rotaviruses	Diarrhea	-	-	-	4·10 ² -8.5·10 ⁴
Adenoviruses	Fever/Bronchitis	-	-	-	-
Hepatitis A	Hepatitis	-	-	-	-
Protozoa					
<i>C. parvum</i>	Diarrhea	0.4-29	0.2-48	0-0.1	0.1-39
<i>Entamoeba histolytica</i>	Amoebic dysentery	-	-	-	0.4
<i>Balantidium coli</i>	Balantidiasis	-	-	-	-
<i>C. cayetanensis</i>	Cyclosporiasis	-	-	-	-
<i>Giarda intestinalis</i>	Diarrhea	0.2-3	0.1-47	0-0.1	12.5-20000
<i>Toxoplasma gondii</i>	Toxoplasmosis	-	-	-	-
Helminths					
<i>Ascaris lumbricoides</i>	Ascariasis	-	-	-	0.5-11
<i>Ancylostoma</i> spp. and <i>Necator</i> sp.	Anemia	-	-	-	0.6-19
<i>Enterobius vermicularis</i>	Enterobiasis	-	-	-	-
<i>Fasciola hepatica</i>	Fasciolosis	-	-	-	-
<i>Hymenolepis nana</i>	Hymenolepiasis	-	-	-	-
<i>Taenia saginata</i>	Taeniasis	-	-	-	-
<i>Taenia solium</i>	Taeniasis	-	-	-	-
<i>Trichuris trichiura</i>	Trichuriasis	-	-	-	1-4

On the other hand, F-RNA coliphages could provide a more specific indicator of faecal pollution than somatic phages. Regarding protozoa, *Cryptosporidium* spp. is one of the most frequently detected in parasitic aetiology outbreaks in developed countries

1. Introduction

(Efstratiou, 2017). It is characterized by a robust infective forms (oocysts), highly resistant to environmental conditions and conventional water disinfection treatments (Rutala, 2004). Nevertheless, due to its laboratory analysis and handling, other alternative indicators of protozoa with similar resistance are also included in water regulations, such as spores of bacteria including *C. perfringens* or spore-forming sulfate-reducing bacteria (EU 2020/741). Currently, the extensive use and misuse of antibiotics has contributed to the development of ARB and ARGs. Antibiotic Resistance (AR) acquisition could be defined as a phenomenon by which a microorganism is no longer affected by an antimicrobial (previously sensitive), so that usual medical treatments become ineffective, infections persist and can be transmitted to other people, having this one higher mortality (Amarasiri, 2020). The World Health Organization (WHO) has declared that antimicrobial resistance is one of the top 10 global public health threats facing humanity and a list of 12 bacteria families which are considered to pose greatest threat to the human health was published (WHO, 2019; 2017). The widespread use of antibiotic has been caused changes in the natural equilibrium between susceptible and resistance bacteria and a significant correlation between antibiotic consumption and resistance phenomenon is generally accepted (Barceló, 2012). Moreover, a correlation between the type and concentration of antibiotics and the number of copies/mL of the corresponding genes detected in UWW has been recently reported (Wang, 2020). Nowadays, different types of ARGs exist in the environment, including genes encoding resistance to quinolone antibiotic class (*qnrS*), sulphonamides (*sulI*), β -lactams (*blaTEM*), cephalosporins (*blaCTX-M32*), tetracycline (*tetM*), and class 1 integron integrase (*intI1*), related with the horizontal transfer of ARGs, whose occurrence in UWWTPs has been reported, as well as the inability of conventional treatment for their removal (Wang, 2020). Conventional UWWTPs may positively affect ARB spread and selection as well as ARGs transfer, due to the simultaneous presence of a high bacterial density, nutrient rich environment and high and wide antibiotics concentration (Rizzo, 2013). In fact, many studies have demonstrated the presence of ARB and ARGs along the water cycle, identifying UWWTPs as hotspots for their spread into the environment, due to the presence of ARB and the associated ARGs in treated UWW (Rizzo, 2013; Wang, 2020). Consequently, ARB and ARGs have been identified as ubiquitous contaminants of municipal sewage, animal manure, treated wastewater, surface water and even drinking water (Dodd, 2012). Moreover, the presence of ARB and ARGs in reclaimed UWW and the potential environmental implications of reusing it for agricultural irrigation have been

reported (Christou, 2017). The impact of reclaimed water irrigation was assessed considering the potential uptake of ARB and ARGs by crops via soil. Contrasting results were obtained according to literature, due to a complex and heterogeneous sample with low amount of ARGs, difficult to correctly be quantified. In any case, a potential risk associate with UWW reuse cannot be excluded and further investigation is necessary (Christou, 2017).

The AR characterization in bacteria involves:

- *Cultivation-based methods*: enumeration and isolation of ARB grown in selective media supplemented with antibiotics at concentrations similar to or above those reported as inhibitory for the target bacteria, provided by EUCAST (European Committee on Antimicrobial Susceptibility Testing) guidelines. The Minimum Inhibitory Concentration (MIC) was determined as the lowest concentration of the antibiotic that inhibits visibly the growth of a target bacterial population, and thus ARB are defined as the bacteria that are able to visibly grow in agar media, in the presence of the determined MIC of the antibiotic of interest. The membrane filtration method is frequently used in the presence of low bacterial concentration.
- *Molecular-based methods*: quantification of genes encoding resistance to antibiotics by using Polymerase Chain Reaction (PCR) methods, detecting the absolute or relative abundance of resistant genes

Widespread dissemination of AR could occur according two mechanisms: (i) vertical transmission (gene mutation and replication of the bacterial chromosome during cell division) and (ii) horizontal gene transfer (with transfer of genetic material from a donor to a recipient). The development of AR include conjugation (with genetic material transfer between donor and recipient cell), transduction (through bacteriophages carrying deoxyribonucleic acid (DNA)), and natural transformation (extracellular DNA originated from a donor cell is taken from the environment by a second cell). Genetic elements (such as plasmids, transposons, and integrons) allow the mobilization and the integration of exogenous DNA into a cell (Dodd, 2012).

1.3.2. Contaminants of Emerging Concern

According to NORMAN (Network of reference laboratories, research centres and related organizations for monitoring of emerging environmental substances) “emerging contaminants” are defined as substances that have been detected in the environment at very

1. Introduction

low concentrations (ng/L- μ g/L), that are currently not included in routine monitoring programs and whose fate, behaviour and (eco)toxicological effects are not well understood (Gogoi, 2018). They are toxic, bio-refractory, bio-accumulative compounds whose fate, behaviour and potential detrimental effect to both aquatic ecosystem and human health are not yet well known, especially considering chronic toxicity and a synergistic harmful effect of a complex chemical mixture.

The population growth and the economic development induce an increase of anthropogenic activities, with higher production and larger use of chemical and consequent widespread occurrence of organic micro pollutants, due to an uncontrolled discharge of these substances into the environment. The main sources of these chemicals are related to (i) agricultural, industrial and hospital activity, (ii) direct release by improper dump and (iii) UWWTPs. As regards the last point, effluents from UWWTPs are considered as one of the main pathways for the introduction of CECs into the aquatic environment, due to their inability to achieve a successful decontamination and in many cases neither an effective disinfection (Michael, 2013).

CECs include pharmaceuticals (antibiotics, Non-Steroidal Anti-Inflammatory Drugs (NSAIDs), hormones, β -blockers, blood lipid regulators) personal care products (PCPs), surfactants, artificial sweeteners, flame retardants, gasoline additives, pesticides and Endocrine Disrupting Compounds (EDCs) (Figure 1.4).

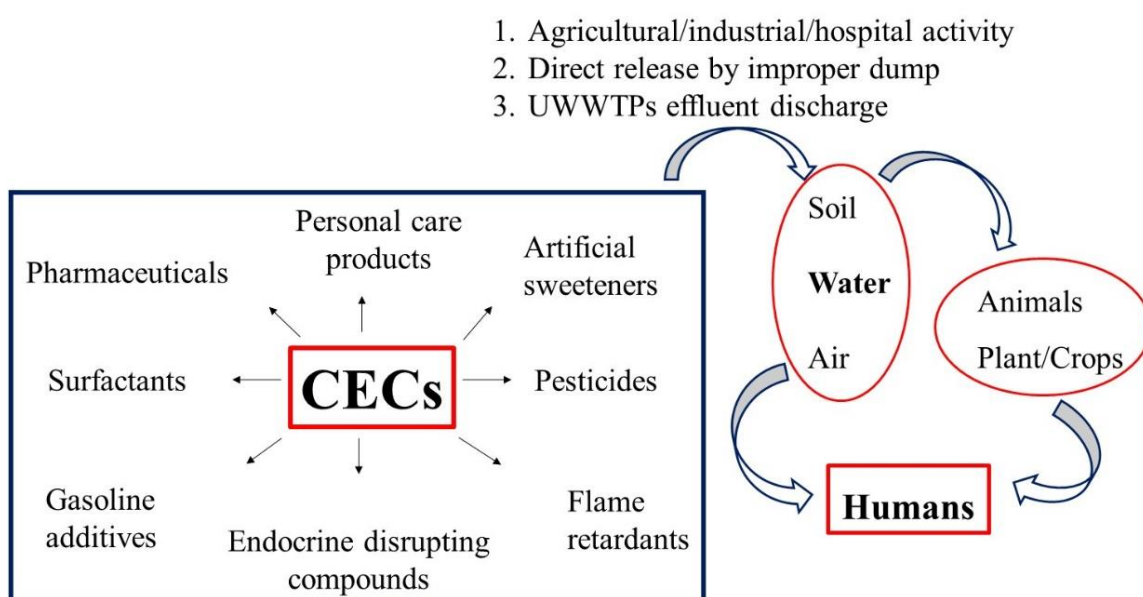


Figure 1.4. CECs classification, sources and accumulation in soil, water and air, impacting on animals, plants and humans.

Although usually present in low concentrations (ng/L- μ g/L), the continuous introduction into the aquatic environment confers some degree of pseudo-persistence and the great technological advances of sensitive analytical techniques, involving high resolution liquid or gas spectrometry, has been allowing the detection of low concentrations of these trace compounds (Gogoi, 2018; Sousa, 2018), enabling the assessment of their occurrence in freshwater resources (groundwaters, surface waters and even drinking waters), as it can be observed in Table 1.6.

Another important concern is related to plant uptake, considering especially the accumulation and translocation of CECs in soil and crops after irrigation with reclaimed UWW (Christou, 2019, 2017; Martínez-Piernas, 2018).

Table 1.6.: Average concentrations of different pharmaceuticals measured in different water matrices in several countries. Adapted from (Montes-Grajales, 2017; Pereira, 2020).

	UWW influent (ng/L)	UWW effluent (ng/L)	Surface water (ng/L)	Other water bodies*** (ng/L)
Pharmaceuticals (Pereira, 2020)				
Anxiolytics	19.9	51.2	5.8	1.9
Antibiotics	502.9	269.5	108/1708**	17.7
Lipid regulators	604.1	319	152.3	22.8
Antiepileptics	513.6	398.4	130.2	59.6
SSRIs*	48.8	38.7	8.6	2.7
Anti-inflammatory	11192.4	564.4	490.9	29.1
Hormones	62.9	23.1	12.6	6.3
Personal care products (PCPs) (Montes-Grajales, 2017)				
Cosmetics, Deodorant stick/Soap, Disinfectant/antiseptic, Fragrances, Insect repellent, Sunscreen, Surfactants, Toothpaste	2238356	159508	nd-1293000	nd-26700

* SSRIs=Selective serotonin reuptake inhibitors; nd= not determined

** 1708.5, if two extremely high average concentrations detected for CIP in surface waters near pharmaceutical industries in Pakistan (1.3 μ g/L) and in India (164 μ g/L) are considered

*** Seawaters, groundwaters, drinking waters and mineral waters

As previously mentioned, currently, the release of CECs from UWWTPs into the environment and the concentration in reclaimed UWW for agricultural reuse have not yet been regulated at European level. Nevertheless, Switzerland is the first country that implemented a legislation for CECs degradation in UWW effluent. Table 1.7 shows the Swiss list that includes 12 indicator substances, with 3-4 compounds belonging to one of the following categories: (i) readily biodegradable, (ii) not biodegradable but amenable to chemical oxidation or sorption to activated carbon and (iii) not biodegradable and not amenable to oxidation or sorption to activated carbon. The main criteria employed in this legislation to evaluate the effectiveness of the tertiary wastewater treatments (mostly

1. Introduction

involving ozonation or powered activated carbon (PAC)) is the removal of at least an average 80 % of the selected indicator substances over the whole treatment (Bourgin, 2018; The Swis Federal Council, 1998).

Table 1.7. List of 12 CECs indicators, class and abatement during ozonation or PAC treatment, according to the New Swiss Water Protection Act.

Substance	Class	Abatement during ozonation or PAC treatment
Amisulpride	Pharmaceutical (antipsychotic)	Very good (>80 %)
Carbamazepine	Pharmaceutical (antiepileptic)	Very good
Citalopram	Pharmaceutical (antidepressant)	Very good
Clarithromycin	Pharmaceutical (macrolide antibacterial)	Very good
Diclofenac	Pharmaceutical (anti-inflammatory / antirheumatic)	Very good
Hydrochlorothiazide	Pharmaceutical (diuretic)	Very good
Metoprolol	Pharmaceutical (beta blocking agent)	Very good
Venlafaxine	Pharmaceutical (antidepressant)	Very good
Benzotriazole	Corrosion inhibitor	Good (50-80 %)
Methylbenzotriazole	Corrosion inhibitor	Good
Candesartan	Pharmaceutical (antihypertensive agent, angiotensin II antagonist)	Good
Irbesartan	Pharmaceutical (antihypertensive agent, angiotensin II antagonist)	Good

1.3.3. Disinfection by Products formation

Chemical oxidant disinfection agents are relatively no selective species that can react with Natural Organic Matter (NOM), producing the well-known Disinfection by Products (DBPs), which are potentially carcinogenic, mutagenic, genotoxic and teratogenic. The formation of DBPs, especially during drinking water disinfection, has been recognized since the 1970s, but advances in analytical techniques and in risk assessment have been allowing to continuously better characterize occurrence, identify and quantify different DBPs, being only a small portion of the potentially formed chemicals identified up to now, as it can be observed in Figure 1.5 (Gil, 2019).

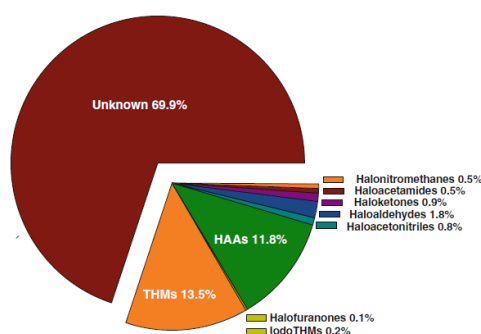


Figure 1.5. Occurrence of DBPs.

It is widely recognized that the use of chemical disinfectants (such as chlorine, ozone, chloramines, and chlorine dioxide) causes the production of DBPs, after the reactions between oxidant and NOM (mostly comprised of humic and fulvic acids) through three main reaction mechanisms: (i) oxidation, (ii) addition (too slow) and (iii) substitution. DBPs include: trihalomethanes (THMs), haloacetic acids (HAAs), haloaldehydes, halo ketones, halonitriles, halogenated acetonitriles, haloamides, halonitromethanes, chlorophenols, nitrogenous DBPs and inorganic DBPs (chlorite ClO_2^- , chlorate ClO_3^- and bromate BrO_3^-). Table 1.8 reports the maximum limit of the regulated DBPs according to U.S. Environmental Protection Agency (USEPA), WHO and European guidelines.

Table 1.8. Maximum Contaminant Level (MCL) ($\mu\text{g/L}$) of regulated DBPs, according to USEPA, WHO and European guidelines in drinking water.

DBPs	Maximum Contaminant Level (MCL) ($\mu\text{g/L}$)
USEPA regulation (USEPA, 1985)	
Total THM (Chloroform, bromodichloromethane, chlorodibromomethane, bromoform)	80
5 HAAs (chloro-, bromo-, dichloro-, dibromo-, trichloro-acetic acid)	60
Bromate	10
Chlorite	1000
WHO guidelines (WHO, 2011)	
Chloroform	300
Bromodichloromethane (BDCM)	60
Dibromochloromethane (DBCM)	100
Bromoform	100
$\frac{\text{Chloroform}}{\text{Chloroform}_{\text{guideline value}}} + \frac{\text{Bromoform}}{\text{Bromoform}_{\text{guideline value}}} + \frac{\text{BDCM}}{\text{BDCM}_{\text{guideline value}}} + \frac{\text{DBCM}}{\text{DBCM}_{\text{guideline value}}} < 1$	
Dichloroacetic acid	50
Trichloroacetic acid	200
Bromate	10
Chlorate	700
Chlorite	700
Dichloroacetonitrile	20
Dibromoacetonitrile	70
2,4,6-trichlorophenol	200
N-Nitrosodimethylamine (NMDA)	0.1
European Union standards (Directive (EU) 2020/2184)	
THMs	100
HAAs	60
Chlorate	250
Chlorite	250
Bromate	10

It is reported that chlorination mainly leads to the formation of THMs, ozonation does not produce halogenated DBPs, but in the presence of Br^- the formation of BrO_3^- and brominated DBPs has been detected, while no evidence of DBPs formation was obtained after UV-C treatment.

1. Introduction

Several factors affect DBPs formation and occurrence including: (i) type of oxidant, (ii) disinfectant dose, (iii) contact time and (iv) water quality (pH, T, type and quantity of NOM and inorganic species concentration). Therefore, the evaluation of potential generation of DBPs during the treatment of UWW by oxidative processes is necessary to ensure a safer reuse.

1.4. Water treatment plants

In water and wastewater management, there are two main industrial strategies: centralized *versus* decentralized treatment plants.

The *centralized treatment (or conventional treatment)* consists of a large-scale plant that treats large volumes of water at high rates and with high efficiency to provide drinking water (DWTPs) or to treat wastewater (UWWTPs). This approach is well developed and installations are generally constructed near the freshwater resources (rivers or lakes). However, the capital investment, operating and maintenance cost can be significant. Another cost is related to water transport to the centralized treatment plant (for wastewater) as well as from the treatment plant to the individual households (for potable water), especially in regions far away from the treatment plant (Kausley, 2019).

The *decentralized treatment (or on-site treatment)* consists of small plant placed close to the water supply, that treats small volumes of water and serves to a more localized area. Decentralized systems are the main treatment options in rural and isolated areas due to lower costs, lower infrastructure complexity (avoiding large initial capital investments, especially for the construction of sewer infrastructure and treatment facilities) and lower operation and maintenance requirements, compared to centralized systems. Moreover, new technologies can be implemented in an easier way, compared to large systems, that treat high volumes of water, being extremely complicated the replace of the already running conventional water treatments.

On the other hand, research on novel or innovative processes are mainly focused on decentralized systems associated to both drinking water treatment (specially for low-income countries) for a local community or even at household level and in less extend to UWW.

1.4.1. Drinking water treatment plants

Drinking water treatments aim to obtain high drinking water quality and they are designed to remove pathogens and macro parameters, such as Total Suspended Solids (TSS), NOM, dissolved iron and manganese.

The treatment process train depends on the water source and on its initial quality, as it can be observed in Figure 1.6 (Barceló, 2012; Gil, 2019). In surface water (Figure 1.6.a) the main processes involve:

- *Coarse Filtration*: for the elimination of larger materials.
- *Coagulation-Flocculation-Sedimentation*: for the elimination of TSS and NOM. Coagulation is a process that consists of decrease the repulsion between particles by adding positively charged ions (Fe(III) or Al(III) salts) in order to promote particles' aggregation (with formation of larger size and weight flocs), capable to settle during a sedimentation step.
- *Filtration*: for the removal of the remained suspended particles, passing the water through a layer of sand, gravel and charcoal. To improve water quality, activated carbon (granular or powdered activated carbon) could be employed, especially to reduce taste and odour, as well as NOM (preventing DBPs formation).
- *Disinfection*: it could be based on (i) chlorination (effective also in controlling microbial post regrowth in the distribution system), (ii) UV-C radiation or (iii) ozonation, followed by activated carbon filtration.

Groundwater's quality is higher than surface water and it is generally easier to condition according to the following main processes (Figure 1.6.b):

- *Aeration*: oxygen or air is added to water in order to eliminate gases (such as CO₂, NH₃, H₂S, CH₄) and volatile organic chemicals and oxidize dissolved metals such as iron and manganese (that after oxidation can precipitate and be removed in the filtration step).
- *Conditioning and softening*: in order to adjust pH, calcium content, bicarbonate concentration and saturation index. Ion exchange (or water softening) processes are used to remove dissolved solid, including carbonate, chloride, bicarbonate and sulfate of calcium and magnesium, but also arsenic, chromium, excess of fluoride, radium, and uranium.
- *Filtration and disinfection*.

1. Introduction

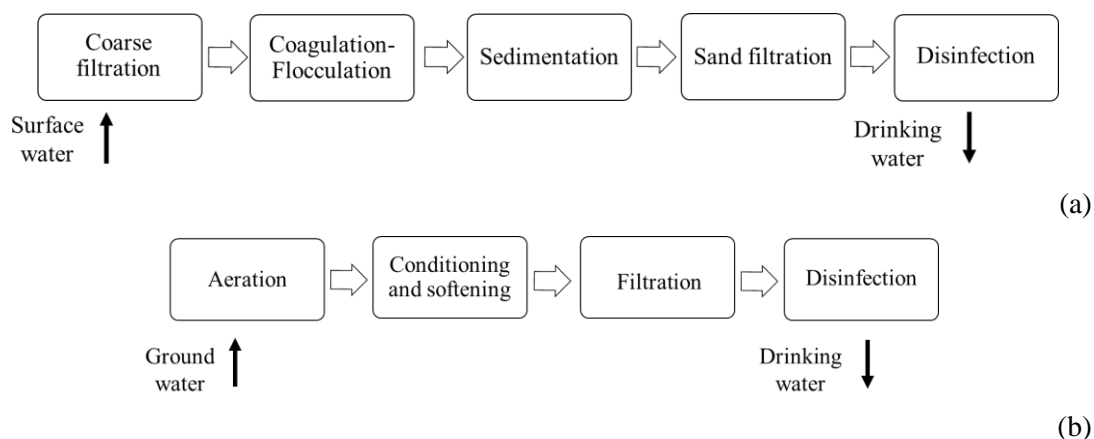


Figure 1.6. Treatment processes train of (a) surface water and (b) groundwater to obtain drinking water.

Conventional water treatments (for both wastewater and drinking water) are not designed and effective enough for CECs removal and a variety of these contaminants has been detected in different environmental matrices including surface, groundwater and drinking water (Barceló, 2012). Coagulation-flocculation is ineffective in removing CECs and only a small % of highly hydrophobic compounds (Octanol-Water Partition Constant $K_{ow} > 5$) could be adsorbed on coagulates particles. An efficient adsorption on activated carbon is reported for pesticides, EDCs and pharmaceuticals (Barceló, 2012), while the removal of these organic pollutants by chemical based-oxidation processes could occur, but kinetic rates are highly dependent on target's compound structure as it will be explained in next sections.

1.4.2. Urban wastewater treatment plants

According to Directive 91/271/EEC, UWW must be treated in UWWTPs, before being discharged into the natural environment in order to protect it from adverse effects. UWWTPs are designed to remove a variety of contaminants and conventional wastewater treatments normally involve a (Gogoi, 2018):

- *Pre-treatment*: for the separation of large objects (rags and plastic) through a bar screens and for grit, oil and grease removal, through grit chamber in order to avoid the clogging and destruction of pumps.
- *Primary treatment*: for the removal of TSS and part of NOM through a primary clarifier, involving coagulation, flocculation and filtration processes.

- *Secondary treatment*: for the removal of the remaining organic matter and/or nutrients, through the action of microorganisms (activated sludge) commonly in the presence of oxygen. Biological treatment techniques used in UWWTPs are Fixed Bed Bioreactors (FBR), Membrane Bioreactors (MBR), Moving Bed Biofilm Reactor (MBBR) and the most well-known Conventional Activated Sludge (CAS). Then, water passes into a second clarifier in order to obtain a further separation of solids from water.

Generally, the secondary effluent is directly discharged into the environment, without further disinfection treatment, causing introduction of pathogens, harmful to public health, into the environment. Additional requirements may be of particular concern and their inclusion in the regulation should be considered, such as (i) CECs, (ii) DBPs and (iii) anti-microbial resistance, whose removal is not achieved in a conventional UWWTP and it could be carried out implementing a tertiary treatment. Figure 1.7 shows UWWTPs train processes and the main parameters of pollution concern (chemical and microbiological), commonly detected in the influent and the secondary effluent.

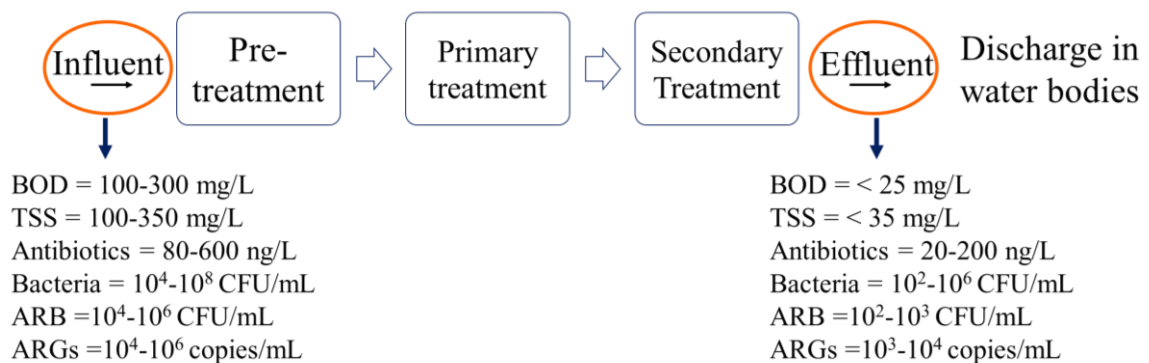


Figure 1.7. Treatment processes train in UWWTPs and influent and effluent main chemical and microbiological parameters of concern (Data according to Wang, 2020).

Consequently, different challenges should be addresses and investigated deeply to not only reach the “reclaimed” status in case of reusing, but also to reduce the impact of direct discharging in the environment:

- Adequate risk assessment of CECs occurrence in the environment, resistance spread and of maximal abundance of CECs, ARB and ARGs (analyzing and minimizing the factors that promote resistance development) to not pose a harmful effect.
- Improvement of the common treatment technologies (chlorination, ozonation and UV-C radiation) or implementation of advanced treatment technologies for CECs,

1. Introduction

ARB and ARGs removal → effective simultaneous disinfection and decontamination process is considered as a possible tool to control the spread of CECs and ARB into the environment, promoting targets removal in UWWTPs.

1.5 Water purification treatments

Water purification treatment is the process of removing undesirable chemicals, biological contaminants, suspended solids, and gases from water in order to produce water fit for specific purposes. Disinfection is a selective process, whose objective is to remove, deactivate or kill pathogenic microorganisms, including bacteria, viruses, protozoa and fungi, in order to prevent the spread of waterborne diseases and guarantee public health. It differs from sterilization, that involves the complete destruction of all microorganisms. Figure 1.8 shows the mostly studied conventional and advanced water treatment technologies up to now:

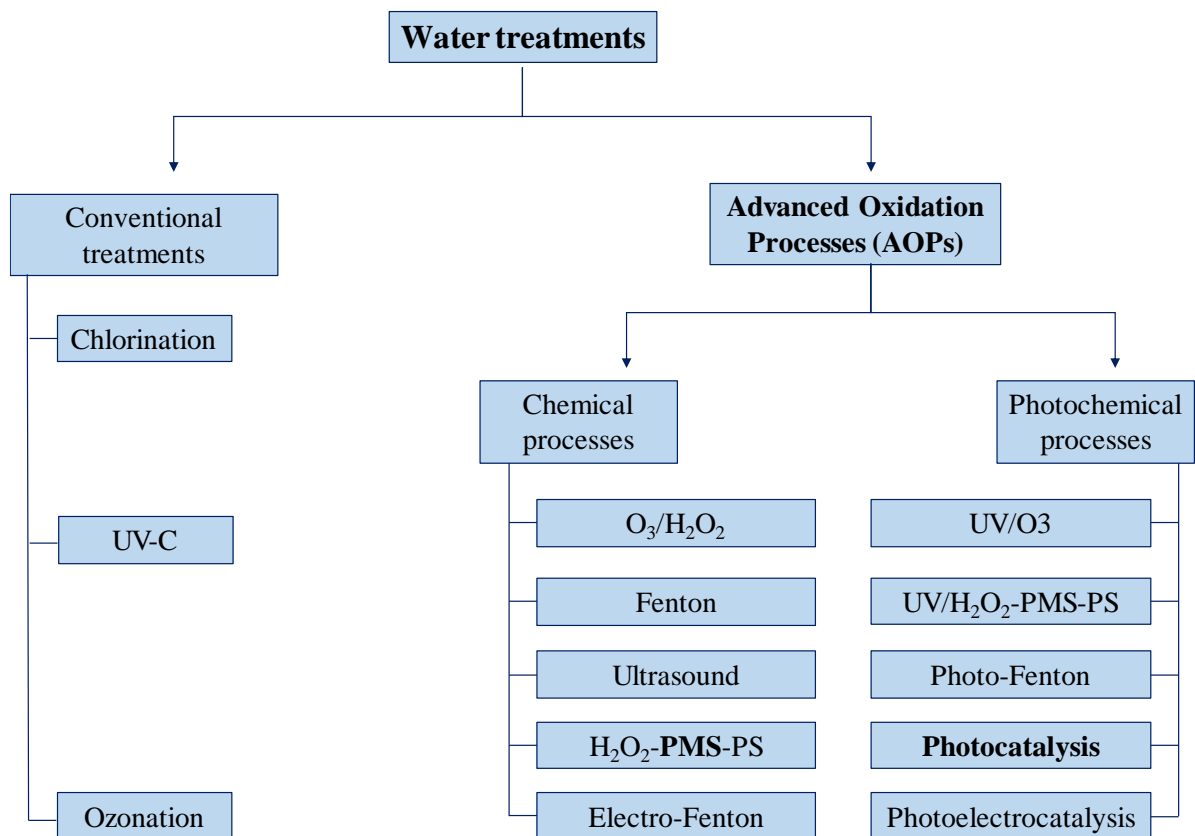


Figure 1.8. Water treatment processes.

1.5.1. Chlorination

Chlorination, involving the use of sodium hypochlorite NaClO, calcium hypochlorite Ca(ClO)₂, chlorine dioxide ClO₂, or gaseous chlorine Cl₂, is the most used process for disinfection in both drinking water and wastewater treatment plants.

It is a simple, consolidated and low-cost technology, that ensures a residual effect and a post treatment microbiological quality. Disinfection efficiency is highly dependent on the microorganism, requiring higher disinfectant doses and contact times to achieve the same degree of inactivation in function of the resistance and the following order was reported: Bacteria > Viruses \cong Fungi > Protozoa (WHO, 2011). The germicidal effect is attributed to the continuous penetration of HClO into the cell, with further reaction with intracellular components, mainly for bacteria, while for other pathogens direct oxidation of membrane components (mainly proteins and enzymes) could be the responsible for their inactivation (Cho, 2010).

An effective inactivation of ARB was reported but requiring higher disinfectant doses (10-100 mg/L) than the usually practiced concentration for UWW treatment (1-10 mg/L), while even higher doses are necessary to remove ARGs (Alaton, 2019; Zheng, 2017). Hypochlorous acid and hypochlorite anion can oxidize ammonia, halides, other anionic inorganic compounds (SO₃²⁻, CN⁻, NO₂⁻ or sulfide), As(III), Fe(II) and Mn(II). Moreover, it is reported that CECs removal efficiency is highly dependent on chemical target structure (and on the presence of reactive sites on the molecule, such as unsaturations, π bonds with delocalized electrons, electron-rich heteroatoms as sulfur or nitrogen and electron-donating group (as -OH or -NH₂ group)) and second-order rate constants for chlorination could vary over 10 orders of magnitude (i.e., < 0.1–10⁹ M⁻¹s⁻¹). Oxidation, addition and electrophilic substitution reactions with organic compounds are possible pathways, but low chlorine reactivity and small modifications in the parent compound's structure are reported, being highly dependent on water pH and on chemical structure (Deborde, 2008). However, the main concern of this treatment relies on DBPs formation (tri-halomethanes) (Rizzo, 2020), the residual effect that could be toxic to different organisms at different trophic levels and it could provoke taste problems.

1.5.2. Ozonation

Ozone (O₃) is a powerful oxidant agent ($E_{\text{red}}(\text{O}_3/\text{O}_2) = 2.1 \text{ V vs Normal Hydrogen Electrode NHE}$), especially employed in DWTPs, characterized by disinfection and decontamination efficiencies even higher than chlorine, because it provides good performances for

1. Introduction

microorganism inactivation and CECs degradation with averaged contact times of 10-30 minutes.

Two types of reactions could take place during ozonation:

- *Direct attack by molecular O₃*: selective attack to organic molecules having nucleophilic moieties, such as carbon double bonds, aromatic rings and functional groups containing sulphur, phosphorous, nitrogen and oxygen. Compounds with these moieties are higher reactive than ones with electron-withdrawing groups. Three types of reactions could occur: (i) cycloadditions, (ii) electrophilic substitutions and (iii) electron-transfer reactions.
- *Secondary reactions with HO[•]*: no selective attack to organic and inorganic species through three main mechanisms (i) hydrogen abstraction, (ii) electron transfer reactions and (iii) addition.

Bactericidal effect is attributed to the ability of destroying bacterial cell wall, with minimal penetration into the cytoplasm, due to rapid oxidant consumption. Oxidation of reactive moieties, contained within the cell envelope by O₃, is possible due to its high reactivity towards amino acids, unsaturated carbon-carbon (C-C) bonds contained in the proteins, in the peptidoglycan layer and in the lipids of the cell wall (Dodd, 2012). Evidence that bacterial inactivation proceeds through oxidation of membrane components was provided by utilizing Scanning Electron Microscopy (SEM) or Transmission Electron Microscopy (TEM) images (Cho, 2010; Dodd, 2012). Once the structural integrity of cell membrane surface is damaged, changes in selective permeability cause the release of intracellular material, ending on cell inactivation.

Rate constants for the reaction between O₃ and CECs can vary more than ten orders of magnitude (from 0.1 to 10¹⁰ M⁻¹s⁻¹), because reactivity is dependent on target chemical structure, being aromatic compounds substituted with electron donor groups, such as -OH or -NH₂ groups, especially susceptible to react with ozone (Lee, 2013). Specific O₃ dose of 0.55 gO₃/gDOC has been found to be effective to achieve the removal of an average 80 % of a broad range of CECs, fulfilling the requirements of the Swiss water protection act (Bourgin, 2018). Moreover, effective inactivation of ARB was also reported, while higher specific ozone doses (0.55 gO₃/gDOC) are necessary to eliminate intracellular ARGs (Czekalski, 2016).

On the other hand, it is an unstable gas that must be generated in situ and used immediately, with high treatment cost (high energy demand and high management costs) and other drawback is related to the potential brominated DBPs formation.

1.5.3. UV-C radiation

UV-C is a physical agent generally recognized as an effective tool for inactivating microorganisms in water, being chemical-free, independent on the pH, without involving the formation of DBPs or generating odours or taste on the treated water. The germicidal effect of UV-C radiation ($\lambda = 254$ nm) is based on light absorption and subsequent direct photoreaction of nucleic acids (maximum absorption at 260 nm), resulting in bacterial DNA damages with eventual inhibition of cell replication. In fact, UV-C radiation can penetrate the cell membrane and cytoplasm and act directly on the purines and pyrimidines nucleobases of DNA or RNA, inducing (i) dimerization of adjacent pyrimidine nucleobases with formation of Cyclobutane Pyrimidine Dimers (CPDs) and (ii) coupling of adjacent pyrimidine nucleobases with generation of pyrimidine (6-4) pyrimidone dimers and its conversion in an isomer (Giannakis, 2016). By analysing the amount and type of proteins and DNA released and morphological changes after UV-C treatment a direct action to the cell wall could be excluded.

It is effective against bacteria, viruses and protozoa and it has been proven to be effective in the elimination of ARB and their associated genetic material, due to direct photolytic deactivation of intracellular ARG-containing DNA during irradiation of ARB, but only when it is applied at higher doses than ones typical for drinking water disinfection (40 mJ/cm^2) (Arslan-Alaton, 2021). UV-C can effectively degrade some organic CECs after absorption of light, breaking chemical bonds, but photolysis is highly dependent on molecule targets and some organic contaminants exhibit low removal capacity (Rizzo, 2020).

The main drawbacks of UV-C radiation are related with the high energy demand (high costs associated) and the effectiveness of the system depends on water matrix characteristics of the wastewater (turbidity, TSS and NOM content), the intensity of UV radiation, the contact time and the reactor configuration. Moreover, microorganisms may recover replication activity, through DNA repair mechanism, and, therefore, water safety during storage cannot be guaranteed.

1.5.4. Solar water disinfection

Solar radiation is the energy radiated from the Sun in the form of electromagnetic waves, corresponding to the UV range (UV-B from 280 to 320 nm and UV-A from 320 to 400 nm), visible range (from 400 to 800 nm) and infrared range (from 800 to 3000 nm). Most of the irradiance is received in the visible and infrared ranges (47.3 and 44.9 %, respectively), while the most energetic part of the spectrum is mostly absorbed by the atmosphere, reaching the Earth's surface only a 7.8 % of UV (distributed around 3 % of UV-B and 97 % of UV-A). The solar radiation is distributed across the electromagnetic spectrum as shown in Figure 1.9.

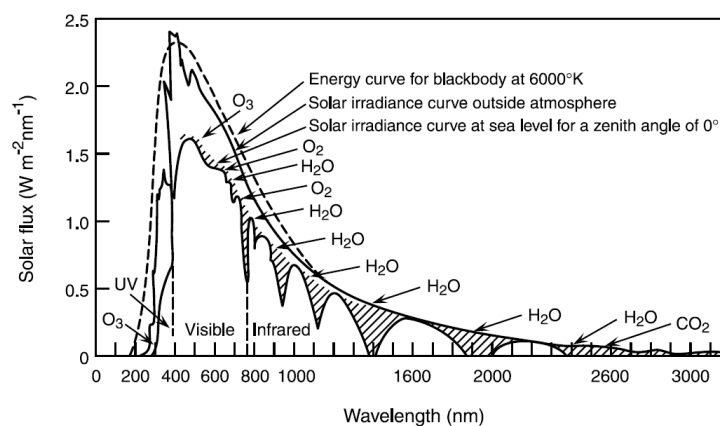


Figure 1.9: Spectrum of solar radiation at the top of Earth and at sea level.

This energy is given by two components: (i) direct radiation, constituted by the rays coming directly from the Sun and (ii) diffuse radiation that comes from different directions and it is scattered by atmosphere particles or by Earth's surface, modifying the original direction of sunlight. The sum of both components (direct and diffuse) is the global radiation reaching the Earth's surface.

One of the most successful applications of sunlight for drinking water disinfection is known as Solar Water Disinfection (SODIS), that is promoted around the world as a low-cost method for household water treatment. It is a practical, simple and low-cost disinfection method, that allows to obtain a safe drinking water by reducing the microorganisms' concentration in water. It consists on the exposition of contaminated water to sunlight in polyethylene terephthalate (PET) bottles for 6 h under full sunshine or 48h under cloudy conditions. A synergistic effect of mild heat and solar UVlight (higher synergistic effect between radiation and T is achieved for T higher than 45 °C) is responsible for the disinfection, being the main inactivation mechanism based on Reactive Oxygen Species

(ROS) generation. The mechanism by which sunlight damages health-relevant microorganisms in water is shown in Figure 1.10 and it can be subdivided into: (i) direct and (ii) indirect effects (Nelson, 2018).

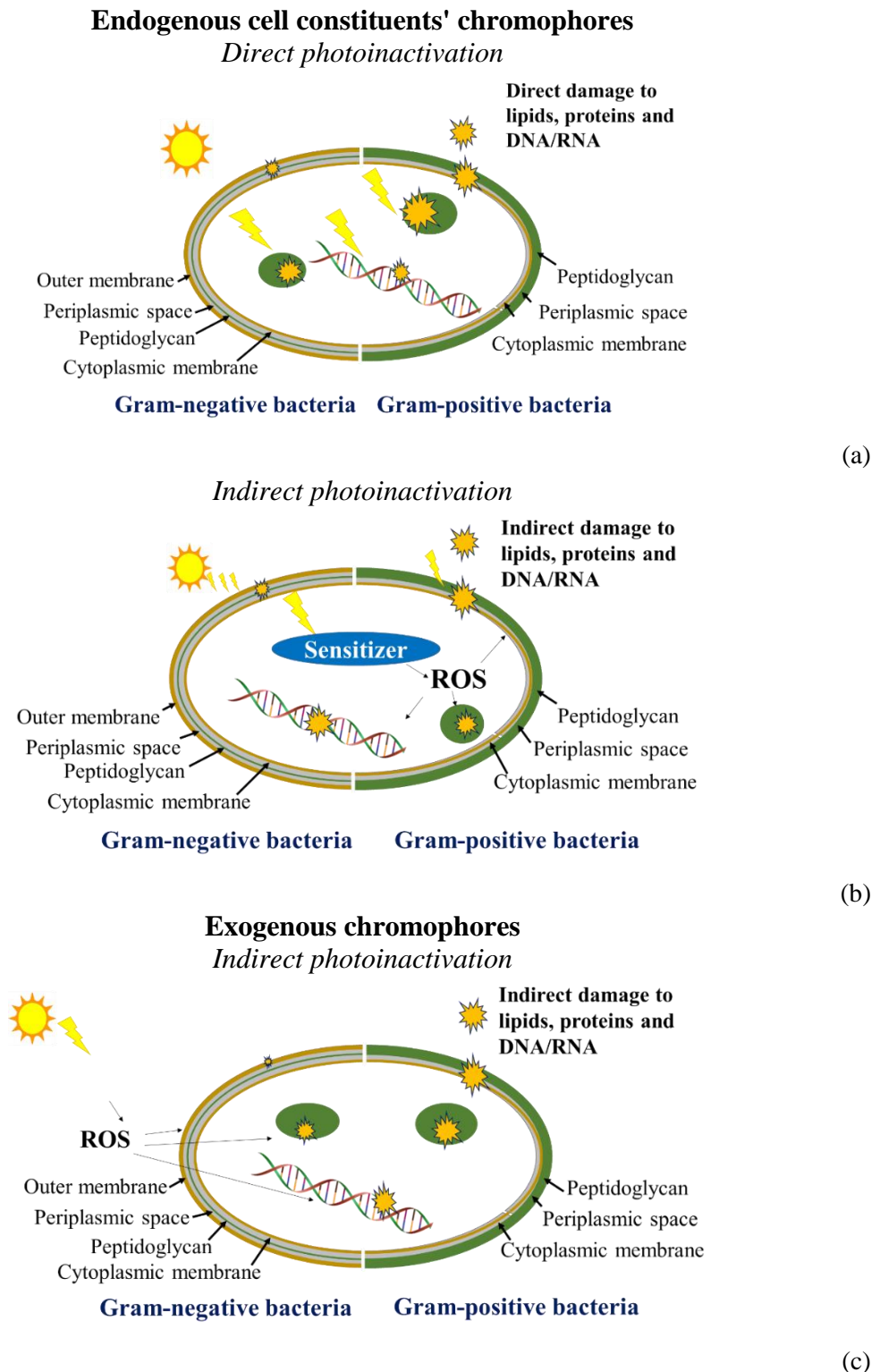


Figure 1.10: Sunlight mediated inactivation mechanism involving photoinactivation of endogeneous cell constituents' chromophore (a) direct effects, (b) indirect effects and (c) indirect photoinactivation of exogeneous chromophore. Adapted from (Nelson, 2018).

1. Introduction

During direct photoinactivation, cellular components (including nucleic acids and proteins) may act as chromophores, directly absorbing radiation (mainly in the UV-B range), suffering a photochemical transformation (Figure 1.10a) (Giannakis, 2016). This type of reactions is promoted by adjacent pyrimidines, that dimerize upon irradiation, leading to the formation of CPDs, Dewar valence isomers and DNA lesions such as Single Strand Breaks (SSBs).

During indirect photoinactivation, intracellular components (microorganism endogenous constituent, such as L-tryptophan, coenzymes and vitamins, Figure 1.10b) and/or natural exogenous photosensitizers present in waters (such as humic acids) (Figure 1.10c) may also absorb radiation (in the UV-B and UV-A range), producing ROS, such as hydroxyl radical HO^\bullet , superoxide radical $\text{O}_2^{\bullet-}$ and singlet oxygen $^1\text{O}_2$, in solution, that in turn attack cellular constituents, leading to cell death. These species have been proven to induce lipids peroxidation, proteins oxidation and DNA damages (Nelson, 2018).

1.6 Advances Oxidation Processes

Advanced Oxidation Processes (AOPs) have been investigated during last decades as possible powerful and effective alternative to conventional processes for water and wastewater disinfection and decontamination (Malato, 2009). These processes rely on the potential generation of highly oxidant, reactive and non-selective ROS, such as hydroxyl radical (HO^\bullet), superoxide radical $\text{O}_2^{\bullet-}$, hydroperoxyl radical (HO_2^\bullet) and alkoxy radical (RO^\bullet). These free-radicals are defined as molecules capable to exist independently and characterized by an unpaired electron. Among them, the HO^\bullet has the key role in AOPs, because it is the second most oxidative ROS (2.8 V *versus* NHE in acid media) after fluorine (3.6 V *versus* NHE) (Legrini, 1993), and it can react with almost any organic compounds, leading eventually the complete mineralization into CO_2 and H_2O (Pera-Titus, 2004; Malato 2009).

The AOPs main applications are as pre-treatment of industrial wastewater to increase biodegradability, before the subsequent conventional biological process; and as an alternative to conventional tertiary treatment, for the improvement of the chemical and microbiological quality of UWWTP effluents.

AOPs are classified as first premise in chemical processes (O_3 , $\text{O}_3/\text{H}_2\text{O}_2$, Fenton ($\text{H}_2\text{O}_2/\text{Fe}^{2+}$), electrochemical oxidation, sonolysis, among others) or photochemical processes, involving the use of a light source (UV/ O_3 , UV/ H_2O_2 -Persulfate (PS)-

Peroxymonosulfate (PMS), UV/H₂O₂/O₃, photocatalysis with semiconductors and photo-Fenton) (Figure 1.8).

Regarding the photochemical AOPs, two main sources of light could be considered, the UV-C radiation and the natural solar radiation.

The benefits of using UV-C radiation as source of light for water purification has been already described. Moreover, the capability to break O-O bond of different oxidative agents, such as H₂O₂, PS, PMS, among others, promoting the generation of ROS in solution, makes its application highly promising in order to overcome the limitations of the use of UV-C alone as tertiary wastewater treatment. The performance of the process is dependent on:

- Type of chemical or biological target: depending on microorganism resistance to oxidation process and on physicochemical properties of chemical contaminants.
- Type and concentration of oxidant: Considering 254 nm UV-C activation method, process efficiency is influenced by oxidant photolysis, leading to the generation of different amounts of radicals in solution. Quantum yield ϕ_{254} and molar absorption coefficient ϵ_{254} of the oxidants commonly employed in combination with UV-C radiation at 254 nm are important factors to evaluate. As it can be observed in Table 1.9, among the different oxidants, the photolysis of chlorine through low-pressure mercury lamps emitting at 254 nm, results in a more efficient production of radicals (high value of ϵ_{254}), while PMS exhibits the lowest one.

Table 1.9. Properties of peroxymonosulfate, persulfate, hydrogen peroxide and free chlorine. References: (Kiejza, 2021; Lee, 2020; Yang, 2019; Wang, 2018; Wacławek, 2017; Guan, 2011; Herrmann, 2007).

Oxidant	Standard reduction potential (V)	O-O bond dissociation energy (kJ/mol)	pKa	ϕ_{254} (mol·Einstein ⁻¹)	Experimental ϵ_{254} (M ⁻¹ cm ⁻¹)
Peroxymonosulfate HSO ₅ ⁻	1.8	377	9.3	0.52	8.8
Persulfate S ₂ O ₈ ²⁻	2.0	92	-3.5	1.4	16.7
Hydrogen peroxide H ₂ O ₂	1.4	213	11.7	1.0	13.1
Free chlorine HClO	1.5	/	7.5	1.0	125.7

- System configuration and operative conditions (batch mode or continuous flow) and contact times.
- Water matrix composition: high organic and inorganic content, turbidity and TSS concentration required higher oxidant doses due to its consumption, light attenuation

1. Introduction

and depletion of active species, because of side reactions with formation of less reactive radicals ($\text{Cl}^\bullet/\text{Cl}_2^{\bullet-}$ and $\text{CO}_3^{\bullet-}$).

On the other hand, the use of natural sunlight as source of photons for AOPs has also been widely investigated during the last decades, looking for treatments with low cost, environmentally friendly, using a renewable energy and reducing the carbon footprint.

In this line, the most investigated AOPs are the solar heterogenous photocatalysis with $\text{TiO}_2\text{-P25}$, and the solar homogenous process, namely photo-Fenton (Malato, 2009). Additionally, based on several drawbacks of the already two most well-known solar AOPs, others water treatments have appearing recently as potential water purification processes, such as solar photo-chemical process based on the use of low concentration of oxidants agents such as H_2O_2 , PS, PMS, among others, which capability for water disinfection has been demonstrated. Nevertheless, all of these water processes still have some limitations, and more research is required in this line to make the use of natural solar radiation a competitive technology. Table 1.10 summarizes main benefits and drawbacks of the most commonly conventional treatments and AOPs investigated to date for water and wastewater disinfection and decontamination.

Table 1.10. Summary of conventional (ozonation, chlorination and UV-C) and advanced water treatment technologies (heterogeneous photocatalysis with TiO₂-P25, H₂O₂/UV-C and H₂O₂/Solar) performances, with main advantages, drawbacks and possible solutions.

	Ozonation	Chlorination	UV-C radiation	Advanced treatment technologies		
				TiO ₂ -P25	H ₂ O ₂ /UV-C	H ₂ O ₂ /Solar
[Reactive]	[O ₃] (g O ₃ /g DOC)= 0.25-0.9	1-10 mg/L	10-140 mJ/cm ²	100-500 mg/L	5-30 mg/L	10-50 mg/L
CECs removal	$k_{O_3,CECs} > 10^3 \text{ M}^{-1}\text{s}^{-1}$ Highly efficient A specific O ₃ dose of 0.55 gO ₃ /gDOC is recommended for 80 % removal of the 12 selected substances, according to the Swiss water protection act.	Poor. Efficiency depends on compound chemical structure, oxidant concentration and pH.	Efficiency depends on chemical structure.	Highly efficient.	Efficient.	Poor.
Microorganisms' inactivation	Mechanism: Disruption of bacterial cell walls, release of intracellular components, damage of nucleic acids, denaturalization of proteins. Efficiency: Effective to decrease pathogens population, depending on: • Target microorganism' susceptibility; • Water type, that influences also O ₃ transfer.	Mechanism: Diffusion of HClO into the cell, with further reaction with intracellular components in bacteria. For viruses, fungi and protozoa, direct oxidation of membrane components. Efficiency: Very effective towards bacteria, moderate towards viruses and fungi while protozoa show high tolerance.	Mechanism: DNA damages after direct absorption. Efficiency: Effective to decrease pathogens population (including bacteria, viruses, spores and cysts).	Mechanism: Generation of ROS, and further reaction with organic compounds and components of microorganisms. Efficiency: Effective to decrease all groups of pathogens.	Mechanism: Generation of ROS and direct DNA damages by absorption of UV-C radiation. Efficiency: Very effective.	Mechanism: H ₂ O ₂ -free diffusion inside microbial cells with the generation of HO• by the so-called internal photo-Fenton reactions with naturally occurring metals and its further attack to cell vital component such as DNA, proteins and enzymes. Efficiency: It is very effective for bacteria, viruses, fungi spores, and lower efficiency against protozoa.

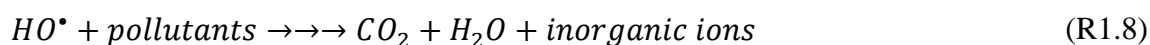
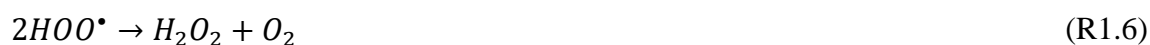
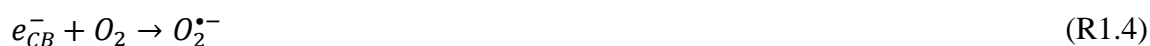
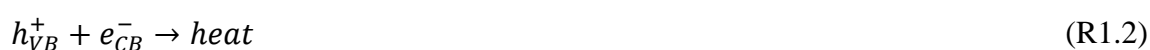
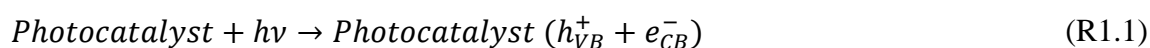
1. Introduction

ARB and ARGs removal	Effective for inactivation of ARB and at some extent for ARGs removal.	Effective to decrease ARB population, while contrasting results were obtained with ARGs, but, at full scale, chlorination did not prove to be effective.	Effective, but strongly dependent on the UV doses: 20-50 mJ/cm ² for ARB. 200-400 mJ/cm ² for ARGs.	Effective for ARB inactivation, but not for ARGs in UWW.	Effective -for ARB inactivation, but inability of the process to prevent the spread of ARGs to the environment.	Effective for ARB inactivation, but low efficiency for ARGs removal.
Advantages	Energy efficient process for CECs removal.	Low cost and simple applicability.	No need to generate, handle and transport chemicals. Short contact times. Low DBPs formation.	Formation of HO [•] capable of oxidizing organic compounds. Nobacterial regrowth.	Formation of HO [•] capable of oxidizing organic compounds. H ₂ O ₂ is a cheap reactive.	Absence of a toxic effect. No potential generation of DBPs. Use of natural solar radiation. H ₂ O ₂ is a cheap reactive.
Drawbacks	Unstable gas generated in situ and used immediately. Low transfer O ₃ into water. High treatment cost. Generation of DBP (N-nitrosodimethylamine NDMA and bromate).	Generation of DBPs (trihalomethanes, chloroamines and haloacetic acids). Higher doses than conventional are necessary to effectively inactivate viruses, spores, ARB and ARGs.	Post treatment regrowth. Low dose could be ineffective. Turbidity and suspended solid could make UV treatment ineffective. Costs.	Technical application still scarce. High costs. Separation of catalyst from water. Lower catalysts efficiency after several cycles.	Relatively high capital and operating costs. High energy consumption of the UV lamps.	Post treatment bacterial regrowth. Low efficiency for CECs and ARGs removal. Low or null HO [•] formation, due to requirements of wavelengths < 290 nm for H ₂ O ₂ homolytic cleavage.
Solution	Post treatment, involving sand or biological activate carbon filter is recommended in order to remove DBPs and TPs.	Post treatment for CECs and DBPs removal.	Combination with oxidizing agents (free chlorine, H ₂ O ₂ , PMS, PS, PAA).	Catalyst immobilization, but obtaining lower performances.	Increase treatment time and/or oxidant concentration.	Combine with metals or other catalyst to promote ROS generation.
Full scale application	Yes, in DWTPs and UWWTPs (UWWTP Neugut with 105000	Yes.	Yes, in DWTPs.	No.	No, but feasible using already working UV-C plants.	No.

	population equivalent in Switzerland).					
References	Bourgin, 2018; Rizzo, 2020; Zheng, 2017; Sgroi, 2021	Fiorentino, 2021; 2015; Pereira, 2013; Zhou, 2014; WHO, 2011; Rizzo, 2020; Zheng, 2017	Rizzo, 2020; Zheng, 2017; USEPA, 1999; Sgroi, 2021	Rizzo, 2020; Agulló-Barceló, 2013; Moreira 2018; Polo-López, 2014; 2010; Aguas, 2017; Malato 2016; Abeledo-Lameiro, 2017	Michael, 2020; Sánchez-Montes, 2020; Cerreta, 2019; Sgroi, 2021	Michael, 2020; Moreira 2018; Polo-López, 2017; 2014; Agulló-Barceló, 2013; Fiorentino, 2015

1.6.1. Solar heterogeneous photocatalysis

Among AOPs, heterogeneous photocatalysis based on semiconductors has been widely investigated since last decades as a promising method for water and wastewater treatment (Byrne, 2018). Heterogeneous photocatalysis can be defined as the acceleration of a photoreaction which occurs at the surface of a catalyst, leading to organic pollutants mineralization into carbon dioxide (CO₂), water (H₂O) and inorganic ions at ambient temperature and atmospheric pressure in the presence of oxygen or air under near UV-irradiation ($\lambda < 400$ nm). In the solar heterogeneous photocatalysis, sunlight is the source of photons that are absorbed by the catalyst. Photocatalysts' reaction mechanism is well known. During the photoexcitation of the semiconductor (with absorption of a photon with an energy $h\nu$ greater or equal to the bandgap energy E_g), electron-hole (e_{CB}^-/h_{VB}^+) pair is created between the Valence Band (VB) and the Conduction Band (CB) (R1.1). These photo-induced species can be trapped and recombined at the surface of the semiconductor, releasing energy in the form of heat (R1.2). However, the reaction between h_{VB}^+ and e_{CB}^- with water molecules (R1.3) and oxygen (R1.4), respectively, leads to the formation of HO[•] and O₂^{•-}, that could attack target molecules yielding to CO₂, H₂O and inorganic ions (R1.8 and R1.10). Moreover, the oxidative potential h_{VB}^+ could allow the direct oxidation of contaminants (R1.9) and further production of HO[•] could be possible (R1.7) after protonation of O₂^{•-} with generation of hydroperoxyl radical HOO[•] (R1.5) and subsequently of H₂O₂ (R1.6) (Figure 1.11) (Nosaka, 2017).



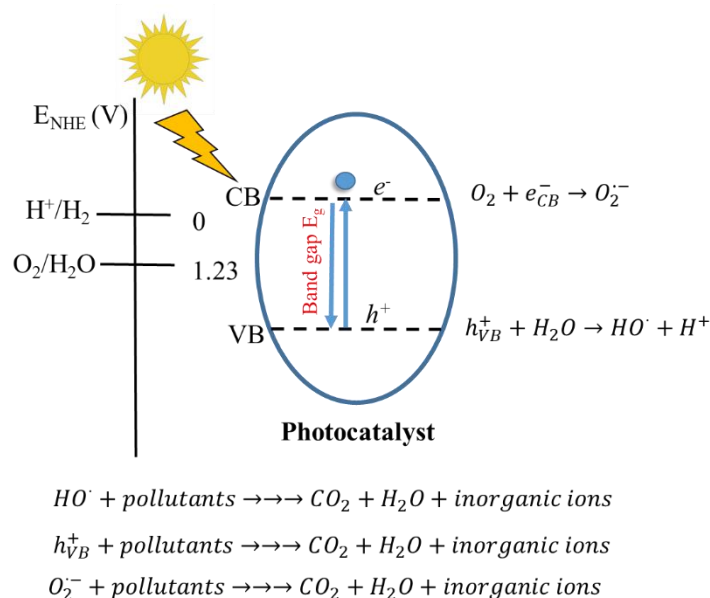


Figure 1.11: Mechanism of photocatalysis.

Generated ROS are therefore responsible for bacteria inactivation and CECs degradation in water during photocatalytic irradiation. As regards pathogens, the first target of the radicals is the surface of the external membrane of the cell wall, causing its disruption with an initial damage on lipopolysaccharides layer and on the peptidoglycan layer, followed by internal components leakage, leading ultimately to the cell death. High reactivity between CECs and ROS (mainly HO^\cdot) leads to their oxidation in solution and high second order kinetic constants for the reaction of different CECs with HO^\cdot are reported in literature (Wols, 2013). Several factors affect photodegradation efficiency, including (Lee, 2016; Malato, 2009):

- *Chemical and biological targets type.*
- *Catalyst concentration:* the increase of catalyst amount leads to an enhancement of the efficiency, due to an increase of catalyst sites on the surface with higher generation of ROS and higher target molecules removal. However, beyond the optimum, a reduced photocatalytic performance has been obtained, due to light scattering, screening effects for higher solution turbidity, inhibiting the penetration of light in the reactor, and agglomeration particle phenomenon, leading to a reduction of surface area. Therefore, an optimum catalyst load should be found, in order to avoid excess usage of catalyst and to ensure maximum absorption of available photons. Moreover, this value is dependent on the radiation incident and path length inside the reactor.

1. Introduction

- *Contaminant target concentration*: an increase of contaminant concentration leads to a decrease in photocatalytic efficiency. In fact, in the presence of the same number of catalyst active site, light irradiation and time, higher target concentration requires a higher amount of ROS.
- *Solution pH*: water pH affects the surface charge of the catalyst particles, the positions of CB and VB in a semiconductor, the size of aggregates, target molecules ionization, influencing the electrostatic interaction between catalyst and surface, which ultimately may affect photocatalytic performances. A parameter that characterizes the surface charge of a catalyst is the Point of Zero Charge (PZC), defined as the pH at which the surface of an oxide is uncharged. Below the pH_{PZC} , semiconductor surface is positively charged, while it is negatively when pH is higher. Moreover, at pH_{PZC} particles are prone to agglomerate, due to the absence of repulsion among particles, affecting catalyst sedimentation, surface area and capability to efficiently absorb light. According to the pK_a value of the organic compounds, the specie could exist as positive, neutral and negative charged and it could be adsorbed or not, according to attraction or repulsion with catalyst surface.
- *Light intensity*: higher light intensity produces more ROS and at lower intensity, reaction rate is proportional to radiant flux.
- *Water matrix components*: NOM, inorganic ions and water turbidity generally lead to a decrease of photocatalytic performances due to different factors acting simultaneously, such as: (i) increase of bacteria viability, serving as nutrient, (ii) photons absorption, (iii) scavengers of photogenerated $h\nu_{\text{VB}}^+$ and ROS, (iv) adsorption on catalyst particles causing agglomeration and inhibition (Rioja, 2016; Tsydenova, 2015).
- *Temperature and oxygen concentration*: the process can operate at room temperature, without the need of heating the water. Higher T is counterproductive, favoring target desorption and decreasing O_2 solubility. Oxygen is necessary for complete mineralization and the reaction rate is independent on its concentration.
- *Type of photoreactor*: its design must guarantee the conversion of incident photons to charge carrier. Turbulent flow in the reactor must be guaranteed in order to avoid sedimentation and deposition of the catalyst. Photoreactors for solar photocatalysis are based on non-concentrating collectors, capable to increase the incident

UV-radiation, both direct and diffuse, on the photo-reactor tube. A wide description of solar photoreactors is reported in section 1.8.1.

Research on solar photocatalysis for water purification has been mainly focused on the use of TiO₂-P25, considered as a reference material, due to its very good photocatalytic properties, high oxidation ability, non-toxic nature, low cost, stability and wide bandgap in the near-UV spectral region (Fanourgiakis, 2014; Fagan, 2016; Malato, 2016; Moreira, 2018; Byrne, 2018; Grilla, 2019).

However, there has been a growing interest on the investigation of other photocatalysts than TiO₂, for example ZnO, ZnS, ZrO₂, semiconductor-graphene, perovskites, MoS₂, WO₃, CdS, Nb₂O₅, V₂O₅ and Fe₂O₃ for water and air treatment (Byrne, 2018).

In particular, ZnO as solar photocatalyst has recently gained the interest of the scientific community due to its wide band-gap in the near-UV spectral region, strong oxidation ability, low cost, good photocatalytic property, chemical and thermal stability and a large free-exciton binding energy. ZnO is a white powder, odourless, insoluble in water and it crystallizes in the wurtzite structure (Lee, 2016). It has a direct band-gap of 3.37 eV, being able to be photoexcited by natural solar radiation. The major drawback of ZnO is the photocorrosion, that leads to the release of Zn²⁺ in solution according to R1.11:



Another disadvantage in semiconductor photocatalysis is related to the recombination of photogenerated h_{VB}^+ and e_{CB}^- , causing a decrease of quantum yield and lowering photocatalysis efficiency. Improvements in photocatalytic activity could be achieved by enhancing the charge separation between h_{VB}^+ and e_{CB}^- through several modifications involving: (i) heterojunction formation and (ii) doping agent (anionic, cation and rare earth dopant) introduction (Lee, 2016). The doping agent may act as electron trapping agent to decrease the h_{VB}^+ and e_{CB}^- recombination rate, leading to an increase in ROS generation and outperforming undoped ZnO performances. Previous studies demonstrated that the addition of a transition metal, such as iron, and of rare earth element, such as Ce or Yb, improve the photocatalytic efficiency under irradiation for water disinfection and decontamination (Bousslama, 2017; Cerrato, 2020b; Paganini, 2016, 2019; Sordello, 2019; Zammit, 2018).

Sunlight-driven ZnO photocatalyst has attracted the attention, because the use of a naturally available, free and renewable source of energy, such as sunlight, to photoexcite a

1. Introduction

semiconductor, for water and wastewater remediation makes the process environmentally sustainable.

The addition of an oxidative agent (H_2O_2 , PMS or PS) has been also investigated as a potential strategy to enhance the efficiency of the photocatalytic processes, by preventing $h\nu_{\text{B}}^+/\text{e}_{\text{CB}}^-$ recombination and increasing the quantum yield. The photodegradation rate could be enhanced due to different factors such as: (i) a more efficient trap of electrons by inorganic oxidant compared to O_2 , minimizing $h\nu_{\text{B}}^+/\text{e}_{\text{CB}}^-$ recombination and (ii) an increase of ROS formation and other oxidizing species (Lee, 2016; Malato, 2009). In this line, the most studied process involves the combination of heterogeneous photocatalysis using TiO_2 -P25 assisted with H_2O_2 (Moreira, 2018; Malato 2009).

However, it has been demonstrated that also the introduction of PMS remarkably enhanced the degradation rate of organic contaminants by simultaneously promoting the charge separation and generating additional $\text{SO}_4^{\bullet-}$, according to the following reaction (R1.12-R1.13). Figure 1.12 shows the schematic diagram of the process Solar/Photocatalysis/PMS. A synergistic effect between PMS and TiO_2 was reported by Rodríguez-Chueca et al. for the removal of methylene blue in water (Rodríguez-Chueca, 2019a), while other studies demonstrated the heterogeneous activation of PMS involving ZnO for bisphenol A degradation (Kong, 2021), with successful degradation rates in comparison with only ZnO (Kong, 2021) and ZnO nanoparticles anchored on a magnetic core/shell structure ($\text{SiO}_2@\text{Fe}_3\text{O}_4$) for diazinon (a pesticide) degradation after PMS activation (Sakineh, 2019).

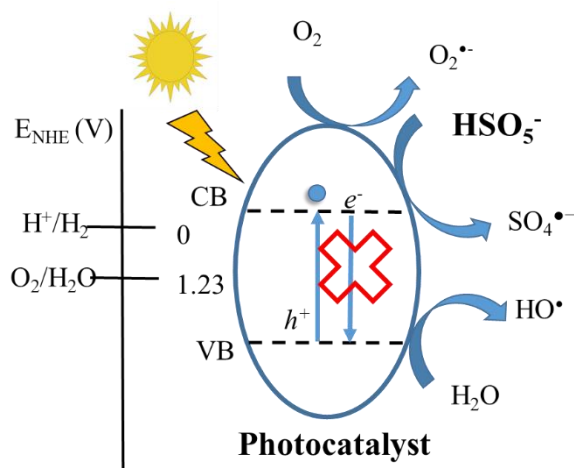
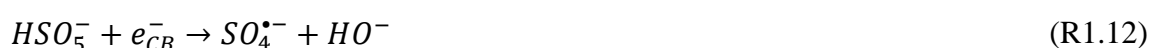


Figure 1.12: Mechanism of photocatalysis in the presence of PMS.

1.7 Sulfate radical Advanced Oxidation Processes

In sulfate radical based AOPs (SR-AOPs) the generation of sulfate radicals $SO_4^{\bullet-}$ is promoted alone or jointly with HO^{\bullet} , presenting similar characteristics to the conventional AOPs. SR-AOPs were firstly introduced for soil and groundwater remediation in the late 1990s, but over the past decades, these processes have drawn a significant attention as a viable alternative to traditional HO^{\bullet} based AOPs in water and wastewater treatment, as it can be observed by the increasing number of documents published since 2000, based on the database Scopus (Figure 1.13) (Lee, 2020).

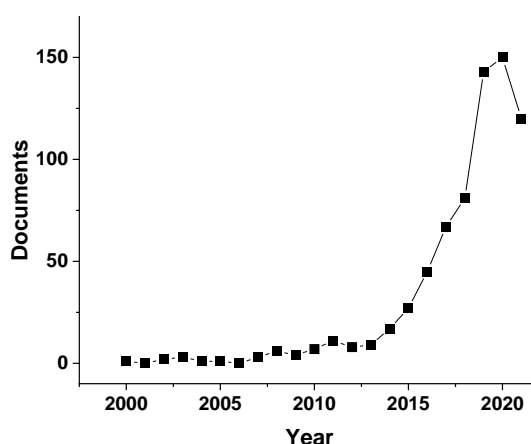


Figure 1.13: Frequency of reports by year (2000 - 2021), dealing with SR-AOPs for water treatment. The search was based on Scopus database using as keywords ‘advanced oxidation processes; sulfate radicals; water including articles, reviews, books, and book chapters.

SR-AOPs are based on the use of a precursor, such as PS ($S_2O_8^{2-}$) or PMS (HSO_5^-) to promote the generation of radicals, through different activation methods, such as UV-radiation, transition metals, heat and alkaline condition (Lee, 2020).

Among them, UV-C radiation (most used wavelength is 254 nm) is one of the most investigated, due to its ability to break O-O bond, leading to the production of $SO_4^{\bullet-}$ and HO^{\bullet} in solution from PMS (R1.14) and $SO_4^{\bullet-}$ from PS (R1.15) with high efficiency (Wang, 2018).



The inactivation of microorganisms and chemical contaminants degradation are based on the reactions between radicals (mainly $SO_4^{\bullet-}$ and HO^{\bullet}) and organic molecules by different

1. Introduction

mechanisms, including electron transfer, addition to a double bond and hydrogen abstraction from aliphatic parts of the molecules (Wojnárovits, 2019).

The HO \cdot unselectively may reacts by any of the three mentioned oxidation mechanisms, while SO $_4^{\bullet-}$ mainly attacks by electron transfer as main reaction. SO $_4^{\bullet-}$ exhibit higher redox potential ($E_0(\text{SO}_4^{\bullet-}/\text{SO}_4^{2-}) = 2.6\text{-}3.1\text{ V} > E_0(\text{HO}\cdot/\text{OH}^-) = 1.9\text{-}2.7\text{ V}$) and longer half-life than HO \cdot . Besides, due its higher selectivity, it is consumed by the main water matrix constituents (Cl $^-$, Br $^-$, HCO $_3^-$ /CO $_3^{2-}$, NOM) with lower kinetic rates (Wacławek, 2017).

Recently the use of PMS as source of sulfate radical in SR-AOPs has gained great attention as a potential and promising wastewater tertiary treatment. PMS is the active ingredient and the component of potassium triple salt with the formula KHSO $_5\cdot 0.5\text{KHSO}_4\cdot 0.5\text{K}_2\text{SO}_4$, known with the tradename Oxone $^{\text{®}}$. It is a white, granular powder, stable, easy to handle and nontoxic compound. The stable triple salt, containing two moles of potassium peroxymonosulfate and one mole of potassium bisulfate and potassium sulfate, has been prepared due to the instability of the corresponding persulfuric acid H $_2\text{SO}_5$ (also known as Caro's acid), firstly described in 1898 by Heinrich Caro. It is used in a variety of industrial and consumer application, such as swimming pool shock oxidizer, electronics-related industries (printed wiring board micro etchant), bleaching cellulose pulp in paper production, control agent in wastewater treatment, bleach component in denture cleanser and laundry formulations and activator in antimicrobial compositions, among others.

Figure 1.14 shows the dissociation equilibria for PMS and the corresponding pKa. The first acid dissociation of peroxymonosulfuric acid (Caro's acid, H $_2\text{SO}_5$) is characterized by a pKa $_1$ of 0.4, at neutral pH it is mainly present in its mono-anionic form (HSO $_5^-$), while at basic pH (pH > 9.4) SO $_5^{2-}$ is the prevailing one (Mao, 2010).

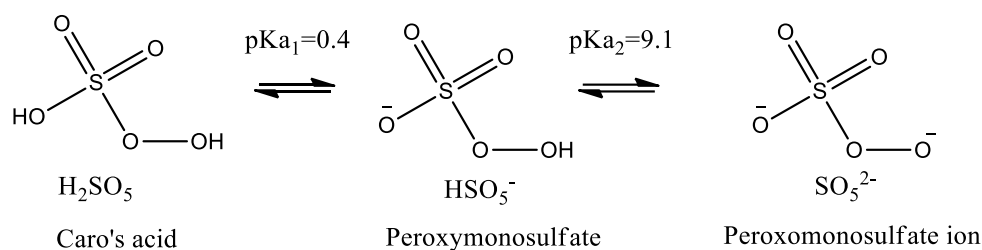


Figure 1.14. Dissociation equilibrium for peroxymonosulfate and corresponding pKa.

The salt mixture is characterized by a theoretical % of active component (PMS) of 42.8 % and 5 % of active oxygen approximately. Moreover, it is highly and readily soluble in water,

with a solubility > 250 g/L (1.6 M) at room temperature. It has been considered a powerful oxidant, whose standard electrode potential ($E^\circ(\text{HSO}_5^-/\text{HSO}_4^-)=1.85$) is given by the following reaction (R1.16):



It has asymmetrical structure, the distance of O-O bond is 1.453 Å and the bond energy is estimated to be 377 kJ/mol. Moreover, singlet oxygen $^1\text{O}_2$ could be generated in solution by its self-decomposition, according to the following reaction (R1.17) (Wang, 2018):



The potential is high enough for many room temperature oxidations, including halide to halogen or hypohalite, ferrous ion to ferric, manganous ion to manganic, oxidation of reduced sulfur and nitrogen compounds, cyanide to cyanate, epoxidation of olefins, Baeyer-Villiger oxidation of ketones, copper metal to cupric ion, etc. (DuPont, 2008). In recent years the use of PMS as a powerful non-chlorine oxidant agent in water purification technologies has been attracted attention. PMS could directly oxidize several organic contaminants, including sulfonamides antibiotics, antipyrine, acetaminophen, doxycycline, ketorolac and caffeine, trimethoprim, ampicillin, carbamazepine, cimetidine, ranitidine, 4-Chlorophenol, 2,4,6-trichlorophenol, furfuryl alcohol, azide ions, and L-histidine (Ji, 2018; Rivas, 2012; Yang, 2021; 2018; Yin, 2018).

Focusing on the combination of PMS with UV-C for water purification, it has showed enhanced removal performance for both disinfection and decontamination in different water matrices, as it can be observed in Table 1.11.

On the other hand, recently, the use of natural solar radiation, as photon source, in combination with PMS has been also investigated for the acceleration of kinetic degradation rates of both microbial and organic contaminants in water, taking also advantage of using a source of renewable and clean energy, saving energy costs by replacing artificial light and making these processes an attractive option for the tertiary treatment of small UWWTPs.

Nevertheless, literature on PMS as oxidative agents in combination with sunlight, as source of photons, for wastewater disinfection and decontamination is quite scarce. Ozores-Diez et al., in an attempt of enhancing SODIS process, evaluated solar light/PMS process for *E. coli* inactivation in different water matrices (such as distilled water, tap water and natural water) in cheap and large-scale plastic vessels (19-L blue poly-carbonate (PC) bottle and 25-L PET jerrycan) (Ozores Diez, 2020).

1. Introduction

Table 1.11. PMS/UV-C literature studies for removal of chemical and microbial targets.

Targets	[PMS] (mM)	Water matrix	Treatment time (min)	Abatement (%)	Reference
Water disinfection					
Fungal spores C ₀ = 2·7·10 ⁵ CFU/mL	0.1	PBS	35-85 mJ/cm ²	99	Wen, 2017
HLS-6 ARB C ₀ = 10 ⁸ CFU/mL ARG <i>sulI/intI1</i>	1 mg/L 20mg/L	DW	10 (60 mJ/cm ²) 30 (180 mJ/cm ²)	5.3 LRV 2.9/3.4LRV	Hu, 2019
<i>Bacillus cereus</i> spores C ₀ = 10 ⁵ -10 ⁶ CFU/mL	50 mg/L	DrW	80 mJ/cm ²	3 LRV	Zeng., 2020
<i>Caenorhabditis elegans</i> C ₀ = 30 nematodes	1	DrW	90	> 99	Chen., 2021
AR <i>E. coli</i> J53/ <i>aphA</i> and <i>tetA</i> C ₀ =3.45· 10 ⁶ CFU/mL	2	UWW	80	6.5 LRV/QL	Arslan-Alaton, 2021
Water decontamination					
2,4- Dichlorophenol C ₀ = 20 mg/L	1.227	DW	60	> 99	Anipsitakis, 2004
Dimethyl phthalate C ₀ = 100 mg/L	40	DW	20	> 95	Olmez-Hanci, 2011
Carbamazepine C ₀ = 5 mg/L	1	DW	90	76	Deng, 2013
Phenol C ₀ = 48 mg/L/TOC	5	DW	40/120	> 99/33	Olmez-Hanci, 2013
Cylindrospermopsin C ₀ = 1 µM	1	5 mM PBS	40 mJ/cm ²	> 99	He, 2013
Atenolol C ₀ = 20 µM	0.08	DW	30	88	Liu, 2013
Ciprofloxacin C ₀ = 50 µM	1	UWW	60	> 99	Mahdi-Ahmed, 2014
Triton X-45/ TOC C ₀ = 20 mg/L/12 mg/L	2.5	DW	7/30	> 99/84	Olmez-Hanci, 2015
Bisphenol-A/TOC C ₀ = 0.22 mM	0.66	DW	360	96.7/72.5	Sharma, 2015
Acid Blue 113 C ₀ = 50 mg/L	4.2	UWW	30	> 99	Shu, 2015
12 sulfonamides C ₀ = 0.2 µg/L	1 mg/L	Dr	30	> 99	Cui, 2016
Lindane C ₀ = 3.43 µM	0.25	DW	-	78.4	Khan, 2016
Sulfamethoxazole C ₀ = 23.69 µM	1	DW	-	97	Ao, 2017
Lindane C ₀ = 3.43 µM	0.25	DW	180	90	Khan, 2017
Sucralose/TOC C ₀ =0.126 mM/18.11 mg/L	1.89	50 mM PBS	60	70	Xu, 2017
25 CECs C ₀ = UWW natural occurring	0.5	UWW	18 s of contact time	48	Rodríguez-Chueca, 2018
Ethyl paraben	0.25	DW	90	81	Dhaka, 2018
7 pharmaceuticals C ₀ = UWW natural occurring	0.5	UWW	0.15-0.5	63-83	Rodríguez-Chueca, 2019b
Dichloroacetonitrile C ₀ = 2 µM	0.3	2mM PBS	30	80	Zhang, 2019
Simultaneous water disinfection and decontamination					
10 antibiotics/ARGs C ₀ = UWW natural occurring	0.5	UWW	7 s of contact time	< 50 %/ 1.4 LRV	Rodríguez-Chueca, 2019c
<i>E. coli</i> K12 & <i>E. faecalis</i> CECs	0.01 5	UWW	3-28 s of contact time	5.7 LRV 90	Rodríguez-Chueca, 2019d

*QL=Quantification Limit; DW= Distilled water; Drinking water= DrW; PBS=Phosphate-Buffered Saline

1.8. Photo-reactors employed for water processes

1.8.1. Compound Parabolic Collector

Compound Parabolic Collectors (CPCs) are static collectors, considered a good option for solar photochemical applications. CPCs are characterized by solar concentration factor of 1 and they are formed by an involute reflective surface around a cylindrical absorber tube, as it can be observed in the schematic drawn showed in Figure 1.15.

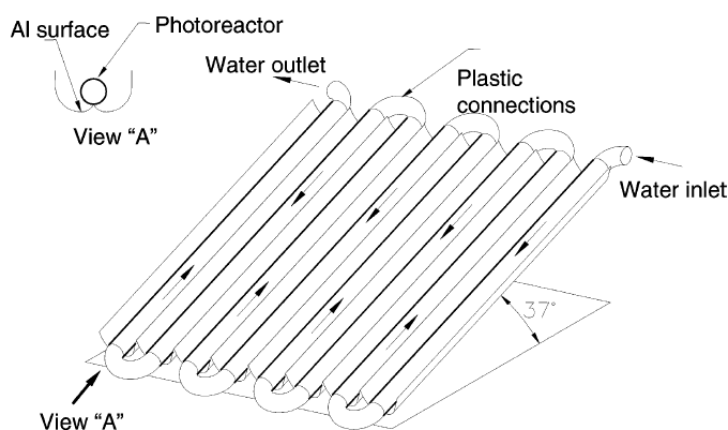


Figure 1.15. Schematic drawing of a CPC. Adapted from (Malato, 2002).

The ideal reflective surface must be highly UV-reflective, low cost and resistance to high solar radiations and adverse weather conditions for long lifetime. Reflectors of anodized aluminium are a good compromise and the design enables to capture almost all the incident UV-radiation, both direct and diffuse, distributing the reflected light homogeneously around the tubes, where water is recirculated under turbulent flow conditions, allowing homogeneity. A centrifugal pump is generally used for the recirculation, whose power is function of the required total reactor volume and flow. The tubes must be weather-resistant, chemically inert, transparent to UV-light, resistant to high or low pH and to high T (temperatures inside solar photochemical reactors can easily reach 40–50 °C). Moreover, the choice of the tube's material is crucial and the enhancement of UV transmissivity and the prevention of UV solarisation lead to processes performances improvement. UV solarisation is a phenomenon in which a change in polyvalent ions charge occurs after radiation absorption (such as photooxidation Fe^{2+} that is converted to Fe^{3+} by photons with a wavelength of less than 400 nm), leading a further decrease of the UV-transmissivity. The best material should have high UV-transmission, elevate resistance to temperature and chemicals, low iron-content and reasonable price. Quartz has low absorption in the solar

1. Introduction

UV range but its high cost makes it completely inadequate. Borosilicate glass is the material commonly used for the absorber tube, due to its transmissivity in the solar range with a cut-off of about 285 nm and proper price. However, it is reported that a strong reduction in iron content in the raw material to 50 mg/kg is necessary to attain an enhancement of transmissivity (Blanco, 1999). The mirror module and the borosilicate-glass tubes are installed on a platform, tilted at the latitude of the place in which the reactor is installed to enhance direct solar radiation capture, maximizing solar irradiance incidence along the year without requiring costly sunrays track system.

The potential of this type of solar reactor for the disinfection and decontamination of water and wastewater has been widely demonstrated (Aguas, 2019; Blanco, 1999; Formisano, 2016; Malato, 2016; 2007; 2002; Martínez-Costa, 2020; McLoughlin, 2004), nevertheless, its extensive use as commercial options is still limited.

1.8.2. UV-C plant

UV-C light radiation has been employed mainly in the field of drinking water treatment for disinfection purposes, involving mostly the use of mercury-vapor lamps, filled with mercury and with an inert gas, mainly argon (Figure 1.16).



Figure 1.16. Water treatment by UV-C radiation.

It is a gas-discharge lamp filled with vaporized mercury that uses an electric arc to generate light. Different lamps are commercially available (Rajkhowa, 2020): (i) low-pressure mercury-vapour lamps (LP) and (ii) medium-pressure mercury-vapor lamps (MP). LP and

MP mercury lamps differ in terms of mercury vapor pressure, emission spectrum, UV flux, wall temperature, lifespan and in particular:

- LP mercury lamps operate at a pressure of approximately 1 Pa (0.01 mbar) and emit UV radiations at 253.7 and 185.0 nm. The output, defined as the intensity of the UV radiation given off, could be high or low. High output lamps have both good germicidal, lower power use and electrical efficiency, while low output ones are less effective (a higher number of lamps is necessary), but more energy efficient.
- MP mercury lamps work at a higher pressure of 100 kPa (1 bar) with emission of lines from 200–600 nm (polychromatic spectrum). They can operate only at high output intensity, they have poor lamp life and the wall temperature could achieve high temperature such as 500-950°C.

Moreover, UV systems could also use Light-Emitting Diode (LED) technology, which recently is gained attention as alternative to conventional UV-C lamps. Its main advantages are related with the absence of harmful mercury content, making them an environmentally friendly option, the small size, the versatility for up-scaling and the lower energy consumption. Nevertheless, as an incipient technology, it still has some drawbacks such as the high cost, and low or reduced yield efficiencies.

1.9. Transformation products and toxicity

Up to date, it is well-known that secondary effluents from UWWTPs continuously dispose CECs into the aquatic ecosystem, posing a potential risk for human health and for the environment. Moreover, the secondary treatment of UWW, as well as a tertiary treatment, may initiate the degradation of CECs, transforming them into the so-called Transformation Products (TPs) (Schollée, 2015). TPs are compounds generated during the applied treatments, that commonly are not detected by conventional analytical procedures and therefore may escape after the treatment, not being totally degraded, and in some cases, they could be even more toxic and persistent than their parent compound, posing a potential ecotoxicological and human health risks.

In fact, the concern of TPs discharge from UWWTPs is related with the wide spectrum of TPs that could be detected, together with the corresponding parent compounds, in rivers, soils and crops irrigated with reclaimed UWW (Chen, 2011; Christou, 2017a; Kinney, 2006; Koba, 2016). Therefore, the analysis of the TPs, generated during any novel water treatment

1. Introduction

under investigation, should be also considered, checking not only proper CECs degradation but also the elimination of the potentially generated TPs, in order to limit further risks associated to the accumulation of such compounds (Brezina et al., 2017).

On the other hand, toxicity is defined as potential adverse effect of a pollutants on organisms, including microorganisms, invertebrates, fish and plants, after short time (acute toxicity) or after a long-term exposure to very low concentration of pollutants (chronic toxicity). Toxicity is commonly measured through different bioassays, and it is considered an effective tool for the assessment of the water and wastewater quality and safety.

Bio-toxicity could be a useful tool to assess water toxicity after the treatment, evaluating the performance, applicability and suitability of AOPs in treating wastewater. The ideal process should yield to completely mineralize the organic pollutant to CO₂ and H₂O. However, the mineralization efficiency is usually low and the partial oxidation of organic contaminants may result in the formation of TPs, that could exhibit equivalent or even higher toxicity than the parent compounds, leading to a toxicity increase. As a consequence, it is important to optimize the proper experimental conditions (in terms of reaction time and oxidant concentration) or combine the process with other treatment (biological, membrane or adsorption process) in order to minimize final toxicity, obtaining a safe effluent (Wang, 2021).

Table 1.12 summarizes the most commonly used tests and organisms to characterize toxicity of water and wastewater and the corresponding standardized protocols that have been developed for ecotoxicological methods by different organization, including International Organization for Standardization (ISO), Organisation for Economic Co-operation and Development (OECD) and U.S. Environmental Protection Agency (USEPA).

Toxicity could be affected by several factors, including: (i) reactive species' type and concentration with formation of different intermediate, due to different degradation mechanism, (ii) structure and concentration of organic pollutants and their TPs, (iii) toxicity assessment method, (iv) experimental parameters (pH, T, oxidant concentration, type of catalyst, reaction time), (v) residual oxidant (Wang, 2021). For this reason, the testing of the treated water is another key aspect in the investigation of water purification treatments.

Table 1.12. Classification of the main toxicity bioassays.

Group	Class	Organisms	Method
Cell	Cell line	Mouse neuroblast N2a	ISO 10993-5:2009
Microorganisms	Bacteria	<i>Aliivibrio fischeri</i>	ISO 11348-3:2007
		Bacteria from activated sludge	OECD209:2010
Invertebrates	Crustaceans	<i>Daphnia magna</i>	ISO 6341:2012 OECD 202:2004
	Earthworms	<i>Eisenia Fetida</i>	ISO 17512-1:2008
Vertebrates	Fish	<i>Danio renio</i> (Zebrafish)	ISO 7346-1:1996
		<i>Oncorhynchus mykiss</i>	OECD 210:1992
Algae	Algae	<i>Pseudokirchneriella subcapitata</i>	ISO 8692:2012 OECD 201:2006
		<i>Scenedesmus subspicatus</i>	
		<i>Selenastrum capricornutum</i>	ISO 8692:1989
Plants	Plants	<i>Latuca sativa</i>	USEPA, 1989
		<i>Lemna minor</i>	ISO 20079:2005 EN ISO 18763:2020

CHAPTER 2
OBJECTIVES AND EXPERIMENTAL
PLAN

2. OBJECTIVES AND EXPERIMENTAL PLAN

2.1 Objectives

The general aim of this work is the assessment of novel AOPs for the simultaneous disinfection and decontamination of water and secondary effluents from urban wastewater treatment plants. The efficiency has been evaluated based on the simultaneous inactivation of three human health impact pathogens (two gram-negative bacteria *E. coli*, *Pseudomonas* spp. and the gram-positive *Enterococcus* spp.) and the degradation of three CECs (Diclofenac DCF, Sulfamethoxazole SMX and Trimethoprim TMP), chosen due to their frequent detection in natural freshwater and wastewater resources. Moreover, *E. coli* and *E. faecalis* were selected because they are commonly used as indicator of faecal contamination, while *P. aeruginosa* has been proposed as supplementary indicator in the analysis of water and wastewater.

To reach the general aim of this study, the following specific objectives were carried out:

- To assess the capability of several photocatalysts involving modified ZnO with Ce, Yb and Fe and the benchmark TiO₂-P25 for solar water and UWW purification.

2. Objectives and experimental plan

- To investigate the fundamental reactivity of PMS based on sulfate radical's generation.
- To assess the effectiveness of non-activated PMS alone under natural solar radiation for water and UWW purification.
- To explore the best-performing photocatalyst for PMS activation under natural solar radiation as an enhanced strategy for UWW purification.
- To investigate the sulfate radical based AOPs (SR-AOPs) driven by UV-C radiation involving PMS as precursor.
- To analyse the global processes performance focused on achieving safer final water quality for reuse in agriculture.

The proof-of-principle was performed for all processes in simple water matrix (such as isotonic water (IW)), the potential effect of organic and inorganic chemical compounds on treatment performances was evaluated in simulated urban wastewater (SUWW) and finally, the process capability was assessed in an actual secondary effluent from the UWWTP of El Bobar (located in Almería, Spain).

2.2 Experimental plan

The experimental plan developed to meet the objectives of this work is explained below.

Objective 1: Assessment of simultaneous disinfection and decontamination of water and wastewater by solar photocatalysis. The evaluation of three modified ZnO material with Ce, Yb or Fe photoactivity for the simultaneous inactivation of the three bacteria (*E. coli*, *E. faecalis* and *P. aeruginosa*) and for the removal of the three CECs (DCF, SMX and TMP) at laboratory scale (200-mL vessel reactors), in suspension mode and under natural sunlight was investigated. Chapter 4 shows all the results related with this objective and, summarizing it contains the following experimental tasks:

- A preliminary analysis of the fundamental efficiency of each photocatalyst for bacteria and contaminants removal was performed in IW and a wide range of photocatalysts concentration (0-500 mg/L) was tested.
- The influence of organic and inorganic chemical compounds on each photocatalyst performance was then investigated by using SUWW, as model of complex water matrix.

2. Objectives and experimental plan

- The bacterial and contaminant abatement mechanisms, based on the characteristics of each photocatalyst, were proposed.
- The capability of the best performing material (ZnO-Ce) in actual UWW, in comparison with the benchmark TiO₂-P25, was finally assessed.

Objective 2: Assessment of PMS and sulfate radical (SO₄^{•-}) reactivity to give an insight into CECs degradation and bacterial inactivation mechanisms in water. Chapter 5 shows in detail all the experimental activities carried out to attain this objective, and briefly it contains the following tasks:

- Assessment of PMS reactivity for the degradation of SMX (as model of organic contaminant) in MilliQ water, in the dark, under simulated solar light and UV-C radiation, evaluating:
 - The effect of different variables, including PMS concentrations, water pH, water temperatures and the presence of common inorganic ions in natural water (chloride and hydrogen carbonate ions).
 - The generation of radical species by reactive species scavenger tests.
 - The generation of radical species by recording EPR spectra.
- A Laser Flash Photolysis (LFP) study to determine the SO₄^{•-} reaction mechanism operating in bacterial inactivation and in CECs degradation. The reactivity was assessed in MilliQ water against different cell-wall model compounds of gram-negative (*E. coli*) and gram-positive (*E. faecalis*) bacteria and CECs (DCF, SMX and TMP).

Objective 3: Assessment of PMS for water and UWW purification under natural solar radiation. Chapter 6 and 7 address the effectiveness of PMS alone as oxidative agent for the simultaneous removal of the three bacteria and CECs at laboratory scale (200-mL vessel reactor) and at pilot plant scale using a 10-L CPC reactor in different water matrices.

- The effectiveness of PMS alone in IW and WeW at laboratory scale is presented in Chapter 6. The following activities were carried out:
 - A preliminary evaluation of the oxidation capability of PMS alone in the dark over all targets investigated was done by testing a wide range of PMS concentration in IW.
 - The capability of PMS alone under natural sunlight in IW was then investigated testing also a wide range of oxidant concentrations (from 0.0001 to 0.01 mM).

2. Objectives and experimental plan

- Then, the influence of inorganic species (chloride and hydrogen carbonate ions) on the PMS/Solar system performance was assessed by testing its effectiveness in natural WeW and diluted well water (d-WeW) at 0.01 mM of oxidant.
- A disinfection and decontamination mechanism was proposed based on all the experimental findings observed.
- The effectiveness of PMS alone in simulated and actual UWW at both laboratory scale and pilot plant scale under natural sunlight is described in detail in Chapter 7. The activities carried out to reach this partial objective were, briefly, the following:
 - The effect of NOM and inorganic ions was preliminary assessed using SUWW as model of actual UWW, at laboratory scale. PMS concentration in this case ranged from 0 to 0.5 mM.
 - The capability of the process in actual UWW was finally assessed by following natural occurring bacteria (*E. coli*, Total coliforms, *Enterococcus* spp. and *Pseudomonas* spp.) and the same spiked CECs (DCF, SMX and TMP) in the presence of different PMS concentration (0-1 mM) at pilot plant scale in CPC reactors.
 - In actual UWW, the inactivation by PMS/Solar of naturally occurring ARB, grown in the presence of sub-minimal inhibitory concentrations of Ampicillin (AMP), Ciprofloxacin (CPX), and Trimethoprim (TMP), and removal of the genes 16S rRNA, *intI1* and selected ARGs commonly found in UWW (*sul1*, *qnrS*, *blaTEM*, *blaCTX-M32*, *tetM*) were also investigated in the presence of the optimal concentration of PMS.

Objective 4: To explore the best-performing photocatalyst for PMS activation under natural solar radiation as an enhanced strategy for UWW purification. The ZnO-Ce material, selected in previous tasks as the best-performing material, was applied for PMS activation under natural solar radiation at laboratory scale. The experimental work performed for this objective is shown in Chapter 7. Briefly, the following activities were carried out:

- The inactivation and degradation of chemical and biological targets by the two stand-alone processes (photocatalysis and PMS direct oxidation) under natural solar radiation, and their combination.
- The synergy of combined process performance for both types of pollutant targets was estimated and analyzed.

2. Objectives and experimental plan

- The release of Zn^{2+} from the catalyst in the presence of the oxidant PMS was analysed by ICP-mass technique.

Objective 5: Assessment of PMS for water and UWW purification under UV-C radiation. Chapter 8 evaluates the effectiveness of SR-AOPs for the simultaneous disinfection and decontamination of water and UWW, generating $SO_4^{\cdot-}$ and HO^{\cdot} in solution through the activation of PMS by UV-C irradiation at pilot plant scale. Specifically, the evaluation was carried out, investigating:

- The capability of PMS/UV-C for the simultaneous removal of biological and chemical targets in IW in the presence of several oxidant concentrations (0-0.01mM) under UV-C radiation at pilot plant scale.
- The effect of inorganic ions and NOM on process performance assessing the efficiency in SUWW.
- The global process ability to obtain reclaimed UWW for its potential reuse in agriculture.
- In actual UWW, the effectiveness of PMS/UV-C process against ARB and ARGs removal.

Objective 6: Comparative evaluation of water processes performances. The promising treatments and operational conditions investigated along the previous objectives were selected and further analyzed as potential tertiary treatments to be implemented in UWWTPs. Accordingly, PMS/Solar and PMS/UV-C processes at oxidant concentration ranged from 0.5 to 1 mM in actual UWW were analyzed. The global analysis, showed in detail in Chapter 9, includes the previous microbial and CECs degradation kinetics, but also the following tasks were performed:

- Transformation Products (TPs) formation and degradation during both processes in the presence of 1 mM of PMS at pilot plant scale in UWW. Preliminary, each CEC was degraded individually in order to identify TPs, in the presence of high compound concentration (1 mg/L) in demineralized water (DW).
- Toxicity: the effect of residual PMS was evaluated in treated UWW involving *Aliivibrio fischeri* (considered as most widely used microorganism to perform a preliminary eco-toxicity assessment for its discharge in the environment) and the germination of three seeds, such as *Sorghum saccharatum*, *Lepidium sativum*, and *Sinapis alba* as models of phytotoxicity.
- Annual Treatment Cost (ATC) for process implementation.

2. Objectives and experimental plan

Finally, a summary of the most important key parameters obtained along the entire study is presented.

CHAPTER 3
MATERIALS AND METHODS

3. MATERIALS AND METHODS

In this chapter, the materials, the laboratory procedures, the analytical techniques, the equipment and the reactors used to carry out the experimental work are explained in detail. All water disinfection and decontamination tests have been performed at the CIEMAT-PSA facilities, nevertheless complementary studies have been done in external institutions and laboratories and therefore the equipment, devices and methodologies employed in those cases are also defined in this chapter.

3.1. Chemicals

Table 3.1 summarizes all the chemicals compounds used along the entire experimental work, including the CAS number, formula and its specific end-use activity. They were used directly as received from the manufacturer.

3. Materials and methods

Table 3.1. Chemicals used in the experimental work.

Compound	CAS number	Formula	Use
Acacia gum powder	9000-01-5	-	SUWW recipe
Acetonitrile	75-05-8	C ₂ H ₃ N	Mobile phase
Ammonium sulfate	7783-20-2	(NH ₄) ₂ SO ₄	SUWW recipe
Beef extract	68990-09-0	-	SUWW recipe /Nutrient both I
Calcium chloride dihydrate	10035-04-8	CaCl ₂ ·2H ₂ O	SUWW recipe
Calcium sulfate dihydrate	10101-41-4	CaSO ₄ ·2H ₂ O	SUWW recipe
3-chloroaniline	108-42-9	C ₆ H ₆ ClN	CO ₃ ^{•-} scavenger
Diclofenac	15307-86-5	C ₁₄ H ₁₁ Cl ₂ NO ₂	Target compound
5,5-dimethyl-1-pyrroline (DMPO) ^a	3317-61-1	C ₆ H ₁₁ NO	Spin-trapping agent to detect OH [•] , SO ₄ ^{•-} or O ₂ ^{•-}
Formic acid	64-18-6	HCOOH	Mobile phase
Furfuryl alcol	98-00-0	C ₅ H ₆ O ₂	¹ O ₂ scavenger
Humic acid	1415-93-6	-	SUWW recipe
Isopropanol	67-63-0	C ₃ H ₈ O	H-donor specie in LFP studies
Magnesium sulfate	7487-88-9	MgSO ₄	SUWW recipe
Magnesium sulfate heptahydrate	10034-99-8	MgSO ₄ ·7H ₂ O	SUWW recipe
Methanol	67-56-1	CH ₃ OH	H-donor specie in LFP studies/HO [•] and SO ₄ ^{•-} scavenger
<i>N</i> -acetylmuramic acid ^b	10597-89-4	C ₁₁ H ₁₉ NO ₈	Cell wall components used in LFP studies
<i>N</i> -acetyl- <i>L</i> -alanine ^b	97-69-8	C ₅ H ₉ NO ₃	
2,6-Diaminopimelic acid ^b	583-93-7	C ₇ H ₁₄ N ₂ O ₄	
<i>N</i> -acetyl- <i>D</i> -glucosamine ^b	7512-17-6	C ₇ H ₁₄ N ₂ O ₄	
<i>N</i> -acetyl- <i>L</i> -lysine ^b	692-04-6	C ₈ H ₁₆ N ₂ O ₃	
<i>N</i> -acetyl- <i>D</i> , <i>L</i> -glutamic ^b	5817-08-3	C ₇ H ₁₁ NO ₅	
<i>N</i> , <i>N</i> -diethyl- <i>p</i> -phenylenediamine ^b	93-05-0	C ₁₀ H ₁₆ N ₂	
OXONE	70693-62-8	KHSO ₅ ·0.5KHSO ₄ ·0.5K ₂ SO ₄	Oxidant for water treatment
Peptone	91079-38-8	-	SUWW recipe/Nutrient both I
Phenol	108-95-2	C ₆ H ₆ O	Cl [•] /Cl ₂ ^{•-} scavenger
Potassium chloride	7440-09-7	KCl	SUWW recipe
Potassium monohydrogen phosphate	7778-77-0	K ₂ HPO ₄	SUWW recipe
Sodium azide	26628-22-8	NaN ₃	e ⁻ -donor specie in LFP studies/HO [•] and SO ₄ ^{•-} scavenger
Sodium bicarbonate	144-55-8	NaHCO ₃	SUWW recipe
Sodium chloride	7440-23-5	NaCl	Isotonic water preparation/ SUWW recipe/ Nutrient both I preparation
Sodium lauryl sulfate	151-21-3	NaC ₁₂ H ₂₅ SO ₄	SUWW recipe
Sodium lignin sulfonate	8061-51-6	C ₂₀ H ₂₄ Na ₂ O ₁₀ S ₂	SUWW recipe
Sodium persulfate	7775-27-1	Na ₂ S ₂ O ₈	Oxidant for LFP studies
Sulfamethoxazole	723-46-6	C ₁₀ H ₁₁ N ₃ O ₃ S	Target compound
Tert-butanol	75-65-0	C ₄ H ₁₀ O	HO [•] scavenger
2,2,6,6-tetramethyl-4-piperidinol (TEMP) ^a	108-42-9	C ₉ H ₁₉ NO	Spin-trapping agent to detect ¹ O ₂
Trimethoprim	738-70-5	C ₁₄ H ₁₈ N ₄ O ₃	Target compound
Triphenyl tetrazolium chloride (TTC) ^c	298-96-4	C ₁₉ H ₁₅ ClN ₄	Supplement of Slanetz & Bartley Agar
Tryptophan methyl ester hydrochloride	7524-52-9	C ₁₂ H ₁₅ ClN ₂ O ₂	Cell wall components used in LFP studies
Urea	57-13-6	CH ₄ N ₂ O	SUWW recipe

All the chemicals were obtained from Merck-Sigma Aldrich (KGaA, Darmstadt, Alemania), except the following: ^a Enzo Life Sciences (New York, USA), ^bFluorochem Limited (UK) and ^cScharlau® (Spain)

3.2. Microbial targets

Safe handling of pathogenic microorganisms was performed inside a laminar flow cabinet class II (Telstar Bio-IIA, Figure 3.1a) to ensure biological safety for the product, the personnel and the environment, according to the European Standard for Microbiological Safety Cabinets (EN 12469:2000). All the materials, culture media and solutions were autoclaved in a Presoclave (Grupo Selecta, Barcelona, Spain) during 15 min at 121 °C to ensure complete sterilization before and after the use (Figure 3.1b).



Figure 3.1. (a) Laminar flow cabinet and (b) autoclave used in this work and available at the laboratory of Solar Treatment of Water (CIEMAT-PSA).

3.2.1 Description of bacterial strains investigated

Three common waterborne bacteria have been used as model for water disinfection tests. Their main characteristics and reasons to select them in this work are summarized as follows:

(i) *Escherichia coli* is a gram-negative, prokariotic, facultative anaerobic, rod-shaped, non-spore forming, animal parasite bacterium, that resides in the intestinal tract of humans and warmed-blood animals. It belongs to the family Enterobacteriaceae and it was chosen because it is the most frequently studied microbial specie in the area of water disinfection and it is commonly used as indicator of faecal contamination, being included in all water regulations. More than 700 serotypes of *E. coli* have been identified and, among of them, *E. coli* O157:H7 is a serotype of the Shiga Toxin-producing *E. coli* (STEC), which expresses somatic (O) antigen 157 and flagellar (H) antigen 7. It is an important food and a waterborne pathogen, that causes diarrhea, haemorrhagic colitis, and haemolytic-uremic syndrome in humans and it is known worldwide from its outbreak in drinking water (Saxena, 2015).

3. Materials and methods

E. coli belongs to other wide group of bacteria namely total coliforms, that is also commonly included in water regulations and legislation as microbial indicator. Total coliforms are a wide range of thermotolerant aerobic and facultative anaerobic, gram-negative, non-spore-forming bacilli, capable of ferment lactose (producing the enzyme β -galactosidase) at high temperatures (44 °C) and of growing in the presence of relatively high concentrations of bile salts. They are excreted in the faeces of humans and animals, they could multiply and grow in water and they occur in sewage, natural waters, in the drinking water distribution system (as biofilm) and in soil (WHO, 2008).

(ii) *Enterococcus faecalis* is a gram-positive, facultative anaerobic bacterium and relatively specific for detection of faecal pollution. It is typically excreted in the faeces of humans and other warm-blooded animals and it is present in large number in sewage, but some strains belonging to this genus have also been detected in soil in the absence of faecal contamination. *E. faecalis* can cause also a variety of infections, including endocarditis, urinary tract infections, prostatitis, intra-abdominal infection, cellulitis, and wound infection as well as concurrent bacteremia (WHO, 2008).

(iii) *Pseudomonas aeruginosa* is an opportunist pathogen for humans, common encapsulated, gram-negative, rod-shaped bacterium, capable of growing in water with a low concentration of nutrients and it is commonly found in feces, soil, water and wastewater. It is responsible of a wide range of infections, but the most commonly affected is the respiratory tract, responsible for 50 % of nosocomial bacterial pneumonia. It has been proposed as supplementary indicator in the analysis of water and wastewater (Gerba, 2009).

3.2.2. Bacterial enumeration and quantification procedure

The water disinfection tests were performed with two different approaches, although in both cases, the same type of bacterial strains was simultaneously monitored and analysed:

- Artificially contaminated water matrices, spiked with laboratory grown bacteria, obtained from the Spanish Culture Collection (Colección Española de Cultivos Tipo CECT) (Table 3.2).
- Actual secondary effluents from a UWWTPs, containing natural occurring bacteria including ARB and ARGs.

For the specific case of culture-collection bacterial strains, the following step are necessary to reactivate and prepare stocks solutions:

- Rehydration of the freeze-dried culture: Bacterial strains were obtained as freeze-dried cultures and they were rehydrated according to CECT instructions. Briefly, lyophilized bacterium was rehydrated and re-suspended in 200 μL of appropriate liquid broth (according to Table 3.2). A drop (ca. 25 μL) of the re-suspended volume was spiked in sterilized bottle, containing 14 mL of the same liquid broth medium, and incubated in a rotary shaker (Heidolph Unimax 1010) coupled to an incubator (Heidolph Inkubator 1000) (Figure 3.2) set at 100 rpm (revolutions per minute) for 20 h at 37 $^{\circ}\text{C}$ (optimum growing temperature for the bacteria). Subsequently, the turbid solution was distributed in sterile vials of cryobeads (Deltalab[®], Spain), that were stored in the freezer at -5 $^{\circ}\text{C}$ for further use.



Figure 3.2. Rotary shaking incubator used in this work for growing of bacteria in liquid culture media.

- Stock preparation: Stock preparation was done streaking a bead onto a Petri dish of Luria-Bertani (LB) agar, contained in the sterile vial, previously unfreezed. The plate was incubated for 24 h at 37 $^{\circ}\text{C}$ to obtain isolated bacteria colonies (Figure 3.3) and it was conserved in the fridge for no longer than 2 weeks.

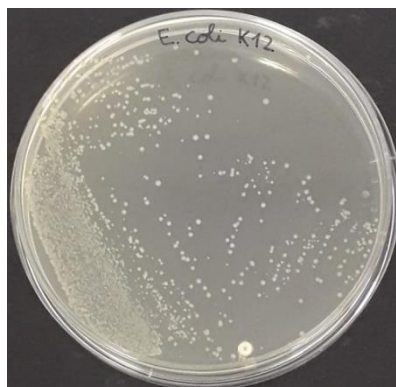


Figure 3.3. Example of a stock plate containing *E. coli* colonies.

- Inoculum preparation: Suspensions of $\sim 10^9$ CFU/mL per bacteria were prepared as follow:

3. Materials and methods

- Transfer 14 mL of proper liquid medium (according to Table 3.2) in a 50-mL bottle.
- Take one colony from the stock plate (Figure 3.3) with a sterilized-loop and transfer it in the liquid, shaking gently the loop in the liquid medium.
- Incubate in a rotary shaking incubator at 100 rpm for 20 h at 37 °C (Figure 3.2).
- Centrifuge the suspension for 15 minutes at 3000 rpm and re-suspend in Phosphate-Buffered Saline (PBS) solution for its further directly dilution in the water intended to be treated.

For the specific case of secondary effluents from UWWTPs, no addition of culture-type bacteria was done, and only the naturally occurring bacteria (*E. coli*/Total coliforms, *Enterococcus* spp. and *Pseudomonas* spp.) as well as the corresponding ARB at the current concentration was monitored. Additionally, in this water matrix, several ARGs were also monitored.

Bacteria enumeration procedures

Quantification of microbial concentration from all water samples was carried out by the Standard Plate Counting Method (SPCM) and the membrane filtration method. SPCM consists of counting the number of Colony Forming Unit (CFU) of organisms, growing on a solid agar medium. Water samples were serial diluted in PBS and 50 µL or 500 µL of samples (diluted or not) were spread on ChromoCult® Coliform Agar (Merck KGaA, Darmstadt, Germany) and Pseudomonas Chromogenic Agar (Conda, Pronadisa, Spain) for *E. coli* (and Total Coliforms) and *Pseudomonas* spp., respectively. For *Enterococcus* spp. detection, 3 drops of 20 µL or 500 µL of samples (diluted or not) were spread on Slanetz&Bartley (SB) agar (Scharlau®, Spain). The agar medium, growth temperature and incubation time for each bacterium are reported in Table 3.2. The Detection Limit (DL) of SPCM was 2 CFU/mL.

The membrane filtration method was used to achieve the lower DL of 1 CFU/100mL, according to the minimum requirements of microbial concentration in water regulations. For this laboratory technique, 100 mL of water samples were filtered using a Microfil® filtration system (Millipore, USA) (Figure 3.4), bacteria were retained using cellulose nitrate filters (0.45 µm, Sartorius Stedim, Spain), followed by incubation of the membranes on same selective media as previously described for each bacterium.



Figure 3.4. Microfil®filtration system.

Table 3.2. CECT number, culture medium, growth temperature and incubation time for each culture-type bacterium.

	<i>E. coli</i> O157:H7	<i>E. faecalis</i>	<i>P. aeruginosa</i>
CECT reference	4972	5143	110
Liquid broth medium	Nutrient broth I	Luria-Bertani broth	Nutrient broth II
Agar medium*	Chromocult	Slanetz & Bartley	Pseudomona Chromogenic
Growth temperature*	37 °C	37 °C	35 °C
Incubation time*	24 h	48 h	48 h

*Same agar medium, growth temperature and incubation time were required for quantification of natural occurring *E. coli*/Total coliforms, *Enterococcus* spp. and *Pseudomonas* spp. in real UWW

Three specific and selective media were used for identification and quantification of each bacterium in both types of experimental approaches, artificially contaminated waters and actual UWW (Figure 3.5):

- ChromoCult® Coliform Agar for the identification of *E. coli* O157:H7, *E. coli* and Total coliforms. It is a selective medium, containing a chromogenic substrate, that is modified by native bacterial enzymes and, after modification, it changes its color enabling bacterial detection. The count of coliform bacteria is based on the presence of the enzyme β -D-galactosidase in the bacteria, capable to cleave the substrate Salmon-GAL (6-Chloro-3-indolyl- β -D-galactopyranoside), forming salmon red colored colonies. *E. coli* can be differentiated from the other thermotolerant coliforms by the ability to produce the enzyme β -glucuronidase, capable to break also the substrates X-glucuronide (X-gluc). In the presence of *E. coli* both substrates are cleaved, resulting in colonies that appear on a dark blue to violet color. Non-coliform bacteria appear as colorless or in rare cases as turquoise colonies, while sodium heptadecylsulfate (Tergitol 7) is present in the formulation as an inhibitor of gram-positive bacteria (Merck, 2008).

3. Materials and methods

- Pseudomonas chromogenic agar for the identification of *P. aeruginosa* and *Pseudomonas* spp. The added chromogenic substrate permits to detect *Pseudomonas* by means of a color change, generating specifically colonies of magenta color. *Pseudomonas* is capable of producing pyocyanin pigment, whose production is enhanced by the presence of potassium sulfate and magnesium chloride, while cetrimide and nalidixic acid inhibit other bacteria growth.
- Slanetz and Bartley Agar, supplemented with Triphenyl tetrazolium chloride (TTC) for the detection and *Enterococcus* spp. and *E. faecalis*. The principle relies on the ability of *Enterococci* to reduce TTC (a redox indicator) to formazan, resulting in the production of red colonies, while sodium azide inhibits the growth of gram-negative and staphylococci bacteria.

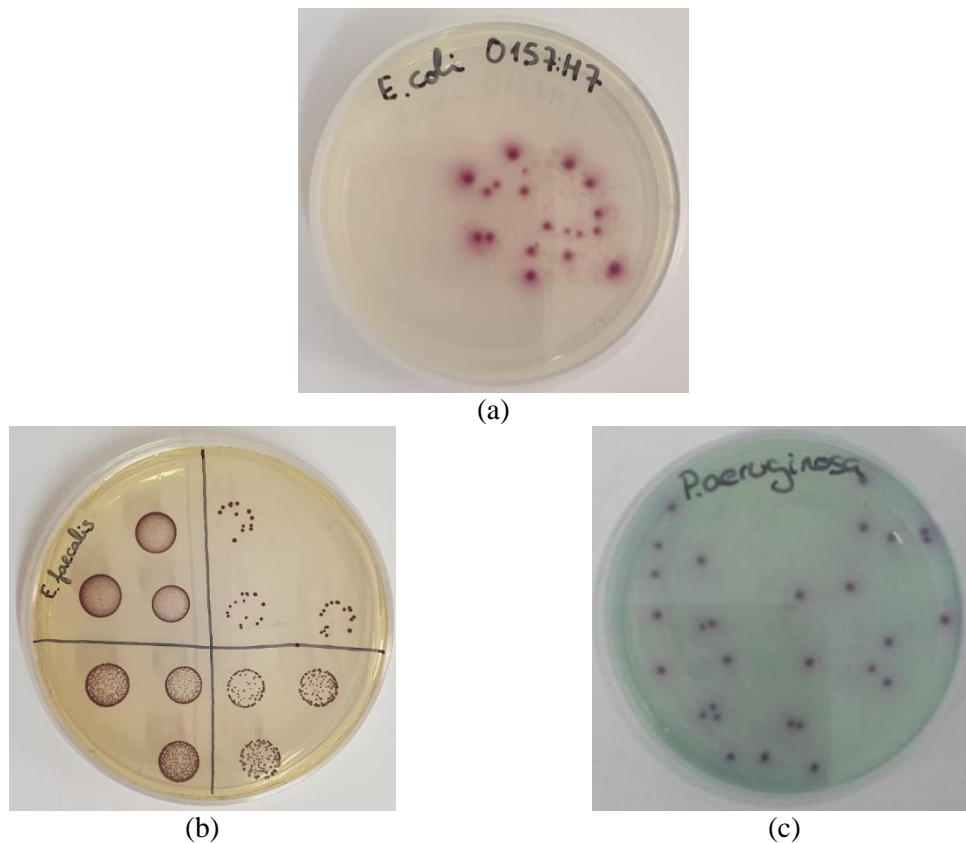


Figure 3.5. (a) *E. coli* O157:H7 cultivated in Chromocult[®] agar, (b) *E. faecalis* in SB agar and (c) *P. aeruginosa* in Pseudomonas chromogenic agar.

Besides, ARB were monitored in UWW following the same procedure described above with selective agar media (Table 3.2), supplemented with three antibiotics according to the respective MIC values available in EUCAST database (<https://mic.eucast.org>). In particular, in this work, the following antibiotics were added: AMP (8 mg/L), CPX (0.5 mg/L) and

TMP (4 mg/L) for AR-*E. coli* and AR-*Pseudomonas* spp.; and AMP (8 mg/L), CPX (4 mg/L) and TMP (1 mg/L) for AR-*Enterococcus* spp. detection.

3.2.3. Antibiotic resistant genes detection procedure

The 16S rRNA gene and several ARGs, including genes encoding resistance to antibiotic classes quinolones (*qnrS*), sulphonamides (*sulI*), β -lactams (*bla_{TEM}*), cephalosporins (*bla_{CTX-M32}*), tetracycline (*tetM*), and class 1 integron integrase (*intI1*), were selected due to their occurrence in UWWTPs (Wang, 2020). They were extracted from the water samples and quantified using real-time quantitative PCR (qPCR), following the steps reported in Figure 3.6.

3. Materials and methods

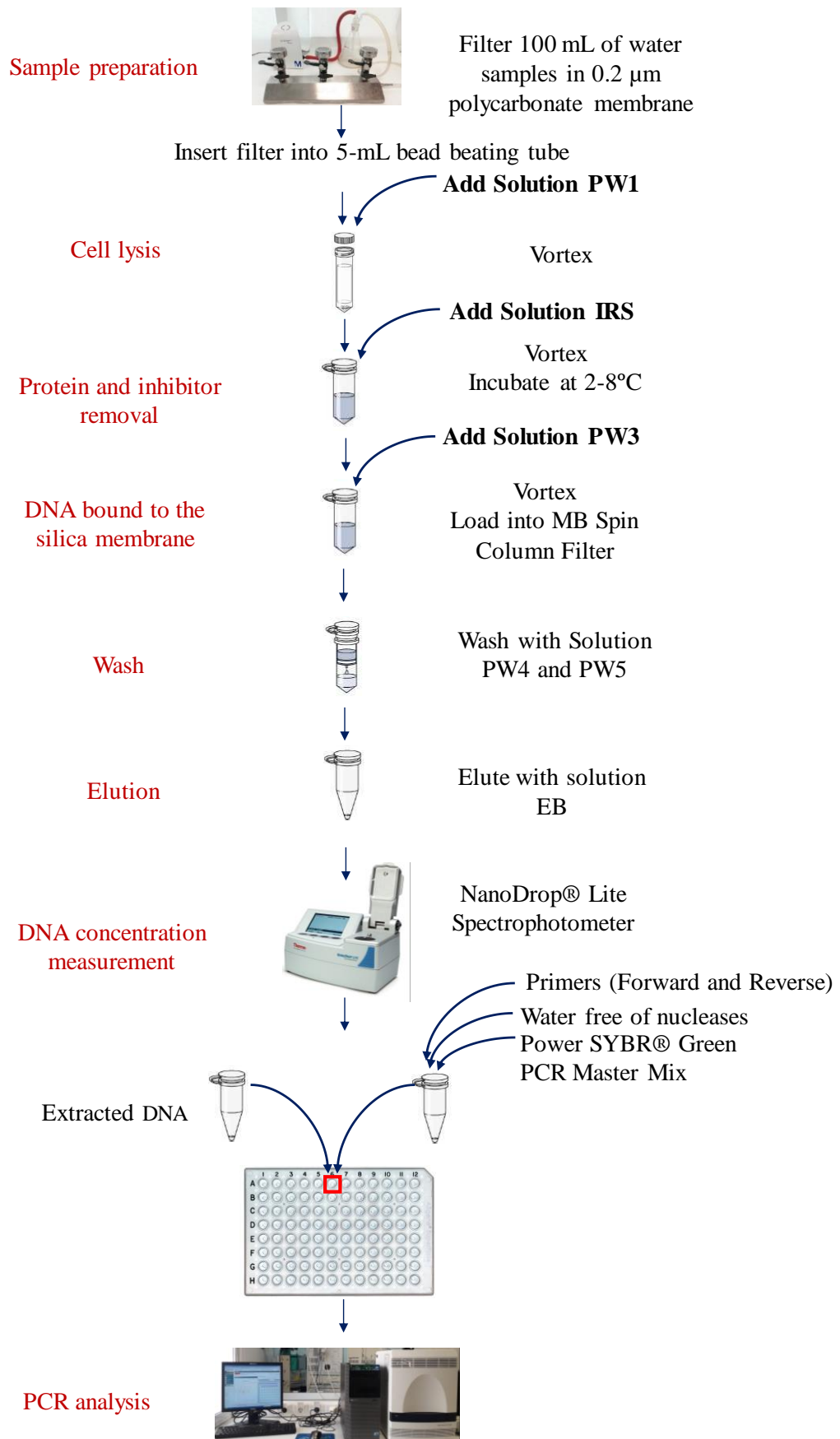


Figure 3.6. DNA extraction of water samples for PCR analysis, according to the commercial DNeasy® PowerWater® Kit.

A volume of 100 mL of each sample was filtered in duplicated through a 0.2 µm polycarbonate membrane (CHMLAB GROUP S.L., Barcelona, Spain), total DNA was extracted with the DNeasy® PowerWater® Kit (QIAGEN Sciences Inc., MD, USA), using a silica membrane in a spin-column format and its concentration was measured using a NanoDrop® Lite Spectrophotometer (Thermo Scientific, MA, USA). All genes were analyzed in duplicated by q-PCR using a 7500 Fast Real-Time PCR Systems (Applied Biosystems, Thermo Fisher Scientific Inc., MA, USA).

The working conditions were done by modifications of reported studies in literature (Das Neves G., 2020; Rocha, 2020) and they are presented in Table 3.3.

Table 3.3. Conditions used in qPCR assays.

Genes	Primers sequence	µM	bp	Conditions	Ref.
16S rRNA	FW: TCCTACGGGAGGCAGCAGT RV: ATTACCGCGGCTGCTGG	0.50	195	50°C - 1 min (1X); 95°C - 3 sec, 60°C - 30 sec (40X); 95°C - 15 sec; 60°C - 1 min; 95°C -15 sec	Modified from (Rocha, 2020)
<i>int11</i>	FW: GATCGGTCTGAATGCGTGT RV: GCCTTGATGTTACCCGAGAG	0.50	196	50°C - 1 min (1X); 95°C - 3 sec, 60°C - 30 sec (40X); 95°C - 15 sec; 60°C - 1 min; 95°C -15 sec	Modified from (Rocha, 2020)
<i>qnrS</i>	FW: GACGTGCTAACTTGCGTG RV: TGGCATTGTTGGAACTT	0.60	118	50°C - 1 min (1X); 95°C - 3 sec, 60°C - 30 sec (40X); 95°C - 15 sec; 60°C - 1 min; 95°C -15 sec	Modified from (Rocha, 2020)
<i>sul1</i>	FW: CGCACCGGAAACATCGCTGCAC RV: TGAAGTTCGCCGCAAGGCTCG	0.30	162	50°C - 1 min (1X); 95°C - 3 sec, 60°C - 30 sec (40X); 95°C - 15 sec; 60°C - 1 min; 95°C -15 sec	Modified from (Rocha, 2020)
<i>bla_{CTX-M32}</i>	FW: CGTCACGCTGTTGTTAGGAA RV: CGCTCATCAGCACGATAAAG	0.30	156	95°C - 10 min (1X); 95°C - 30 sec; 55°C - 1 min; 72°C - 1 min (40X); 72°C - 7 min; 60°C - 10 sec; 95°C - 10 sec (1X)	(Das Neves G., 2020)
<i>Tet(M)</i>	FW: GCAATTCTACTGATTTCTGC RV: CTGTTTGATTACAATTTCCGC	0.20	186	50°C - 1 min (1X); 95°C - 3 sec, 60°C - 30 sec (40X); 95°C - 15 sec; 60°C - 1 min; 95°C -15 sec	Modified from (Rocha, 2020)
<i>bla_{TEM}</i>	FW: TTCCTGTTTTTGTCTACCCAG RV: CTCAAGGATCTTACCGCTGTTG	0.20	113	50°C - 1 min (1X); 95°C - 3 sec, 60°C - 30 sec (40X); 95°C - 15 sec; 60°C - 1 min; 95°C -15 sec	Modified from (Rocha, 2020)

3. Materials and methods

Five ingredients are necessary to perform a PCR analysis:

- DNA template.
- Forward and reverse primers: short nucleic acid sequences that provide a starting point for DNA synthesis (they are specifically for each gene).
- DNA nucleotide bases (adenine (A), guanine (G), cytosine (C) and thymine (T)): building blocks necessary to construct the new strand of DNA.
- Taq polymerase enzyme: it is an enzyme originally isolated from the bacteria *Thermus aquaticus*, that is capable to tolerate temperatures above 80 °C and it is necessary to build the complementary DNA strand.
- Buffer to ensure the right conditions for the reaction.

A commercial premix of the components, Power SYBR Green PCR Master Mix, was used and it contains: (i) SYBR Green I Dye (providing a fluorescent signal after the binding to the double-stranded DNA), (ii) AmpliTaq Gold DNA Polymerase, (iii) nucleotide bases, (iv) passive reference (to normalize the fluorescence signal variations) and (v) a buffer.

A series of temperature changes allows the amplification of a particular gene and the main stages, repeated for several times, are:

- DNA polymerase activation (50-95°C).
- Denaturation (95 °C): for the separation of DNA strands.
- Annealing stage (50-65°C): for the attachment of the primers to a sequence of DNA.
- Extending stage (72°C): for the addition of DNA bases to the new complementary strand of DNA by DNA-polymerase.

Amplification data were analysed calculating the ratio between each analysed ARG and 16S rRNA gene (indicator for the total microbial abundance) using the Cycle Threshold (Ct) value. Figure 3.7 shows the amplification plot obtained over the duration of a real-time PCR experiment, in which the normalized fluorescence signal (relative to the baseline) generated by the reporter (fluorescent dye that binds to the double-stranded DNA; SYBR Green) is plotted against cycle number.

The Ct value is defined as the number of amplification cycles needed to detect the fluorescence PCR product (from the target amplification), crossing a pre-established threshold above the background signal (the baseline signal that is present in any assay regardless of whether target is present, also known as negative control). Therefore, the detection of the investigated gene is considered positive if the threshold of fluorescence is

reached, and the corresponding Ct value obtained was used for calculation of genes presence/absence.

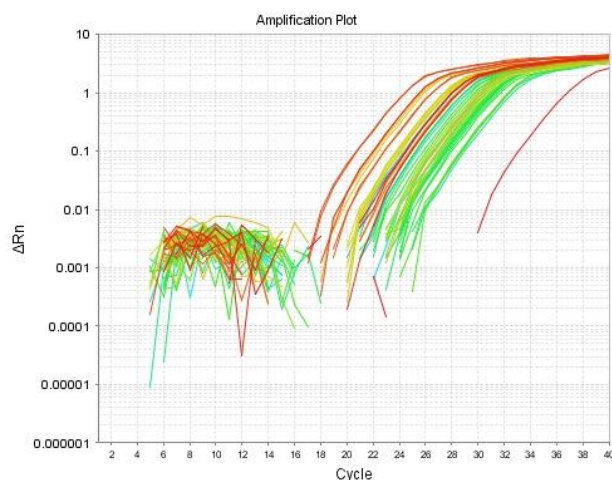


Figure 3.7. Amplification plot obtained over the duration of a real-time PCR experiment. ΔR_n : baseline-corrected normalized reporter.

3.3 Organic chemical targets

3.3.1 Contaminants of Emerging Concern description

Three model of chemical pollutants have been selected and monitored in this experimental work, due to their intensive use, low biodegradability and chemical stability: Diclofenac (DCF), Sulfamethoxazole (SMX) and Trimethoprim (TMP), which main physicochemical properties are summarized in Table 3.4. Besides, as a consequence of these properties, commonly they are incompletely removed in UWWTPs (Michael 2013), with subsequent detection and spreading in environmental compartments, including the possible uptake and bioaccumulation in the edible parts of food crops, after irrigation with reclaimed UWW (Christou 2017b).

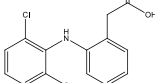
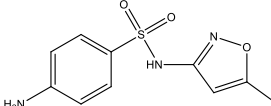
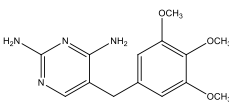
- **Diclofenac (DCF)** is a NSAID used to treat pain and inflammatory diseases. DCF is ubiquitously present in several environmental compartments, due to its high human consumption and low removal in UWWTPs. Main removal pathway is related to its high K_{ow} , being adsorbed preferably on the sludge. Primary treatment, involving sedimentation, coagulation and sorption to the activated sludge during secondary treatment could lead to 30–70 % of removal of DCF (Lonappan, 2016).
- **Sulfamethoxazole (SMX)** is a sulphonamide antimicrobial agent, that prevents the formation of dihydropteroic acid, a precursor of folic acid, which is required for bacterial growth, competitively inhibiting dihydropteroate synthase. It is rapidly absorbed on oral administration; metabolism is mainly hepatic, with the formation

3. Materials and methods

of predominantly N4-acetyl-SMX (NAcSMX) and glucuronide conjugates (GluSMX). Removal percentages of SMX between 50 to > 90 % are reported by different studies in the literature (Hoffmann-La Roche, 2020, Wang, 2020; Michael, 2013). This removal could be attained in actual UWWTPs with sufficient activated sludge retention times. However, both NAcSMX and GluSMX can be back transformed to SMX, which is one of the reasons that apparent SMX removal rates may varied widely.

- **Trimethoprim (TMP)** is a diaminopyrimidine antimicrobial agent, used in combination with SMX, which is effective against a wide range of gram-positive and gram-negative microorganisms. It prevents the conversion of folic acid into folinic acid in the bacterial or protozoal cell, by inhibiting the enzyme dihydrofolate reductase and consequently affecting DNA synthesis. The UWWTPs average removal rates reported for this compound is 25 % (Hoffmann-La Roche, 2020), but highly variable data (13-94 %) are reported by Michael et al (Michael, 2013).

Table 3.4. Physicochemical properties and detection parameters of DCF, SMX and TMP.

Physicochemical properties	CECs		
	DCF	SMX	TMP
Formula	C ₁₄ H ₁₁ Cl ₂ NO ₂	C ₁₀ H ₁₁ N ₃ O ₃ S	C ₁₄ H ₁₈ N ₄ O ₃
Structure			
Molecular weight (g/mol)	296.15	253.28	290.32
Water solubility (mg/L)	10 (at 25°C)	610 (at 37°C)	400 (at 25°C)
log _{k_{ow}}	4.51	0.89	0.91
Φ ₂₅₄ (mol/Einstein)	0.292	0.038	0.001
ε ₂₅₄ (1/M·cm)	4770	13200	2940
pK _a	4	1.6/5.7	7.1
Detection parameters*			
λ (nm)	285	267	273
Retention time(min)	8.8	4.7	3.2
LOQ (mg/L)	8	8	20

* Values measured in this experimental work.

3.3.2. CECs preparation and quantification

Stock solution with each CEC was prepared at 8 mg/L in MilliQ water and stored at 4 °C, and directly diluted in the different water matrices to reach an initial concentration of 100 µg/L each.

Concentration profiles of each CEC were monitored by Ultra-Performance Liquid Chromatography with Ultraviolet-Diode Array Detection (UPLC-UV-DAD) (Agilent Technologies, Series 1260, Palo Alto, CA, USA, Figure 3.8).

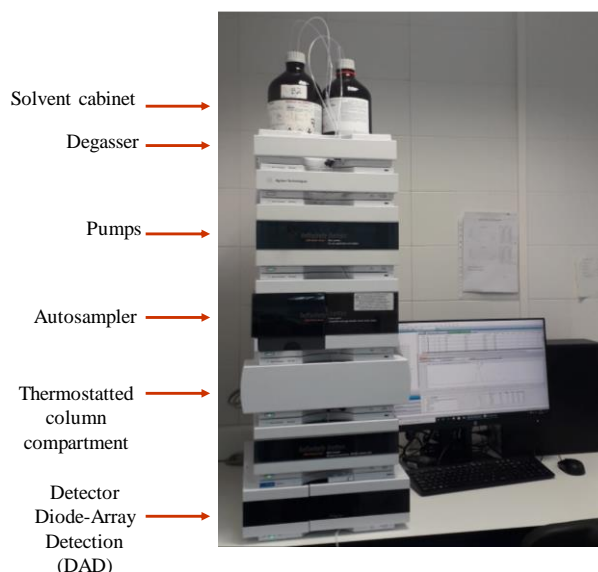


Figure 3.8. UPLC-UV-DAD used for CECs quantification.

High-Performance Liquid Chromatography (HPLC) is a liquid chromatography technique, whose separation principle is based on the distribution of the analyte between a mobile phase (eluent) and a stationary phase (column absorbent material). Depending on the chemical structure of the analyte and on the type of stationary phase, the molecules are eluted at different times.

Typically, Reversed-Phase Liquid Chromatography (RP-LC) is employed and the separation mode involves the use of a nonpolar and hydrophobic stationary phase (most frequently an octadecyl carbon chain (C18)-bonded silica) and a polar mobile phase constituted by water and at least a water-miscible organic solvent.

The system contains the following modules: a solvent reservoir, pumps, an injection valve, a column, a detector unit and the software for instrument control, data acquisition and data evaluation. The eluent is delivered by the pump at high pressure and constant speed through the system, the analyte is introduced by an injection valve into the column, that allows compounds separation. A detector recognizes the analytes present in the eluent coming from the HPLC column, converting the signals, recorded by a data management system (computer software) and shown in a chromatogram in the form of peak (intensity of signal plotted against retention time). Different type of detector could be used: (i) Ultraviolet (UV)

3. Materials and methods

detector, (ii) infrared detector, (iii) refractive index detector, (iv) mass spectrometer, (v) fluorescence detector and (vi) electrochemical detector.

The basic principles of UPLC are the same as HPLC, but involving smaller length of the column, smaller sized particles (less than 2 μm) and, consequently, higher pressure to drive the mobile phase through the column, acquiring better resolution, speed, sensitivity and leading to time saving and reduction in the consumption of solvent. Moreover, UPLC is characterized by lower injection volume, resulting in higher resolution, and higher column temperature that, reducing the mobile phase viscosity, leads to an increase of the diffusion coefficient and of the flow rate.

The separation efficiency is proportional to column length and inversely to the radius of the particles. Consequently, smaller sizes particles lead to higher efficiency, minimizing H, according to the Van Deemter equation (Eq. 3.1):

$$H = A + \frac{B}{v} + (C_S + C_M)v \quad \text{Eq. 3.1}$$

Where H represents Height Equivalent to the Theoretical Plate (HETP), A (related to eddy diffusion), B (related to longitudinal molecular diffusion along the column axis) and C (related to mass transfer of the analyte between the mobile and the stationary phase) are constants and v is the flow rate of the carrier gas.

In a UPLC system is possible to pass from commonly used 3.5 μm and 5 μm particle sizes (in HPLC) to 1.8 μm . This allows the use of shorter columns, without significantly affecting resolution and hence the analysis time is reduced.

Smaller and more uniform particles (1.8 μm in UPLC vs 5 μm in HPLC) lead to:

- A rapid increase in back pressure (up to 1000 bars in UPLC vs up to 400 bars in HPLC).
- An increase of efficiency, resolution and a performance improvement.
- Reduction of multiple flow paths (minimizing A term).
- Reduction of mass transfer times (minimizing C).
- Possibility to use shorter columns, without affecting efficiency (50 mm in UPLC vs 150 mm in HPLC).
- Possibility to work at higher flow rate (shortening analysis time), without obtaining a remarkable loss efficiency.

For the quantification of the selected CECs, volumes of 4.5 mL of water samples were filtered through a 0.2 mm syringe-driven filter (Merck Millipore filter hydrophobic polytetrafluoroethylene (PTFE)) and washed with 0.5 mL of acetonitrile (ACN), to remove any absorbed organic compounds, and immediately analyzed by UPLC-UV-DAD array according to the following working conditions: A C-18 analytical column (ZORBAX Eclipse XDB-C18, 600 Bar, 4.6x50 mm, 1.8 μm , fully porous, 80 \AA), 100 μL of injection volume and flow rate of 1 mL/min, 95 % water with 25 mM formic acid (mobile phase A) and 5 % ACN (mobile phase B). A linear gradient progressed from 5 % to 90 % of B in 12 minutes and then to 100 % for 1 minute. The re-equilibration time was 3 minutes with a flow of 1 mL/min. Detection wavelength (λ), retention time and Limit of Quantification (LOQ) for each CEC are reported in Table 3.4.

CECs concentration in water samples was then calculated against previously performed calibration lines. For that, 6 standard solutions, containing the three CECs at different concentration in the range 0-120 $\mu\text{g/L}$ were analysed. A linear relationship between the CECs concentration and the peak area was obtained and the calibration lines for each CEC are shown in Figure 3.9.

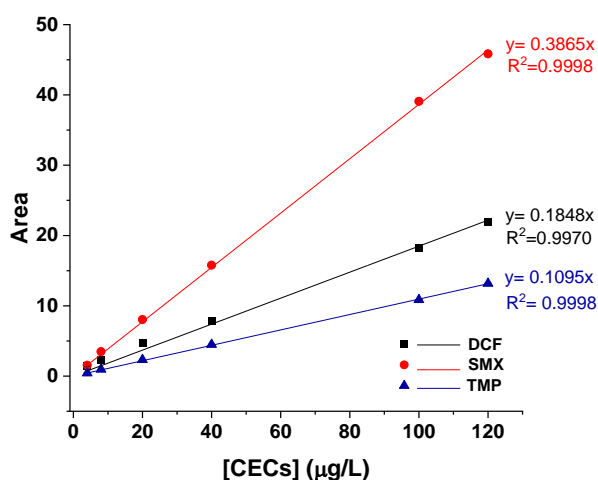


Figure 3.9. Calibration lines of DCF, SMX and TMP (0-120 $\mu\text{g/L}$).

3.4. Water matrices

3.4.1 Isotonic water

IW was chosen as simple matrix to investigate the processes' efficiency for the simultaneous disinfection and decontamination of water, excluding the effect of inorganic ions and organic matter, but avoiding an osmotic bacterial stress condition. IW was prepared by dissolving NaCl 0.9 % (w/v) in sterile demineralized water (DW) and autoclaved at 121°C

3. Materials and methods

for 15 minutes. IW main physicochemical characteristics are shown in Table 3.5. DW was supplied by a plant installed at Plataforma Solar de Almeria (PSA), obtained following these steps:

- Silex filter: to remove the solid particles.
- Pre-treatment with dosages of hypochlorite, sodium bisulfite (to control chlorine), hydrochloric acid (to control pH) and anti-fouling (to avoid calcification in the membranes) followed by a 5 μm filtration.
- Inverse osmosis: it takes place in three modules with 3 semi-permeable polyamide membranes each module. Two modules work in parallel and the third one uses the rejection of the other two modules. The flow production is around 1400 L/h with a rejection of 700 L/h.
- Electro-deionization: to retain the salts that were not retained in the inverse osmosis. The plant uses ion exchange resins and electric currents to regenerate the resins. The flow production is around 1000 L/h with a rejection of 150 L/h.

3.4.2 Well water

Well water, obtained from a well hole located at Plataforma Solar de Almeria (PSA) (Spain), was used as natural water and also to assess the influence of $\text{HCO}_3^-/\text{CO}_3^{2-}$ on the treatment's performance. Due to the high concentration of $\text{HCO}_3^-/\text{CO}_3^{2-}$ naturally present in the well water, actual well water (WeW) and ten-fold diluted well water (d-WeW) were used. Their physicochemical characteristics are shown in Table 3.5.

3.4.3 Simulated Urban Wastewater

Simulated Urban Wastewater (SUWW) was chosen as model of secondary effluents from UWWTPs, to guarantee the reproducibility and comparability of results among the different experiments, avoiding the fluctuations on the water composition of actual effluents. Two different recipes were followed:

1. SUWW-1, with the absence of humic acids: NaHCO_3 (96 mg/L); $\text{CaSO}_4 \cdot 2\text{H}_2\text{O}$ (60 mg/L); MgSO_4 (60 mg/L); KCl (4 mg/L); NaCl (400 mg/L); $\text{MgSO}_4 \cdot 2\text{H}_2\text{O}$ (2 mg/L); $\text{CaCl}_2 \cdot 2\text{H}_2\text{O}$ (4 mg/L); Peptone (32 mg/L), Beef extract (22 mg/L); Urea (6 mg/L) (Polo-Lopez, 2011).
2. SUWW-2, with the presence of humic acids: NaHCO_3 (96 mg/L); MgSO_4 (60mg/L), NaCl (580 mg/L), and K_2HPO_4 (7.0 mg/L); $\text{CaSO}_4 \cdot 2\text{H}_2\text{O}$ (60 mg/L); $(\text{NH}_4)_2\text{SO}_4$ (23.6 mg/L); KCl (4 mg/L); Beef extract (1.8 mg/L); peptone (2.7 mg/L); humic acid (4.2 mg/L), sodium lignin sulfonate (2.4 mg/L); sodium lauryl sulphate

(0.9 mg/L); tannic acid (4.2 mg/L) and acacia gum powder (4.7 mg/L) (Sánchez-Montes, 2020).

3.4.4 Urban Wastewater

Secondary effluents from the UWWTP El Bobar (Almeria, Spain) were freshly collected and used without additional modifications. This UWWTP is a conventional plant consisting of a pre-treatment step, primary and secondary treatment, based on CAS. It treats the sewage collected from the municipality of Almeria with a capacity of 315000 p.e. and entering 256582 population equivalent (p.e). The physicochemical and microbiological characteristics of the batches used in this work are shown in Table 3.5.

3.5 Water characterization

Water matrices were characterized using several devices (explained below) and the main physicochemical parameters are reported in Table 3.5.

Table 3.5. Physicochemical characteristics of the water matrices used in this work.

	IW	WeW	d- WeW	SUWW ¹	SUWW ²	UWW
Physicochemical parameters						
DOC (mg/L)	< 0.5	5.9±3.5	<0.5	20.7 ± 2.2	11.1±2.5	19.6±2.8
[HCO ₃ ⁻] (mg/L)	-	828±592	82.5±2.5	70.8 ± 13.9	69.5±7.3	370.0±28.0
Turbidity (NTU)	< 0.5	1.6±0.9	0.3±0.1	1.9 ± 0.1	2.5±0.2	9.1±9.3
pH	5.8±0.1	7.6±0.3	7.9±0.2	7.7 ± 0.2	7.4±0.2	7.6±0.1
Conductivity (mS/cm)	16.1±0.2	2.6±0.9	0.6±0.4	1.3 ± 0.1	1.5±0.1	2.4±0.1
Ionic content (mg/L)						
Cl ⁻	5400±10	346±172	64.3±49.7	247.4 ± 11.6	356.7±4.4	436.7±80.0
NO ₃ ⁻	-	24±20	5.6±4.9	-	2.7±0.9	4.0±0.9
NO ₂ ⁻	-	0.8±0.1	0.1±0.0	-	-	6.0±±3.1
PO ₄ ³⁻	-	-	-	-	4.0±1.6	3.4±1.5
Br ⁻	-	2.5±0.5	0.4±0.2	-	-	2.8±0.1
SO ₄ ²⁻	-	283±180	56.8±48.8	86.2 ± 2.8	99.1±0.8	101.5±22.7
Na ⁺	3542±5	371±138	56.1±26.6	182.1 ± 15.2	255.2±1.6	252.0±13.4
NH ₄ ⁺	-	2.3±0.6	0.4±0.2	-	7.6±1.0	39.3±7.7
K ⁺	-	7.4±3.3	0.9±0.3	3.2 ± 0.4	9.5±2.3	27.8±1.0
Ca ²⁺	-	101±53	18.7±15.0	17.2 ± 1.2	18.6±3.4	88.5±11.5
Mg ²⁺	-	68±33	12.5±9.7	13.0 ± 1.2	13.3±1.6	46.7±7.5
Microbial content (CFU/mL)						
<i>E. coli</i>	-	-	-	-	-	4.49·10 ³ ±7.56·10 ³
<i>Enterococcus</i> spp.	-	-	-	-	-	5.83·10 ² ±7.65·10 ²
<i>Pseudomonas</i> spp.	-	-	-	-	-	1.61·10 ⁴ ±2.28·10 ⁴
Total coliforms	-	-	-	-	-	3.19·10 ⁴ ±4.64·10 ⁴
Antibiotic Resistance Bacteria (CFU/mL)						
AR- <i>E. coli</i>	-	-	-	-	-	8·10 ¹
AR- <i>Enterococcus</i> spp.	-	-	-	-	-	3.2·10 ¹
AR- <i>Pseudomonas</i> spp.	-	-	-	-	-	5.4·10 ²

3. Materials and methods

3.5.1. Conductivity, pH, and turbidity

Water conductivity was monitored using a conductometer (GLP31 CRISON, Figure 3.10a) and pH through a pH-meter (GLP22, CRISON, Figure 3.10b), calibrated accordingly to manufacturer.

Turbidity (expressed in Nephelometric Turbidity Units (NTU)) was measured with a turbidimeter (Hach Model 2100N, with a detection range from 0.1 to 4000 NTU, Figure 3.10c). The optical system is composed by a tungsten-filament lamp, lenses and aperture to focus light, a 90° detector, forward-scatter light detector and a transmitted-light detector. The analysis is based on measuring the weakening of light intensity (as a function of the dispersed phase concentration), due to absorption and scattering of light by solid or colloidal particles suspended in solution. Briefly, the turbidity of water samples was measured in a cylindrical vial, recording the value of turbidity immediately to avoid effects of particles precipitation. Calibration was performed using the kit Hach 2100AN (IS Stablcal® Stabilized Formazin standards), containing 5 sealed vials of Formazin (< 0.1, 20, 200, 1000 and 4000 NTU).

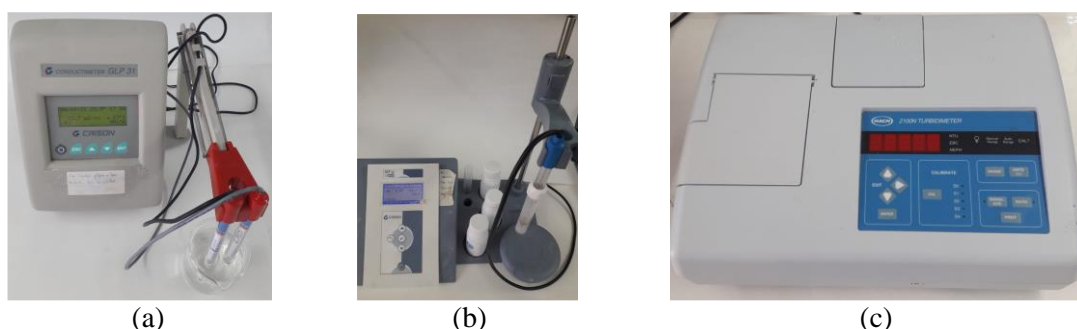


Figure 3.10. (a) Conductometer, (b) pH meter and (c) turbidimeter.

3.5.2 Dissolved organic carbon

Dissolved Organic Carbon (DOC), Inorganic Carbon (IC) and Total Carbon (TC) were measured using a Shimadzu Total Organic Carbon analyzer TOC-L with an autosampler ASI-L (Figure 3.11).

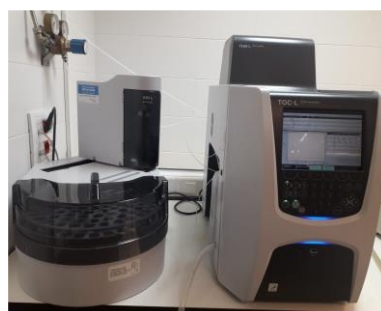


Figure 3.11. Shimadzu Total Organic Carbon analyzer TOC-L with an autosampler ASI-L.

TC (mg/L) of the samples is converted to CO_2 through the $680\text{ }^\circ\text{C}$ combustion catalytic oxidation method in the presence of a platinum catalyst supported on aluminum oxide spheres in an oxygen-rich environment. CO_2 is cooled, dehumidified, it passes in a halogen scrubber and then it is detected by the Non-Dispersive Infrared (NDIR) gas analyzer. The analog detection signal forms a peak, that is proportional to the TC concentration of the samples. IC (comprising CO_3^{2-} , HCO_3^- and dissolved CO_2) (mg/L) is obtained, acidifying the sample with HCl 2N, sparging, obtaining $\text{HCO}_3^-/\text{CO}_3^{2-}$ conversion into CO_2 , that is detected by NDIR detector. DOC (mg/L) is then calculated by subtracting the IC concentration from the obtained TC concentration (Figure 3.12).

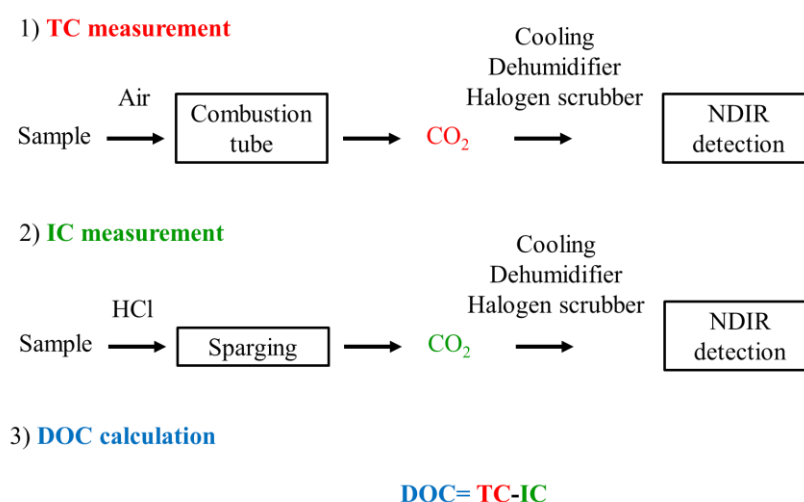


Figure 3.12. TC, IC and DOC measurements.

Samples were filtered through a $0.45\text{ }\mu\text{m}$ nylon syringe filters. In the presence of extremely high IC content, significant errors may result using the aforementioned method for DOC measurement. Therefore, in such cases, after samples filtering, a previous removal of $\text{HCO}_3^-/\text{CO}_3^{2-}$ was performed adding H_2SO_4 concentrated under atmospheric condition, followed by the analysis.

The calibration of the TOC analyser used is regularly performed to ensure correct and accurate data from water samples. Potassium hydrogen phthalate and $\text{NaHCO}_3/\text{Na}_2\text{CO}_3$ in MilliQ water for TC and IC standards solutions are used for the calibration tests, respectively. Five calibration lines are estimated: 0-10, 10-50, 50-250, 250-1000, 1000-2500 mg/L for TC concentration and 0-5, 5-20, 20-80, 80-200 and 200-500 mg/L for IC concentration.

3. Materials and methods

3.5.3. Ion chromatography

Ion chromatography is a method for separating ions, based on their interactions with resin (stationary phase) and the eluent (mobile phase). Ions move through the separation column of the ion chromatographer at different speeds depending on their affinity for the specific resin and the separation is based on the differences in ion charge and size. Ions with smaller size and charge are eluted first due to the weaker affinity for the resin, while ions with a stronger affinity for the column are more retained and they elute later. Then, they are measured by an electrical conductivity detector, obtaining a peak whose area is dependent on the relative ion concentration in the injected solution.

The equipment used in this work to analyze anions and cations in water samples was an 850 Professional IC (Metrohm AG, Switzerland) (Figure 3.13).

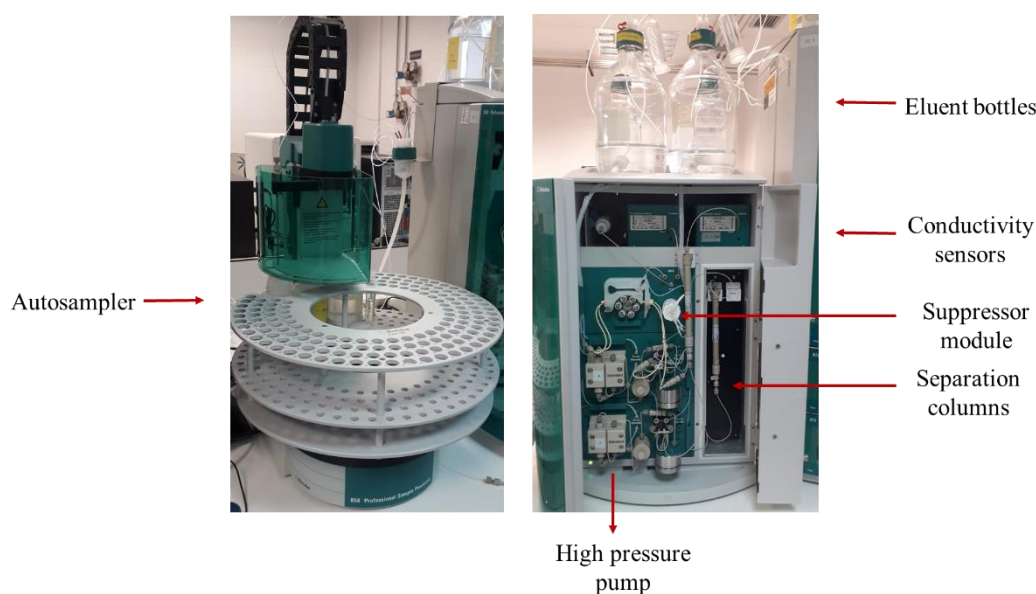


Figure 3.13. 850 Professional IC.

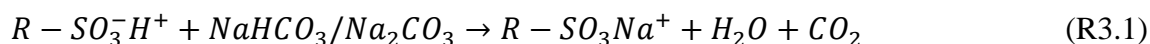
Samples were filtered with a 0.45 μ m nylon filters and introduced into a sample loop to be carried by an eluent into a column, that contains the stationary phase material.

For the determination of monovalent and bivalent cations, a silica gel with carboxyl groups was used, being a cationic ion exchange resins with negatively charged anchor groups, capable of attracting cationic species (Metrosep C6-150/4.0 at room temperature, particle size of 5 μ m, flow 0.9 mL/min). The eluent was a mixture containing 1.7 mM nitric acid and 1.7 mM pyridine-2,6-dicarboxylic acid (dipicolinic acid).

For the determination of inorganic and low-molecular organic anions with chemical suppression, a polyvynil alcohol with quaternary ammonium group (Metrosep A Supp 7 - 150/4.0, thermostatted at 45°C, particle size of 5 μ m, 0.8 mL/min), being anionic ion

exchange resins with positively charged anchor groups, capable of attracting anionic species. The eluent was Na_2CO_3 (3.6 mM).

A suppressor module is necessary for anion analysis, due to the high eluent conductivity. It consists of three cartridges filled with cation exchanger material used in rotation for: (i) suppression (ions in the eluent are replaced with a non-ionic species; R3.1), (ii) regeneration with sulphuric and oxalic acid and (iii) rinsing with MilliQ water.



Cation's eluent has a low conductivity and the use of a suppressor is not necessary.

Guard columns, containing the same stationary phase of separation columns in a reduced amount, are used to protect separation columns and to remove critical contaminants, that could affect column material.

The calibration of IC against each ion in the range 0-20 mg/L is performed regularly to ensure good and accurate results. Besides, a standard solution of 10 mg/L of each anion and cation was always checked before the samples measurements as control of the experimental data.

3.6. Reactors for water purification

3.6.1. 200-mL solar vessel reactor

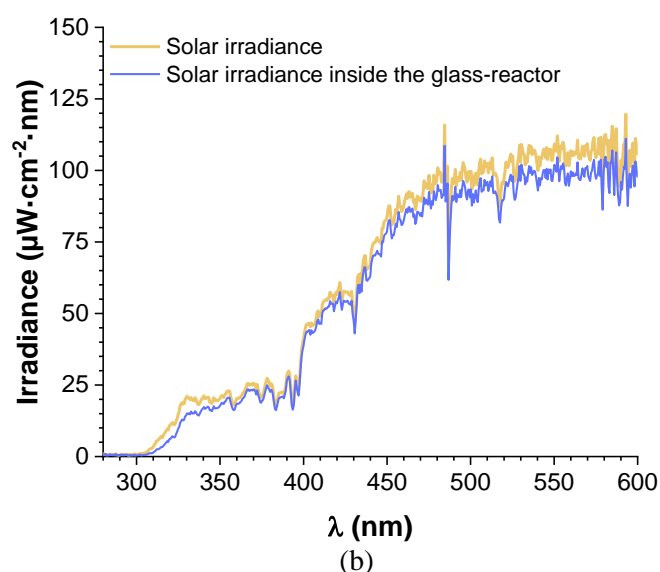
200-mL batch-vessels (DURAN Glass, Schott, Germany) made of borosilicate glass were used for laboratory scale studies and they were placed on magnetic stirrers (at 350 rpm) and covered by a glass cover (Schott) to allow the solar radiation entering from all directions (Figure 3.14). The main technical specifications of this solar reactor are reported in Table 3.6.

The transmittance of the glass composing the solar vessel reactor was determined using a spectrometer (AvaSpec-ULS2048 AVANTES). Solar irradiance was measured outside and inside the glass reactor and no significant differences were obtained regarding the incident irradiance, as it can be observed in Figure 3.14b.

3. Materials and methods



(a)



(b)

Figure 3.14. (a) 200-mL vessel reactor used in a photocatalytic test under natural sunlight. (b) Outside and inside natural solar irradiance profile, measured through the solar-glass vessel reactor used in this study. Measurements obtained with a spectrometer (AvaSpec-ULS2048 AVANTES) at 10:50 am local time in a sunny day at CIEMAT-PSA location (South East of Spain).

Table 3.6. Technical characteristics and specification of solar water reactors used in this experimental work.

	200-mL solar vessel reactor	10-L CPC
UV-A borosilicate transmission	90 % (cut-off at 280 nm)	87 % (cut-off at 280 nm)
Total volume (L)	0.2	10
Irradiated volume (L)	0.2	5
Length (m)	0.15	1.50 per tube
Water high (m)	0.055	0.05
Internal diameter (m)	0.055	0.05
Wall thickness (m)	0.002	0.0025
Irradiated area (m ²)	0.0095	0.44
Concentration factor	-	1
Agitation /Flow rate	350 rpm	30 L/min

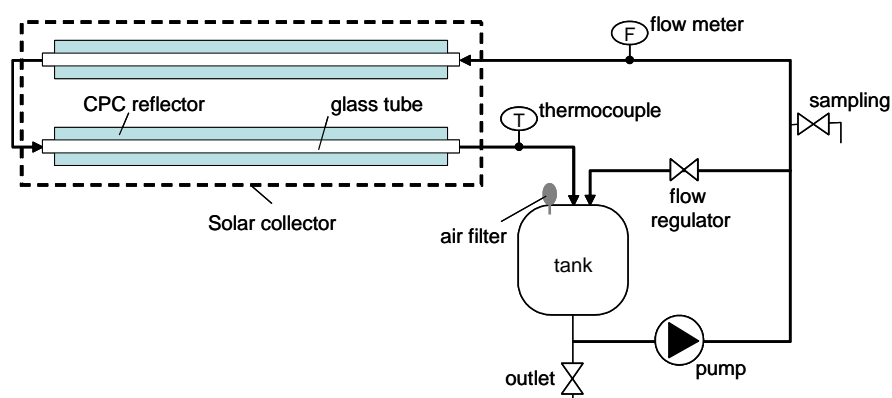
3.6.2. 10-L Compound Parabolic Collector reactor

The CPC photoreactor used in this work consists of a mirror module, made of highly reflective anodized aluminum (ca. 87 % on the UV-A range) (MiroSun, Alanod, Germany), with 2 independent systems composed by 2 borosilicate-glass tubes, each one placed on a platform titled at 37°, value that allows to enhance direct solar radiation capture, being coincident with the latitude of the place in which the reactor is installed (at Plataforma Solar de Almería: latitud: 37°84' N, longitud: 2°34' W) (Figure 3.15a). The water is recirculated through the tubes by a centrifugal pump (70 W, Mod.NH-50 PX PanWorld, USA) with a flow rate of 30 L/min, according to the flow diagram reported in Figure 3.15b. The main

technical specifications are reported in Table 3.6. The ratio between the illuminated and the total volume in this system is 0.5.



(a)



(b)

Figure 3.15. (a) 10-L CPC installed at PSA-CIEMAT facilities and used in this work and (b) reactor flow diagram.

3.6.3. 80-L UV-C pilot plant

The UV-C pilot plant used in this experimental study consists of three independent lowpressure UV-C lamps (max. flow rate 25m³/h, 254 nm peak wavelength, 230 W) protected by quartz tubes and axially located each one in a stainless steel cylindrical photoreactor (Figure 3.16). The flexible design of the system allows the use of one, two or three lamps in batch or continuous flow mode. The water re-circulated from a hold tank (200-250 L of maximum volume capacity) to the UV-lamps chambers by a centrifugal pump (0.55 kW, Lowara, CEA 120/3N/A) which provides a flow rate of 36 L/min. The system contains a long term-stable UV-C detector (ProMinent[®] Iberia S.A., Spain), placed in the inner wall of the cylindrical photochemical reactor (Figure 3.16), that provides continuously irradiance values, expressed in W/m². Table 3.7 summarizes the main technical specifications

3. Materials and methods

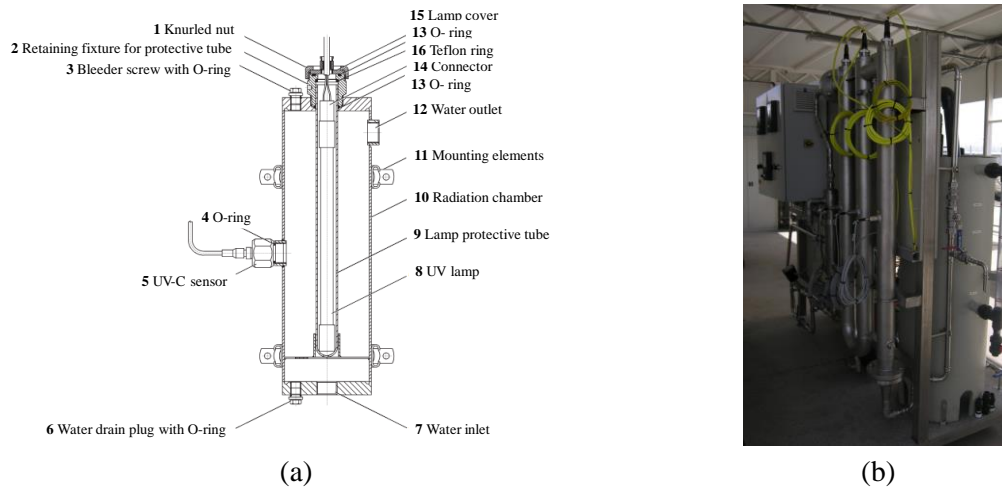


Figure 3.16. (a) Schematic configuration of the reactor containing the UV-C lamp and (b) UV-C pilot plant installed at PSA-CIEMAT facilities.

Table 3.7. 80-L UV-C pilot plant main technical specifications.

λ_{\max} (nm)	254
Total volume (L)	80
Irradiated volume (L)	6.21
Chamber Length (m)	1.61
Chamber diameter (m)	0.0889
Lamp length (m)	1.21
Lamp diameter (m)	0.0370
Irradiated area (m ²)	0.34
Flow rate (L/min)	36

In this study, the water disinfection and decontamination tests with UV-C radiation were done by using only one UV-C lamp. UV-C irradiance was recorded along all the experiments and the profiles of irradiance in W/m² in the different water matrices are shown in Figure 3.17.

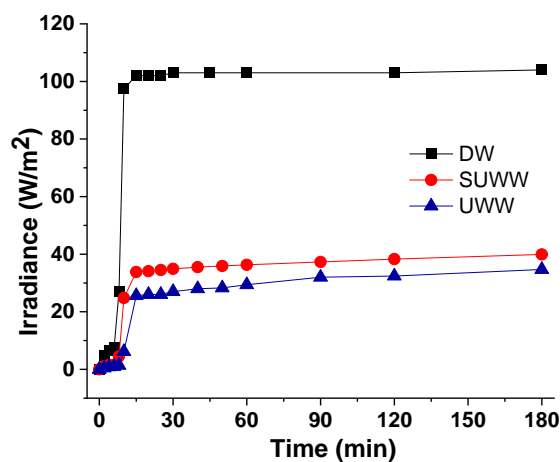


Figure 3.17. Irradiance profiles of UV-C lamp in different water matrices (DW, SUWW and UWW).

3.7. Water disinfection and decontamination tests

3.7.1. Experimental procedure

The experimental procedure was similar for all water treatments investigated in this study, where microbial and CECs targets were simultaneously monitored. Briefly it consists of the following sequential steps:

- Fill the corresponding reactor with the water matrix (IW, WeW, d-WeW, SUWW or UWW).
- Add CECs and bacteria from the previously prepared stocks solutions/suspensions to obtain the desired initial concentrations (100 µg/L and 10⁶ CFU/mL for CECs and bacteria, respectively). In UWW, only CECs were added, as natural occurring bacteria were the microbial target monitored in this water matrix.
- Homogenize in dark and take a sample as control to probe the right initial concentration of pathogens and contaminants.
- Add reagent (PMS and/or photocatalysts) and collect the initial sample (time 0 minute).
- Switch-on the UV-C lamp or expose the reactors to natural solar radiation.
- Take water samples at regular time intervals for bacterial and CECs quantification and monitoring along the experimental time the following parameters: T with a thermometer (Checktemp, Hanna, Spain), pH with a pH-meter (110-K, Horiba Laqua act), solar irradiance with a pyranometer (Section 3.7.2) and PMS concentration by spectrophotometric procedure (Section 3.7.3).

At least two replicated experiments of each operational condition were done and results of targets concentrations detected at any time are presented in graphs (Origin[®] 2021, Electronic Arts) as the averaged values with their corresponding standard deviation as error.

The experimental tests performed in this study include also the assessment of boundary effects, needed to read into the results obtained under radiation. These control tests included:

- Dark tests: they were performed under darkness, in the same conditions of the experiments employing light, in order to assess a potential toxic effect of oxidant/catalyst on bacteria viability and CECs.
- Irradiation tests: they were performed under the same irradiation source (solar and UV-C) to assess the mere effect of each radiation on bacteria viability (photo-inactivation) and CECs degradation (photolysis).

3.7.2. Solar radiation analysis

All solar experiments started between 10:30-11:00 am at local time. The analysis of the incident solar radiation during treatment time in terms of solar radiant energy rate incident on a surface (W/m^2) was done using UV-A pyranometers. They are connected to a computer by a data logger, that records the sensor measurements along the day. Two UV-A pyranometers placed near the solar reactors at 3 m of high were used (Figure 3.18); one located horizontally (Kipp & Zonen CUV-5 (280-400 nm)) for horizontally placed systems (200-mL vessel reactor) and the other one inclined 37° (Kipp & Zonen CUV4 (300-400nm)) for 10-L CPC reactor.

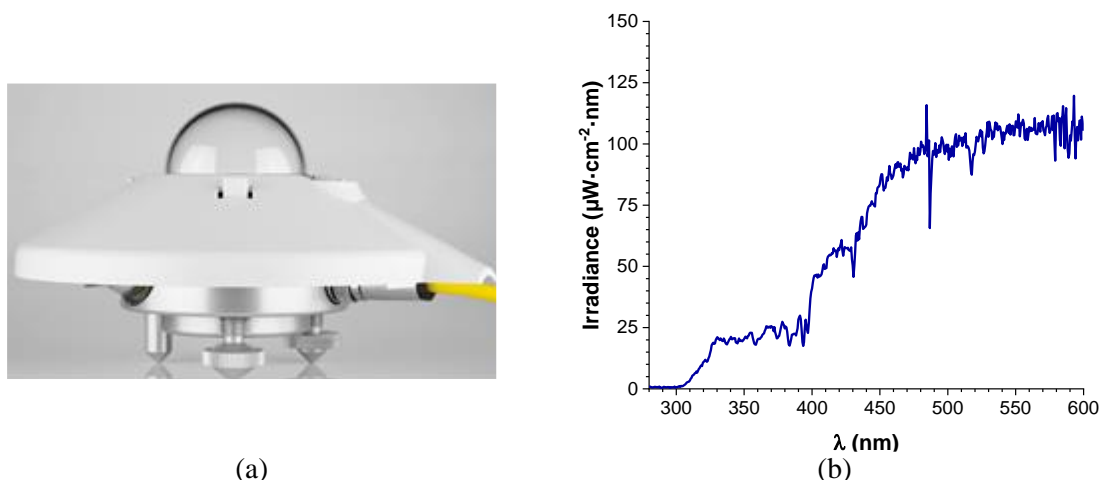


Figure 3.18. (a) UV-A pyranometer located at PSA facilities and (b) typical solar irradiance profile at the PSA location.

The accumulative energy per unit of volume Q_{UV} (kJ/L) parameter was estimated using the solar irradiance data. It was used to compare experimental results under different operational conditions (including different irradiances and solar reactors). It was calculated according to the following equation (Eq. 3.1).

$$Q_{UV,n} = Q_{UV,n-1} + \Delta t_n UV_n \frac{A_i}{V_t} \quad (\text{Eq. 3.1})$$

where $Q_{UV,n}$ and $Q_{UV,n-1}$ are the UV accumulated energy per liter (kJ/L) at time n and $n-1$; Δt_n is the experimental time of each sample ($\Delta t_n = t_n - t_{n-1}$); UV_n is the average incident radiation on the irradiated area; A_i illuminated area (m^2); V_t the total volume (L) (Polo-López, 2010).

3.7.3. Analytical determination of PMS in water

PMS concentration, expressed in mM, was measured by a colorimetric method according to the Hach Method 10070.

It is based on the oxidation of the N,N'-diethyl-p-phenylenediamine (DPD) reagent, with generation of an intermediate with a pinkish colour development, according to the reaction shown in Figure 3.19a. PMS concentration was quantified mixing 5 mL of the sample with the contents of one DPD Total Chlorine Powder Pillow. After 3 minutes of reaction time, the absorbance of the sample was measured at 530 nm with a UV-Vis spectrophotometer Evolution 220 (Thermo scientific, Massachusetts, USA, Figure 3.19b). To determine the concentration of each sample, an external standard curve was prepared in the range of PMS concentration from 0.001 mM to 0.1 mM.

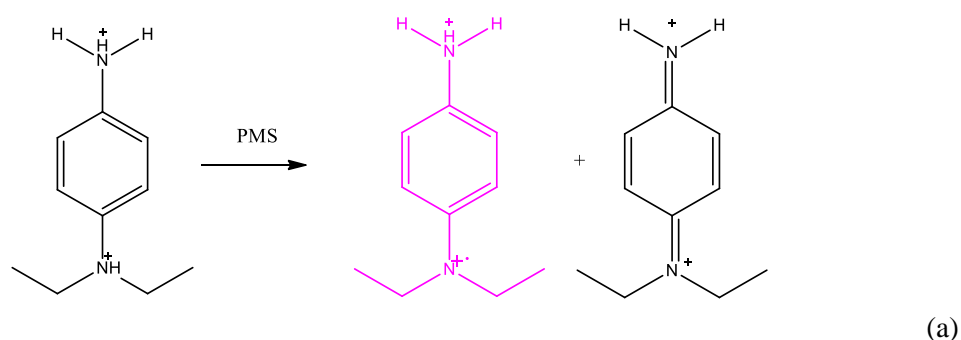


Figure 3.19. (a) Oxidation of DPD by PMS and (b) spectrophotometer Evolution 220.

3.7.4. Photocatalysts

Three different modified ZnO photocatalysts with cerium (ZnO-Ce) (1 %), ytterbium (ZnO-Yb) (1 %) and iron (ZnO-Fe) (0.5 %) were evaluated in this study and the performances were compared with the benchmark TiO₂ Evonik-P25.

The preparation methods, characterization and the photocatalytic performances of each ZnO catalyst under artificial light for pollutants abatement are reported elsewhere (Cerrato, 2018a,b; Paganini, 2019; Cerrato, 2020b, Sordello 2019). Briefly, they were synthesized starting from a 1M water solution of Zn(NO₃)₂·6H₂O and kept under stirring in the presence of the stoichiometric amount of doping agent (Ce(NO₃)₃·6H₂O, Yb(NO₃)₃·6H₂O and FeCl₃ for ZnO-Ce, for ZnO-Yb and for ZnO-Fe, respectively). Then pH was modified to 10–11 using a solution of NaOH 4M. The solution was transferred into

3. Materials and methods

a PTFE lined stainless steel 100-mL autoclave (70 % of filling) and treated at 175 °C overnight. The product was centrifuged and washed with deionized water, then dried at 70 °C. SEM, TEM, X-rays powder diffraction (XRD), Brunauer–Emmett–Teller (BET) and Diffuse Reflectance DR-UV–vis characterization results of the used photocatalysts are reported in previous works (Cerrato, 2018b; 2020b; Paganini, 2019) and summarized in Annex A. UV-visible absorbance profiles of the different photocatalysts at 100 mg/L and the solar emission spectrum at ground level (measured at CIEMAT-PSA facilities) are reported in Figure 3.20.

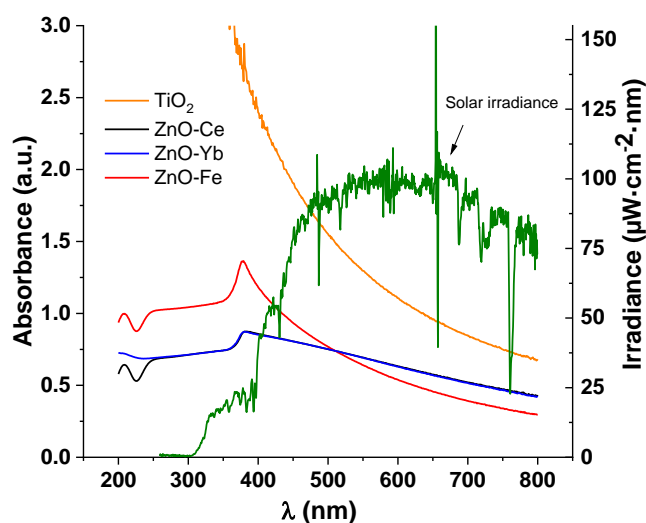


Figure 3.20. UV-visible absorbance profiles of the different photocatalysts at 100 mg/L and solar emission spectrum at ground level (measured at CIEMAT-PSA facilities).

Moreover, the release of Zn^{2+} was analyzed by ICP-MS (iCAP TQ, Thermo Scientific) by an external service at University of Almeria (Almería, Spain).

3.8. Kinetics analysis models

The inactivation and degradation kinetic constants of each bacterium and CEC investigated along the disinfection and decontamination experiments of this study were determined by fitting the results with different mathematical models available in literature and according to the high R^2 value obtained. The kinetic constants were calculated, considering the treatment time, to compare the efficiency of the different treatments and conditions studied.

- Microbial kinetics models:

Like most of the biological processes, microbial inactivation follows a first-order reaction with respect to bacterial concentration as a function of time, according to Chick's law (Eq. 3.2):

$$\text{Log} \left(\frac{N_t}{N_0} \right) = -k \cdot t \quad (\text{Eq. 3.2})$$

Inactivation profiles could be fitted also by another model with a ‘shoulder phase’ given by constant bacteria concentration followed by a log-linear decrease (Eq. 3.3):

$$\text{Log} \left(\frac{N_t}{N_0} \right) = -k \cdot t \begin{cases} 0; N = N_0 \\ -k(t - SL); N < N_0 \end{cases} \quad (\text{Eq. 3.3})$$

Experimental data could follow also a double log-linear kinetics, with a first stage very fast (k_1) and a second phase of attenuated inactivation (k_2) ($k_1 \gg k_2$) (Eq. 3.4):

$$\begin{aligned} \text{Log} \left(\frac{N_t}{N_0} \right) &= -k_1 \cdot \lambda t \quad t = (0, t_1) \\ \text{Log} \left(\frac{N_t}{N_0} \right) &= -k_2 \cdot \lambda t \quad t = (t_1, t_2) \end{aligned} \quad (\text{Eq. 3.4})$$

where N_0 and N_t correspond to the bacterial concentration (expressed in CFU/mL) at time 0 min and at any specific time (t), respectively, k is the kinetic constant (k, min^{-1}), and SL is the shoulder length in the lag phase (SL, min).

- CECs kinetic:

Contaminant's degradation obeys pseudo-first order kinetics (Eq. 3.5 and Eq. 3.6):

$$\frac{dC}{dt} = -kC \quad (\text{Eq. 3.5})$$

$$\ln \left(\frac{C_t}{C_0} \right) = -kt \quad (\text{Eq. 3.6})$$

where C_0 and C_t are initial and sampling time concentrations of CECs, respectively. The slope of the regression line, k (min^{-1}) is the pseudo-first order rate constant.

3.9. Transformation Products analysis and quantification

The identification of TPs, formed as consequence of the degradation of each CEC during the different treatments, was done in collaboration with the research group FQM374 “Análisis ambiental y tratamiento de aguas”, belonging to the research centre CIESOL (joint research centre formed by University of Almería (UAL) and CIEMAT).

The analysis of the TPs was conducted with:

- Direct sample injection analysis: for TPs identification in DW at high concentration of each pollutant (1 mg/L).
- Pre-concentration of samples through Solid Phase Extraction (SPE): to concentrate the formed TPs and to avoid interference from other non-desired compounds present in the sample in UWW spiked with the three CECs at the concentration of 100 µg/L each.

3. Materials and methods

The procedure for the pre-concentration of water samples with SPE is reported in Figure 3.21.

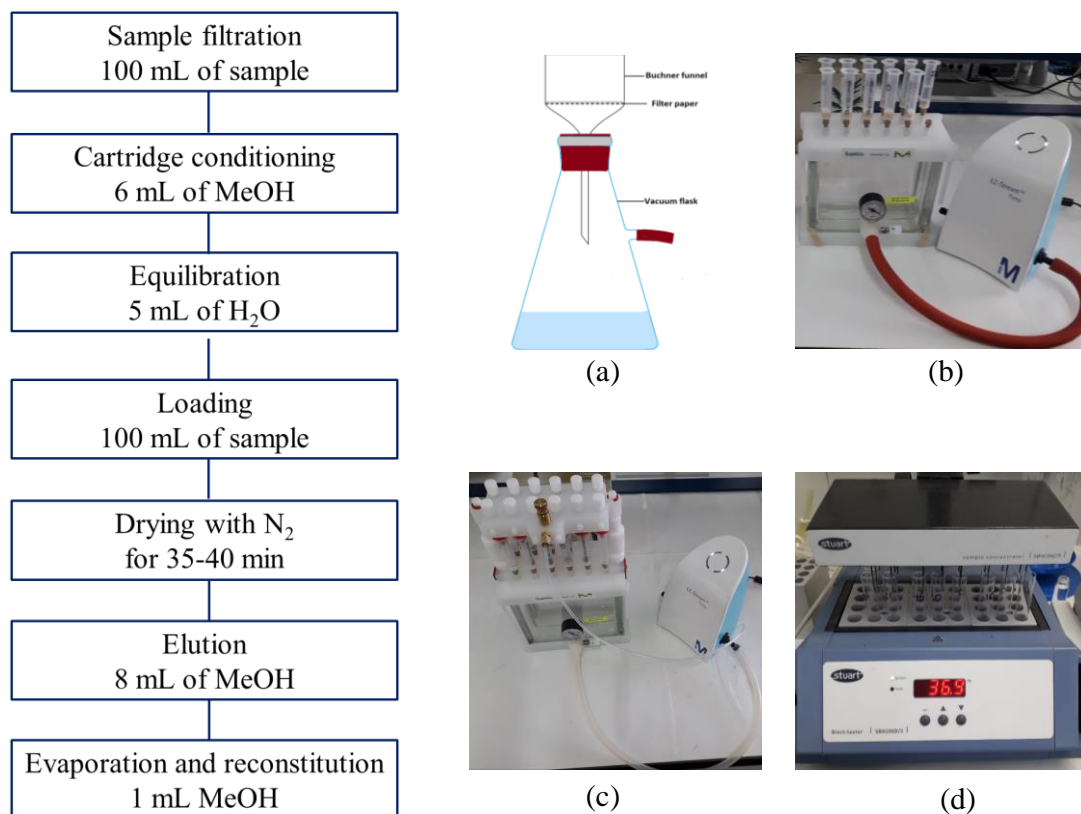


Figure 3.21. SPE procedure: (a) sample filtration, (b) cartridge conditioning, equilibration, loading and elution, (c) cartridge drying under N₂ and (d) sample evaporation.

It consisted of their preliminary filtering in a vacuum filter with 1- μ m glass microfibre filter (Albet Labscience, Barcelona, Spain). Then, 100 mL of sample were extracted using SPE Oasis HLB cartridges (6 cc, 200 mg; Waters, Miliford, MA, USA), that were previously conditioned with 6 mL of MeOH and 5 mL of Milli-Q water. After sample loading, cartridges were dried with N₂ for 30-45 minutes and the elution of the analytes was performed with 2 x 4 mL of MeOH and collected in glass tubes. The eluted sample was dried under a gentle N₂ stream and reconstituted with 1 mL of MeOH (Figure 3.21).

Then, TPs from water samples (both approaches, direct sampling or pre-concentrated by SPE) were analysed by Liquid Chromatography-Quadrupole Time of Flight-Mass Spectrometry (LC-QTOF-MS). Chromatographic separation was carried out using a HPLC 1260 Infinity (Agilent Technologies, Palo Alto, CA, USA) system with the working conditions summarized in Table 3.8.

Table 3.8. Working conditions used for TPs analysis in HPLC.

Column	Eclipse C18 (4.6x150 mm, 5 μ m particle size) (Agilent Technologies)				
Mobile phases	Solvent A: 0.1 % formic acid in water				
	Solvent B: ACN				
	Step	Time (min)	Flow rate (mL/min)	% A	% B
	1	Initial	0.5	90	10
	2	2	0.5	90	10
	3	38	0.5	0	100
	4	48	0.5	0	100
5	48.1	0.5	90	10	
Analysis Time (min)	48.1 min; Re-equilibration time: 15 min				
Injection volume	20 μ L				
Oven Temperature	30 $^{\circ}$ C				

The outlet of the analytical column was connected to a QTOF mass analyzer (Quadrupole time-of-flight) (Triple TOF 5600+, Sciex Instruments, Foster City, CA, USA, Figure 3.22a), used for the structural elucidation of TPs during water treatment processes.

The system consists of the following parts (Figure 3.22b):

- *Ion source*: after chromatographic separation, analytes are introduced into the ion source for their conversion into ions, before entering in the mass spectrometer. A dual source was used: (i) an Atmospheric Pressure Chemical Ionization interface (APCI) for calibrant delivery and (ii) an electrospray ionization source (ESI) interface for sample injection, capable of operating in either positive or negative modes to generate positively or negatively charged ions. The ESI source parameters are shown in Table 3.9.

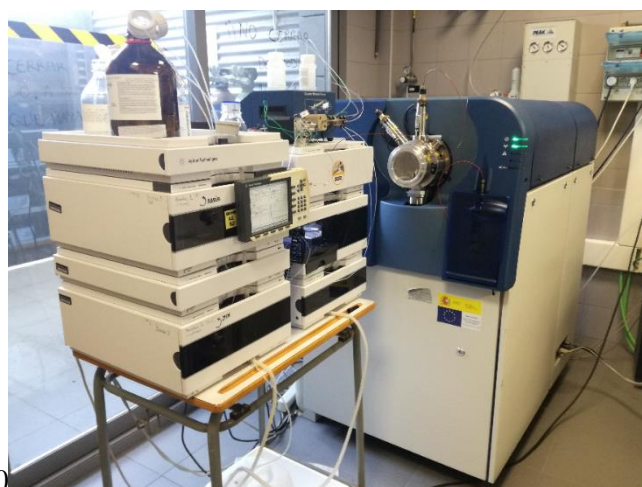
Table 3.9. ESI source parameters.

Parameter	Setting Value
Ionization mode	ESI+ and ESI-
Ion spray voltage	4500 V
Curtain gas	30 psi
Ion Source Gas 1 (GS1)	60 psi
Ion Source Gas 1 (GS2)	60 psi
Declustering potential	80 V
Source temperature	575 $^{\circ}$ C
Nebulizer, curtain and collision gas	N ₂

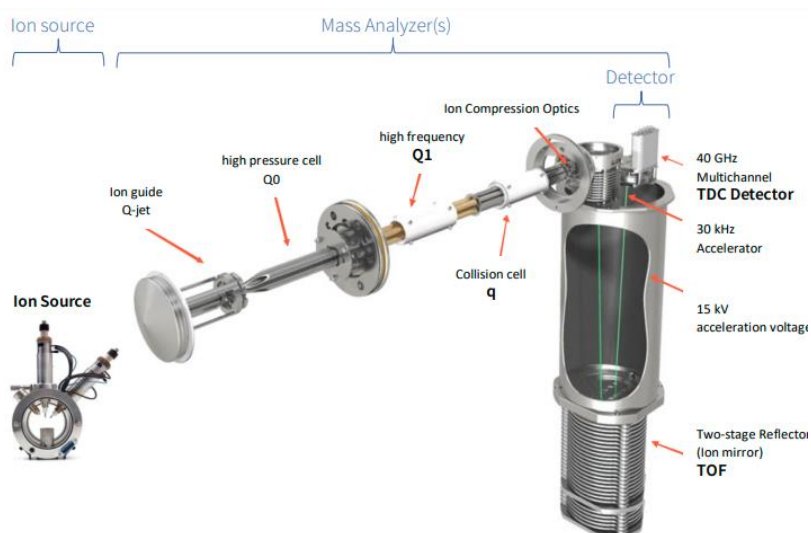
- *QToF mass analyzer*: a series of quadrupole filters which transmit ions according to their mass-to-charge ratio (m/z) values:
 - QJet ion guide and Q0: does not filter ions, but focus them, in order to increase instrument sensitivity and improve the signal-to-noise ratio.
 - Q1 quadrupole: sorts the ions within a specified m/z range.

3. Materials and methods

- Q2 collision cell: an inert gas is introduced in order to fragment the receiving ions to produce product ions.
- TOF region: for the separation of the resulting ions according to their m/z values.
- *Detector*: ions reach the detector at different times (representing a specific m/z value), where they create a current that is converted into a voltage pulse. These voltage pulses are counted and the number of pulses is directly proportional to the quantity of ions entering the detector (representing ion intensity). A mass spectrum plots the intensity versus m/z .



(a)



(b)

Figure 3.22. (a) HPLC 1260 Infinity- QTOF mass analyzer Triple TOF 5600+ and (b) scheme of a QTOF instrument.

The acquisition method consisted in a full-scan survey (TOF-MS) followed by five TOF-MS/MS scans carried out by Information Dependent Acquisition (IDA) of the five more

intense ions in each TOF-MS scan. Scanned mass range was from 50 to 1000 m/z , either in TOF-MS (resolving power of 30,000) or TOF-MS/MS experiments. An accumulation time of 250 ms was applied in TOF-MS and 100 ms for IDA scan. IDA criteria considered dynamic background subtraction. Collision energy of 35 eV with a ± 15 eV spread was used for MS/MS fragmentation. Data acquisition was carried out by Analyst TF 1.5, and data processing by PeakView™ 2.2 and MasterView 1.1.

A suspect compound list based on TPs found in literature was built for each CEC considering TPs' formula. Then, a suspect screening workflow to identify tentative candidates was applied using the parameters explained in Figure 3.23.

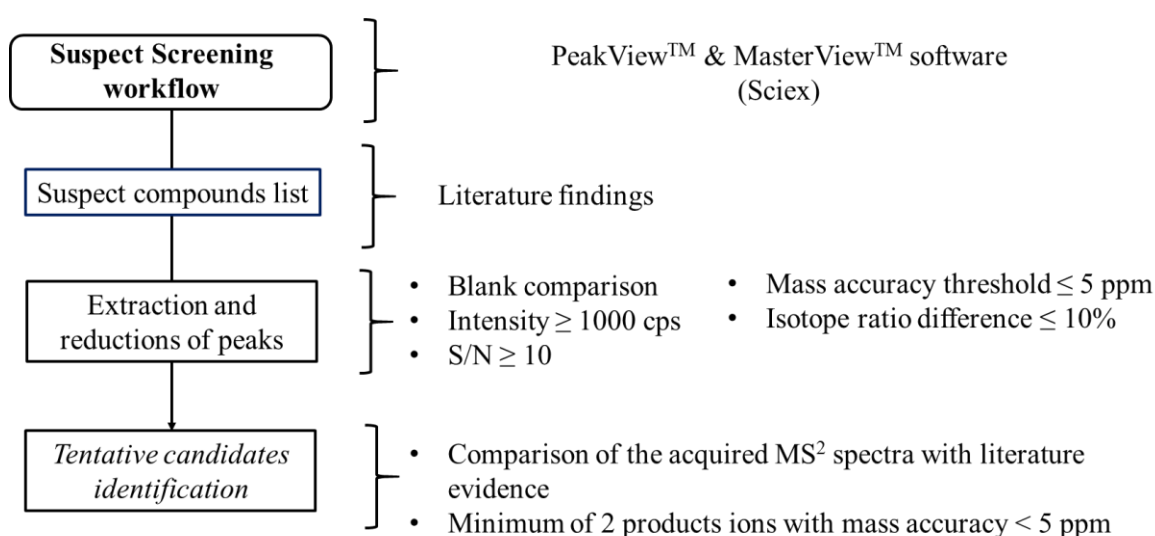


Figure 3.23. Suspect screening workflow.

3.10. Toxicity tests

3.10.1. *Aliivibrio fischeri*

A. fischeri (NRRL B-11177) is a psychrophilic marine bacterium of the family Vibrionaceae, widely used for acute toxicity determination of environmental samples (Wang, 2021). The determination of the inhibitory effect of water samples on the light emission of *A. fischeri* was evaluated according to ISO-11348-3:2007. In this study, the assessment of acute toxicity was carried out using the commercial kit BioFix Lumi-10, by monitoring changes in the bacteria bioluminescence after 30 minutes of exposure of the samples compared to a control, according to the following steps:

3. Materials and methods

- *Sample preparation*: prior to the test, the samples were filtered with 0.2 µm syringe-driven filters (Millex, Millipore), salinity adjusted to 2 % (w/v) with NaCl to avoid bacterial stress conditions and correction of pH between 6.0-8.5.
- *Reactivation of the freeze-dried bacteria* (-20 °C): bacteria were reactivated by adding BioFix Lumi Reactivation solution for “Multi shot” luminescent bacteria, dissolving the bacteria contained in the vial by shaking and stabilizing the reactivated bacteria for 5 minutes in the refrigerator (at 2-8 °C). 0.5 mL of reactivated luminescent bacteria suspension were introduced into each cuvette and they were left for 10 minutes at 15 °C.
- *Bioluminescence measurement*: All the samples (including control test) were tested in triplicate and kept on at 15 °C (in a thermostatic plate) along the test duration. *A. fischeri* bioluminescence was measured with a BioFix® Lumi-10 luminometer (Macherey-Nagel GmbH & Co. KG, Duren, Germany) after 30 minutes of sample exposure.

Samples toxicity results were expressed as bioluminescence inhibition percentage (BI %), in comparison to an uninhibited control.

3.10.2. Phytotoxicity

Phytotoxicity tests were performed following standard procedures (EN ISO 18763:2020) for root lengths assessment in monocotyl sorgho (*Sorghum saccharatum*), in dicotyls garden cress (*Lepidium sativum*) and in mustard (*Sinapis alba*), using seeds provided by a commercial kit (Phytotoxkit liquid samples, Microbiotests Gent, Belgium) (Figure 3.24).

The following steps were performed to conduct the toxicity test:

- Prepare 140 mm-diameter Petri dishes lined with sterilized filter paper layers (0.39 mm thick).
- Add 8 mL of each water sample on the Petri dishes: urban wastewater (UWW) (negative control), ZnSO₄·7H₂O (Zn²⁺ 100 mg/L) (positive control) and water samples. Each sample was analyzed in triplicate.
- Place 10 seeds (only 5 for *S. saccharatum*) on the filter.
- Incubate for 72 h in darkness at 25 °C.

- Then, the root length was measured to calculate the Relative Growth Index (RGI) as a ratio of radicle length of samples/negative control, according following equation (Eq. 3.7).

$$RGI = \frac{RLS}{RLC} \quad (\text{Eq. 3.7})$$

Where RLS is the radicle length of the sample plants and RLC is the radicle length in the negative control (UWW). Results can be classified as: (i) inhibition of the root elongation (toxic effect) for $0 < RGI < 0.8$; (ii) no significant effect for $0.8 \leq RGI \leq 1.2$; and (iii) stimulation (benefit): $RGI > 1.2$ (Young, 2012).

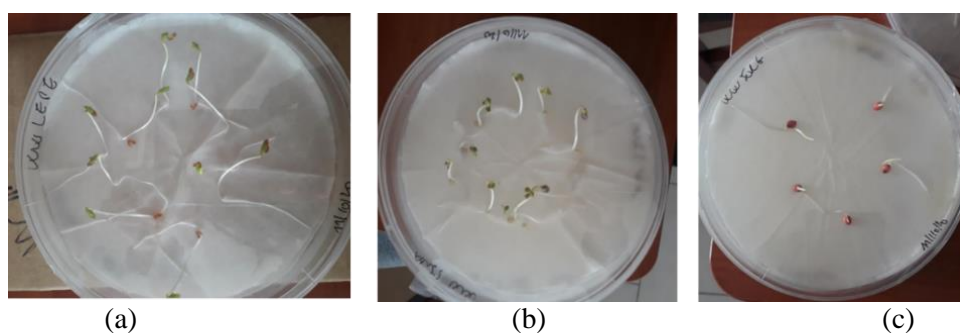


Figure 3.24. Germination of *L. sativum* (a), *S. alba* (b) and *S. saccharatum* (c).

3.11. Laser Flash Photolysis technique

In collaboration with the Universitat Politècnica de València (UPV) at Instituto de Tecnología Química (ITQ), the technique of LFP was used in this experimental study. It is useful for studying transient absorption of species (singlet or triplet excited species and radicals) generated by a short intense light pulse from a pulsed laser source ('pump source'). In particular, LFP was used for the assessment of several chemical compound's reactivity with $\text{SO}_4^{\cdot-}$, in order to elucidate the degradation or disinfection reaction mechanism.

LFP experiments were carried out with a pulsed ND:YAG SL404G-10 Spectron Laser System consisting of a pulsed laser ND:YAG SL404G-10, a pulsed Lo255 Oriel Xenon lamp, a 77200 Oriel monochromator, an Oriel photomultiplier tube (PMT) housing, a 70705 PMT power supply and a TDS-640A Tektronix oscilloscope. The output signal from the oscilloscope was transferred to a computer (Figure 3.25).

3. Materials and methods

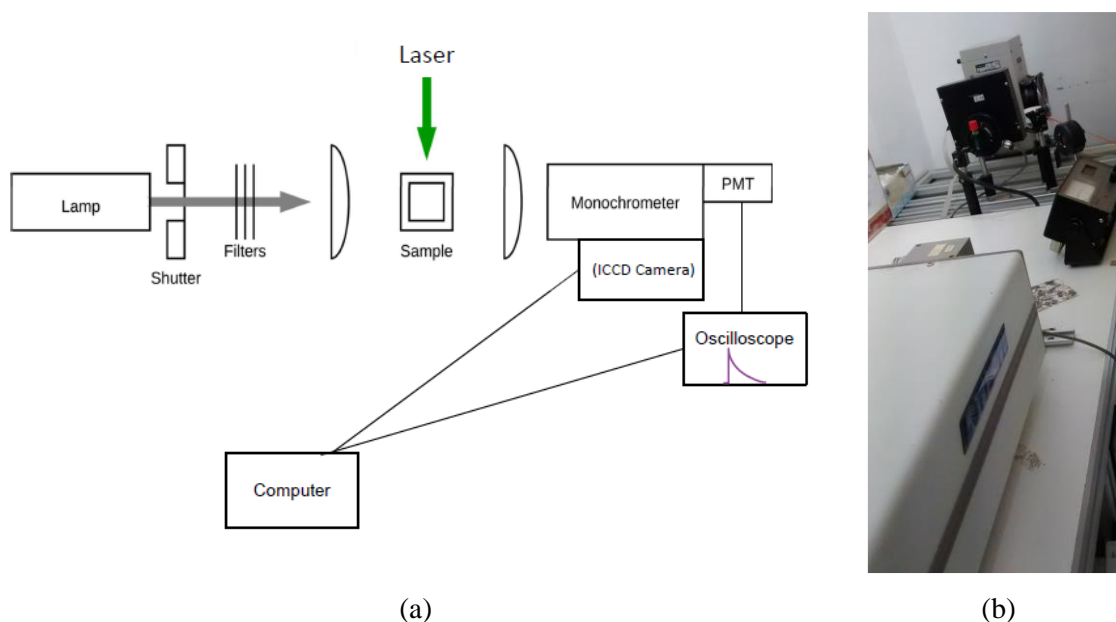


Figure 3.25. (a) LFP diagram and (b) ND:YAG SL404G-10 Spectron Laser System.

LFP was used to generate $\text{SO}_4^{\bullet-}$ from a solution of sodium persulfate PS ($\text{Na}_2\text{S}_2\text{O}_8$), at the excitation wavelength of 266 nm and at pulse energy of 30 mJ.

An appropriate volume of stock solution of PS, to reach an initial concentration of 0.1 M, was mixed with different Quenchers (Q) (compounds investigated) at several concentrations in a quartz cells of 1 cm optical path-length with a total volume of 3 mL.

The lifetime of $\text{SO}_4^{\bullet-}$ was recorded upon addition of increasing concentrations of each Q , and the bimolecular rate constants $k_{\text{SO}_4^{\bullet-}, Q}$ ($\text{M}^{-1} \text{s}^{-1}$) were determined applying the Stern-Volmer equation and by using a linear regression of the decay rate of $\text{SO}_4^{\bullet-}$ versus Q concentration (Stern-Volmer plot) (Eq. 3.8). The slope of the straight line yielded the bimolecular rate constant k_Q ($\text{M}^{-1} \text{s}^{-1}$):

$$\frac{1}{\tau} = \frac{1}{\tau_0} + k_Q \cdot [Q] \quad (\text{Eq. 3.8})$$

where, τ = lifetime of $\text{SO}_4^{\bullet-}$ recorded at a given concentrations of quencher Q ; τ_0 = Lifetime of $\text{SO}_4^{\bullet-}$ recorded in the absence of quencher (s); $[Q]$ = Quencher concentration (M); k_Q = bimolecular reaction rate constant $k_{\text{SO}_4^{\bullet-}, Q}$ ($\text{M}^{-1} \text{s}^{-1}$).

Reaction rate between several Q species and $\text{SO}_4^{\bullet-}$ were determinate to elucidate:

- $\text{SO}_4^{\bullet-}$ mechanism of reaction:
 - H-abstraction: by involving two electron donor species: isopropanol and methanol (MeOH).
 - e^- transfer: by involving sodium azide as electron donor.

- Bacterial inactivation mechanism mediated by $\text{SO}_4^{\cdot-}$: studying several bacterial cell wall constituents, such as *N*-acetylmuramic acid, *N*-acetyl-*L*-alanine, 2,6-Diaminopimelic acid, *N*-acetyl-*D*-glucosamine, *N*-acetyl-*L*-lysine, *N*-acetyl-*D,L*-glutamic acid, Tryptophan, Tyrosine and Phenylalanine.
- CECs degradation mechanism mediated by $\text{SO}_4^{\cdot-}$, studying DCF, SMX and TMP.

3.12. Radical's generation analysis

The assessment of radical's generation during the water treatments investigated in this experimental work was done by performing scavenger's tests and Electron Paramagnetic Resonance (EPR). Both types of analysis were done in collaboration with Dipartimento di Chimica at Università di Torino (UNITO) (Italy) and described in detail below.

3.12.1. Radical scavenger's tests

Radical scavenger's tests are based on the addition of a scavenger specie, that is a chemical substance able to react with high rate with a reactive radical specie, consuming it and suppressing its chemical reaction with the target. Radical species, generated during the oxidative process, are indirectly detected by evaluating the degradation profile of a model target compound in the presence of different radical's scavengers.

Different radical scavengers were used to identify the species involved in the processes:

- Methanol (MeOH): it reacts rapidly with $\text{SO}_4^{\cdot-}$ and HO^{\cdot} .
- Tert Butanol (TBA): it reacts rapidly with HO^{\cdot} .
- Furfuryl alcohol (FFA): it reacts rapidly with singlet oxygen $^1\text{O}_2$.
- Sodium azide (NaN_3): it could directly react with PMS by donating an electron or with $^1\text{O}_2$.
- Phenol: it was used to investigate the reactivity in the presence of Cl^- to have a proof of $\text{Cl}^{\cdot}/\text{Cl}_2^{\cdot-}/\text{ClOH}^{\cdot-}$ generation.
- 3-chloroaniline: it was used to investigate the reactivity in the presence of HCO_3^- to have a proof of $\text{CO}_3^{\cdot-}$ formation.

Tests using SMX or TMP ($C_0 = 1 \cdot 10^{-5}$ M) as model substrate were carried out under different conditions, summarized briefly as follows:

- *Darkness*: in a beaker with a total volume of 200 mL, at room temperature and magnetically stirred to ensure the correct homogenization of the samples along the entire experimental time.

3. Materials and methods

- *UV-C radiation*: in a beaker with a total volume of 200 mL by using a Philips TUV PL-S 9Watt Hg lamp (254 nm of peak wavelength) placed 25 cm over the beaker (4 W/m^2).
- *Simulated sunlight*: in magnetically stirred air-saturated pyrex glass cells (dimensions: 4.0 cm diameter and 2.5 cm height; cut-off at 295 nm), containing 5 mL of total volume. Experiments were conducted in a COFOMEGRA Solarbox system (Italy) equipped with a Xenon arc lamp (1500 W) and glass filters, cutting the transmission of wavelengths below 280 nm. The light irradiance on the cell from 295–400 nm was $39.3 \pm 0.8 \text{ W/m}^2$, measured with a radiometer (model PMA2111, Solar Light Co., Inc, Philadelphia) and temperature reached $52 \pm 1 \text{ }^\circ\text{C}$ after few minutes (remaining constant during the experiment).

All water samples were collected at defined times for SMX quantification and they were supplemented with 60 μL of NaN_3 0.25 M to quench the remaining PMS.

The concentrations of SMX and TMP were measured through a YL HPLC system 9300 with a YL9330 Column Compartment and a YL9150 autosampler. The following measurement conditions were used: a C-18 analytical column (RP C18 LiChroCART[®] - LiChrosphere[®] with 5 μm particles), 50 μL of injection volume and flow rate at 1 mL/min with H_3PO_4 4.4 mM/MeOH (75/25) and H_3PO_4 4.4 mM/ACN (40/60) for SMX and TMP, respectively. SMX was detected at 267 nm at the retention time of 7.3 minutes, while TMP at 273 nm and 6.2 minutes.

3.12.2. Electron paramagnetic resonance

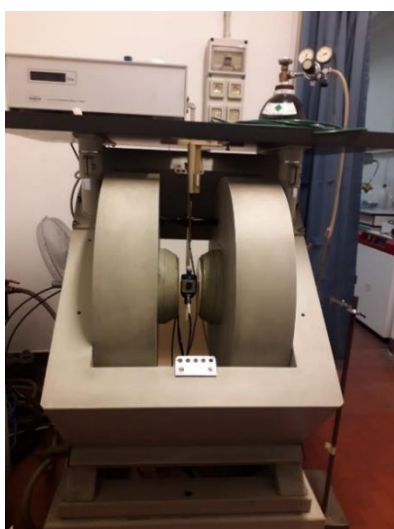
EPR is a technique used to study chemical species with unpaired electrons. It was used to investigate the radical species generated under the studied treatment processes. EPR spectra were recorded at room temperature with a X-band Bruker EMX spectrometer equipped with a cylindrical cavity (Figure 3.26a).

Free radicals generated in solution at room temperature commonly have very short lives and therefore, they are not readily detectable by conventional EPR spectroscopy. Indirect analytical method, using spin trapping agent, has been used to identify such labile species, consisting of reactions between short-lived free radicals and diamagnetic nitroso or nitrono compounds spin trap. As a result, relatively stable aminoxyl radicals, spin adducts, are formed and they can be measured by EPR spectroscopy, enabling the identification of the original free radicals (Makino, 1991).

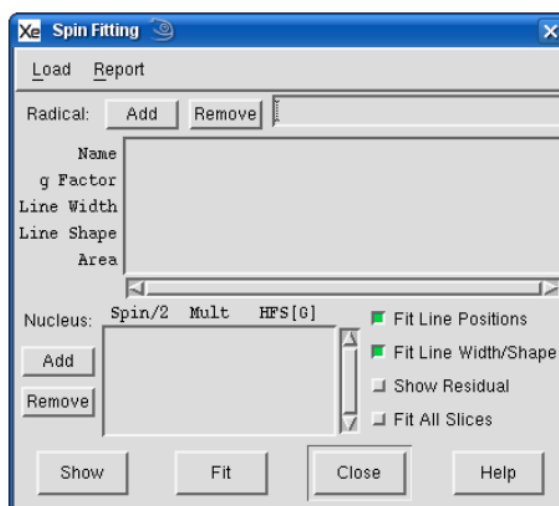
In this study, 5,5-dimethyl-1-pyrroline N-oxide (DMPO) was used as a spin-trapping agent to detect HO^\bullet , $\text{SO}_4^{\bullet-}$ or $\text{O}_2^{\bullet-}$, and 2,2,6,6-tetramethyl-4-piperidinol (TEMP) for the detection of singlet oxygen ($^1\text{O}_2$), both at a concentration of $1.7 \cdot 10^{-2}$ M.

Measurements were carried out in quartz capillary tubes and the following parameters were set: microwave frequency 9.86 GHz; microwave power 2.7 mW; modulation frequency 100 kHz; modulation amplitude 2 Gauss; time constant 0.01 ms. In all experiments, the spin trap (DMPO or TEMP) was added to the cell before irradiating.

Moreover, SpinFit software was used to obtain reliable and accurate EPR spectrum simulations. The g-Factor, the spin of the nucleus and the HFS (Hyper Fine Splittings) (according to literature data) were inserted in the software window (Figure 3.26b) and through the fitting tool all the parameters were optimized to minimize the difference between the simulated and experimental spectrum. The area values were obtained, reflecting the concentration of the radical species.



(a)



(b)

Figure 3.26. (a) X-band Bruker EMX spectrometer and (b) the SpinFit window.

CHAPTER 4

ASSESSMENT OF SIMULTANEOUS

DISINFECTION AND

DECONTAMINATION OF WATER BY

SOLAR PHOTOCATALYSIS

4. ASSESSMENT OF SIMULTANEOUS DISINFECTION AND DECONTAMINATION OF WATER BY SOLAR HETEROGENEOUS PHOTOCATALYSIS

In this chapter the photoactivity of three modified ZnO materials with Ce, Yb or Fe was assessed for the simultaneous inactivation of three bacteria (*E. coli*, *E. faecalis* and *P. aeruginosa*) and for the removal of three CECs (DCF, SMX and TMP) at laboratory scale, in suspension mode and under natural sunlight.

The proof-of-principle of all photocatalysts was investigated in a wide range of concentration (0-500 mg/L) in simple matrix (IW), the potential effect of organic and inorganic chemical compounds on photocatalytic performances was evaluated in SUWW and finally the capability of the best performing material was assessed in an actual secondary effluent of UWWTP, in comparison with the benchmark TiO₂-P25.

4.1. Proof-of-principle studies in isotonic water

4.1.1. Dark assessment of ZnO materials.

Preliminary tests with the different modified ZnO photocatalysts were performed in the dark at 500 mg/L to assess the viability of each bacterium (*E. coli*, *E. faecalis* and *P. aeruginosa*) and the adsorption of each CEC (TMP, SMX and DCF). Figure 4.1 shows that the concentration of the three bacteria remained almost constant along the contact time, achieving an averaged 0.5 ± 0.4 LRV for the three bacteria after 120 minutes (Figure 4.1a), demonstrating that none of the catalysts (including the components used for doping) generated a toxic effect over the bacterial viability. For CECs, no adsorption was observed in any case (Figure 4.1b). Besides, it is important to note that these results indicate that no interference in the analytical measurements of the targets is occurring during the experiments, discarding a toxic effect of CECs over bacterial viability and CECs hydrolysis and allowing the simultaneous analysis of all bacteria and CECs investigated in this experimental study.

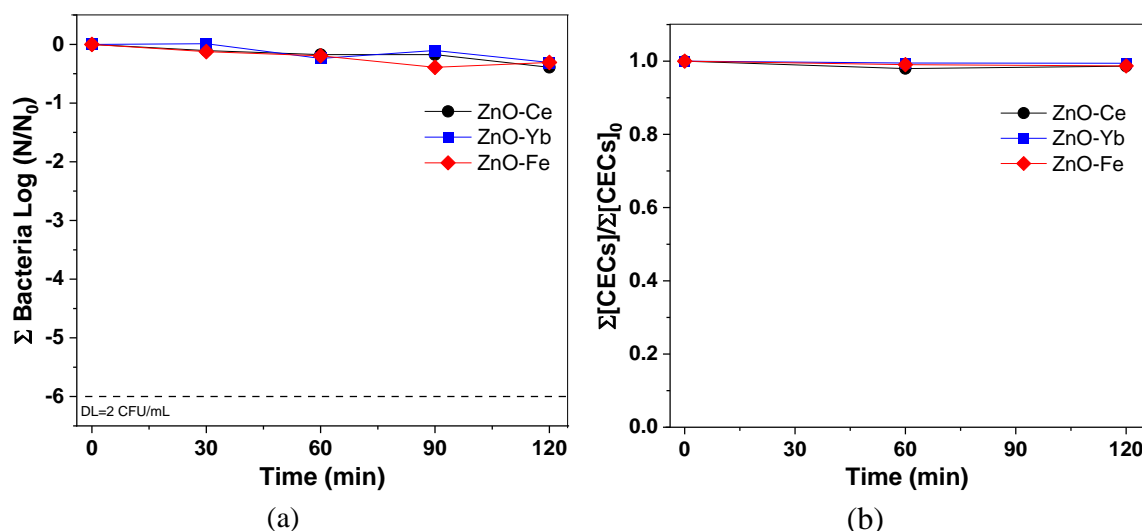


Figure 4.1: (a) Viability of sum of bacteria and (b) adsorption of total CECs in IW in the presence of modified ZnO with Ce, Fe and Yb at 500 mg/L. Tests performed in the dark, at room temperature and under constant agitation (350 rpm).

These preliminary results allow to demonstrate that the removal of the targets (bacteria and CECs) in the presence of modified ZnO materials under natural sunlight can be exclusively attributed to the action of solar photons and to the photocatalysts' activity.

4.1.2. Photocatalytic activity in isotonic water.

The photocatalytic capability of modified ZnO with Ce, Yb and Fe at different catalyst concentrations (100, 200 and 500 mg/L) was assessed under natural solar radiation for the simultaneous bacteria and CECs removal in IW. The assessment of different concentrations of catalyst was done considering that the optimization of the photocatalyst load is fundamental and it could be influenced by several parameters such as (i) the amount of catalyst particles in suspension, (ii) water path-length of photons (absence of darkness areas), (iii) type of targets (microbial particles or dissolved organic and CECs) and the (iv) complexity of the water matrices (Lee, 2016). Therefore, the catalyst concentrations selected and tested were 0, 100, 200 and 500 mg/L, according to previous works carried out in similar solar vessels reactors with TiO₂-P25 for bacterial inactivation and CECs degradation (Agulló-Barceló, 2013; García-Fernández, 2015; Grilla, 2019). In addition, the well-known mere effect of solar radiation over the bacterial viability (from now “solar inactivation”) and the CECs degradation (from now “solar photolysis”) was also assessed, as reference and baseline to analyze the photocatalysis’ performance. Along the treatment time, the water T, pH and solar UV-A radiation were monitored. Figure 4.2 shows the average value of these parameters, highlighting that the water T ranged between 24 to 40.9 °C, pH between 7.5 and 8.5, and the minimum and maximum values recorded of solar UV-A dose was 33.4 and 50.5 W/m², respectively. Thermal contribution to solar photo-inactivation of pathogens in this study can be excluded, being significant for temperature higher than 40 °C (Castro-Alfárez, 2016).

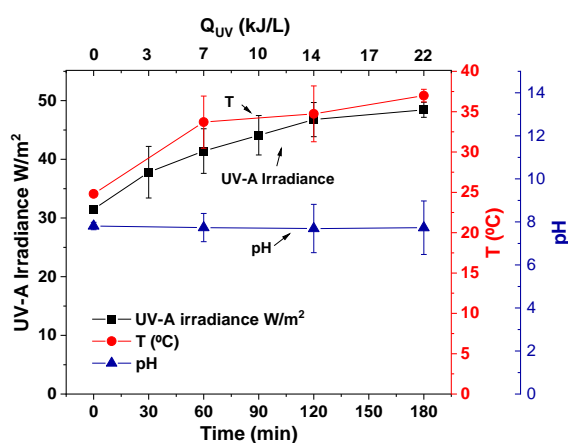


Figure 4.2. T, pH and UV-A irradiance profiles during solar experiments.

Figure 4.3 shows the photocatalytic inactivation profiles of *E. coli*, *E. faecalis* and *P. aeruginosa* and the sum of bacteria; while Figure 4.4 shows the simultaneous degradation profiles of DCF, SMX and TMP and total CECs with all modified ZnO materials at

4. Solar heterogeneous photocatalysis

100, 200 and 500 mg/L of catalyst concentration. The corresponding kinetics data are summarized in Table B.1 and B.2 of Annex B.

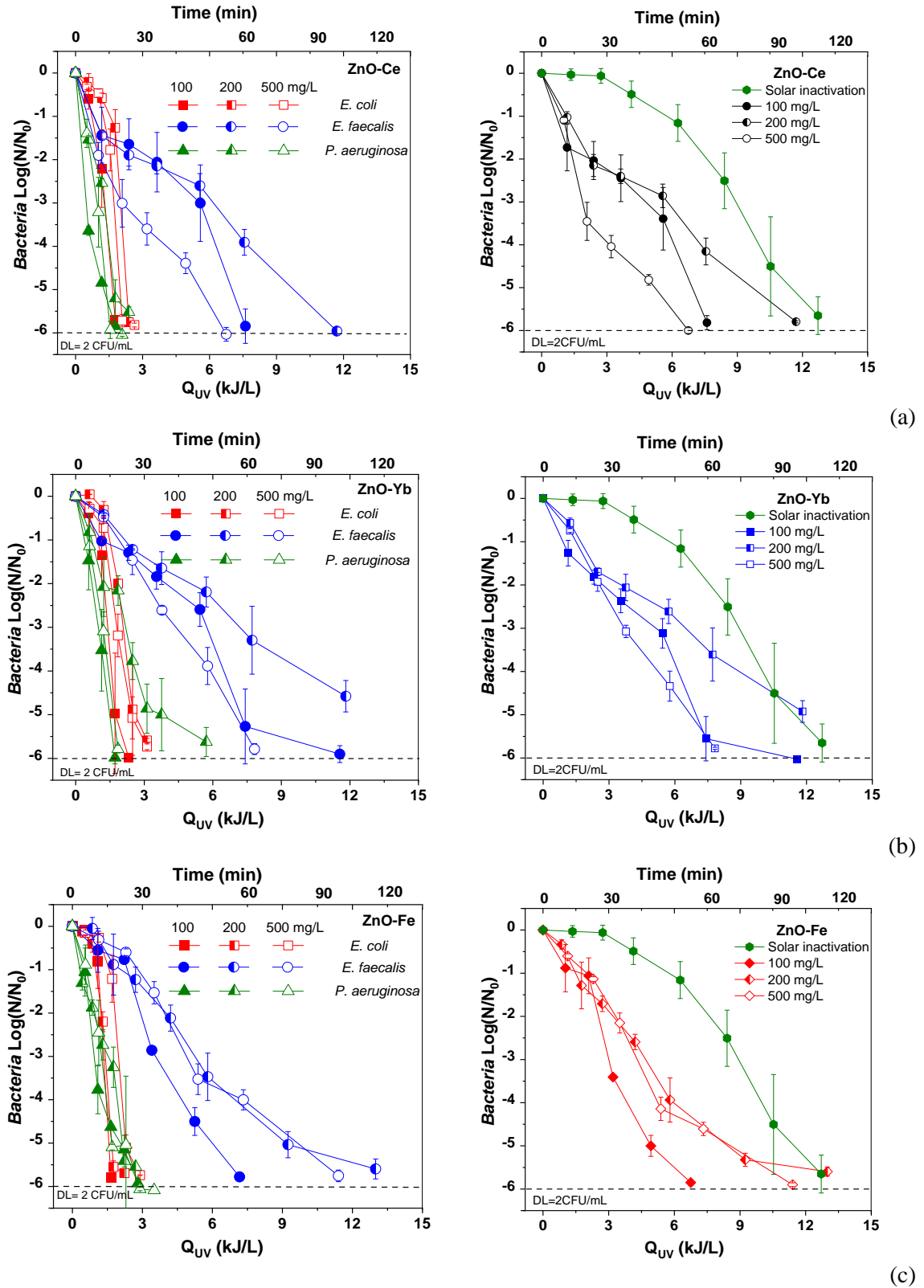


Figure 4.3. Inactivation profiles of *E. coli*, *E. faecalis* and *P. aeruginosa* (left) and sum of bacteria with solar inactivation (for comparison purposes) (right) by modified ZnO with Ce (a), Yb (b), and Fe (c) at 100, 200 and 500 mg/L under natural solar radiation in IW.

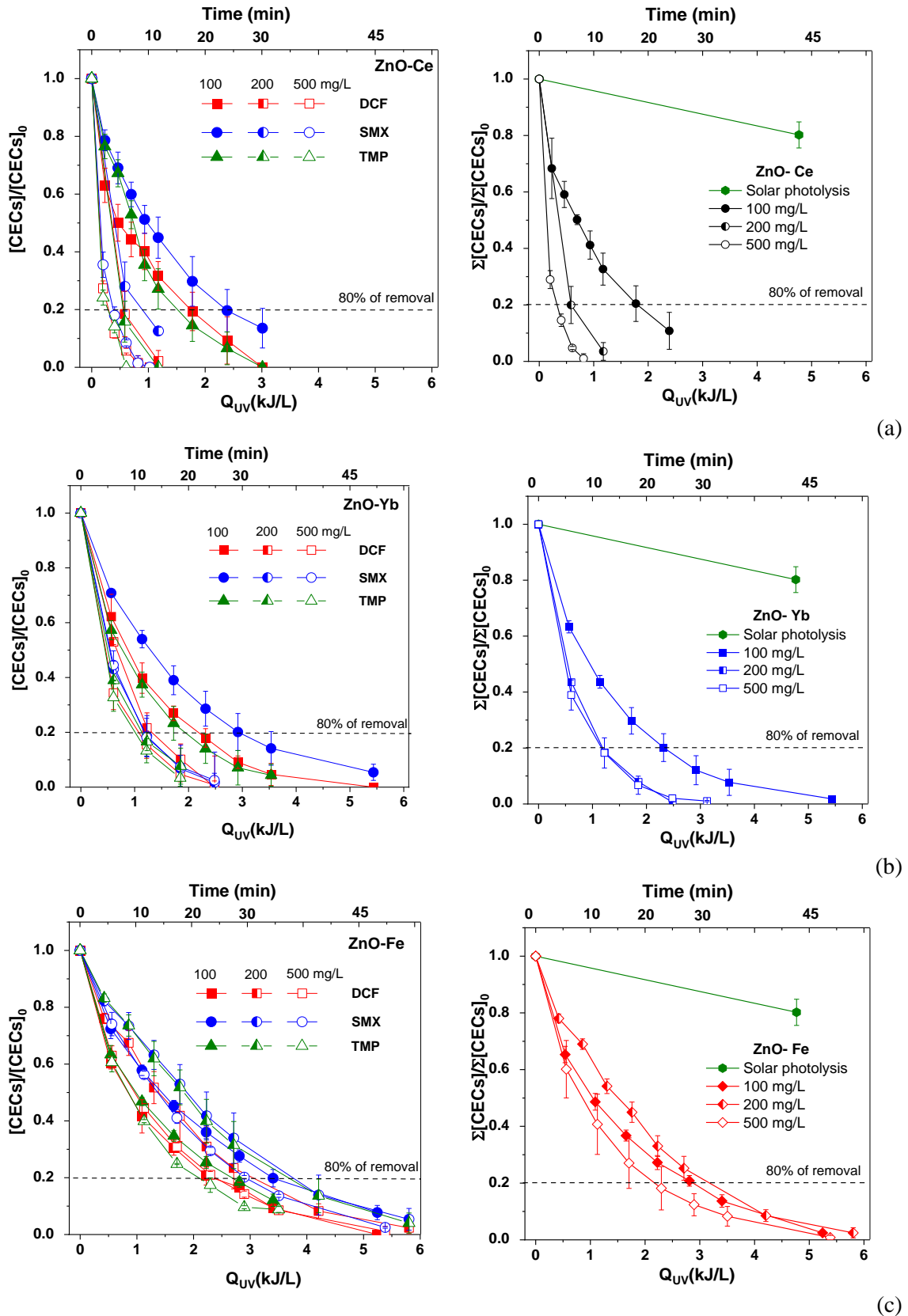


Figure 4.4. Degradation profiles of DCF, SMX and TMP (left) and total CECs with solar photolysis (for comparison purpose) (right) by modified ZnO with Ce (a), Yb (b) and Fe (c) at 100, 200 and 500 mg/L in IW under natural solar radiation.

4. Solar heterogeneous photocatalysis

From these results, the capability of all the modified ZnO materials for water purification could be initially confirmed. More than 5 LRV of bacteria and 80 % CECs removal were obtained in all cases by adding the investigated photocatalysts, enhancing both the bacterial inactivation and CECs degradation, compared to the mere effect of sunlight. The order of bacterial reactivity observed was: *P. aeruginosa* (gram-negative) \cong *E. coli* (gram-negative) $>$ *E. faecalis* (gram-positive). Gram-positive bacteria are less susceptible to the photocatalytic treatment due to a thicker membrane, requiring a larger number of radicals to attain complete inactivation (Marugán, 2010). Regarding CECs, the following reactivity order was obtained: TMP \cong DCF $>$ SMX. It could be explained considering the reactivity of the different CECs with HO \cdot formed during the treatment, considering the second order kinetic constants for the reaction between the three CECs and HO \cdot . Values of $(8.2 \pm 0.3) \cdot 10^9 \text{ M}^{-1}\text{s}^{-1}$, $(8.0 \pm 0.7) \cdot 10^9 \text{ M}^{-1}\text{s}^{-1}$ and $(6.3 \pm 0.5) \cdot 10^9 \text{ M}^{-1}\text{s}^{-1}$ are reported for DCF, TMP and SMX, respectively, in line with the reactivity order found elsewhere (Wols, 2013). Focusing on the catalyst load, the kinetic constants (min^{-1}) (Table B.1 and B.2) of each target investigated in the presence of the three modified ZnO catalysts have been plotted, for a better comparison, in Figure 4.5.

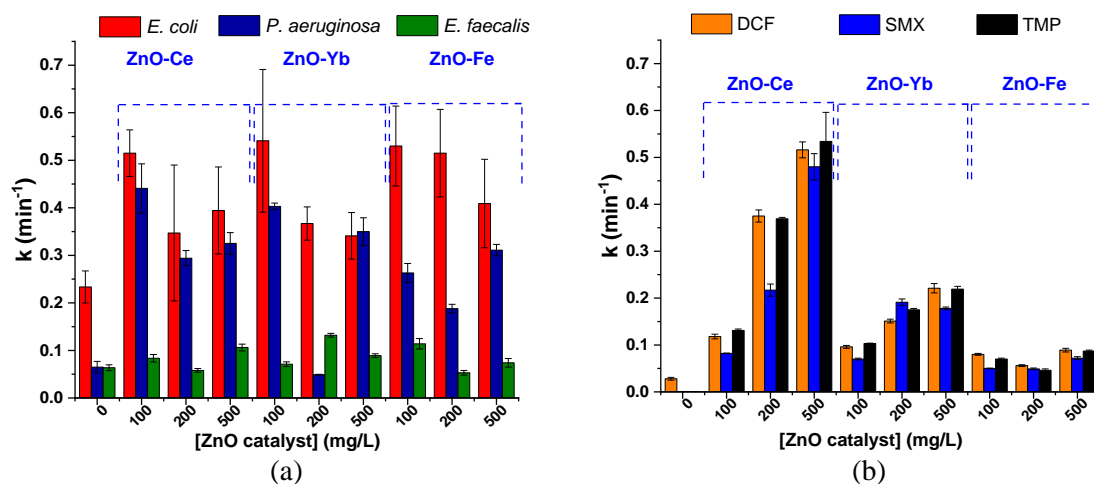


Figure 4.5. (a) Inactivation kinetic constants of *E. coli*, *P. aeruginosa* and *E. faecalis* and (b) CECs degradation kinetic constants in the presence of modified ZnO with Ce, Yb and Fe at concentration of 100, 200 and 500 mg/L in IW under natural solar radiation.

The simultaneous analysis of biological and chemical contaminants highlights that the faster photocatalytic performance is obtained with different catalyst concentrations, being 100 mg/L the best load for the bacteria inactivation (Figure 4.5a), while better results were obtained with 500 mg/L for CEC removal in IW (Figure 4.5b).

A catalyst concentration far from the considered as the optimum, according to principles explained before, could affect the photocatalytic efficiency, effect that is independent from the type of catalyst. From a general point of view, catalyst concentrations lower than the optimum will generate limited performances, based on a low radical's generation rate. Nevertheless, concentrations higher than the optimal also will be negative for the process performance. To understand the optimum of both type of targets, obtained in this study, and the influence of a higher amount of particles in suspension over the bacteria and CECs removal, it is necessary to know the different mechanism that governs the inactivation of bacteria and the degradation of CECs by solar photocatalysis.

Bacterial inactivation mechanisms: It is well known that a reduction of microorganisms' concentration is obtained, due to the bactericidal effect of solar radiation, mainly attributed to generation of intracellular ROS (such as O_2^{\cdot} , HO^{\cdot} and HO_2^{\cdot}) that can attack DNA, proteins, lipids and enzymes, accumulating damages and eventually leading to the cell death.

The effect of natural solar radiation on bacteria viability showed that DL (2 CFU/mL) was reached after 45, 75 and 90 minutes of solar exposure (6.2, 10.5 and 12.7 kJ/L of Q_{UV}) for *E. coli*, *P. aeruginosa* and *E. faecalis*, respectively.

However, the use of photocatalytic material (particles in suspension) in water under solar radiation accelerated the inactivation of microorganisms (considered also as particles in suspension), according to a mechanism based on the generation of ROS under UV-A radiation at the semiconductor particle-solution interface. These species immediately oxidize the outer cell wall components of microorganisms in water, with formation of pores in the cytoplasmic membrane, loss of fluidity, increase of ion permeability with a further direct attack to intracellular components, resulting in loss of microorganism viability (Malato, 2016). However, a higher amount of catalyst particles could have a detrimental effect, attributed to a shadowing or screening effects that protect bacteria from light. This negative effect for bacterial inactivation has been reported previously by Helali et al. at catalyst concentration higher than 0.5 g/L, at which the kinetic rate of *E. coli* in IW by TiO_2 -P25, PC500, Ruana and Bi_2WO_6 photocatalysts was not enhanced (Helali, 2013).

CECs degradation mechanisms: In this case, the contact phases are different considering that CECs are dissolved in the solution. Therefore, the higher the surface contact (in terms of catalyst particles in suspension), the higher the number of active sites on the material, higher photon absorption and, consequently, more electron-hole pairs formation and higher

4. Solar heterogeneous photocatalysis

reaction rates. However, for CECs, also higher amounts that the optimum could be detrimental, leading to scattering effect and to a decrease in the process efficiency, as it has been reported in literature (Abellán, 2009; Tsydenova, 2015). Tsydenova et al. showed that concentration higher than 0.5 g/L did not improved the degradation rate of SMX and TMP in the range of 0.1-2 g/L of TiO₂ (Tsydenova, 2015).

4.1.3. Interpretation of modified ZnO photocatalytic activity

Another key result clearly observed in Figure 4.5 is the different efficiency of each modified ZnO material, showing the following order of photocatalytic activity: ZnO-Ce > ZnO-Yb > ZnO-Fe. The different efficiency exhibited by each ZnO material can be attribute to their different physicochemical properties (Annex A, Table A.1), affecting, therefore, their capability of forming HO[•] after light excitation.

In general, all photocatalysts have similar values of band gap: ZnO-Ce (3.273 eV), ZnO-Yb (3.284 eV) and ZnO-Fe (3.275 eV), compared to the bare ZnO (3.278 eV) (Table A.1), which indicates that the insertion of the dopant in the ZnO matrix did not dramatically affect electronic transition from the VB to CB on ZnO particles (Cerrato, 2018a). Besides, the EPR spectroscopy analysis for each material, reported in previous works (Cerrato, 2020b; 2020a; 2018a; 2018b), demonstrated no significant differences in the EPR signals related to the dopant ions (Ce, Yb and Fe). The EPR analysis evidenced in all cases a charge carrier generation by detecting EPR signal of the paramagnetic species O⁻ and Zn⁺, which is related to the stabilization of photoinduced holes by oxygen ions and the electrons by Zn²⁺, respectively. Nevertheless, at the same time, a different relative EPR signal growth was also detected and reported, which could give an insight into the different operating mechanism of each modified ZnO material, explaining the different performance results obtained in this study. The interpretation of the HO[•] generation for each material is schematically represented in Figure 4.6, and explained in detail as follows:

- The presence in ZnO-Ce of a new crystalline phase, CeO₂, has been reported via XRD patterns and TEM (Annex A, Figure A.1 and A.2) and, therefore, ZnO-Ce could be considered a biphasic solid rather than a doped system (Cerrato, 2020a; 2018a; 2018b). In the EPR spectra, a growth of signal was observed, obtaining a higher number of trapped holes upon light irradiation than that of trapped electrons, due to the presence of Ce⁴⁺ (Annex A, Figure A.4). According to reported Density Functional Theory (DFT) calculations, a smaller number of visible photoexcited electrons to EPR technique was recorded due to an electronic transition from ZnO CB to the empty,

localized, 4f levels of Ce^{4+} , that would be reduced to the paramagnetic species Ce^{3+} (not recorded) (Cerrato, 2018b).

- In the case of ZnO-Yb, a new crystalline phase formed (Yb_2O_3) was also detected, but it was lower and visible only by using a high-resolution TEM technique (Cerrato, 2020b) (Annex A, Figure A.3). Moreover, in the EPR spectra the amount of trapped electrons is higher than that of trapped holes (Cerrato, 2020a; 2020b) (Annex A, Figure A.5). In this case, the above-mentioned electron transfer is prevented because, unlike Ce, Yb has the 4f level fully occupied by electrons. A hypothetical working mechanism was suggested based on the hole transfer, from ZnO VB to Yb_2O_3 VB, improving charge carrier separation (Cerrato, 2020b).
- As regards ZnO-Fe, a new phase was not created and iron ions entered in the structure of ZnO. Charge carrier separation could be made possible considering the reactions R4.1-R4.4. The oxide CB has an energy close to the redox potential of the Fe^{3+}/Fe^{2+} pair and Fe^{3+} ion can be reduced to Fe^{2+} by the photogenerated electrons (Paganini, 2019):

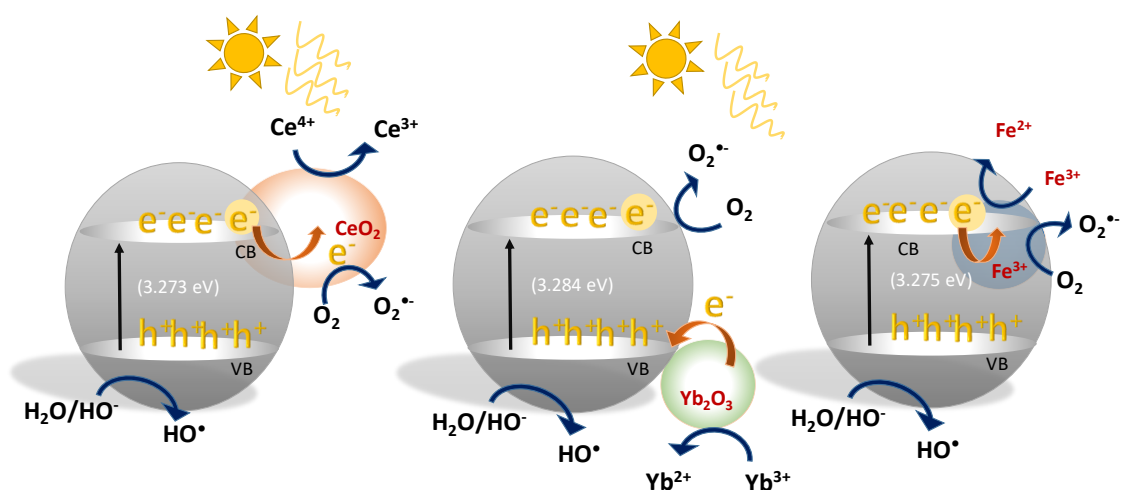


Figure 4.6. Schematic representation of ROS generation by the modified ZnO catalysts with Ce, Yb and Fe in water and irradiated by natural solar radiation.

This interpretation of the photocatalytic activity could help to explain the better kinetics results obtained by ZnO-Ce in comparison with the other modified materials. Nevertheless,

4. Solar heterogeneous photocatalysis

to proof the participation of HO^{*} in disinfection and decontamination of water by ZnO-Ce as the most promising material obtained, a radical scavenger's experiments using SMX as target reference was carried out. Figure 4.7 shows SMX degradation curves ($C_0=25$ mg/L) in MilliQ water under simulated sunlight (photolysis), in the presence of ZnO-Ce at 50 mg/L, with or without HO^{*} scavenger' species (MeOH and TBA at 0.1 M). SMX did not undergo photolysis under simulated sunlight and an enhancement of its degradation was achieved in the presence of ZnO-Ce, obtaining 70 % of removal after 30 minutes. On the other hand, in the presence of both MeOH and TBA, no removal of SMX was observed, demonstrating the participation of HO^{*} in the degradation of this compound. Therefore, it can be concluded that HO^{*} can be the responsible of bacteria inactivation and CECs degradation in the presence of ZnO-Ce and natural solar radiation.

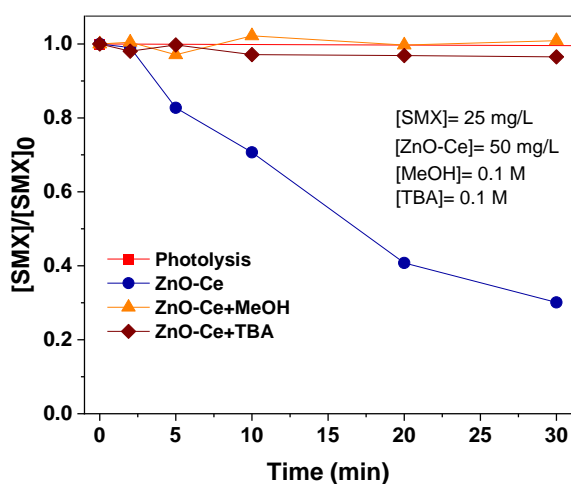


Figure 4.7. SMX degradation curves ($C_0=25$ mg/L) under simulated sunlight (photolysis), in the presence of ZnO-Ce at 50 mg/L, with or without MeOH and TBA at 0.1 M.

4.2. Proof-of principle in simulated urban wastewater

The photocatalytic performance under natural sunlight of all the modified ZnO photocatalysts was investigated in SUWW-1 to assess the effect of NOM (DOC content of ~ 20 mg/L). Bacteria inactivation and CECs degradation profiles in the presence of 100 and 500 mg/L of each photocatalyst, the benchmark TiO₂-P25 (at same concentrations) and the mere effect of solar radiation as references are shown in Figure 4.8 and 4.9, respectively.

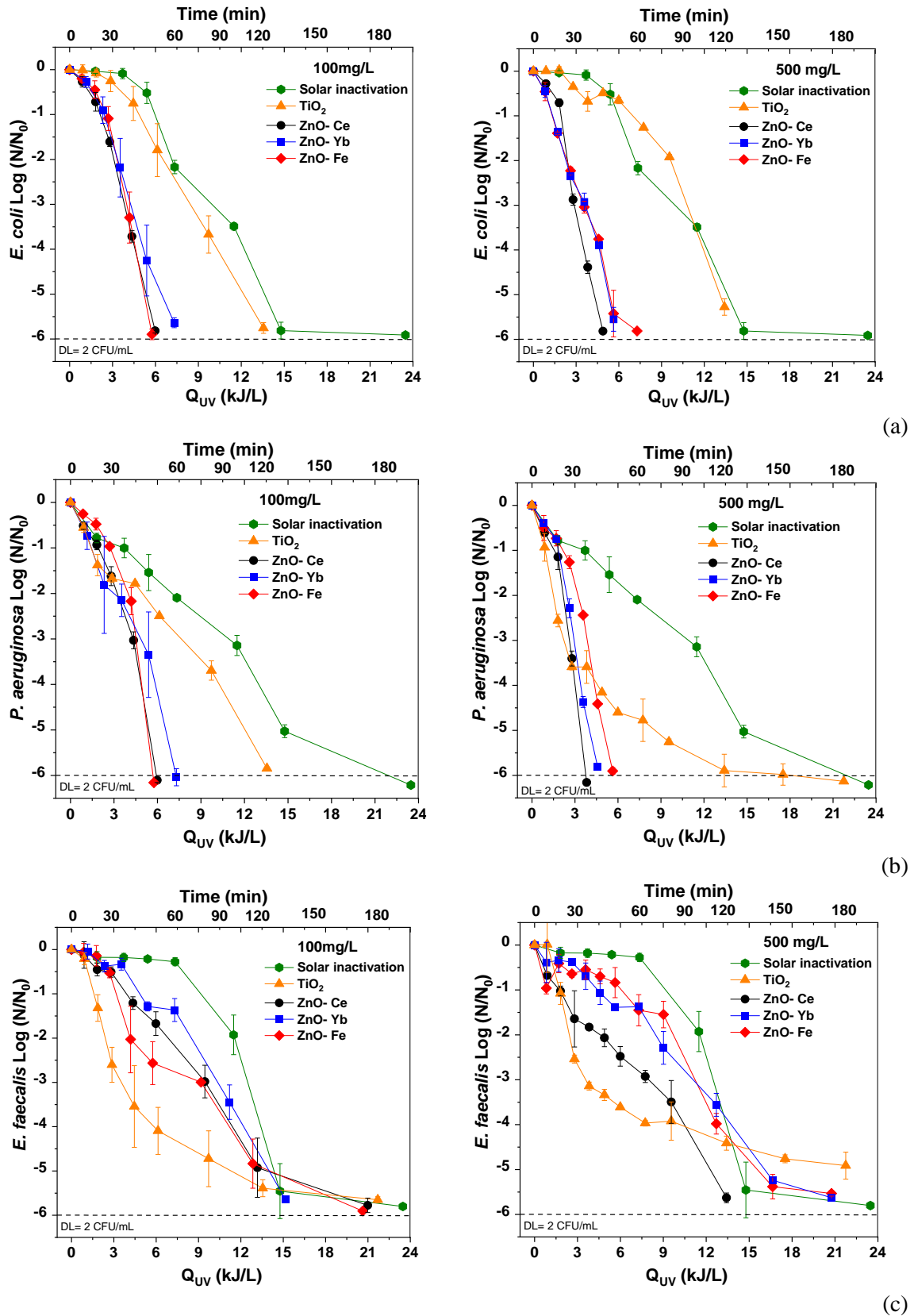


Figure 4.8. Inactivation profiles of *E. coli* (a), *P. aeruginosa* (b) and *E. faecalis* (c) in SUWW in the presence of modified ZnO with Ce, Fe and Yb and TiO_2 -P25 at 100 (left) and 500 mg/L (right).

4. Solar heterogeneous photocatalysis

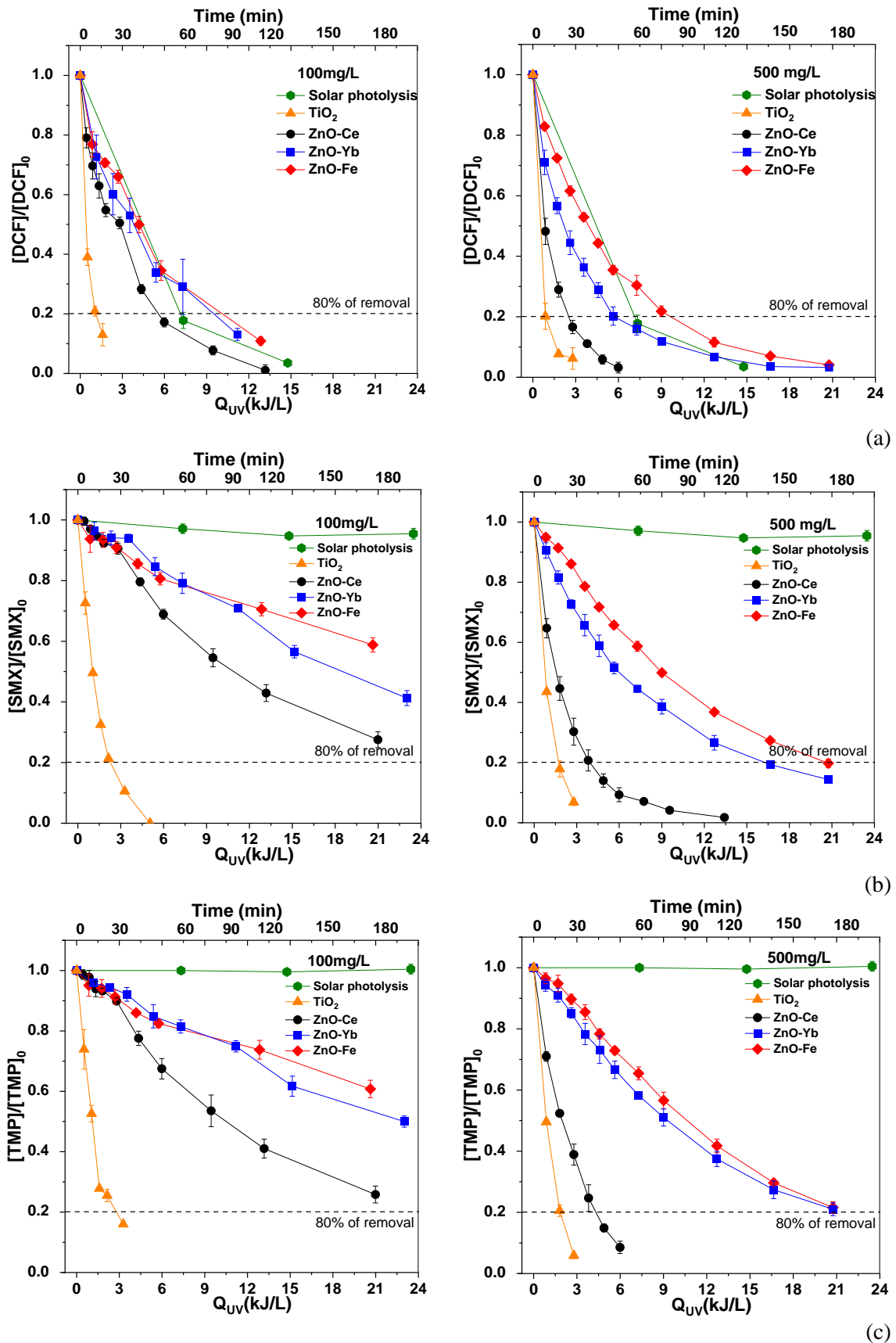


Figure 4.9. Degradation profiles of DCF (a), SMX (b) and TMP (c) in the presence of modified ZnO with Ce, Yb and Fe and TiO₂-P25 at concentration of 100 (left) and 500 mg/L (right) in SUWW under natural solar radiation.

The concentration of 100 mg/L was chosen as optimum for bacteria inactivation, while the higher value (500 mg/L) was considered as the best dosage for CECs degradation. The kinetics data from the analysis of these results are summarized in Table B.1 and B.2 and the corresponding pseudo first-order inactivation kinetic constants are shown in Figure 4.10. The DOC was measured for all solar test, and it remained almost constant at 20 mg/L along the treatment time.

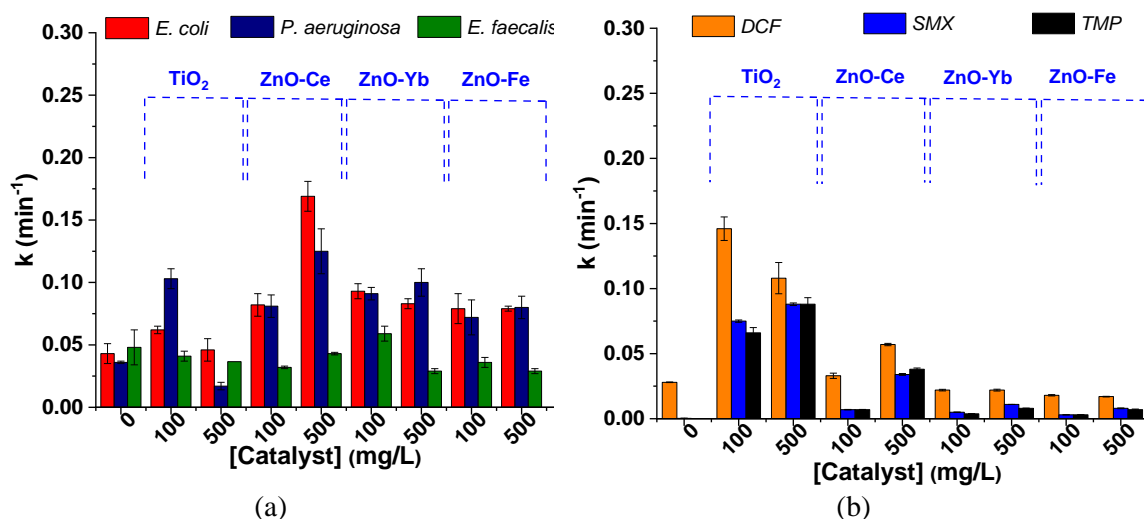


Figure 4.10. (a) Pseudo first-order inactivation kinetic constants of *E. coli*, *P. aeruginosa* and *E. faecalis* and (b) degradation constants of DCF, SMX and TMP in the presence of modified ZnO with Ce, Yb and Fe and TiO₂-P25 at concentration of 100 and 500 mg/L in SUWW under natural solar radiation.

The results obtained for modified ZnO materials in SUWW showed a similar trend that the observed for IW, i.e., the best disinfection and decontamination efficiency was also obtained with ZnO-Ce (at 500 mg/L of concentration), with similar bacteria and CECs reactivity order: *P. aeruginosa* \cong *E. coli* > *E. faecalis* and DCF > TMP > SMX. On the other hand, as expected, slower kinetics rates were obtained in comparison with IW and it could be attributed to the more physico-chemical complexity of SUWW. The DL (2 CFU/mL) in SUWW was obtained after 40, 50 and 120 minutes (3.8, 4.9 and 13.4 kJ/L) for *P. aeruginosa*, *E. coli* and *E. faecalis*, respectively, and 80 % removal of total CECs was attained after 37 minutes (3.6 kJ/L) of treatment time.

It is well-known that NOM and inorganic ions negatively affect photocatalytic performances (Rioja, 2016). The main effect of NOM could be summarized as follows: (i) it serves as nutrients for bacteria, helping to maintain their viability, (ii) it can absorb photons

4. Solar heterogeneous photocatalysis

competitively, (iii) it can act as scavengers of ROS, (iv) it can be absorbed on catalyst surface, inhibiting the material photoactivity.

Moreover, inorganic ions, such as $\text{HCO}_3^-/\text{CO}_3^{2-}$ and Cl^- negatively affect the performance of photocatalysis, due to HO^\bullet scavenger effect, and also water turbidity may hinder light transmission in the bulk of the solution (Tsydenova, 2015; Rioja, 2016).

Besides, it can be observed that decontamination kinetics are more influenced by the presence of NOM than the microbial inactivation kinetics. In fact, comparing the results of ZnO-Ce (500 mg/L) in IW and in SUWW, an average reduction of 92 % and 59 % in the efficiency was observed (kinetic constant 12 and 2 times lower in SUWW) for CECs and bacteria, respectively. Specifically, a reduction of 57 %, 59 % and 62 % was observed for *E. coli*, *E. faecalis* and *P. aeruginosa*, respectively, while 89 %, 93 % and 93 % for DCF, SMX and TMP, respectively.

These differences could be attributed to the different removal mechanisms already explained for both type of targets and their different physical phases, i.e, bacteria are suspended particles, while CECs are dissolved organic compound. In the case of bacteria, the adsorption of photocatalyst particles to the cell-wall membrane, with direct generation of radicals on the cell-wall surface, is an important way of inactivation (Blanco, 2007). Therefore, the HO^\bullet radical scavenging by inorganic compounds and by NOM could have less importance, due to the proximity of the radical species generated on the catalyst surface, and directly in contact with the bacteria cell-wall.

Nevertheless, CECs are in solution (and a low adsorption between the CECs investigated and the modified ZnO-Ce was already reported in control tests (Figure 4.1)) as well as the NOM and inorganic ions. Therefore, in this case, the generated radicals have to migrate from catalyst' surface to the solution to react with CECs, thus a higher competitive effect for radicals may occur due to the higher probability to be scavenged by NOM and inorganic ions than in the case of bacteria.

In comparison with the benchmark $\text{TiO}_2\text{-P25}$, the results revealed that it was the most efficient photocatalyst for the degradation of CECs, but it exhibited a lower efficiency toward disinfection. In fact, 80 % of total CECs was effectively removed after 17 minutes (1.6 kJ/L) (obtaining similar results with both, 100 and 500 mg/L), but 120 minutes (13.5 kJ/L) for *E. coli* and *P. aeruginosa* and 180 minutes for *E. faecalis* were necessary to reach DL at 500 mg/L.

As regards bacteria inactivation, the effect could be correlated with the PZC of the two catalysts. At the pH of SUWW (7.5-8), a favoured adsorption effect between the negatively charged bacteria occurs on the surface of the positively charged particle of ZnO-Ce (PZC around 8.6-8.9), compared to the repulsion effect with the negatively charged TiO₂ surface at this pH (PZC for TiO₂ is 6.2) (Chou, 2005).

The importance of a good adsorption and the effect of the PZC on disinfection performances has been outlined by Abbaszadegan et al. and by Marugán et al. (Abbas Abbaszadegan, 2014; Marugán, 2010). Abbaszadegan et al., investigated the influence of different surface charges of silver nanoparticles (positive, neutral, and negative) on their antibacterial effectiveness against a panel of human pathogens, including gram-positive (i.e., *Staphylococcus aureus*, *Streptococcus mutans*, and *Streptococcus pyogenes*) and gram-negative (i.e., *E. coli*) bacteria. These authors showed that positively-charged silver nanoparticles had the highest bactericidal activity against all microorganisms tested (Abbas Abbaszadegan, 2014). Marugán et al., reported TiO₂ disinfection rates significantly lower in the presence of Na₃PO₄ as a consequence of an increasing bacterial repulsion for PO₄³⁻ adsorption on the catalyst surface (Marugán, 2010). Finally, it can be highlighted that ZnO-Fe and Zn-Yb showed again lower removal rates in comparison with ZnO-Ce, and, therefore, only the latter one was selected as potentially the best photocatalyst for a further investigation in UWW.

4.3. Disinfection and decontamination of urban wastewater

The simultaneous disinfection and decontamination of actual UWW was assessed with ZnO-Ce in comparison with the benchmark TiO₂-P25 at 100 and 500 mg/L of photocatalyst concentration. Individual profiles of each natural occurring bacterium tested in UWW (*E. coli*, Total Coliforms, *Enterococcus* spp. and *Pseudomonas* spp. at the natural initial concentration (Table 3.5)) and of each spiked CEC (at 100 µg/L) are shown in Figure 4.11 and 4.12, respectively. Kinetic data analysis is summarized in Table B.1 and B.2 and plotted in Figure 4.13.

The DOC concentration (ca. 22 mg/L) along the treatment time remained constant in all cases, no exhibiting any significant differences.

4. Solar heterogeneous photocatalysis

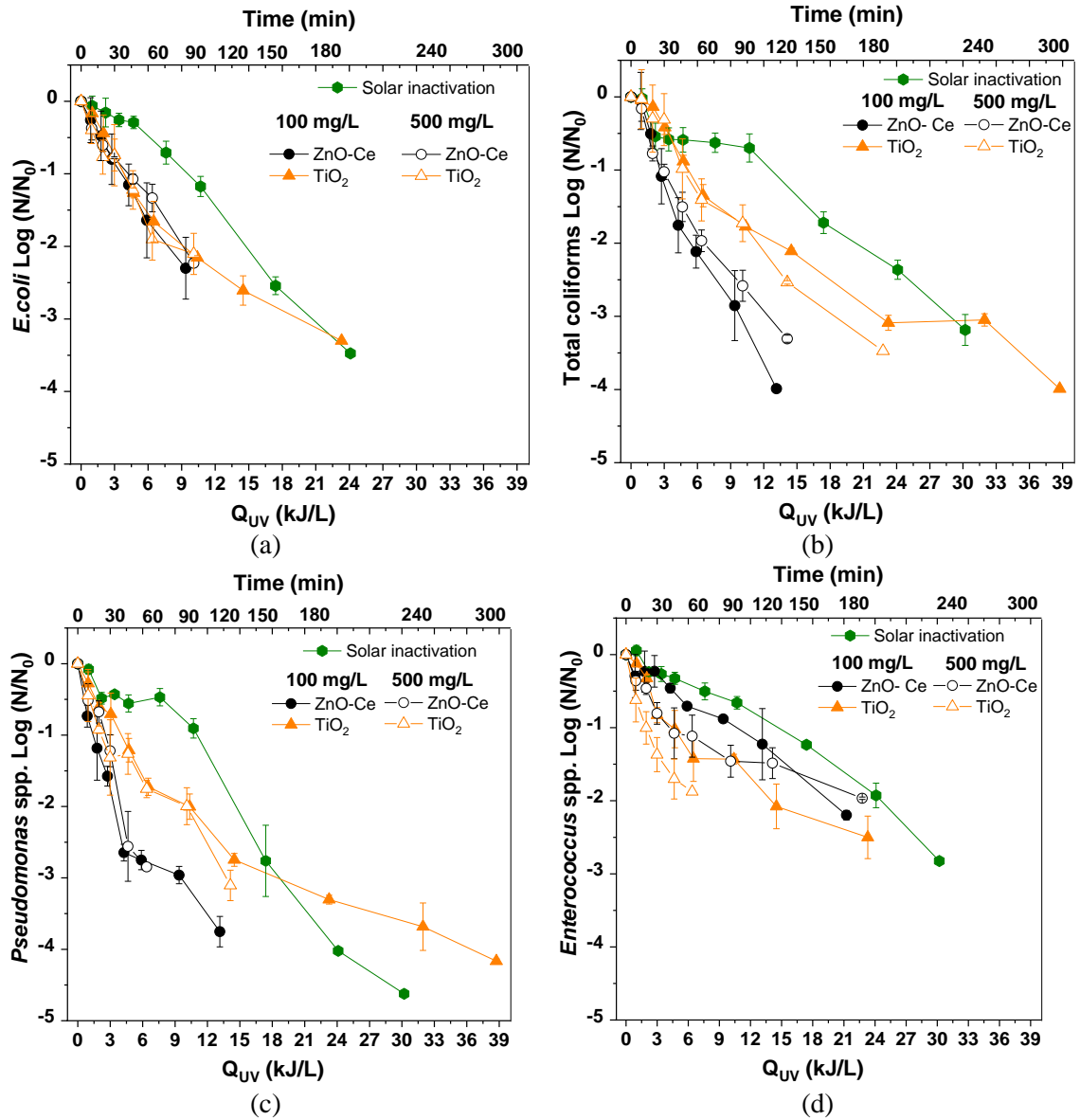


Figure 4.11. Inactivation profiles of *E. coli* (a), Total coliforms (b), *Pseudomonas* spp. (c) and *Enterococcus* spp. (d) in UWW in the presence of TiO₂-P25 and modified ZnO-Ce at 100 and 500 mg/L.

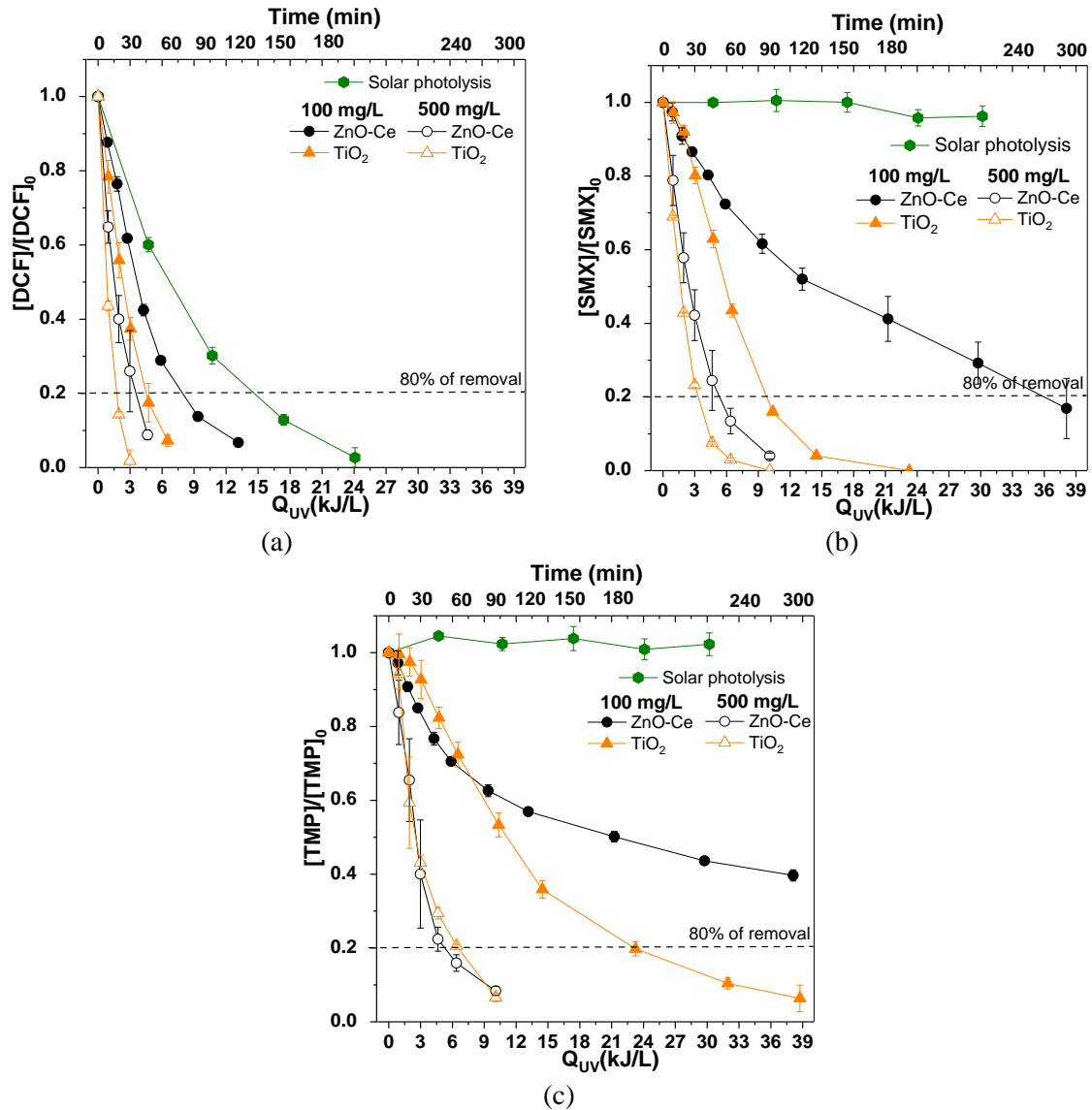


Figure 4.12. Degradation profiles of DCF (a), SMX (b) and TMP (c) in the presence of modified ZnO-Ce and TiO₂-P25 at concentration of 100 and 500 mg/L in UWW under natural solar radiation.

The best performance for the simultaneous water disinfection and decontamination was obtained at 500 mg/L for both catalysts, at which DL for the sum of all bacteria was attained after 120 minutes (14 kJ/L) and 80 % removal of total CECs after 45 minutes (4.4 kJ/L) and 37 minutes (3.4 kJ/L), for ZnO-Ce and TiO₂-P25, respectively. At lower catalyst dosage (100 mg/L) a difference in disinfection efficiency could be highlighted, obtaining higher kinetic rates in the presence of ZnO-Ce, while better decontamination performances were obtained with TiO₂, similarly to the previous results obtained for SUWW.

4. Solar heterogeneous photocatalysis

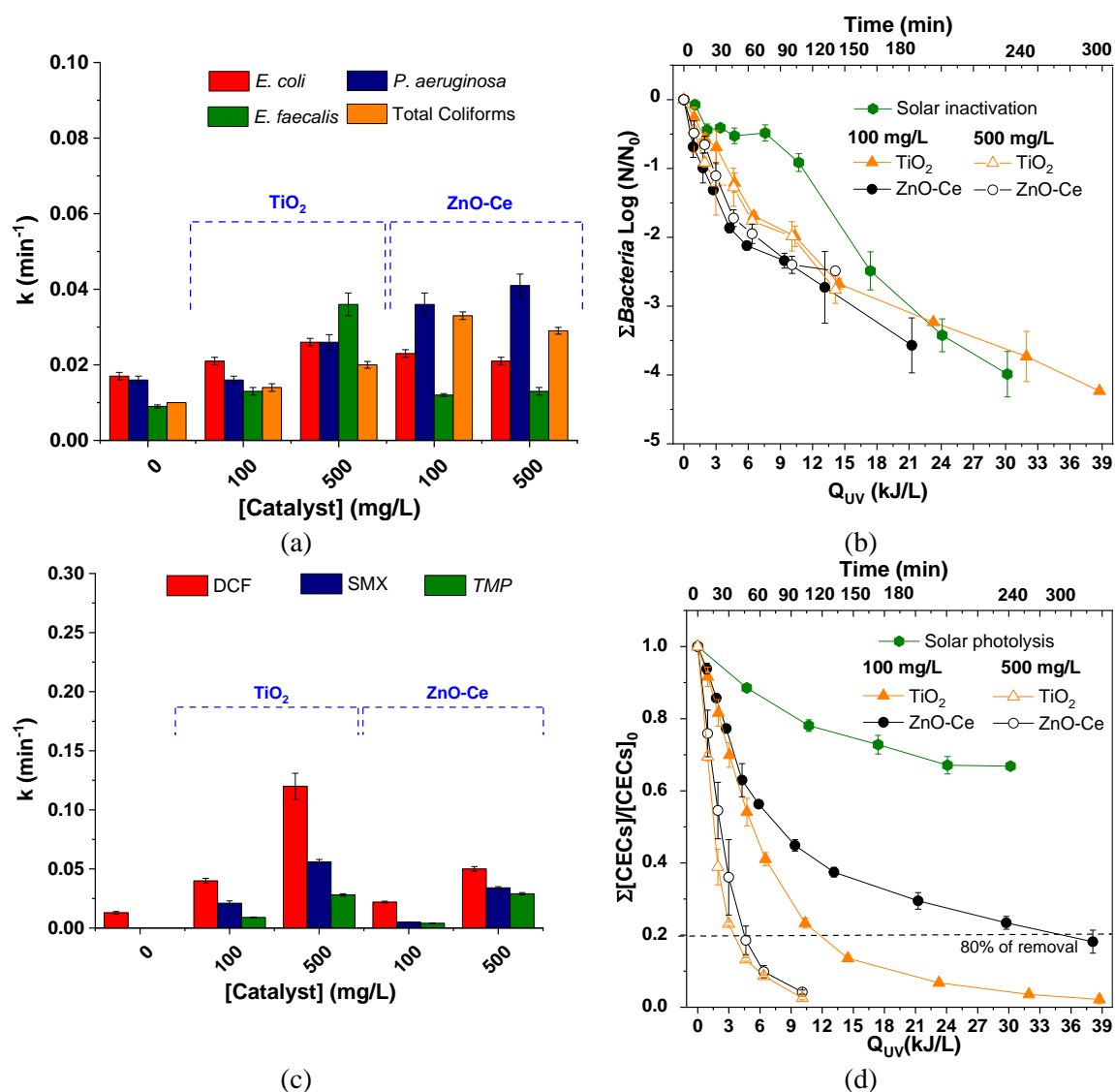


Figure 4.13. (a) Inactivation kinetic constants of UWW natural occurring *E. coli*, Total coliforms, *Enterococcus* spp., and *Pseudomonas* spp., (b) inactivation bacteria summation profiles, (c) degradation kinetic constants of DCF, SMX and TMP and (d) total CECs degradation curves in the presence of ZnO-Ce and TiO₂-P25 at concentration of 100 and 500 mg/L under natural solar radiation.

In UWW, lower reaction rates (three/four times lower than in SUWW) were obtained due to a more complex physicochemical and microbial scenario of UWW, with (i) different family of pathogens and chemical species simultaneously present, competing for catalyst active sites and reactive species, (ii) higher inorganic and organic matter complexity (with differences in humic-substances type), (iii) higher turbidity ((1.9 ± 0.1) NTU and (9.1 ± 9.3) NTU in SUWW and UWW, respectively) (Table 3.5, Chapter 3) and, (iv) higher resistance to inactivation of naturally occurring bacteria than commercial cultures (laboratory grown microorganisms (García-Fernández, 2015)).

On the other hand, it could be noted that ZnO-Ce is less influenced by complex matrix than TiO₂. Therefore, to analyse this difference, the ratio k_{UWW}/k_{SUWW} only for CECs removal was calculated and the results are shown in Figure 4.14. The same criterion was not applied for bacterial inactivation due to the potential significant different behaviour of culture (collection type-, analysed in SUWW) and naturally occurring bacterium (analysed in UWW) which could give uncertain and ambiguous conclusions.

A higher decrease in kinetic constants in UWW compared to SUWW was observed for TiO₂-P25. This effect could be related to its possible higher affinity towards NOM, compared to ZnO-Ce, that leads to a higher NOM adsorption on its surface. Consequently, the specific CECs removal could be limited due to the higher competition for the active sites between targets and NOM in the TiO₂ surface, in comparison with ZnO-Ce. However, further investigation is necessary to obtain experimental evidences on this matter.

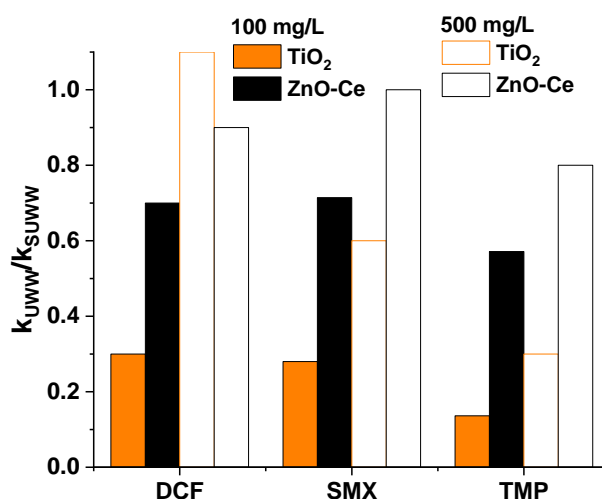


Figure 4.14. Ratio between kinetic constants in UWW and SUWW of DCF, SMX and TMP in the presence of ZnO-Ce and TiO₂-P25 at concentration of 100 and 500 mg/L.

The capability of the ZnO-Ce for wastewater disinfection and decontamination has been previously reported, but studying individually each target removal and using mainly lamps and simulated solar radiation. The inactivation of an isolated-UWW *E. coli* strain in IW under UV-A lamp (365 nm peak) with 100 mg/L was reported by Zammit et al, achieving the DL after 135 minutes and exceeding the efficiency of the standard TiO₂-P25 in the same conditions (Zammit, 2018). Higher removal efficiency of a cocktail of carbamazepine, atenolol, sulfamethoxazole, bisphenol A, diclofenac, ibuprofen and caffeine (at 2 mg/L of each) in MilliQ water and UWW was obtained for ZnO-Ce at 1 g/L, compared to TiO₂-P25 (Fabbri, 2019). Good performances for acesulfame K abatement by ZnO-Ce were obtained

4. Solar heterogeneous photocatalysis

also in the presence of organic matter, in a complex matrix such as river water, compared to ultrapure water, both under UV–vis and visible light (Calza, 2017).

Finally, the release of Zn^{2+} from ZnO particles could be a concern, leading to be a potential source of toxicity. Therefore, the concentration of dissolved Zn^{2+} was analyzed by ICP-MS (external services of the University of Almeria) from samples containing 500mg/L of ZnO- Ce under darkness and exposed to natural sunlight for 180 minutes, selected as the most stressful conditions for the catalyst stability investigated in this study. The concentration detected was 1.70 mg/L and 3.63 mg/L for dark and sunlight samples, respectively, while the concentration of cerium in solution was negligible.

The maximum permissible concentration of Zn^{2+} in potable water is 5 mg/L according to the drinking water guidelines established by WHO (WHO, 2011) and similar values are recommended by the U.S. EPA on National Secondary Drinking Water Regulations (USEPA, 2009). Therefore, the use of ZnO-Ce could not be considered a potential source of toxicity for human or environmental health, according to the Zn^{2+} release detected even at the higher and the optimal concentration obtained for the simultaneous disinfection and decontamination of UWW (500 mg/L).

However, focusing on the criteria established by the regulation (EU) 2020/741 for UWW reclamation, where only *E. coli* is established as microbial indicator and CEC removal are not included, the ZnO-Ce concentration exhibiting the best *E. coli* inactivation kinetics was 100 mg/L. Therefore, from this perspective, the use of a lower catalyst load will benefit the process allowing to reduce costs and the release of Zn^{2+} in solution.

4.4. Concluding remarks

The photoactivity of ZnO with Ce, Yb and Fe for water and wastewater treatment has been demonstrated against several waterborne pathogens and CECs by exciting the semiconductors with natural solar radiation, an economically and ecologically source of light.

Proof-in-principle in IW and SUWW have outlined that the most performing material for an overall application in UWW purification could be ZnO-Ce, while ZnO-Fe and ZnO-Yb were discarded due to their low efficiencies obtained in SUWW, in comparison with the benchmark TiO₂-P25.

Best results were obtained with ZnO-Ce at 500 mg/L, at which 80 % of the mixture of CECs was removed after 45 minutes (4.4 kJ/L of accumulated UV energy), obtaining similar

results with the benchmark TiO₂-P25. On the other hand, best inactivation kinetics of wild bacteria present in UWW was achieved with ZnO-Ce at 100 mg/L after 180 minutes (21 kJ/L of Q_{UV}), slightly better than the kinetics obtained for TiO₂-P25.

The mechanisms of bacteria inactivation and CECs degradation by ZnO-Ce was proved to be based on HO• generation, confirmed by EPR and scavengers' experiments. The release of Zn²⁺ during the irradiation time was below to the established in guidelines and regulation, excluding a toxic effect.

However, the up-scale of this photocatalytic material was not considered in this study due to: (i) the photocatalyst preparation effort (and further associated costs) and (ii) the no significant enhancement kinetics in comparison with the benchmark TiO₂-P25.

CHAPTER 5
ASSESSMENT OF
PEROXYMONOSULFATE AND SULFATE
RADICAL REACTIVITY

5. ASSESSMENT OF PEROXYMONOSULFATE AND SULFATE RADICAL REACTIVITY

This chapter looks at the reactivity of PMS and sulfate radical anion $\text{SO}_4^{\bullet-}$, being the main responsible of CECs degradation and bacterial inactivation in PMS-based water treatment systems. The studies were done in MilliQ water and following two different experimental approaches.

Firstly, the reactivity of PMS was evaluated using SMX as model substrate under dark, simulated solar light and UV-C radiation. The effect of several parameters on SMX removal was determined, evaluating different PMS concentrations, water pH, temperatures and presence of chloride and hydrogen carbonate ions. Moreover, proper reactive species scavengers, together with the recorded EPR spectra, allowed to give an insight into the radical species involved in SMX degradation. This study was entirely conducted during a secondment carried out for three months at Università di Torino, Italy.

Secondly, LFP technique was employed to assess $\text{SO}_4^{\bullet-}$ reaction mechanism operating in bacteria inactivation and in CECs degradation, evaluating its reactivity against cell-wall

5. PMS and sulfate radical reactivity

model compounds of gram-negative (*E. coli*) and gram-positive (*E. faecalis*) bacteria and CECs (DCF, SMX and TMP). This study was entirely conducted during another secondment carried out for three months at Universidad Politécnica de Valencia, Spain.

5.1 Peroxymonosulfate reactivity

5.1.1 Parameters affecting PMS reactivity under dark conditions

The potential activation of PMS alone by several chemical parameters and thermal effect was initially assessed in the dark. For this purpose, the reactivity of PMS with SMX ($1 \cdot 10^{-5}$ M initial concentration), as model of substrate, was assessed following the kinetic degradation of SMX under several operational conditions.

The influence of the following parameters was investigated: (i) PMS dosage (from $2.5 \cdot 10^{-4}$ - $2 \cdot 10^{-3}$ M), (ii) water T (from 20 to 70 °C), (iii) water pH (from 3 to 11) and (iv) the role of the inorganic ions (Cl^- and HCO_3^-).

(i) Role of PMS dosage: Figure 5.1a shows the SMX degradation profiles at room temperature in the presence of different initial PMS concentrations ($2.5 \cdot 10^{-4}$ - $2 \cdot 10^{-3}$ M), selected based on previous results (Yang, 2018; Yang, 2021). A significant degradation of SMX in the presence of PMS alone was observed, with degradation profiles following an exponential decay. A linear relationship between the pseudo first order reaction kinetics k_{obs} (min^{-1}) vs [PMS] (M) was observed, obtaining from the slope of the linear fit the second order kinetic constant value of $(0.096 \pm 0.005) \text{ M}^{-1} \text{ s}^{-1}$ for the reaction between SMX and PMS. According to these results, the PMS concentration chosen to investigate the other variables' effect was $1 \cdot 10^{-3}$ M.

(ii) Role of water T: Figure 5.1b shows SMX transformation rate in the presence of PMS ($1 \cdot 10^{-3}$ M), investigated in the water T range of 293-343 K (20-70 °C). In the absence of the oxidant and at the highest T (70 °C), SMX concentration showed a stable profile, indicating its non-thermal degradation. Nevertheless, an enhancement in SMX removal was obtained by increasing T in the presence of PMS. At the lowest T (20 °C) the observed initial reaction rate was $(6.0 \pm 0.3) \cdot 10^{-8} \text{ M min}^{-1}$ compared to $(5.0 \pm 0.2) \cdot 10^{-7} \text{ M min}^{-1}$ for the highest T (70 °C). To determine the activation energy of this process, the data were fitted through the Arrhenius equation (Eq. 5.1).

$$\ln(k_{obs}) = \ln A + \frac{E_a}{RT} \quad (\text{Eq. 5.1})$$

where k_{obs} is the observed kinetic constant of SMX at the temperature T (in K), $\ln A$ is the natural logarithm of the pre-exponential factor A , R is the molar gas constant (8.314 J/K·mol) and E_a is the activation energy of the reaction between SMX and PMS.

A linear relationship was observed plotting $\ln(k_{obs})$ as a function of $1/T$ (Arrhenius plot) and from the slope of the linear fitting an activation energy equal to 36.0 ± 1.6 kJ/mol was estimated. Therefore, these results demonstrated that PMS even under dark conditions is an efficient oxidant for the direct or mediated removal of SMX. Moreover, thermal effects should be considered as an important key parameter on PMS performance for water purification, carried out under strong natural sunlight incidence, due to the increase of T via infrared wavelengths.

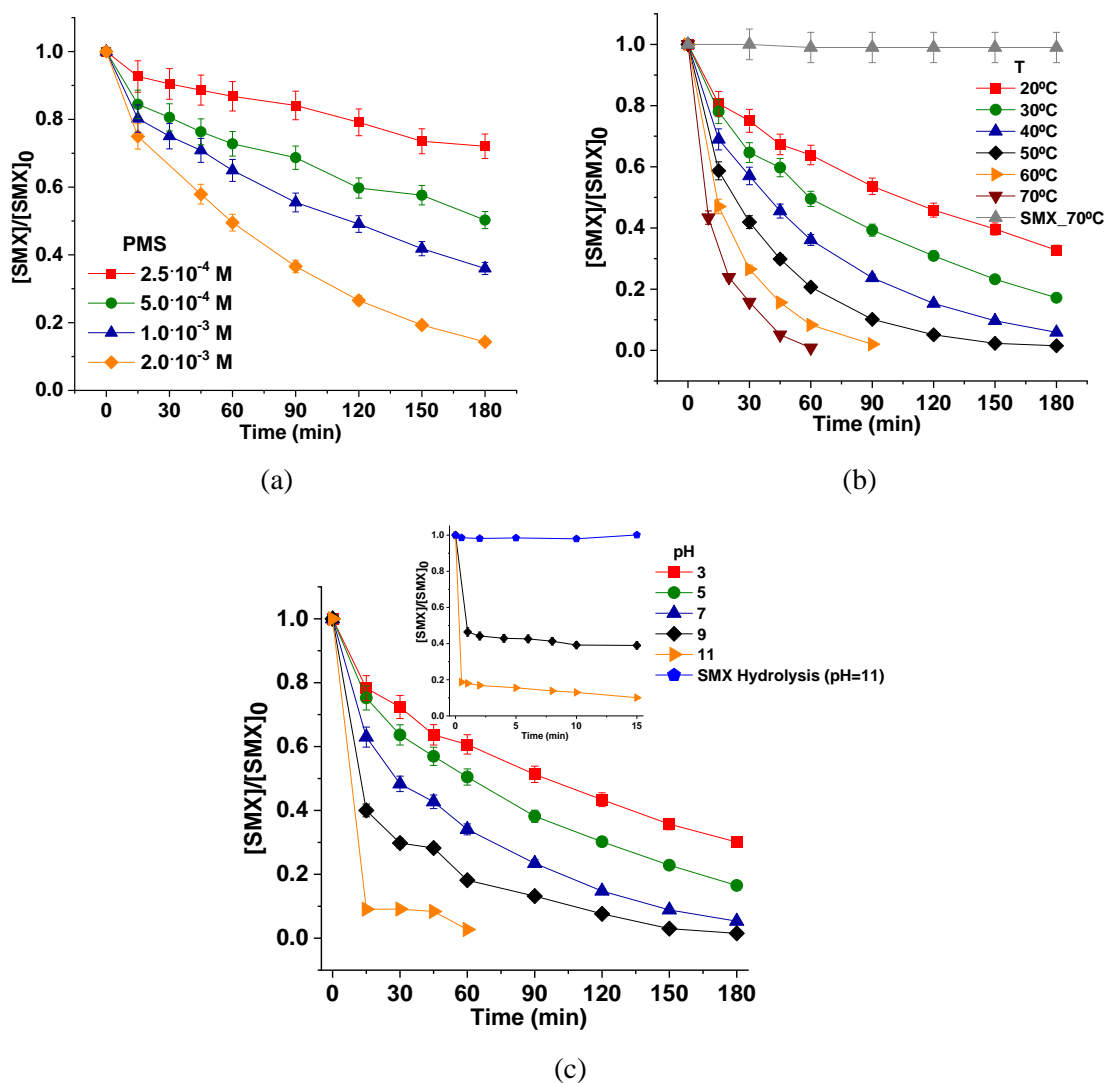


Figure 5.1: SMX ($C_0 = 1 \cdot 10^{-5}$ M) degradation profiles under dark conditions in the presence of different (a) concentration of PMS, (b) T and (c) pH.

5. PMS and sulfate radical reactivity

(iii) Role of water pH: This parameter strongly affects SMX and PMS speciation in water as it is shown in Figure 5.2.

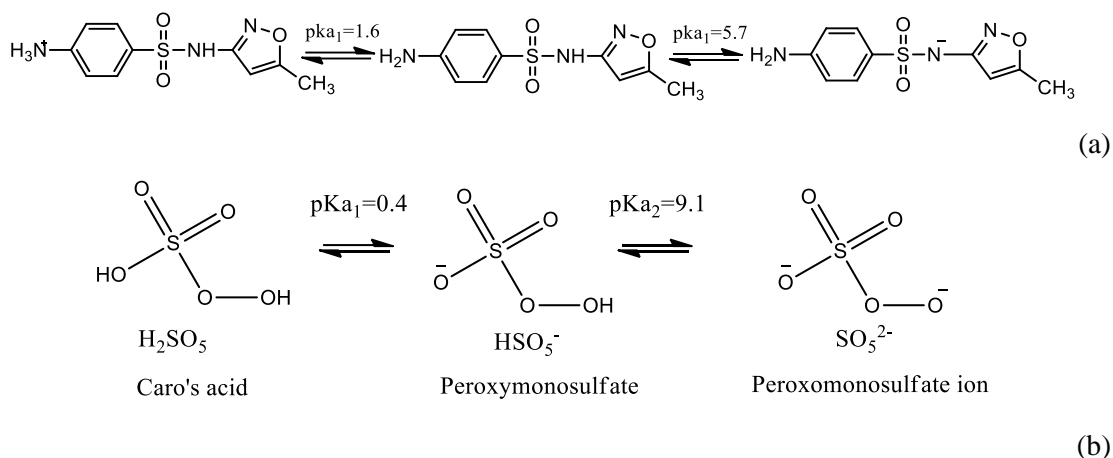
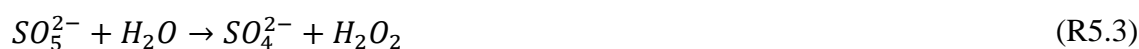


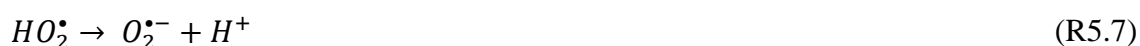
Figure 5.2: Acid-base speciation for SMX (a) and for PMS (b).

Therefore, the effect of pH on SMX degradation was evaluated using phosphate buffer solutions adjusting the pH to values ranging from 3 to 11 and in the presence of PMS ($1 \cdot 10^{-3}$ M). In addition, SMX hydrolysis at pH 11 and in the absence of oxidant was also investigated. Results obtained (Figure 5.1c) demonstrated a no significant degradation without oxidant, while removal rates increased by increasing pH in the presence of PMS. At acidic and neutral pH (3, 5 and 7) a single exponential decay was observed, while at basic pH (9 and 11), a double kinetics was obtained with a sharp decrease of SMX concentration immediately after oxidant addition (Figure 5.1c), followed by a progressive exponential decay up to the total degradation.

The faster kinetics at basic pH could be related to:

- *Production of highly reactive species* (HO[•] and ¹O₂): alkaline activation of PMS has been reported to be an effective way for the degradation of organic contaminants, leading mainly to the formation of singlet oxygen (¹O₂) and HO[•] in solution, according to R5.1-5.9 (Xia, 2020).





Moreover, PMS self-decomposes spontaneously in water, especially at slightly alkaline pH, to form 1O_2 , according to reaction R5.10 (Wang, 2018).



- *Acid-basic speciation*: SMX mono-anionic specie (that prevails at $pH > 5.7$) reacts faster than the neutral and cationic ones (that prevails at $pH < 1.6$) with both HO^\bullet and 1O_2 , as it can be observed in Table 5.1. PMS at $pH < 9.4$ is in its mono-anion form (HSO_5^-), while for higher pH values the dianion form (SO_5^{2-}) prevails, with lower oxidant capacity.

Table 5.1. Second order kinetic constants for the reaction with OH^\bullet and 1O_2 with the different SMX species at different pH (Ge, 2019).

Species	$k_{OH,SMX}, M^{-1} s^{-1}$	$k_{1O_2,SMX}, M^{-1} s^{-1}$
SMX ⁺	$8.2 \cdot 10^8$	$9.16 \cdot 10^7$
SMX	$6.66 \cdot 10^9$	$4.18 \cdot 10^6$
SMX ⁻	$6.58 \cdot 10^9$	$1.92 \cdot 10^9$
pH	$k_{OH,SMX}, M^{-1} s^{-1}$	$k_{1O_2,SMX}, M^{-1} s^{-1}$
2	$3.74 \cdot 10^9$	$2.91 \cdot 10^7$
5	$6.50 \cdot 10^9$	$2.52 \cdot 10^7$
8	$6.50 \cdot 10^9$	$1.9 \cdot 10^8$

(iv) *Role of inorganic ions*: The effect of different concentrations of commonly inorganic ions (Cl^- and HCO_3^-) on the degradation of SMX ($C_0 = 1 \cdot 10^{-5}$ M) was also investigated to give insights into the operative transformation mechanism activated in the dark by PMS and to highlight the possible interferences of these species in a real treatment scenario.

Figure 5.3a shows SMX profiles in the presence of increasing amount of sodium chloride (from 0 to $1.5 \cdot 10^{-1}$ M) and a positive effect on SMX removal was observed with the increment of the Cl^- concentration. PMS is capable to oxidize Cl^- , promoting the generation of active chlorine and in particular $Cl_2/HClO$ (R5.15-5.16) (Ding, 2020), while the formation radical $Cl_2^{\bullet-}$ is not possible from a thermodynamic point of view, due to the higher redox potential ($E^\circ = 2.09$ V vs NHE), compared to PMS one.

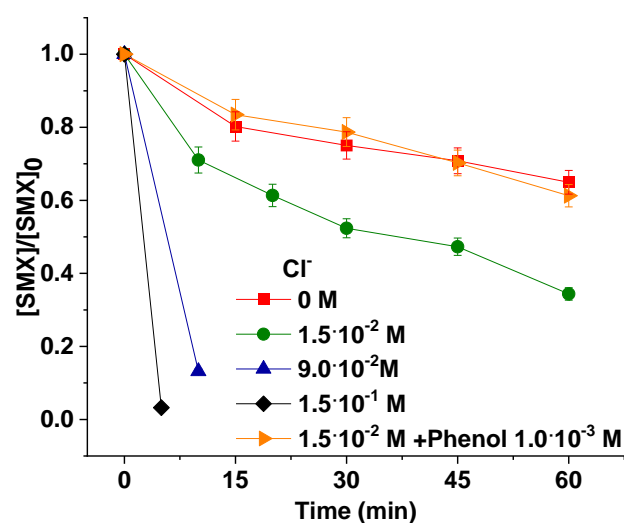
5. PMS and sulfate radical reactivity



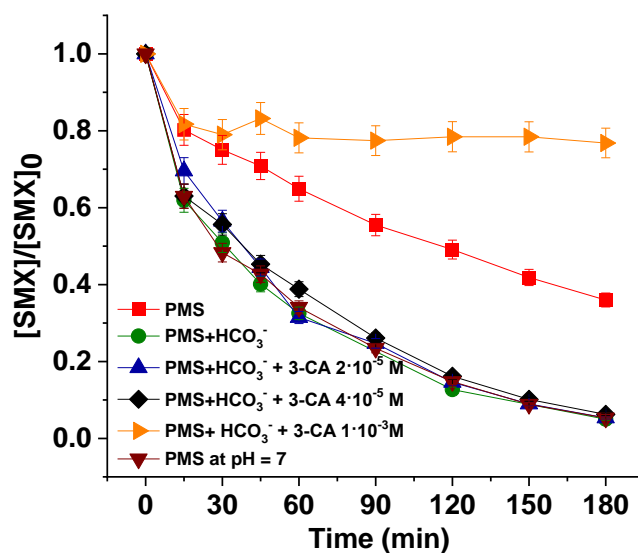
Previous studies in literature have also reported about the effect of adding Cl^- with opposite conclusions. Zhou et al. observed an accelerated degradation of steroid estrogens in the presence of both Br^- and Cl^- (at environmentally relevant concentrations) with the formation of halogenated aromatic products (Zhou, 2018); while Nihemaiti et al. did not observe any effect on the degradation of ciprofloxacin with Cl^- ($5 \cdot 10^{-3}$ M) at pH 8.2 using borate buffer (Nihemaiti, 2020). This agrees with the lower oxidative properties of the hypochlorite ion (R5.13) with respect to the hypochlorous acid ($\text{pK}_a = 7.52$) (Harris, 2010).

In addition, to have a proof of active chlorine generation, experiments were performed in the presence of phenol, considered an effective scavenger of these species, being easily monoelectronically oxidized by HClO (especially at acidic pH) (Acero, 2005). Results in Figure 5.3a showed that the addition of phenol ($1 \cdot 10^{-3}$ M) in the presence of chloride ($1.5 \cdot 10^{-2}$ M) led to a significant decrease in SMX degradation rate (around 3 times lower, with rates of $(7.0 \pm 0.2) \cdot 10^{-8}$ M min^{-1} and $(2.2 \pm 0.2) \cdot 10^{-7}$ M min^{-1} in the presence and absence of phenol, respectively), attributed to the scavenging effect of chlorine species. Therefore, it can be assumed that the main mechanism of compounds degradation in the presence of PMS (at acid pH) and chloride is the bi-electronic oxidation of Cl^- with formation of Cl_2/HClO by PMS; while at basic pH, the same mechanism could be silent.

On the other hand, the effect of HCO_3^- on the transformation rate of SMX ($C_0 = 1 \cdot 10^{-5}$ M) in the presence and absence of PMS ($1 \cdot 10^{-3}$ M) was also investigated. Results reported in Figure 5.3b revealed that the addition of HCO_3^- ($4 \cdot 10^{-3}$ M) increased the reaction rate 3-times with respect to the experiment with PMS alone, suggesting two possible effects in which HCO_3^- could act in the system: (i) as source of carbonate radical $\text{CO}_3^{\bullet-}$ or (ii) as pH modifier.



(a)



(b)

Figure 5.3: SMX ($C_0 = 1 \cdot 10^{-5}$ M) degradation profiles under dark conditions in the presence of different concentration of (a) Cl^- and Cl^- in the presence of phenol ($1 \cdot 10^{-3}$ M) and (b) HCO_3^- $4 \cdot 10^{-3}$ M, adding different concentrations of 3-Chloroaniline ($2 \cdot 10^{-5}$, $4 \cdot 10^{-5}$ and $1 \cdot 10^{-3}$ M), and in the presence of PMS alone $1 \cdot 10^{-3}$ M in milliQ water at pH 3 and at pH 7 for phosphate buffer.

The second order kinetic constant for the reaction between $\text{CO}_3^{\bullet-}$ and 3-chloroaniline has not been reported yet, but the value $4.3 \cdot 10^8 \text{ M}^{-1} \text{ s}^{-1}$ was measured for the reaction between $\text{CO}_3^{\bullet-}$ and 4-chloroaniline (Neta, 1979; Wojnárovits, 2020). SMX is quite easily oxidized by $\text{CO}_3^{\bullet-}$ with a kinetic constant equal to $2.68 \cdot 10^8 \text{ M}^{-1} \text{ s}^{-1}$ (Zhang, 2015). In this light, if the $\text{CO}_3^{\bullet-}$ was formed, it would oxidize easily both SMX and 3-chloroaniline, with a branching ratio for the reaction with 3-chloroaniline and SMX equal to $\alpha = k_{\text{CO}_3^{\bullet-}, 3\text{-chloroaniline}} / k_{\text{CO}_3^{\bullet-}, \text{SMX}} \approx 1.5$ if 3-CA and SMX were at the same concentration, leading to a suppression of SMX degradation rate, due to the reaction between $\text{CO}_3^{\bullet-}$ and 3-CA.

5. PMS and sulfate radical reactivity

The results obtained suggested that an active role of this radical specie can be ruled out, according to the observing small decrease in the SMX removal rate (Figure 5.3b). A significant decrease in the SMX degradation rate in the presence of 3-chloroaniline ($1 \cdot 10^{-3}$ M) could be related not to a scavenger effect of the aniline towards $\text{CO}_3^{\bullet-}$, but toward PMS, that at this concentration reacted mainly with 3-CA than with SMX.

On the other hand, the increment of SMX reaction rate in the presence of HCO_3^- was explained by the effect of pH increase to 7.

In MilliQ water, the oxidant addition caused a drop of pH to 3, due to the composition of the triple potassium salt OXONE® ($\text{HSO}_5^-:\text{HSO}_4^-:\text{SO}_4^{2-}=2:1:1$), leading to the simultaneous release of the weak acid HSO_4^- ($\text{pK}_a=2$) (Lide, 2004), while by adding HCO_3^- water pH increased to pH 7.

Therefore, to evaluate the effect of HCO_3^- as pH modifier, experiments were conducted in the absence of HCO_3^- in phosphate buffer (total concentration = $4.4 \cdot 10^{-3}$ M).

Similar SMX degradation profiles were obtained, comparing the experiments with $4 \cdot 10^{-3}$ M of HCO_3^- in MilliQ water (alone or with 3-chloroaniline $2 \cdot 10^{-5}$ or $4 \cdot 10^{-5}$ M) and in phosphate buffer (in the absence of HCO_3^-), highlighting an important effect of pH on the reaction rate increase.

Therefore, the role of the $\text{CO}_3^{\bullet-}$ for SMX degradation could be excluded, mainly because in the dark there was no evidence of the formation of this specie.

5.1.2. Reactive Oxygen Species determination by scavenger experiments

Several radical scavengers' species (Q) were used for the identification of the potential ROS involved in the PMS reactivity processes in the dark, under light irradiation by artificial solar radiation (39.3 ± 0.8 W/m²) and UV-C radiation (4 W/m²). The scavengers used and their corresponding second-order kinetic constant $k_{ROS,Q}$ (M⁻¹ s⁻¹) against specific ROS are summarized in Table 5.2. Quenching experiments with TBA and MeOH were performed in order to highlight the specific contributions of HO^{\bullet} and $\text{SO}_4^{\bullet-}$ radicals. TBA is an efficient scavenger toward HO^{\bullet} (reacting with $\text{HO}^{\bullet} \approx 700$ times higher than with $\text{SO}_4^{\bullet-}$, $k_{\text{SO}_4^{\bullet-},\text{TBA}} 8.4 \cdot 10^5$ M⁻¹ s⁻¹); while MeOH is effective toward both radicals ($\text{SO}_4^{\bullet-}$ and HO^{\bullet}). FFA is usually applied as scavengers of $^1\text{O}_2$ and azide ions N_3^- could directly react with PMS by donating an electron.

Table 5.2. Radicals, quenching agent and corresponding $k_{ROS,Q}$ ($M^{-1} s^{-1}$) (Acero, 2005; Neta, 1988; Appiani, 2017).

Reactive Oxygen Species (ROS)	Radical scavenger specie Q	$k_{ROS,Q}$ ($M^{-1} s^{-1}$)
$SO_4^{\cdot-}$	MeOH	$1 \cdot 10^7$
HO^{\cdot}	MeOH	$9.7 \cdot 10^8$
	TB)	$6 \cdot 10^8$
HClO	Phenol	$3.0 \cdot 10^4$
$HCO_3^-/CO_3^{\cdot-}$	4-chloroaniline	$4.8 \cdot 10^8$
1O_2	FFA	$1.0 \cdot 10^8$
PMS	NaN_3	-

5.1.2.1 Reactive species under dark condition

Figure 5.4a shows SMX degradation in the presence of PMS ($1 \cdot 10^{-3}$ M) in the dark without scavengers and in the presence of MeOH (1 M), TBA (1 M), NaN_3 ($1.5 \cdot 10^{-2}$ M) and FFA ($1 \cdot 10^{-5}$ M) as scavengers.

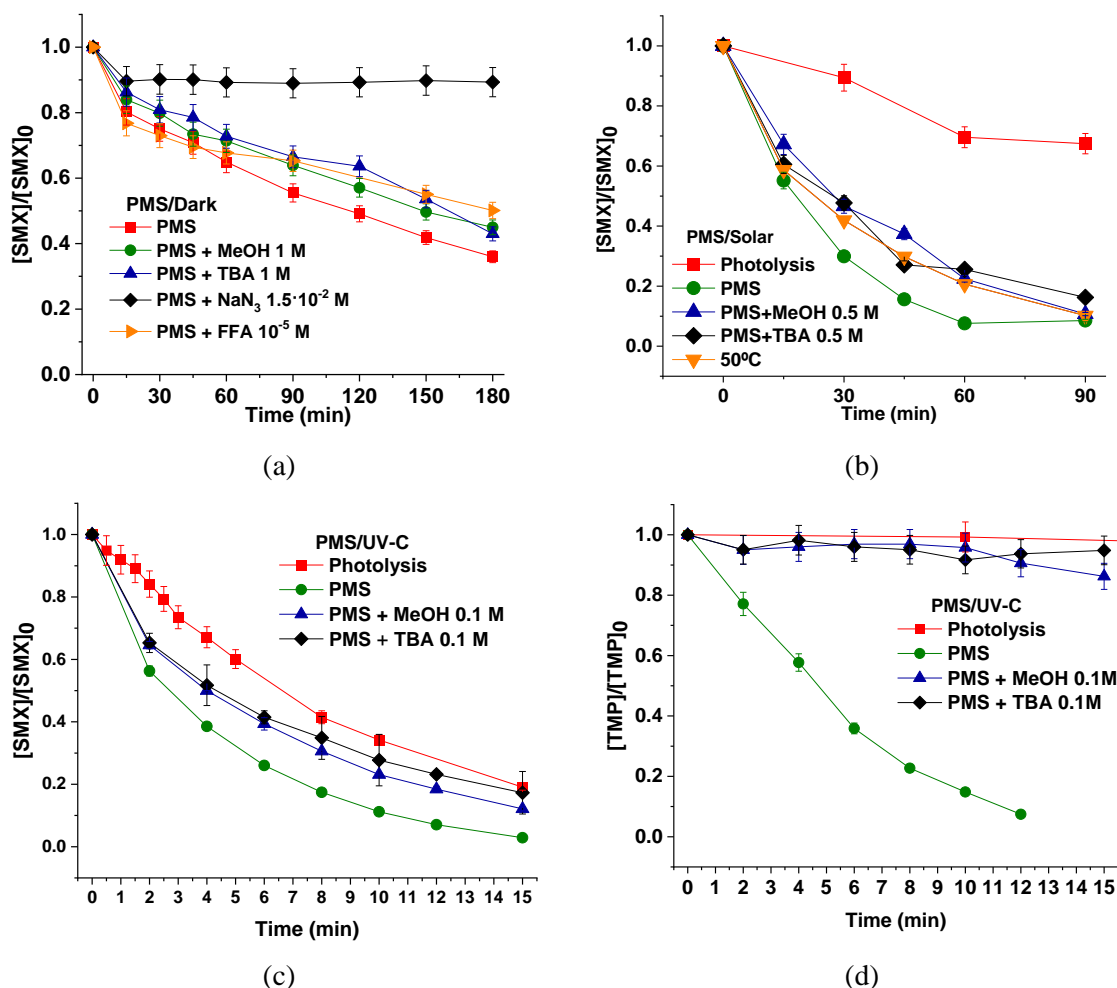
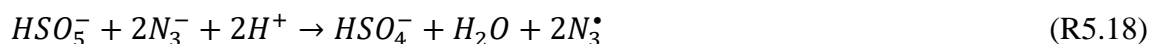


Figure 5.4. SMX degradation profiles in the presence of PMS $1 \cdot 10^{-3}$ M (a) under dark condition and (i) without scavengers, (ii) with MeOH 1 M, (iii) with TBA 1 M, (iv) NaN_3 $1.5 \cdot 10^{-2}$ M and (v) FFA $1 \cdot 10^{-5}$ M; (b) under simulated solar radiation (280 nm filter) and (i) without scavengers, (ii) with MeOH 0.5 M, (iii) with TBA 0.5 M and at 50°C under dark conditions and SMX (c) and TMP (d) degradation profiles under UV-C light in the presence PMS $3 \cdot 10^{-3}$ M and MeOH 0.1 M or TBA 0.1 M.

5. PMS and sulfate radical reactivity

Results shows that the addition of MeOH, TBA and FFA scarcely affected SMX degradation, excluding therefore the role of HO[•], ¹O₂ or SO₄^{•-} in the target oxidation. On the other hand, the addition of sodium azide (NaN₃) completely quenched SMX degradation, due to PMS consumption, that directly oxidized N₃⁻ according to the following reaction (R 5.18):



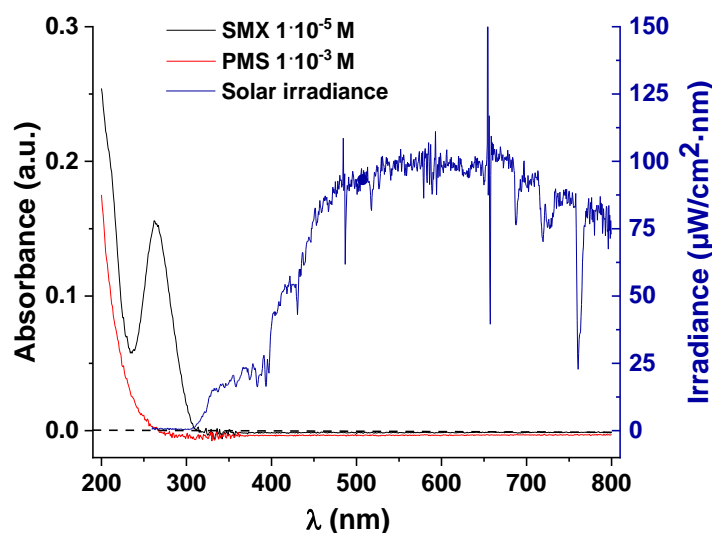
5.1.2.2 Reactive species under simulated solar radiation

SMX degradation was carried out in the absence of PMS (photolysis), and with PMS in the presence and absence of MeOH and TBA. Maximum temperature recorded during experiments involving simulated solar radiation was 50 °C. Figure 5.4b shows an enhancement on SMX degradation rate by combining PMS (1·10⁻³ M) and simulated solar radiation, obtaining 90 % of removal after 90 minutes, compared to photolysis that led only a 25 % of degradation.

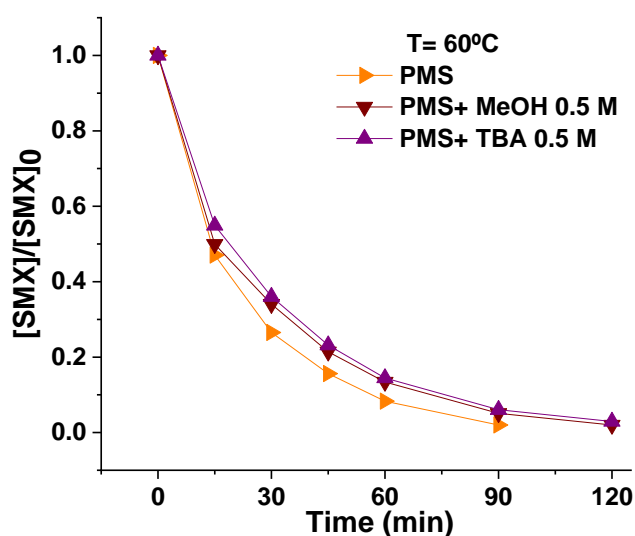
The addition of MeOH and TBA as scavengers showed only a very slight inhibition, suggesting that under simulated solar radiation neither HO[•] nor SO₄^{•-} radicals were the main responsible of SMX oxidation. PMS direct oxidation of SMX under sunlight could be enhanced due to an increase of T, as it can be highlighted observing the similar degradation profiles obtained under simulated solar radiation and under dark conditions at 50 °C (Figure 5.4b).

In addition to these results, the absence of HO[•] and SO₄^{•-} radical's generation by PMS under the mere effect of solar radiation wavelengths could be also explained by:

- The absence of overlap between the solar emission spectrum and the absorption spectrum of PMS, preventing the occurrence of a photo-chemical reaction with peroxy-bond O-O break (Figure 5.5a).
- The absence of a quenching effect by MeOH and TBA under dark conditions and at 60 °C, being this temperature not enough to promote the peroxy-bond break (Figure 5.5b), and not being typical water T reached in solar photochemical or photocatalytic water treatments (T < 50 °C).



(a)



(b)

Figure 5.5. (a) Absorption spectra of SMX $1 \cdot 10^{-5}$ M and PMS $1 \cdot 10^{-3}$ M on an optical length ($b=1\text{cm}$) and solar emission spectrum at ground level (measured at CIEMAT-PSA facilities) and (b) SMX degradation profiles in the presence of PMS $1 \cdot 10^{-3}$ M in dark at 60°C and with and without MeOH and TBA 0.5 M as radical's scavengers.

5.1.2.3 Reactive species under UV-C radiation

SMX degradation was finally also evaluated under UV-C radiation (254 nm), a source of photons capable to break the peroxy-bond of PMS, generating $\text{SO}_4^{\cdot-}$ and HO^\cdot radicals. The degradation rate was assessed in the absence and in the presence of PMS ($3 \cdot 10^{-3}$ M), with or without MeOH or TBA. Figure 5.4c shows that the removal of SMX was strongly affected by the mere effect of UV-C wavelengths, almost complete disappearance in the first 15 minutes was observed in the presence of the oxidant and the degradation rate decreased in the presence of both scavenger's species, i.e., MeOH and TBA.

5. PMS and sulfate radical reactivity

Based on the quick effect of the UV-C photolysis of SMX, similar experiments were therefore conducted with a substrate less prone to direct photolysis, such as TMP (Figure 5.4d). Photolysis was negligible in this case, the addition of PMS led to TMP degradation in a few minutes and the addition of scavengers largely quenched target degradation, highlighting the strong role played by $\text{SO}_4^{\bullet-}$ and HO^{\bullet} during the TMP degradation.

Table 5.3 summarizes the measured first order kinetic constants (min^{-1}) for the different processes.

Table 5.3. Experimentally measured first order kinetic constants.

Scavenger	SMX			
	k (min^{-1}) R^2	k (min^{-1}) R^2	k (min^{-1}) R^2	k (min^{-1}) R^2
	PMS/Dark	PMS/Dark/60 °C	PMS/Solar	PMS/UV-C
-	$0.006 \pm 3 \cdot 10^{-4}$ 0.983	$0.043 \pm 6 \cdot 10^{-4}$ 0.999	$0.034 \pm 3 \cdot 10^{-3}$ 0.947	$0.237 \pm 5 \cdot 10^{-3}$ 0.994
MeOH	$0.005 \pm 2 \cdot 10^{-4}$ 0.981	$0.033 \pm 6 \cdot 10^{-4}$ 0.998	$0.025 \pm 5 \cdot 10^{-4}$ 0.998	$0.144 \pm 4 \cdot 10^{-3}$ 0.995
TBA	$0.005 \pm 2 \cdot 10^{-4}$ 0.982	$0.031 \pm 6 \cdot 10^{-4}$ 0.997	0.017 ± 0.001 0.968	$0.125 \pm 5 \cdot 10^{-3}$ 0.990
NaN_3	NA	-	-	-
FFA	$0.004 \pm 5 \cdot 10^{-4}$ 0.898	-	-	-

5.1.3. Electron paramagnetic resonance detection

EPR spectra were also recorded in this study to further clarify the reactive species involved in reactivity of PMS. DMPO was used to reveal the presence of HO^{\bullet} , obtaining the typical 1:2:2:1 spectrum of DMPO-OH $^{\bullet}$, and $\text{SO}_4^{\bullet-}$ with the formation of DMPO- $\text{SO}_4^{\bullet-}$ (Figure 5.6a). TEMP was used to detect the presence of $^1\text{O}_2$ after the formation of 2,2,6,6-tetramethyl-4-piperidone-N-oxyl (TEMPO), which could be detected by EPR spectroscopy with an intensive 1:1:1 signal (Figure 5.6b).

PMS concentration used for all spectra analysis was $3 \cdot 10^{-3}$ M, while the spin trap (DMPO or TEMP) was added to the sample before irradiating at a concentration of $1.7 \cdot 10^{-2}$ M.

Under dark conditions, the EPR spectra obtained by PMS alone at pH 3 (Figure 5.7a) with DMPO revealed the absence of DMPO-OH $^{\bullet}$ and DMPO- $\text{SO}_4^{\bullet-}$, confirming the exclusion of an active role of HO^{\bullet} or $\text{SO}_4^{\bullet-}$ in the target oxidation. On the other hand, at pH 11 (Figure 5.7b), the presence of HO^{\bullet} was detected, in line with the reactions reported above (R5.1-5.9) during PMS alkaline activation.

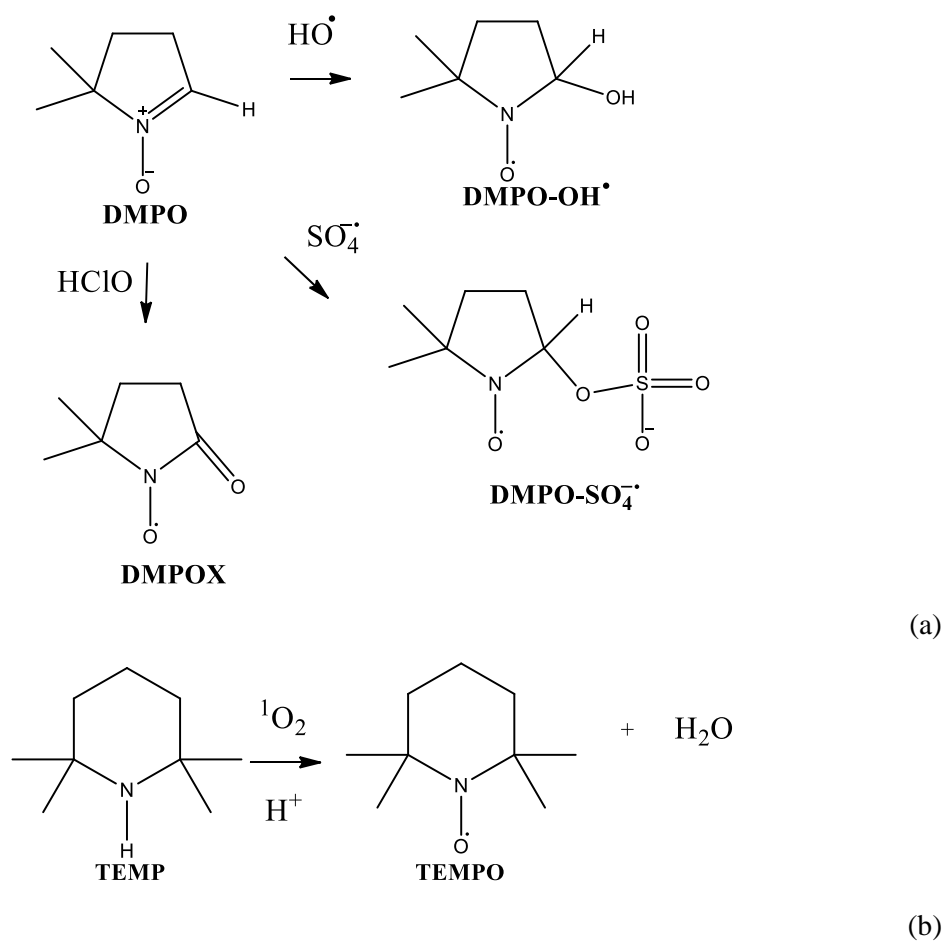


Figure 5.6. Reactions between the spin trap (a) DMPO and HO^\bullet , $\text{SO}_4^{\bullet-}$ and HClO and (b) TEMP and $^1\text{O}_2$.

Under dark conditions and in the presence of sodium azide an intense signal of the DMPO-N_3^\bullet adduct ($a_{\text{N}(\text{NO})} = 14.7$ Gs; $a_{\text{H}} = 14.2$ Gs; $a_{\text{N}(\text{N}_3)} = 3.1$ Gs (Kalyanaraman, 1985)) was recorded (Figure 5.7c) and compared to the simulated spectrum obtained by the Spinfit software (Figure 5.7d). In the absence of PMS, no EPR signal was recorded in the presence of DMPO and NaN_3 alone, confirming the oxidation of N_3^- to N_3^\bullet by PMS with a direct electron transfer mechanism.

In the presence of Cl^- ions, EPR analysis revealed an intense signal attributable to 5,5-dimethyl-2-pyrrolidone-N-oxyl (DMPOX, $a_{\text{N}} = 7.2$ Gs; $2a_{\text{H}} = 4.1$ Gs species (Figure 5.7e), supporting the formation of HClO in the sample (Bernofsky, 1990).

5. PMS and sulfate radical reactivity

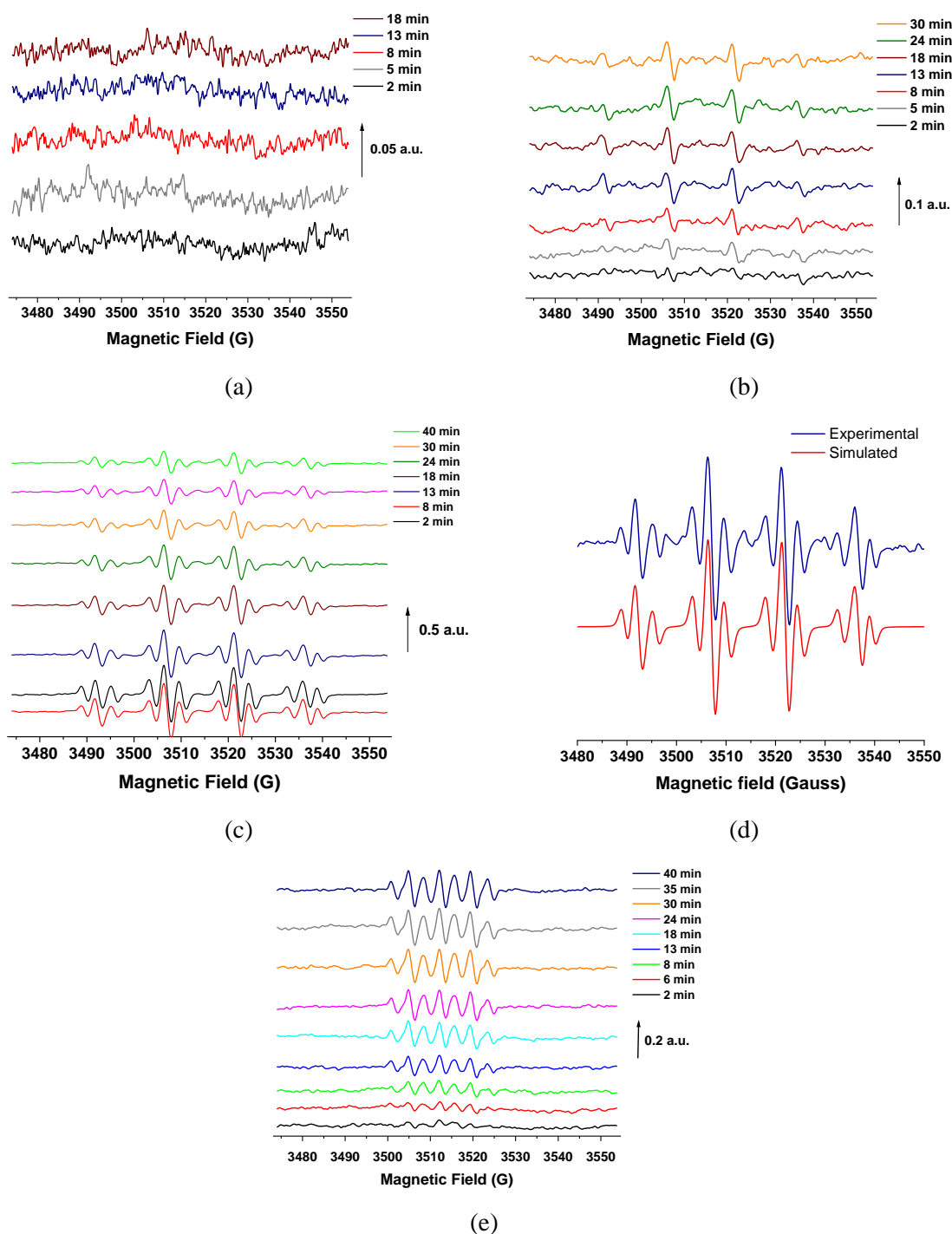


Figure 5.7. EPR spectra of DMPO adducts formed by PMS in the dark (a) at pH 3; (b) pH 11; (c) in the presence of NaN_3 ($1.5 \cdot 10^{-2}$ M) at different times, (d) simulation by Spinfit software and (e) EPR spectra of DMPOX formed by PMS in the dark and in the presence of chloride ions $1.5 \cdot 10^{-1}$ M at different times.

EPR spectra obtained after 10 minutes of irradiation of PMS under UV-C light and the correspondent simulation are reported in Figure 5.8, revealing the presence of two radical species that can be assigned to DMPO-OH^{\bullet} (Tummino, 2017) ($a_N = 15.0$ Gs; $a_H = 14.7$ Gs) and $\text{DMPO-SO}_4^{\bullet-}$ adducts ($a_N = 13.9$ Gs; $a_H = 9.7$ Gs (Liu, 2017; Zamora and Villamena,

2012). Moreover, the simulation of EPR spectra allowed to observe that, in these experimental conditions, the ratio $\text{DMPO-SO}_4^{\bullet-}/\text{DMPO-HO}^{\bullet}$ was quite independent from the type and intensity of irradiation and it was estimated in 1.2:1 (standard deviation 3 %).

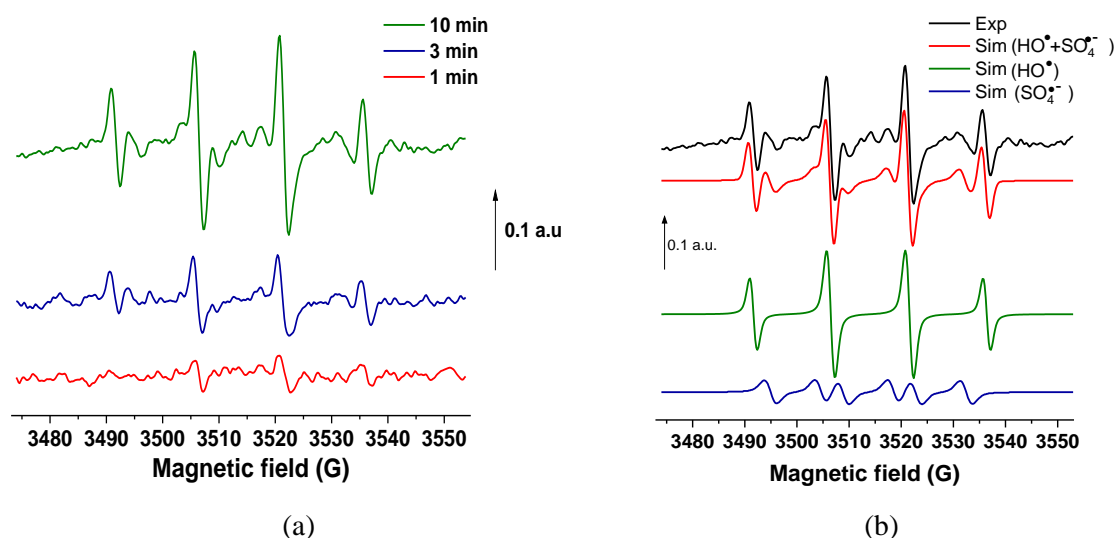


Figure 5.8. (a) EPR spectra of DMPO adducts formed by PMS under UV-C radiation at different times; (b) its simulation by Spinfit software as sum of two species: DMPO-OH^{\bullet} and $\text{DMPO-SO}_4^{\bullet-}$ adducts. Simulated spectra of the two species are also shown separately in the lower part of the figure.

Figure 5.9 shows the EPR spectra obtained with simulated solar radiation of DMPO in the presence of PMS. The EPR patterns of DMPO-OH^{\bullet} and $\text{DMPO-SO}_4^{\bullet-}$ adducts, observed by irradiating for a few minutes, were progressively substituted by DMPOX spectrum, indicating a progressive enhancement of oxidation environment induced by long-time irradiation (more than 15 minutes). The direct electron transfer promoted by the interaction of PMS with the spin trap led to the formation of the oxidized product.

Addition of TEMP to PMS solutions allowed to reveal the formation of the typical three-lines EPR spectrum, characteristic of TEMPO, resulting from the addition of singlet oxygen to the nitrogen atom in TEMP (Figure 5.10). Experiments were conducted in the dark at pH 3 in the presence of dissolved oxygen and under anoxic conditions and $^1\text{O}_2$ was formed in any case, confirming its formation from decomposition of PMS and not from the reaction of PMS with the dissolved oxygen. At pH 11 the concentration of $^1\text{O}_2$ was particularly high, as it can be observed in the relative EPR spectra intensity shown in Figure 5.10b. $^1\text{O}_2$ could be generated in solution by the self-decomposition, according to the reaction (R5.10) (Wang, 2018) and a higher amount could be formed at basic pH according to the reactions R5.8 and R5.9, reported above during alkaline activation of PMS.

5. PMS and sulfate radical reactivity

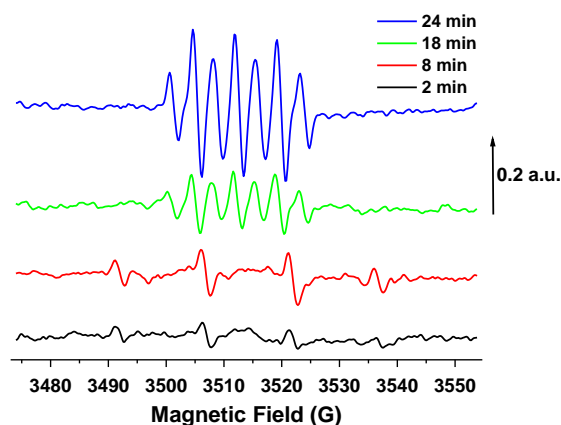


Figure 5.9. EPR spectra of DMPOX formed by PMS under simulated sunlight at different times.

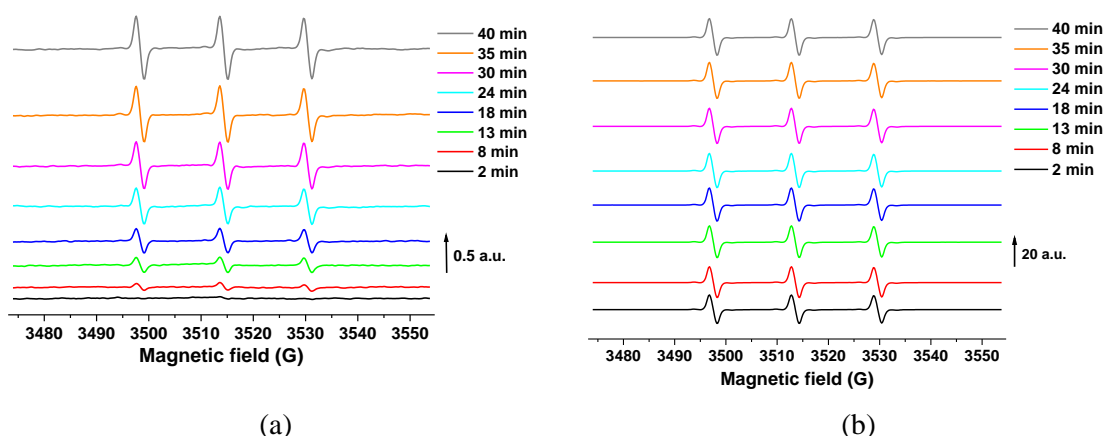


Figure 5.10. EPR spectra of TEMP adducts formed by PMS at different times in the dark (a) at pH = 3 and (b) at pH = 11.

5.2 Radical sulfate reactivity

5.2.1 Radical sulfate $SO_4^{\cdot-}$ generation

The UV photo-dissociation of PS anion $S_2O_8^{2-}$ was used as sulfate radical source in solution (R 5.19) (Herrman, 2007). The $SO_4^{\cdot-}$ generation was promoted *in situ* upon LFP irradiation (at 266 nm) of an aqueous solution of sodium persulfate (0.1 M).



PS was chosen as source of $SO_4^{\cdot-}$, due to the production of two moles of $SO_4^{\cdot-}$ per mol of $S_2O_8^{2-}$ reacted, with higher absolute effective quantum yield for $SO_4^{\cdot-}$, compared to PMS (Table 1.9 in the section “Introduction”; 1.4 vs 0.52 mol/Einstein), leading to a higher signal in LFP experiments, and allowing therefore to investigate the reactivity of $SO_4^{\cdot-}$. Initially,

the transient absorption spectrum of $\text{SO}_4^{\cdot-}$ was recorded between 700 and 300 nm (Figure 5.11a), showing a maximum absorption wavelength at 450 nm and a second less intense maximum at 320 nm, as it is also reported in literature (Ivanov, 2000). Therefore, the working conditions fitted in the LFP for evaluating $\text{SO}_4^{\cdot-}$ were the following: laser excitation of PS at 266 nm and $\text{SO}_4^{\cdot-}$ detection at 450 nm.

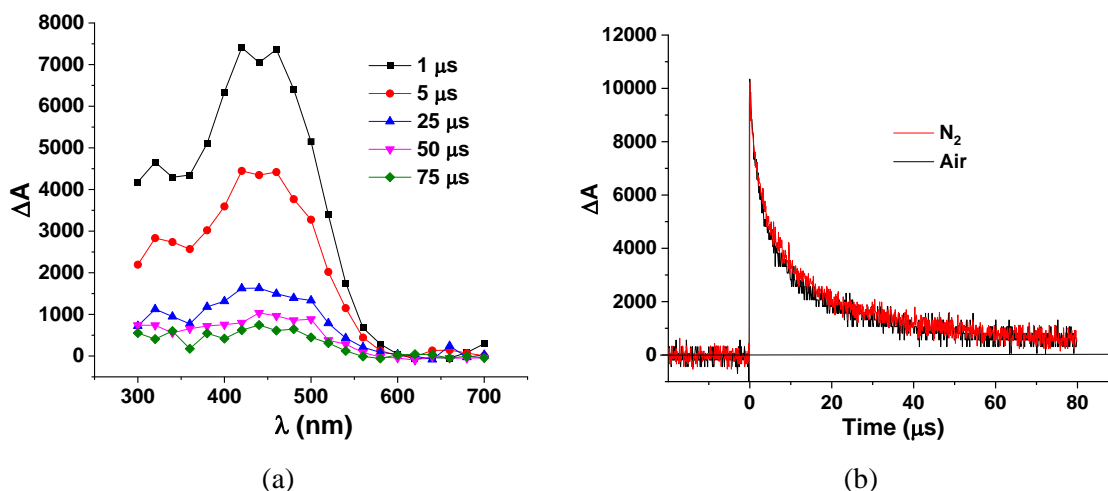


Figure 5.11. (a) Transient absorption spectra of $\text{SO}_4^{\cdot-}$, generated upon LFP irradiation ($\lambda_{\text{exc}} = 266$ nm) of aqueous solutions of PS (0.1 M) and (b) decay of $\text{SO}_4^{\cdot-}$ monitored at 450 nm in the absence or presence of air.

Figure 5.11b shows the decay traces, monitored at 450 nm in the absence and presence of air, highlighting the lack of influence of O_2 on $\text{SO}_4^{\cdot-}$ reactivity and allowing the monitoring of $\text{SO}_4^{\cdot-}$ transient decay under air. The decrease of the transient species was fitted with a pseudo first order constant of $1.3 \cdot 10^5 \text{ s}^{-1}$ and a lifetime τ_0 of *ca.* 6-8 μs was calculated, in agreement with literature data (Wu, 2018; 2015).

5.2.2 Elucidation of the $\text{SO}_4^{\cdot-}$ mechanism of reaction

In general, radicals could react with organic molecules by one of the following three possible mechanisms: (i) H-abstraction, (ii) electron transfer and (iii) addition to double bond (Wojnárovits, 2019). $\text{SO}_4^{\cdot-}$ is known to react with organic molecules mainly by hydrogen abstraction and electron transfer. The main characteristics of $\text{SO}_4^{\cdot-}$ in comparison with HO^{\cdot} could be summarized as follows (Guerra-Rodríguez, 2018; Wojnárovits, 2019):

- Higher oxidation potential $E_{\text{red}}(\text{SO}_4^{\cdot-}/\text{SO}_4^{2-}) = 2.5\text{-}3.1 \text{ V vs NHE}$, compared to $E_{\text{red}}(\text{HO}^{\cdot}/\text{H}_2\text{O}) = 2.8 \text{ vs NHE}$.
- Higher half-life time compared to HO^{\cdot} .
- Strong selectivity with electron-rich moieties, reacting more efficiently via electron

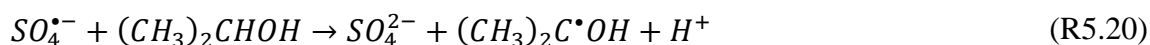
5. PMS and sulfate radical reactivity

transfer. By contrast, HO[•] is a non-selective radical, that could react by the three mechanisms, being consumed at higher rate by water matrix constituents (Wacławek, 2017).

To elucidate the type of reaction mechanism between SO₄^{•-} and each target investigated (constituents of bacterial cell wall and CECs), initially, the reactivity of well-known model compounds (isopropanol, MeOH and NaN₃) was determined by LFP under the experimental conditions selected previously. The obtained kinetic rate constants values were taken as the typical values range associated to each mechanism (H-abstraction and electron transfer process). Therefore, second-order rate constants $k_{SO_4^{\bullet-}, Q}$ (M⁻¹ s⁻¹) for the reactions of SO₄^{•-} with these substrates (Q) were determined by measuring the first-order rate constants for the decay of SO₄^{•-} ($k_{SO_4^{\bullet-}}$, s⁻¹) in the presence of various amounts of added Q.

5.2.2.1 H-abstraction reaction

For this purpose, LFP experiments were performed with two alcohols as H donor species. SO₄^{•-} reacts abstracting an H in C-H bond of isopropanol and MeOH, according to reaction R5.20 and R5.21, respectively:



SO₄^{•-} decays in the presence of increasing concentrations of isopropanol (a) or MeOH (b) (range 0-1·10⁻² M) are shown in Figure 5.12.

The slope of the corresponding Stern-Volmer plots yielded the bimolecular rate constant k_Q (M⁻¹ s⁻¹), obtaining $(6.8 \pm 0.1) \cdot 10^7$ M⁻¹s⁻¹ and $(1.0 \pm 0.1) \cdot 10^7$ M⁻¹s⁻¹ for isopropanol and MeOH, respectively. The bimolecular rate constant value for MeOH was lower than the one obtained for isopropanol, as expected from a primary alcohol compared to the secondary one (Clifton, 1989).

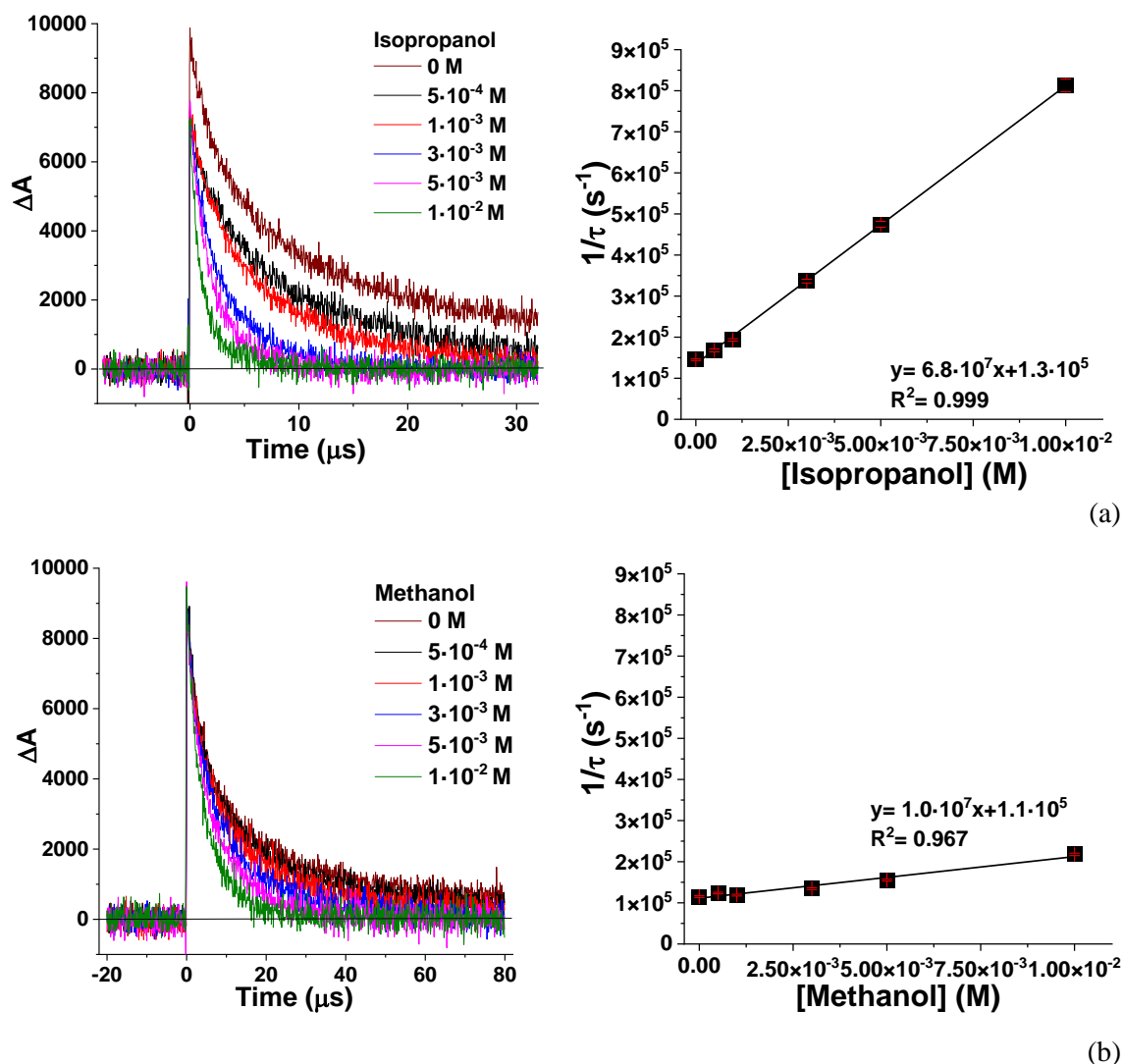


Figure 5.12. Left: Decay of $\text{SO}_4^{\bullet-}$, monitored at 450 nm, obtained from laser flash excitation ($\lambda_{\text{exc}} = 266$ nm) of aerated solutions of PS (0.1 M), in the presence of increasing concentrations of isopropanol (a) or methanol (b). Right: Corresponding Stern-Volmer plots.

5.2.2.2 Electron transfer reaction

NaN_3 was chosen as electron donor to investigate the electron transfer mechanism ($E_{\text{red}}(\text{N}_3^{\bullet-}/\text{N}_3^-) = 1.35 \pm 0.02$ V (vs NHE) (Zeev, 1987). Figure 5.13 shows the decay of $\text{SO}_4^{\bullet-}$, in the presence of increasing concentrations of NaN_3 (range of 0 - $1.33 \cdot 10^{-3}$ M), and the corresponding Stern-Volmer plot. The determined bimolecular rate constant value was $(1.2 \pm 0.03) \cdot 10^9 \text{ M}^{-1} \text{ s}^{-1}$, in good agreement with data reported in the literature (Huie, 1990). It can be observed that $\text{SO}_4^{\bullet-}$ reacts via H-atom abstraction with rate of 2-3 order of magnitude smaller than those of direct electron transfer.

5. PMS and sulfate radical reactivity

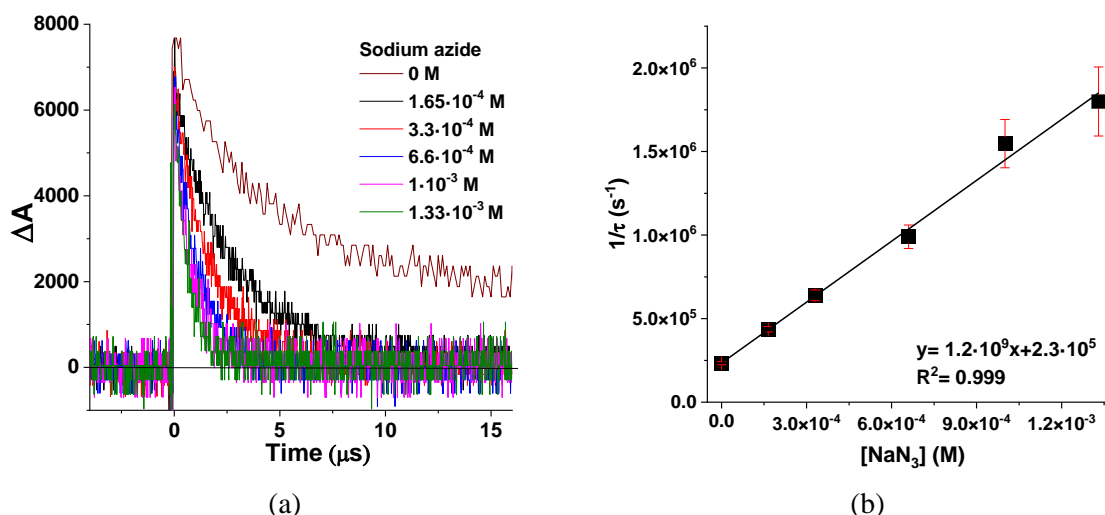


Figure 5.13. (a) Decay of $\text{SO}_4^{\bullet-}$, monitored at 450 nm, obtained from laser flash excitation ($\lambda_{\text{exc}} = 266$ nm) of deaerated solutions of PS (0.1 M), in the presence of increasing concentrations of NaN_3 . (b) Corresponding Stern-Volmer plot.

5.2.3. Determination of the bimolecular rate constants ($k_{\text{SO}_4^{\bullet-}}$) between cell wall constituents and $\text{SO}_4^{\bullet-}$

It is well-known that $\text{SO}_4^{\bullet-}$ initiates oxidative reactions on the cell wall, with deformation, pore-forming, and fracture of membrane cells, as it has been demonstrated by Xiao *et al.*, through SEM imaging of bacteria (Xiao, 2020). Therefore, LFP technique was used to investigate $\text{SO}_4^{\bullet-}$ reactivity against cell-wall model compounds of gram-negative (*E. coli*) and gram-positive (*E. faecalis*) bacteria.

Bacteria cell wall is constituted by peptidoglycan layer, an inner membrane and the periplasmic space in between these membranes. The thickness of peptidoglycan layer allows to distinguish between gram-positive and gram-negative bacteria, being the first ones characterized by a thicker layer. Peptidoglycan layer surrounds the cytoplasmic membrane, protecting the bacterium, providing structural integrity and it is considered the main site of attack by different oxidative agents. The structure of muramic acid subunit in the peptidoglycan of *E. coli* is shown in Figure 5.14.

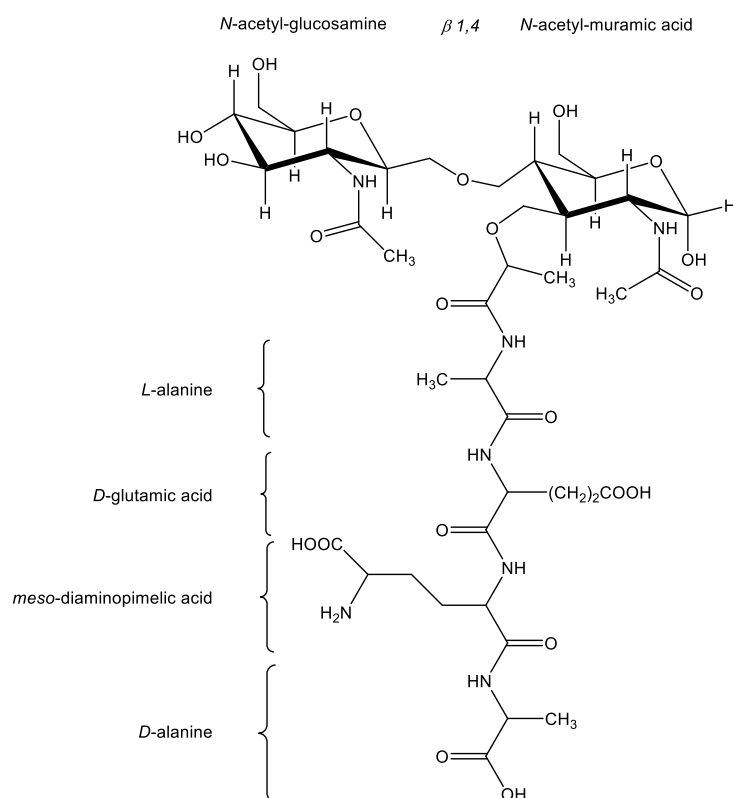


Figure 5.14. Structure of the muramic acid subunit in the peptidoglycan of *E. coli*.

The mechanisms of the oxidation reactions between $\text{SO}_4^{\cdot-}$ and bacteria was investigated using the following typical constituents of bacterial cell wall: *N*-acetylmuramic acid, *N*-acetyl-*L*-alanine, 2,6-Diaminopimelic acid, *N*-acetyl-*D*-glucosamine, *N*-acetyl-*L*-lysine and *N*-acetyl-*D,L*-glutamic acid.

The decays of $\text{SO}_4^{\cdot-}$, monitored at 450 nm, in the presence of increasing amounts of all membrane cell constituents (range $5 \cdot 10^{-4}$ to $5 \cdot 10^{-3}$ M) with the corresponding Stern-Volmer plots are shown in Figure 5.15. The experimental values of $k_{\text{SO}_4^{\cdot-}, Q}$ ($\text{M}^{-1}\text{s}^{-1}$) are in the range $7.1 \cdot 10^6$ - $7.1 \cdot 10^7$ $\text{M}^{-1}\text{s}^{-1}$, as it can be observed in Table 5.4. These values were in the order of those obtained with H-donor species (isopropanol and MeOH) and, therefore, the inactivation mechanism could initiate with a H-transfer to $\text{SO}_4^{\cdot-}$ involving C-H bond in the cell wall membrane compounds, damaging the membrane integrity and permeability, ultimately leading to microorganism's inactivation.

5. PMS and sulfate radical reactivity

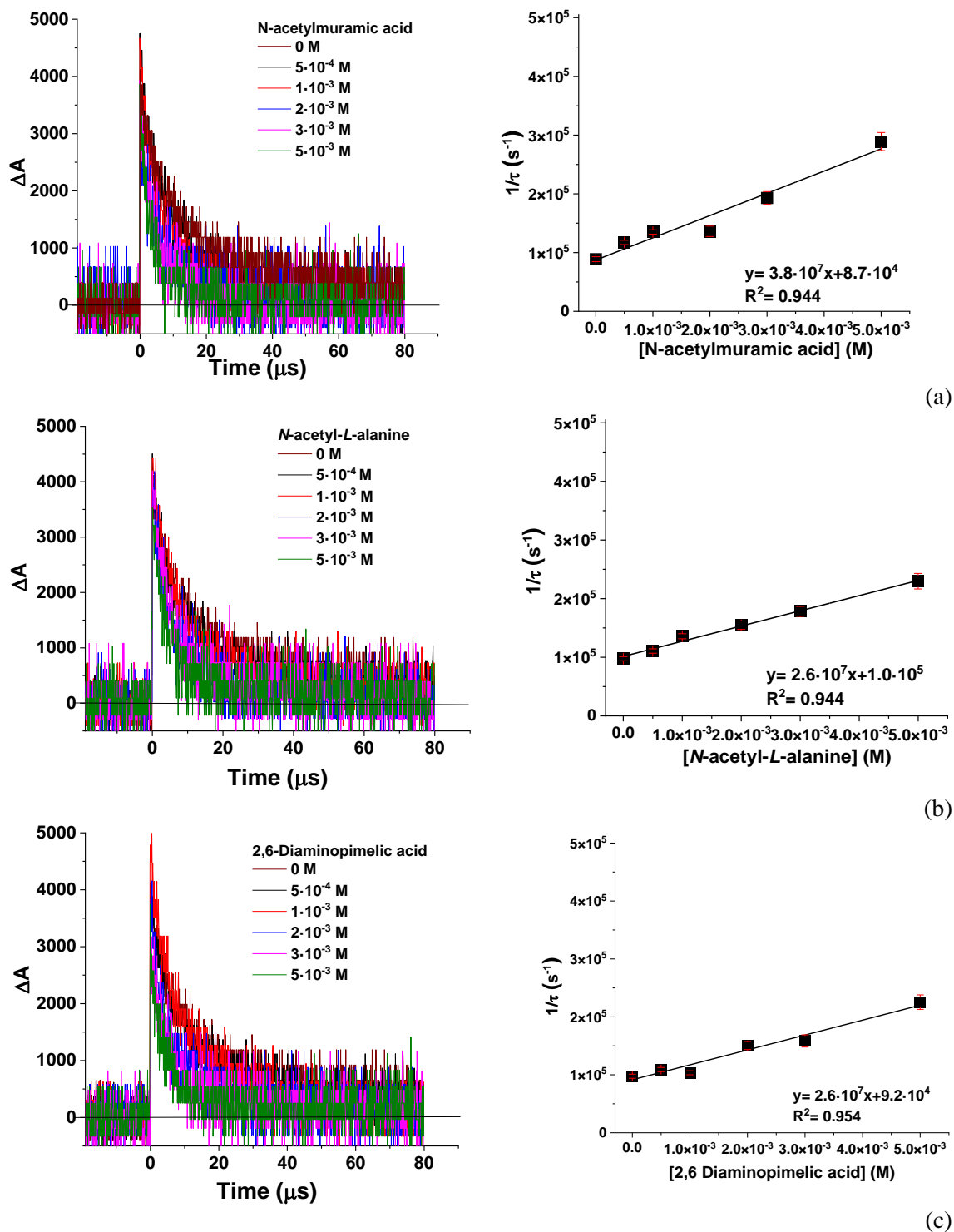


Figure 5.15. Left: Decay of $\text{SO}_4^{\bullet-}$, monitored at 450 nm, obtained from laser flash excitation ($\lambda_{\text{exc}} = 266$ nm) of deaerated solutions of PS (0.1 M), in the presence of increasing concentrations of cell wall constituents: *N*-acetylmuramic acid (a); *N*-acetyl-*L*-alanine (b); 2,6-Diaminopimelic acid (c); *N*-acetyl-*D*-glucosamine (d); *N*-acetyl-*L*-lysine (e); *N*-acetyl-*D,L*-glutamic acid (f). Right: corresponding Stern-Volmer plots.

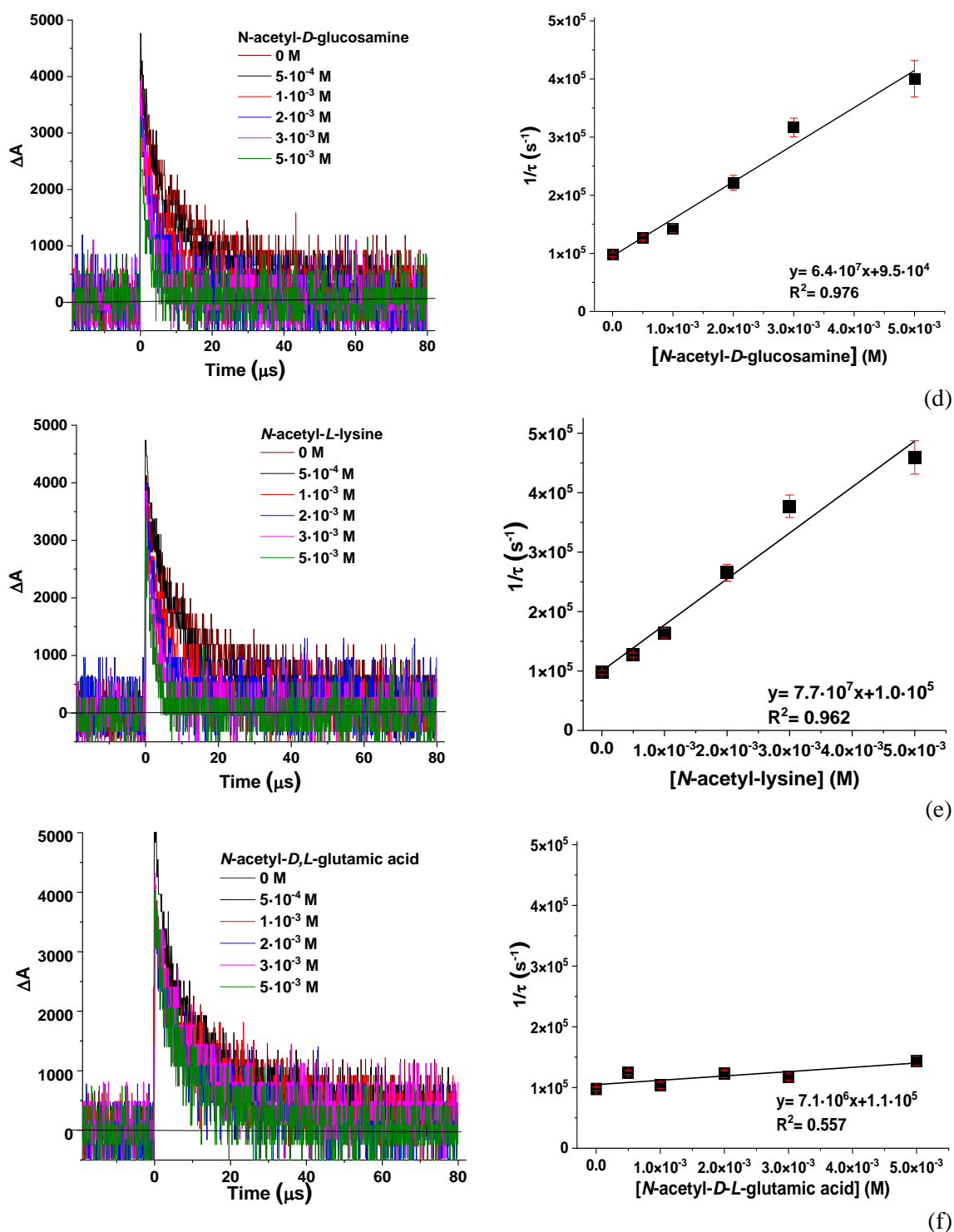


Figure 5.15. (Continued) Left: Decay of $\text{SO}_4^{\cdot-}$, monitored at 450 nm, obtained from laser flash excitation ($\lambda_{\text{exc}} = 266 \text{ nm}$) of deaerated solutions of PS (0.1 M), in the presence of increasing concentrations of cell wall constituents: *N*-acetylmuramic acid (a); *N*-acetyl-*L*-alanine (b); 2,6-Diaminopimelic acid (c); *N*-acetyl-*D*-glucosamine (d); *N*-acetyl-*L*-lysine (e); *N*-acetyl-*D,L*-glutamic acid (f). Right: corresponding Stern-Volmer plots.

5. PMS and sulfate radical reactivity

Table 5.4. Second order rate constants $k_{SO_4^{\cdot-}, Q}$ ($M^{-1}s^{-1}$) between $SO_4^{\cdot-}$ and cell wall constituents investigated.

Cell wall constituents	$k_{SO_4^{\cdot-}} (M^{-1}s^{-1})$
<i>N</i>-acetylmuramic acid	$(3.8 \pm 0.4) \cdot 10^7$
<i>N</i>-acetyl-<i>L</i>-alanine	$(2.6 \pm 0.1) \cdot 10^7$
2,6-Diaminopimelic acid	$(2.6 \pm 0.3) \cdot 10^7$
<i>N</i>-acetyl-<i>D</i>-glucosamine	$(6.4 \pm 0.4) \cdot 10^7$
<i>N</i>-acetyl-<i>L</i>-lysine	$(7.7 \pm 0.7) \cdot 10^7$
<i>N</i>-acetyl-<i>D,L</i>-glutamic acid	$(7.1 \pm 3.0) \cdot 10^6$
Tryptophan	$(6.7 \pm 1) \cdot 10^9$
Tyrosine	$(1.0 \pm 0.1) \cdot 10^9$
Phenylalanine	$(1.4 \pm 0.4) \cdot 10^9$

In general, the reactivity order obtained in this study was: *N*-acetyl-*L*-lysine > *N*-acetyl-*D*-glucosamine > *N*-acetylmuramic acid > 2,6-Diaminopimelic acid \cong *N*-acetyl-*L*-alanine > *N*-acetyl-*D,L*-glutamic acid.

In literature, it is described that after H-abstraction, a carbon-centered radical is formed, whose stability, depending on the type of substituents, determines the efficiency of the H-transfer (Clifton, 1989). Besides, it is also reported that electron donating groups (OH- and NH₂- group) enhance H abstraction of α C-H, while an opposite effect of withdrawing electron group (such as -COOH) could cause a decrease of the H-transfer efficiency (Macinnes, 1987). Among the studied compounds, similar second order kinetic constants, in the range of $10^7 M^{-1}s^{-1}$, were obtained and only *N*-acetyl-*D,L*-glutamic acid reacted with $SO_4^{\cdot-}$ with one order of magnitude smaller. Higher reactivity of the different component could be related to the presence of C-H bond adjacent to the amino or hydroxyl group, while *N*-acetyl-*D,L*-glutamic acid could transfer H with a lower efficiency due to the absence of e- donating groups and the presence of -COOH group in the structure. Therefore, the presence of two -COOH groups in *N*-acetyl-*D,L*-glutamic acid structure could explain the lower kinetic constant observed.

On the other hand, gram-negative bacteria are also characterized by an additional outer membrane, that constitutes the first line of defense, forming a physical and mechanical barrier that protects the cell. It contains proteins (porins), that mediate the passive or active uptake of small molecules for growth and cell functions. *E. coli* produces three majors trimeric porins: OmpC and OmpF (selective for cationic molecules), and PhoE, (selective for anionic molecules) (Vergalli, 2020). Porin structures contain, around the trimer peripheral surface, aromatic amino acids, such as phenylalanine (Phe) and tryptophan (Trp),

pointing towards the hydrophobic phase, and tyrosine (Tyr), characterized by hydroxyl groups that point towards the aqueous phase (Welte, 1995). Therefore, in order to find differences into the reactivity of gram-positive and gram-negative bacteria, LFP analysis were also performed with the aromatic amino acids Trp, Tyr and Phe. Firstly, the transient absorption spectrum of Trp (at concentration of $2 \cdot 10^{-4}$ M) was recorded by LFP, and results are shown in Figure 5.16a. It is clear that Trp presents two maxima absorptions at *ca.* 320 nm and 550 nm.

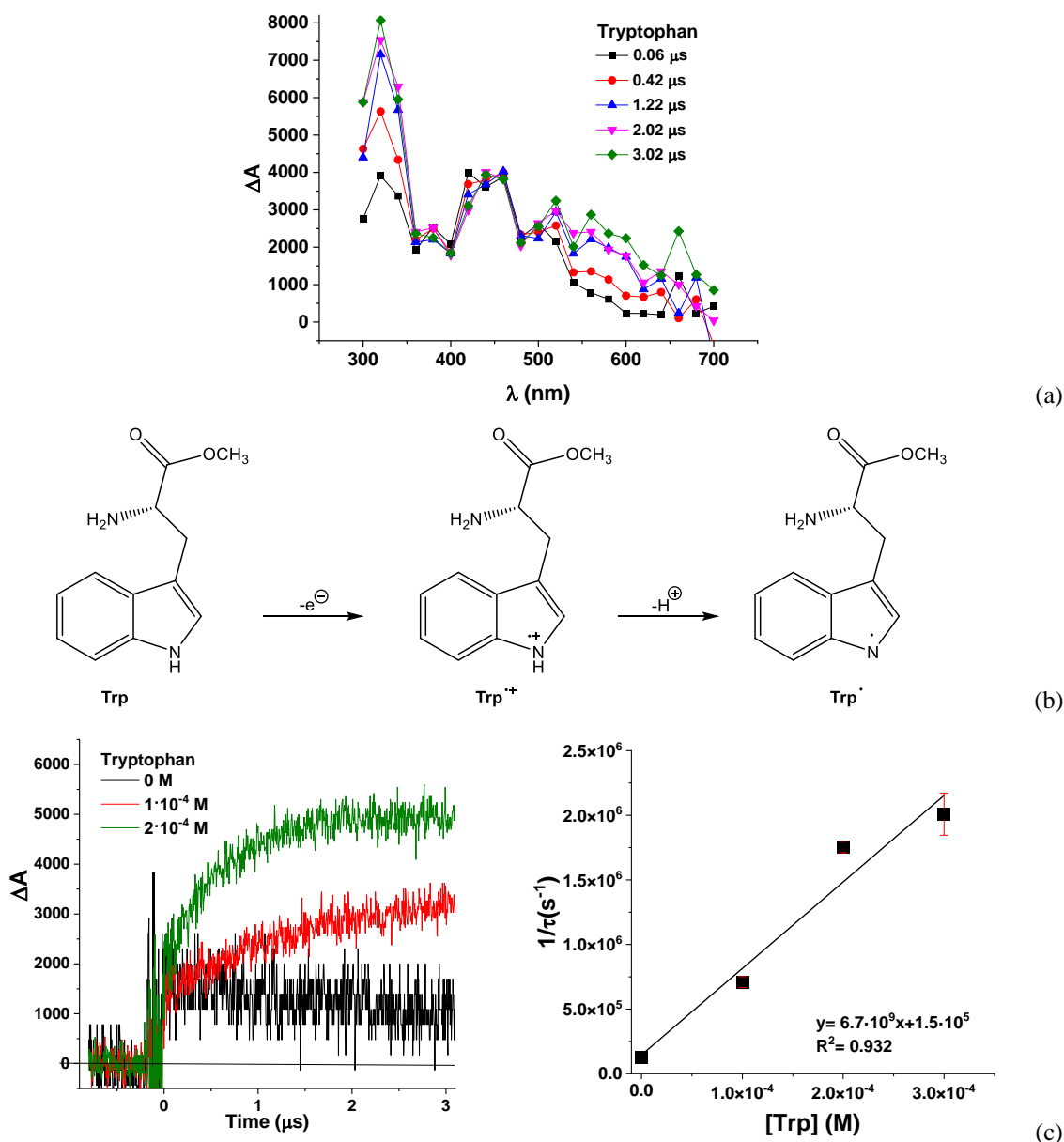


Figure 5.16: (a) Transient absorption spectra obtained from a solution of PS (0.1 M) in the presence of Trp ($2 \cdot 10^{-4}$ M), recorded at different times after the laser pulse ($\lambda_{\text{exc}} = 266$ nm). (b) Oxidation of L-tryptophan methyl ester by e^- transfer followed by proton transfer (PCET mechanism). (c) Left: Transient absorption traces monitored at 550 nm, obtained upon laser pulse ($\lambda_{\text{exc}} = 266$ nm) from a solution of PS (0.1 M) with different concentrations of Trp. Right: Corresponding Stern-Volmer plot.

5. PMS and sulfate radical reactivity

This effect could be explained by the reaction between Trp with $\text{SO}_4^{\cdot-}$ via Proton Coupled Electron Transfer (PCET), according to Figure 5.16b. The electron transfers from Trp to $\text{SO}_4^{\cdot-}$ leads to the formation of an intermediate specie $\text{Trp}^{+\cdot}$, that subsequently deprotonates to yield the much longer-lived radical Trp^{\cdot} , being this specie the one detected by LFP at these two maxima absorption, in accordance with literature (Teixeira, 2019).

Due to the impossibility to follow $\text{SO}_4^{\cdot-}$ decay at 450 nm, the quenching rate constant for the reaction between the $\text{SO}_4^{\cdot-}$ and Trp, was determined from the growth corresponding to the formation of the Trp^{\cdot} , recorded in a clean region of the available spectral window (550 nm), (Figure 5.16c). Thus, the corresponding Stern-Volmer analysis gave a $k_{\text{SO}_4^{\cdot-}, \text{Trp}}$ value of $(6.7 \pm 1) \cdot 10^9 \text{ M}^{-1} \text{ s}^{-1}$.

Similar experiments were also performed with Tyr and Phe (Figure 5.17), obtaining the second-order kinetic constants reported in Table 5.4, which correspond to the electron transfer mechanism.

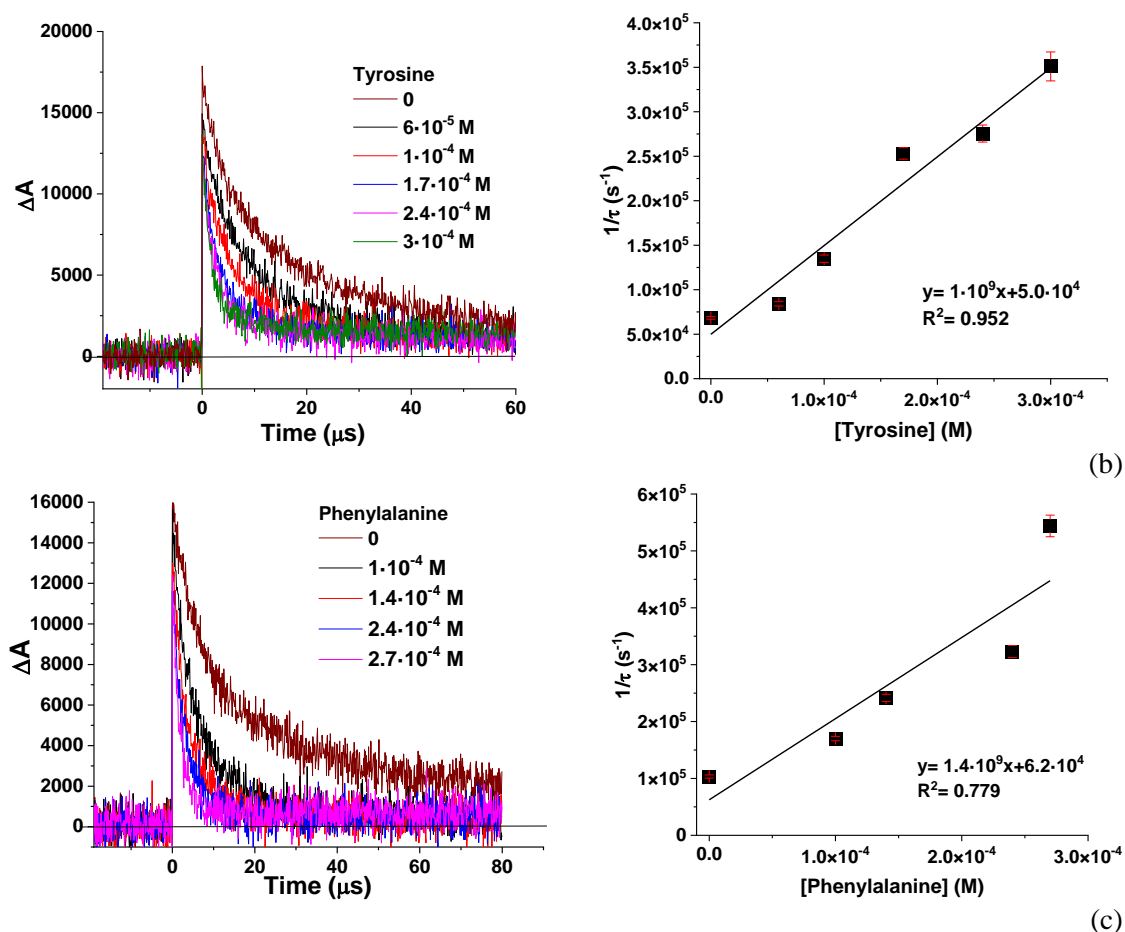


Figure 5.17: Left: Decay of $\text{SO}_4^{\cdot-}$, monitored at 450 nm, obtained from laser flash excitation ($\lambda_{\text{exc}} = 266 \text{ nm}$) of aerated solutions of PS (0.1 M), in the presence of increasing concentrations of tyrosine (a) and phenylalanine (b). Right: Corresponding Stern-Volmer plot.

With this scenario, cell wall components in peptidoglycan layer, in both gram-negative and gram-positive bacteria, predominantly react, at rates 10^6 - 10^7 $M^{-1}s^{-1}$, by H-abstraction mechanism. Higher inactivation rates of gram-negative bacteria could be obtained, for the presence of some biomolecules in the outer membrane (proteins such as porins containing aromatic amino acids), capable of reacting at higher rates 10^9 $M^{-1}s^{-1}$ with $SO_4^{\bullet-}$ by electron transfer mechanism. Following these findings, a schematic drawing of gram-negative and gram-positive bacteria cell wall and the main site of attack of $SO_4^{\bullet-}$ has been proposed and shown in Figure 5.18.

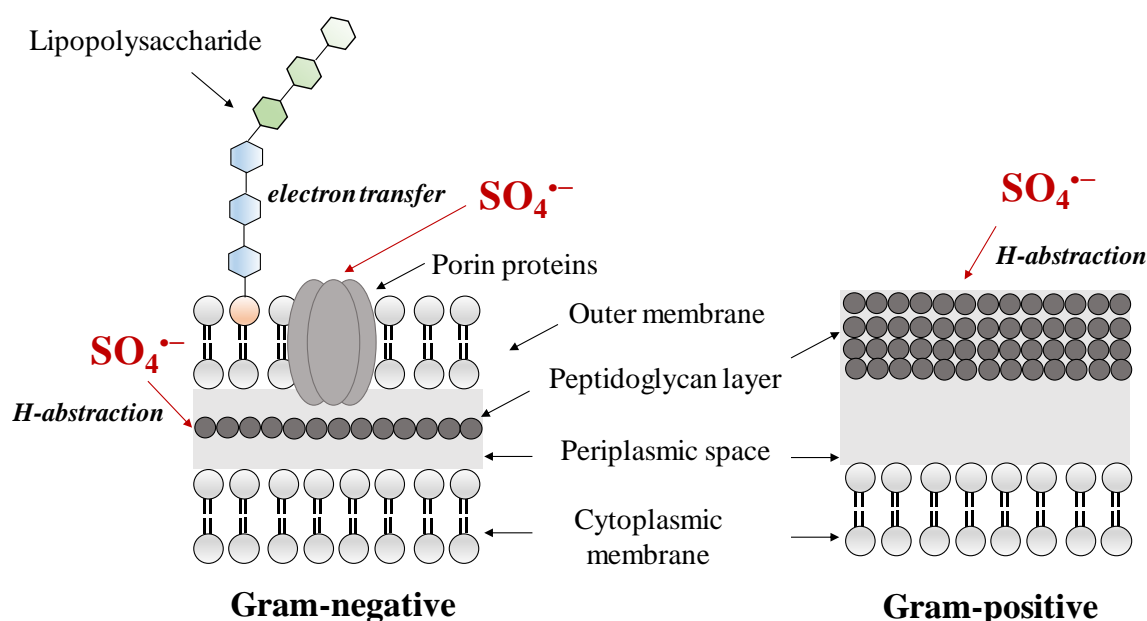


Figure 5.18: Schematic drawing of gram-negative and gram-positive bacteria cell wall and $SO_4^{\bullet-}$ main attack sites.

5.2.4. Determination of the bimolecular rate constants between $SO_4^{\bullet-}$ and CECs.

The reactivity between $SO_4^{\bullet-}$ and the selected CECs (DCF, SMX and TMP) was also assessed. LFP experiments were preliminary performed with each CEC in the absence of PS and no significant absorption at 450 nm was detected, excluding interference of other transient species absorbing at this wavelength and attributing the decay only to the generated radical anion specie. Figure 5.19 shows the decays of $SO_4^{\bullet-}$, monitored at 450 nm in the presence of different concentrations of DCF, SMX and TMP (0 - $5 \cdot 10^{-5}$ M), respectively.

5. PMS and sulfate radical reactivity

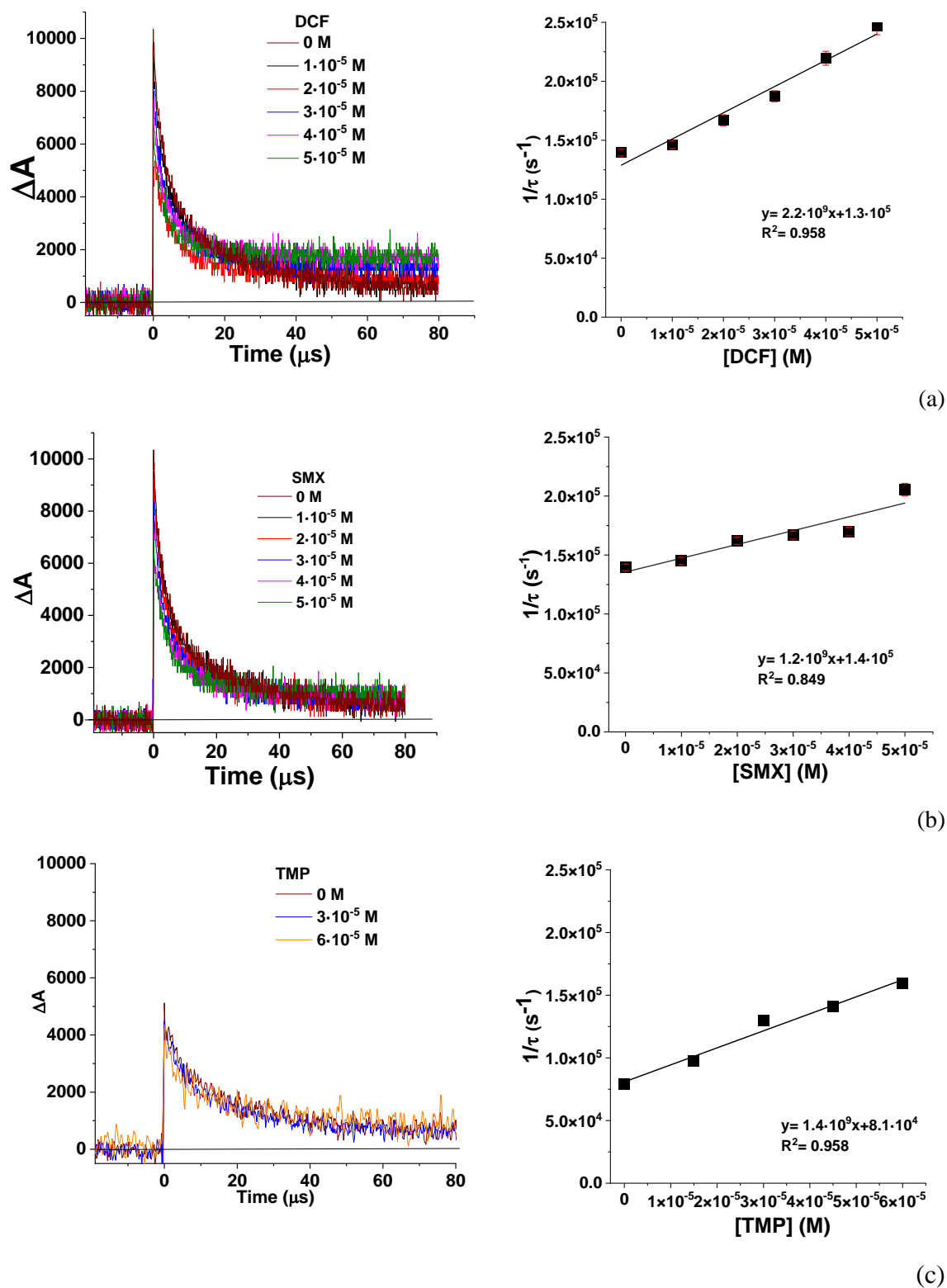


Figure 5.19. Left: Decay of $\text{SO}_4^{\bullet-}$, obtained from laser flash excitation ($\lambda_{\text{exc}} = 266 \text{ nm}$) of a solution of PS (0.1 M), in the presence of different concentrations of DCF (a), SMX (b) and TMP (c), monitored at 450 nm. Right: corresponding Stern-Volmer plot.

The slope of Stern-Volmer plots provided $k_{\text{SO}_4^{\cdot-}}$ with the following reactivity order: DCF $((2.2 \pm 0.2) \cdot 10^9 \text{ M}^{-1}\text{s}^{-1}) > \text{TMP} ((1.4 \pm 0.1) \cdot 10^9 \text{ M}^{-1}\text{s}^{-1}) \cong \text{SMX} ((1.2 \pm 0.2) \cdot 10^9 \text{ M}^{-1}\text{s}^{-1})$, in accordance with literature data (Wojnárovits, 2019; Wu, 2018). It can be highlighted that the kinetic constants obtained are in the order of the electron transfer mechanism, concluding that CECs quickly react with $\text{SO}_4^{\cdot-}$ by electron transfer process, as starting point of the degradation pathways.

Interestingly, although Mahdi Ahmed et al. determined, by using competition kinetics technique, higher values for the bimolecular rate constants of $\text{SO}_4^{\cdot-}$ with DCF and SMX $((12.5 \pm 3.1) \cdot 10^9$ and $(9.2 \pm 2.6) \cdot 10^9 \text{ M}^{-1} \text{ s}^{-1}$, respectively), the same reactivity order than that determined in the present study was obtained. Moreover, they postulated that the formation of an *N*-centred radical, through probably a one-electron transfer mechanism, was the starting point of the degradation pathways of both compounds (Mahdi-Ahmed, 2012). With the results obtained here with CECs is not possible to discard that at least part of the reactivity determined by LFP was produced by the addition of $\text{SO}_4^{\cdot-}$ to a double bond of CECs.

5.3 Concluding remarks

PMS can induce direct oxidation of some organic pollutants with electron-rich moieties through a no-radical pathway, involving direct electron transfer in the absence of both a catalytic and/or photochemical activation. EPR experiments and tests with active scavenger species (i.e. MeOH, TBA, FFA and NaN_3) confirm the absence of ROS in solution. Target removal was enhanced in the presence of higher T, pH and in the presence of chloride and bicarbonate ions. HO^{\cdot} and $^1\text{O}_2$ could be the main reactive species under alkaline pH, while the formation of active chlorine (e.g. Cl_2/HClO) is promoted in the presence of chloride ions. Under artificial solar irradiation, photochemical processes did not occur, without formation of $\text{SO}_4^{\cdot-}$ and HO^{\cdot} , due to the impossibility to break O-O bond, and an enhancement in degradation rate of organic compounds could be explained with the increment of the temperature of the solution. Homolytic break of the PMS O-O bond with the formation of the strong $\text{SO}_4^{\cdot-}$ and HO^{\cdot} occurs under UV-C radiation, with a ratio 1.2:1 (experimentally evaluated comparing the EPR DMPO- $\text{SO}_4^{\cdot-}$ / DMPO- HO^{\cdot} signals).

On the other hand, LFP technique was used to investigate $\text{SO}_4^{\cdot-}$ reactivity against cell-wall model compounds commonly found in gram-negative (such as *E. coli*) and gram-positive (such as *E. faecalis*) bacteria and CECs (DCF, SMX and TMP). $\text{SO}_4^{\cdot-}$ reacts with typical

5. PMS and sulfate radical reactivity

constituents of bacteria cell wall via H-abstraction mechanism (10^6 - 10^7 $M^{-1}s^{-1}$). Nevertheless, an additional electron transfers at higher rate (10^9 $M^{-1}s^{-1}$) could occur with aromatic amino acids (Trp, Tyr and Phe) contained in the skeleton of porins, proteins of outer membrane of gram-negative bacteria, suggesting a more susceptibility of these type of bacteria to $SO_4^{\bullet-}$. Finally, CECs also quickly react with $SO_4^{\bullet-}$ by electron transfer process ($k_{SO_4^{\bullet-},CECs}, 10^9$ $M^{-1}s^{-1}$).

CHAPTER 6
ASSESSMENT OF
PEROXYMONOSULFATE FOR WATER
PURIFICATION UNDER NATURAL
SOLAR RADIATION

6. ASSESSMENT OF PEROXYMONOSULFATE FOR WATER PURIFICATION UNDER NATURAL SOLAR RADIATION

In this chapter the effectiveness of non-activated PMS alone as oxidative agent for water purification in the absence and in the presence of natural solar radiation was assessed for the simultaneous inactivation of three pathogens (*E. coli*, *E. faecalis* and *P. aeruginosa*) and for the degradation of three CECs (DCF, SMX and TMP).

A wide range of PMS concentrations (from 0.0001 to 0.01 mM) was tested in IW at laboratory scale in 200-mL vessel reactors. Moreover, the influence of inorganic species on the global PMS/Solar system performance was assessed by testing its effectiveness in DW, WeW and d-WeW at 0.01 mM of oxidant.

6.1 PMS/Dark system

To determine the capability of non-activated PMS alone as oxidative agent over the targets investigated in this work, a wide range of PMS concentrations from 0 to 0.01 mM was evaluated in the dark for 3 hours of contact time.

6. PMS/Solar for water purification

Abatement profiles of each individual bacterium, each CEC and their corresponding sum in PMS/Dark system in IW are shown in Figure 6.1 and Figure 6.2, respectively. Water temperature ranged between 20 to 25 °C, discarding thermal effects on microbial targets inactivation (Berney, 2006). Water pH was 6.5-7 in all cases, remaining constant along the treatment time, excluding therefore pH effects on CEC degradation by dissociation modifications or over bacterial viability (Nahim-Granados, 2019; Martínez-García, 2020). Values obtained for both parameters also could be discarded as activation factors of PMS according to literature (Wang, 2018) and to the results showed in Chapter 5.

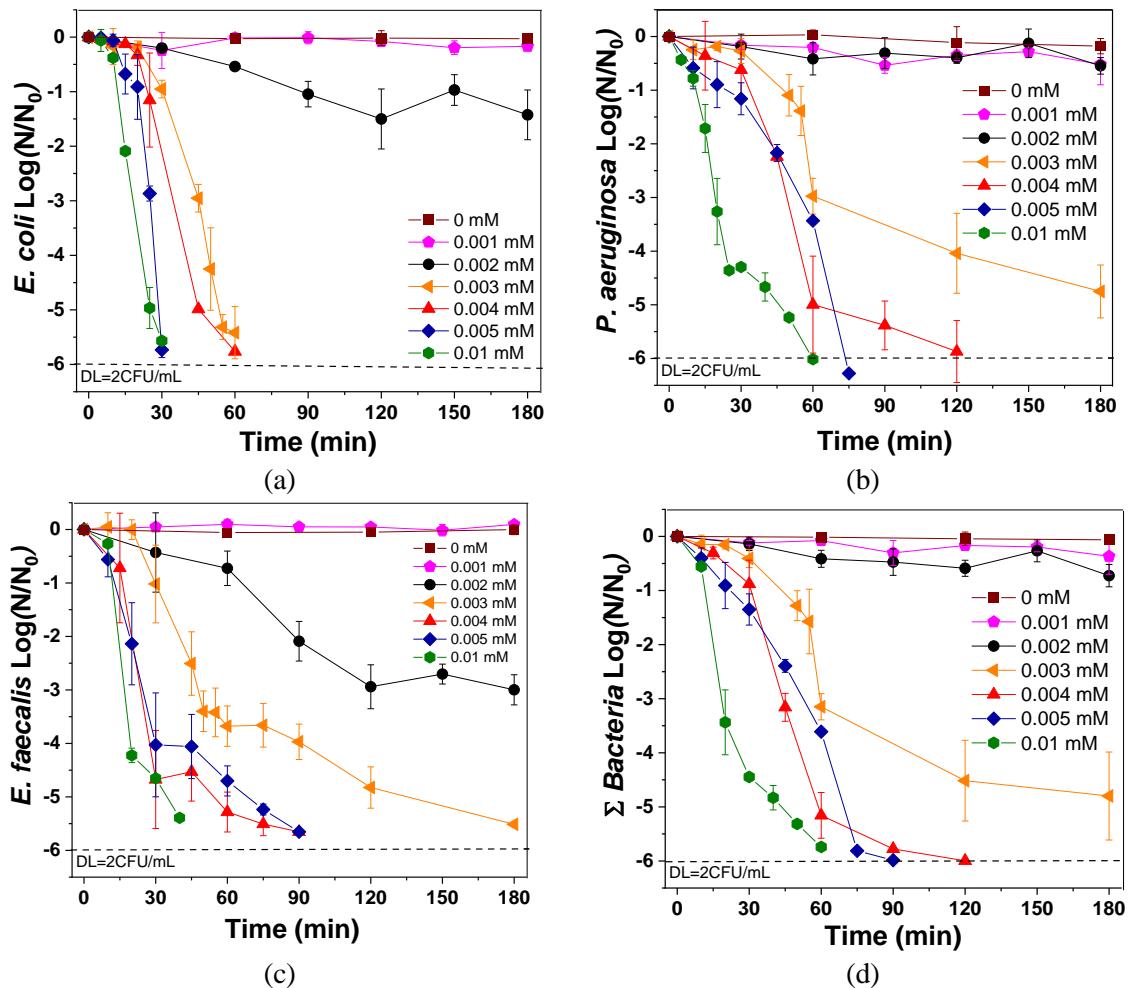


Figure 6.1. Inactivation profiles of (a) *E. coli*, (b) *P. aeruginosa*, (c) *E. faecalis* and (d) the sum of bacteria in the presence of different concentrations of PMS (0-0.01 mM) at 25 °C in IW and in the dark.

The bacterial inactivation results (Figure 6.1) showed that the increasing dose of PMS, the higher the inactivation kinetics (Table B.3 Annex B), reaching > 5 LRV for all bacteria with PMS concentration higher than 0.004 mM. At this condition, the DL for all bacteria was

reached after 120 minutes and, particularly, for *E. coli*, *E. faecalis* and *P. aeruginosa* after 60, 90 and 120 minutes, respectively.

The individual CECs degradation profiles and their sum in PMS/Dark system in IW (Figure 6.2) show that 80 % of removal of total CECs was achieved only in the presence of 0.01 mM of PMS after 120 minutes and, particularly, after 45, 120 and 173 minutes for SMX, DCF and TMP, respectively.

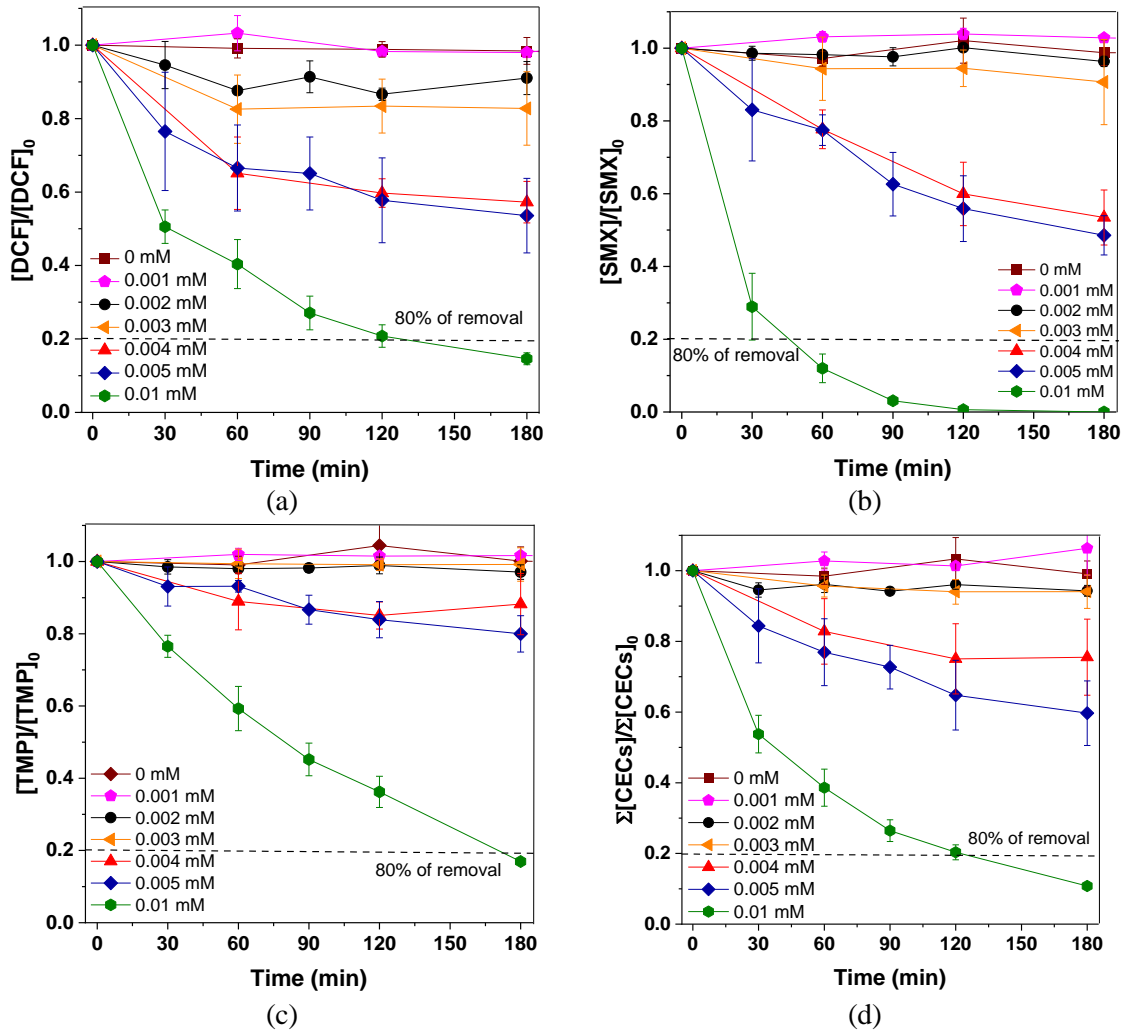


Figure 6.2. Degradation profiles of (a) DCF, (b) SMX, (c) TMP and (d) total CECs in the presence of different concentrations of PMS (0-0.01 mM) at 25 °C in IW and in the dark.

Table B.3 reports bacterial inactivation and CECs pseudo-first order degradation kinetic constants obtained in these experimental conditions and Figure 6.3 plots these kinetic constants against PMS concentration.

6. PMS/Solar for water purification

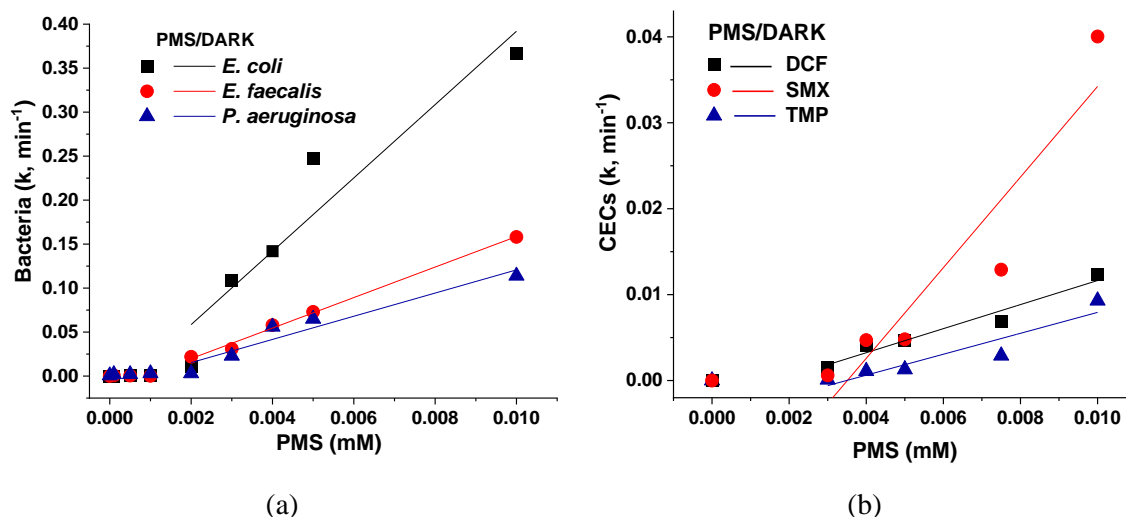


Figure 6.3: Kinetic constant values (min⁻¹) of (a) bacterial inactivation and (b) CEC degradation by PMS/Dark in IW.

The results demonstrate the capability of non-activated PMS at very low concentrations for the simultaneous water disinfection and decontamination. In literature, similar results have been reported individually for bacteria and CECs (mainly pharmaceuticals) abatement from water. Rodríguez-Chueca et al., reported a total inactivation of *E. coli* K12 after 240 minutes using $9 \cdot 10^{-5}$ M of PMS in the dark (Rodríguez-Chueca, 2019e). Among CECs, sulphonamide antibiotics have been also investigated, highlighting that more than 65 % of SMX at concentration of 15 μ M (3.795 mgL^{-1}) could be degraded within 80 minutes by 1 mM PMS at pH 7 in milliQ water under dark conditions (Ji, 2018).

The PMS efficiency for water purification is attributed to the high oxidation potential of HSO_5^- ($E^0_{\text{HSO}_5^-/\text{HSO}_4^-}=1.82\text{V}$), that permits the direct oxidation of organic compounds containing electron-rich moieties (heteroatoms such as N, O and S) (Ding, 2021), while those containing electron withdrawing group (such as nitro and carboxyl functional groups) may exhibit low reactivity with PMS. In the literature, it has been reported three mechanisms for organic compounds direct oxidation by PMS: (i) two electron oxidation with cleavage of the peroxo bond and oxygen atoms transfer from PMS to organic pollutants, (ii) one electron oxidation with the formation of organic radical cations and (iii) singlet oxygen oxidation (Ding, 2021). In the previous Chapter 5, the LFP results revealed that the initial degradation mechanism of the investigated CECs could be based on electron transfer process.

As observed in Figure 6.3b, CECs were degraded by non-activated PMS in the dark but a different trend was obtained for each CEC. In general, a linear trend was observed in the

range from 0.003 to 0.01 mM, with the following fitted k values against PMS concentration: SMX ($5.3 \pm 1.1 \text{ min}^{-1} \text{ mM}^{-1}$) > DCF ($1.4 \pm 0.2 \text{ min}^{-1} \text{ mM}^{-1}$) \geq TMP ($1.2 \pm 0.3 \text{ min}^{-1} \text{ mM}^{-1}$). These differences could be attributed to CECs respective chemical structure, and briefly explained as follows:

- The electron donating amino group present on the benzene ring of SMX is considered the preferential site of attack by PMS, that, donating electrons to the oxidant, is oxidized, forming sequentially N-OH-, NO- and NO₂- adducts, that are more recalcitrant and toxic than the parent compound (Yin, 2018).
- DCF structure is composed by a more susceptible amino group, but carboxylic acid and chlorinated groups (electron withdrawing groups) could decrease the nucleophilic character of the amino group.
- TMP structure is composed by 2,4-diamino-pyrimidine (DAPD) and the more refractory to the degradation 1,2,3-trimethoxybenzene (TMBz) linked by a methylene bridge. DAPD is the more reactive moiety, containing in its structure two electron rich amine group, that are easily attacked by PMS to form N-OH-TMP. It was found to not be further oxidized to nitro or nitroso derivatives, due to an energy barrier that PMS is not able to overcome (Yang, 2021).

Regarding bacterial abatement, the lower membrane redox potential (characterized by a number of compounds such as transpeptidases, amino groups, lipopolysaccharides, etc.) compared to PMS, could make possible cell wall direct oxidation by PMS (Rivas, 2012; Ji, 2018; Rodríguez-Chueca, 2019e). Moreover, the generation and accumulation of free chlorine (HClO/Cl₂) (according to R5.11-R5.17) in the presence of high Cl⁻ content typical of IW (9 g/L) could result in an enhancement in inactivation kinetics.

Disinfection results (Figure 6.3a) clearly demonstrated that inactivation kinetics significantly increased by increasing PMS from 0.002 to 0.01 mM for all bacteria, although different susceptibilities were observed. The linear fitting of bacterial inactivation kinetics showed the following order: *E. coli* ($41.7 \pm 7.7 \text{ min}^{-1} \text{ mM}^{-1}$) > *E. faecalis* ($17.3 \pm 0.7 \text{ min}^{-1} \text{ mM}^{-1}$) > *P. aeruginosa* ($13.2 \pm 2.1 \text{ min}^{-1} \text{ mM}^{-1}$). This difference could be attributed to their cell-wall architecture. Gram-negative bacteria (*E. coli* and *P. aeruginosa*) are more susceptible to oxidative processes than gram-positive bacteria (*E. faecalis*) in good agreement with results from LFP (Chapter 5), being characterized by a thinner peptidoglycan layer (Van Grieken, 2010). Nevertheless, in spite of its gram-negative cell wall architecture, *P. aeruginosa* exhibited the higher resistance to PMS in the PMS/dark system. This

6. PMS/Solar for water purification

unexpected result could be explained by the well-known capability of this bacterium to generate and exudate extracellular polymeric substances (EPS). Xue et al. reported that the capsular EPS (with acidic polysaccharide alginate as mayor ESP) generated by *P. aeruginosa* PAO1 strain increased its resistance to direct oxidants, such as chlorine and monochloramine. This resistance was explained by the higher disinfectant consumption and/or the limited direct cell membrane access for the oxidants (Xue, 2013).

6.2 PMS/Solar system

The effect of the combination between PMS and natural solar radiation was assessed for the simultaneous disinfection and decontamination of water. The water T, pH and UV-A irradiance measured during the experiments are shown in Figure 6.4. It can be observed that water T ranged between 25 to 40 °C and water pH was 6.5 remaining constant along the treatment time. Higher values of pH are necessary to promote PMS activation and higher T values than 50 °C are necessary to promote the fission of O-O bond in PMS, with $\text{SO}_4^{\cdot-}$ generation, discarding, therefore, their effect on oxidant activation in these results (Wang, 2018).

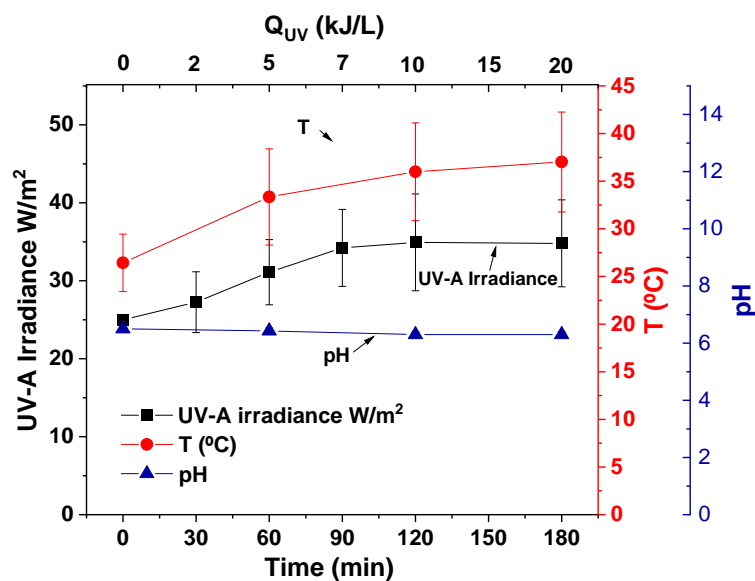


Figure 6.4: Temperature, pH and UV-A irradiance profiles during solar experiments.

Figure 6.5 shows the inactivation profiles of *E. coli* (a), *P. aeruginosa* (b), *E. faecalis* (c) and the sum of bacteria (d) by PMS/Solar treatment with concentrations ranged from 0 to 0.01 mM. Corresponding kinetic rates are summarized in Table B.4 (Annex B).

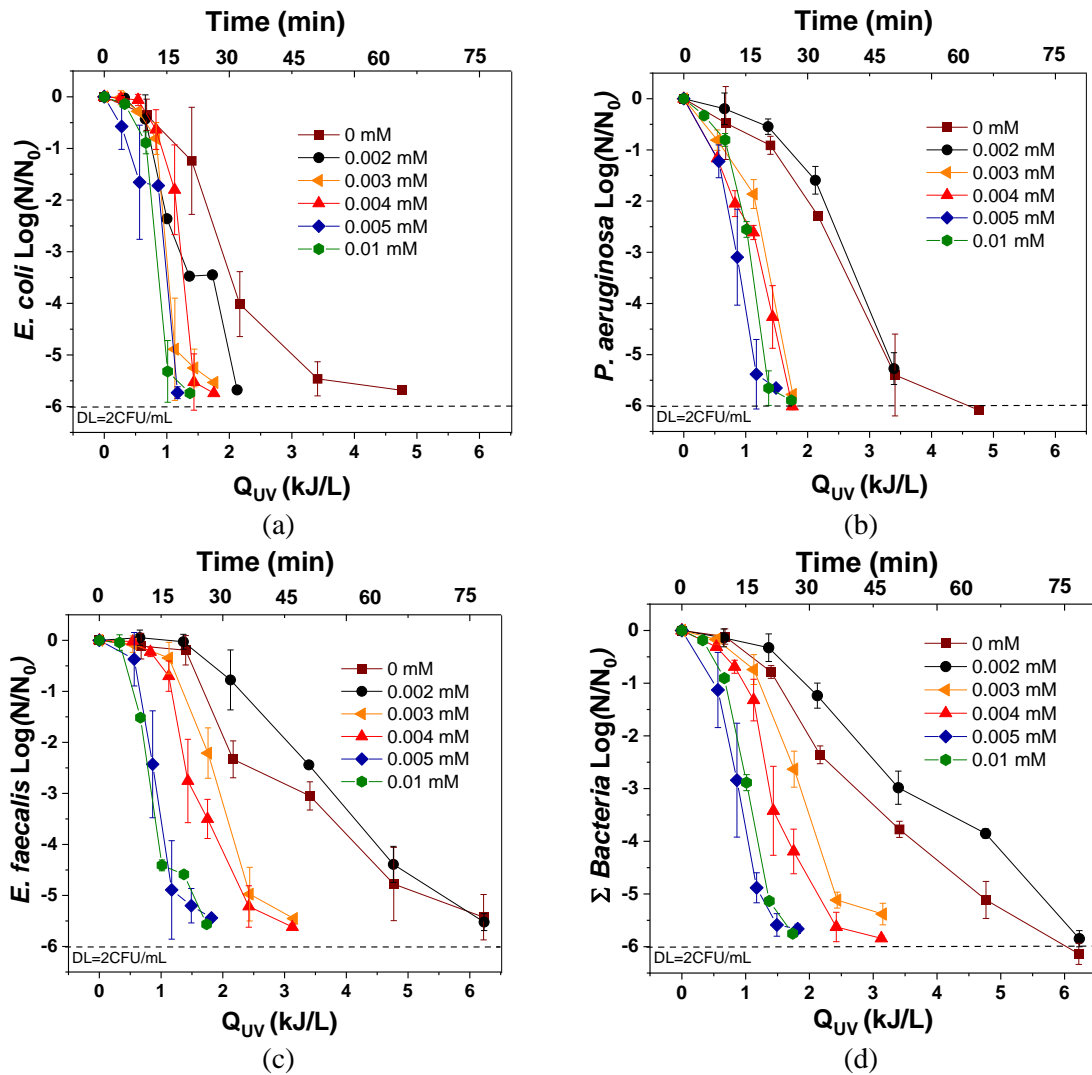


Figure 6.5. Inactivation profiles of (a) *E. coli*, (b) *E. faecalis*, (c) *P. aeruginosa* and (d) sum of bacteria by PMS/Solar system at different PMS concentrations (0-0.01 mM) in IW and under natural sunlight.

The DL was reached after 60 minutes (4.8 kJ/L) for *E. coli* and *P. aeruginosa*, and in 75 minutes (6.2 kJ/L) for *E. faecalis* with solar photo-inactivation process. For PMS concentration lower than 0.002 mM, bacterial inactivation did not enhance in comparison with solar photo-inactivation results, while for higher concentration an enhancement was clearly observed. Best inactivation performance was obtained at 0.005 mM of PMS, at which DL was achieved in 20 minutes (1.2 kJ/L of Q_{UV}), 25 minutes (1.5 kJ/L of Q_{UV}), and 30 minutes (1.8 kJ/L of Q_{UV}) for *E. coli*, *P. aeruginosa* and *E. faecalis*, respectively. Concentration of 0.01 mM did not significantly enhance the inactivation kinetics, suggesting that, once the optimal condition has been reached, higher oxidative conditions are not required.

6. PMS/Solar for water purification

These results agree with other studies reported in literature. Rodríguez-Chueca et al. reported an enhancement on the inactivation of *E. coli* K12 under artificial solar light by the addition of $9 \cdot 10^{-5}$ M of PMS (DL in 45 minutes) in comparison with the solely effect of artificial light (2.8-LRV in 300 minutes) (Rodríguez-Chueca, 2019e). Ozores-Diez et al. reported the efficiency of PMS/Solar (36 $\mu\text{mol/L}$) in 19L-polycarbonate bottles in different water matrices, compared to solar only disinfection. It was shown a significant increase in *E. coli* K12 inactivation kinetics, reaching DL after 60 minutes in the presence of PMS, compared to 90 minutes with the solar only inactivation process in distilled water. Higher treatment time was necessary with tap water, reaching 6 LRV after 90 and 180 minutes for PMS/Solar and only solar, respectively (Ozores Diez, 2020).

The degradation profiles and kinetic rates of DCF (a), SMX (b) and TMP (c) and total CECs (d) with different concentrations of PMS under natural solar radiation are shown in Figure 6.6 and Table B.5 (Annex B), respectively.

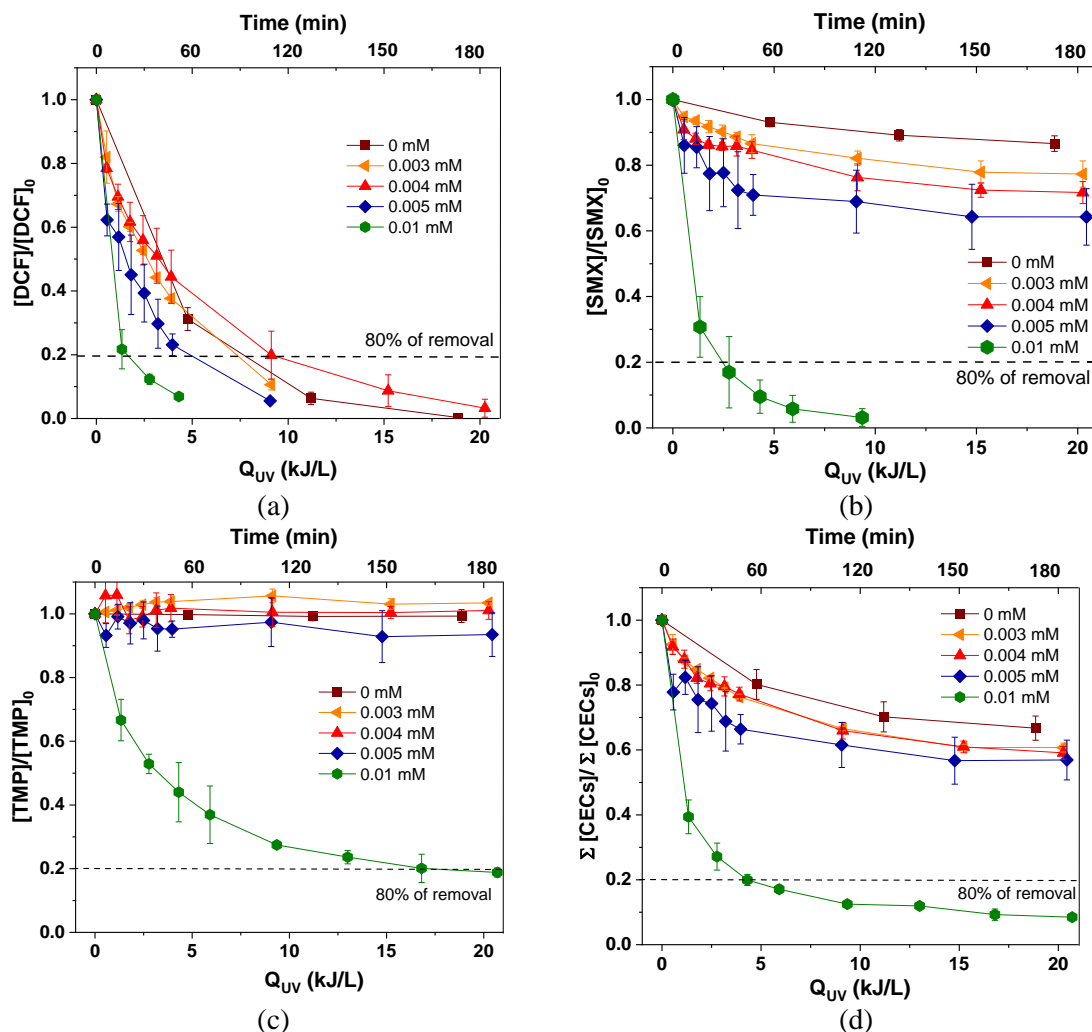


Figure 6.6. Degradation profiles of (a) DCF, (b) SMX, (c) TMP and (d) total CECs by PMS/Solar system at different PMS concentrations in IW and under natural solar radiation.

The effect of solar radiation on CECs was also reported (0 mM) and it can be observed that DCF was the only compound that underwent photolysis under sunlight, due to the overlapping of the compound spectrum with the solar region between 300 nm and 330 nm (Agüera, 2005). Nevertheless, the addition of PMS significantly enhanced CECs degradation and the best performance was obtained with 0.01 mM of PMS, achieving 80 % removal in all cases (4.3 kJ/L and 45 minutes for 80 % of total CECs abatement), with the following order of reactivity: DCF (16 minutes, Q_{UV} = 1.5 kJ/L) > SMX (27 minutes, Q_{UV} = 2.5 kJ/L) > TMP (150 minutes, Q_{UV} = 16.8 kJ/L).

6.3 Interpretation of abatement mechanisms by PMS/Solar radiation

Figure 6.7 shows a comparison between the different kinetic constants found in (i) PMS/Dark, (ii) only solar radiation and (iii) PMS/Solar process at the best PMS concentration obtained for bacterial inactivation (0.005 mM) and CEC degradation (0.01 mM). For comparison purposes, $k_{PMS/dark}$ and k_{Solar} have been calculated considering the same treatment time of PMS/Solar process required to reach the DL for each bacterial target or 80 % removal of each CEC.

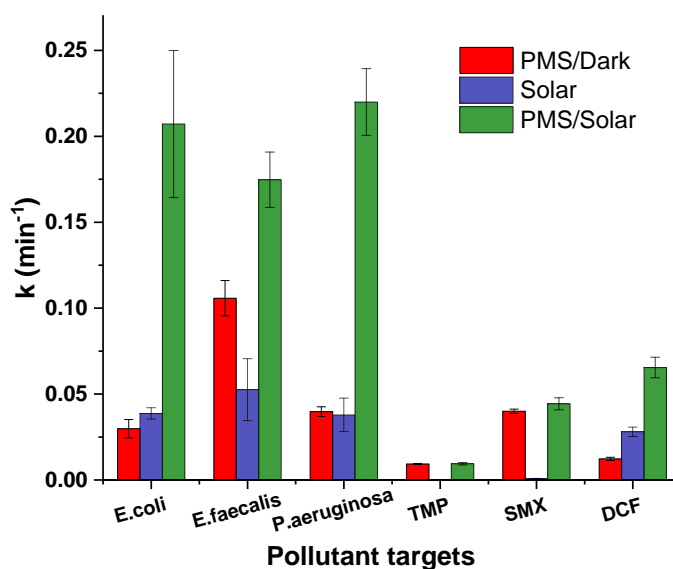


Figure 6.7. Kinetic constant values of bacterial inactivation at 0.005 mM of PMS and CECs degradation at 0.01 mM of PMS, in the dark and under natural solar radiation in IW.

A significant enhancement of the efficiency in the system PMS/Solar compared to solar photo-inactivation and PMS/Dark was obtained for bacteria and a relevant increase in the inactivation constant was obtained with a factor of 5.4, 3.3 and 5.8, compared to only solar

6. PMS/Solar for water purification

radiation, and 6.9, 1.7 and 5.5, compared to PMS/Dark, for *E. coli*, *E. faecalis* and *P. aeruginosa*, respectively.

For CECs (Figure 6.7), degradation rates in PMS/Solar system increased of a factor equal to 2, 55 and 100 times for DCF, SMX and TMP, respectively, compared to solar photolysis. On the other hand, similar kinetic constants were obtained for PMS/Solar and PMS/Dark for SMX and TMP, while DCF had a degradation rate 5 times higher.

The synergy index (SI) was calculated, according to Eq. 6.1, in order to determine the effect of the combination of sunlight and PMS (Mecha, 2017).

$$SI = \frac{k_{PMS/Solar}}{k_{Solar} + k_{PMS/dark}} \quad \text{Eq. 6.1}$$

Where $k_{PMS/Solar}$ is the constant value obtained with PMS/Solar, k_{solar} is the constant value obtained by solar-inactivation or photolysis and $k_{PMS/dark}$ is the constant value obtained by PMS/Dark for each target analysed. $SI \leq 1$ no synergy and $SI > 1$ means synergy effect for PMS/Solar system.

SI values for *E. coli*, *P. aeruginosa* and *E. faecalis* were 3.0, 2.8 and 1.1, respectively, with a greater effect for the two gram-negative bacteria, *E. coli* and *P. aeruginosa*, than *E. faecalis* (gram-positive).

On the other hand, SI values for TMP, SMX and DCF were 1.0, 1.1 and 1.6, respectively for PMS/Solar system, revealing a very slight synergistic effect between solar radiation and PMS. In fact, the main operating mechanism is direct target oxidation by PMS both under dark conditions and under natural solar radiation.

This difference on the synergistic degradation between CECs and bacteria could be attributed to the different mechanism by which each type of pollutant is abated. In the removal mechanism of both bacteria and CECs, $SO_4^{\cdot-}$ radicals' generation by activation of PMS with the solar wavelengths reaching the Earth's surface (> than 300 nm) could be discarded, as it has been explained in Chapter 5, confirming the absence of synergies in the PMS/Solar system for CEC removal. However, the inactivation mechanism of bacteria is more complex and the higher performances observed by PMS/Solar process could be related to the following different factors (simplified in Figure 6.8), operating simultaneously and in a synergistic way:

- Effect of solar photons with formation of intracellular ROS (according to the mechanism reported in Figure 1.10) and inactivation of key enzymes such as catalase and superoxide dismutase (Nelson, 2018).
- Direct oxidative effect of PMS over the cell wall components, including lipids peroxidation, inhibiting normal metabolism, changing membrane permeability and ultimately leading to cell death (Xiao, 2019).
- Possible penetration of HClO, formed after oxidation of Cl⁻ contained in IW.

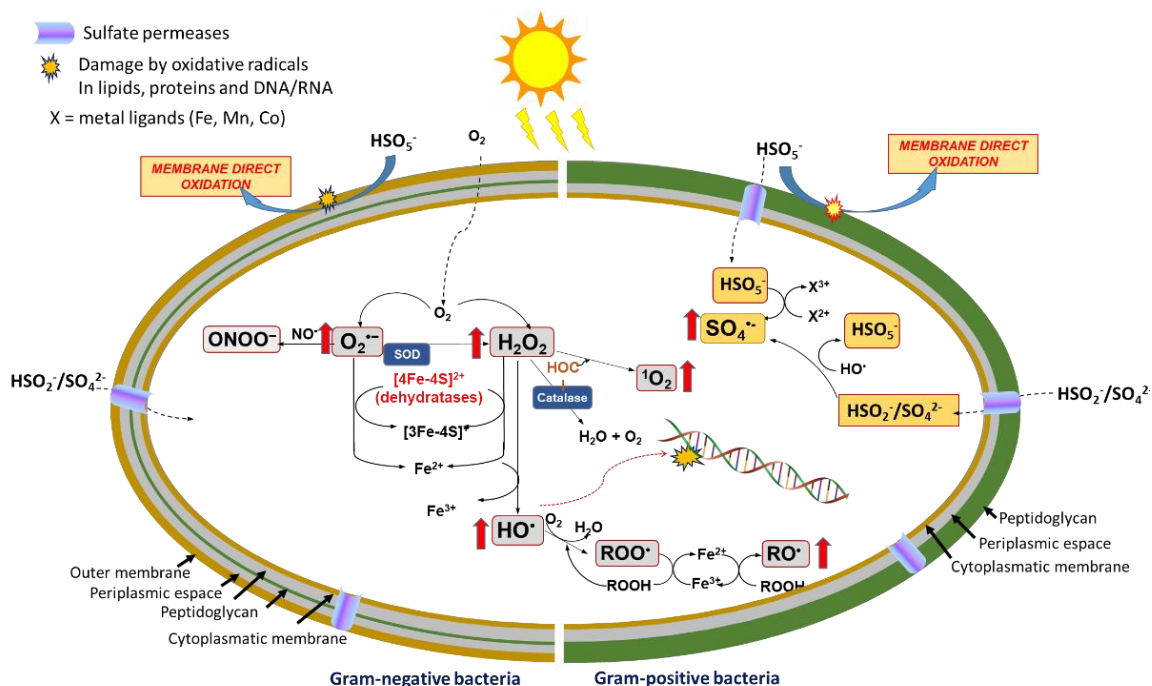


Figure 6.8. Proposed inactivation mechanism of bacteria by PMS/Solar treatment.

Additionally, and although not experimentally demonstrated, internal damages in bacteria in the presence of sulfate species could be also considered. This damage on internal cell components, such as enzymes and genetic material, could be attributed to the potential diffusion or penetration of sulfate species through membrane-protein transporters (such as sulphate permeases, well defined in gram-negative bacterium such as *E. coli* and *Salmonella* spp.) (Aguilar-Barajas, 2011). Moreover, their further plausible reactions with metals (such as iron, cobalt or manganese, naturally occurring in cells and whose release is particularly increased during solar exposure (Giannakis, 2016)), could occur, making the promotion of SO₄^{•-} generation inside cells possible (Xiao, 2019).

Finally, higher susceptibility of gram-negative bacteria (*E. coli* and *P. aeruginosa*) than the gram-positive one (*E. faecalis*) to PMS/Solar treatment has been obtained, attributed mainly

6. PMS/Solar for water purification

to the thicker cell-wall structure of the gram-positive bacteria. This behaviour trend has been also widely reported for other solar photo-chemical (PS/Solar, H₂O₂/Solar) and photocatalytic (TiO₂ and photo-Fenton) treatments (Van Grieken, 2010).

6.4 Disinfection and decontamination performances in natural well water

The efficiency of PMS/Solar process for the simultaneous disinfection and decontamination in natural well water was also assessed. The main physicochemical characteristics of this water matrix are reported in Table 3.5, highlighting the low presence of organic matter (DOC < 6 mg/L) and the high concentration of bicarbonates ([HCO₃⁻] ~ 800 mg/L). Therefore, natural diluted WeW (d-WeW) was also investigated as model of a softer well water ([HCO₃⁻] ~ 80 mg/L).

Figure 6.9 shows the individual bacterium and CEC removal profiles obtained in WeW and d-WeW in the absence (only solar radiation) and in the presence of PMS (at 0.01 mM) under natural solar radiation. Kinetic rates are summarized in Table B.6.

A significant enhancement in kinetic rates was observed by adding PMS in both water matrices, compared to solar only radiation. DL in the presence of PMS was achieved after 50, 50 and 90 minutes (4.2, 4.2 and 8.2 kJ/L) for *E. coli*, *P. aeruginosa* and *E. faecalis*, while in the absence of oxidant more than 180 minutes were necessary to reach DL (except for *E. coli*, that was inactivated in 120 minutes). Higher inactivation rates were obtained in diluted matrix and DL in the presence of PMS was achieved after 15, 15 and 60 minutes (1.3, 1.3 and 5.2 kJ/L) for *E. coli*, *P. aeruginosa* and *E. faecalis*. Regarding CECs, 80 % of removal was achieved only for DCF after 45 minutes (3.7 kJ/L), while 60 % and 17 % of degradation of SMX and TMP, respectively, were observed after 180 minutes (16.8 kJ/L), obtaining similar performances in the two water matrices.

These results evidence the efficient disinfection obtained by PMS/Solar process with 0.01 mM, while higher oxidant demand is necessary for an effective decontamination. Moreover, no regrowth after 24-48 h of storage was observed, highlighting the benefits of using PMS to control post-treatment reactivation of bacteria, during both storage or in the distribution systems. Moreover, significant differences in comparison with IW can be observed, and therefore a more exhaustive analysis of the inorganic ions effect on the performance of this solar process was done and the results are shown in the next section.

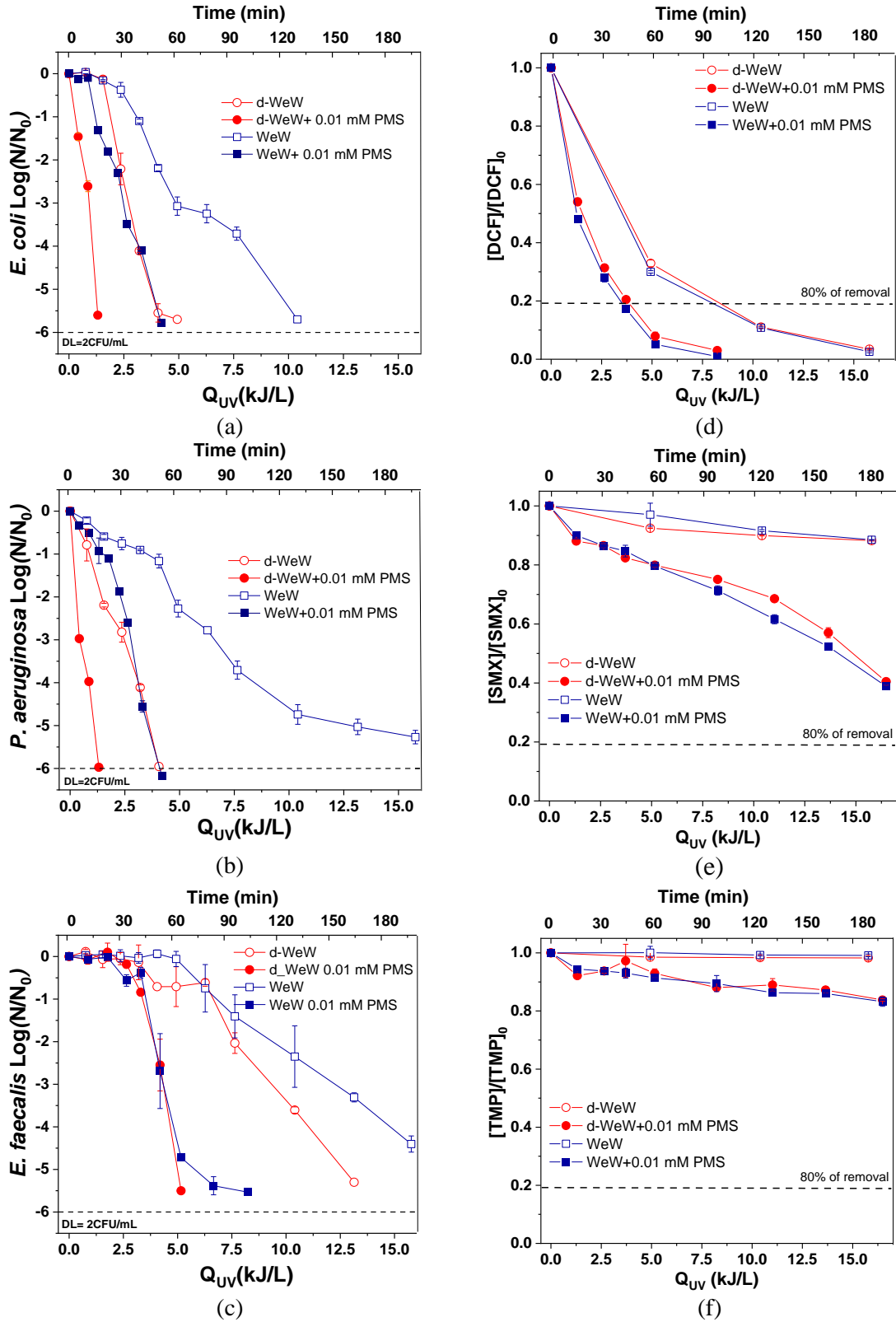


Figure 6.9: Inactivation profiles of *E. coli* (a), *P. aeruginosa* (b), *E. faecalis* (c) and degradation profiles of DCF (d), SMX (e), TMP (f) in diluted well water (d-WeW) and well water (WeW) by PMS/Solar at 0.01 mM of oxidant.

6.5. Effect of inorganic species on PMS/Solar system performance

To evaluate the effect of Cl^- and HCO_3^- (two chemical inorganic species commonly present in surface and well waters) on the PMS/Solar system performance, a comparative analysis of the results previously obtained with PMS (0.01mM) and without oxidant (solar only radiation) were accomplished. The following water matrices were used: (i) IW ($[\text{Cl}^-]=9\text{g/L}$), (ii) d-WeW ($[\text{HCO}_3^-] \sim 80 \text{ mg/L}$), (iii) WeW ($[\text{HCO}_3^-] \sim 800 \text{ mg/L}$) and (iv) distilled water (DW) (as model of water matrix without inorganic ions). In the specific case of bacteria, experiments in DW were not carried out, due to the well-known osmotic stress generated on microbial cells. The individual bacterial inactivation and CECs pseudo-first order degradation kinetic necessary to achieve DL of 2 CFU/mL for each microbial target and 80 % of removal of each CEC are summarize in Table B.6 (Annex B).

The inactivation profiles of the sum of all bacteria are shown in Figure 6.10a, while the degradation profiles of total CECs can be observed in Figure 6.10b.

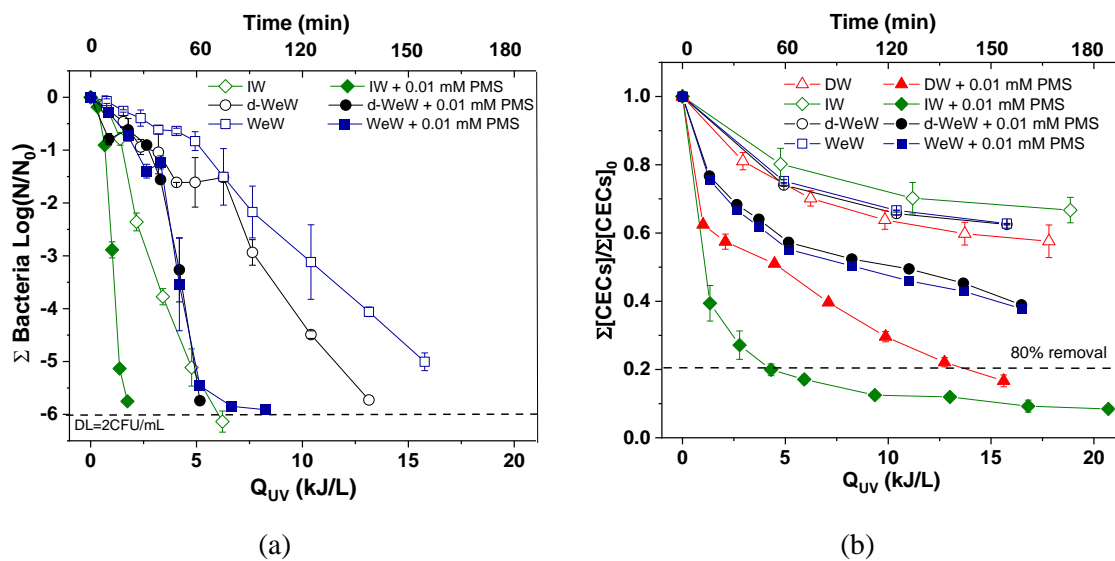


Figure 6.10. (a) Inactivation profiles of the sum of all bacteria and (b) degradation profiles of total CECs in DW, IW, d-WeW and WeW by solar only radiation and PMS/Solar at 0.01 mM under natural solar radiation.

Considering the solar only disinfection processes, the composition of the water matrix had a significant impact on the inactivation of bacteria in water and higher treatment times were required to achieve DL, following the order of water matrix complexity $\text{IW} < \text{d-WeW} < \text{WeW}$. Opposite result is clearly observed for CECs, as almost no differences on the degradation profiles were obtained (Figure 6.10).

On the other hand, a significant enhancement of chemical and microbiological targets removal rates was observed adding PMS in all water matrices, while the main effects of inorganic ions on disinfection and decontamination performance could be summarized as follow:

- Positive effect of the presence of chloride ions (9 g/L), provoking faster microbial inactivation and CECs degradation, due to direct oxidation of Cl^- by PMS with generation of HClO/Cl_2 , as it has been explained in Chapter 5. As regard CECs, 80 % removal of total CECs degradation was achieved in 45 minutes in IW, compared to 145 minutes in DW.
- Lower efficiency of the process in the real water matrix WeW, in comparison to both DW and IW, due to its higher complexity in chemical composition with different inorganic ions present simultaneously.
- Low influence of HCO_3^- concentration: despite an enhanced disinfection performance in d-WeW (characterized by a lower concentration of these ions), a scavenging effect of these ions was excluded, comparing the inactivation profile in the absence of PMS. In fact, the low conductivity of d-WeW (Table 3.5) could be the responsible of higher inactivation rate, creating an osmotic stress condition that leads to cell death. Moreover, it could be observed that the two gram-negative bacteria (*E. coli* and *P. aeruginosa*) were more affected by osmotic stress, while no significant differences between the two matrices were obtained for the more resistant gram-positive *E. faecalis*. As regards CECs, overlapped degradation profiles confirms the absence of HCO_3^- scavenging effect, as a proof also of the no generation of $\text{SO}_4^{\cdot-}$ and HO^{\cdot} in solution. The feasibility of the PMS/Solar process to treat matrices with different loads of $\text{HCO}_3^-/\text{CO}_3^{2-}$ has been demonstrated.

6.6 Concluding remarks

The feasibility of non-activated PMS as oxidant agent at very low concentrations and its combination with a renewable source of energy, such as natural solar radiation, for simultaneous water disinfection and decontamination has been demonstrated. A significant oxidative effect of PMS in darkness was obtained for both bacteria and CECs abatement and an enhancement of all targets removal kinetic rates (especially microbial ones) were obtained under natural solar radiation, reaching > 5 LRV in 30 minutes (1.5 kJ/L of Q_{UV}) (with the optimal load of 0.005 mM), while 80 % of total CECs was removed after

6. PMS/Solar for water purification

45 minutes (4.3 kJ/L) at the optimal dose of 0.01 mM, being TMP the most refractory compound (requiring 150 minutes, 16.8 kJ/L to reach 80 % of removal). A direct oxidative mechanism has been proposed for the inactivation and degradation of all targets, discarding $\text{SO}_4^{\cdot-}$ and HO^{\cdot} generation in solution. The effect of commonly present inorganic ions was evaluated and results revealed that (i) high Cl^- concentration (IW) enhanced the process, (ii) the presence of a complex inorganic chemical water composition reduced the system efficiency (WeW) and (iii) no differences were obtained in the presence of different concentration of HCO_3^- (WeW versus d-WeW), obtaining the following global PMS/Solar efficiency performance order: $\text{IW} > \text{DW} > \text{WeW} = \text{d-WeW}$.

As a conclusion, PMS/Solar system could be applied for a wide range of water, containing different inorganic ion concentrations and it could be an efficient and promising process for groundwater treatment.

CHAPTER 7

**ACTUAL WASTEWATER PURIFICATION
BY PEROXYMONOSULFATE AND SOLAR
RADIATION AT PILOT PLANT SCALE**

7. ACTUAL WASTEWATER PURIFICATION BY PEROXYMONOSULFATE AND SOLAR RADIATION AT PILOT PLANT SCALE

In this chapter, the already demonstrated capability of PMS alone in combination with natural sunlight for disinfection and decontamination of clear water (Chapter 6) has been furthermore investigated simulating a scenario close to a real implementation. To that, more complex water matrices (simulated UWW and actual UWW) were used to assess the simultaneous removal of microbial and chemical targets. A preliminary study was performed in SUWW in the presence of several PMS concentrations to evaluate the effect of NOM and inorganic ions on process performance. Then, experimental assays in UWW were carried out at pilot plant scale using a solar CPC reactor to elucidate the up-scaling of this type of solar process. The capability of the PMS/Solar process was evaluated in actual UWW by following the inactivation of several natural occurring bacteria (*E. coli*, Total coliforms, *Enterococcus* spp. and *Pseudomonas* spp.) and the degradation of CECs

7. PMS/Solar for wastewater purification

(DCF, SMX and TMP) in the presence of different PMS concentration (0-1 mM) under natural solar radiation.

Moreover, inactivation of naturally occurring ARB, grown in the presence of sub-minimal inhibitory concentrations of AMP, CPX and TMP and removal of the genes 16S rRNA, *intI1* and selected ARGs commonly found in UWW (*sul1*, *qnrS*, *blaTEM*, *blaCTX-M32*, *tetM*) were also investigated in the presence of the best concentration of PMS previously obtained.

Finally, in this chapter the testing at laboratory scale of the best-performing photocatalytic material (ZnO-Ce from Chapter 4) is also included in combination with PMS as a strategy to enhance the solar system for UWW purification.

7.1 PMS/Solar process performance in simulated urban wastewater

7.1.1 Assessment of microbial and CECs abatement

Disinfection and decontamination performances of the PMS/Solar process were preliminarily assessed in SUWW to evaluate the influence of the organic matter under controlled conditions in 200-mL solar vessel reactors at laboratory scale. The first difference observed in comparison with clear waters (IW, DW and WW, Chapter 6) was the required PMS initial concentration to detect an effective target (both microbial and chemical) abatement. In SUWW, concentrations of PMS lower than 0.01 mM are not expected to determine any significant CECs removal (according results obtained in IW), and therefore concentrations from 0.01 mM to 0.5 mM were investigated. The inactivation and degradation profiles of each microbial and chemical target and their summation in the presence of these PMS concentrations are shown in Figures 7.1 and 7.2, respectively; and Tables B.4 and B.5 (Annex B) summarize the corresponding pseudo-first order kinetic constants. Water temperature ranged between 25 to 37 °C and solar UV-A irradiance between 25 to 45 W/m², while water pH was 8-8.5 in all cases, remaining constant along the treatment time. At this pH, PMS still exists in its monoanionic form (HSO₅⁻) (Figure 5.2, Chapter 5), and a significant effect of pH could be excluded.

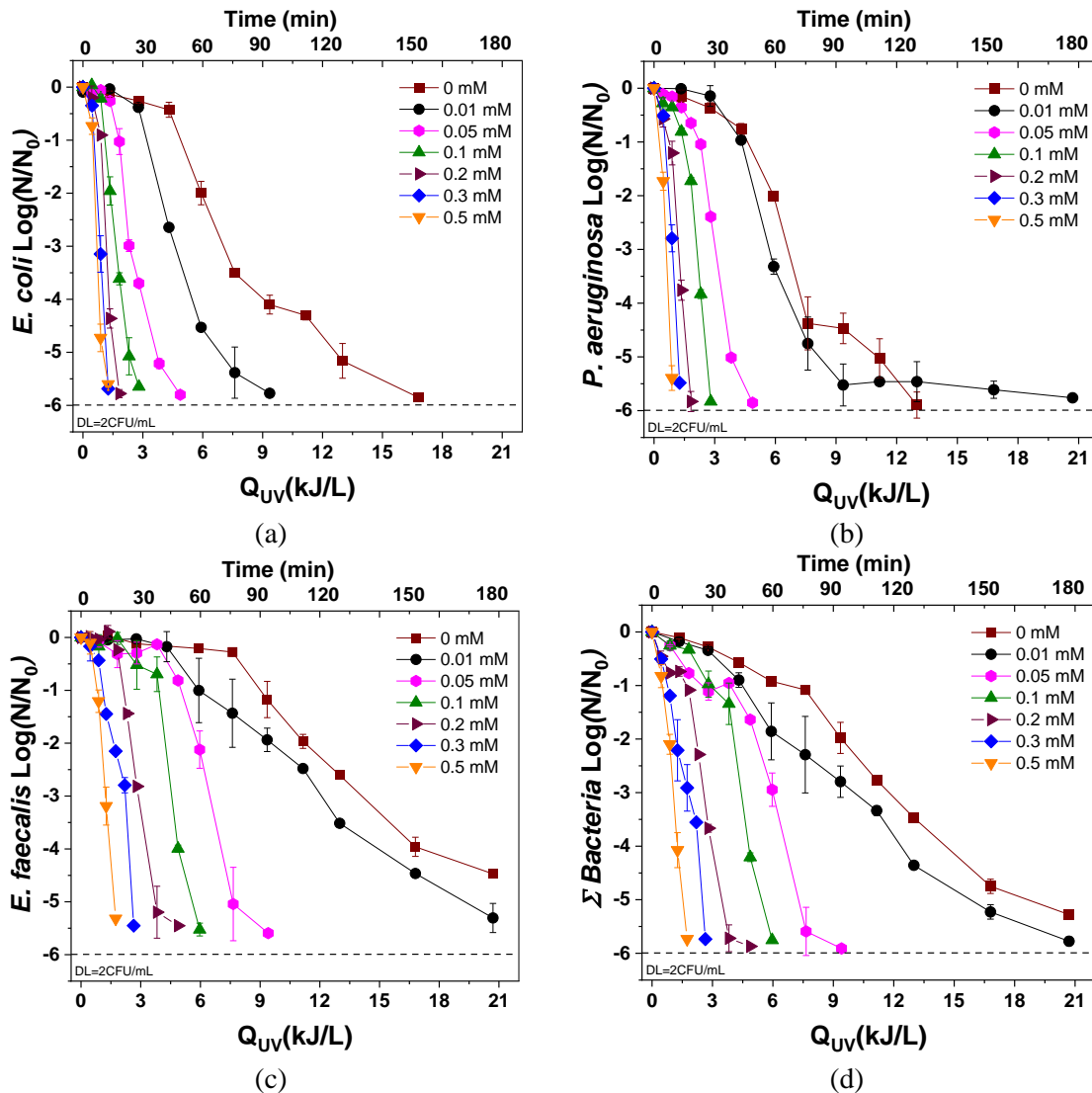


Figure 7.1: Inactivation profiles of *E. coli* (a), *P. aeruginosa* (b), *E. faecalis* (c) and sum of bacteria (d) in SUWW by PMS/Solar (0-0.5 mM).

These results confirm the effectiveness of the PMS/Solar process for water purification even in the presence of organic matter (DOC in SUWW-2 of 11.1 ± 2.5 mg/L), and the required increase oxidant concentration. As expected, the lowest treatment efficiency was obtained in the presence of only natural solar radiation (0 mM of PMS), achieving 6 LRV for *E. coli* and *P. aeruginosa* after 150 minutes, 4 LRV for the more resistant gram-positive bacterium *E. faecalis* and 30 % of removal of total CECs after 180 minutes, being only DCF effectively removed (reasons already explained in Chapter 6). The addition of increasing concentrations of PMS determined better performances for both bacteria inactivation (Figure 7.1) and CECs removal (Figure 7.2). It can be observed that the higher the PMS concentration added, the higher the inactivation/degradation rates obtained, obtaining the best process

7. PMS/Solar for wastewater purification

performance at 0.5 mM of PMS: 6-LRV of bacteria reached after 20 minutes (1.7 kJ/L of Q_{UV}), and 80 % average degradation of CECs after 78 minutes (6.5 kJ/L of Q_{UV}).

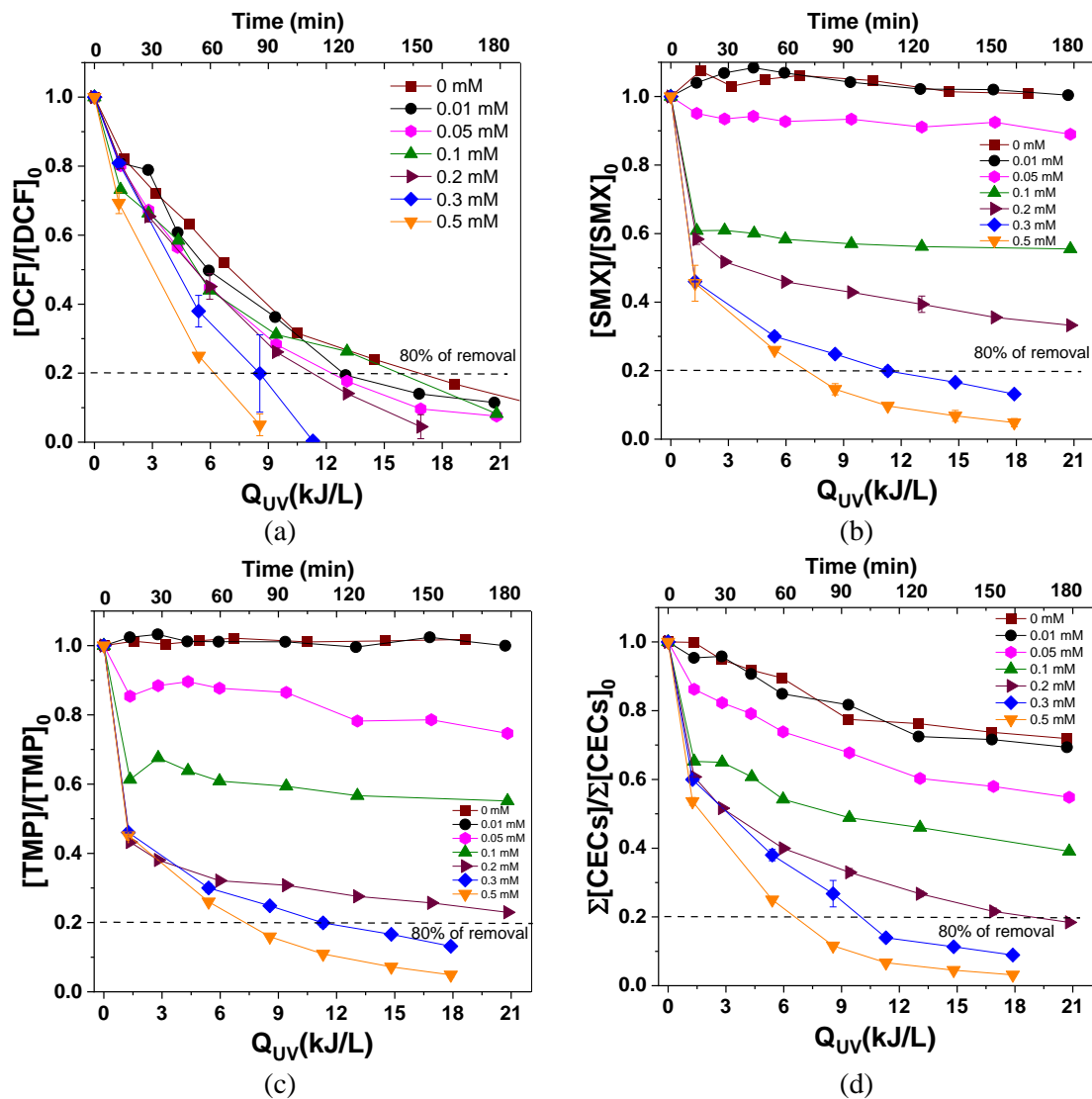


Figure 7.2: Degradation profiles of DCF (a), SMX (b), TMP (c) and total CECs (d) in SUWW by PMS/Solar (0-0.5 mM).

In addition, to exclude an aggressive effect of 0.5 mM of PMS concentration on the targets, considering the previous results in IW, a dark control test at this concentration was performed. Figure 7.3 shows the comparison between the inactivation profiles of the total concentration of bacteria and total CECs degradation in SUWW by only solar radiation, PMS/Dark and PMS/Solar at 0.5 mM. The results show that in the presence of the same oxidant concentration, lower efficiencies were obtained under darkness than under solar radiation: DL was achieved after 75 minutes and only 67 % of CECs removal after 180 minutes for PMS/Dark, compared to 20 minutes for bacterial inactivation and to 80 % of removal after 70 minutes for PMS/Solar. Besides, a similar synergetic effect than the

obtained in IW is again observed herein (i.e., higher SI indexes for microbial targets (4, 7 and 50 for *P. aeruginosa*, *E. coli* and *E. faecalis*, respectively) than for chemical ones (1, 2 and 3 for SMX, TMP and DCF, respectively), reinforcing therefore the insights of the mechanism governing the inactivation and CEC degradation by PMS alone with natural sunlight already described in Chapter 6.

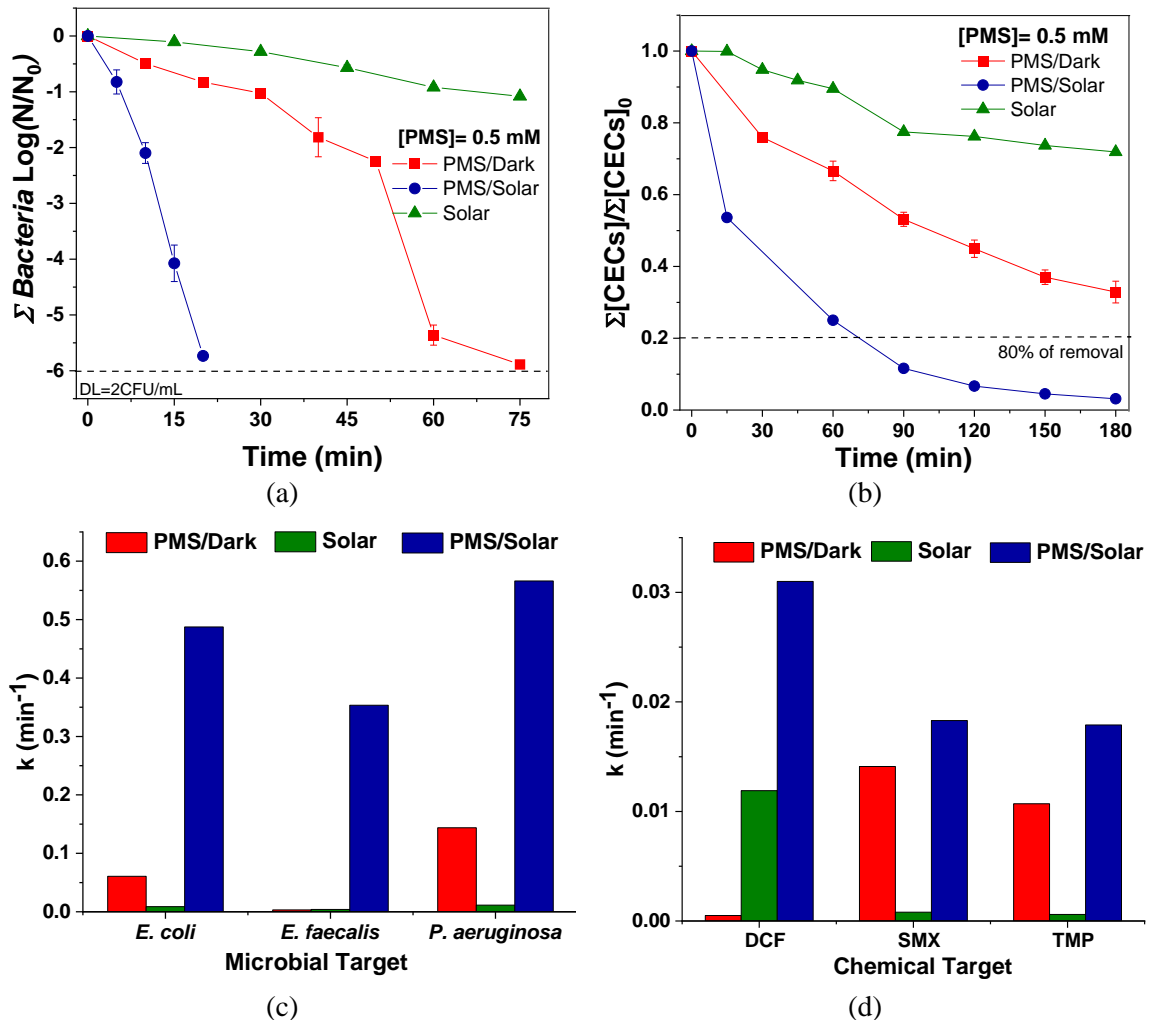


Figure 7.3. (a) Inactivation profiles of the total concentration of bacteria, (b) total CECs degradation and inactivation (c) and degradation (d) kinetic constant values in SUWW by PMS at 0.5 mM under darkness and under natural solar radiation.

7.1.2 Assessment of organic matter influence

It has been clearly demonstrated that the water matrix significantly affected both disinfection and decontamination efficiency and lower degradation and inactivation performances were obtained in SUWW, compared to IW, requiring higher treatment time to achieve targets' removal or needing higher oxidant dosage. This lower efficiency could be related mostly to oxidant consumption by water components, because as it has been

7. PMS/Solar for wastewater purification

demonstrated in previous chapters, under natural solar radiation the generation of $\text{SO}_4^{\cdot-}$ and HO^{\cdot} could be discarded, excluding also radical scavenging effect by water matrix species.

Therefore, the PMS concentration profiles measured at all oxidant concentration tested in SUWW are shown in Figure 7.4a. Besides, PMS consumption was followed under dark conditions in three different matrices characterized by increasing complexity, such as DW, SUWW and UWW (Figure 7.4b), and in the presence of different components of organic matter (contained in the SUWW receipt) (Figure 7.4c).

These results show that, higher PMS consumption was observed with the increase of water matrix complexity, as a consequence of a possible oxidation of organic matter, with a significant effect of tannic acid on PMS concentration decrease. In the present results, the DOC did not show any decrease in its concentration along the treatment time, nevertheless modifications of the nature or structure of the NOM contained in UWW cannot be discarded, being its presence the main reason to explain the increase oxidant concentration required to achieve good performance on microbial and CECs removal.

Similar results have been reported in the literature regarding the influence of the organic matter by PMS/Solar process. Solís et al. investigated the degradation of a mixture of six CECs (100 $\mu\text{g/L}$ each, caffeine, primidone, *N,N*-diethyl-3-methylbenzamide (DEET), methylparaben, clofibrac acid and ibuprofen), using simulated solar radiation, achieving the complete degradation after 90 minutes in the presence of 0.5 mM of PMS in ultrapure water. However, to obtain similar performances in a complex matrix, such as UWW, an increasing PMS concentration of ten times was required, observing a significant water matrix effect (Solís, 2020).

Moreover, Zhang et al highlighted an inhibition in the oxidation of para-aminobenzoic acid (PABA) in the presence of NOM, due to an oxidant consumption by humic-like substances (containing phenolic groups). Less PMS residual concentration was observed when NOM concentration was higher, suggesting that the lower PABA oxidation by PMS was due to the competition for PMS between organic matter and PABA (Zhang, 2020).

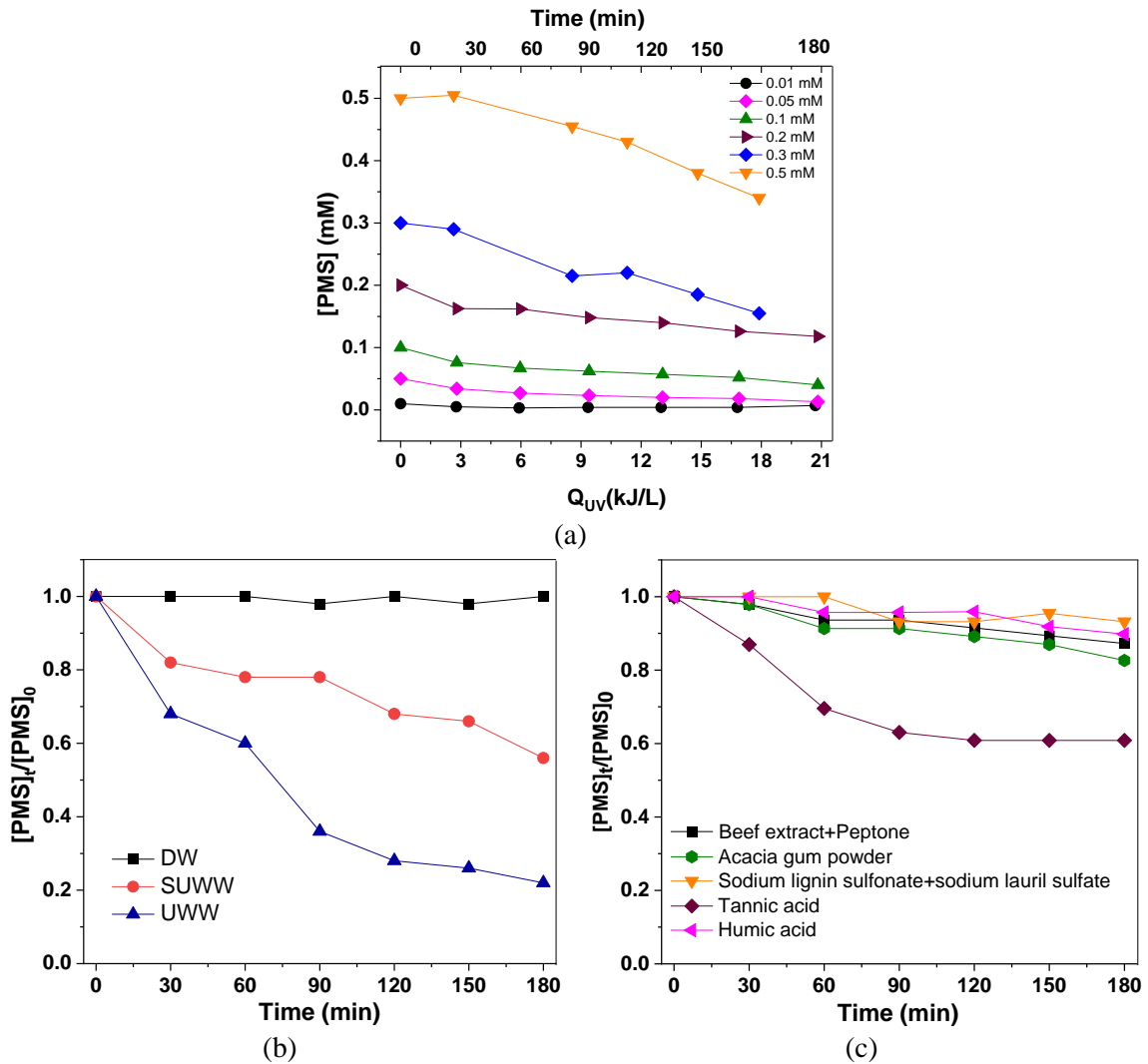


Figure 7.4. PMS concentration profiles along: (a) all solar treatments in SUWW (0.01-0.5 mM); (b) at 0.05 mM in the dark and with different water matrixes (DW, SUWW and UWW); (c) at 0.05 mM with different organic matter components (concentration according to SUWW recipe).

7.2 PMS/Solar process performance in actual urban wastewater

Subsequently, disinfection and decontamination performances by PMS/Solar were evaluated in actual UWW at pilot plant scale, to assess the capability of the process to obtain water with a quality enough to be reused in agriculture. A solar CPC photo-reactors with a total volume of 10 L and 5 L of illuminated volume was used in recirculation batch mode at 30 L/min of flow-rate. Water temperature ranged between 22 to 39 °C and solar UV-A irradiance between 25 to 45 W/m², while water pH was 8-8.5 in all cases, remaining constant along the treatment time.

The microbial inactivation of naturally occurring bacteria including *E. coli*, *Enterococcus* spp., *Pseudomonas* spp., Total coliforms and their corresponding ARB

7. PMS/Solar for wastewater purification

counterparts, the removal of naturally present ARGs and the degradation of spiked CECs (at 100 µg/L each) were simultaneously monitored along the solar tests. In this case, to determine the optimal concentration in UWW and considering the previous oxidant consumption profile of 0.5 mM observed in Figure 7.4b and on the base of other study (Solis, 2020), the tested PMS concentrations ranged from 0 (solar only) to 1 mM.

PMS consumption during all the solar experiments is shown in Figure 7.5. It is observed a sharp decrease of all the initial added PMS concentrations, and only in the case of 1 mM initial concentration, a significant residual PMS concentration is detected at the end of the process, which is key to avoid post-treatment regrowth. Nevertheless, no bacteria regrowth was observed for any microbial targets after 24h and 48h from the treatment in the presence of initial concentrations higher than 0.5 mM. DOC concentration remained constant for dosage ≤ 0.75 mM, while at 1 mM 9 % of removal was observed after 180 minutes, highlighting the need of more oxidative conditions to attain organic matter oxidation.

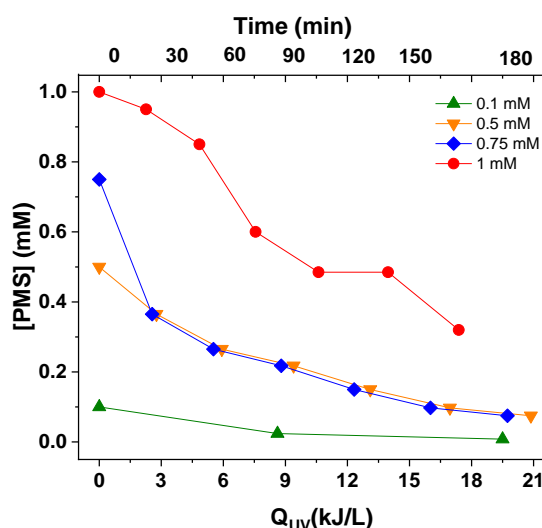


Figure 7.5: PMS concentration profiles measured along PMS/Solar treatments in UWW (0.1-1 mM).

7.2.1 Bacterial inactivation kinetics

Figure 7.6 and Table B.4 shows the microbial inactivation profiles and kinetic data obtained in actual UWW in the presence of increasing concentration of PMS (in the range 0.1-1 mM), respectively.

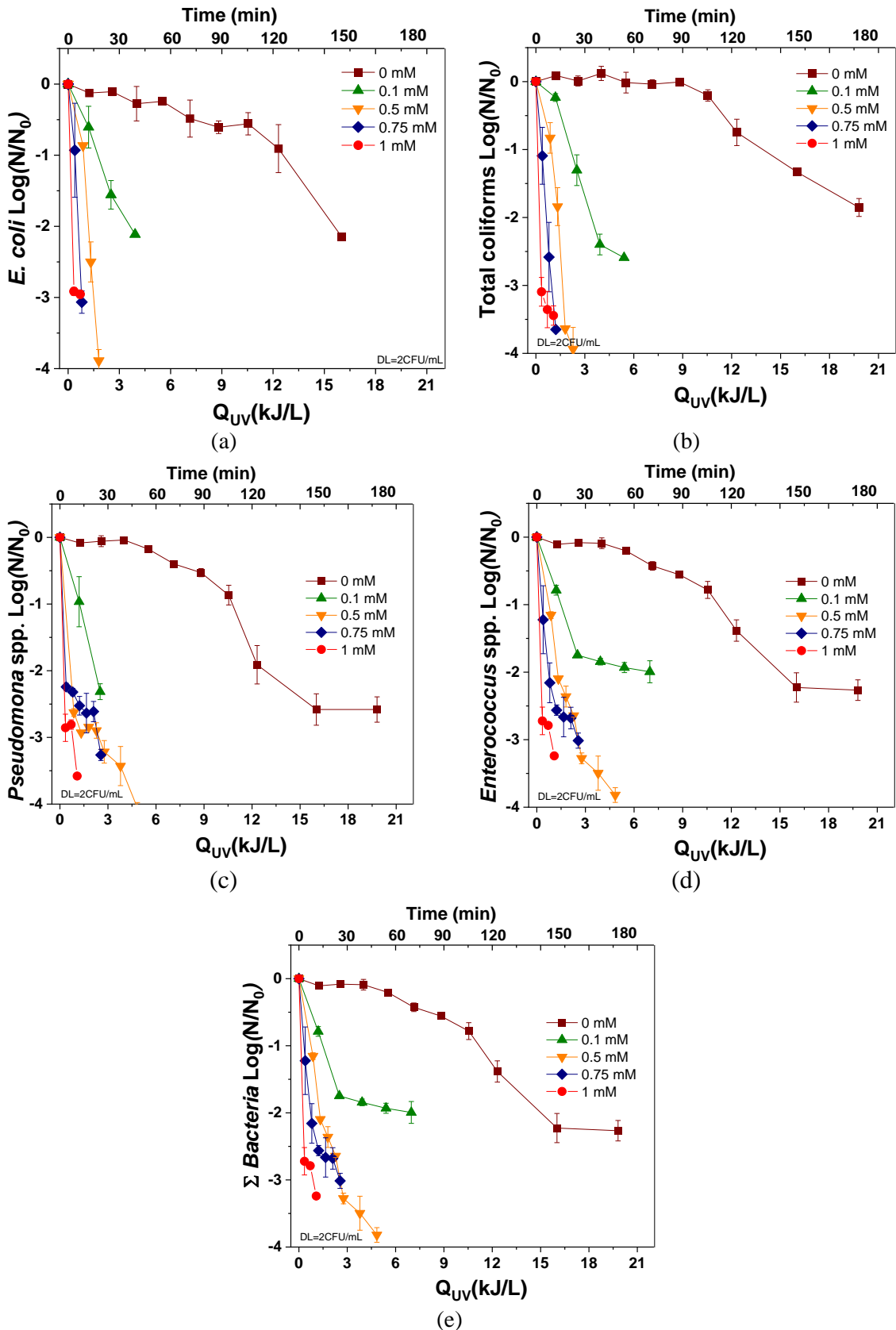


Figure 7.6: Inactivation profiles of *E. coli* (a), Total coliforms (b), *Pseudomonas* spp. (c), *Enterococcus* spp. (d) and sum of bacteria (e) in UWW by PMS/Solar (0-1 mM).

7. PMS/Solar for wastewater purification

An enhancement in process performance was obtained in the presence of increasing oxidant concentrations and best results were obtained with 1 mM, at which DL of 2 CFU/mL was reached for all microbial target after 15 minutes (1.1 kJ/L of Q_{UV}) of treatment time. For comparison with only solar radiation, 180 minutes (20 kJ/L of Q_{UV}) were necessary to reach DL for bacteria.

Currently, the regulation for UWW reuse (EU 2020/741) includes only *E. coli* as main indicator for the microbial assessment. However, focusing only on this microbial target, no significant differences were obtained between 0.5, 0.75, and 1 mM of PMS, indicating that 0.5 mM was enough to guarantee bacterium inactivation, avoiding post-treatment regrowth and allowing to meet minimum quality criteria imposed by the regulation.

The individual bacterial behavior revealed the following order (according also to kinetic data reported in Table B.4 of Annex B): *Pseudomonas* spp. (gram negative) \approx *E. coli* (gram-negative) > Total coliforms (gram-negative) > *Enterococcus* spp. (gram-positive), in line with gram-negative bacteria higher susceptibility, mainly attributed to a thinner peptidoglycan layer (Van Grieken, 2010).

7.2.2 CECs degradation kinetics

Figure 7.7 and Table B.5 (Annex B) show the CECs profiles and kinetic data, respectively, obtained in actual UWW in the presence of increasing concentration of PMS (in the range 0.1-1 mM). A significant enhancement in comparison with only solar radiation (only 40 % of the total CEC removal after 180 minutes or 20 kJ/L of Q_{UV}) was obtained in the presence of added PMS. Concentrations higher than 0.75 mM were necessary to attain good removal efficiency for the more refractory TMP and the best CECs results were obtained with 1 mM, at which total CECs degradation (> 80 % removal) was achieved after 27 minutes (2 kJ/L of Q_{UV}).

In particular, the following CECs reactivity order was found: SMX (17 minutes, Q_{UV} = 1.2 kJ/L) > DCF (30 minutes, Q_{UV} = 2.3 kJ/L) > TMP (40 minutes, Q_{UV} =3.2 kJ/L).

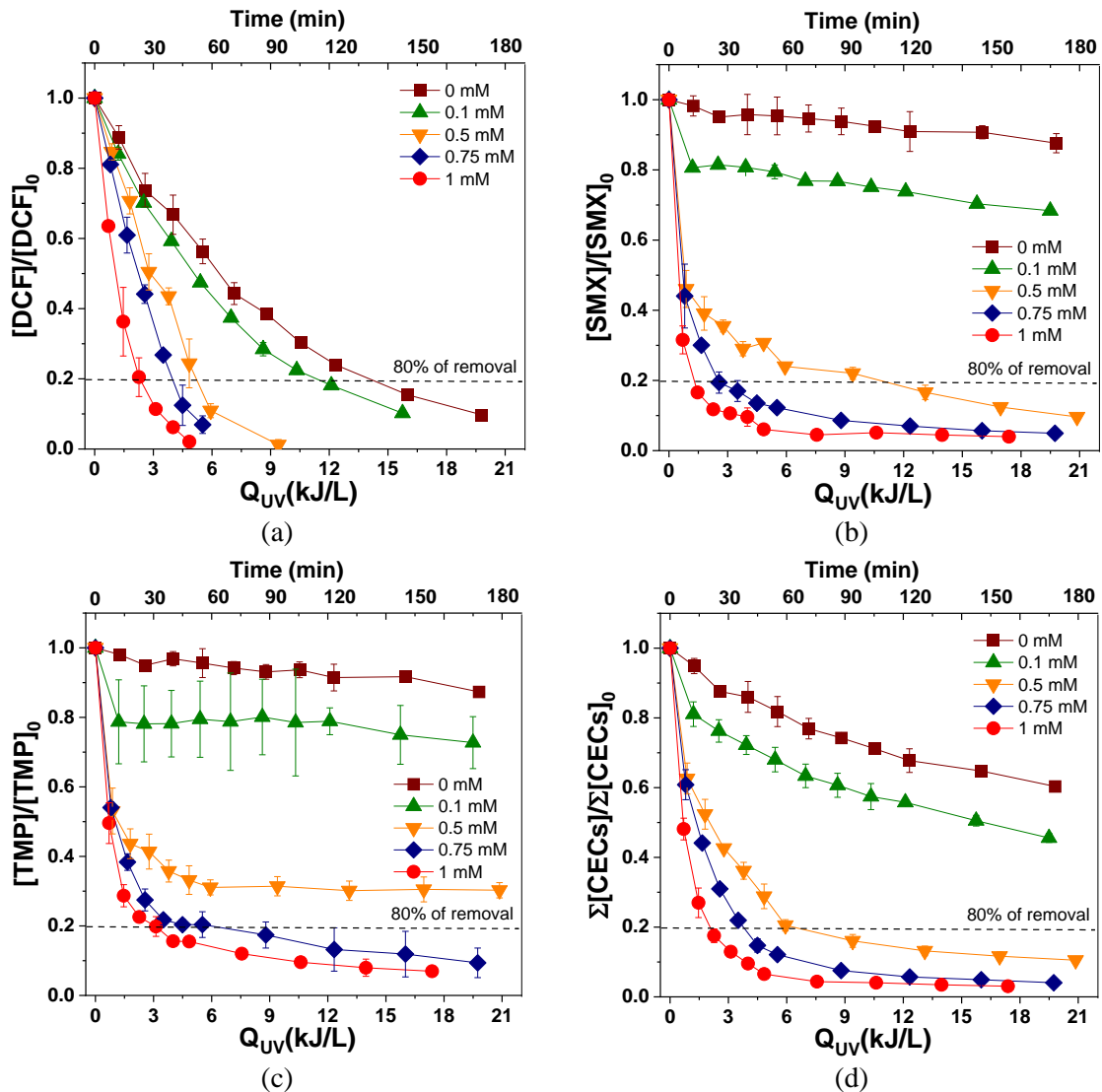


Figure 7.7: Degradation profiles of DCF (a), SMX (b), TMP (c) and total CECs (d) in UWW by PMS/Solar (0-1 mM).

Regarding literature, PMS has been mainly investigated in combination with lamps or solar simulators. Guerra-Rodríguez et al., reported the simultaneous degradation of 20 micropollutants (antibiotics, beta-blockers, other pharmaceuticals, pesticides, and herbicides) in secondary treated wastewater involving UV-A lamps (using four LEDs at λ_{max} of 385 nm) in a 1 L cylindrical glass reactor under magnetic stirring (Guerra-Rodríguez, 2021). These authors obtained an average degradation of 80 % of spiked targets after 60 minutes in the presence of 0.1 mM. The results differ from the obtained in this work carried out at pilot plant scale and under natural solar radiation, as in the presence of the same amount of PMS only 32 % of total CECs were degraded after 60 minutes, which could be attributed mainly to difference on UWW characteristics

7. PMS/Solar for wastewater purification

(affecting PMS consumption as it has been described previously), type of irradiation and reactor configuration.

7.2.3 Antibiotic Resistant Bacteria and Genes removal

The co-presence of bacteria, antibiotics and a nutrients rich environment in UWWTPs promotes the development and the proliferation of ARB and ARGs, posing an additional health risk. Although actually ARB and ARGs are not yet regulated, it is important to find a solution for these targets' removal, because they are recognized as public concern worldwide. In this line, ARB and ARGs were also simultaneously monitored in UWW during PMS/Solar treatment at the highest PMS concentration tested, 1 mM.

The removal efficiency of *E. coli*, *Enterococcus* spp, *Pseudomonas* spp. and their AMP, CPX and TMP antibiotic resistant counterpart is shown in Figure 7.8a.

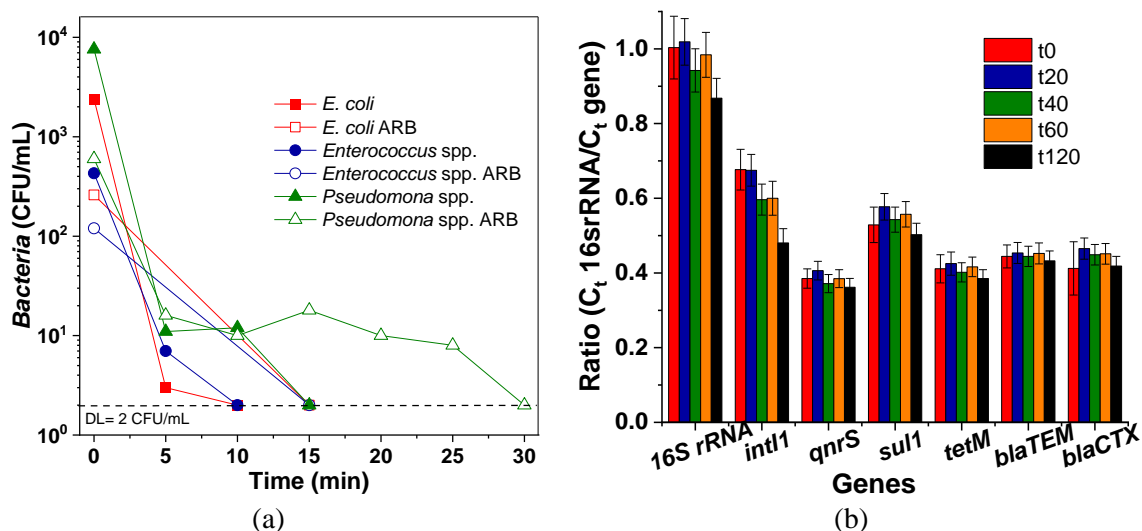


Figure 7.8. (a) Inactivation profiles of *E. coli*, *Enterococcus* spp. and *Pseudomonas* spp. and their resistant TMP, AMP and CPX counterparts and (b) ARGs removal in the presence of 1 mM of PMS under natural solar radiation in UWW.

No significant differences in the inactivation of wild and AR-bacteria were observed and DL of 2 CFU/mL was reached within 30 minutes of treatment for all microbial targets. These results agree with other studies, recently pointing out that the real challenge on the AR phenomenon lies in the removal of the genetic material that encode the AR instead of the mere inactivation of ARB (Polo-López, 2021). This is explained considering that the acquisition of the “AR status” by bacteria is not directly related in any case with a higher resistance to oxidative processes, including in this line similar results on ARB and wild

bacteria inactivation kinetics for solar photo-Fenton process (Fiorentino, 2019; Giannakis, 2018), H₂O₂/Solar process (Michael, 2020), among others.

As regards genes, it has been reported that different types of ARGs exist in the environment, such as genes conferring resistance to quinolone, tetracycline, sulfonamide, β -lactams, cephalosporine, due to the widespread use of antibiotics to treat bacterial infections in both human and animal (Carvalho and Santos, 2016; Michael, 2020; Narciso-Da-Rocha, 2014). Moreover, the gene of class 1 integron integrase, *intI1*, was considered in the present study also because it is an indicator of horizontal gene transfer, encoding a protein involved in the integration of DNA into the cell and whose removal can be considered as fundamental to control the AR phenomenon spread (Gillings, 2015; Kampouris, 2021).

The occurrence ratio of different ARGs naturally present in the secondary effluents of UWW was calculated by means of their relative abundance by analyzing the 16S rRNA gene, which represents the microbiological abundance in UWW. The following rank was preliminary obtained: *intI1* (0.654 ± 0.021) > *sulI* (0.530 ± 0.014) > *blaTEM* (0.443 ± 0.042) > *tetM* (0.440 ± 0.049) > *blaCTX-M32* (0.408 ± 0.091) > *qnrS* (0.384 ± 0.021). It is important to highlight that this rank was calculated as baseline for the determination of the % of degradation, but it could be highly variable considering the fluctuations in the same effluents (season dependency) and differences between different UWWTPs (Wang, 2021). The relative abundance of each ARG (ratio 16S rRNA/ARG) during the treatment PMS/Solar at a concentration of PMS of 1 mM is shown in Figure 7.8b and summarized in Table 7.1.

Table 7.1. ARGs mean and standard deviation of the ratio detected in this study.

Time (min)	16s rRNA	<i>intI1</i>	<i>sulI</i>	<i>blaCTX-M32</i>	<i>blaTEM</i>	<i>tetM</i>	<i>qnrS</i>
Raw	1.00±0.01	0.65±0.02	0.53±0.01	0.41±0.09	0.44±0.04	0.44±0.05	0.38±0.02
0	1.00±0.08	0.68±0.05	0.53±0.05	0.41±0.07	0.44±0.03	0.41±0.04	0.39±0.03
20	1.02±0.06	0.67±0.04	0.58±0.04	0.47±0.03	0.45±0.03	0.43±0.03	0.41±0.02
40	0.94±0.06	0.60±0.04	0.54±0.03	0.45±0.03	0.44±0.03	0.40±0.03	0.37±0.02
60	0.98±0.06	0.60±0.05	0.56±0.03	0.45±0.03	0.45±0.03	0.42±0.03	0.38±0.02
120	0.87±0.05	0.48±0.05	0.50±0.02	0.42±0.03	0.43±0.03	0.39±0.02	0.36±0.02

7. PMS/Solar for wastewater purification

A decrease of 13 % and 30 % was observed after 120 minutes of treatment (11.5 kJ/L of Q_{UV}) for 16S rRNA and *IntI1*, respectively, while no significant changes in relative abundance were detected for the other genes. These results are in accordance with the low removal efficiency for ARGs (0.3-1.7 LRV) obtained under natural solar radiation in combination with another oxidant, such as H₂O₂ (Michael, 2020), highlighting the resistance of this type of pollutants to be removed by solar processes.

7.3 Photocatalytic performance of ZnO-Ce with peroxymonosulfate in UWW

The combination of the best-performing photocatalytic material (ZnO-Ce) (Chapter 4) with the oxidant PMS was investigated as potential enhancement strategy for UWW purification, considering the presence of PMS as a dual role: for one hand, acting as electron acceptor, it leads to the simultaneous enhancement of photocatalytic process by preventing recombination electron-hole; and for the other hand, due to the possible generation of SO₄^{•-} as an additional reactive species in the solution. Table B.7 (Annex B) summarizes the obtained inactivation and degradation kinetic constants obtained in the following conditions: ZnO-Ce (100 mg/L), PMS alone (0.2, 0.3 and 0.4 mM) and the combination of PMS/ZnO-Ce (0.2, 0.3, 0.4 mM of PMS with 100 mg/L of ZnO-Ce) under natural solar radiation. All concentrations have been chosen in order to decrease each reactive concentration, with the aim of obtaining good performances by combining the photocatalyst and PMS.

The concentration of 100 mg/L for ZnO-Ce was selected as it was found to be effective for bacterial inactivation, but not suitable for CECs degradation (Chapter 4). It was tested in combination with PMS to enhance the process performance including also chemical targets removal, without the need to increase up to 5 times its concentration (500 mg/L). As regards PMS, 0.1 mM was found to be ineffective for disinfection and decontamination of UWW. Therefore, concentrations between 0.1 and 0.5 mM were evaluated to assess the effect of catalysts combination. Figure 7.9 shows the comparison of the inactivation kinetic constants (k , min⁻¹) for each individual bacterium and CEC.

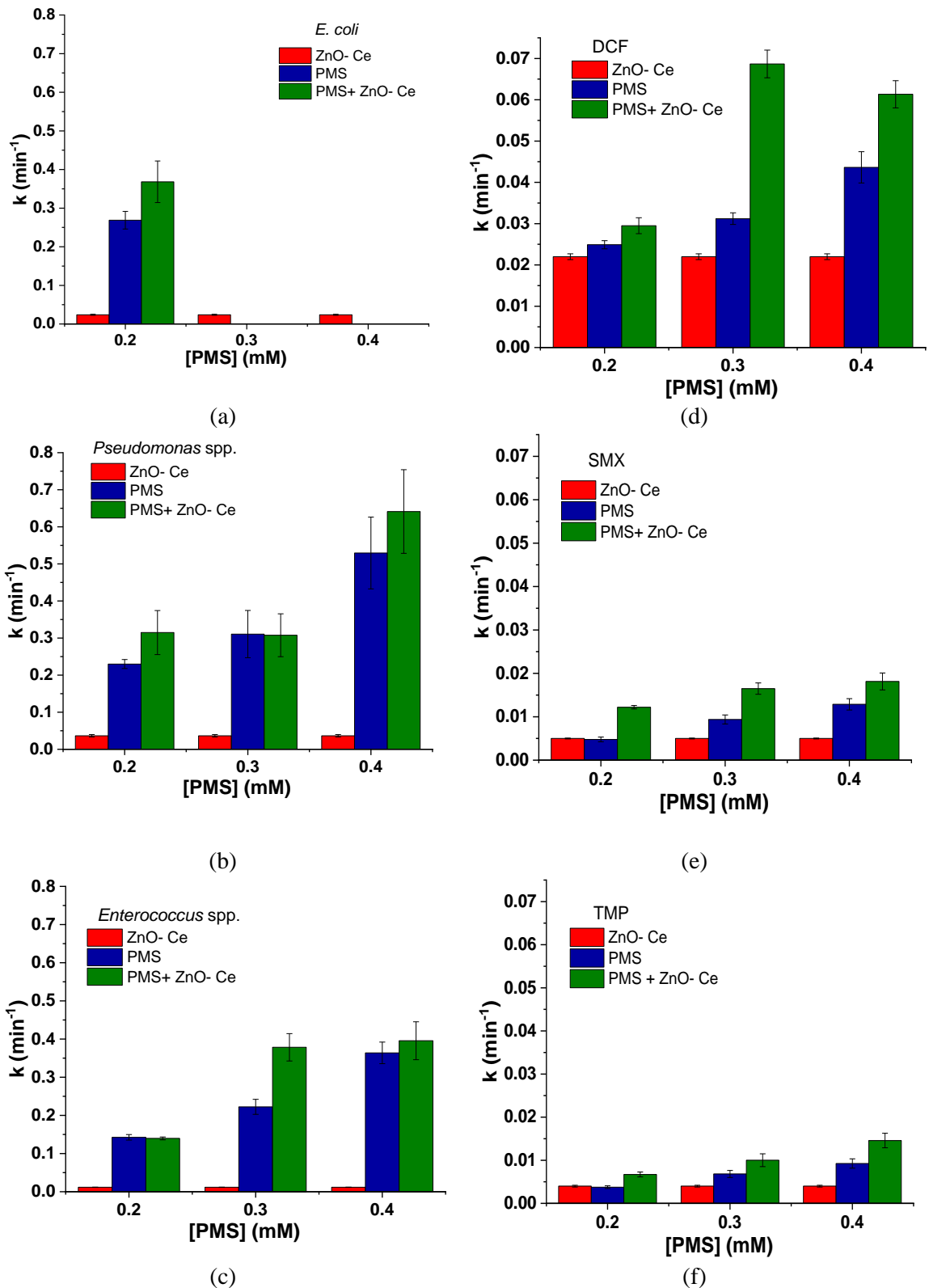


Figure 7.9: Comparison of the inactivation constants for *E. coli* (a), *Pseudomonas spp.* (b), *Enterococcus spp.* (c), DCF (d), SMX (e) and TMP (f) by ZnO-Ce (100 mg/L), PMS/Solar (0.2, 0.3 and 0.4 mM) and their combination PMS/ZnO-Ce (0.2, 0.3, 0.4 mM with 100 mg/L) under natural solar radiation.

7. PMS/Solar for wastewater purification

To quantify the effectiveness of the solar process with PMS and ZnO-Ce, the SI was calculated according to Eq. 7.1 (Mecha, 2017).

$$SI = \frac{k_{PMS/ZnO-Ce}}{k_{ZnO-Ce} + k_{PMS}} \quad \text{Eq. 7.1}$$

where k_{ZnO-Ce} is the constant value obtained with ZnO-Ce (100 mg/L), k_{PMS} is the constant value obtained by PMS/Solar and $k_{PMS/ZnO-Ce}$ is the constant value obtained by the combination. Interpretation of SI values is performed as following stated: $SI \leq 1$ no synergy and $SI > 1$ means synergy effect for PMS/radiation system.

A significant oxidative effect of PMS alone was observed for *E. coli* at oxidant concentration higher than 0.3 mM, reaching the DL after 1-2 minutes of treatment. For this reason, the comparison of kinetic rates is presented only at 0.2 mM, due to the impossibility to calculate the inactivation constant for the higher concentrations tested.

Table 7.2 shows the synergistic factor calculated for microbial (*E. coli*, Total coliforms, *Enterococcus* spp. and *Pseudomonas* spp.) and chemical targets (DCF, SMX and TMP) in the presence of the different concentration of PMS. A significant synergistic factor was obtained for Total coliforms and *Enterococcus* spp. at concentration of PMS of 0.3 mM, while for *E. coli* and *Pseudomonas* spp. the optimal load for an enhancement in the process was obtained in the presence of 0.2 mM. At 0.3 mM, DL was reached after 8 minutes (0.9 kJ/L of Q_{UV}) for each microbial target in the presence of PMS/ZnO-Ce/Solar, while 15 minutes (1.7 kJ/L of Q_{UV}) were necessary in the presence of only PMS. Nevertheless, it is clearly that PMS effect is dominating the inactivation kinetic rates when in combination with the catalyst. As regards CECs, an enhanced degradation was observed for all chemical targets, compared to the stand-alone processes, but a significant synergistic effect was obtained only for DCF in the presence of 0.3 mM of PMS. At these conditions, 80 % of total CECs removal was observed after 60 minutes (7.1 kJ/L of Q_{UV}), while more than 180 minutes are necessary for PMS and ZnO-Ce alone.

Table 7.2: Synergistic factor calculated for microbial and chemical targets in the presence of the different concentrations of PMS.

[PMS] (mM)	Synergistic index						
	Microbial target				Chemical target		
	<i>E. coli</i>	Total coliforms	<i>Enterococcus</i> spp.	<i>Pseudomonas</i> spp.	DCF	SMX	TMP
0.2	1.3	1.2	0.9	1.2	0.6	1.2	0.9
0.3	/	1.6	1.6	0.9	1.3	1.1	0.9
0.4	/	1.0	1.1	1.1	0.9	1.0	1.1

Nevertheless, and despite the good performance observed by the combination of ZnO-Ce and PMS, the release of Zn²⁺ detected (500 mg/L for ZnO-Ce and 0.5 mM for PMS) by ICP-MS, revealed a very high Zn²⁺ concentration in solution after the treatment (20 mg/L). Therefore, it could be concluded that this approach of combination is not useful to obtain a safe treated wastewater.

7.4 Conclusions

The simultaneous removal of microbial and chemical targets in UWW at pilot plant scale has been demonstrated by combining PMS and natural solar radiation. Optimal load of PMS was found to be 1 mM, at which DL of 2 CFU/mL was achieved for all microbial targets after 15 minutes (1.1 kJ/L of Q_{UV}) and 80 % of CECs removal was reached after 27 minutes (2.0 kJ/L of Q_{UV}) and no bacterial regrowth was observed after 48h. The inactivation of ARB was successfully achieved, obtaining no significant difference with wild bacteria and discarding the need to follow these targets removal in actual monitoring UWW programs. On the other hand, PMS/Solar process was demonstrated to be ineffective to prevent the spread of ARGs to the environment, highlighting the need to find more oxidative conditions in view of future regulations.

Finally, the combination of ZnO-Ce with PMS could allow to increase treatment performances using lower reactive concentrations, but results demonstrated that a significant synergistic effect was not observed for any target removal and the release of a high amount of Zn²⁺ in solution (20 mg/L in the presence of very high reactive concentrations) leads to discard this process as feasible for water treatment, due to an important post-contamination effect.

CHAPTER 8
WATER AND WASTEWATER
PURIFICATION BY
PEROXYMONOSULFATE AND UV-C
RADIATION

8. WATER AND WASTEWATER PURIFICATION BY PEROXYMONOSULFATE AND UV-C RADIATION

In this chapter the effectiveness of SR-AOPs has been evaluated for water and wastewater purification, generating $\text{SO}_4^{\cdot-}$ and HO^{\cdot} in solution through the activation of PMS by UV-C irradiation at pilot plant scale. The assessment was carried out throughout the testing of a wide range of PMS concentrations and monitoring simultaneously the abatement of the three microbial pathogens and CECs targets investigated in this study. Besides, in this chapter, the capability of PMS/UV-C process for ARB and ARGs removal has been also investigated.

The efficacy and limitations of this process was evaluated using different water matrices:

- IW: to evaluate the fundamental capability of the process.
- Simulated UWW: complex matrix in order to investigate the effect of inorganic ions and NOM on process performance.
- Actual UWW: assessing process ability to obtain high water quality for its potential reuse in agriculture, according to the (EU) 2020/741 regulation.

8.1 Disinfection and decontamination performances in isotonic water

The inactivation profiles of the culture-type strains *E. coli*, *P. aeruginosa*, *E. faecalis*, all at an initial concentration of 10^6 CFU/mL, and the sum of all bacteria by PMS/UV-C process in IW are shown in Figures 8.1. Different oxidant concentrations, ranging from 0.003 to 0.005 mM (according to previous results obtained in Chapter 6) were tested in comparison with UV-C alone (as baseline of the well-known capability of UV-C photons for bacterial abatement).

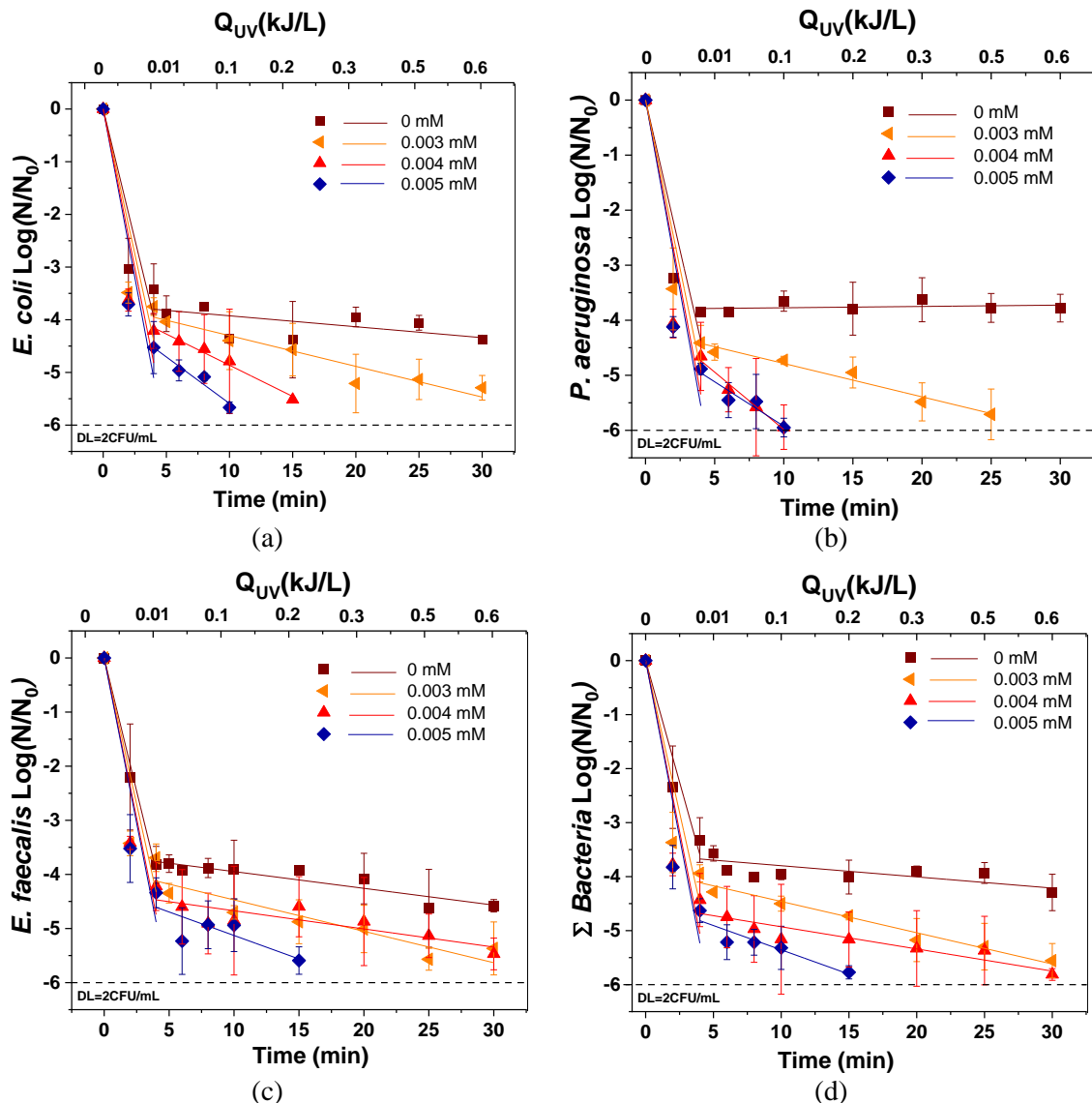


Figure 8.1. Linear fitting of the inactivation profiles of (a) *E. coli*, (b) *P. aeruginosa*, (c) *E. faecalis* and (d) sum of bacteria by PMS/UV-C system at different PMS concentrations (0-0.005 mM) in IW under UV-C radiation.

Table B.8 (Annex B) reports the bacteria inactivation kinetic constants for each condition tested and the value of Q_{UV} (kJ/L) needed for achieving the DL (2 CFU/mL). Water T ranged

between 20.1 and 30 °C, while water pH was 6.5-7 in all cases, remaining constant along the treatment time.

The inactivation profile of each bacterium showed a double log-linear kinetic, with a rapid loss of bacteria viability, k_1 (> 3 LRV in the first 2 minutes) followed by a tail shape ($k_2 \ll k_1$, Table B.8, Annex B). This bacterial inactivation profile (observed in all UV-C results, including in the presence of PMS) is similar to the reported in previous studies using the same UV-C pilot plant with different oxidants such as PS (Sánchez-Montes, 2020), indicating an independence from the type of oxidant employed. In fact, the first k_1 is attributed to the well-known efficiency for microbial inactivation of UV-C, based on the direct photo-absorption of nucleic acids (maximum absorption at 260 nm), and consequent bacterial DNA damages. Regarding k_2 values with the mere effect of UV-C wavelengths, no significant differences were observed for the three bacteria (DL of 2 CFU/mL (6 LRV) was not achieved). The slower k_2 can be explained considering the engineering of the plant design, in terms of the low ratio between the illuminated volume (V_i 6.21 L) and the total volume (V_t 80L) of the reactor, and, therefore, a photo-limitation of UV-C process and the re-circulation flow-mode could be the responsible of not reaching the DL, favouring bacterial auto-reparation mechanism or regrowth in the dark zones. Besides, a post-treatment regrowth was detected after 24 and 48h, detecting a final concentration after 48h of 6, 10 and 400 CFU/mL for *E. faecalis*, *E. coli* and *P. aeruginosa*, respectively.

The addition of very low concentration of PMS and its combination with UV-C irradiation enhanced the disinfection performances, obtaining higher inactivation kinetic rates and requiring lower treatment times or Q_{UV} to inactivate these pathogens. The enhancement in the inactivation kinetics could be attributed to the photolysis of PMS, with the subsequent generation of $SO_4^{\cdot-}$ and HO^{\cdot} in solution. These ROS initiate oxidative stress by attacking firstly the cell membrane, altering its permeability, with further reaction with cellular components (enzymes and genetic materials) after diffusion through the cell-wall membrane, inhibiting normal metabolism and thus leading cells inactivation (Xiao, 2019). Focusing on the enhancement of UV-C process performance by PMS dose, the main advantage can be observed for k_2 in comparison with k_1 values for all bacteria. This difference is due to the fast inactivation generated initially by UV-C wavelengths, superposing and limiting the effect of PMS. Nevertheless, once the process starts to show a photo-limitation, the presence of PMS and the radicals generated clearly led to an enhancement based on: (i) the higher the PMS dose, the faster the inactivation kinetics,

8. PMS/UV-C for water and wastewater purification

(ii) the DL was attained in all cases, and (iii) the post-treatment bacteria regrowth after 24h and 48h of storage in the dark was prevented, guaranteeing safe water reuse. Among all the concentrations of PMS tested in IW, the best results were obtained with 0.005 mM, which allows to reach > 6 LRV and the DL (2 CFU/mL) with the following individual reactivity order: *E. coli* \approx *P. aeruginosa* (both gram-negative bacteria) after 10 minutes (0.1 kJ/L of Q_{UV}) $>$ *E. faecalis* (gram-positive-bacteria) after 15 minutes (0.2 kJ/L of Q_{UV}). Figure 8.2 shows the degradation profiles of DCF (a), SMX (b), TMP (c) and total CECs (d) by PMS/UV-C system, while the pseudo first order kinetic constants and the Q_{UV} (kJ/L) value for the 80 % removal are shown in Table B.9. In the absence of oxidant, 80 % of DCF and SMX removal was obtained after 5 minutes (0.01 kJ/L of Q_{UV}) and 10 minutes (0.1 kJ/L of Q_{UV}) of treatment time, respectively, while 78 % of TMP was degraded after 180 minutes (4.5 kJ/L of Q_{UV}). The order of CECs reactivity found was: DCF $>$ SMX $>$ TMP.

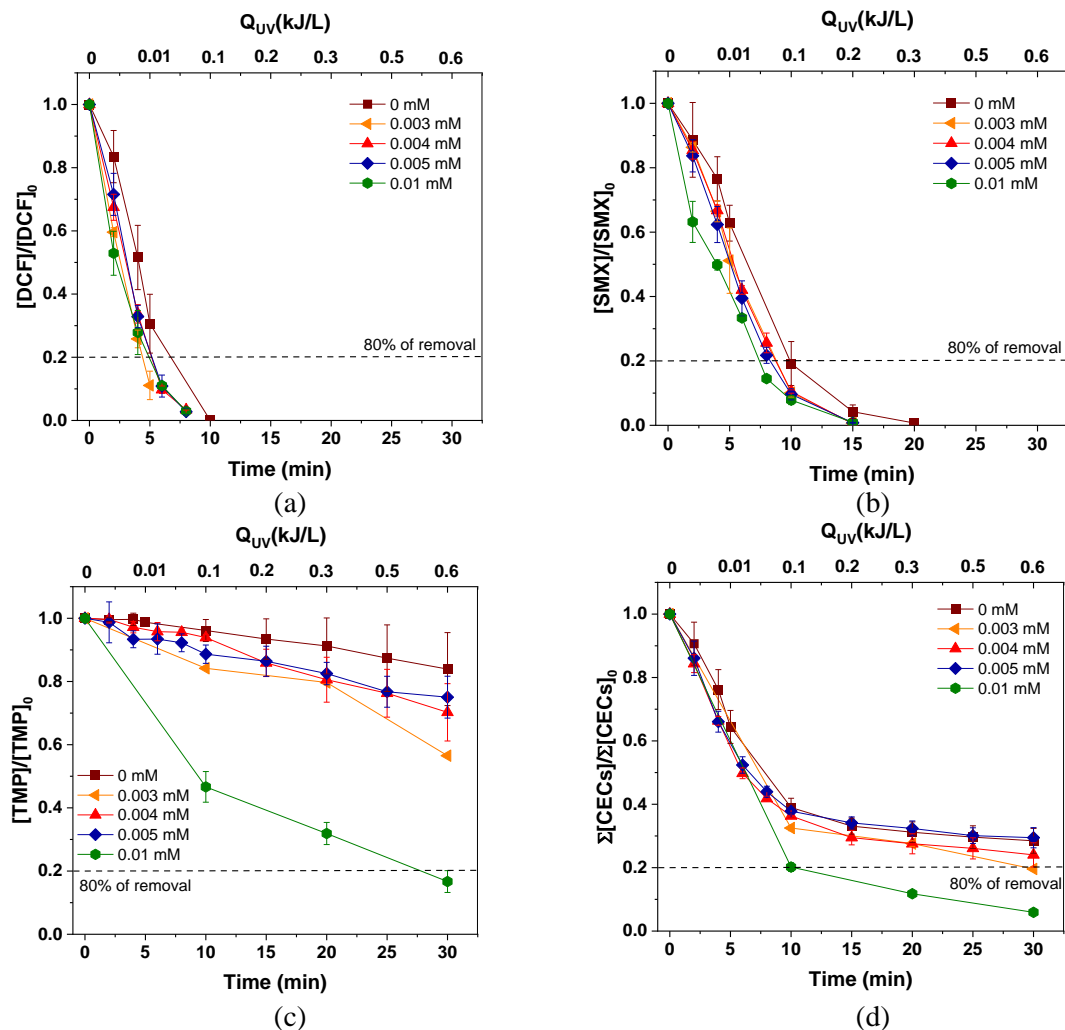


Figure 8.2. Degradation profiles of (a) DCF, (b) SMX, (c) TMP and (d) total CECs by PMS/UV-C system at different PMS concentrations (0-0.01 mM) in IW and under UV-C radiation.

The efficiency of CECs removal under UV-C is highly dependent on the type of compound, being mainly affected by its molar absorption coefficients ϵ_{254} and by the quantum yield Φ_{254} at the same wavelength of the lamp emission (254 nm). Table 8.1 summarizes the main values (experimentally measured and found in literature) related to optical absorption characteristics of DCF, SMX and TMP (Sanchez-Montes, 2020).

Table 8.1. Main parameters related to optical absorption characteristics of DCF, SMX, TMP (at 1 mg/L) and PMS (at 1 mM) of concentration.

Compound	λ_{\max} (nm)	A_{254} (a.u)	ϵ_{254}^* L/(mol·cm)	Φ_{254}^* mol/Einstein	Time (min)	Q_{UV} (kJ/L)
DCF	276	0.022	4770	0.292	7	0.02
SMX	262	0.053	13200	0.038	10	0.1
TMP	278	0.015	2940	0.0011	> 180	> 4.5

*=Literature values λ_{\max} = maximum absorption wavelength (nm), A_{254} = experimental value of absorbance at 254 (a.u.), ϵ_{254} = Molar absorption coefficients ($l \cdot mol^{-1} \cdot cm^{-1}$) at 254 nm, Φ_{254} = quantum yield at 254 nm (mol/Einstein), Time (min) and Q_{UV} (kJ/L) necessary to achieve 80 % removal of the compound.

The optical absorption characteristics shows that DCF has lower molar absorption coefficient, but 8-fold lower quantum yield at 254 nm than SMX and for this reason it exhibits a higher photolysis efficiency. On the contrary, TMP values of ϵ_{254} , Φ_{254} and A_{254} are low, which could explain its refractoriness to UV-C treatment, and therefore the lower degradation of this compound in comparison with DCF and SMX.

Opposite to the results obtained with bacteria, the initial investigated PMS concentrations did not enhance DCF, SMX or TMP degradation. For this reason, an additional higher PMS concentration (0.01 mM) was also tested in IW. Results again revealed a no significant enhancement for DCF and SMX removal, achieving in all cases 80 % of removal after 5 minutes (0.01 kJ/L of Q_{UV}) and 8 minutes (0.03 kJ/L of Q_{UV}) of treatment time, respectively. Nevertheless, as regards TMP, 80 % of removal was attained with a concentration of PMS of 0.01 mM after 28 minutes (0.54 kJ/L of Q_{UV}).

Therefore, summarizing the results obtained in IW, it can be concluded that the combination of PMS with UV-C wavelengths could enhance the process performance. Nevertheless, for actual waters, an optimization of the PMS concentration is required to ensure a complete simultaneous removal of waterborne pathogens and CECs.

8.2 Disinfection and decontamination performances in simulated urban wastewater

The effect of organic matter on the performance of PMS under UV-C radiation for the simultaneous wastewater disinfection and decontamination was evaluated in SUWW-2 (DOC content of 11.1 ± 2.5 mg/L, Table 3.5).

Figure 8.3 shows the inactivation of *E. coli* (a), *P. aeruginosa* (b), *E. faecalis* (c) and the sum of the bacteria (d) in SUWW by PMS/UV-C with concentrations of PMS ranged from 0 to 0.5 mM. Tables B.8 (Annex B) reports the corresponding inactivation kinetic constants and the PMS concentration monitored during the treatment at each tested condition is shown in Figure 8.4.

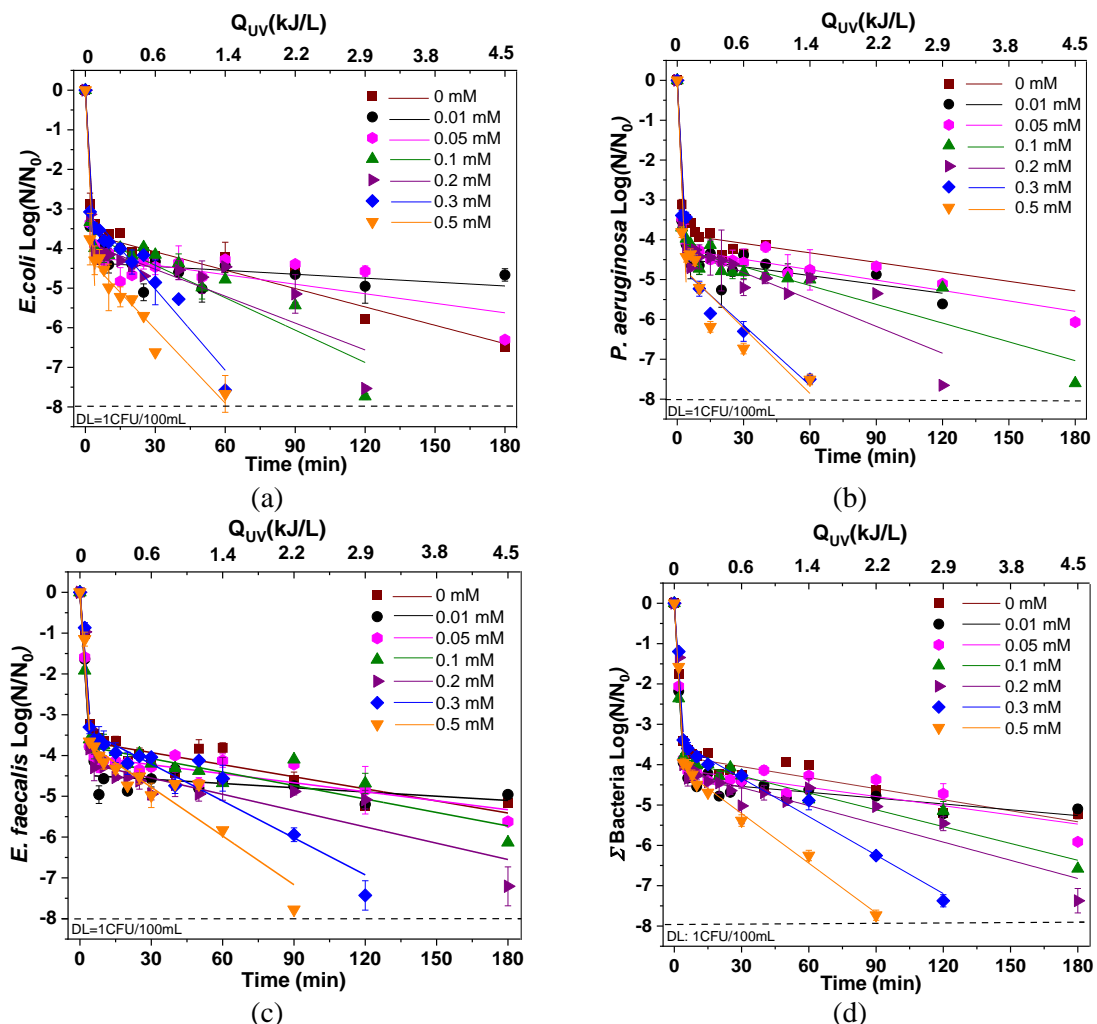


Figure 8.3. Inactivation profiles of (a) *E. coli*, (b) *P. aeruginosa*, (c) *E. faecalis* and (d) sum of bacteria by PMS/UV-C system at different PMS concentrations (0-0.5 mM) in SUWW and under UV-C radiation.

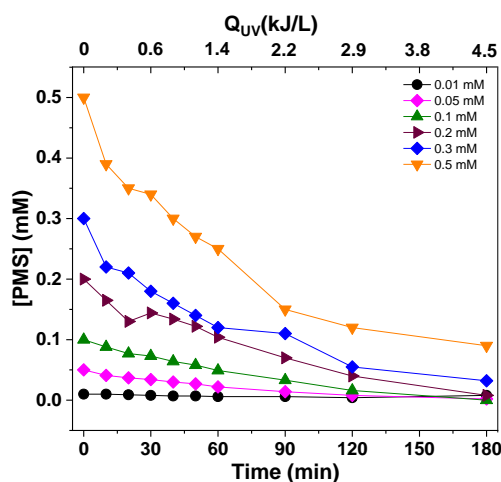


Figure 8.4. PMS concentration decrease in function of time (minutes) and accumulative UV energy Q_{UV} (kJ/L) under UV-C treatment at different PMS concentrations in SUWW (0.01-0.5 mM).

As observed previously, a significant effect of UV-C radiation was observed in the first minutes of treatment, achieving 3.4 LRV after 4 minutes, while the remaining microbial concentration (up to 4 LRV) was inactivated with a second slower kinetic rate (k_2). DL of 1 CFU/100 mL was not achieved for any of the bacteria investigated and a post-treatment bacterial regrowth analysis after 24-48h revealed the presence of all bacteria.

A significant enhancement in bacteria inactivation was obtained adding PMS, in the range from 0.01 to 0.5 mM. A minimum dosage of PMS equal to 0.2 mM was necessary for achieving DL of 1 CFU/100 mL (8 LRV) and for not observing bacterial regrowth after 24 and 48h. No significant differences in k_1 values were obtained in the presence of the oxidant, compared with UV-C alone process (3.4 LRV and a k_1 of 0.85 min^{-1}), achieving (4.0 ± 0.2) LRV of total bacteria with a k_1 of $(0.90 \pm 0.2) \text{ min}^{-1}$. A significant positive effect is observed in the second phase of the process (k_2), similarly to the process trend observed in IW.

Figure 8.5 shows the degradation profiles of DCF (a), SMX (b), TMP (c) and total CECs (d) by PMS/UV-C process, and the pseudo first order kinetic constants are reported in Table B.9 (Annex B). The 80 % removal of total CECs was attained after 120 minutes (2.9 kJ/L of Q_{UV}) by UV-C alone and the order of susceptibility was confirmed as above for IW, being independent from the water matrix: DCF > SMX > TMP.

Increasing PMS concentration, SMX and DCF degradation rate did not improve, highlighting the effectiveness of UV-C technology for some compounds susceptible to this type of radiation. On the other hand, for refractory compounds, such as TMP, the

8. PMS/UV-C for water and wastewater purification

degradation mediated by $\text{SO}_4^{\cdot-}$ and OH^{\cdot} determines a significant enhancement by increasing PMS concentration, as a consequence of a higher amount of radical species in solution.

Considering the simultaneous water disinfection and decontamination, best performance was reached at 0.5 mM of PMS, obtaining 8 LRV for total bacteria after 90 minutes (2.1 kJ/L of Q_{UV}) and 80 % of CECs removal after 8 minutes (0.02 kJ/L of Q_{UV}). The enhanced water purification by PMS/UV-C process was attributed to the generation of $\text{SO}_4^{\cdot-}$ and OH^{\cdot} radicals by PMS photolysis.

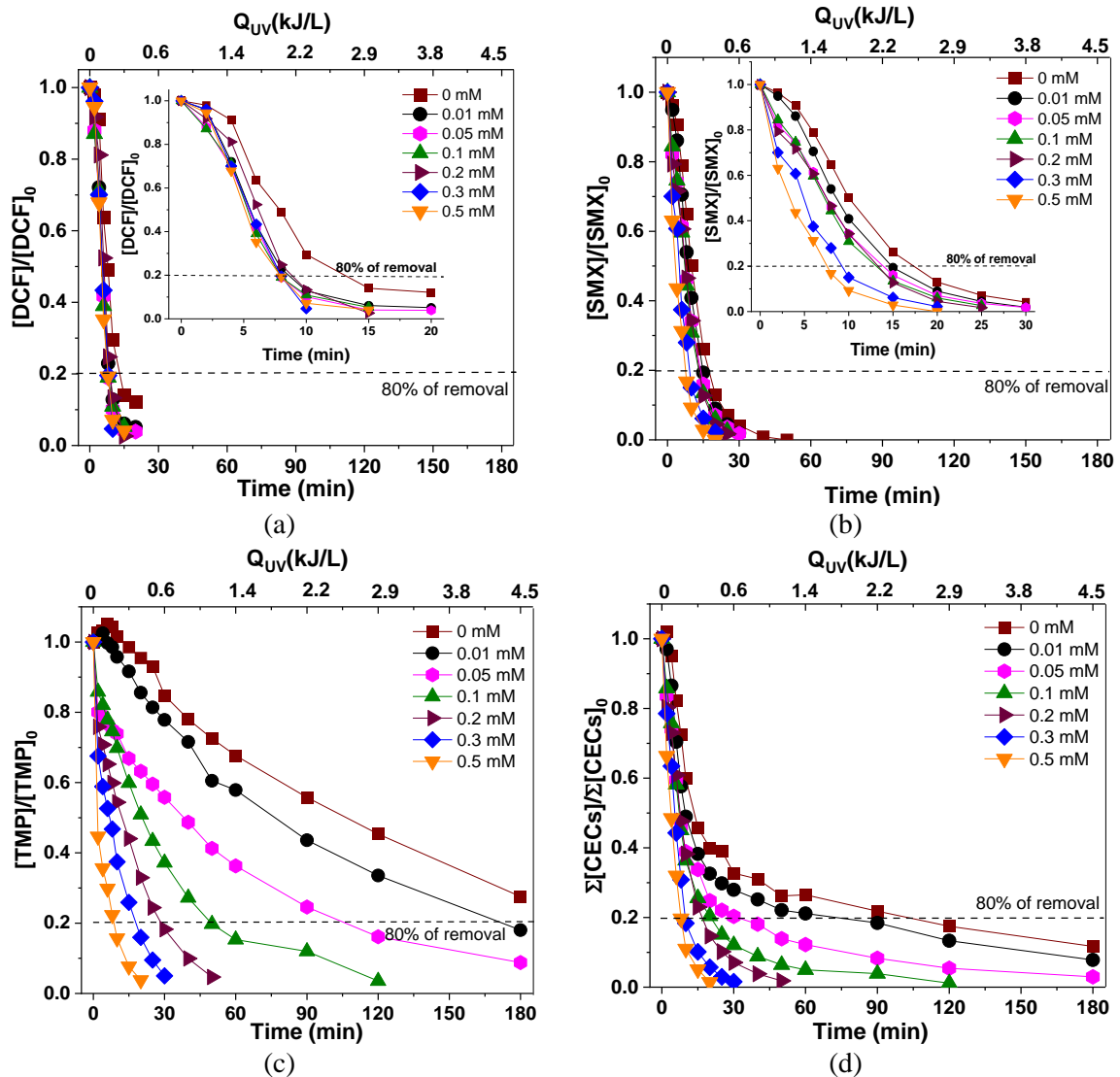


Figure 8.5. Degradation profiles of (a) DCF, (b) SMX, (c) TMP and (d) total CECs by PMS/UV-C system at different PMS concentrations (0-0.5 mM) in SUWW under UV-C radiation.

8.3 Disinfection and decontamination performances in urban wastewater

Afterwards, process capability was assessed for the treatment of actual UWW, characterized by a higher chemical and microbiological complexity and physico-chemical variations than SUWW. The inactivation profiles of natural occurring *E. coli*, *Pseudomonas* spp.,

Enterococcus spp., Total coliforms and the sum of all bacteria under UV-C radiation and PMS/UV-C at oxidant concentrations ranging from 0 to 1 mM in UWW are shown in Figure 8.6.

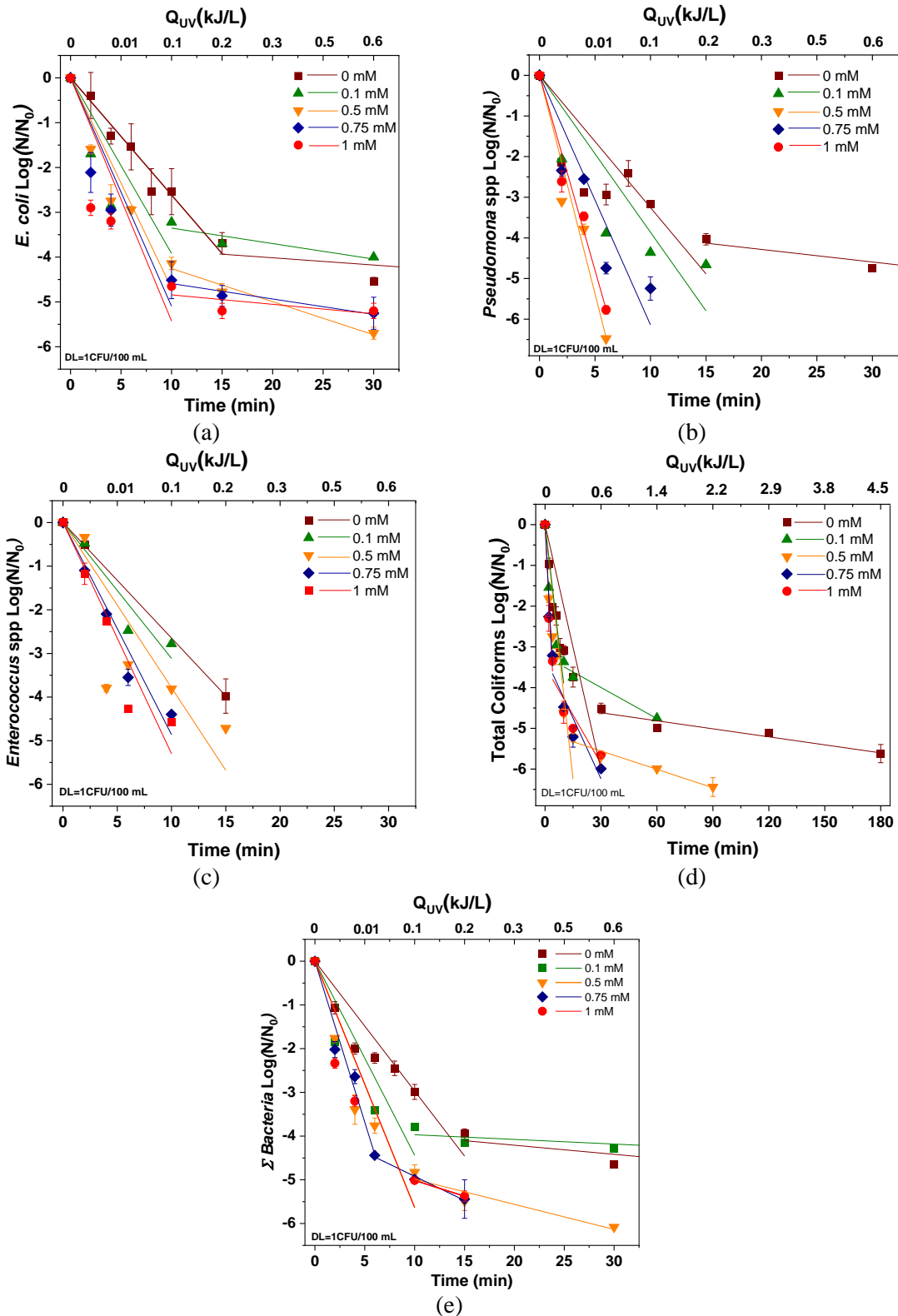


Figure 8.6. Inactivation profiles of (a) *E. coli*, (b) *Pseudomonas* spp., (c) *Enterococcus* spp., (d) Total coliforms and (e) sum of bacteria by PMS/UV-C system at different PMS concentrations (0-1 mM) in UWW under UV-C radiation.

8. PMS/UV-C for water and wastewater purification

Kinetic rate analysis is reported in Table B.8 (Annex B) and the PMS decrease during the treatment at each condition is showed in Figure 8.7.

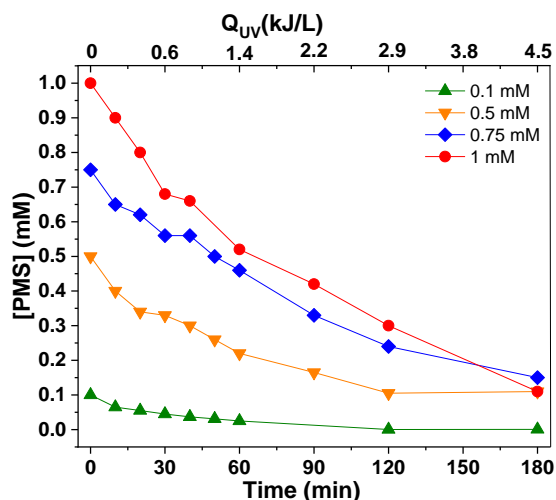


Figure 8.7. PMS concentration decrease in function of time (minutes) and accumulative UV energy Q_{UV} (kJ/L) under UV-C treatment at different PMS concentrations in UWW (0.1-1 mM).

Figure 8.8 shows the degradation profiles of DCF (a), SMX (b), TMP (c) and total CECs (d) by PMS/UV-C system, while the pseudo first order kinetic constants and the Q_{UV} (kJ/L) value for 80 % of removal are reported in Table B.9 (Annex B).

A decrease of all the initial PMS concentrations could be observed during time, due to the simultaneous oxidant consumption by water matrix and radicals' generation (Figure 8.7). The presence of a correct initial dosage of oxidant is an important factor, that should be optimized to guarantee the (i) efficient removal of the chemical and biological targets and (ii) presence of a residual PMS concentration, needed to avoid post-treatment regrowth.

Considering the simultaneous UWW disinfection and decontamination (Figure 8.6 and 8.8), the best PMS concentration was obtained with 0.5 mM. At this condition, 4.7 LRV (concentration < 10 CFU/100 mL) was achieved after 10 minutes of treatment (0.1 kJ/L of Q_{UV}) for all bacteria, no regrowth of microbial target was detected (with a residual concentration of 0.1 mM at the end of the treatment) and 80 % of total CECs was removed after 15 minutes (0.2 kJ/L of Q_{UV}).

Increasing oxidant concentration up to 1 mM did not enhance performance, observing better degradation only for TMP, for which PMS dosage higher than 0.5 mM was necessary for achieving 80 % of removal. This result demonstrated that beyond the optimum, possible reactions between oxidant and radicals and self-recombination of active species could lead to a decrease in degradation rates, as it is reported elsewhere (Yang, 2019). Therefore, the optimization of the oxidative agent concentration is important and it could vary depending

on the quality requirements established by reclamation guidelines, affecting also the treatment cost.

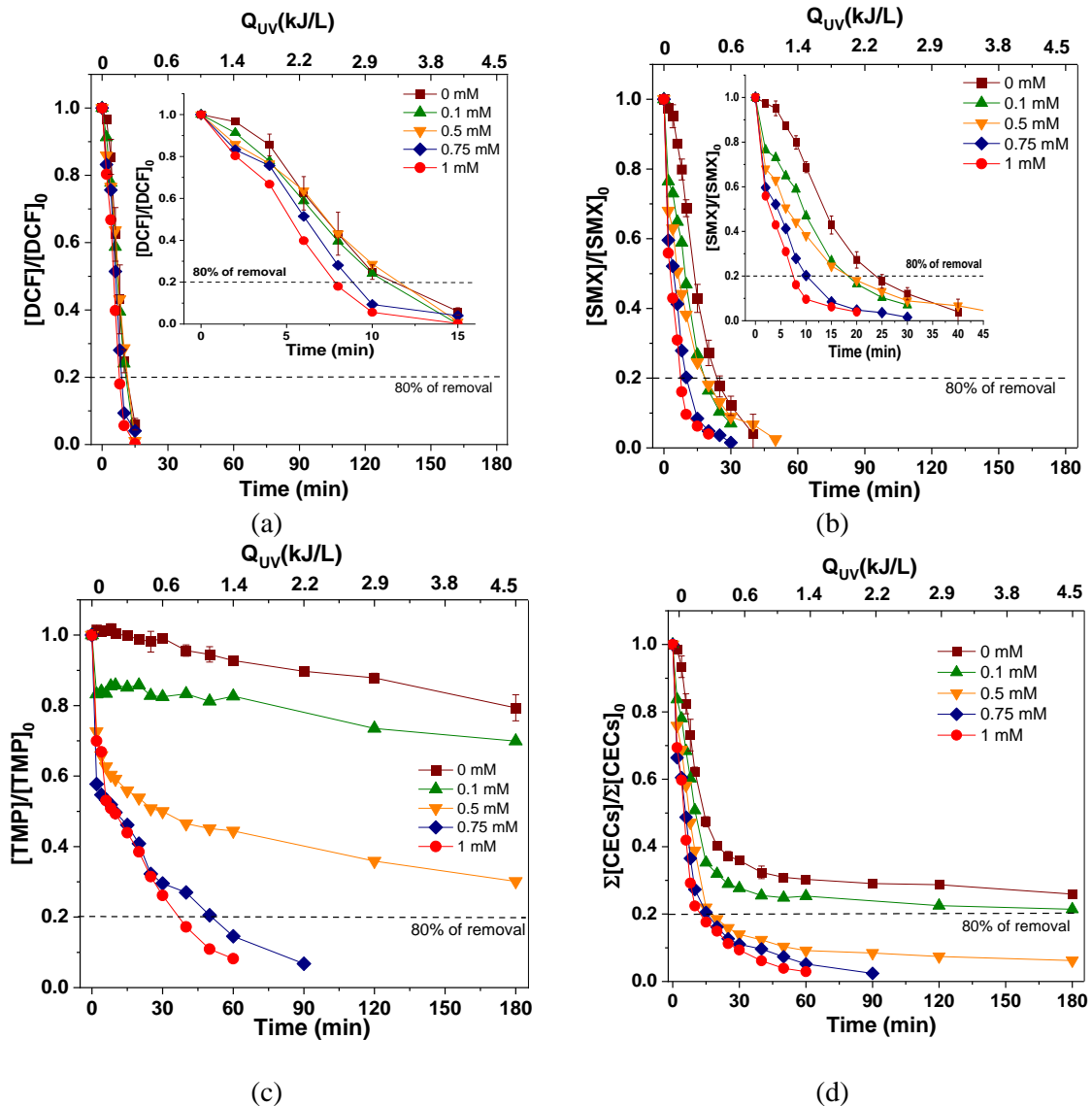


Figure 8.8. Degradation profiles of (a) DCF, (b) SMX, (c) TMP and (d) total CECs by PMS/UV-C system at different PMS concentrations (0-1 mM) in UWW under UV-C radiation.

Rodriguez-Chueca et al. reported a full-scale application of this process, investigating the removal of 25 CECs (including antibiotics, pesticides, flame retardants, corrosion inhibitors, and synthetic fragrances) detected at trace level (1–4 $\mu\text{g/L}$) in continuous flow mode by UV-C/SR-AOPs in the presence of different oxidant concentrations (0.05, 0.2, and 0.5 mM of PMS, PS and also in comparison with H_2O_2) and contact times (4–18 s). An average removal rates of CECs of 55 %, 48 %, and 10 % for H_2O_2 , PMS, and PS, respectively, compared to 13 % with only UV-C radiation were reported (Rodriguez-Chueca, 2018), being lower than the ones obtained in the present study conducted in batch flow-mode. The

8. PMS/UV-C for water and wastewater purification

use of a continuous flow mode system, implies low contact times and it could lead to obtain lower removal efficiencies compared to a batch mode.

Currently UV systems in continuous flow-mode are commonly used for disinfection purposes in DWTPs, treating high-quality water characterized by low turbidity, a small content of suspended solids and NOM. However, it is necessary to take into account several factors for the treatment of a complex matrix and optimizing them, in order to achieve good performances:

- Low intensity of radiation (high intensity increases costs).
- Incorrect operational conditions: optimize contact times and oxidant concentration (it has been seen that PMS concentration higher than 0.5 mM did not promote an effective enhancement, increasing only the total cost).
- Reactor configuration.
- Composition of the water matrix: light absorption by water constituents.

Rodriguez-Chueca et al. in a latter work, also pointed out that the process efficiency depends on the target compound and the experimental conditions (contact time and oxidant concentration) by studying the degradation of several pharmaceuticals and their transformation products with low dosage of oxidant (0.5 mM) and obtaining good removal efficiencies only for some of them (Rodriguez-Chueca, 2019b).

8.4 Comparison of process performance: analysing the effect of natural organic matter and inorganic species

Along the different water matrices investigated, it has been clearly observed that the presence of NOM and inorganic species (such as Cl^- , $\text{CO}_3^{2-}/\text{HCO}_3^-$, SO_4^{2-} and NO_3^-), ubiquitous in natural waters at different concentrations, highly affects process performances and the efficiency obtained in this study decreases as matrix complexity increased (Yang, 2019), according to the following order: IW > SUWW > UWW.

The effect of NOM on the process was evaluated comparing the results in the different water matrices investigated in this work (IW, SUWW and UWW), keeping constant the time to achieve a desired targets removal (> 5 LRV of bacteria in 20 minutes (0.3 kJ/L of Q_{UV}) and 80 % of CECs removal after 10 minutes (0.1 kJ/L of Q_{UV})) and estimating the required oxidant concentration to achieve the goal in the different matrices

These results are shown in Figure 8.9 and demonstrate that similar performances in the different water matrices could be achieved but increasing PMS dosage, with the aim of achieving disinfection and decontamination after a fixed time. For bacteria, 0.003 mM was needed in IW, but 0.5 mM of PMS was necessary in SUWW and in UWW. Similarly, for CECs, 0.01, 0.3 and 1 mM of PMS was needed in IW, SUWW and UWW, respectively.

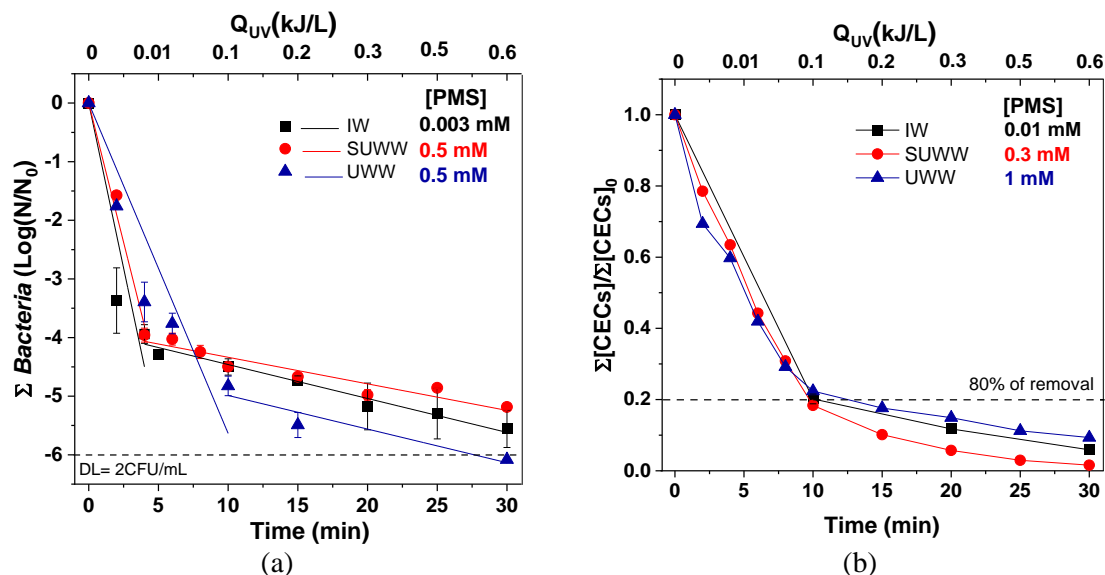


Figure 8.9. Bacteria inactivation (a) and CECs degradation (b) profiles by PMS/UV-C in IW, SUWW and UWW in the presence of PMS concentration necessary to achieve > 5 LRV in 20 minutes and 80 % of CECs removal in 10 minutes.

Several factors affect disinfection and decontamination capability in complex matrix, inhibiting the process, such as:

- Oxidant consumption by water constituents: PMS is able to directly oxidize Cl^- into less reactive chlorine species (such as Cl_2 and ClO^-) and it can react with NOM, as it has been described in the previous chapter and reported in the literature (Yang, 2019; Zhang, 2020).
- Light attenuation: NOM highly absorbs light at 254 nm, reducing the amount of photons available for the process. The filtering effect is clearly observed in Figure 3.17, showing different irradiance (W/m^2) profiles under UV irradiation in DW, SUWW and UWW.
- Decrease of the active species ($\text{SO}_4^{\cdot-}$ and HO^{\cdot}) generated in solution as a consequence of: (i) lower oxidant availability due to its consumption (ii) light attenuation and (iii) scavenging effect, that implies the conversion of active radicals into less reactive species. In fact, in complex matrix, side reactions between inorganic species (mainly Cl^- and $\text{CO}_3^{2-}/\text{HCO}_3^-$, while SO_4^{2-} is not considered a

8. PMS/UV-C for water and wastewater purification

robust radical scavenger) and NOM with active radicals ($\text{SO}_4^{\bullet-}$ and HO^\bullet), convert them into $\text{Cl}^\bullet/\text{Cl}_2^{\bullet-}$ and $\text{CO}_3^{\bullet-}$, characterized by lower reactivity with target compounds (Wacławek, 2017).

On the other hand, it could be mentioned that NO_3^- and NOM may contribute to increase degradation rates under certain conditions, acting as photosensitizers, absorbing light and generating ROS in solution (Yang, 2019). Nevertheless, under the experimental conditions of the present study, the presence of NOM and other inorganic substances has clearly shown a reduction but not limitation of the PMS/UV-C process performance.

8.5 Antibiotic Resistant Bacteria and Genes removal

The inactivation of ARB and the removal of ARGs by PMS/UV-C have been also assessed. Figure 8.10 shows the inactivation of *E. coli*, *Enterococcus* spp., and *Pseudomonas* spp. and their antibiotic-resistant counterpart under UV-C irradiation in the presence of PMS at an initial concentration of 1 mM, chosen on the base of previous results (Chapter 7) in UWW.

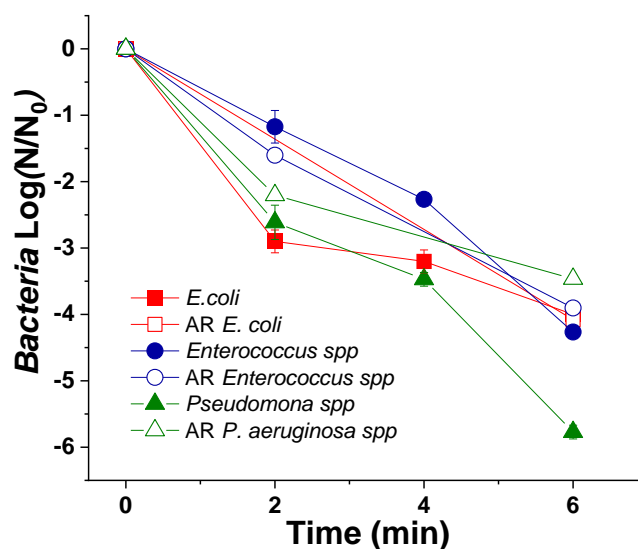


Figure 8.10. Inactivation of *E. coli*, *Enterococcus* spp., and *Pseudomonas* spp. and their AMP, CPX and TMP-AR counterpart by PMS/UV-C with 1 mM in UWW.

Wild and AR-bacteria reached the DL (1 CFU/100 mL) in 6 minutes (Q_{UV} of 0.01kJ/L), obtaining no significant differences in the inactivation. Other authors have also reported the capability of PMS/UV-C for ARB inactivation (Hu, 2019; Arslan-Aton, 2021). Hu et al., reported 5.3 LRV of AR-*Pseudomonas* spp. HLS-6 after 10 minutes of treatment (60 mJ/cm²) in the presence of 1 mg/L of oxidant in UWW (Hu, 2019), while Arslan-Aton

et al., reported > 6.5 LRV of resistant *E. coli* J53 after 80 minutes of treatment, but obtaining only slight difference with only UV-C (Arslan-Aton, 2021).

The set of ARGs, including the 16S rRNA, *intI1*, *qnrS*, *sul1*, *bla_{TEM}*, *bla_{CTX-M32}* and *tetM*, was analyzed. Figure 8.11 and Table 8.2 show the relative abundance of each ARG investigated (with respect to 16S rRNA) as a function of time under UV-C irradiation with and without PMS (1 mM).

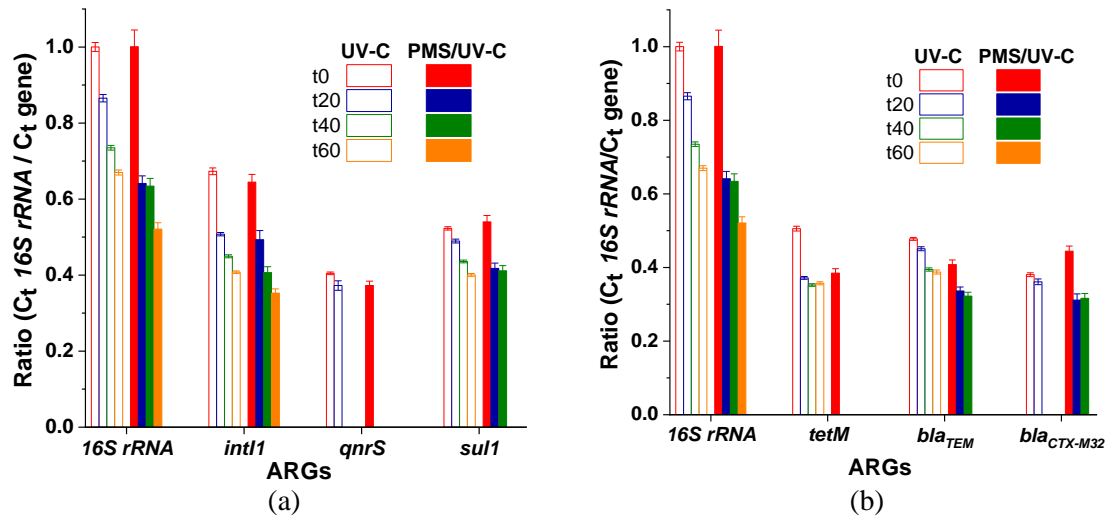


Figure 8.11. Relative abundance of ARGs detected by PMS/UV-C (1 mM) and UV-C alone.

Table 8.2. ARGs mean and standard deviation of the ratio detected in this study.

	16s rRNA	<i>intI1</i>	<i>sul1</i>	<i>bla_{CTX-M32}</i>	<i>bla_{TEM}</i>	<i>tetM</i>	<i>qnrS</i>
Time (min)	Mean±SD	Mean±SD	Mean±SD	Mean±SD	Mean±SD	Mean±SD	Mean±SD
UV-C							
0	1.00±0.01	0.67±0.01	0.52±0.00	0.38±0.01	0.48±0.00	0.51±0.01	0.40±0.00
20	0.87±0.01	0.51±0.00	0.49±0.01	0.36±0.01	0.45±0.01	0.37±0.00	0.37±0.01
40	0.73±0.01	0.45±0.00	0.44±0.00	QL	0.39±0.00	0.35±0.00	QL
60	0.67±0.01	0.41±0.00	0.40±0.00	QL	0.39±0.00	0.36±0.00	QL
PMS/UV-C							
0	1.00±0.04	0.64±0.02	0.54±0.02	0.44±0.01	0.41±0.01	0.38±0.01	0.37±0.01
20	0.64±0.02	0.49±0.02	0.42±0.01	0.31±0.01	0.34±0.01	QL	QL
40	0.63±0.02	0.41±0.02	0.41±0.01	0.32±0.01	0.32±0.01	QL	QL
60	0.52±0.02	0.35±0.01	QL	QL	QL	QL	QL

QL, quantification limit

For UV-C alone, the quantification limit (QL) is only reached for the *qnrS* and *bla_{CTX-M32}* genes after 40 minutes (0.9 kJ/L of Q_{UV}), while for the other genes, degradation percentages of 38.8 %, 33 %, 29.4%, 23 % and 18.8 % were obtained after 60 minutes of treatment for *intI1*, 16S rRNA, *tetM*, *sul1* and *bla_{TEM}*, respectively.

For PMS/UV-C, the QL was achieved after 20 minutes of treatment (0.3 kJ/L) for *tetM* and *qnrS* genes, after 60 minutes (1.4 kJ/L of Q_{UV}) for *sul1*, *bla_{TEM}*, and *bla_{CTX-M32}*, while 50 % of degradation was observed for the 16S rRNA and *intI1* genes after 60 minutes of treatment

8. PMS/UV-C for water and wastewater purification

time, highlighting the enhanced removal in the presence of the oxidant. The higher efficiency of ARGs reduction by PMS/UV-C process could be related to the direct attack to DNA of $\text{SO}_4^{\cdot-}$ and HO^{\cdot} generated in solution, and to the oxidative effect of this oxidant over bacteria containing the genetic material. It should be also noted here that this analysis (and the one presented in Chapter 7) was performed using the total contents of material genetic from UWW samples after application of the DNA extraction method, without considering the differences between external and internal genetic material. Therefore, it cannot be excluded that the degradation % obtained could be related with the available external genetic material (considered as easier to degrade for proximity with radical's generation in the solution) instead of the internal one present in bacteria at the moment of the samples analysis.

Regarding previous results reported in literature, better performances in the presence of PMS/UV-C (20 mg/L) were also obtained by Hu et al., achieving 2.9 and 3.4 LRV, compared to UV-C alone that attained 1.2 and 0.8 LRV for *sulI* and *intI1* genes, respectively, after 30 minutes of treatment (180 mJ/cm^2) in phosphate buffer saline solution (Hu, 2019). Arslan-Alaton et al. also reported that the addition of PMS (2 mM) enhanced the removal of ARGs in UWW compared to UV-C radiation alone, achieving QL for 16S rRNA, *aphA* and *tetA* after 80 minutes (Arslan-Alaton, 2021).

On the other hand, a detrimental effect of the oxidant addition was reported by Rodríguez-Chueca et al., analyzing several ARGs (*sulI*, *sul2*, *qnrS*, *bla_{TEM}*, *bla_{OXA-A}* and *intI1*) in UWW by different oxidation processes (UV-C alone, UV-C/ H_2O_2 and PMS/UV-C). These authors obtained after 4 s of contact time < 1 LRV for each gene by UV-C alone, while a reduced ARGs removal efficiency was observed by PMS/UV-C (at 0.5 mM). This effect was attributed to the competition between DNA and oxidant species in the absorption of UV photons, reducing the direct damage to the genes in the presence of the oxidant. Moreover, low performances in genes removal could be attributed to the very low contact time (4 s (Rodríguez-Chueca, 2019c) *versus* 300 s of the present study with 1 mM of PMS).

8.6 Concluding remarks

The disinfection and decontamination results obtained in this chapter demonstrated the capability of PMS/UV-C for both groundwater treatment and for the reclamation of urban wastewater, overcoming the limitations of UV-C system, such as post-treatment regrowth and limited CECs removal. On the other hand, wastewater reuse challenges, involving fecal

bacterial load (*E. coli*, *Pseudomonas* spp., and *Enterococcus* spp.), ARB and ARGs removal and CECs degradation, were successfully addressed by combining UV-C irradiation with the oxidative agent PMS.

The best PMS concentration was found to be 1 mM, at which bacterial concentration < 10 CFU/100 mL (maximum permissible *E. coli* concentration for the most restrictive reuse category) was obtained after 6 minutes of treatment (0.01 kJ/L of Q_{UV}) for all bacteria investigated. Regarding organic chemical pollutants, 80 % of the total CECs analyzed was removed after 12 minutes (0.13 kJ/L of Q_{UV}).

Significant differences in the inactivation of wild and AR-bacteria were not observed, and DL of 1 CFU/100 mL was also reached after 6 minutes of treatment (0.01 kJ/L of Q_{UV}) for all microbial targets in the presence of higher oxidant load (1 mM). The QL of the genes *sul1*, *blaTEM*, *blaCTX-M32*, *qnrS*, and *tetM* genes was reached within 60 minutes of treatment, while only 50 % of the 16S rRNA and *intI1* was removed, obtaining higher removal efficiency compared with UV-C alone.

It is important to highlight that the inactivation of ARB does not guarantee DNA damage, which could still contribute to AR spread through different transmission mechanisms and highlight that ARB inactivation is not the challenge on UWW; rather, it is the removal of ARGs.

Therefore, the PMS/UVC process could be a suitable option to be implemented in UWWTPs, allowing to obtain a higher-quality water suitable to be reused in agriculture.

CHAPTER 9

COMPARATIVE EVALUATION OF

PHOTO-CHEMICAL PROCESSES

9. COMPARATIVE EVALUATION OF PHOTO-CHEMICAL PROCESSES

This chapter tackles a comparative evaluation of photo-chemical processes, namely PMS/Solar and PMS/UV-C, for water purification taking into the analysis of: (i) TPs generation and process capability to attain their efficient degradation, (ii) eco-toxicity of treated UWW effluent and (iii) ATC for process implementation.

Finally, a comparison of both water processes has been done using the data obtained in the aforementioned analysis, but also including the capability for the simultaneous disinfection and decontamination, regrowth of bacteria during post-treatment storage, and the influence on the antibiotic resistant phenomenon control, all of them considered as key parameters needed to determine the proper suitability and safety of the water treatments investigated along this study.

9.1 Transformation Products assessment

9.1.1 Identification of TPs and degradation routes

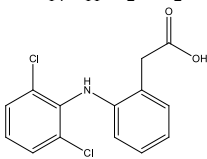
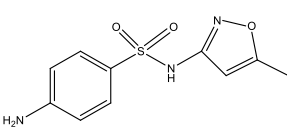
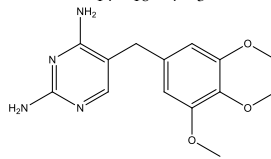
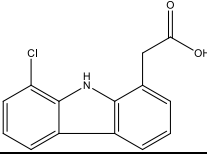
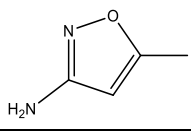
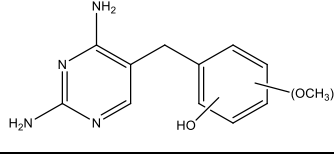
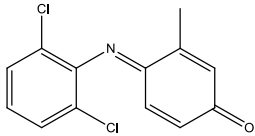
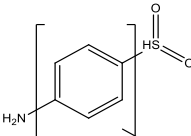
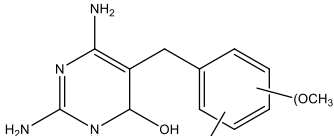
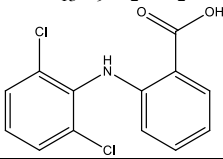
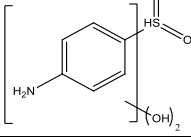
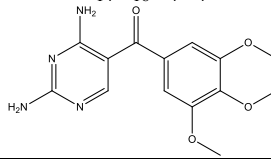
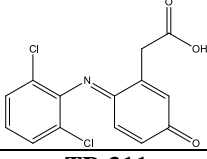
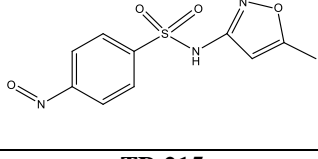
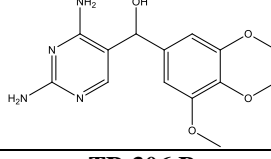
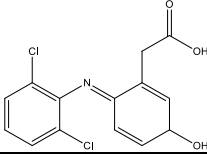
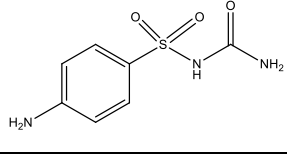
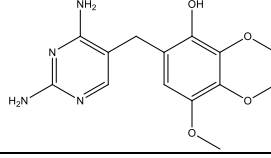
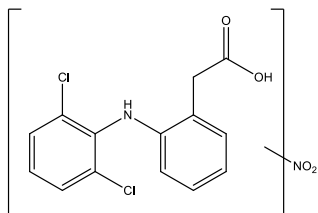
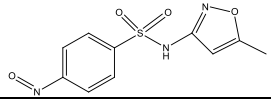
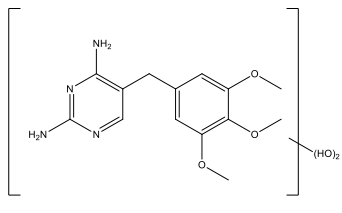
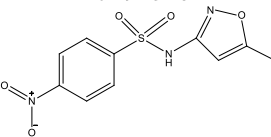
The identification of the TPs was preliminarily carried out in pure water in the presence of each CEC at 1 mg/L, individually degraded by either PMS/Solar and PMS/UV-C in the presence of 1 mM of oxidant. Then, TPs generation was evaluated in actual UWW in the presence of 1 mM of PMS, spiking the matrix with the mix of CECs, containing 100 µg/L each, and assessing processes capability to achieve their degradation.

Analysis by LC–QTOF–MS allowed to elucidate the structure of unknown TPs, based on accurate mass measurements, through the application of suspect screening workflow (Figure 3.23 in Chapter 3).

The main TPs identified for each CEC are summarized in Table 9.1 and further details and more complete information are shown in Table C.1 (Annex C), which sets out the information about structure, retention time, MS/MS fragmentation pattern, the theoretical formula of both protonated molecules $[M+H]^+$ and ion fragments and the data regarding relative mass error between the measured and calculated mass and the DBE (Double Bond Equivalents).

9. Comparative evaluation of photo-chemical processes

Table 9.1. List of TPs tentatively identified in samples for DCF, SMX and TMP.

<p>DCF C₁₄H₁₁Cl₂NO₂</p> 	<p>SMX C₁₀H₁₁N₃O₃S</p> 	<p>TMP C₁₄H₁₈N₄O₃</p> 
<p>TP-259 C₁₄H₁₀ClNO₂</p> 	<p>TP-98 C₄H₆N₂O</p> 	<p>TP-276 C₁₃H₁₆N₄O₃</p> 
<p>TP-265 C₁₃H₉Cl₂NO</p> 	<p>TP-173 C₆H₇NO₃S</p> 	<p>TP-294 C₁₃H₁₈N₄O₄</p> 
<p>TP-281 C₁₃H₉Cl₂NO₂</p> 	<p>TP-189 C₆H₇NO₄S</p> 	<p>TP-304 C₁₄H₁₆N₄O₄</p> 
<p>TP-309 C₁₄H₉Cl₂NO₃</p> 	<p>TP-197 C₇H₇N₃O₂S</p> 	<p>TP-306 A C₁₄H₁₈N₄O₄</p> 
<p>TP-311 C₁₄H₁₁Cl₂NO₃</p> 	<p>TP-215 C₇H₉N₃O₃S</p> 	<p>TP-306 B C₁₄H₁₈N₄O₄</p> 
<p>TP-340 A/B C₁₄H₁₀Cl₂N₂O₄</p> 	<p>TP-267 C₁₀H₉N₃O₄S</p> 	<p>TP-322 A/B/C C₁₄H₁₈N₄O₅</p> 
	<p>TP-283 C₁₀H₉N₃O₅S</p> 	

9. Comparative evaluation of photo-chemical processes

Diclofenac degradation route: The degradation pathway of DCF in the presence of PMS both under natural solar radiation and UV-C irradiation in UWW is shown in Figure 9.1 and transformation routes included:

- Photocyclisation: elimination of the chlorine substituent, followed by ring closure to form monohalogenated carbazole-1-acetic acid (**TP-259**), previously identified as main photolytic degradation product in other studies (Alharbi, 2017; Aguera, 2005).
- Hydroxylation of the aromatic ring: leading to the generation of 5-hydroxy-DCF (**TP-311**), as the most probable option based on reactivity sites and previous literature (Jewell, 2016; Kosjek, 2008; Pérez-Estrada, 2005).
- Oxidation by dehydrogenation: the monohydroxylated derivatives (**TP-311**) is further oxidized into the corresponding quinone imine (**TP-309**) (Jewell, 2016; Kosjek, 2008; Pérez-Estrada, 2005).
- Decarboxylation and oxidation of the aliphatic $-CH_2$ moiety to a carboxylic acid group with formation of DCF-benzoic acid (**TP-281**) (Jewell, 2016; Aguera, 2005).
- Incorporation of nitro group ($-NO_2$) into aromatic ring: substitution of hydrogen atom by $-NO_2$ group, leading to the generation of DCF-nitro derivate (**TP-340 A/B**, being not possible to obtain the exact position of the nitro group in the molecule from the MS/MS data). It has previously been reported by Kosjek et al. (Kosjek, 2008).
- Further decarboxylation of the phenylacetic acid group of TP-309 to generate **TP-265** (Pérez-Estrada, 2005).

This primary degradation route with formation of the stable TP-309 was suggested also during $SO_4^{\cdot-}$ oxidation of DCF (Mahdi-Ahmed, 2012) and during solar photo-Fenton treatment (Pérez-Estrada, 2005). In fact, it has been reported that the main degradation mechanism could be based on an electron transfer from the N atom to $SO_4^{\cdot-}$ leading to a N-centered radical cation, with stabilization of the positive charge on C-5 position of aromatic ring, followed by hydroxylation yielding to a hydroxylamine derivative (**TP-311**), further oxidized to quinone imine structure (**TP-309**) (Mahdi-Ahmed, 2012).

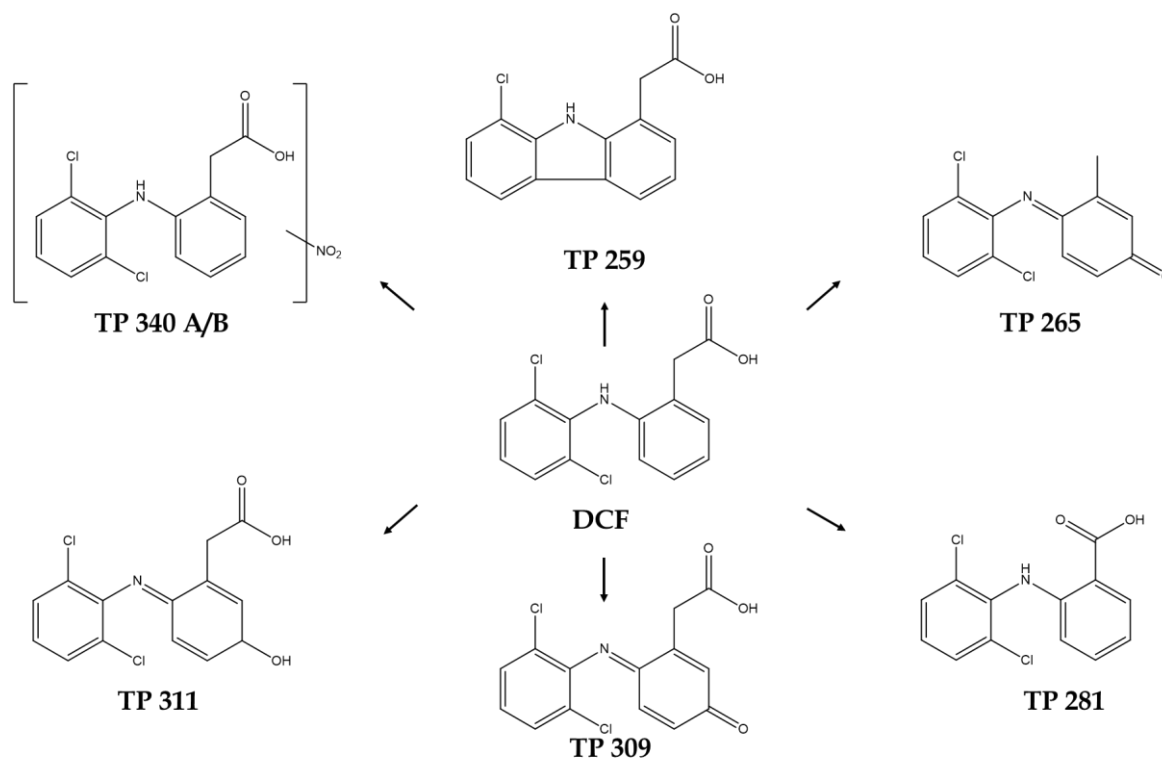


Figure 9.1: Degradation pathway of DCF.

Sulfamethoxazole degradation route: SMX degradation upon PMS/Solar and PMS/UV-C generated six TPs, according to the degradation pathway shown in Figure 9.2, which included:

- Cleavage of sulphonamide bond S–N, resulting in the formation of 3-amino-5-methyl-isoxazole (**TP-98**) (Trovó, 2009).
- Monohydroxylation (**TP-173**) and bihydroxylation (**TP-189**) of p-sulfoaniline moiety after cleavage of sulphonamide bond S–N (Trovó, 2009).
- Subsequent oxidation of the p-sulfoaniline moiety (amine group at the benzene ring) to nitroso NO-SMX (**TP-267**) and nitro derivate NO₂-SMX (**TP-283**) (Gmurek, 2015; Gómez-Ramos, 2011).
- Isoxazole ring opening and rearrangement (**TP-197** and **TP-215**) (Trovó, 2009).

9. Comparative evaluation of photo-chemical processes

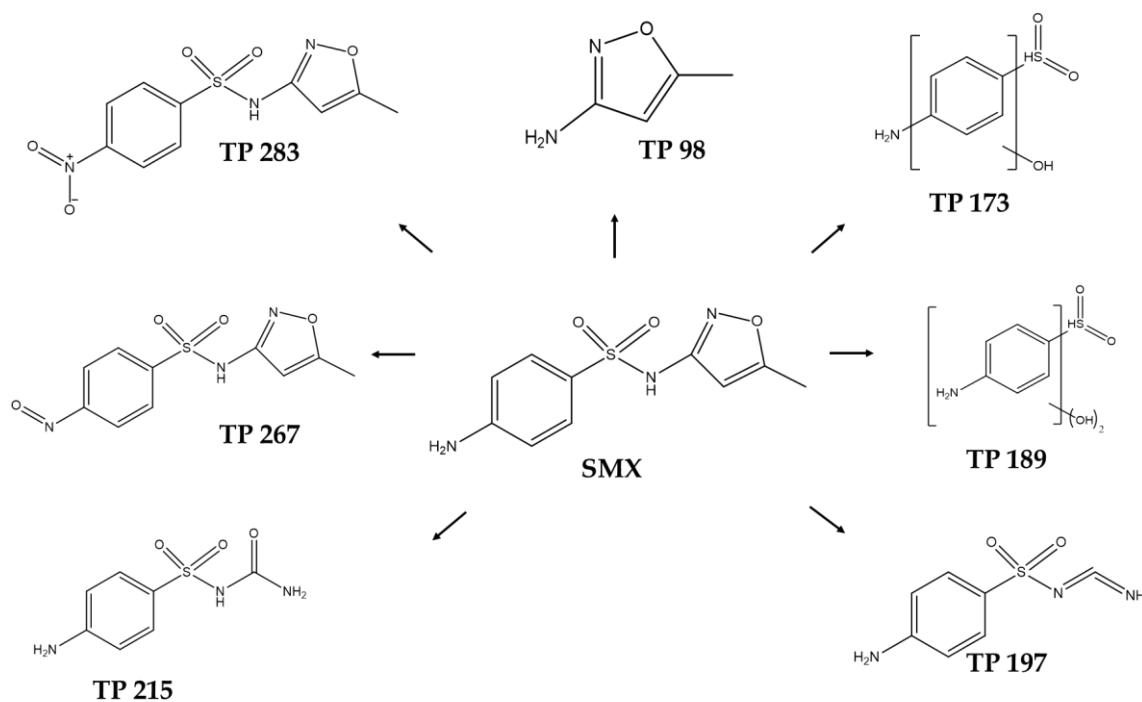


Figure 9.2: Degradation pathway of SMX.

During $\text{SO}_4^{\cdot-}$ oxidation of SMX the predominance of the degradation pathway involving oxidation of the amine group to yield the nitro-SMX derivative has been reported by several authors (Yang, 2017; Mahdi-Ahmed, 2012). The mechanism postulated was based on generation of a N-centered radical as a first intermediate after electron-transfer from N to $\text{SO}_4^{\cdot-}$ (acting as selective electrophile), its subsequent conversion to hydroxy (-N-OH), nitroso (-NO) and finally nitro-SMX (-NO₂) (Mahdi-Ahmed, 2012). Moreover, 3-amino-5-methylisoxazole (**TP-98**), formed after cleavage of sulphonamide bond, has been reported as main photolysis product by Zhang et al. (Zhang, 2016).

Mostly of the identified TPs of SMX retained the amino group in their molecule, still exhibiting, therefore, antibacterial properties, being possibly biologically active and inducing antimicrobial resistance. Majewsky et al. found that all breakdown products (such as **TP-98**, **TP-173** and **TP-189**) were less active than SMX, indicating the loss of the bacteriostatic mechanism of action. On the contrary, TPs modified at the para-amino group, such as NO-SMX (**TP-267**) and NO₂-SMX (**TP-283**), still exhibited antibacterial effects, being more toxic relative to SMX (Majewsky, 2014).

Trimethoprim degradation route: TMP photo-transformation pathway proposed is shown in Figure 9.3, involving:

- Hydroxylation: generating the mono-hydroxylated derivatives (**TP-306A/B**) in which hydroxyl group could be attached to the methylene group (**TP-306A**) and to the ring of TMP molecule (**TP-306B**). Further hydroxylation could occur forming the bi-hydroxylated (**TP-322 A/B**), whose differentiation was not feasible and the hydroxyl groups could be connected to both rings of the TMP molecule (Sirtori, 2010; Arvaniti, 2020).
- Carbonylation at the methylene bridge with formation of **TP-305** (Sirtori, 2010; Arvaniti, 2020).
- Demethylation accompanied with hydroxylation (**TP-276** and **TP-294**): loss of one methoxy group (-OCH₃) and addition of hydroxyl one (-OH) to generate **TP-276** and further attack to the diaminopyrimidine moiety to form **TP-294**.

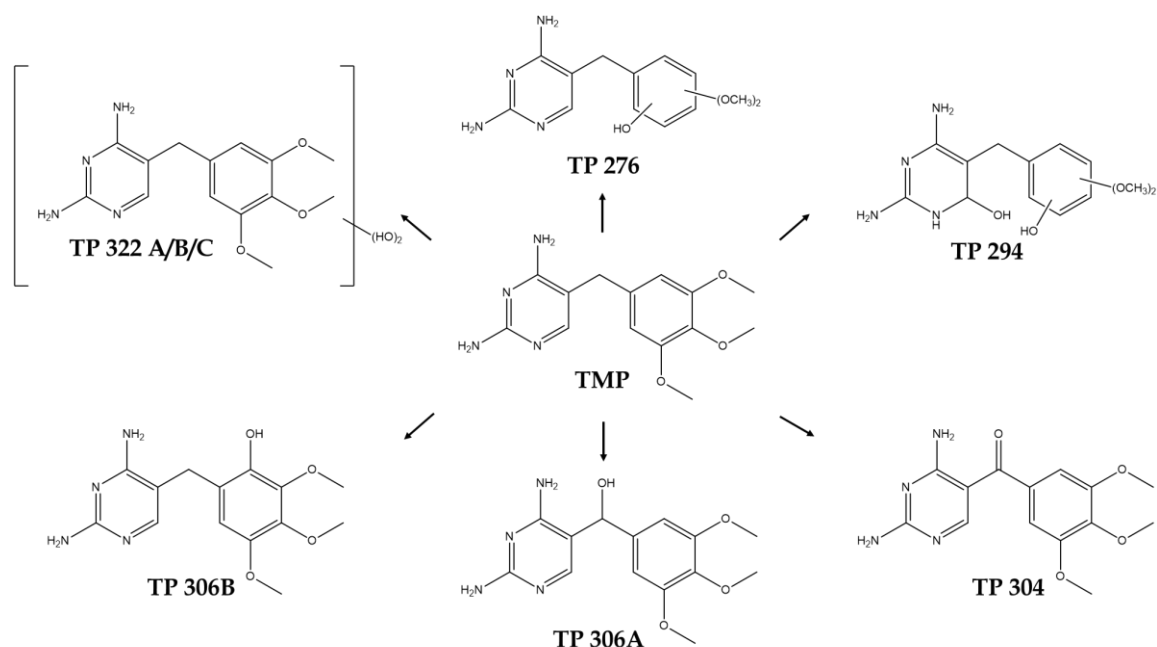


Figure 9.3: Degradation pathway of TMP.

It has been reported that $\text{SO}_4^{\bullet-}$ primarily attacks the pyrimidine ring via electron transfer mechanism, leading to the generation of a radical intermediate with a positive charge, stabilized at the methylene bridge and at the trimethoxybenzene ring through resonance. A carbon-center radical on methylene group could be formed, transformed to superoxide with the presence of dissolved oxygen and to a hydroxyl moiety yielding **TP-306A** and a carbonyl moiety yielding **TP-304**, reported as major products by $\text{SO}_4^{\bullet-}$ (Ji, 2016; Zhang, 2016). A direct H abstraction mechanism at bridging methylene by $\text{SO}_4^{\bullet-}$ was considered to be less probable to occur in comparison to electron transfer mechanism

9. Comparative evaluation of photo-chemical processes

(Ji, 2016). Same TPs were previously identified by solar-photo Fenton and ozonation (Kuang, 2013; Michael, 2012).

In all cases, the cleavage of the methylene group was not observed and TPs maintained the two-ring TMP structure, with major changes occurring in the trimethoxybenzyl moiety, as it has been also reported during the solar photo-degradation of TMP by Sirtori et al. (Sirtori, 2010). The antimicrobial activity has been attributed to the presence of pyrimidine group, maintained in all TPs detected (Ji, 2016).

9.1.2 TPs detection during PMS/Solar versus PMS/UV-C process

The evolution of DCF, SMX and TMP and their major photolytic transformation products in UWW in the presence of 1 mM of PMS under natural solar radiation (left) and UV-C irradiation (right) is shown in Figure 9.4.

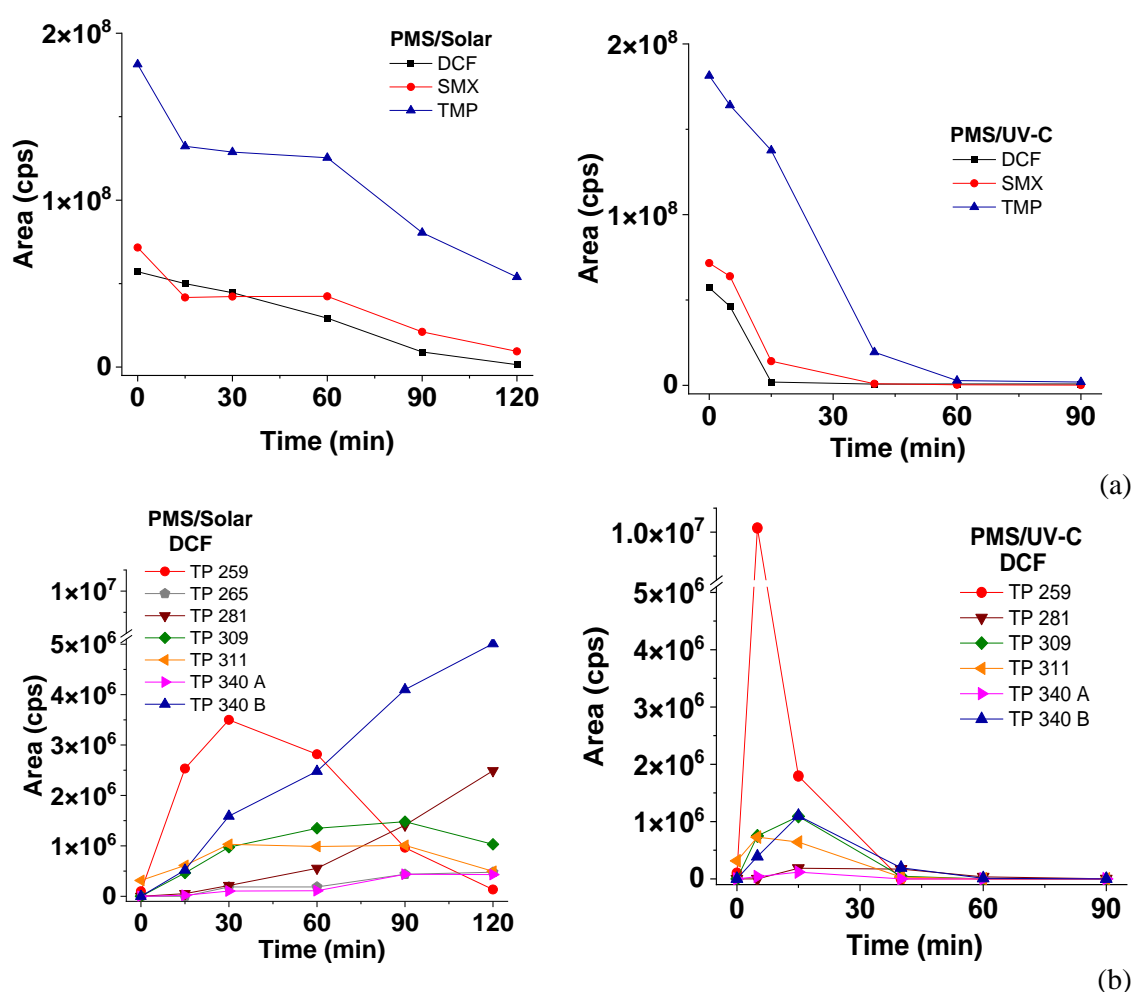


Figure 9.4: Degradation of DCF, SMX and TMP (a) and evolution of their major photolytic TPs (b, c and d) in UWW with 1 mM of PMS under natural solar radiation (left) and UV-C radiation (right) in SPE-enriched sample.

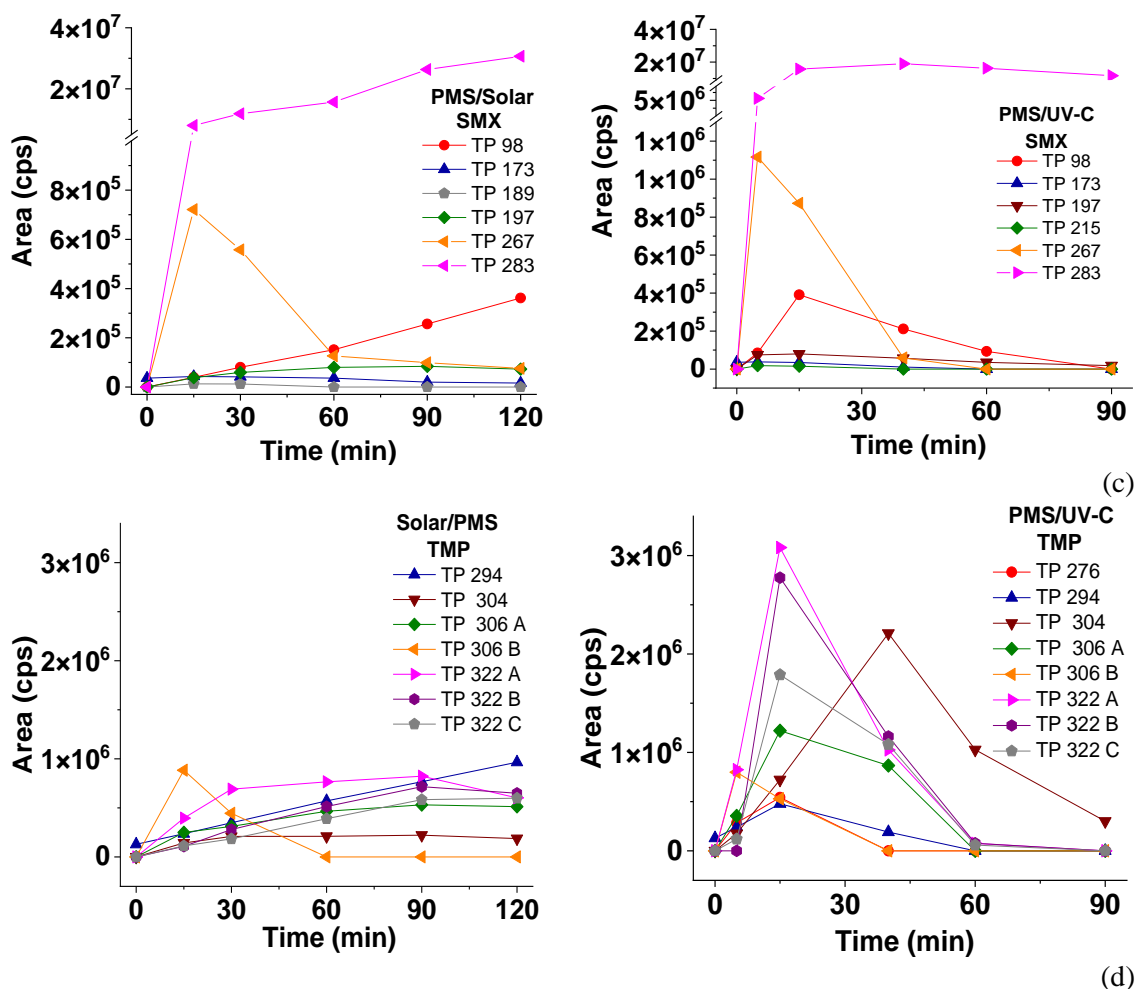


Figure 9.4 (Continued): Degradation of DCF, SMX and TMP (a) and evolution of their major photolytic TPs (b, c and d) in UWW with 1 mM of PMS under natural solar radiation (left) and UV-C radiation (right) in SPE-enriched sample.

The time-evolution profile of DCF shows that it was effectively removed both under UV-C and natural solar radiation in the presence of PMS, achieving > 95 % after 15 and 120 minutes by PMS/UV-C and PMS/Solar, respectively. The most predominant TP formed under UV-C radiation was **TP-259**, whose concentration sharply increased at a considerable concentration after 5 minutes, obtaining a complete removal after 40 minutes of treatment time.

In the case of SMX, more than 95 % was removed after 40 and 120 minutes by PMS/UV-C and PMS/Solar, respectively. Oxidation of the amine group $-NH_2$ to yield the nitro-SMX derivative was found to be the predominance degradation pathway, generating firstly the nitroso-derivate (**TP-267**), that is gradually converted into the most abundant nitro-intermediate (**TP-283**) and remaining in the solution until the end of the experiments. **TP-267** reached its maximum concentration after 5 and 15 minutes of UV and solar exposure time, respectively, and an almost complete removal was observed after 60 minutes

9. Comparative evaluation of photo-chemical processes

in both processes. **TP-283** increased in the first minutes (5 minutes for PMS/UV-C and 15 minutes for PMS/Solar) and then reached a plateau, not being susceptible to be photodegraded under both processes and considered more recalcitrant than the parent compound (Yin, 2018). Other interesting TP detected is 3-amino-5-methylisoxazole (**TP-98**), formed after cleavage of sulphonamide bond. It needed the longest time (15 minutes) to reach its maximum concentration, being totally degraded by PMS/UV-C, while its concentration increased along the PMS/Solar process. Time-trend profiles of this TP was in good agreement with Muhl et al. (Muhl, 2020), which indicated that the slow formation of this products could be related to the degradation of SMX and of other TPs, formed later during SMX degradation, by heat-activated PS oxidation.

Finally, TMP was efficiently removed by PMS/UV-C (> 95 %), while approximately only 70 % was degraded after 120 minutes under solar exposure. The major products of TMP degradation were monohydroxylated derivates (**TP-306A/B**), the carbonyl form (**TP-304**) and the dihydroxylated isomers (**322 A/B/C**), which agree with Zang et al., that identified the same TPs as main products during oxidation of TMP by UV activated PS in synthetic human urine (Zhang, 2016).

As showed in Figure 9.4d, TMP-OH (**TP-306A**) reached the maximum detection rapidly (ca.15 minutes) after the reaction was initialized under UV-C radiation, while the carbonyl form TMP=O (**TP-304**) reached the highest concentration after 40 minutes (indicating a later conversion of **TP-306** into **TP-304**) and then gradually decreased. This tendency has been reported also by Ji et al. during TMP degradation by thermo-activated PS oxidation (Ji, 2016). On the other hand, the hydroxylated form (**TP-306A**) was formed in a lower quantity during PMS/Solar and it was not degraded during the treatment time, highlighting lower TMP removal and less aggressive oxidative conditions. Regarding the **TP-322 A/B/C**, a maximum was reached in 15 minutes and then diminished quickly under UV-C radiation; while 90 minutes were necessary to achieve the maximum concentration by PMS/Solar, decaying much slowly.

Summarizing the comparison of the TPs generated by PMS/UV-C and PMS/Solar, it could be highlighted that:

- Similar intermediates were generated under UV-C light and natural solar radiation in the presence of PMS, involving analogous degradation pathways.
- Most of the TPs identified throughout the experiments were completely degraded during PMS/UV-C, while some of them were not removed under natural solar

radiation during the treatment time, highlighting a higher oxidative capacity of PMS/UV-C by involving radical generation and greater efficiency in TPs removal.

- A total of 7 intermediate products of DCF was detected via mass spectrometry and TP most abundant was **TP-259** in both systems. The highest removal of DCF and the lowest final concentration of its degradation products was observed under UV-C radiation, while concentration of **TP-281** and **TP-340B** did not show any decrease in their concentrations by PMS/Solar.
- A total of 6 intermediate products of SMX was detected via mass spectrometry and the TP most abundant was **TP-283** in both systems, being refractory to degradation by both systems, whereas others were apparently formed only in traces.
- A total of 8 intermediate products of TMP was detected via mass spectrometry and the TPs most abundant produced were **TP-304** and **TP-322A/B/C** in UV-C system, while lower amount of intermediates was generated under sunlight, probably as a consequence of parent compound's lower degradation rate.

9.2 Eco-toxicological assessment of treated UWW

The potential toxic post-treatment effect of the treated UWW by PMS under both irradiation sources (UV-C and sunlight) has been also analysed. Samples from UWW being treated by each process at 1 mM initial concentration of PMS were assessed following two main toxicological analyses: *A. fisheri* commonly used as model of the potential environmental impact associated with the direct discharge; and phytotoxicity (with several species) to assess potential effects associate to the reuse in agriculture. The residual concentration of PMS in the tested samples for toxicity was not eliminated to determine the real potential toxic effect derived from treated UWW (containing oxidant), discharged into the receiving environment or reused in agriculture.

Figure 9.5 shows the BI results towards *A. fisheri*. In this case, samples were diluted 1:10 (v/v), being this dilution factor below the range of 1:80 to 1:100 v/v usually considered in real UWW coastal discharge (Aude, 1995). BI < 20 % indicates that the discharge does not pose a harmful effect to the receiving aquatic environment (Persoone, 2003). The results obtained showed that the mere effect of PMS addition (t0) led to a slight BI (an average 2 %), while stimulation effect was observed for both, untreated UWW (-45.5 BI %) and treated UWW by PMS/Solar (-10 % after 120 minutes) and PMS/UV-C processes (-18.5 %

9. Comparative evaluation of photo-chemical processes

after 90 minutes). Therefore, these results demonstrated that the process investigated with PMS will not generate a toxic effect and an environmental risk can be discarded when considering direct discharges. Similar results have been also reported in river water treated with PMS at 1 mM, i.e., an initial toxic effect after oxidant addition and its decrease along the treatment time (Deng, 2017).

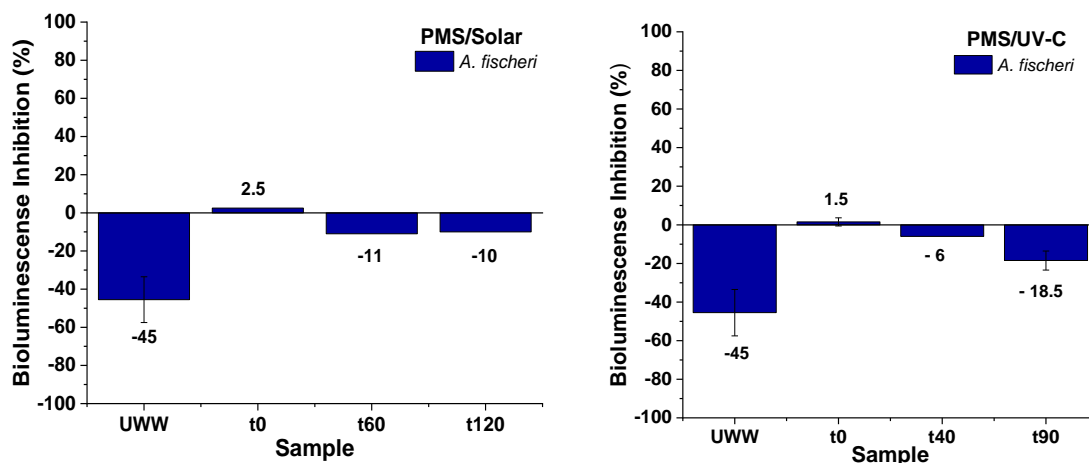


Figure 9.5. BI results towards *A. fischeri* in untreated and treated UWW by PMS/Solar and PMS/UV-C (1 mM).

The phytotoxicity results from the root growth of *S. saccharatum*, *S. alba* and *L. sativum* seeds are shown in Figure 9.6. In this case, three conditions were simultaneously analysed: (i) a positive control (Zn^{2+} solution at 100 mg/L), (ii) a negative control (with untreated UWW) and (iii) treated UWW by PMS/Solar and PMS/UV-C at 1 mM of PMS. The interpretation of the parameter RGI values is: (i) phytotoxicity for $0 < RGI < 0.8$; (ii) no significant effect for $0.8 \leq RGI \leq 1.2$; and (iii) stimulation (benefit): $RGI > 1.2$. Therefore, results showed that immediately after the addition of PMS to the UWW sample (t=0 minute), a slightly reduction on the RGI (values below 0.8) was observed only for *S. alba* and *L. sativum* whereas, *S. saccharatum* RGI value was 1, meaning no effect.

Moreover, different trends for each specie were observed for PMS/Solar treatment (after 60 minutes of treatment time) and PMS/UV-C (after 40 minutes):

- No significant effect for *S. saccharatum* (RGI between 0.8 and 1.2) in all cases.
- Very slight inhibition for *S. alba* and similar than the t0 sample for PMS/Solar (RGI: 0.78), while for PMS/UV-C, an additional increment on the phytotoxicity (ca. 10 %) was observed (RGI: 0.65).

- *L. sativum* showed no phytotoxicity for PMS/Solar treatment (RGI: 0.9); while an increased phytotoxicity (RGI: 0.58) was observed in comparison with t0 sample (RGI: 0.69).

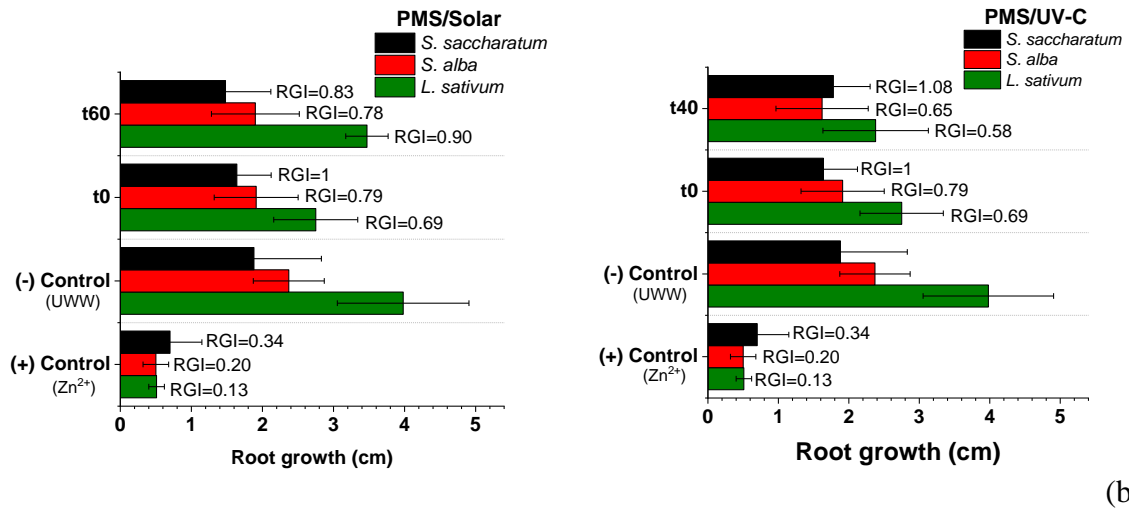


Figure 9.6: Phytotoxicity results for *S. saccharatum*, *S. alba* and *L. sativum* in the positive (+) control (Zn²⁺ solution at 100 mg/L), negative (-) control (untreated UWW), and treated UWW by PMS/Solar and PMS/UV-C (1 mM).

Therefore, summarizing, reclaimed UWW obtained by both PMS/Solar and PMS/UV-C process showed no toxicity towards *A. fischeri*, excluding a harmful effect toward the receiving aquatic environment after effluent discharge, and a very slightly toxic effect for growth of two out of the three seeds tested (*L. sativum* and *S. alba*), compared to the positive control Zn²⁺, indicating the suitability of this water for its subsequent reuse for agriculture.

Additionally, to the toxicity results, there are other aspects that in this line should be also mentioned. For one hand, it is important to note that considering the PMS as oxidative agent for reclamation of UWW and reuse in agriculture, the residual PMS concentration (0.3 and 0.1 mM for PMS/Solar and PMS/UV-C, respectively, starting from an initial concentration of 1 mM) could not be considered as a matter of concern. It is well-known that PMS salt suffers, upon contact with soils, a quickly abiotic decomposition (half-lives < 11 minutes and no detection after 1 hour) into products of no concern and ubiquitously present in the environment (such as potassium hydrogensulfate, hydrogen peroxide and oxygen) (ECHA, European Chemicals Agency).

On the other hand, and due to PMS composition, a release of SO₄²⁻ after oxidant addition could eventually cause a problem of post-contamination. Although, no health-based guidelines have been derived for SO₄²⁻, values less than 250 mg/L were established by USEPA for potable water (Watson, 2016) and lower than 1000 mg/L are generally

9. Comparative evaluation of photo-chemical processes

recommended for reclaimed water according to USEPA guidelines for water reuse (USEPA, 2012). Under the experimental conditions tested herein with a maximum concentration of 1 mM of PMS, an increase in the UWW concentrations of SO_4^{2-} (101.5 ± 22.7 mg/L, Table 3.5) of ca. 193 mg/L was detected at the end experiment, being therefore lower than the level to impart undesirable taste in drinking water (250-500 mg/L) and to cause illnesses such as diarrhea (> 1000 mg/L) (WHO, 2004). Besides, the presence of a higher concentration of potassium ion (increase in a concentration of ca. 80 mg/L) and SO_4^{2-} could be an added benefit for crop fertigation, saving of essential fertilizers (FAO, 1985).

9.3 Annual Treatment Cost

The evaluation of technology costs, expressed as Annual Treatment Cost (ATC), was performed to assess process feasibility and it includes: (i) Investment Cost (InC) (equipment and construction costs) and (ii) Operation and Maintenance cost (OC and MC).

9.3.1 PMS/Solar

The ATC to treat UWW (bacteria and CECs removal) by the PMS/Solar process was estimated for three concentrations (0.5 mM, 0,75 mM and 1 mM) (experimental data obtained from Chapter 7), being 0.5 mM the minimum tested dosage needed to achieve an effective disinfection and 1 mM the optimal load to reach also good decontamination performances. The following assumptions were considered:

- Treatment of 1000 m³/day in a small UWWTP, working 365 days/year with a 5000 p.e. (150 L/ day per p.e) and the UWW flow of the USEPA category 3 (0.27 Million Gallons per Day MGD) (British Water, 2013; USEPA, 1996).
- A Capital Recovery Factor (CRF) of 0.117 (cost amortized at 10 % interest rate for 20 years): the annual cost was found by multiplying the capital cost by the amortization factor.
- The InC includes (i) the cost of the CPC field required, including the cost of land for their installation (150 €/m²) (BOE, 2021) and (ii) the cost of CPC reactors (648 and 513 €/m², updating prices (+ 5.9 %) based on consumer price index 2015-2021, with lower price for > 1000 m²) (Nahim-Granados, 2020; Miralles-Cuevas 2016).

9. Comparative evaluation of photo-chemical processes

- The MC was calculated as the 2.5 % of the estimated annual InC and the OC was estimated as the summation of the electricity costs for water pumping (0.12 €/kWh, 0.22 + 0.44 kWh/m³ for fill and recirculation, respectively) and reagent costs (PMS, 0.61 €/m³) (Sbardella, 2020).
- The CPC field (A_{CPC} , m²) needed for each treatment condition was calculated according to the Eq. 9.1 (Malato, 2009).

$$A_{CPC} = \frac{Q_{UV} \cdot V_{tot}}{T_s \cdot UV_g} \quad \text{Eq. 9.1}$$

Where Q_{UV} (J/L) is the UV-A energy values needed to achieve the treatment goal (2 CFU/mL and 80 % CECs abatement), V_{tot} is the annual volume of treated water (365 x 10⁶ L/year), T_s is the annual operation time (157.68 x 10⁵ s for 12 h/day) and UV_G is the average of local solar UV-A radiation (36.8 W/m²).

The ATC values resulting are shown in Table 9.2.

Table 9.2. Annual treatment costs to disinfect and remove CECs from UWW by the PMS/Solar process at 0.5, 0.75 and 1 mM.

	Bacteria			CECs		
[PMS] (mM)	0.5	0.75	1	0.5	0.75	1
Q_{UV} (J/L)	4840	2560	1080	6000	3800	2000
CPC field (m²)	3045	1610	679	3774	2390	1258
Investment Costs (IC) (€)	236164	124913	63428	292765	185418	97588
O & M costs (€)	146137	199019	253144	147552	200531	253998
Electricity	28908	28908	28908	28908	28908	28908
Reagents	111325	166988	222650	111325	166988	222650
Maintenance (2.5 % IC)	5904	3123	1586	7319	4635	2440
Total annual cost (€)	382301	323932	316572	440317	385949	351586
€/m³	1.05	0.89	0.87	1.21	1.06	0.96

The CPC field required for 1 and 0.5 mM of PMS was 679 and 3045 m², respectively, leading to a treatment cost for UWW disinfection from 0.87 to 1.05 €/m³. For CECs removal (implicit disinfection), the cost may vary from 0.96 to 1.21 €/m³ (corresponding CPC area of 1258 and 3774 m²) for 1 and 0.5 mM of PMS, respectively. Therefore, according to total cost, the best treatment condition for PMS/Solar process was found to be 1 mM of oxidant: 0.87 or 0.96 €/m³, requiring 679 or 1258 m² of CPC for only disinfection or for the simultaneous removal of chemical and biological targets, respectively.

Other studies using solar processes and CPC reactors reported data that varied among 1-3 €/m³, depending on the type of treatment, targets removal (disinfection or also decontamination), type of water matrix and land cost consideration. The treatment cost

9. Comparative evaluation of photo-chemical processes

obtained was 0.92 €/m³ - without disinfection and land cost consideration - for solar photo-Fenton at neutral pH (Miralles-Cuevas, 2016) and 1.50 €/m³ for the disinfection of synthetic fresh-cut wastewater and 3.04 €/m³ for its simultaneous disinfection and decontamination by H₂O₂/Solar (Nahim-Granados, 2020), compared to other conventional disinfection processes (0.64 €/m³ for ozonation and 0.23 €/m³ for chlorination) (Miralles-Cuevas, 2016; Plappally, 2013).

9.3.2 PMS/UV-C

The ATC analysis for the implementation of PMS/UV-C as tertiary treatment in a UWWTPs was performed according to the USEPA, considering the scaling up of the UV-C pilot plant used in the study and the obtained results in Chapter 8. The following assumptions were taken into account:

- UV-C pilot plant used in the study characterized by: (i) total volume of 80 L, (ii) flow-rate of 36 L/min and, (iii) illuminated volume of 6 L.
- Contact time of 10 s with a dose of 0.2 Wh/m² (12 mJ/cm²), reached with 6 lamps (calculated according to the USEPA in which to deliver 40 mJ/cm², 24 lamps would be necessary) (USEPA, 1996).
- Treatment of 1000 m³/day (0.27 MGD) of water in a continuous flow UV-C reactor (USEPA flow category 3) for a population range of 500-1000 p.e.
- CRF of 0.117 (cost amortized at 10 % of interest for 20 years): the annual cost was found by multiplying the capital cost by the amortization factor.
- Investment cost (InC) is the sum of the equipment cost (EC) and of its 20 % related to engineering and installation costs (IC= EC+0.2·EC, 20 % of EC corresponds to: engineering 10 %, legal fiscal and administrative 3 %, site work and interconnecting piping 6 % and contingencies 1 %).
- Operation and maintenance cost includes (i) elements replacement (lamps) (USEPA, 1999), (ii) electric power consumption (Pabi, 2013) and (iii) labor.
- Reagent cost (2 €/kg or 0.61 €/mol of commercial PMS salt). Costs associated to an intermediate tank (to dissolve PMS salt) and a dispenser pump were not considered, being much lower than the reagent costs.

Table 9.3 shows the estimation of the ATC for UWW treatment by UV-C alone and PMS/UV-C at 0.5, 0.75 and 1 mM of oxidant concentration in a continuous flow reactor. Treatment costs were 0.02, 0.33, 0.48 and 0.63 €/m³ for 0, 0.5, 0.75 and 1 mM of PMS,

respectively, in agreement with previous studies in literature reporting treatment cost for UWW of 0.012 and 0.585 €/m³ for UV-C and UV-C/PMS (at 0.5 mM) (Rodríguez-Chueca, 2018).

Therefore, the PMS/UV-C process seems to be a promising alternative to UV-C alone for a near future, avoiding bacterial regrowth, degrading more than 80 % of total CECs and promoting AR phenomenon disappearance.

Table 9.3. Estimated ATC for UWW treatment by UV-C and PMS/UV-C in a continuous flow reactor.

INVESTMENT COSTS	1301 €
Equipment cost (EC)	1085 €
Engineering and installation (20 % of EC)	216 €
OPERATIONAL AND MAINTENANCE COSTS	7213 €
Replacement (lamps): 6 UV-C lamps (8760 h) x 820 €/lamp	4920 €
Power: 4468 kWh (lamps) & 11643 kWh (pumping) = 16111 kWh x 0.12 €/m ³	1933 €
Labour (36 h) (0.5 h per month per lamp for cleaning and repair) x 10 €/h	360 €
UV-C TOTAL COST	8514 €
	0.02 €/m ³
UV-C + 0.5 mM PMS	120450 €
	0.33 €/m ³
UV-C + 0.75 mM PMS	176414 €
	0.48 €/m ³
UV-C + 1 mM PMS	231164 €
	0.63 €/m ³

9.4 Comparative evaluation and concluding remarks

Two oxidation processes, PMS/Solar and PMS/UV-C, have been evaluated as possible tertiary treatment methods for UWW to meet water quality limits for its reuse in agriculture. In this final comparison analysis, the following key parameters, considered determinant to select a promising UWW treatment technology, have been considered: (i) the capability to perform simultaneous disinfection and chemical decontamination, (ii) the post treatment storage (guaranteeing water safety without bacteria regrowth), (iii) the efficiency on antimicrobial resistant bacterial and gene loads reduction, (iv) the TPs generation and their elimination and (v) the techno-economic evaluation. Table 9.4 summarizes all the data regarding these parameters, obtained from Chapter 7, 8 and 9.

The PMS/UV-C treatment in the presence of 1 mM of PMS was found capable of inactivating natural occurring bacteria and their resistant counterparts (achieving a concentration < 10 CFU/100 mL after 6 minutes, 0.01 kJ/L), without observing bacterial regrowth after 48h, removing ARGs (within 60 minutes, 1.4 kJ/L) eliminating CECs (12 minutes, 0.13 kJ/L) and their TPs (with 90 minutes of treatment, except for the refractory **SMX-TP 283**). Toxicity studies revealed that a significant potential toxicity towards

9. Comparative evaluation of photo-chemical processes

A. fischeri was not observed, excluding a harmful effect toward the receiving aquatic environment after effluent discharge. The growth of *L. sativum* and *S. alba* was little affected, but rapid PMS abiotic decomposition upon contact with soils making the effluent suitable for its reuse in agriculture. An increment in the cost for PMS/UV-C process (0.63 €/m³, compared to 0.02 €/m³) is totally due to the reagent price, but the higher efficiency in the simultaneous removal of chemical and biological targets by PMS/UV-C, makes this process a suitable option to be implemented in an already working UWWTPs, provided with a UV-C lamp technology.

Table 9.4. Summary of the comparative evaluation of PMS/Solar and PMS/UV-C processes in the actual UWW from El Bobar (Almería).

	PMS/Solar	PMS/UV-C
Experimental set up	10-L CPC Natural solar radiation [PMS]= 1 mM pH=7.5-8	80-L UV-C plant UV-C radiation [PMS]= 1 mM pH=7.5-8
80 % total CECs removal (Spiked DCF, SMX and TMP, 100 µg/L-each)	27 min (2.0 kJ/L)	12 min (0.13 kJ/L)
Bacteria inactivation (UWW natural occurring <i>E. coli</i> , Total coliforms, <i>Enterococcus</i> spp. and <i>Pseudomonas</i> spp.)	DL 2 CFU/mL 15 min (1.1 kJ/L)	< 10 CFU/100 mL 6 min (0.01 kJ/L)
ARB inactivation	DL 2 CFU/mL 30 min (2.6 kJ/L)	DL 1 CFU/100 mL 6 min (0.01 kJ/L)
ARGs reduction	Low removal	QL in 60 min (1.4 kJ/L)
Post treatment regrowth	No, for [PMS] ₀ > 0.5 mM	No, for [PMS] ₀ > 0.5 mM
TPs generation	7 DCF-TPs (only TP-259 degraded) 6 SMX-TPs (only TP-189 degraded) 7 TMP-TPs (only TP-306B degraded)	6 DCF-TPs (all degraded) 6 SMX-TPs (all degraded, except for TP-283) 8 TMP-TPs (all degraded)
Toxicity	Slightly toxic effect detected towards <i>L. sativum</i> and <i>S. alba</i> No toxic effect on <i>A. fischeri</i>	Slightly toxic effect detected towards <i>L. sativum</i> and <i>S. alba</i> No toxic effect on <i>A. fischeri</i>
Costs	0.96 €/m ³	0.63 €/m ³

Regarding PMS/Solar treatment, 1 mM of PMS allowed to achieve the inactivation of natural occurring bacteria and their resistant counterparts (DL of 2 CFU/mL after 30 minutes, 2.6 kJ/L), without observing bacterial regrowth after 48h, eliminating CECs (27 minutes, 2.0 kJ/L), but it was ineffective for ARGs removal and for TPs degradation.

9. Comparative evaluation of photo-chemical processes

Moreover, TPs identified for the two antibiotics, SMX and TMP, still retained the moieties (amino and pyrimidine group, respectively) that confer antibacterial activity, possibly leading to antimicrobial resistance spread, aspect that should be further investigated with the correct optimization of treatment time (or accumulative energy) necessary to achieve proper TPs removal. Toxicity studies revealed that a significant potential toxicity towards *A. fischeri* was not observed and a slight toxic effect was detected towards *L. sativum* and *S. alba*, indicating the suitability of the UWW treated by PMS/Solar for its subsequent agriculture reuse. Therefore, this solar process could be an attractive, suitable and sustainable option to be applied for the treatment of small water volumes in decentralized systems in areas with a high solar radiation incidence, saving energy costs by using natural solar radiation.

CHAPTER 10
CONCLUSIONS

10. CONCLUSIONS

The main conclusions obtained from the entire experimental study are summarized as follows:

1. The photoactivity of ZnO modified with Ce, Yb and Fe for water and UWW treatment has been assessed against several waterborne pathogens and CECs by exciting the semiconductors with natural solar radiation, an economic and ecological source of light. The HO[•] generation was considered responsible of bacteria inactivation and CECs degradation, confirmed by EPR and scavengers' experiments. From all tested photocatalysts, ZnO-Ce exhibited the most promising performance, obtaining similar results with the benchmark TiO₂-P25 for UWW purification.
2. Despite of the promising findings obtained with ZnO-Ce photocatalyst, its further up-scaling was discarded as a feasible approach for UWW treatment, due to the following main considerations: (i) the high amount of photocatalyst needed per liter (and treatment cost associated) and (ii) the treatment effectiveness in comparison with the already commercial TiO₂-P25 and other conventional treatments, making its use non-competitive enough for this application.

10. Conclusions

3. The tested strategy of ZnO-Ce photocatalyst activity enhancement *via* its combination with PMS under natural sunlight showed great preliminary results for UWW treatment. However, opposite to the detected Zn^{2+} release during the irradiation time with the photocatalyst alone (below to the established in guidelines and regulations), when combining with PMS, a significant increased concentration (up to 20 mg/L) was detected, making this strategy an invalid option from an environmental point of view. Nevertheless, for future analysis, the combination with other lower oxidative agents such as H_2O_2 or PS cannot be discarded.
4. The use of PMS alone has been proven to be effective as oxidant agent for water and UWW treatment increasing its effectiveness when illuminated with photons from UV-C lamps and natural sunlight. Nevertheless, different inactivation and CECs degradation mechanisms have been postulated for each type of irradiation, and according to the activation of PMS (with UV-C photons) or non-activation (under natural sunlight).
5. Under UV-C radiation the homolytic break of the O-O bond in PMS occurs, with the formation of the strong $\text{SO}_4^{\bullet-}$ and HO^{\bullet} with a ratio 1.2:1 (experimentally evaluated comparing the EPR DMPO- $\text{SO}_4^{\bullet-}$ / DMPO- HO^{\bullet} signals), being the main responsible for pollutants removal.
6. The reactivity of $\text{SO}_4^{\bullet-}$ generated upon UV-C irradiation against cell-wall model compounds commonly found in gram-negative (such as *E. coli*) and gram-positive (such as *E. faecalis*) bacteria has been assessed for the first time through LFP, a time-resolving technique. It was proven that $\text{SO}_4^{\bullet-}$ reacts (i) via H- abstraction mechanism ($k_{\text{SO}_4^{\bullet-}}, 10^6\text{-}10^7 \text{ M}^{-1}\text{s}^{-1}$) with cell wall components in both type of bacteria, (ii) via electron transfer with amino acids typically present in outer-membrane proteins of gram-negative bacteria ($k_{\text{SO}_4^{\bullet-}}, 10^9 \text{ M}^{-1}\text{s}^{-1}$) and (iii) via electron transfer with CECs (DCF, SMX and TMP) ($k_{\text{SO}_4^{\bullet-}}, 10^9 \text{ M}^{-1}\text{s}^{-1}$).
7. Under natural sunlight, the PMS alone was proven not to be activated, meaning that $\text{SO}_4^{\bullet-}$ and HO^{\bullet} are not generated in the solution, as confirmed by EPR experiments and tests with active scavenger species. Therefore, a non-radical pathway involving direct electron transfer pollutants with electron-rich moieties was postulated with an additional synergistic effect for bacterial inactivation, attributed to the potential damages occurring inside cells.

8. The testing of different types of water matrices has permitted to discern that PMS/Solar process efficiency is (i) affected by a complex inorganic chemical water composition (WeW), but no significant differences were obtained in the presence of different concentration of HCO_3^- , (ii) markedly increased in the presence of chloride ions (IW – due to HClO formation) and (iii) decreased in the presence of organic matter content (SUWW and actual UWW).
9. Reclaimed UWW obtained by both PMS/Solar and PMS/UV-C processes showed no toxicity towards *A. fischeri*, excluding a harmful effect towards the receiving aquatic environment after an effluent discharge, and a very slightly toxic effect for growth of two out of the three seeds tested (*L. sativum* and *S. alba*), proving the suitability of this water for its subsequent reuse for agriculture.
10. PMS/UV-C process (at 1 mM of oxidant concentration) has been demonstrated to be a suitable option to be implemented in UWWTPs, allowing to obtain a high-quality water and addressing other wastewater reuse challenges, such as limiting the spread of the antibiotic resistant phenomenon through the inactivation of natural occurring ARB and efficient removal of ARGs, avoiding bacterial regrowth after 48h post-treatment, degrading CECs original compounds efficiently and also most of their TPs generated during the treatment time.
11. The PMS/Solar process (at 1 mM of oxidant concentration) has been demonstrated to be an attractive, suitable and sustainable option to be applied for the treatment of UWW, achieving successful inactivation of natural occurring bacteria and their antibiotic resistant counterparts, without observing bacterial regrowth after 48h and efficiently eliminating CECs. However, ARGs removal and an effective TPs degradation are still challenges to be addressed in this case.
12. The analysis of the treatment cost revealed that this key factor could be an important barrier for implementation of PMS/Solar process in large centralized UWW treatment plants. Nevertheless, its consideration as decentralized systems associated to small volume of water in areas with a high solar radiation incidence, saving energy costs by using natural solar radiation, could be a real and affordable option.

CHAPTER 11
REFERENCES

11. REFERENCES

- Abbaszadegan, A., Ghahramani, Y., Gholami, A., Hemmateenejad, B., Dorostkar, S., Nabavizadeh, M., Sharghi, H., 2014. The Effect of Charge at the Surface of Silver Nanoparticles on Antimicrobial Activity against Gram-Positive and Gram-Negative Bacteria: A Preliminary Study Abbas. *Journals Nanomater.* 48, 395–400. <https://doi.org/10.1155/2015/720654>
- Abeledo-Lameiro, M.J., Reboredo-Fernández, A., Polo-López, M.I., Fernández-Ibáñez, P., Ares-Mazás, E., Gómez-Couso, H., 2017. Photocatalytic inactivation of the waterborne protozoan parasite *Cryptosporidium parvum* using TiO₂/H₂O₂ under simulated and natural solar conditions. *Catal. Today* 280, 132–138. <https://doi.org/10.1016/j.cattod.2016.05.046>
- Abellán, M.N., Giménez, J., Esplugas, S., 2009. Photocatalytic degradation of antibiotics: The case of sulfamethoxazole and trimethoprim. *Catal. Today.* <https://doi.org/10.1016/j.cattod.2009.01.051>
- Acero, J.L., Piriou, P., Von Gunten, U., 2005. Kinetics and mechanisms of formation of bromophenols during drinking water chlorination: Assessment of taste and odor development. *Water Res.* 39, 2979–2993. <https://doi.org/10.1016/j.watres.2005.04.055>
- Aguas, Y., Hincapie, M., Martínez-Piernas, A.B., Agüera, A., Fernández-Ibáñez, P., Nahim-Granados, S., Polo-López, M.I., 2019. Reclamation of Real Urban Wastewater Using Solar Advanced Oxidation Processes: An Assessment of Microbial Pathogens and 74 Organic Microcontaminants Uptake in Lettuce and Radish. *Environ. Sci. Technol.* 53, 9705–9714. <https://doi.org/10.1021/acs.est.9b00748>
- Aguas, Y., Hincapie, M., Fernández-Ibáñez, P., Polo-López, M.I., 2017. Solar photocatalytic disinfection of agricultural pathogenic fungi (*Curvularia* sp.) in real urban wastewater. *Sci. Total Environ.* 607–608, 1213–1224. <https://doi.org/10.1016/j.scitotenv.2017.07.085>
- Agüera, A., Perez Estrada, L.A., Ferrer, I., Thurman, E.M., Malato, S., Fernandez-Alba, A.R., 2005. Application of time-of-flight mass spectrometry to the analysis of phototransformation products of diclofenac in water under natural sunlight. *J. Mass Spectrom.* 40, 908–915. <https://doi.org/10.1002/jms.867>
- Aguilar-Barajas, E., Díaz-Pérez, C., Ramírez-Díaz, M.I., Riveros-Rosas, H., Cervantes, C., 2011. Bacterial transport of sulfate, molybdate, and related oxyanions. *BioMetals* 24, 687–707. <https://doi.org/10.1007/s10534-011-9421-x>
- Agulló-Barceló, M., Polo-López, M.I., Lucena, F., Jofre, J., Fernández-Ibáñez, P., 2013. Solar Advanced Oxidation Processes as disinfection tertiary treatments for real wastewater: Implications for water reclamation. *Appl. Catal. B Environ.* 136–137, 341–350. <https://doi.org/10.1016/j.apcatb.2013.01.069>
- Alharbi, S.K., Kang, J., Nghiem, L.D., van de Merwe, J.P., Leusch, F.D.L., Price, W.E., 2017. Photolysis and UV/H₂O₂ of diclofenac, sulfamethoxazole, carbamazepine, and trimethoprim: Identification of their major degradation products by ESI–LC–MS and assessment of the toxicity of reaction mixtures. *Process Saf. Environ. Prot.* 112, 222–234. <https://doi.org/10.1016/j.psep.2017.07.015>

11. References

- Alharbi, S.K., Price, W.E., Kang, J., Fujioka, T., Nghiem, L.D., 2016. Ozonation of carbamazepine, diclofenac, sulfamethoxazole and trimethoprim and formation of major oxidation products. *Desalin. Water Treat.* 57, 29340–29351. <https://doi.org/10.1080/19443994.2016.1172986>
- Amarasiri, M., Sano, D., Suzuki, S., 2020. Understanding human health risks caused by antibiotic resistant bacteria (ARB) and antibiotic resistance genes (ARG) in water environments: Current knowledge and questions to be answered. *Crit. Rev. Environ. Sci. Technol.* 50, 2016–2059. <https://doi.org/10.1080/10643389.2019.1692611>
- Arslan-Alaton, I., Karatas, A., Pehlivan, Ö., Koba Uçun, O., Ölmez-Hancı, T., 2021. Effect of UV-A-assisted iron-based and UV-C-driven oxidation processes on organic matter and antibiotic resistance removal in tertiary treated urban wastewater. *Catal. Today* 361, 152–158. <https://doi.org/10.1016/j.cattod.2020.02.037>
- Anipsitakis, G.P., Dionysiou, D.D., 2004. Transition metal/UV-based advanced oxidation technologies for water decontamination. *Appl. Catal. B Environ.* 54, 155–163. <https://doi.org/10.1016/j.apcatb.2004.05.025>
- Ao, X., Liu, W., 2017. Degradation of sulfamethoxazole by medium pressure UV and oxidants: Peroxymonosulfate, persulfate, and hydrogen peroxide. *Chem. Eng. J.* 313, 629–637. <https://doi.org/10.1016/j.cej.2016.12.089>
- Appiani, E., Ossola, R., Latch, D.E., Erickson, P.R., McNeill, K., 2017. Aqueous singlet oxygen reaction kinetics of furfuryl alcohol: Effect of temperature, pH, and salt content. *Environ. Sci. Process. Impacts* 19, 507–516. <https://doi.org/10.1039/c6em00646a>
- Arslan-Alaton, I., Karatas, A., Pehlivan, Ö., Koba Uçun, O., Ölmez-Hancı, T., 2021. Effect of UV-A-assisted iron-based and UV-C-driven oxidation processes on organic matter and antibiotic resistance removal in tertiary treated urban wastewater. *Catal. Today* 361, 152–158. <https://doi.org/10.1016/j.cattod.2020.02.037>
- Arvaniti, O.S., Frontistis, Z., Nika, M.C., Aalizadeh, R., Thomaidis, N.S., Mantzavinos, D., 2020. Sonochemical degradation of trimethoprim in water matrices: Effect of operating conditions, identification of transformation products and toxicity assessment. *Ultrason. Sonochem.* 67. <https://doi.org/10.1016/j.ultsonch.2020.105139>
- AUDE Orden de 13 de Julio de 1993 Por la Que se Aprueba la Instrucción Para el Proyecto de Conducciones de Vertidos Desde Tierra al Mar. 1995. Available online: <https://www.boe.es/buscar/doc.php?id=BOE-A-1993-19593>
- Barceló, D., Kostianoy, A.G., (ed.), 2012. *The Handbook of Environmental Chemistry: Emerging Organic Contaminants and Human Health*, Springer-Verlag.
- Berney, M., Weilenmann, H.U., Simonetti, A., Egli, T., 2006. Efficacy of solar disinfection of *Escherichia coli*, *Shigella flexneri*, *Salmonella Typhimurium* and *Vibrio cholerae*. *J. Appl. Microbiol.* 101, 828–836. <https://doi.org/10.1111/j.1365-2672.2006.02983.x>
- Bernofsky, C., Bandara, B.M.R., Hinojosa, O., 1990. Electron spin resonance studies of the reaction of hypochlorite with 5,5-dimethyl-1-pyrroline-N-oxide. *Free Radic. Biol. Med.* 8, 231–239. [https://doi.org/10.1016/0891-5849\(90\)90068-T](https://doi.org/10.1016/0891-5849(90)90068-T)

- Blanco, J., Fernández-Ibáñez, P., Malato-Rodríguez, S., 2007. Solar photocatalytic detoxification and disinfection of water: Recent overview. *J. Sol. Energy Eng. Trans. ASME* 129, 4–15. <https://doi.org/10.1115/1.2390948>
- Blanco, J., Malato, S., Fernández, P., Vidal, A., Morales, A., Trincado, P., Oliveira, J.C., Minero, C., Musci, M., Casalle, C., Brunotte, M., Tratzky, S., Dischinger, N., Funken, K.H., Sattler, C., Vincent, M., Collares-Pereira, M., Mendes, J.F., Rangel, C.M., 1999. Compound parabolic concentrator technology development to commercial solar detoxification applications. *Sol. Energy* 67, 317–330. [https://doi.org/10.1016/s0038-092x\(00\)00078-5](https://doi.org/10.1016/s0038-092x(00)00078-5)
- BOE, 2021. Spanish government. Average price per square meter of urban land by autonomous communities and provinces, <https://apps.fomento.gob.es/BoletinOnline2/?nivel=2&orden=36000000>
- Boretti, A., Rosa, L., 2019. Reassessing the projections of the World Water Development Report. *npj Clean Water* 2. <https://doi.org/10.1038/s41545-019-0039-9>
- Bourgin, M., Beck, B., Boehler, M., Borowska, E., Fleiner, J., Salhi, E., Teichler, R., von Gunten, U., Siegrist, H., McArdell, C.S., 2018. Evaluation of a full-scale wastewater treatment plant upgraded with ozonation and biological post-treatments: Abatement of micropollutants, formation of transformation products and oxidation by-products. *Water Res.* 129, 486–498. <https://doi.org/10.1016/j.watres.2017.10.036>
- Bousslama, W., Elhouichet, H., Férid, M., 2017. Enhanced photocatalytic activity of Fe doped ZnO nanocrystals under sunlight irradiation. *Optik (Stuttg.)* 134, 88–98. <https://doi.org/10.1016/j.ijleo.2017.01.025>
- Brezina, E., Prasse, C., Meyer, J., Mückter, H., Ternes, T.A., 2017. Investigation and risk evaluation of the occurrence of carbamazepine, oxcarbazepine, their human metabolites and transformation products in the urban water cycle. *Environ. Pollut.* 225, 261–269. <https://doi.org/10.1016/j.envpol.2016.10.106>
- British Water, 2013. Code of practice- flows and loads 4: sizing criteria, treatment capacity for small wastewater treatment systems. ISBN 978-1-903481-10-3, Available online: <https://www.britishwater.co.uk/code-of-practise-flows-and-loads-4-on-sizing-criteria-treatm.aspx>
- Byrne, C., Subramanian, G., Pillai, S.C., 2018. Recent advances in photocatalysis for environmental applications. *J. Environ. Chem. Eng.* 6, 3531–3555. <https://doi.org/10.1016/j.jece.2017.07.080>
- Calza, P., Gionco, C., Giletta, M., Kalaboka, M., Sakkas, V.A., Albanis, T., Paganini, M.C., 2017. Assessment of the abatement of acelsulfame K using cerium doped ZnO as photocatalyst. *J. Hazard. Mater.* 323, 471–477. <https://doi.org/10.1016/j.jhazmat.2016.03.093>
- Carvalho, I.T., Santos, L., 2016. Antibiotics in the aquatic environments: A review of the European scenario. *Environ. Int.* 94, 736–757. <https://doi.org/10.1016/j.envint.2016.06.025>
- Castro-Alfárez, M., Polo-López, M.I., Fernández-Ibáñez, P., 2016. Intracellular mechanisms of solar water disinfection. *Sci. Rep.* 6. <https://doi.org/10.1038/srep38145>

11. References

- Cerrato, E., Gionco, C., Berruti, I., Sordello, F., Calza, P., Paganini, M.C., 2018a. Rare Earth ions doped ZnO: Synthesis, characterization and preliminary photoactivity assessment. *J. Solid State Chem.* 264, 42–47. <https://doi.org/10.1016/j.jssc.2018.05.001>
- Cerrato, E., Gionco, C., Paganini, M.C., Giamello, E., Albanese, E., Pacchioni, G., 2018b. Origin of Visible Light Photoactivity of the CeO₂/ZnO Heterojunction. *ACS Appl. Energy Mater.* 1, 4247–4260. <https://doi.org/10.1021/acsaem.8b00887>
- Cerrato, E., Paulo, N., Gonçalves, F., Calza, P., Paganini, M.C., 2020a. Comparison of the photocatalytic activity of ZnO/CeO₂ and ZnO/Yb₂O₃ mixed systems in the phenol removal from water: a mechanistic approach. *Catalysts* 10, 1–15. <https://doi.org/10.3390/catal10101222>
- Cerrato, E., Zickler, G.A., Paganini, M.C., 2020b. The role of Yb doped ZnO in the charge transfer process and stabilization. *J. Alloys Compd.* 816, 152555. <https://doi.org/10.1016/j.jallcom.2019.152555>
- Cerreta, G., Roccamante, M.A., Oller, I., Malato, S., Rizzo, L., 2019. Contaminants of emerging concern removal from real wastewater by UV/free chlorine process: A comparison with solar/free chlorine and UV/H₂O₂ at pilot scale. *Chemosphere* 236, 124354. <https://doi.org/10.1016/j.chemosphere.2019.124354>
- Chen, F., Ying, G.G., Kong, L.X., Wang, L., Zhao, J.L., Zhou, L.J., Zhang, L.J., 2011. Distribution and accumulation of endocrine-disrupting chemicals and pharmaceuticals in wastewater irrigated soils in Hebei, China. *Environ. Pollut.* 159, 1490–1498. <https://doi.org/10.1016/j.envpol.2011.03.016>
- Chen, T., Li, J., Xu, L., Zhang, D., Wang, Z., Chen, H., 2021. Deactivation of *Caenorhabditis elegans* nematodes in drinking water by PMS/UV-C: efficiency and mechanisms. *Environ. Sci. Pollut. Res.* <https://doi.org/10.1007/s11356-021-14312-8>
- Chen, T., Wang, R., Zhang, A., Xu, T., Xiao, R., Chu, W., Yin, D., 2020. Peroxymonosulfate/chloride disinfection versus sodium hypochlorite disinfection in terms of the formation and estimated cytotoxicity of CX3R-type disinfection by-products under the same dose of free chlorine. *Chem. Eng. J.* 391, 123557. <https://doi.org/10.1016/j.cej.2019.123557>
- Chesney, Alexandra, Booth, Clarissa, Li, Lingjun, P.J., 2016. Peroxymonosulfate rapidly inactivates the disease-associated prion protein. *Env. Sci Technol* 50, 7095–7105. <https://doi.org/10.1021/acs.est.5b06294>. Peroxymonosulfate
- Cho, M., Kim, J., Kim, J.Y., Yoon, J., Kim, J.H., 2010. Mechanisms of *Escherichia coli* inactivation by several disinfectants. *Water Res.* 44, 3410–3418. <https://doi.org/10.1016/j.watres.2010.03.017>
- Chou, J.C., Liao, L.P., 2005. Study on pH at the point of zero charge of TiO₂ pH ion-sensitive field effect transistor made by the sputtering method. *Thin Solid Films* 476, 157–161. <https://doi.org/10.1016/j.tsf.2004.09.061>
- Christou, A., Papadavid, G., Dalias, P., Fotopoulos, V., Michael, C., Bayona, J.M., Piña, B., Fatta-Kassinou, D., 2019. Ranking of crop plants according to their potential to uptake and accumulate contaminants of emerging concern. *Environ. Res.* 170, 422–432. <https://doi.org/10.1016/j.envres.2018.12.048>

- Christou, A., Agüera, A., Bayona, J.M., Cytryn, E., Fotopoulos, V., Lambropoulou, D., Manaia, C.M., Michael, C., Revitt, M., Schröder, P., Fatta-Kassinos, D., 2017a. The potential implications of reclaimed wastewater reuse for irrigation on the agricultural environment: The knowns and unknowns of the fate of antibiotics and antibiotic resistant bacteria and resistance genes – A review. *Water Res.* 123, 448–467. <https://doi.org/10.1016/j.watres.2017.07.004>
- Christou, A., Karaolia, P., Hapeshi, E., Michael, C., Fatta-kassinos, D., 2017b. Long-term wastewater irrigation of vegetables in real agricultural systems: Concentration of pharmaceuticals in soil, uptake and bioaccumulation in tomato fruits and human health risk assessment. *Water Res.* 109, 24–34. <https://doi.org/10.1016/j.watres.2016.11.033>
- Clifton, C.L., Huie, R.E., 1989. Rate constants for hydrogen abstraction reactions of the sulfate radical, $\text{SO}_4^{\cdot-}$ Alcohols. *Int. J. Chem. Kinet.* 21, 677–687. <https://doi.org/10.1002/kin.550210807>
- Cui, C., Jin, L., Jiang, L., Han, Q., Lin, K., Lu, S., Zhang, D., Cao, G., 2016. Removal of trace level amounts of twelve sulfonamides from drinking water by UV-activated peroxymonosulfate. *Sci. Total Environ.* 572, 244–251. <https://doi.org/10.1016/j.scitotenv.2016.07.183>
- Czekalski, N., Imminger, S., Salhi, E., Veljkovic, M., Kleffel, K., Drissner, D., Hammes, F., Bürgmann, H., Von Gunten, U., 2016. Inactivation of Antibiotic Resistant Bacteria and Resistance Genes by Ozone: From Laboratory Experiments to Full-Scale Wastewater Treatment. *Environ. Sci. Technol.* 50, 11862–11871. <https://doi.org/10.1021/acs.est.6b02640>
- Das Neves G., 2020. Expression of *bla_{CTX-M2}* and *invA* genes of *Salmonella heidelberg* isolated from poultry by qPCR. *Ann. Mol. Genet. Med.* 4, 006–011. <https://doi.org/10.17352/amgm.000006>
- Deborde, M., von Gunten, U., 2008. Reactions of chlorine with inorganic and organic compounds during water treatment-kinetics and mechanisms: A critical review. *Water Res.* 42, 13–51. <https://doi.org/10.1016/j.watres.2007.07.025>
- Deng, J., Ge, Y., Tan, C., Wang, H., Li, Q., Zhou, S., Zhang, K., 2017. Degradation of ciprofloxacin using A-MnO₂ activated peroxymonosulfate process: Effect of water constituents, degradation intermediates and toxicity evaluation. *Chem. Eng. J.* 330, 1390–1400. <https://doi.org/10.1016/j.cej.2017.07.137>
- Deng, J., Shao, Y., Gao, N., Xia, S., Tan, C., Zhou, S., Hu, X., 2013. Degradation of the antiepileptic drug carbamazepine upon different UV-based advanced oxidation processes in water. *Chem. Eng. J.* 222, 150–158. <https://doi.org/10.1016/j.cej.2013.02.045>
- Dhaka, S., Kumar, R., Lee, S. hun, Kurade, M.B., Jeon, B.H., 2018. Degradation of ethyl paraben in aqueous medium using advanced oxidation processes: Efficiency evaluation of UV-C supported oxidants. *J. Clean. Prod.* 180, 505–513. <https://doi.org/10.1016/j.jclepro.2018.01.197>
- Ding, Y., Wang, X., Fu, L., Peng, X., Pan, C., Mao, Q., Wang, C., Yan, J., 2020. Nonradicals induced degradation of organic pollutants by peroxydisulfate (PDS) and peroxymonosulfate (PMS): Recent advances and perspective. *Sci. Total Environ.* 765, 142794. <https://doi.org/10.1016/j.scitotenv.2020.142794>

11. References

- Dodd, M.C., 2012. Potential impacts of disinfection processes on elimination and deactivation of antibiotic resistance genes during water and wastewater treatment. *J. Environ. Monit.* 14, 1754–1771. <https://doi.org/10.1039/c2em00006g>
- DuPont, 2008. Dupont™ Oxone® monopersulfate compound: General technical attributes 1–4. <http://www.waterguardinc.com/files/90708730.pdf>
- EN ISO 18763:2020 - Soil quality - Determination of the toxic effects of pollutants on germination, n.d. URL <https://standards.iteh.ai/catalog/standards/cen/520f9488-9609-48d2-a11b-d3b06f16bb68/en-iso-18763-2020> (accessed 7.4.21).
- Eckers, C., Monaghan, J.J., Wolff, J.C., 2005. Fragmentation of trimethoprim and other compounds containing alkoxy-phenyl groups in electrospray ionisation tandem mass spectrometry. *Eur. J. Mass Spectrom.* 11, 73–82. <https://doi.org/10.1255/ejms.719>
- Efstratiou, A., Ongerth, J.E., Karanis, P., 2017. Waterborne transmission of protozoan parasites: Review of worldwide outbreaks - An update 2011–2016. *Water Res.* 114, 14–22. <https://doi.org/10.1016/j.watres.2017.01.036>
- Eichhorn, P., Ferguson, P.L., Pérez, S., Aga, D.S., 2005. Application of ion trap-MS with H/D exchange and QqTOF-MS in the identification of microbial degradates of trimethoprim in nitrifying activated sludge. *Anal. Chem.* 77, 4176–4184. <https://doi.org/10.1021/ac050141p>
- European Parliament and the Council of the European Union, 2020. Directive (EU) 2020/2184, EU (revised) Drinking Water Directive. Annex 1. Part B. Off. J. Eur. Communities 2019, 35.
- EN 12469:2000 - Biotechnology - Performance criteria for microbiological safety cabinets
- Fabbri, D., López-Muñoz, M.J., Daniele, A., Medana, C., Calza, P., 2019. Photocatalytic abatement of emerging pollutants in pure water and wastewater effluent by TiO₂ and Ce-ZnO: Degradation kinetics and assessment of transformation products. *Photochem. Photobiol. Sci.* 18, 845–852. <https://doi.org/10.1039/c8pp00311d>
- Fagan, R., McCormack, D.E., Dionysiou, D.D., Pillai, S.C., 2016. A review of solar and visible light active TiO₂ photocatalysis for treating bacteria, cyanotoxins and contaminants of emerging concern. *Mater. Sci. Semicond. Process.* 42, 2–14. <https://doi.org/10.1016/j.mssp.2015.07.052>
- Fanourgiakis, S., Frontistis, Z., Chatzisyneon, E., Venieri, D., Mantzavinos, D., 2014. Simultaneous removal of estrogens and pathogens from secondary treated wastewater by solar photocatalytic treatment. *Glob. Nest J.* 16, 543–552. <https://doi.org/10.30955/gnj.001389>
- FAO. 2011. The state of the world's land and water resources for food and agriculture (SOLAW) – Managing systems at risk. Food and Agriculture Organization of the United Nations, Rome and Earthscan, London.
- FAO, 1985. Water Quality for Agriculture. Available online: <http://www.fao.org/3/T0234E/T0234E00.htm>
- Fiorentino, A., Lofrano, G., Cucciniello, R., Carotenuto, M., Motta, O., Proto, A., Rizzo, L., 2021. Disinfection of roof harvested rainwater inoculated with *E. coli* and *Enterococcus* and post-treatment

- bacterial regrowth: Conventional vs solar driven advanced oxidation processes. *Sci. Total Environ.* 801, 149763. <https://doi.org/10.1016/j.scitotenv.2021.149763>
- Fiorentino, A., Esteban, B., Garrido-Cardenas, J.A., Kowalska, K., Rizzo, L., Aguera, A., Sánchez-Pérez, J.A., 2019. Effect of solar photo-Fenton process in raceway pond reactors at neutral pH on antibiotic resistance determinants in secondary treated urban wastewater. *J. Hazard. Mater.* 378, 120737. [10.1016/j.jhazmat.2019.06.014](https://doi.org/10.1016/j.jhazmat.2019.06.014)
- Fiorentino, A., Ferro, G., Alferez, M.C., Polo-López, M.I., Fernández-Ibañez, P., Rizzo, L., 2015. Inactivation and regrowth of multidrug resistant bacteria in urban wastewater after disinfection by solar-driven and chlorination processes. *J. Photochem. Photobiol. B Biol.* 148, 43–50. <https://doi.org/10.1016/j.jphotobiol.2015.03.029>
- Formisano, F., Fiorentino, A., Rizzo, L., Carotenuto, M., Pucci, L., Giugni, M., Lofrano, G., 2016. Inactivation of *Escherichia coli* and *Enterococci* in urban wastewater by sunlight/PAA and sunlight/H₂O₂ processes. *Process Saf. Environ. Prot.* 104, 178–184. <https://doi.org/10.1016/j.psep.2016.09.003>
- García-Fernández, I., Fernández-Calderero, I., Inmaculada Polo-López, M., Fernández-Ibañez, P., 2015. Disinfection of urban effluents using solar TiO₂ photocatalysis: A study of significance of dissolved oxygen, temperature, type of microorganism and water matrix. *Catal. Today* 240, 30–38. <https://doi.org/10.1016/j.cattod.2014.03.026>
- Ge, L., Zhang, P., Halsall, C., Li, Y., Chen, C.E., Li, J., Sun, H., Yao, Z., 2019. The importance of reactive oxygen species on the aqueous phototransformation of sulfonamide antibiotics: kinetics, pathways, and comparisons with direct photolysis. *Water Res.* 149, 243–250. <https://doi.org/10.1016/j.watres.2018.11.009>
- Geneva: World Health Organization, 2017. *Microbial aspects. Guidel. Drink. Qual. Fourth Ed. Inc. First Add.* 49.
- Gerba, C.P., 2009. *Indicator Microorganisms, Second Edition. Environmental Microbiology.* Elsevier Inc. <https://doi.org/10.1016/B978-0-12-370519-8.00023-7>
- Giakoumis, T., Vaghela, C., Voulvoulis, N., 2020. *The role of water reuse in the circular economy, 1st ed, Wastewater treatment and Reuse – Present and future perspectives in technological developments and management issues.* Elsevier Inc. <https://doi.org/10.1016/bs.apmp.2020.07.013>
- Giannakis, S., Le, T.T.M., Entenza, J.M., Pulgarin, C., 2018. Solar photo-Fenton disinfection of 11 antibiotic-resistant bacteria (ARB) and elimination of representative AR genes. Evidence that antibiotic resistance does not imply resistance to oxidative treatment. *Water Res.* 143, 334–345. <https://doi.org/10.1016/j.watres.2018.06.062>
- Giannakis, S., López, M.I.P., Spuhler, D., Pérez, J.A.S., Ibañez, P.F., Pulgarin, C., 2016. Solar disinfection is an augmentable, in situ-generated photo-Fenton reaction-Part 2: A review of the applications for drinking water and wastewater disinfection. *Appl. Catal. B Environ.* 198, 431–446. <https://doi.org/10.1016/j.apcatb.2016.06.007>

11. References

- Gil, A., Galeano, L.A., Vicente, M.Á. (Eds.), 2019. Applications of Advanced Oxidation Processes (AOPs) in drinking water treatment. The Handbook of Environmental Chemistry 67. <https://doi.org/10.1007/978-3-319-76882-3>
- Gillings, M.R., Gaze, W.H., Pruden, A., Smalla, K., Tiedje, J.M., Zhu, Y.G., 2015. Using the class 1 integron-integrase gene as a proxy for anthropogenic pollution. *ISME J.* 9, 1269–1279. <https://doi.org/10.1038/ismej.2014.226>
- Gmurek, M., Horn, H., Majewsky, M., 2015. Phototransformation of sulfamethoxazole under simulated sunlight: Transformation products and their antibacterial activity toward *Vibrio fischeri*. *Sci. Total Environ.* 538, 58–63. <https://doi.org/10.1016/j.scitotenv.2015.08.014>
- Gogoi, A., Mazumder, P., Tyagi, V.K., Tushara Chaminda, G.G., An, A.K., Kumar, M., 2018. Occurrence and fate of emerging contaminants in water environment: A review. *Groundw. Sustain. Dev.* 6, 169–180. <https://doi.org/10.1016/j.gsd.2017.12.009>
- Gómez-Ramos, M. del M., Mezcua, M., Agüera, A., Fernández-Alba, A.R., Gonzalo, S., Rodríguez, A., Rosal, R., 2011. Chemical and toxicological evolution of the antibiotic sulfamethoxazole under ozone treatment in water solution. *J. Hazard. Mater.* 192, 18–25. <https://doi.org/10.1016/j.jhazmat.2011.04.072>
- Greene, J., C. Bartels, W. Warren-Hicks, B. Parkhurst, AND G. Linder, 1988. Protocols for short term toxicity screening of hazardous waste sites. U.S. Environmental Protection Agency, Washington, D.C., EPA/600/3-88/029 (NTIS PB88235510)
- Grilla, E., Matthaïou, V., Frontistis, Z., Oller, I., Polo, I., Malato, S., Mantzavinos, D., 2019. Degradation of antibiotic trimethoprim by the combined action of sunlight, TiO₂ and persulfate: A pilot plant study. *Catal. Today* 328, 216–222. <https://doi.org/10.1016/j.cattod.2018.11.029>
- Guan, Y.H., Ma, J., Li, X.C., Fang, J.Y., Chen, L.W., 2011. Influence of pH on the formation of sulfate and hydroxyl radicals in the UV/Peroxymonosulfate system. *Environ. Sci. Technol.* 45, 9308–9314. <https://doi.org/10.1021/es2017363>
- Guerra-Rodríguez, S., Ribeiro, A.R.L., Ribeiro, R.S., Rodríguez, E., Silva, A.M.T., Rodríguez-Chueca, J., 2021. UV-A activation of peroxymonosulfate for the removal of micropollutants from secondary treated wastewater. *Sci. Total Environ.* 770, 145299. <https://doi.org/10.1016/j.scitotenv.2021.145299>
- Guerra-Rodríguez, S., Oulego, P., Rodríguez, E., Singh, D.N., Rodríguez-Chueca, J., 2020. Towards the implementation of circular economy in the wastewater sector: Challenges and opportunities. *Water (Switzerland)* 12. <https://doi.org/10.3390/w12051431>
- Guerra-Rodríguez, S., Rodríguez, E., Singh, D.N., Rodríguez-Chueca, J., 2018. Assessment of sulfate radical-based advanced oxidation processes for water and wastewater treatment: A review. *Water (Switzerland)* 10. <https://doi.org/10.3390/w10121828>
- Harris, D. C., 2010. Quantitative Chemical Analysis 8th edition, W.H. Freeman & Co Ltd, New York.

- He, X., De La Cruz, A.A., Dionysiou, D.D., 2013. Destruction of cyanobacterial toxin cylindrospermopsin by hydroxyl radicals and sulfate radicals using UV-254 nm activation of hydrogen peroxide, persulfate and peroxymonosulfate. *J. Photochem. Photobiol. A Chem.* 251, 160–166. <https://doi.org/10.1016/j.jphotochem.2012.09.017>
- Helali, S., Polo-López, M.I., Fernández-Ibáñez, P., Ohtani, B., Amano, F., Malato, S., Guillard, C., 2013. Solar photocatalysis: A green technology for *E. coli* contaminated water disinfection. Effect of concentration and different types of suspended catalyst. *J. Photochem. Photobiol. A Chem.* 276, 31–40. <https://doi.org/10.1016/j.jphotochem.2013.11.011>
- Herrmann, H., 2007. On the photolysis of simple anions and neutral molecules as sources of O[•]/OH, SO_x⁻ and Cl in aqueous solution. *Phys. Chem. Chem. Phys.* 9, 3935–3964. <https://doi.org/10.1039/b618565g>
- Hoffmann-La Roche F. Ltd, 2020. Environmental Risk Assessment Summary Sulfamethoxazole 1–7.
- Hoffmann-La Roche F. Ltd, 2020. Environmental Risk Assessment Summary Trimethoprim 1–7.
- Hu, Y., Zhang, T., Jiang, L., Yao, S., Ye, H., Lin, K., Cui, C., 2019. Removal of sulfonamide antibiotic resistant bacterial and intracellular antibiotic resistance genes by UVC-activated peroxymonosulfate. *Chem. Eng. J.* 368, 888–895. <https://doi.org/10.1016/j.cej.2019.02.207>
- Huie, R.E., Herron, J.T., 1990. Temperature dependence of the rate constants for reactions of ozone with some olefins. *J. Phys. Chem.* 94, 8561–8567.
- ISO 17512-1:2008(en), Soil quality — Avoidance test for determining the quality of soils and effects of chemicals on behaviour — Part 1: Test with earthworms (*Eisenia fetida* and *Eisenia andrei*) n.d. URL <https://www.iso.org/obp/ui/#iso:std:iso:17512:-1:ed-1:v1:en> (accessed 9.28.21).
- ISO 7346-1:1996(en), Water quality — Determination of the acute lethal toxicity of substances to a freshwater fish [*Brachydanio rerio* Hamilton-Buchanan (Teleostei, Cyprinidae)] — Part 1: Static method, n.d. URL <https://www.iso.org/obp/ui/#iso:std:iso:7346:-1:ed-2:v1:en> (accessed 9.26.21).
- ISO 10993-5:2009 - Biological evaluation of medical devices — Part 5: Tests for in vitro cytotoxicity [WWW Document], n.d. URL <https://www.iso.org/standard/36406.html> (accessed 9.26.21).
- ISO 11348-3:2007 - Water quality — Determination of the inhibitory effect of water samples on the light emission of *Vibrio fischeri* (Luminescent bacteria test) — Part 3: Method using freeze-dried bacteria [WWW Document], URL <https://www.iso.org/standard/40518.html> (accessed 8.21.21).
- ISO 20079:2005 - Water quality — Determination of the toxic effect of water constituents and waste water on duckweed (*Lemna minor*) — Duckweed growth inhibition test [WWW Document], n.d. URL <https://www.iso.org/standard/34074.html> (accessed 9.26.21).
- ISO 6341:2012 - Water quality — Determination of the inhibition of the mobility of *Daphnia magna* Straus (Cladocera, Crustacea) — Acute toxicity test [WWW Document], n.d. URL <https://www.iso.org/standard/54614.html> (accessed 8.21.21).

11. References

ISO 8692:1989 - Water quality — Fresh water algal growth inhibition test with *Scenedesmus subspicatus* and *Selenastrum capricornutum* [WWW Document], n.d. URL <https://www.iso.org/standard/16096.html> (accessed 9.26.21).

ISO 8692:2012 - Water quality — Fresh water algal growth inhibition test with unicellular green algae [WWW Document], n.d. URL <https://www.iso.org/standard/54150.html> (accessed 8.21.21).

Ivanov, K.L., Glebov, E.M., Plyusnin, V.F., Ivanov, Y. V., Grivin, V.P., Bazhin, N.M., 2000. Laser flash photolysis of sodium persulfate in aqueous solution with additions of dimethylformamide. *J. Photochem. Photobiol. A Chem.* 133, 99–104. [https://doi.org/10.1016/S1010-6030\(00\)00218-5](https://doi.org/10.1016/S1010-6030(00)00218-5)

Jewell, K.S., Falås, P., Wick, A., Joss, A., Ternes, T.A., 2016. Transformation of diclofenac in hybrid biofilm-activated sludge processes. *Water Res.* 105, 559–567. <https://doi.org/10.1016/j.watres.2016.08.002>

Ji, Y., Lu, J., Wang, L., Jiang, M., Yang, Y., Yang, P., Zhou, L., Ferronato, C., Chovelon, J.M., 2018. Non-activated peroxymonosulfate oxidation of sulfonamide antibiotics in water: Kinetics, mechanisms, and implications for water treatment. *Water Res.* 147, 82–90. <https://doi.org/10.1016/j.watres.2018.09.037>

Ji, Y., Xie, W., Fan, Y., Shi, Y., Kong, D., Lu, J., 2016. Degradation of trimethoprim by thermo-activated persulfate oxidation: Reaction kinetics and transformation mechanisms. *Chem. Eng. J.* 286, 16–24. <https://doi.org/10.1016/j.cej.2015.10.050>

Kalyanaraman, B., Janzen, E.G., Mason, R.P., 1985. Spin trapping of the azidyl radical in azide/catalase/H₂O₂ and various azide/peroxidase/H₂O₂ peroxidizing systems. *J. Biol. Chem.* 260, 4003–4006. [https://doi.org/10.1016/s0021-9258\(18\)89222-5](https://doi.org/10.1016/s0021-9258(18)89222-5)

Kampouris, I.D., Agrawal, S., Orschler, L., Cacace, D., Kunze, S., Berendonk, T.U., Klümper, U., 2021. Antibiotic resistance gene load and irrigation intensity determine the impact of wastewater irrigation on antimicrobial resistance in the soil microbiome. *Water Res.* 193. <https://doi.org/10.1016/j.watres.2021.116818>

Kausley, S.B., Dastane, G.G., Kumar, J.K., Desai, K.S., Doltade, S.B., Pandit, A.B., 2019. Clean water for developing countries: Feasibility of different treatment solutions, 2nd Edition. ed, *Encyclopedia of Environmental Health*. Elsevier. <https://doi.org/10.1016/B978-0-12-409548-9.11079-6>

Khan, S., He, X., Khan, J.A., Khan, H.M., Boccelli, D.L., Dionysiou, D.D., 2017. Kinetics and mechanism of sulfate radical- and hydroxyl radical-induced degradation of highly chlorinated pesticide lindane in UV/peroxymonosulfate system. *Chem. Eng. J.* 318, 135–142. <https://doi.org/10.1016/j.cej.2016.05.150>

Khan, S., Han, C., Khan, H.M., Boccelli, D.L., Dionysiou, D.D., 2016. Efficient degradation of lindane by visible and simulated solar light-assisted S-TiO₂/peroxymonosulfate process: Kinetics and mechanistic investigations. *J. Mol. Catal. A, Chem.* <https://doi.org/10.1016/j.molcata.2016.11.035>

Kiejza, D., Kotowska, U., Polińska, W., Karpińska, J., 2021. Peracids - New oxidants in advanced oxidation processes: The use of peracetic acid, peroxymonosulfate, and persulfate salts in the

- removal of organic micropollutants of emerging concern – A review. *Sci. Total Environ.* 790. <https://doi.org/10.1016/j.scitotenv.2021.148195>
- Kinney, C.A., Furlong, E.T., Werner, S.L., Cahill, J.D., 2006. Presence and distribution of wastewater-derived pharmaceuticals in soil irrigated with reclaimed water. *Environ. Toxicol. Chem.* 25, 317–326. <https://doi.org/10.1897/05-187R.1>
- Koba, O., Golovko, O., Kodesova, R., Klement, A., Grabic, R., 2016. Transformation of atenolol, metoprolol, and carbamazepine in soils: The identification, quantification, and stability of the transformation products and further implications for the environment. *Environ. Pollut.* 218, 574–585. <https://doi.org/10.1016/j.envpol.2016.07.041>
- Kong, L., Fang, G., Fang, Z., Zou, Y., Zhu, F., Zhou, D., 2021. Peroxymonosulfate activation by localized electrons of ZnO oxygen vacancies for contaminant degradation. *Chem. Eng. J.* 416, 128996. <https://doi.org/10.1016/j.cej.2021.128996>
- Kong, J., Li, R., Wang, F., Chen, P., Liu, H., Liu, G., Lv, W., 2018. Sulfate radical-induced transformation of trimethoprim with CuFe₂O₄/MWCNTs as a heterogeneous catalyst of peroxymonosulfate: mechanisms and reaction pathways. *RSC Adv.* 8, 24787–24795. <https://doi.org/10.1039/c8ra04103b>
- Kosjek, T., Žigon, D., Kralj, B., Heath, E., 2008. The use of quadrupole-time-of-flight mass spectrometer for the elucidation of diclofenac biotransformation products in wastewater. *J. Chromatogr. A* 1215, 57–63. <https://doi.org/10.1016/j.chroma.2008.10.111>
- Kuang, J., Huang, J., Wang, B., Cao, Q., Deng, S., Yu, G., 2013. Ozonation of trimethoprim in aqueous solution: Identification of reaction products and their toxicity. *Water Res.* 47, 2863–2872. <https://doi.org/10.1016/j.watres.2013.02.048>
- Lee, J., Von Gunten, U., Kim, J.H., 2020. Persulfate-Based Advanced Oxidation: Critical Assessment of Opportunities and Roadblocks. *Environ. Sci. Technol.* 54, 3064–3081. <https://doi.org/10.1021/acs.est.9b07082>
- Lee, K.M., Lai, C.W., Ngai, K.S., Juan, J.C., 2016. Recent developments of zinc oxide based photocatalyst in water treatment technology: A review. *Water Res.* 88, 428–448. <https://doi.org/10.1016/j.watres.2015.09.045>
- Lee, Y., Gerrity, D., Lee, M., Bogeat, A.E., Salhi, E., Gamage, S., Trenholm, R.A., Wert, E.C., Snyder, S.A., Von Gunten, U., 2013. Prediction of micropollutant elimination during ozonation of municipal wastewater effluents: Use of kinetic and water specific information. *Environ. Sci. Technol.* 47, 5872–5881. <https://doi.org/10.1021/es400781r>
- Legrini, O., Oliveros, E., Braun, A.M., 1993. Photochemical Processes for Water Treatment. *Chem. Rev.* 93, 671–698. <https://doi.org/10.1021/cr00018a003>
- Lide, D. R. (Ed), 2004. *CRC Handbook of Chemistry and Physics*, 84th Edition, CRC Press LLC, Boca Raton, 2616, ISBN 0-8493-0484-9

11. References

- Liu, G., You, S., Tan, Y., Ren, N., 2017. In Situ Photochemical Activation of Sulfate for Enhanced Degradation of Organic Pollutants in Water. *Environ. Sci. Technol.* 51, 2339–2346. <https://doi.org/10.1021/acs.est.6b05090>
- Liu, X., Zhang, T., Zhou, Y., Fang, L., Shao, Y., 2013. Degradation of atenolol by UV/peroxymonosulfate: Kinetics, effect of operational parameters and mechanism. *Chemosphere* 93, 2717–2724. <https://doi.org/10.1016/j.chemosphere.2013.08.090>
- Liu, Y., Guo, H., Zhang, Y., Cheng, X., Zhou, P., Deng, J., Wang, J., Li, W., 2019. Highly efficient removal of trimethoprim based on peroxymonosulfate activation by carbonized resin with Co doping: Performance, mechanism and degradation pathway. *Chem. Eng. J.* 356, 717–726. <https://doi.org/10.1016/j.cej.2018.09.086>
- Luo, T., R. Young, P. Reig. 2015. Aqueduct Projected Water Stress Country Rankings. Technical Note. Washington, D.C.: World Resources Institute. Available online at: www.wri.org/publication/aqueduct-projected-water-stresscountry-rankings
- Macinnes, I., Walton, J.C., Nonhebel, D.C., 1987. Hydrogen abstraction from primary amines. Substituent effects on the carbon-nitrogen bond rotation barriers in aminoalkyl radicals. *J. Chem. Soc. Perkin Trans. 2* 1789–1794. <https://doi.org/10.1039/p29870001789>
- Magana-Arachchi, D.N., Wanigatunge, R.P., 2020. Ubiquitous waterborne pathogens. *Waterborne Pathog.* 15–42. <https://doi.org/10.1016/b978-0-12-818783-8.00002-5>
- Mahdi-Ahmed, M., Chiron, S., 2014. Ciprofloxacin oxidation by UV-C activated peroxymonosulfate in wastewater. *J. Hazard. Mater.* 265, 41–46. <https://doi.org/10.1016/j.jhazmat.2013.11.034>
- Mahdi Ahmed, M., Barbati, S., Doumenq, P., Chiron, S., 2012. Sulfate radical anion oxidation of diclofenac and sulfamethoxazole for water decontamination. *Chem. Eng. J.* 197, 440–447. <https://doi.org/10.1016/j.cej.2012.05.040>
- Malato, S., Maldonado, M.I., Fernández-Ibáñez, P., Oller, I., Polo, I., Sánchez-Moreno, R., 2016. Decontamination and disinfection of water by solar photocatalysis: The pilot plants of the Plataforma Solar de Almeria. *Mater. Sci. Semicond. Process.* 42, 15–23. <https://doi.org/10.1016/j.mssp.2015.07.017>
- Malato, S., Fernández-Ibáñez, P., Maldonado, M.I., Blanco, J., Gernjak, W., 2009. Decontamination and disinfection of water by solar photocatalysis: Recent overview and trends. *Catal. Today* 147, 1–59. <https://doi.org/10.1016/j.cattod.2009.06.018>
- Malato, S., Blanco, J., Alarcón, D.C., Maldonado, M.I., Fernández-Ibáñez, P., Gernjak, W., 2007. Photocatalytic decontamination and disinfection of water with solar collectors. *Catal. Today* 122, 137–149. <https://doi.org/10.1016/j.cattod.2007.01.034>
- Malato, S., Blanco, J., Vidal, A., Richter, C., 2002. Photocatalysis with solar energy at a pilot-plant scale: An overview. *Appl. Catal. B Environ.* 37, 1–15. [https://doi.org/10.1016/S0926-3373\(01\)00315-0](https://doi.org/10.1016/S0926-3373(01)00315-0)

- Makino, K., Hagiwara, T., Murakami, A.Z.A., 1991. A Mini Review: fundamental aspects of spin trapping with DMPO 37, 657–665. [https://doi.org/10.1016/1359-0197\(91\)90164-W](https://doi.org/10.1016/1359-0197(91)90164-W)
- Mao, J., Jacob, D.J., Evans, M.J., Olson, J.R., Ren, X., Brune, W.H., St. Clair, J.M., Crouse, J.D., Spencer, K.M., Beaver, M.R., Wennberg, P.O., Cubison, M.J., Jimenez, J.L., Fried, A., Weibring, P., Walega, J.G., Hall, S.R., Weinheimer, A.J., Cohen, R.C., Chen, G., Crawford, J.H., McNaughton, C., Clarke, A.D., Jaeglé, L., Fisher, J.A., Yantosca, R.M., Le Sager, P., Carouge, C., 2010. Chemistry of hydrogen oxide radicals (HOx) in the Arctic troposphere in spring. *Atmos. Chem. Phys.* 10, 5823–5838. <https://doi.org/10.5194/acp-10-5823-2010>
- Martínez-Costa, J.I., Maldonado Rubio, M.I., Leyva-Ramos, R., 2020. Degradation of emerging contaminants diclofenac, sulfamethoxazole, trimethoprim and carbamazepine by bentonite and vermiculite at a pilot solar compound parabolic collector. *Catal. Today* 341, 26–36. <https://doi.org/10.1016/j.cattod.2018.07.021>
- Martínez-Costa, J.I., Rivera-Utrilla, J., Leyva-Ramos, R., Sánchez-Polo, M., Velo-Gala, I., Mota, A.J., 2018. Individual and simultaneous degradation of the antibiotics sulfamethoxazole and trimethoprim in aqueous solutions by Fenton, Fenton-like and photo-Fenton processes using solar and UV radiations. *J. Photochem. Photobiol. A Chem.* 360, 95–108. <https://doi.org/10.1016/j.jphotochem.2018.04.014>
- Martínez-García, A., Vincent, M., Rubiolo, V., Domingos, M., Canela, M.C., Oller, I., Fernández-Ibáñez, P., Polo-López, M.I., 2020. Assessment of a pilot solar V-trough reactor for solar water disinfection. *Chem. Eng. J.* 399, 125719. <https://doi.org/10.1016/j.cej.2020.125719>
- Martínez-Piernas, A.B., Polo-López, M.I., Fernández-Ibáñez, P., Agüera, A., 2018. Validation and application of a multiresidue method based on liquid chromatography-tandem mass spectrometry for evaluating the plant uptake of 74 microcontaminants in crops irrigated with treated municipal wastewater. *J. Chromatogr. A* 1534, 10–21. <https://doi.org/10.1016/j.chroma.2017.12.037>
- Marugán, J., van Grieken, R., Pablos, C., Sordo, C., 2010. Analogies and differences between photocatalytic oxidation of chemicals and photocatalytic inactivation of microorganisms. *Water Res.* 44, 789–796. <https://doi.org/10.1016/j.watres.2009.10.022>
- Majewsky, M., Wagner, D., Delay, M., Bräse, S., Yargeau, V., Horn, H., 2014. Antibacterial activity of sulfamethoxazole transformation products (TPs): General relevance for sulfonamide TPs modified at the para position. *Chem. Res. Toxicol.* 27, 1821–1828. <https://doi.org/10.1021/tx500267x>
- McLoughlin, O.A., Fernández Ibáñez, P., Gernjak, W., Malato Rodriguez, S., Gill, L.W., 2004. Photocatalytic disinfection of water using low cost compound parabolic collectors. *Sol. Energy* 77, 625–633. <https://doi.org/10.1016/j.solener.2004.05.017>
- Mecha, A.C., Onyango, M.S., Ochieng, A., Momba, M.N.B., 2017. Evaluation of synergy and bacterial regrowth in photocatalytic ozonation disinfection of municipal wastewater. *Sci. Total Environ.* 601–602, 626–635. <https://doi.org/10.1016/j.scitotenv.2017.05.204>
- Merck, 2008. Chromocult ® Coliform Agar 49, 1–8.

11. References

- Michael, I., Rizzo, L., McArdell, C.S., Manaia, C.M., Merlin, C., Schwartz, T., Dagot, C., Fatta-Kassinos, D., 2013. Urban wastewater treatment plants as hotspots for the release of antibiotics in the environment: A review. *Water Res.* 47, 957–995. <https://doi.org/10.1016/j.watres.2012.11.027>
- Michael, I., Hapeshi, E., Osorio, V., Perez, S., Petrovic, M., Zapata, A., Malato, S., Barceló, D., Fatta-Kassinos, D., 2012. Solar photocatalytic treatment of trimethoprim in four environmental matrices at a pilot scale: Transformation products and ecotoxicity evaluation. *Sci. Total Environ.* 430, 167–173. <https://doi.org/10.1016/j.scitotenv.2012.05.003>
- Michael, S.G., Michael-Kordatou, I., Nahim-Granados, S., Polo-López, M.I., Rocha, J., Martínez-Piernas, A.B., Fernández-Ibáñez, P., Agüera, A., Manaia, C.M., Fatta-Kassinos, D., 2020. Investigating the impact of UV-C/H₂O₂ and sunlight/H₂O₂ on the removal of antibiotics, antibiotic resistance determinants and toxicity present in urban wastewater. *Chem. Eng. J.* 388, 124383. <https://doi.org/10.1016/j.cej.2020.124383>
- Milh, H., Schoenaers, B., Stesmans, A., Cabooter, D., Dewil, R., 2020. Degradation of sulfamethoxazole by heat-activated persulfate oxidation: Elucidation of the degradation mechanism and influence of process parameters. *Chem. Eng. J.* 379, 122234. <https://doi.org/10.1016/j.cej.2019.122234>
- Miralles-Cuevas, S., Oller, I., Agüera, A., Sánchez-Pérez, J. A., Sánchez-Moreno, R., Malato, S., 2016. Is the combination of nanofiltration membranes and AOPs for removing microcontaminants cost effective in real municipal wastewater effluents?. *Environmental Science: Water Research & Technology*, 2(3), 511-520. <https://doi.org/10.1039/C6EW00001K>
- Montes-Grajales, D., Fennix-Agudelo, M., Miranda-Castro, W., 2017. Occurrence of personal care products as emerging chemicals of concern in water resources: A review. *Sci. Total Environ.* 595, 601–614. <https://doi.org/10.1016/j.scitotenv.2017.03.286>
- Moreira, N.F.F., Narciso-da-Rocha, C., Polo-López, M.I., Pastrana-Martínez, L.M., Faria, J.L., Manaia, C.M., Fernández-Ibáñez, P., Nunes, O.C., Silva, A.M.T., 2018. Solar treatment (H₂O₂, TiO₂-P25 and GO-TiO₂ photocatalysis, photo-Fenton) of organic micropollutants, human pathogen indicators, antibiotic resistant bacteria and related genes in urban wastewater. *Water Res.* 135, 195–206. <https://doi.org/10.1016/j.watres.2018.01.064>
- Nahim-Granados, S., Rivas-Ibáñez, G., Antonio Sánchez Pérez, J., Oller, I., Malato, S., Polo-López, M.I., 2020. Fresh-cut wastewater reclamation: Techno-Economical assessment of solar driven processes at pilot plant scale. *Appl. Catal. B Environ.* 278, 119334. <https://doi.org/10.1016/j.apcatb.2020.119334>
- Narciso-Da-Rocha, C., Varela, A.R., Schwartz, T., Nunes, O.C., Manaia, C.M., 2014. *bla*_{TEM} and *vanA* as indicator genes of antibiotic resistance contamination in a hospital-urban wastewater treatment plant system. *J. Glob. Antimicrob. Resist.* 2, 309–315.
- Nahim-Granados, S., Oller, I., Malato, S., Sánchez Pérez, J.A., Polo-Lopez, M.I., 2019. Commercial fertilizer as effective iron chelate (Fe³⁺-EDDHA) for wastewater disinfection under natural sunlight for reusing in irrigation. *Appl. Catal. B Environ.* 253, 286–292. <https://doi.org/10.1016/j.apcatb.2019.04.041>

- USEPA, National Primary Drinking Water Regulations [WWW Document], n.d. URL <https://www.epa.gov/ground-water-and-drinking-water/national-primary-drinking-water-regulations#Byproducts> (accessed 9.28.21).
- Nelson, K.L., Boehm, A.B., Davies-Colley, R.J., Dodd, M.C., Kohn, T., Linden, K.G., Liu, Y., Maraccini, P.A., McNeill, K., Mitch, W.A., Nguyen, T.H., Parker, K.M., Rodriguez, R.A., Sassoubre, L.M., Silverman, A.I., Wigginton, K.R., Zepp, R.G., 2018. Sunlight-mediated inactivation of health-relevant microorganisms in water: a review of mechanisms and modeling approaches. *Environ. Sci. Process. Impacts* 20, 1089–1122. <https://doi.org/10.1039/c8em00047f>
- Neta, P., Huie, R.E., Ross, A.B., 1988. Rate Constants for Reactions of Inorganic Radicals in Aqueous Solution 17.
- Nihemaiti, M., Permala, R.R., Croué, J.P., 2020. Reactivity of unactivated peroxymonosulfate with nitrogenous compounds. *Water Res.* 169. <https://doi.org/10.1016/j.watres.2019.115221>
- Nosaka, Y., Nosaka, A.Y., 2017. Generation and detection of Reactive Oxygen Species in photocatalysis. *Chem. Rev.* <https://doi.org/10.1021/acs.chemrev.7b00161>
- OECD, (2010)., *Test No. 209: Activated Sludge, Respiration Inhibition Test (Carbon and Ammonium Oxidation)*, OECD Guidelines for the Testing of Chemicals, Section 2, OECD Publishing, Paris, <https://doi.org/10.1787/9789264070080-en>
- OECD, 2006. *Test No. 201: Alga, Growth Inhibition Test*, 2006. OECD Guidelines for the Testing of Chemicals, Section 2: Effects on Biotic Systems. <https://doi.org/10.1787/9789264069923-EN>
- OECD, 2004. *Test No. 202: Daphnia sp. Acute Immobilisation Test*, 2004. OECD Guidelines for the Testing of Chemicals, Section 2. <https://doi.org/10.1787/9789264069947-EN>
- OECD, 1992. *Test No. 210: Fish, Early-Life Stage Toxicity Test.*, 1992. Test No. 210 Fish, Early-Life Stage Toxic. Test. <https://doi.org/10.1787/9789264070103-EN>
- Olmez-Hanci, T., Arslan-Alaton, I., Dursun, D., Genc, B., Mita, D.G., Guida, M., Mita, L., 2015. Degradation and toxicity assessment of the nonionic surfactant TritonTM X-45 by the peroxymonosulfate/UV-C process. *Photochem. Photobiol. Sci.* 14, 569–575. <https://doi.org/10.1039/c4pp00230j>
- Olmez-Hanci, T., Arslan-Alaton, I., 2013. Comparison of sulfate and hydroxyl radical based advanced oxidation of phenol. *Chem. Eng. J.* 224, 10–16. <https://doi.org/10.1016/j.cej.2012.11.007>
- Olmez-Hanci, T., Imren, C., Kabdaşlı, I., Tünay, O., Arslan-Alaton, I., 2011. Application of the UV-C photo-assisted peroxymonosulfate oxidation for the mineralization of dimethyl phthalate in aqueous solutions. *Photochem. Photobiol. Sci.* 10, 408–413. <https://doi.org/10.1039/c0pp00173b>
- Ozores Diez, P., Giannakis, S., Rodríguez-Chueca, J., Wang, D., Quilty, B., Devery, R., McGuigan, K., Pulgarin, C., 2020. Enhancing solar disinfection (SODIS) with the photo-Fenton or the Fe²⁺/peroxymonosulfate-activation process in large-scale plastic bottles leads to toxicologically safe drinking water. *Water Res.* 186. <https://doi.org/10.1016/j.watres.2020.116387>

11. References

Pabi, S.; Reekie, L.; Amarnath, A.; Goldstein, R. Electric Power Research Institute Water Research Foundation Electricity Use and Management in the Municipal Water Supply and Wastewater Industries; EPRI: Palo Alto, CA, USA; Water Research Foundation: Denver, CO, USA, 2013.

Paganini, M.C., Giorgini, A., Gonçalves, N.P.F., Gionco, C., Bianco Prevot, A., Calza, P., 2019. New insight into Zinc Oxide doped with iron and its exploitation to pollutants abatement. *Catal. Today* 328, 230–234. <https://doi.org/10.1016/j.cattod.2018.10.054>

Paganini, M.C., Dalmasso, D., Gionco, C., Polliotto, V., Mantilleri, L., Calza, P., 2016. Beyond TiO₂: Cerium-doped Zinc Oxide as a new photocatalyst for the photodegradation of persistent pollutants. *Chemistry Select* 1, 3377–3383. <https://doi.org/10.1002/slct.201600645>

Pera-Titus, M., García-Molina, V., Baños, M.A., Giménez, J., Esplugas, S., 2004. Degradation of chlorophenols by means of advanced oxidation processes: A general review. *Appl. Catal. B Environ.* 47, 219–256. <https://doi.org/10.1016/j.apcatb.2003.09.010>

Pereira, A., Silva, L., Laranjeiro, C., Lino, C., Pena, A., 2020. Selected pharmaceuticals in different aquatic compartments: Part I—Source, fate and occurrence. *Molecules* 25. <https://doi.org/10.3390/molecules25051026>

Pereira, V.J., Marques, R., Marques, M., Benoliel, M.J., Barreto Crespo, M.T., 2013. Free chlorine inactivation of fungi in drinking water sources. *Water Res.* 47, 517–523. <https://doi.org/10.1016/j.watres.2012.09.052>

Pérez-Estrada, L.A., Malato, S., Gernjak, W., Agüera, A., Thurman, E.M., Ferrer, I., Fernández-Alba, A.R., 2005. Photo-Fenton degradation of diclofenac: Identification of main intermediates and degradation pathway. *Environ. Sci. Technol.* 39, 8300–8306. <https://doi.org/10.1021/es050794n>

Persoone, G., Marsalek, B., Blinova, I., Törökne, A., Zarina, D., Manusadzianas, L., Nalecz-Jawecki, G., Tofan, L., Stepanova, N., Tothova, L., Kolar, B., 2003. A practical and user-friendly toxicity classification system with microbiotests for natural waters and wastewaters. *Environ. Toxicol.* 18, 395–402. <https://doi.org/10.1002/tox.10141>

Plappally, A.K., Lienhard V, J.H., 2013. Costs for water supply, treatment, end-use and reclamation. *Desalin. Water Treat.* 51, 200–232. <https://doi.org/10.1080/19443994.2012.708996>

Polo-López, M.I., Sánchez Pérez, J.A., 2021. Perspectives of the solar photo-Fenton process against the spreading of pathogens, antibiotic-resistant bacteria and genes in the environment. *Curr. Opin. Green Sustain. Chem.* 27, 100416. <https://doi.org/10.1016/j.cogsc.2020.100416>

Polo-López, M.I., Castro-Alfárez, M., Nahim-Granados, S., Malato, S., Fernández-Ibáñez, P., 2017. *Legionella jordanis* inactivation in water by solar driven processes: EMA-qPCR versus culture-based analyses for new mechanistic insights. *Catal. Today* 287, 15–21. <https://doi.org/10.1016/j.cattod.2016.10.029>

Polo-López, M.I., Castro-Alfárez, M., Oller, I., Fernández-Ibáñez, P., 2014. Assessment of solar photo-Fenton, photocatalysis, and H₂O₂ for removal of phytopathogen fungi spores in synthetic and real effluents of urban wastewater. *Chem. Eng. J.* 257, 122–130. <https://doi.org/10.1016/j.cej.2014.07.016>

- Polo-López M. I., García-Fernández I., Oller I., Fernández-Ibáñez, P., 2011. Solar disinfection of fungal spores in water aided by low concentrations of hydrogen peroxide. *Photochem. Photobiol. Sci.* 10, 332–337. <https://doi.org/10.1039/c0pp00158a>
- Polo-López, M.I., Fernández-Ibáñez, P., García-Fernández, I., Oller, I., Salgado-Tránsito, I., Sichel, C., 2010. Resistance of *Fusarium* sp spores to solar TiO₂ photocatalysis: Influence of spore type and water (scaling-up results). *J. Chem. Technol. Biotechnol.* 85, 1038–1048. <https://doi.org/10.1002/jctb.2397>
- ECHA. Pentapotassium Bis(peroxymonosulphate). -Registration Dossier-ECHA. Available online: <https://echa.europa.eu/es/registration-dossier/-/registered-dossier/15990/7/3/1>
- Radjenović, J., Godehardt, M., Petrović, M., Hein, A., Farré, M., Jekel, M., Barceló, D., 2009. Evidencing generation of persistent ozonation products of antibiotics roxithromycin and trimethoprim. *Environ. Sci. Technol.* <https://doi.org/10.1021/es900965a>
- Rajkhowa, S., 2020. Heat, solar pasteurization, and ultraviolet radiation treatment for removal of waterborne pathogens, *Waterborne Pathogens*. Elsevier. <https://doi.org/10.1016/b978-0-12-818783-8.00009-8>
- Rioja, N., Zorita, S., Peñas, F.J., 2016. Effect of water matrix on photocatalytic degradation and general kinetic modeling. *Appl. Catal. B Environ.* 180, 330–335. <https://doi.org/10.1016/j.apcatb.2015.06.038>
- Rivas, F.J., Gimeno, O., Borallho, T., 2012. Aqueous pharmaceutical compounds removal by potassium monopersulfate. Uncatalyzed and catalyzed semicontinuous experiments. *Chem. Eng. J.* 192, 326–333. <https://doi.org/10.1016/j.cej.2012.03.055>
- Rizzo, L., Gernjak, W., Krzeminski, P., Malato, S., McArdell, C.S., Perez, J.A.S., Schaar, H., Fatta-Kassinos, D., 2020. Best available technologies and treatment trains to address current challenges in urban wastewater reuse for irrigation of crops in EU countries. *Sci. Total Environ.* 710, 136312. <https://doi.org/10.1016/j.scitotenv.2019.136312>
- Rizzo, L., Manaia, C., Merlin, C., Schwartz, T., Dagot, C., Ploy, M.C., Michael, I., Fatta-Kassinos, D., 2013. Urban wastewater treatment plants as hotspots for antibiotic resistant bacteria and genes spread into the environment: A review. *Sci. Total Environ.* 447, 345–360. <https://doi.org/10.1016/j.scitotenv.2013.01.032>
- Rocha, J., Cacace, D., Kampouris, I., Guilloteau, H., Jäger, T., Marano, R.B.M., Karaolia, P., Manaia, C.M., Merlin, C., Fatta-Kassinos, D., Cytryn, E., Berendonk, T.U., Schwartz, T., 2020. Inter-laboratory calibration of quantitative analyses of antibiotic resistance genes. *J. Environ. Chem. Eng.* 8, 102214. <https://doi.org/10.1016/j.jece.2018.02.022>
- Rodríguez-Chueca, J., Alonso, E., Singh, D.N., 2019d. Photocatalytic mechanisms for peroxymonosulfate activation through the removal of methylene blue: A case study. *Int. J. Environ. Res. Public Health* 16. <https://doi.org/10.3390/ijerph16020198>
- Rodríguez-Chueca, J., Garcia-Cañibano, C., Sarro, M., Encinas, Á., Medana, C., Fabbri, D., Calza, P., Marugán, J., 2019b. Evaluation of transformation products from chemical oxidation of

11. References

micropollutants in wastewater by photoassisted generation of sulfate radicals. *Chemosphere* 226, 509–519. <https://doi.org/10.1016/j.chemosphere.2019.03.152>

Rodríguez-Chueca, J., Varella della Giustina, S., Rocha, J., Fernandes, T., Pablos, C., Encinas, Á., Barceló, D., Rodríguez-Mozaz, S., Manaia, C.M., Marugán, J., 2019c. Assessment of full-scale tertiary wastewater treatment by UV-C based-AOPs: Removal or persistence of antibiotics and antibiotic resistance genes? *Sci. Total Environ.* 652, 1051–1061. <https://doi.org/10.1016/j.scitotenv.2018.10.223>

Rodríguez-Chueca, J., García-Cañibano, C., Lepistö, R.J., Encinas, Pellinen, J., Marugán, J., 2019d. Intensification of UV-C tertiary treatment: Disinfection and removal of micropollutants by sulfate radical based Advanced Oxidation Processes. *J. Hazard. Mater.* 372, 94–102. <https://doi.org/10.1016/j.jhazmat.2018.04.044>

Rodríguez-Chueca, J., Giannakis, S., Marjanovic, M., Kohantorabi, M., Gholami, M.R., Grandjean, D., de Alencastro, L.F., Pulgarín, C., 2019e. Solar-assisted bacterial disinfection and removal of contaminants of emerging concern by Fe²⁺-activated HSO₅⁻ vs. S₂O₈²⁻ in drinking water. *Appl. Catal. B: Environ.* 248, 62–72. <https://doi.org/10.1016/j.apcatb.2019.02.018>

Rodríguez-chueca, J., Laski, E., García-Cañibano, C., Vidales, M.J.M. De, Encinas, Á., 2018. Micropollutants removal by full-scale UV-C/sulfate radical based Advanced Oxidation Processes. *Sci. Total Environ.* 630, 1216–1225. <https://doi.org/10.1016/j.scitotenv.2018.02.279>

Ruiz, M., Yang, Y., Lochbaum, C.A., Delafield, D.G., Pignatello, J.J., Li, L., Pedersen, J.A., 2019. Peroxymonosulfate oxidizes amino acids in water without activation. *Environ. Sci. Technol.* 53, 10845–10854. <https://doi.org/10.1021/acs.est.9b01322>

Rutala, W. A., Weber D. J., 2004. Selection of the ideal disinfectant. *Infection Control and Hospital Epidemiology*, 25, 333-341. <https://doi.org/10.1086/676877>

Sakineh, S., Dehghanifard, E., Noorisepehr, M., 2019. Efficient clean-up of waters contaminated with diazinon pesticide using photo-decomposition of peroxy-monosulfate by ZnO decorated on a magnetic core/shell structure. *J. Environ. Manage.* 250, 109472. <https://doi.org/10.1016/j.jenvman.2019.109472>

Sánchez-Montes, I., Salmerón García, I., Rivas Ibañez, G., Aquino, J.M., Polo-López, M.I., Malato, S., Oller, I., 2020. UVC-based advanced oxidation processes for simultaneous removal of microcontaminants and pathogens from simulated municipal wastewater at pilot plant scale. *Environ. Sci. Water Res. Technol.* 6, 2553–2566. <https://doi.org/10.1039/d0ew00279h>

Saxena, T., Kaushik, P., Krishna Mohan, M., 2015. Prevalence of *E. coli* O157: H7 in water sources: An overview on associated diseases, outbreaks and detection methods. *Diagn. Microbiol. Infect. Dis.* <https://doi.org/10.1016/j.diagmicrobio.2015.03.015>

Sbardella, L., Gala, I.V., Comas, J., Carbonell, S.M., Rodríguez-Roda, I., Gernjak, W., 2020. Integrated assessment of sulfate-based AOPs for pharmaceutical active compound removal from wastewater. *J. Clean. Prod.* 260, 121014. <https://doi.org/10.1016/j.jclepro.2020.121014>

Schollée, J.E., Schymanski, E.L., Avak, S.E., Loos, M., Hollender, J., 2015. Prioritizing Unknown Transformation Products from Biologically-Treated Wastewater Using High-Resolution Mass

- Spectrometry, Multivariate Statistics, and Metabolic Logic. *Anal. Chem.* 87, 12121–12129. <https://doi.org/10.1021/acs.analchem.5b02905>
- Sgroi, M., Snyder, S.A., Roccaro, P., 2021. Comparison of AOPs at pilot scale: Energy costs for micro-pollutants oxidation, disinfection by-products formation and pathogens inactivation. *Chemosphere* 273, 128527. <https://doi.org/10.1016/j.chemosphere.2020.128527>
- Sharma, J., Mishra, I.M., Dionysiou, D.D., Kumar, V., 2015. Oxidative removal of Bisphenol A by UV-C/peroxymonosulfate (PMS): Kinetics, influence of co-existing chemicals and degradation pathway. *Chem. Eng. J.* <https://doi.org/10.1016/j.cej.2015.04.021>
- Shu, H.-Y., Chang, M.-C., Huang, S.-W., 2015. Decolorization and mineralization of azo dye Acid Blue 113 by the UV/Oxone process and optimization of operating parameters. *New pub Balaban* 57, 7951–7962. <https://doi.org/10.1080/19443994.2015.1031188>
- Sirtori, C., Agüera, A., Gernjak, W., Malato, S., 2010. Effect of water-matrix composition on Trimethoprim solar photodegradation kinetics and pathways. *Water Res.* 44, 2735–2744. <https://doi.org/10.1016/j.watres.2010.02.006>
- Solís, R.R., Rivas, F.J., Chávez, A.M., Dionysiou, D.D., 2020. Peroxymonosulfate/solar radiation process for the removal of aqueous microcontaminants. Kinetic modeling, influence of variables and matrix constituents. *J. Hazard. Mater.* 400, 123118. <https://doi.org/10.1016/j.jhazmat.2020.123118>
- Sordello, F., Berruti, I., Gionco, C., Paganini, M.C., Calza, P., Minero, C., 2019. Photocatalytic performances of rare earth element-doped zinc oxide toward pollutant abatement in water and wastewater. *Appl. Catal. B Environ.* 245, 159–166. <https://doi.org/10.1016/j.apcatb.2018.12.053>
- Sousa, J.C.G., Ribeiro, A.R., Barbosa, M.O., Pereira, M.F.R., Silva, A.M.T., 2018. A review on environmental monitoring of water organic pollutants identified by EU guidelines. *J. Hazard. Mater.* 344, 146–162. <https://doi.org/10.1016/j.jhazmat.2017.09.058>
- Teixeira, R.I., Goulart, J.S., Corrêa, R.J., Garden, S.J., Ferreira, S.B., Netto-Ferreira, J.C., Ferreira, V.F., Miro, P., Marin, M.L., Miranda, M.A., De Lucas, N.C., 2019. A photochemical and theoretical study of the triplet reactivity of furano- and pyrano-1,4-naphthoquinones towards tyrosine and tryptophan derivatives. *RSC Adv.* 9, 13386–13397. <https://doi.org/10.1039/c9ra01939a>
- The Swis Federal Council, 1998 (Status as of 1 January 2021) Waters Protection Ordinance (WPO) 1–70.
- Tortora, G.J., Funke, B.R., Case, C.L., 2007. *Microbiology: an introduction* 958.
- Trovó, A.G., Nogueira, R.F.P., Agüera, A., Sirtori, C., Fernández-Alba, A.R., 2009. Photodegradation of sulfamethoxazole in various aqueous media: Persistence, toxicity and photoproducts assessment. *Chemosphere* 77, 1292–1298. <https://doi.org/10.1016/j.chemosphere.2009.09.065>
- Tsydenova, O., Batoev, V., Batoeva, A., 2015. Solar-enhanced advanced oxidation processes for water treatment: Simultaneous removal of pathogens and chemical pollutants. *Int. J. Environ. Res. Public Health* 12, 9542–9561. <https://doi.org/10.3390/ijerph120809542>

11. References

- Tummino, M.L., Laurenti, E., Deganello, F., Bianco Prevot, A., Magnacca, G., 2017. Revisiting the catalytic activity of a doped SrFeO₃ for water pollutants removal: Effect of light and temperature. *Appl. Catal. B Environ.* 207, 174–181. <https://doi.org/10.1016/j.apcatb.2017.02.007>
- UNEP, 2017. Freshwater Strategy 2017-2021. Report 21.
- United Nation, Water, 2019. <https://www.un.org/en/global-issues/water>
- United Nation, 2018. SDG 6 Synthesis Report 2018 on Water and Sanitation, 2018. SDG 6 Synthesis Report 2018 on Water and Sanitation. <https://doi.org/10.18356/e8fc060b-en>
- USEPA 2012. Guidelines for Water Reuse. *Development* 26, 252. <https://doi.org/EPA16251R-921004>
- USEPA, 2009. Drinking Water Regulations and Contaminants. URL <https://www.epa.gov/sdwa/drinking-water-regulations-and-contaminants>
- USEPA. 1999. Wastewater Technology Fact Sheet: Ultraviolet Disinfection. Available online: <https://www3.epa.gov/npdes/pubs/uv.Pdf>.
- USEPA. 1996. Ultraviolet Light Disinfection Technology in Drinking Water Application—An Overview. EPA 811-R-96-002. Science Applications International Corporation, McLean, Va.
- USEPA, 1985. National Primary Drinking Water Regulations. Available online: <https://www.epa.gov/ground-water-and-drinking-water/national-primary-drinking-water-regulations>
- Van Grieken, R., Marugán, J., Pablos, C., Furones, L., López, A., 2010. Comparison between the photocatalytic inactivation of Gram-positive *E. faecalis* and Gram-negative *E. coli* faecal contamination indicator microorganisms. *Appl. Catal. B Environ.* 100, 212–220. <https://doi.org/10.1016/j.apcatb.2010.07.034>
- Vergalli, J., Bodrenko, I. V., Masi, M., Moynié, L., Acosta-Gutiérrez, S., Naismith, J.H., Davin-Regli, A., Ceccarelli, M., van den Berg, B., Winterhalter, M., Pagès, J.M., 2020. Porins and small-molecule translocation across the outer membrane of Gram-negative bacteria. *Nat. Rev. Microbiol.* 18, 164–176. <https://doi.org/10.1038/s41579-019-0294-2>
- Wacławek, S., Lutze, H. V., Grübel, K., Padil, V.V.T., Černík, M., Dionysiou, D.D., 2017. Chemistry of persulfates in water and wastewater treatment: A review. *Chem. Eng. J.* 330, 44–62. <https://doi.org/10.1016/j.cej.2017.07.132>
- Wang, R., Ji, M., Zhai, H., Guo, Y., Liu, Y., 2021. Occurrence of antibiotics and antibiotic resistance genes in WWTP effluent-receiving water bodies and reclaimed wastewater treatment plants. *Sci. Total Environ.* 796, 148919. <https://doi.org/10.1016/j.scitotenv.2021.148919>
- Wang, J., Wang, S., 2021. Toxicity changes of wastewater during various advanced oxidation processes treatment: An overview. *J. Clean. Prod.* 315, 128202. <https://doi.org/10.1016/j.jclepro.2021.128202>

- Wang, J., Chu, L., Wojnárovits, L., Takács, E., 2020. Occurrence and fate of antibiotics, antibiotic resistant genes (ARGs) and antibiotic resistant bacteria (ARB) in municipal wastewater treatment plant: An overview. *Sci. Total Environ.* 744, 140997. <https://doi.org/10.1016/j.scitotenv.2020.140997>
- Wang, J., Wang, S., 2018. Activation of persulfate (PS) and peroxymonosulfate (PMS) and application for the degradation of emerging contaminants. *Chem. Eng. J.* 334, 1502–1517. <https://doi.org/10.1016/j.cej.2017.11.059>
- Watson, J., Hassinger E., 2016. Drinking water standards. College of Agriculture and Life Sciences, University of Arizona (Tucson, AZ)
- Welte, W., Nestel, U., Wacker, T., Diederichs, K., 1995. Structure and function of the porin channel. *Kidney Int.* 48, 930–940. <https://doi.org/10.1038/ki.1995.374>
- Wen, G., Xu, X., Zhu, H., Huang, T., Ma, J., 2017. Inactivation of four genera of dominant fungal spores in groundwater using UV and UV/PMS: Efficiency and mechanisms. *Chem. Eng. J.* 328, 619–628. <https://doi.org/10.1016/j.cej.2017.07.055>
- World Health Organization WHO, 2021. Guidelines on Recreational Water Quality: Volume 1 Coastal and Fresh Waters. Geneva: World Health Organization; 2021, Chapter 4: Faecal pollution <https://www.who.int/publications/i/item/9789240031302>
- WHO, 2019. New report calls for urgent action to avert antimicrobial resistance crisis. Available online: <https://www.who.int/news/item/29-04-2019-new-report-calls-for-urgent-action-to-avert-antimicrobial-resistance-crisis>
- WHO, 2017. WHO publishes list of bacteria for which new antibiotics are urgently needed. Available online: <https://www.who.int/news/item/27-02-2017-who-publishes-list-of-bacteria-for-which-new-antibiotics-are-urgently-needed>
- WHO, 2011. Guidelines for Drinking-water Quality: Fourth edition. Available online: <https://www.who.int/publications/i/item/9789241549950>
- WHO, 2008. Guidelines for drinking-water quality: Third edition (incorporating the first and second addenda). Chapter 7: Microbial fact sheets, Chapter 11: Microbial fact sheets. Geneva, Switzerland
- WHO, 2006. Guidelines for Drinking-water Quality first addendum to third edition Volume 1 Recommendations WHO Library Cataloguing-in-Publication Data.
- WHO. 2004. Sulfate in Drinking-Water Background Document for Development of WHO Guidelines for Drinking-Water Quality; WHO: Geneva, Switzerland
- WHO. 2003. Guidelines for safe recreational water environments. Volume 1, Coastal and fresh waters. World Health Organization. <https://apps.who.int/iris/handle/10665/42591>
- Wojnárovits, L., Takács, E., 2019. Rate constants of sulfate radical anion reactions with organic molecules: A review. *Chemosphere.* <https://doi.org/10.1016/j.chemosphere.2018.12.156>

11. References

- Wols, B.A., Hofman-Caris, C.H.M., Harmsen, D.J.H., Beerendonk, E.F., 2013. Degradation of 40 selected pharmaceuticals by UV/H₂O₂. *Water Res.* 47, 5876–5888. <https://doi.org/10.1016/j.watres.2013.07.008>
- Wu, Y., Bianco, A., Brigante, M., Dong, W., De Sainte-Claire, P., Hanna, K., Mailhot, G., 2015. Sulfate radical photogeneration using Fe-EDDS: Influence of critical parameters and naturally occurring scavengers. *Environ. Sci. Technol.* 49, 14343–14349. <https://doi.org/10.1021/acs.est.5b03316>
- Wu, Y., Shi, Y., Chen, H., Zhao, J., Dong, W., 2018. Activation of persulfate by magnetite: Implications for the degradation of low concentration sulfamethoxazole. *Process Saf. Environ. Prot.* 116, 468–476. <https://doi.org/10.1016/j.psep.2018.03.020>
- Xia, X., Zhu, F., Li, J., Yang, H., Wei, L., Li, Q., Jiang, J., Zhang, G., Zhao, Q., 2020. A Review Study on Sulfate-Radical-Based Advanced Oxidation Processes for Domestic/Industrial Wastewater Treatment: Degradation, Efficiency, and Mechanism. *Front. Chem.* 8. <https://doi.org/10.3389/fchem.2020.592056>
- Xiao, R., Liu, K., Bai, L., Minakata, D., Seo, Y., Kaya Göktaş, R., Dionysiou, D.D., Tang, C.J., Wei, Z., Spinney, R., 2019. Inactivation of pathogenic microorganisms by sulfate radical: Present and future. *Chem. Eng. J.* 371, 222–232. <https://doi.org/10.1016/j.cej.2019.03.296>
- Xu, X., Ran, Z., Wen, G., Liang, Z., Wan, Q., 2020. Efficient inactivation of bacteria in ballast water by adding potassium peroxydisulfate alone: Role of halide ions. *Chemosphere* 253, 126656. <https://doi.org/10.1016/j.chemosphere.2020.126656>
- Xu, Y., Lin, Z., Wang, Y., Zhang, H., 2017. The UV/peroxydisulfate process for the mineralization of artificial sweetener sucralose. *Chem. Eng. J.* <https://doi.org/10.1016/j.cej.2017.02.058>
- Xue, Z., Hessler, C.M., Panmanee, W., Hassett, D.J., Seo, Y., 2013. *Pseudomonas aeruginosa* inactivation mechanism is affected by capsular extracellular polymeric substances reactivity with chlorine and monochloramine. *FEMS Microbiol. Ecol.* 83, 101–111. <https://doi.org/10.1111/j.1574-6941.2012.01453.x>
- Yang, Q., Ma, Y., Chen, F., Yao, F., Sun, J., Wang, S., Yi, K., Hou, L., Li, X., Wang, D., 2019. Recent advances in photo-activated sulfate radical-advanced oxidation process (SR-AOP) for refractory organic pollutants removal in water. *Chem. Eng. J.* 378, 122149. <https://doi.org/10.1016/j.cej.2019.122149>
- Yang, X., Ding, X., Zhou, L., Zhao, Q., Ji, Y., Wang, X., Chovelon, J.M., Xiu, G., 2021. Direct oxidation of antibiotic trimethoprim by unactivated peroxydisulfate via a nonradical transformation mechanism. *Chemosphere* 263, 128194. <https://doi.org/10.1016/j.chemosphere.2020.128194>
- Yang, Y., Banerjee, G., Brudvig, G.W., Kim, J., Pignatello, J.J., 2018. Oxidation of organic compounds in water by unactivated peroxydisulfate. *Environ. Sci. Technol.* 52, 5911–5919. <https://doi.org/10.1021/acs.est.8b00735>

- Yang, Y., Lu, X., Jiang, J., Ma, J., Liu, G., Cao, Y., Liu, W., Li, J., Pang, S., Kong, X., Luo, C., 2017. Degradation of sulfamethoxazole by UV, UV/H₂O₂ and UV/persulfate (PDS): Formation of oxidation products and effect of bicarbonate. *Water Res.* 118, 196–207. <https://doi.org/10.1016/j.watres.2017.03.054>
- Yin, R., Guo, W., Wang, H., Du, J., Zhou, X., Wu, Q., Zheng, H., Chang, J., Ren, N., 2018. Selective degradation of sulfonamide antibiotics by peroxymonosulfate alone: Direct oxidation and nonradical mechanisms. *Chem. Eng. J.* 334, 2539–2546. <https://doi.org/10.1016/j.cej.2017.11.174>
- Young, B.J., Riera, N.I., Beily, M.E., Bres, P.A., Crespo, D.C., Ronco, A.E., 2012. Toxicity of the effluent from an anaerobic bioreactor treating cereal residues on *Lactuca sativa*. *Ecotoxicol. Environ. Saf.* 76, 182–186. <https://doi.org/10.1016/j.ecoenv.2011.09.019>
- Zammit, I., Vaiano, V., Iervolino, G., Rizzo, L., 2018. Inactivation of an urban wastewater indigenous: *Escherichia coli* strain by cerium doped zinc oxide photocatalysis. *RSC Adv.* 8, 26124–26132. <https://doi.org/10.1039/c8ra05020a>
- Zamora, P.L., Villamena, F.A., 2012. Theoretical and experimental studies of the spin trapping of inorganic radicals by 5,5-dimethyl-1-pyrroline N-oxide (DMPO). 3. Sulfur dioxide, sulfite, and sulfate radical anions. *J. Phys. Chem. A* 116, 7210–7218. <https://doi.org/10.1021/jp3039169>
- Zeev, B., 1987. The Redox Potential of the Azide/Azldyl Couple. *J. Phys. Chem.* 91, 2120–2122
- Zeng, F., Cao, S., Jin, W., Zhou, X., Ding, W., Tu, R., Han, S.F., Wang, C., Jiang, Q., Huang, H., Ding, F., 2020. Inactivation of chlorine-resistant bacterial spores in drinking water using UV irradiation, UV/Hydrogen peroxide and UV/Peroxymonosulfate: Efficiency and mechanism. *J. Clean. Prod.* 243, 118666. <https://doi.org/10.1016/j.jclepro.2019.118666>
- Zhang, Y., Wang, B., Hu, X., Li, H., 2020. Non-activated peroxymonosulfate oxidation of p-aminobenzoic acid in the presence of effluent organic matter. *Chem. Eng. J.* 384, 123247. <https://doi.org/10.1016/j.cej.2019.123247>
- Zhang, X., Yao, J., Zhao, Z., Liu, J., 2019. Degradation of haloacetonitriles with UV/peroxymonosulfate process: Degradation pathway and the role of hydroxyl radicals. *Chem. Eng. J.* 364, 1–10. <https://doi.org/10.1016/j.cej.2019.01.029>
- Zhang, R., Yang, Y., Huang, C.H., Li, N., Liu, H., Zhao, L., Sun, P., 2016. UV/H₂O₂ and UV/PDS treatment of trimethoprim and sulfamethoxazole in synthetic human urine: Transformation products and toxicity. *Environ. Sci. Technol.* 50, 2573–2583. <https://doi.org/10.1021/acs.est.5b05604>
- Zhang, R., Sun, P., Boyer, T.H., Zhao, L., Huang, C.H., 2015. Degradation of pharmaceuticals and metabolite in synthetic human urine by UV, UV/H₂O₂, and UV/PDS. *Environ. Sci. Technol.* 49, 3056–3066. <https://doi.org/10.1021/es504799n>
- Zheng, J., Su, C., Zhou, J., Xu, L., Qian, Y., Chen, H., 2017. Effects and mechanisms of ultraviolet, chlorination, and ozone disinfection on antibiotic resistance genes in secondary effluents of municipal wastewater treatment plants. *Chem. Eng. J.* 317, 309–316. <https://doi.org/10.1016/j.cej.2017.02.076>

11. References

Zhou, P., Di Giovanni, G.D., Meschke, J.S., Dodd, M.C., 2014. Enhanced inactivation of *Cryptosporidium parvum* oocysts during solar photolysis of free available chlorine. *Environ. Sci. Technol. Lett.* 1, 453–458. <https://doi.org/10.1021/ez500270u>

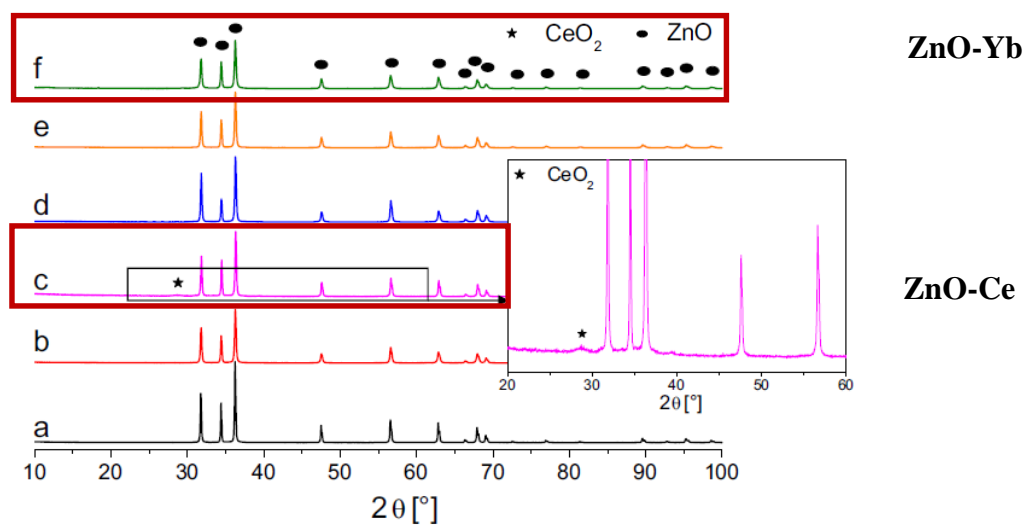
Zhou, Y., Jiang, J., Gao, Y., Pang, S.Y., Ma, J., Duan, J., Guo, Q., Li, J., Yang, Y., 2018. Oxidation of steroid estrogens by peroxymonosulfate (PMS) and effect of bromide and chloride ions: Kinetics, products, and modeling. *Water Res.* 138, 56–66. <https://doi.org/10.1016/j.watres.2018.03.045>

CHAPTER 12

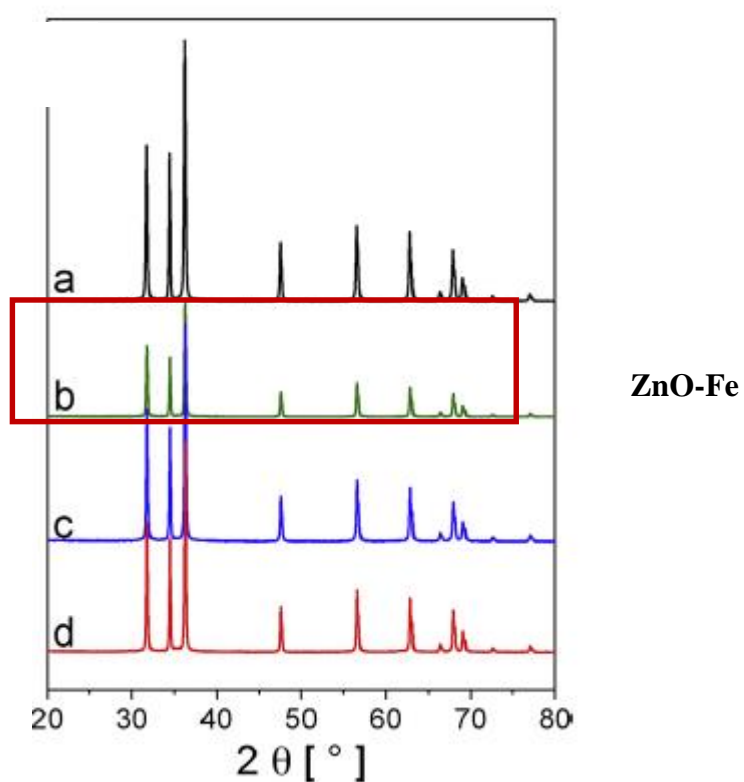
ANNEXES

12. ANNEXES

ANNEX A. Modified ZnO photocatalyst characterization



(a)



(b)

Figure A.1. XRD patterns of several rare earth ions modified ZnO and among them (a) ZnO-Ce (trace c) and ZnO-Yb (trace f). Inset: enlargement of the ZnO-Ce pattern and of (b) ZnO-Fe with different iron contents; ZnO-Fe (0.5 %) (trace b). Adapted from (Cerrato, 2018; Paganini, 2019).

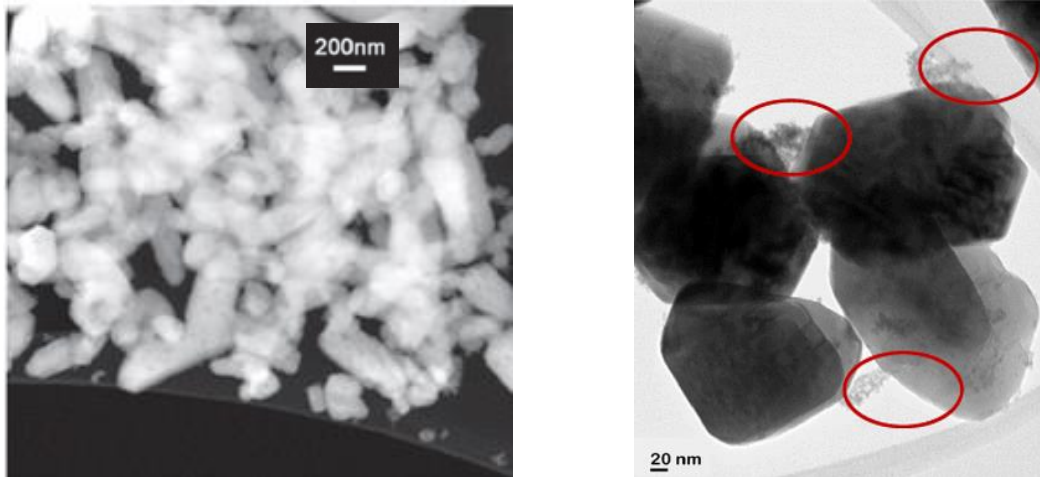


Figure A.2. (a) SEM micrographs, (b) TEM images of ZnO-Ce. Adapted from (Cerrato, 2018; Cerrato, 2020).

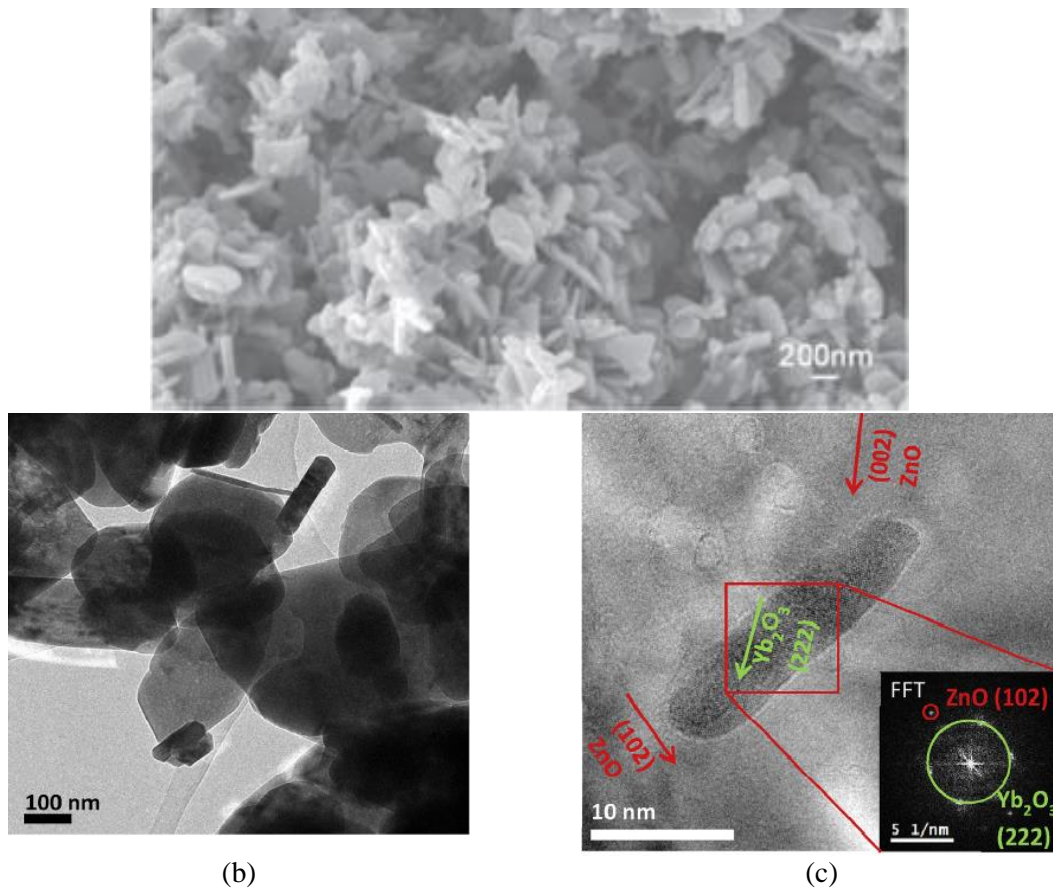


Figure A.3. (a) SEM micrographs, (b) TEM images and (c) High Resolution TEM (HR-TEM) image of ZnO-Yb. Adapted from (Cerrato, 2018; Cerrato, 2020).

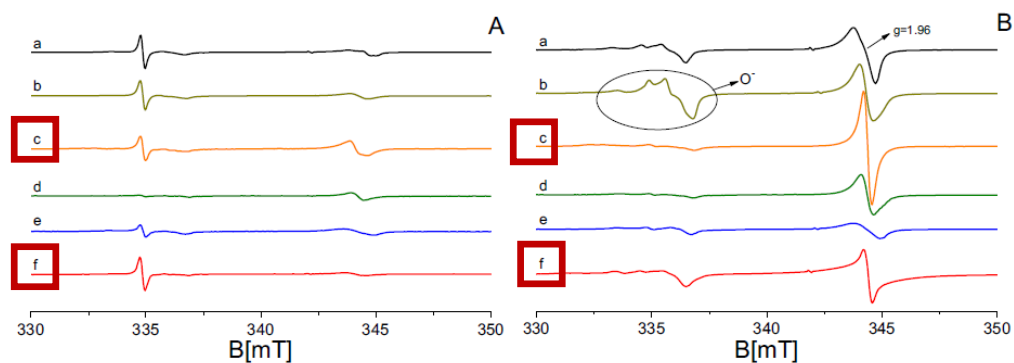


Figure A.4. EPR spectra recorded at 77 K of activated samples before (Panel A) and during (Panel B) UV irradiation of several rare earth ions modified ZnO and among of them: c) ZnO-Ce and ZnO-Yb. Adapted from (Cerrato, 2018).

Table A.1. Crystallite's size, and calculated energy gap for ZnO and modified samples (Cerrato, 2018b; 2020b; Paganini, 2019).

Catalyst	d ZnO (nm)	d dopant (nm)	Energy gap (eV)
ZnO	256±25	-	3.278
ZnO-Ce	163±16	10±2	3.273
ZnO-Yb	93±9	*	3.284
ZnO-Fe	112±17	n.a.	3.275

* Yb is present with nanorods shape, of about 100-200 nm of length and 10-30 nm of width.

ANNEX B. Kinetic constants evaluation

Table B.1. Bacteria inactivation kinetic constants in IW, SUWW and UWW at different concentrations of modified ZnO catalysts under natural sunlight (Data belong to Chapter 4).

Catalyst (mg/L)		Bacteria								
		<i>E. coli</i>			<i>E. faecalis</i>			<i>P. aeruginosa</i>		
		k (min ⁻¹) R ²	SL (min)	Q_{UV} (kJ/L)	k (min ⁻¹) R ²	SL (min)	Q_{UV} (kJ/L)	k (min ⁻¹) R ²	SL (min)	Q_{UV} (kJ/L)
Isotonic water (IW)										
Solar inactivation	0	0.233±0.034 0.959	20	6.2	0.064±0.006 0.965	30	12.7	0.065±0.012 0.853	-	10.5
ZnO-Ce	100	0.515±0.049 0.981	5	1.8	0.084±0.008 0.950	-	11.8	0.441±0.052 0.947	-	1.8
	200	NF			0.058±0.004 0.969	-	16.0	0.294±0.016 0.985	-	2.4
	500	0.394±0.092 0.854	10	2.6	0.106±0.007 0.974	-	6.7	0.325±0.023 0.976	-	2.1
ZnO-Fe	100	0.530±0.084 0.985	10	1.7	0.114±0.011 0.985	10	7.2	0.263±0.02 0.972	-	2.8
	200	0.515±0.092 0.939	10	1.8	0.053±0.005 0.957	20	13.0	0.188±0.009 0.984	-	2.7
	500	0.409±0.093 0.860	10	2.9	0.074±0.009 0.938	20	11.4	0.311±0.012 0.992	-	2.3
ZnO-Yb	100	0.541±0.150 0.858	5	1.7	0.071±0.005 0.960	-	11.6	0.403±0.007 0.999	-	1.7
	200	0.367±0.035 0.973	10	3.1	0.049±8E ⁻⁴ 0.998	-	16.0	0.132±0.004 0.994	-	5.7
	500	0.341±0.049 0.941	10	3.1	0.089±0.004 0.989	-	7.8	0.350±0.029 0.972	-	1.8
Simulated urban wastewater (SUWW)										
Solar inactivation	0	0.043±0.008 0.844	30	23.5	0.048±0.014 0.771	60	23.5	0.036±0.001 0.991	-	23.5
TiO ₂	100	0.062±0.003 0.989	30	13.5	0.041±0.004 0.915	-	21.7	0.046±0.002 0.987	-	13.5
	500	0.046±0.009 0.793	20	13.4	0.074±0.096 0.964 0.013±0.001 0.944	-	21.8	0.103±0.008 0.967 0.017±0.003 0.865	-	13.5
ZnO-Ce	100	0.082±0.009 0.935	-	6.0	0.032±0.001 0.985	-	21.0	0.081±0.009 0.922	-	6.0
	500	0.169±0.012 0.985	20	4.9	0.043±0.001 0.989	-	13.4	0.125±0.018 0.907	-	3.8
ZnO-Fe	100	0.079±0.012 0.883	-	5.8	0.036±0.004 0.934	20	20.6	0.072±0.014 0.800	-	5.8
	500	0.079±0.002 0.993	-	7.3	0.029±0.002 0.927	-	20.8	0.080±0.009 0.922	-	5.6
ZnO-Yb	100	0.093±0.006 0.973	-	7.3	0.059±0.006 0.961	30	15.1	0.091±0.005 0.979	-	7.3
	500	0.083±0.004 0.981	-	5.6	0.029±0.002 0.965	-	20.8	0.100±0.011 0.933	-	4.6
Urban wastewater (UWW)										
		<i>E. coli</i>		Total coliforms		<i>Enterococcus</i> spp.		<i>Pseudomonas</i> spp.		
		k (min ⁻¹) R ²	Q_{UV} (kJ/L)	k (min ⁻¹) R ²	Q_{UV} (kJ/L)	k (min ⁻¹) R ²	Q_{UV} (kJ/L)	k (min ⁻¹) R ²	Q_{UV} (kJ/L)	
Solar inactivation	0	0.017±0.001* 0.976	24.1	0.001±5E ⁻⁴ 0.977	/	0.009±4E ^{-4**} 0.980	/	0.016±0.001** 0.935	30.2	
TiO ₂	100	0.021±0.001 0.978	23.3	0.014±0.00 0.930	/	0.013±0.001 0.944	23.3	0.016±0.001 0.952	38.7	
	500	0.026±0.001 0.980	10.1	0.020±9E ⁻⁴ 0.984	22.8	0.036±0.003 0.968	4.6	0.026±0.002 0.966	14.1	
ZnO-Ce	100	0.023±0.001 0.978	9.4	0.033±0.001 0.992	13.1	0.012±4E ⁻⁴ 0.989	21.3	0.036±0.003 0.937	13.1	
	500	0.024±0.001 0.982	10.1	0.029±9E ⁻⁴ 0.992	14.1	0.013±0.001 0.902	22.8	0.041±0.003 0.958	6.4	

NF= no fitting (for R² < 0.7); SL=Shoulder Length (min); *SL= 30 min **SL= 15 min; Q_{UV} (kJ/L) = Cumulative energy at which the DL was reached; / = no DL reached.

Table B.2. CECs degradation constants in IW, SUWW and UWW at different concentrations of modified ZnO catalysts under natural sunlight (Data belong to Chapter 4).

Catalyst (mg/L)		CECs								
		DCF			SMX			TMP		
		k , (min ⁻¹)	R ²	Q_{UV} kJ/L	k , (min ⁻¹)	R ²	Q_{UV} kJ/L	k , (min ⁻¹)	R ²	Q_{UV} kJ/L
Isotonic water (IW)										
Solar photolysis	0	0.028±0.003	0.965	7.6	8E ⁻⁴ ±3E ⁻⁵	0.992		9E ⁻⁵ ±1E ⁻⁵	0.890	
ZnO-Ce	100	0.118±0.005	0.988	1.8	0.082±7E ⁻⁴	0.999	2.4	0.131±0.003	0.996	1.5
	200	0.375±0.013	0.996	0.6	0.217±0.013	0.989	0.9	0.369±0.003	1.000	0.6
	500	0.516±0.017	0.995	0.3	0.480±0.028	0.983	0.4	0.534±0.062	0.960	0.3
ZnO-Fe	100	0.080±0.002	0.996	2.2	0.050±7E ⁻⁴	0.998	3.4	0.07±0.002	0.998	2.6
	200	0.056±0.002	0.983	3.0	0.049±0.002	0.977	3.8	0.046±0.003	0.971	3.6
	500	0.089±0.004	0.987	2.3	0.072±0.003	0.981	2.9	0.087±0.002	0.995	2.1
ZnO-Yb	100	0.096±0.003	0.995	2.2	0.070±0.002	0.992	2.9	0.103±0.001	0.999	1.9
	200	0.151±0.004	0.997	1.3	0.191±0.007	0.993	1.2	0.175±0.003	0.999	1.1
	500	0.221±0.010	0.997	1.1	0.148±0.003	0.998	1.2	0.219±0.006	0.989	1.0
Simulated urban wastewater (SUWW)										
Solar photolysis	0	0.028±2E ⁻⁴	0.999	7.1	3E ⁻⁴ ±5E ⁻⁵	0.893	/	NF		/
TiO ₂	100	0.146±0.009	0.986	1.0	0.075±9E ⁻⁴	0.999	2.3	0.066±0.004	0.982	2.9
	500	0.108±0.012	0.948	0.8	0.088±0.001	0.999	1.7	0.088±0.005	0.988	1.9
ZnO-Ce	100	0.033±0.002	0.976	5.6	0.007±2E ⁻⁴	0.988	/	0.007±2E ⁻⁴	0.989	/
	500	0.057±9E ⁻⁴	0.998	2.7	0.034±7E ⁻⁴	0.996	3.9	0.038±0.001	0.990	4.2
ZnO-Fe	100	0.018±5E ⁻⁴	0.993	10.1	0.003±9E ⁻⁵	0.992	/	0.003±9E ⁻⁵	0.992	/
	500	0.017±2E ⁻⁴	0.999	9.5	0.008±3E ⁻⁴	0.989	20.8	0.007±4E ⁻⁴	0.968	20.7
ZnO-Yb	100	0.022±6E ⁻⁴	0.993	9.5	0.005±2E ⁻⁴	0.984	/	0.004±1E ⁻⁴	0.991	/
	500	0.022±7E ⁻⁴	0.999	5.7	0.011±5E ⁻⁵	0.999	16.6	0.008±2E ⁻⁴	0.990	20.7
Urban wastewater (UWW)										
Solar photolysis	0	0.013±0.001	0.965	14.6	NF		/	NF		/
TiO ₂ -25	100	0.040±0.002	0.982	4.6	0.021±0.002	0.906	9.8	0.009±3E ⁻⁴	0.986	23.3
	500	0.120±0.011	0.965	1.8	0.056±0.002	0.990	3.4	0.028±0.001	0.991	6.4
ZnO-Ce	100	0.022±7E ⁻⁴	0.992	7.8	0.005±1E ⁻⁴	0.993	36.9	0.004±2E ⁻⁴	0.962	/
	500	0.050±0.002	0.991	3.5	0.034±0.001	0.994	5.3	0.029±0.001	0.991	5.3

NF= no fitting (for R² < 0.7); Q_{UV} (kJ/L) = Cumulative energy at which 80 % of CECs removal was reached; / = 80 % of removal not reached.

Table B.3. Bacteria inactivation and CECs degradation pseudo-first order kinetic constants (k , min^{-1}) by PMS/Dark in the presence of several oxidant concentrations in IW and SUWW (Data belong to Chapter 6 and 7).

PMS/Dark [PMS] in mM	Bacteria								
	<i>E. coli</i>			<i>E. faecalis</i>			<i>P. aeruginosa</i>		
	k , (min^{-1})	R^2	SL, min	k , (min^{-1})	R^2	SL, min	k , (min^{-1})	R^2	SL, min
Isotonic water (IW)									
0	NF			NF			$6E^{-4} \pm 1E^{-4}$	0.866	0
0.0001	NF			NF			$0.002 \pm 5E^{-4}$	0.758	0
0.0005	NF			NF			$0.002 \pm 3E^{-4}$	0.848	0
0.001	NF			NF			$0.003 \pm 5E^{-4}$	0.837	0
0.002	$0.010 \pm 5E^{-4}$	0.950	0	0.022 ± 0.002	0.937	0	$0.003 \pm 4E^{-4}$	0.896	0
0.003	0.117 ± 0.015	0.904	20	0.031 ± 0.006	0.717	20	0.023 ± 0.003	0.883	0
0.004	0.142 ± 0.018	0.940	15	NF			0.056 ± 0.004	0.952	0
0.005	NF			0.073 ± 0.004	0.968	0	0.065 ± 0.007	0.922	0
0.01	0.367 ± 0.055	0.936	10	NF			0.114 ± 0.007	0.961	0
Simulated urban wastewater (SUWW)									
0.5	0.130 ± 0.012 24	-	-	0.126 ± 0.023 0.876	30	-	0.184 ± 0.021 0.925	-	-
PMS/Dark [PMS] in mM	CECs								
	DCF		SMX		TMP				
	k , (min^{-1})	R^2	k , (min^{-1})	R^2	k , (min^{-1})	R^2			
Isotonic water (IW)									
0	$1E^{-4} \pm 2E^{-5}$	0.880		NF			NF		
0.003	$0.002 \pm 3E^{-5}$	0.998		$6E^{-4} \pm 2E^{-5}$	0.989		$1E^{-4} \pm 1E^{-5}$	0.980	
0.004	0.004 ± 0.001	0.850		$0.005 \pm 6E^{-4}$	0.937		$0.001 \pm 2E^{-4}$	0.896	
0.005	$0.005 \pm 6E^{-4}$	0.921		$0.005 \pm 4E^{-4}$	0.971		$0.001 \pm 1E^{-4}$	0.967	
0.01	$0.012 \pm 9E^{-4}$	0.966		0.040 ± 0.001	0.978		$0.009 \pm 3E^{-4}$	0.995	
Simulated urban wastewater (SUWW)									
0.5	$0.002 \pm 2E^{-4}$ 0.900	-		$0.014 \pm 6E^{-4}$ 0.988	-		$0.011 \pm 6E^{-4}$ 0.978	-	

NF= no fitting (for $R^2 < 0.7$); SL=Shoulder Length (min); Q_{UV} (kJ/L) = Cumulative energy at which the DL/80% of removal was reached; / = no DL/80% reached.

Table B.4. Bacteria inactivation pseudo-first order kinetic constants (k , min^{-1}) by PMS/Solar in the presence of several oxidant concentrations in IW, SUWW and UWW (Data belong to Chapter 6 and 7).

PMS/Solar [PMS] in mM	Bacteria								
	<i>E. coli</i>			<i>E. faecalis</i>			<i>P. aeruginosa</i>		
	k (min^{-1}) R^2	SL, min	Q_{UV} , kJ/L	k (min^{-1}) R^2	SL, min	Q_{UV} , kJ/L	k (min^{-1}) R^2	SL, min	Q_{UV} , kJ/L
Isotonic water (IW)									
0	0.103±0.010 0.947	0	4.8	0.089±0.011 0.937	20	7.8	0.132±0.018 0.927	10	4.8
0.0001	0.110±0.011 0.935	5	6.0	0.061±0.006 0.952	20	13.3	0.123±0.009 0.970	10	6.0
0.0005	0.110±0.013 0.922	15	4.8	0.062±0.006 0.951	20	11.3	0.113±0.008 0.973	15	6.3
0.001	0.116±0.014 0.938	15	4.5	0.068±0.005 0.977	45	10.7	0.084±0.003 0.989	15	7.4
0.002	0.242±0.043 0.885	10	2.4	0.105±0.005 0.990	20	6.8	0.079±0.006 0.963	0	6.8
0.003	0.259±0.044 0.871	5	1.8	0.152±0.023 0.914	10	3.2	0.155±0.025 0.880	0	1.8
0.004	NF			0.160±0.016 0.946	10	3.1	0.166±0.014 0.962	0	1.8
0.005	0.207±0.043 0.809	0	1.2	0.176±0.016 0.952	0	1.8	0.220±0.019 0.962	0	1.5
0.01	0.422±0.102 0.842	5	1.4	0.283±0.050 0.887	5	1.7	0.223±0.026 0.923	0	1.7
Simulated urban wastewater (SUWW)									
0	0.050±0.006 0.921	30	16.8	0.040±0.003 0.969	60	/	0.050±0.009 0.822	45	16.8
0.01	0.089±0.015 0.892	30	9.4	0.039±0.002 0.987	45	20.7	0.099±0.010 0.961	30	9.4
0.05	0.164±0.023 0.910	15	4.9	0.119±0.013 0.956	40	9.4	0.105±0.011 0.907	/	4.9
0.1	0.279±0.025 0.970	10	2.8	0.186±0.042 0.859	30	6.0	0.155±0.019 0.899	/	2.8
0.2	0.405±0.071 0.913	5	1.8	0.183±0.028 0.914	20	4.9	0.287±0.019 0.978	/	1.8
0.3	0.534±0.008 0.999	5	1.3	0.237±0.051 0.840	10	2.6	0.363±0.032 0.969	/	1.3
0.5	0.488±0.175 0.771	5	1.3	0.353±0.036 0.970	5	1.7	0.566±0.043 0.983	/	0.9
Urban wastewater (UWW)									
	<i>E. coli</i>		Total Coliforms		<i>Enterococcus</i> spp.		<i>Pseudomonas</i> spp.		
	k (min^{-1}) R^2	Q_{UV} kJ/L	k (min^{-1}) R^2	Q_{UV} kJ/L	k (min^{-1}) R^2	Q_{UV} kJ/L	k (min^{-1}) R^2	Q_{UV} kJ/L	
0	0.009±0.001 0.810	16.0	0.022±0.001* 0.991	23.6	0.009±0.001 0.928	19.8	0.022±0.003** 0.909	16.0	
0.1	0.045±0.001 0.996	3.9	0.045±0.004 0.968	5.4	0.013±0.002 0.879	7.0	0.073±0.006 0.980	2.5	
0.5	0.171±0.021 0.943	1.8	0.151±0.001 0.976	2.8	0.065±0.005 0.955	3.8	0.216±0.022 0.969 0.033±0.006 0.858	4.8	
0.75	0.279±0.041 0.937	0.8	0.240±0.007 0.997	1.2	0.090±0.005 0.979	2.1	0.275±0.062 0.863 0.040±0.012 0.706	2.6	
1	0.362±0.077 0.875	0.7	0.285±0.065 0.818	1.1	0.258±0.035 0.946	0.7	0.274±0.048 0.886	1.1	

NF= no fitting (for $R^2 < 0.7$); SL=Shoulder Length (min); Q_{UV} (kJ/L) = Cumulative energy at which the DL was reached; / = no DL reached.

Table B.5. CECs degradation pseudo-first order kinetic constants (k , min^{-1}) by PMS/Solar in the presence of several oxidant concentrations in IW, SUWW and UWW (Data belong to Chapter 6 and 7).

PMS/Solar [PMS] in mM	CECs								
	DCF			SMX			TMP		
	k , (min^{-1})	R^2	Q_{UV} , kJ/L	k , (min^{-1})	R^2	Q_{UV} , kJ/L	k , (min^{-1})	R^2	Q_{UV} , kJ/L
Isotonic water (IW)									
0	0.028±0.003	0.965	7.6	0.001±3E ⁻⁵	0.991	/	9E-5±1E-5	0.890	/
0.003	0.018±4E ⁻⁴	0.995	7.3	0.001±9E ⁻⁵	0.918	/	NF		/
0.004	0.013±2E ⁻⁴	0.996	8.9	0.001±2E ⁻⁴	0.855	/	NF		/
0.005	0.024±7E ⁻⁴	0.989	4.8	0.002±4E ⁻⁴	0.729	/	NF		/
0.01	0.065±0.006	0.963	1.5	0.044±0.004	0.964	2.5	0.011±9E ⁻⁴	0.944	16.8
Simulated urban wastewater (SUWW)									
0	0.012±2E ⁻⁴	0.998	15.0	NF		/	NF		/
0.01	0.012±3E ⁻⁴	0.993	13.0	NF		/	NF		/
0.05	0.015±3E ⁻⁴	0.997	12.3	7E ⁻⁴ ±1E ⁻⁴	0.850	/	0.002±2E ⁻⁴	0.900	/
0.1	0.013±5E ⁻⁴	0.990	15.7	NF		/	0.005±1E ⁻³	0.737	/
0.2	0.018±0.001	0.971	11.1	0.008±0.001	0.873	/	0.010±0.002	0.838	/
0.3	0.036±0.007	0.819	8.5	0.013±6E ⁻⁴	0.975	11.3	0.012±7E ⁻⁴	0.976	11.2
0.5	0.031±0.003	0.963	6.1	0.018±0.001	0.980	7.2	0.018±0.001	0.979	7.4
Urban wastewater (UWW)									
0	0.012±3E ⁻⁴	0.993	13.9	9E-4±3E ⁻⁵	0.982	/	7E-4±3E ⁻⁵	0.981	/
0.1	0.014±4E ⁻⁴	0.993	11.2	0.002±1E ⁻⁴	0.942	/	0.002±1E ⁻⁴	0.849	/
0.5	0.039±0.004	0.903	5.3	0.028±0.003	0.914	10.6	0.024±0.003	0.917	/
0.75	0.049±0.005	0.925	3.9	0.042±0.0019	0.898	2.5	0.033±0.003	0.948	4.5
1	0.058±0.003	0.984	2.3	0.054±0.005	0.937	1.2	0.043±0.004	0.958	3.2

NF= no fitting (for $R^2 < 0.7$); Q_{UV} (kJ/L) = Cumulative energy at which 80 % of CECs removal was reached; / = 80 % of removal not reached.

Table B.6. Kinetics data of bacteria and CECs obtained in isotonic water (IW), diluted well water (d-WeW) and well water (WeW) under natural sunlight with and without 0.01 mM of PMS (Data belong to Chapter 6).

Matrix	Bacteria								
	<i>E. coli</i>			<i>E. faecalis</i>			<i>P. aeruginosa</i>		
	$k, (\text{min}^{-1})$ R^2	SL, min	Q_{UV} , kJ/L	$k, (\text{min}^{-1})$ R^2	SL, min	Q_{UV} , kJ/L	$k, (\text{min}^{-1})$ R^2	SL, min	Q_{UV} , kJ/L
Sunlight, [PMS]=0 mM									
IW	0.103±0.01 0.947	0	4.8	0.089±0.011 0.937	20	7.8	0.132±0.018 0.927	10	4.8
d-WeW	0.145±0.022 0.916	20	4.9	0.048±0.005 0.942	40	13.1	0.108±0.005 0.987	0	4.1
WeW	0.055±0.004 0.960	20	10.4	0.036±9E ⁻⁴ 0.997	60	/	0.033±0.002 0.977	0	/
Sunlight, [PMS]=0.01 mM									
IW	0.422±0.102 0.842	5	1.4	0.283±0.050 0.887	5	1.7	0.223±0.026 0.923	0	1.7
d-WeW	0.335±0.030 0.969	0	1.3	0.175±0.040 0.861	30	5.2	0.412±0.029 0.980	0	1.3
WeW	0.134±0.008 0.976	10	4.2	0.102±0.028 0.750	40	8.2	0.124±0.012 0.929	0	4.2
Matrix	CECs								
	DCF		SMX		TMP				
	$k, (\text{min}^{-1})$ R^2	Q_{UV} , kJ/L	$k, (\text{min}^{-1})$ R^2	Q_{UV} , kJ/L	$k, (\text{min}^{-1})$ R^2	Q_{UV} , kJ/L			
Sunlight, [PMS]=0 mM									
DW	0.026±5E ⁻⁴ 0.998	6.2	0.002±3E ⁻⁵ 0.998	/	6E-4±4E-5 0.971	/			
IW	0.028±0.003 0.965	7.6	8E-4±3E-5 0.991	/	NF	/			
d-WeW	0.019±1E ⁻⁴ 0.999	8.1	8E-4±1E-4 0.944	/	1E-4±2E-5 0.870	/			
WeW	0.020±5E ⁻⁴ 0.998	7.7	6E-4±1E-4 0.913	/	NF	/			
Sunlight, [PMS]=0.01 mM									
DW	0.081±0.001 0.947	0.9	0.020±0.002 0.922	9.1	0.003±3E-4 0.869	/			
IW	0.065±6E ⁻⁴ 0.963	1.5	0.044±0.004 0.964	2.5	0.011±9E ⁻⁴ 0.944	16.8			
d-WeW	0.039±0.001 0.996	3.7	0.004±3E ⁻⁴ 0.957	/	0.001±1E ⁻⁴ 0.911	/			
WeW	0.049±0.002 0.990	3.4	0.005±1E ⁻⁴ 0.984	/	0.001±8E ⁻⁵ 0.954	/			

NF= no fitting (for $R^2 < 0.7$); SL=Shoulder Length (min); Q_{UV} (kJ/L) = Cumulative energy at which the DL or 80 % of CECs removal was reached; / = no DL or 80 % of removal reached.

Table B.7. Bacteria and CECs kinetic constants in UWW at different concentrations of PMS (0, 0.2, 0.3 and 0.4 mM) in the absence and in the presence of ZnO-Ce in UWW under natural sunlight (Data belong to Chapter 7).

PMS (mM)	ZnO-Ce (mg/L)	Bacteria								
		<i>E. coli</i>			<i>Enterococcus</i> spp.			<i>Pseudomonas</i> spp.		
		k (min ⁻¹) R ²	R ²	Q_{UV} kJ/L	k (min ⁻¹)	R ²	Q_{UV} kJ/L	k (min ⁻¹)	R ²	Q_{UV} kJ/L
0.2	0	0.269±0.023	0.972	1.7	0.142±0.007	0.987	2.3	0.304±0.046	0.916	1.7
	100	0.368±0.054	0.939	1.2	0.140±0.004	0.996	2.3	0.315±0.059	0.871	1.7
0.3	0	NF		0.2	0.222±0.020	0.955	1.1	0.311±0.064	0.765	1.7
	100	NF		0.2	0.378±0.036	0.965	0.7	0.308±0.058	0.796	1.7
0.4	0	NF		0.1	0.364±0.028	0.959	0.6	0.529±0.097	0.783	0.8
	100	NF		0.1	0.396±0.050	0.912	0.5	0.641±0.113	0.818	0.6
PMS (mM)	ZnO-Ce (mg/L)	CECs								
		DCF			SMX			TMP		
		k (min ⁻¹)	R ²	Q_{UV} kJ/L	k (min ⁻¹)	R ²	Q_{UV} kJ/L	k (min ⁻¹)	R ²	Q_{UV} kJ/L
0	100	0.022±7E ⁻⁴	0.992	7.8	0.005±1E ⁻⁴	0.993	36.1	0.004±2E ⁻⁴	0.962	/
0.2	0	0.025±1E ⁻³	0.989	8.5	0.005±5E ⁻⁴	0.916	/	0.004±3E ⁻⁴	0.955	/
	100	0.030±0.002	0.971	6.5	0.012±4E ⁻⁴	0.993	19.0	0.007±6E ⁻⁴	0.953	/
0.3	0	0.031±0.001	0.986	5.2	0.009±0.001	0.908	/	0.007±8E ⁻⁴	0.898	/
	100	0.069±0.003	0.991	3.0	0.016±0.001	0.952	11.9	0.01±0.001	0.848	/
0.4	0	0.044±0.004	0.963	4.7	0.013±0.001	0.923	16.3	0.009±1E ⁻³	0.901	/
	100	0.061±0.003	0.989	3.1	0.018±0.002	0.924	10.5	0.015±2E ⁻³	0.914	/

NF= no fitting (for R² < 0.7); Q_{UV} (kJ/L) = Cumulative energy at which the DL or 80 % of removal was reached. / DL or 80 % was not reached.

Table B.8. Bacteria inactivation kinetic constants (k , min^{-1}) by PMS/UV-C in the presence of several oxidant concentrations in IW, SUWW and UWW (Data belong to Chapter 8).

PMS/UV-C [PMS] in mM	Bacteria								
	<i>E. coli</i>			<i>E. faecalis</i>			<i>P. aeruginosa</i>		
	k_1 (min^{-1}) k_2 (min^{-1})	R^2	Q_{UV} kJ/L	k_1 (min^{-1}) k_2 (min^{-1})	R^2	Q_{UV} kJ/L	k_1 (min^{-1}) k_2 (min^{-1})	R^2	Q_{UV} kJ/L
Isotonic water (IW)									
0	0.987±0.188 0.021±0.012	0.899 0.228	/	0.985±0.041 0.031±0.005	0.995 0.826	/	1.093±0.187 NF	0.917	2.9
0.003	1.099±0.228 0.058±0.008	0.881 0.897	0.6	1.081±0.223 0.058±0.012	0.881 0.800	0.6	1.225±0.173 0.061±0.005	0.942 0.962	0.5
0.004	1.205±0.215 0.118±0.009	0.910 0.976	0.2	1.186±0.185 0.034±0.009	0.930 0.662	0.6	1.337±0.248 0.209±0.022	0.906 0.966	0.1
0.005	1.276±0.204 0.177±0.030	0.927 0.921	0.1	1.220±0.191 0.087±0.038	0.930 0.510	0.2	1.389±0.237 0.161±0.036	0.917 0.866	0.1
Simulated urban wastewater (SUWW)									
0	0.960±0.162 0.016±0.002	0.9190. 866	> 4.5	0.747±0.084 0.010±0.002	0.963 0.753	> 4.5	1.01±0.194 0.008±0.002	0.847 0.648	> 4.5
0.01	1.13±0.210 0.003±0.002	0.884 0.139	> 4.5	0.921±0.036 0.004±0.002	0.995 0.214	> 4.5	1.17±0.206 0.009±0.002	0.913 0.556	> 4.5
0.05	1.11±0.193 0.008±0.002	0.915 0.375	> 4.5	0.911±0.041 0.007±0.002	0.994 0.691	> 4.5	1.14±0.210 0.009±0.001	0.896 0.833	> 4.5
0.1	1.12±0.191 0.027±0.004	0.918 0.820	2.9	0.911±0.017 0.011±0.002	0.999 0.797	> 4.5	1.17±0.241 0.021±0.003	0.881 0.817	4.5
0.2	1.14±0.154 0.022±0.005	0.947 0.724	2.9	0.864±0.134 0.013±0.002	0.931 0.774	> 4.5	1.20±0.199 0.023±0.003	0.922 0.776	2.9
0.3	1.00±0.189 0.067±0.007	0.900 0.916	1.4	0.752±0.110 0.031±0.003	0.938 0.903	2.9	1.03±0.237 0.047±0.017	0.856 0.742	1.4
0.5	1.24±0.219 0.062±0.005	0.911 0.944	1.4	0.845±0.098 0.040±0.005	0.960 0.871	2.2	1.27±0.226 0.057±0.011	0.910 0.790	2.2
Urban wastewater (UWW)									
	<i>E. coli</i>		Total Coliforms		<i>Enterococcus</i> spp.		<i>Pseudomonas</i> spp.		
	k (min^{-1}) R^2	Q_{UV} kJ/L	k (min^{-1}) R^2	Q_{UV} kJ/L	k (min^{-1}) R^2	Q_{UV} kJ/L	k (min^{-1}) R^2	Q_{UV} kJ/L	
0	0.193±0.023 0.900 0.003±4E ⁻⁴	4.5	0.202±0.031 0.841 0.007±0.001 0.876	4.5	0.271±6E ⁻⁴ 0.999	0.2	NF		
0.1	0.392±0.091 0.815 0.035±0.015 0.681	0.6	0.390±0.05 0.926 0.026±0.00 0.937	1.4	0.311±0.035 0.952	0.01	0.686±0.081 0.959 0.085±0.017 0.926	0.2	
0.5	0.464±0.046 0.952 0.077±0.012 0.954	0.6	0.416±0.045 0.933 0.015±0.002 0.938	2.1	0.379±0.062 0.860	0.6	1.075±0.083 0.976	0.01	
0.75	0.519±0.084 0.902 0.035±0.008 0.889	0.6	0.518±0.096 0.876 0.071±0.017 0.887	0.6	0.485±0.032 0.979	0.01	0.624±0.068 0.944	0.01	
1	0.416±0.076 0.851 0.007±0.003 0.786	1.4	0.896±0.082 0.975 0.080±0.024 0.766	1.4	0.530±0.053 0.952	0.07	0.958±0.056 0.987	0.01	

NF= no fitting (for $R^2 < 0.7$); SL=Shoulder Length (min); SL= 30 min **SL= 15 min; Q_{UV} (kJ/L) = Cumulative energy at which the DL was reached; / = no DL reached.

12. Annexes

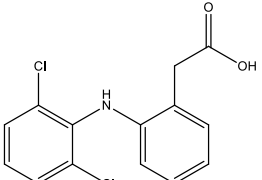
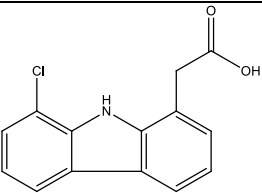
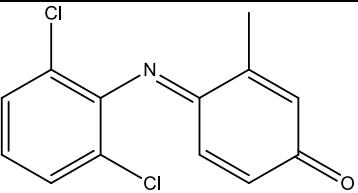
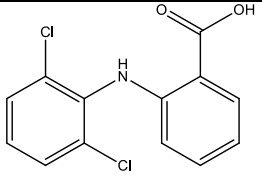
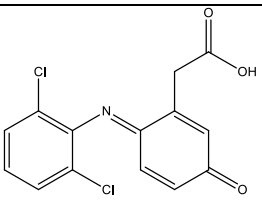
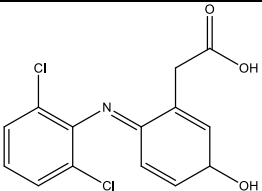
Table B.9. CECs degradation pseudo-first order kinetic constants (k , min^{-1}) by PMS/UV-C in the presence of several oxidant concentrations in IW, SUWW and UWW (Data belong to Chapter 8).

PMS/UV-C [PMS] in mM	CECs								
	DCF			SMX			TMP		
	k (min^{-1})	R^2	Q_{UV} kJ/L	k (min^{-1})	R^2	Q_{UV} kJ/L	k (min^{-1})	R^2	Q_{UV} kJ/L
Isotonic water (IW)									
0	0.197±0.029	0.920	0.02	0.217±0.018	0.952	0.1	0.008±2E ⁻⁴	0.985	/
0.003	0.389±0.036	0.968	0.01	0.281±0.034	0.967	0.03	0.013±0.001	0.976	/
0.004	0.385±0.030	0.970	0.01	0.271±0.037	0.883	0.05	0.012±2E ⁻⁴	0.996	/
0.005	0.392±0.036	0.959	0.01	0.261±0.028	0.924	0.03	0.007±3E ⁻⁴	0.975	/
0.01	0.398±0.024	0.982	0.01	0.273±0.019	0.969	0.01	0.068±0.004	0.953	0.54
Simulated urban wastewater (SUWW)									
0	0.113±0.012	0.927	0.15	0.107±0.005	0.978	0.25	0.007±2E ⁻⁴	0.978	> 4.5
0.01	0.166±0.010	0.970	0.02	0.121±0.006	0.978	0.20	0.009±1E ⁻⁴	0.997	4.32
0.05	0.185±0.012	0.966	0.02	0.129±0.006	0.974	0.16	0.015±6E ⁻⁴	0.974	2.57
0.1	0.195±0.012	0.974	0.02	0.136±0.005	0.986	0.14	0.028±4E ⁻⁴	0.997	1.14
0.2	0.204±0.021	0.930	0.02	0.147±0.008	0.975	0.12	0.059±0.001	0.996	0.55
0.3	0.229±0.036	0.869	0.02	0.184±0.005	0.995	0.06	0.096±0.002	0.995	0.28
0.5	0.214±0.025	0.918	0.02	0.230±0.005	0.996	0.02	0.175±0.008	0.985	0.06
Urban wastewater (UWW)									
0	0.110±0.018	0.903	0.01	0.071±0.004	0.968	0.4	0.001±6E ⁻⁵	0.957	/
0.1	0.119±0.013	0.925	0.10	0.088±0.004	0.974	0.3	NF		/
0.5	0.205±0.040	0.779	0.12	0.076±0.003	0.986	0.3	NF		/
0.75	0.197±0.018	0.943	0.04	0.144±0.004	0.993	0.07	0.033±0.002	0.935	1.1
1	0.314±0.039	0.900	0.02	0.185±0.010	0.970	0.02	0.045±0.002	0.974	0.8

NF= no fitting (for $R^2 < 0.7$); Q_{UV} (kJ/L) = Cumulative energy at which 80 % of CECs removal was reached; / = 80 % of removal not reached.

ANNEX C. TPs identification

Table C.1. List of TPs tentatively identified in samples. Chromatographic and spectral information.

Compound	Structure	RT (min)	Theoretical [M+H] ⁺ (m/z)	Assigned formula	RDB ^b	Error (ppm)	Reference
DCF		29.77	294.0094 250.0196 214.0429 178.0662	C₁₄H₁₁Cl₂NO₂ C ₁₃ H ₁₁ Cl ₂ N C ₁₃ H ₁₀ CIN C ₁₃ H ₉ N	9 8 9 10	-3.9 -1.9 -1.9 -2.4	
TP-259		27.94	258.0327 214.0429 178.0662	C₁₄H₁₀ClNO₂ C ₁₃ H ₁₀ CIN C ₁₃ H ₉ N	10 9 10	-3.4 0.1 -1.8	(Agüera, 2005)
TP-265		24.50	266.0134 230.0367 202.0418 195.0679 167.0730	C₁₃H₉Cl₂NO C ₁₃ H ₈ ClNO C ₁₂ H ₈ CIN C ₁₃ H ₉ NO C ₁₂ H ₉ N	9 10 9 10.5 9.5	-1.9 -0.5 0.1 2.2 3.9	(Pérez-Estrada, 2005; Agüera, 2005)
TP-281		26.21	282.0083 263.9977 236.0028 234.9950 229.0289 201.0340 200.0262 194.0600 166.0651 140.0495	C₁₃H₉Cl₂NO₂ C ₁₃ H ₇ Cl ₂ NO C ₁₂ H ₇ Cl ₂ N C ₁₂ H ₇ Cl ₂ N C ₁₃ H ₈ ClNO C ₁₂ H ₈ CIN C ₁₂ H ₆ CIN C ₁₃ H ₇ NO C ₁₂ H ₇ N C ₁₀ H ₅ N	9 10 9 9.5 10.5 9.5 10 11 10 9	-4.4 -2.8 -3.5 -4.7 -5.6 -4.9 -1.3 -4.8 -2.6 -3.4	(Jewell, 2016)
TP-309		24.47	310.0032 291.9927 263.9977 236.0028 234.9950 229.0289 201.0340 194.0600 166.0651	C₁₄H₉Cl₂NO₃ C ₁₄ H ₇ Cl ₂ NO ₂ C ₁₃ H ₇ Cl ₂ NO C ₁₂ H ₇ Cl ₂ N C ₁₂ H ₇ Cl ₂ N C ₁₃ H ₈ ClNO C ₁₂ H ₈ CIN C ₁₃ H ₇ NO C ₁₂ H ₇ N	10 11 10 9 9.5 10.5 9.5 11 10	-3.3 -3.6 -0.6 -0.6 -4.3 -2.6 0.1 -2.3 1.7	(Jewell, 2016; Pérez-Estrada, 2005)
TP-311		24.82	312.0188 294.0083 266.0134 231.0445 230.0367 214.0418 196.0757 195.0679 167.0730	C₁₄H₁₁Cl₂NO₃ C ₁₄ H ₉ Cl ₂ NO ₂ C ₁₃ H ₉ Cl ₂ NO C ₁₃ H ₁₀ ClNO C ₁₃ H ₈ ClNO C ₁₃ H ₈ CIN C ₁₃ H ₉ NO C ₁₃ H ₉ NO C ₁₂ H ₉ N	9 10 9 9.5 10 10 10 10.5 9.5	-2.8 1.3 -1.1 -1.1 1.2 2.3 4.6 4.8 6.3	(Jewell, 2016)

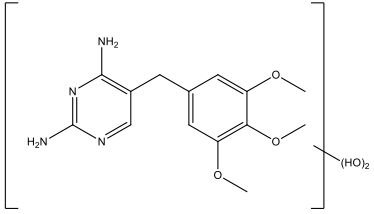
12. Annexes

TP-340 A		27.72	341.0090 322.9985 295.0036 260.0347 259.0269 249.0107 248.0028 225.0659 215.0371 213.0340	C₁₄H₁₀Cl₂N₂O₄ C ₁₄ H ₈ Cl ₂ N ₂ O ₃ C ₁₃ H ₈ Cl ₂ N ₂ O ₂ C ₁₃ H ₉ ClN ₂ O ₂ C ₁₃ H ₇ ClN ₂ O ₂ C ₁₃ H ₉ Cl ₂ N C ₁₃ H ₇ Cl ₂ N C ₁₃ H ₈ N ₂ O ₂ C ₁₂ H ₇ ClN ₂ C ₁₃ H ₈ ClN	10 11 10 10.5 11 9.5 10 11 10 10.5	-2.7 -2.4 -2.9 -1.6 -1.9 1.0 2.7 -5.6 -0.2 -0.4	(Kosjek, 2008)
TP-340 B		28.45	341.0090 324.0063 322.9985 305.9957 295.0036 275.9977 260.0347 259.0269 248.0028 241.0289 225.0659 213.0340 178.0651	C₁₄H₁₀Cl₂N₂O₄ C ₁₄ H ₁₀ Cl ₂ N ₂ O ₃ C ₁₄ H ₈ Cl ₂ N ₂ O ₃ C ₁₄ H ₈ Cl ₂ N ₂ O ₂ C ₁₃ H ₈ Cl ₂ N ₂ O ₂ C ₁₄ H ₇ Cl ₂ NO C ₁₃ H ₉ ClN ₂ O ₂ C ₁₃ H ₇ ClN ₂ O ₂ C ₁₃ H ₇ Cl ₂ N C ₁₄ H ₈ ClNO C ₁₃ H ₈ N ₂ O ₂ C ₁₃ H ₈ ClN C ₁₃ H ₇ N	10 10.5 11 11.5 10 11 10.5 11 10 11.5 11 10.5 11	-4.8 -3.1 -5.8 -2.1 -4.3 -3.4 -3.5 -4.2 -6.2 -3.3 -3.8 -5.1 -4.1	(Kosjek, 2008)
SMX		17.57	254.0593 188.0818 160.0869 156.0114 147.0791 108.0444 92.0495	C₁₀H₁₁N₃O₃S C ₁₀ H ₉ N ₃ O C ₉ H ₉ N ₃ C ₆ H ₅ NO ₂ S C ₈ H ₉ N ₃ C ₆ H ₅ NO C ₆ H ₅ N	7 8 7 5 6.5 5 5	-2.5 -2.3 -3.9 -2.4 -0.7 3.8 5.7	
TP-98		6.57	99.0552 72.0444	C₄H₆N₂O C ₃ H ₅ NO	3 2	1.8 -2.6	(Michael, 2020; Trovó, 2009)
TP-173		4.29	174.0219 108.0444 156.0114 93.0573 92.0495	C₆H₇NO₃S C ₆ H ₅ NO C ₆ H ₅ NO ₂ S C ₆ H ₇ N C ₆ H ₅ N	4 5 5 4.5 5	-2.3 1.9 4.6 2.1 -12.8	(Trovó, 2009)
TP-189		2.9	190.0168 172.0063 124.0393 122.,237 109.0522 96.0444	C₆H₇NO₄S C ₆ H ₅ NO ₃ S C ₆ H ₅ NO ₂ C ₆ H ₃ NO ₂ C ₆ H ₇ NO C ₅ H ₅ NO	4 5 5 6 4.5 4	-1.1 -2.9 6.4 -3.7 3.5 -3.0	(Trovó, 2009)
TP-197		4.32	196.0186 156.0125 155.0046 132.0567 131.0489 108.9866 107.0377	C₇H₇N₃O₂S C ₆ H ₇ NO ₂ S C ₆ H ₅ NO ₂ S C ₇ H ₇ N ₃ C ₇ H ₅ N ₃ C ₄ H ₂ N ₂ S C ₆ H ₅ NO	6 4 4.5 6 6.5 5 4.5	0.9 -0.5 -5.5 -5.5 1.6 5.6 1.3	(Trovó, 2009)
TP-215		7.37	216.0437 156.0114 108.0444 92.0495	C₇H₉N₃O₃S C ₆ H ₅ NO ₂ S C ₆ H ₅ NO C ₆ H ₅ N	5 5 5 5	-1.1 -1.8 1.9 14.4	(Trovó, 2009)

TP-267		16.01	266.0241 237.0227 199.0421 170.0030 155.9873 79.9574	C₁₀H₉N₃O₄S C ₉ H ₇ N ₃ O ₂ S C ₇ H ₉ N ₃ O ₂ S C ₅ H ₅ N ₃ O ₂ S C ₄ H ₃ N ₃ O ₂ S SO ₃	8 7.5 4.5 5 5 0.5	-0.8 5.6 8.1 3.7 5.6 0.5	(Gmurek, 2015)
TP-283		23.6	282.0190 185.9867 138.0197 122.0248	C₁₀H₉N₃O₅S C ₆ H ₅ NO ₄ S C ₆ H ₅ NO ₃ C ₆ H ₅ NO ₂	8 5 5 5	-0.6 -4 -0.5 -0.4	(Gómez-Ramos, 2011)
TMP		11.29	291.1452 275.1139 261.0982 258.1111 257.1033 245.1033 230.1176 187.0978 123.0665 110.0587	C₁₄H₁₈N₄O₃ C ₁₃ H ₁₄ N ₄ O ₃ C ₁₂ H ₁₂ N ₄ O ₃ C ₁₃ H ₁₃ N ₄ O ₂ C ₁₃ H ₁₂ N ₄ O ₂ C ₁₂ H ₁₂ N ₄ O ₂ C ₁₄ H ₁₅ NO ₂ C ₁₀ H ₁₀ N ₄ C ₅ H ₆ N ₄ C ₄ H ₆ N ₄	8 9 9 9.5 10 9 8 8 5 4.5	-0.9 0.8 0.3 -0.5 0.8 1.6 -5 -3.3 2.3 8.2	(Eckers, 2005)
TP-276		8.82	277.1295 262.1060 261.0982 247.0826 245.1033 233.1033 219.0877 187.0978 173.0822 123.0665	C₁₃H₁₆N₄O₃ C ₁₂ H ₁₄ N ₄ O ₃ C ₁₂ H ₁₂ N ₄ O ₃ C ₁₁ H ₁₀ N ₄ O ₃ C ₁₂ H ₁₂ N ₄ O ₂ C ₁₁ H ₁₂ N ₄ O ₂ C ₁₀ H ₁₀ N ₄ O ₂ C ₁₀ H ₁₀ N ₄ C ₉ H ₈ N ₄ C ₅ H ₆ N ₄	8 8.5 9 9 9 8 8 8 8 5	-1.8 -1.3 -2 3.4 -2.9 -3.4 -2.5 -1.2 -7.4 -1.8	(Kuang, 2013; Michael, 2012; Sirtori, 2010; Zhang, 2016)
TP-294		8.79	295.1401 278.1135 263.0901 253.1183 205.0720 181.0846 148.0505 113.0458	C₁₃H₁₈N₄O₄ C ₁₃ H ₁₅ N ₃ O ₄ C ₁₂ H ₁₃ N ₃ O ₄ C ₁₂ H ₁₆ N ₂ O ₄ C ₉ H ₈ N ₄ O ₂ C ₈ H ₁₁ N ₃ O ₃ C ₇ H ₅ N ₃ O C ₃ H ₄ N ₄ O	7 8 8.5 6 8 5.5 7 4	-0.8 -1.6 -4 -4.7 -5.4 7.9 8.5 -1.7	(Alharbi, 2017, 2016; Kuang, 2013; Michael, 2012; Radjenović, 2009; Sirtori, 2010; Zhang, 2016)
TP-304		12.86	305.1244 289.0931 275.0775 271.0826 244.0968 215.0927 201.0771 137.0458 95.0240	C₁₄H₁₆N₄O₄ C ₁₃ H ₁₂ N ₄ O ₄ C ₁₂ H ₁₀ N ₄ O ₄ C ₁₃ H ₁₀ N ₄ O ₃ C ₁₄ H ₁₃ NO ₃ C ₁₁ H ₁₀ N ₄ O C ₁₀ H ₈ N ₄ O C ₅ H ₄ N ₄ O C ₄ H ₂ N ₂ O	9 10 10 11 9 9 9 6 5	-1.0 0.6 0.4 -1.7 -6.6 -0.6 -0.4 0.8 10.6	(Alharbi, 2017; Arvaniti, 2020; Ji, 2016; Kong, 2018; Liu, 2019; Martínez-Costa, 2018; Michael, 2012; Sirtori, 2010)

12. Annexes

TP-306 A		9.09	307.1401 289.1295 274.1060 259.0826 243.0877 231.0877 200.0693 187.0614	C₁₄H₁₈N₄O₄ C ₁₄ H ₁₆ N ₄ O ₃ C ₁₃ H ₁₄ N ₄ O ₃ C ₁₂ H ₁₀ N ₄ O ₃ C ₁₂ H ₁₀ N ₄ O ₂ C ₁₁ H ₁₀ N ₄ O ₂ C ₁₀ H ₈ N ₄ O C ₉ H ₆ N ₄ O	8 9 9.5 10 10 9 9.5 9	-1.0 -0.4 2.4 0.1 -1 -2.8 -1.3 16.9	(Alharbi, 2017; Arvaniti, 2020; Eichhorn, 2005; Ji, 2016; Kong, 2018; Kuang, 2013; Liu, 2019; Martínez-Costa, 2018; Michael, 2012; Sirtori, 2010; Zhang, 2016)
TP-306 B		11.43	307.1401 292.1166 277.0931 275.1139 260.0666 259.0826 245.0669 231.0877 218.0448 203.0927 123.0665	C₁₄H₁₈N₄O₄ C ₁₃ H ₁₆ N ₄ O ₄ C ₁₂ H ₁₂ N ₄ O ₄ C ₁₃ H ₁₄ N ₄ O ₃ C ₁₂ H ₉ N ₃ O ₄ C ₁₂ H ₁₀ N ₄ O ₃ C ₁₁ H ₈ N ₄ O ₃ C ₁₁ H ₁₀ N ₄ O ₂ C ₁₁ H ₇ NO ₄ C ₁₀ H ₁₀ N ₄ O C ₅ H ₆ N ₄	8 8.5 9 9 10 10 10 9 9 8 5	-0.4 -3.1 -3 -0.2 0.8 -2.2 -0.1 0.2 2.8 3.3 -5.1	(Arvaniti, 2020; Liu, 2019; Martínez-Costa, 2018; Michael, 2012; Sirtori, 2010; Zhang, 2016)
TP-322 A		10.80	323.1350 291.1088 263.1139 259.0826 249.0982 231.0877 216.0642 199.0614 189.0771 173.0822 160.0743 147.0665 123.0665	C₁₄H₁₈N₄O₅ C ₁₃ H ₁₄ N ₄ O ₄ C ₁₂ H ₁₄ N ₄ O ₃ C ₁₂ H ₁₀ N ₄ O ₃ C ₁₁ H ₁₂ N ₄ O ₃ C ₁₁ H ₁₀ N ₄ O ₂ C ₁₀ H ₈ N ₄ O ₂ C ₁₀ H ₆ N ₄ O C ₉ H ₈ N ₄ O C ₉ H ₈ N ₄ C ₈ H ₈ N ₄ C ₇ H ₆ N ₄ C ₅ H ₆ N ₄	8 9 8 10 8 9 9.5 10 8 8 7.5 7 5	-1 -1 -0.6 0.5 0.3 -2.4 3.4 -0.7 1.7 -1 0.3 -7 6.3	(Alharbi, 2017, 2016; Ji, 2016; Kong, 2018; Kuang, 2013; Michael, 2012; Radjenović, 2009; Sirtori, 2010; Zhang, 2016)
TP-322 B		12.12	323.1350 291.1088 263.1139 259.0826 249.0982 231.0877 216.0642 199.0614 189.0771 173.0822 160.0743	C₁₄H₁₈N₄O₅ C ₁₃ H ₁₄ N ₄ O ₄ C ₁₂ H ₁₄ N ₄ O ₃ C ₁₂ H ₁₀ N ₄ O ₃ C ₁₁ H ₁₂ N ₄ O ₃ C ₁₁ H ₁₀ N ₄ O ₂ C ₁₀ H ₈ N ₄ O ₂ C ₁₀ H ₆ N ₄ O C ₉ H ₈ N ₄ O C ₉ H ₈ N ₄ C ₈ H ₈ N ₄	8 9 8 10 8 9 9.5 10 8 8 7.5	-0.7 1.4 -3.7 0.1 -0.1 -0.2 2 -1.2 -2.6 -1.6 2.2	(Alharbi, 2017, 2016; Ji, 2016; Kong, 2018; Kuang, 2013; Michael, 2012; Radjenović, 2009;

			123.0665	$C_5H_6N_4$	5	6.3	Sirtori, 2010; Zhang, 2016)
TP-322 C		13.21	323.1350 291.1088 263.1139 259.0826 249.0982 231.0877 216.0642 189.0771 173.0822 160.0743 123.0665	$C_{14}H_{18}N_4O_5$ $C_{13}H_{14}N_4O_4$ $C_{12}H_{14}N_4O_3$ $C_{12}H_{10}N_4O_3$ $C_{11}H_{12}N_4O_3$ $C_{11}H_{10}N_4O_2$ $C_{10}H_8N_4O_2$ $C_9H_8N_4O$ $C_9H_8N_4$ $C_8H_8N_4$ $C_5H_6N_4$	8 9 8 10 8 9 9.5 8 8 7.5 5	-0.6 0.1 2.0 -1 -0.5 -2.4 11.6 -3.1 -1.6 -4 1.4	(Alharbi, 2017, 2016; Ji, 2016; Kong, 2018; Kuang, 2013; Michael, 2012; Radjenović, 2009; Sirtori, 2010; Zhang, 2016)